AGARD

ADVISORY GROUP FOR AEROSPACE RESEARCH & DEVELOPMENT

7 RUE ANCELLE 92200 NEUILLY SUR SEINE FRANCE

AGARD LECTURE SERIES No.133

Advances in Strapdown Inertial Systems

NORTH ATLANTIC TREATY ORGANIZATION

DISTRIBUTION AND AVAILABILITY
ON BACK COVER

COMPONENT PART NOTICE

THIS PAPER IS A COMPONENT PART OF THE FOLLOWING COMPILATION REPORT:

(TITLE): Advances in Strapdown Inertial Systems. Lecture Series Held in Athens, Greece on 14-15 May 1984, in Rome, Italy on 17-18 May 1984 and in Copenhagen, Denmark on 21-22 May 1984.

(SOURCE): Advisory Group for Aerospace Research and Development, Neuilly-Sur-Seine (France).

TO ORDER THE COMPLETE COMPILATION REPORT USE AD-A143 244.

THE COMPONENT PART IS PROVIDED HERE TO ALLOW USERS ACCESS TO INDIVIDUALLY AUTHORED SECTIONS OF PROCEEDINGS, ANNALS, SYMPOSIA, ETC. HOWEVER, THE COMPONENT SHOULD BE CONSIDERED WITHIN THE CONTEXT OF THE OVERALL COMPILATION REPORT AND NOT AS A STAND-ALONE TECHNICAL REPORT.

THE FOLLOWING COMPONENT PART NUMBERS COMPRISE THE COMPILATION REPORT:

AD#:	TITLE:
AD-P003 619	Advances in Strapdown Inertial Systems-Introduction and Overview.
AD-P003 620	Advances in Strapdown Sensors.
AD-P003 621	Strapdown System Algorithms.
AD-P003 622	Requirements, Applications, and Results of Strapdown Inertial Technology to Commercial Airplanes.
AD-P003 623	Strapdown Inertial Systems for Tactical Missiles Using Mass Unbalanced Two-Axis Rate Gyros.
AD-P003 624	Modular Strapdown Guidance Unit with Embedded Microprocessors.
AD-P003 625	Application of Multifunction Strapdown Inertial System.
AD-P003 626	Initial Alignment and Augmentation of the Arinc 750 Strapdown Attitude and Heading Reference System (AHRS) LTR-81.

COMPONENT PART NOTICE (CON'T)

AD#: TITLE:

NORTH ATLANTIC TREATY ORGANIZATION

ADVISORY GROUP FOR AEROSPACE RESEARCH AND DEVELOPMENT

(ORGANISATION DU TRAITE DE L'ATLANTIQUE NORD)

AGARD Lecture Series No.133

ADVANCES IN STRAPDOWN INERTIAL SYSTEMS

The material in this publication was assembled to support a Lecture Series under the sponsorship of the Guidance and Control Panel and the Consultant and Exchange Programme of AGARD on 14 15 May 1984 in Athens, Greece; 17 18 May 1984 in Rome, Italy; and 21 22 May 1984

THE MISSION OF AGARD

The mission of AGARD is to bring together the leading personalities of the NATO nations in the fields of science and technology relating to aerospace for the following purposes:

- Exchanging of scientific and technical information;
- Continuously stimulating advances in the aerospace sciences relevant to strengthening the common defence posture;
- Improving the co-operation among member nations in aerospace research and development;
- Providing scientific and technical advice and assistance to the North Atlantic Military Committee in the field of aerospace research and development;
- Rendering scientific and technical assistance, as requested, to other NATO bodies and to member nations in connection with research and development problems in the aerospace field;
- Providing assistance to member nations for the purpose of increasing their scientific and technical potential;
- Recommending effective ways for the member nations to use their research and development capabilities for the common benefit of the NATO community.

The highest authority within AGARD is the National Delegates Board consisting of officially appointed senior representatives from each member nation. The mission of AGARD is carried out through the Panels which are composed of experts appointed by the National Delegates, the Consultant and Exchange Programme and the Aerospace Applications Studies Programme. The results of AGARD work are reported to the member nations and the NATO Authorities through the AGARD series of publications of which this is one.

Participation in AGARD activities is by invitation only and is normally limited to citizens of the NATO nations.

Published April 1984

ISBN 92-835-0351-1

Printed by Specialised Printing Services Limited

PREFACE

This Lecture Series is intended to address the advances in strapdown inertial system technology during the last five years. Areas that are addressed include advances in strapdown instruments and computational algorithms and the application to commercial aircraft, remotely piloted vehicles, flight controls, instrumentation, and navigation problems in general. This provides one document which covers the present state-of-the-art in strapdown systems technology.

The material in this publication was assembled to support a Lecture Series under the sponsorship of the Guidance and Control Panel and the Consultant and Exchange Programme of AGARD.

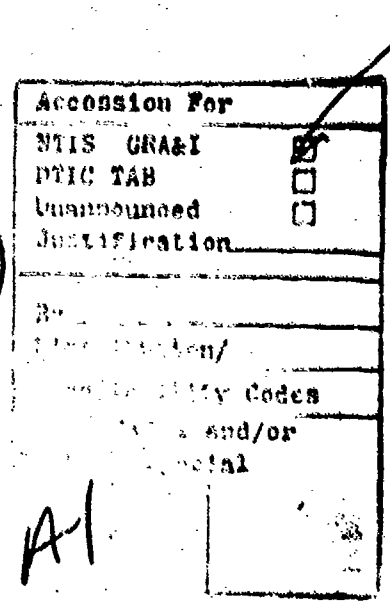

LIST OF SPEAKERS

Lecture Series Director: Dr G.T.Schmidt
Charles Stark Draper Laboratory, Inc.
555 Technology Square
Cambridge, MA 02139
USA

SPEAKERS

Mr P.Fenner
Boeing Commercial Aircraft Co.
Seattle, WA 98124
USA

Mr J.Gilmore
Charles Stark Draper Laboratory, Inc.
555 Technology Square
Cambridge, MA 02139
USA

Mr W.Hassenpflug
LITEF
Lörracher Strasse 18
7800 Freiburg
Germany

Mr J.Michelin
S.F.I.M
13 Avenue Marcel Ramolfo Garnier
91300 Massy
France

Mr P.Savage
Strapdown Associates, Inc.
620 Mendelssohn Avenue, N
Golden Valley, MN 55427
USA

Mr D.L.Sebring
McDonnell Aircraft Company
Building 74, P.O. Box 516
St. Louis, MO 63166
USA

CONTENTS

ADVANCES IN STRAPDOWN INERTIAL SYSTEMS - INTRODUCTION AND OVERVIEW

George T. Schmidt
Leader, G&N Advanced Programs Division
The C.S. Draper Laboratory, Inc., Cambridge, MA, U.S.A.

SUMMARY

This Lecture Series is intended to present the significant advances in strapdown inertial system technology since the last Lecture Series (No. 95) in 1978 on the subject. Areas that will be addressed in the Lecture Series include advances in strapdown instruments and computational algorithms and the applications to commercial aircraft, remotely piloted vehicles, flight controls, instrumentation, and navigation problems in general. This introductory paper will give an overview of these lectures.

1. INTRODUCTION

In June and October of 1978, an AGARD Lecture Series (No. 95)[1] on strapdown inertial system technology was held in seven NATO countries. This present Lecture Series (No. 133) is again sponsored by the Guidance and Control Panel of AGARD whose members felt it was timely to review the state-of-the-art in strapdown systems. The intent of this lecture is to provide some overall background and introductory material and an overview of the following lectures.

Traditionally, inertial navigation systems have been categorized into (1) those that employ gimbals to isolate the inertial instruments from some vehicle motions, (2) those that mount (or strapdown) the inertial instruments directly to the vehicle and (3) others where the gimbals may be replaced by a fluid or where the system may be partially strapped-down and partially gimbaled. Figure 1 illustrates some applications of these types. A brief description of types (1) and (2) follows.

INERTIAL SYSTEM TYPE		
Gimbal	F-15, F-16	ALCM
Strapdown	737, 757, 767	MRASM
Other	Peacemaker (MX)	Reentry Vehicles

Figure 1. Typical Inertial System Applications

In inertial-platform gimbal mechanizations, the gyroscopes mounted on a stable platform measure angular rates, and gimbal-drive systems can use the angular-rate information to null the angular motion sensed by the gyroscopes. In this manner, the gyroscopes and accelerometers on the stable platform are inertially stabilized from the vehicle motion, and the stable member physically represents an inertial reference frame. By double integration of the specific-force indications from the accelerometers, with a correction for gravity, position determination is possible. Figure 2 illustrates this approach.

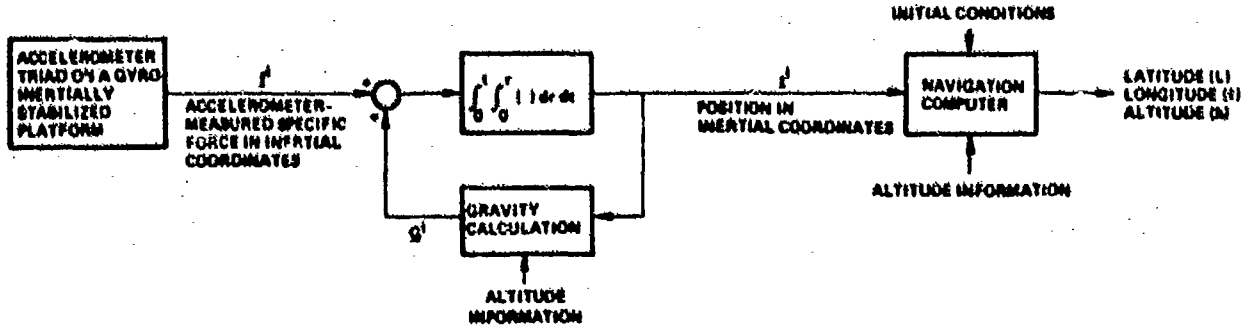

Gimbal systems provide a good dynamic environment for inertial instruments, particularly in severe angular oscillatory cases, since the gimbals isolate the gyros from the environment. In fact, the state-of-the-art is such that navigation performance of gimbal systems can approach almost error-free instrument operation to the point where uncertainties in the knowledge of the gravity field become the dominant sources of navigational error.

In strapdown inertial systems, the sensors are mounted directly (or perhaps with vibration isolators) to the vehicle. Inertial-sensor outputs now represent specific force and angular rate with respect to inertial space coordinatized in vehicle body axes. Therefore, to maintain an inertial reference frame, a computer-generated transformation-matrix algorithm between body and inertial frames must be used to process the gyro outputs as the vehicle moves and its orientation changes. Then, the accelerometer information must be transformed from the body frame to the inertial reference frame. Figure 3 illustrates this mechanization. Other reference frames, such as local vertical, may also be used for navigation.[1]

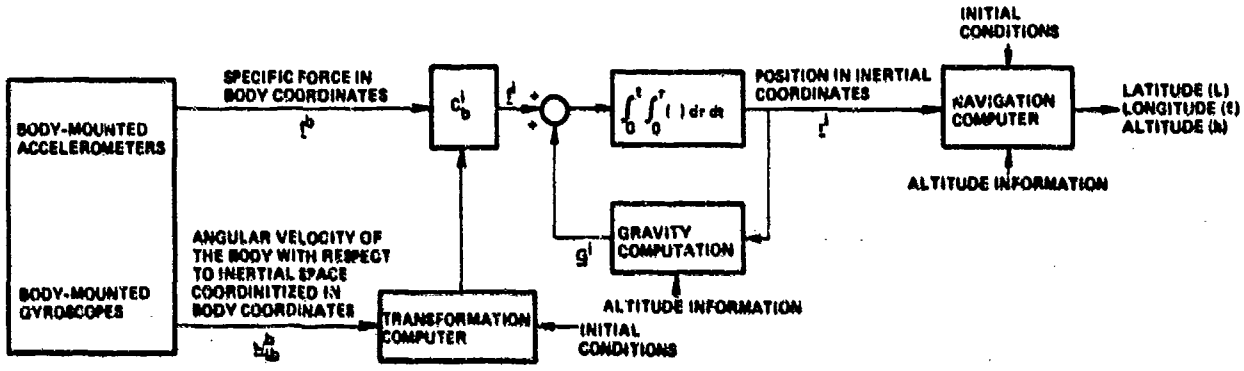

Figure 3. Strapdown System Computing in Inertial Coordinates

In addition to the added computations of a strapdown system, the inertial sensors require a large dynamic range. They are now subjected to the entire vehicle dynamic environment and, in general, will not perform as well had they been isolated from it. Much of the work, in fact, on laser gyros (to be discussed in following papers) stems from their reputed insensitivity to dynamically induced errors, although single-degree-of-freedom gyros, tuned-rotor two-degree-of-freedom gyros, and other gyros have had strapdown applications.

Strapdown systems are of interest for all but the most demanding performance missions since elimination of the gimbals could possibly result in easier maintenance, less cost, and perhaps improved reliability. If aided-inertial systems such as Global Positioning System (GPS)-inertial are considered, performance differences between gimbal and strapdown systems are even less. The increased computational requirements of strapdown systems appear less important with each advance in computer technology. Furthermore, the strapdown instruments' outputs are in body coordinates, which is desirable for autopilot functions. Since 1978, a new generation of commercial aircraft (757,767), tactical missiles (NRASM) and other systems have committed to the use of strapdown inertial systems. Consequently, much interest and ongoing activity exists in strapdown sensor and system development, and this Lecture Series has been motivated by these activities.

2. OVERVIEW OF THE LECTURES*

The first two lectures are by Mr. P. Savage. His first paper on strapdown sensor advances will update his strapdown sensor paper presented in AGARD Lecture Series 95. Principle areas to be addressed in strapdown gyro technology will be the state-of-the-art is floated rate integrating and tuned-rotor strapdown gyros; performance advances in laser gyros; special design considerations associated with mechanical dither; square versus triangular laser gyros; the state-of-the-art in multi-oscillator and magnetic mirror laser gyros; present and projected application areas for laser gyros related to size, performance, and cost; the theory of operation and state-of-the-art in fiber optics laser interferometer rate sensor technology; and the fundamental distinctions between the laser gyro and interferometer rate sensor. Basic areas to be addressed in strapdown accelerometer technology will be performance advances in pendulous accelerometers, and the theory of operation and state-of-the-art in vibrating beam accelerometer technology.

*Presentation of these lectures is, as of this writing (2/84), still subject to review by the appropriate national authorities.

His second paper on strapdown system algorithms will address the attitude determination, acceleration transformation, and attitude/heading output computational operations used in modern-day strapdown inertial navigation systems and the contemporary iterative algorithms for implementing these operations in real-time computers. The emphasis will be on two-speed algorithms in which coning and sculling vibration induced effects are handled by simplified high speed algorithms with results fed into lower speed higher-order attitude updating/acceleration transformation algorithms. Design equations will be presented for evaluating the performance of the strapdown computer algorithms as a function of computer execution speed and sensor assembly vibration amplitude/frequency/phase environment. Direction cosine and quaternion based algorithms will be described and compared for accuracy and computer loading in light of modern day algorithm capabilities for overall strapdown operations. Orthogonality and normalization operations will be addressed for potential attitude algorithm accuracy enhancement including a discussion on the question of need for such algorithms, potential pitfalls if used, and tradeoffs for direction cosine matrix row versus column orthogonality/normalization control. The section on attitude data output algorithms (i.e., Euler angle extraction) will include a discussion on roll/yaw output algorithms near high/low pitch angle conditions.

The next lecture by Mr. P. Fenner will describe the application of laser strapdown technology to commercial aircraft. Background will be provided on design requirements and design synthesis. Specific application of the Honeywell laser Inertial Reference System (IRS) will be described for the Boeing 737, 757, and 767 commercial airplanes. Redundancy, safety, and reliability considerations will be described along with the highly integrated aspects of the system design. A review will be given of the IRS architecture, performance, requirements, operation modes, and a top level description of the processing algorithms. The test program and methodology employed by both Boeing and Honeywell to ensure the system design satisified all performance requirements and that the software was exhaustively verified and validated prior to initiation of flight testing will be described. A special flight test program conducted in cooperation with American Airlines to obtain navigation performance data to support the use of the IRS as a certified long range navigation system will be described along with the test results. The results of the Boeing flight program with 757 and 767 airplanes will also be described as well as unique problems that were encountered. In-service experience, both MTBF and performance, will be provided from the first year of air-line experience. These results will show the "payoff" from laser strapdown technology is substantially better than predicted.

The following lecture by Mr. R. Acker will describe GN&C for remotely piloted vehicles. Major system elements include: an on-board computer, strapdown inertial sensor, air data sensor, data link, flight control, propulsion control, and payload control. His paper will concentrate on the system architecture, design tradeoffs, error sources and digital processing techniques utilized to tie together these major systems to meet RPV requirements. Inertial sensor error sources and accuracy will be related to mission requirements with respect to payload pointing, data link acquisition after loss, silent run periods, and flight control. Techniques for use of the air data system information will be described and evaluated for expanding mission flexibility. The Kalman filter utilized in the onboard computer to process inertial, data link, and air data system data will be described with emphasis on the relationship between system error sources, filter complexity, and mission performance parameters. Data link parameters, their need and accuracy requirements with respect to mission performance will be quantatively evaluated. The onboard computer software will be described with respect to functions and their time and memory loading per function. Results of 16 flight tests will be presented and compared to simulation data for mission effectiveness determination and assessment of ability to predict performance. The remaining flight test program and objectives will be reviewed. With perspective gained from the design pha and a flight test program the effectiveness of the digital control techniques employed will be evaluated and future trends projected.

The next paper by Mr. J. Michelin and Mr. Senneville will describe the application of a strapdown system to tactical missiles and builds upon an application presented in Lecture Series No. 95. A mass unbalanced rate gyro which also provides specific force measurements, a totally computerized system, and an optimal data processing system are some of the features described. The test methods and results of a prototype system are also described.

The following lecture by Mr. J. Gilmore will describe the Low-cost Inertial Guidance System (LCIGS) which is a modular strapdown implementation of attitude (gyro) and velocity (accelerometer) axes that permits the interchangeable use of different manufacturer's instruments without affecting the system's electronic or mechanical interfaces or processing software. This design flexibility is made possible by the use of microprocessors for processing and control. The microprocessors are embedded in each module and five are used: one per accelerometer triad, one each per gyro module, and one in the service module. The processors effect on-line digital torquing control of the gyros, active instrument error model compensation, including modeling for temperature sensivitity effects, temperature control, self-testing, etc. Adaptation of processing and calibration algorithms to accommodate for instrument changes or sensed environmental variations is achieved through the use of an alterable read-only data base that may be updated by the LCIGS support equipment as required at calibrations or upon an instrument replacement. This data base is accessed by the microprocessors and used to compute coefficient corrections for the processing algorithms. The system architecture is presented and the microprocessor software partitioning and functions are described.

The next paper presented by Mr. D. Sebring will describe the Multifunction Flight Control Reference System (MFCRS) program. The MFCRS program uses two highly modified ring laser gyro navigation units developed by Honeywell Inc. to perform the flight control reference and navigation functions onboard a F-15 fighter aircraft. The two units are separated by nine feet to provide survivability and one is skewed with respect to the other to provide required redundant inertial information. Technical information on the actual flight control and redundancy management designs, including the unique electronic alignment procedure, will be given. Appropriate data from the flight control analyses, man-in-the-loop simulation, redundancy management Monte Carlo simulations, and laboratory tests will also be included to substantiate the design.

The final lecture presented by Mr. W. Hassenpflug and Dr. Kleinschmidt describes the initial alignment and augmentation of a strapdown attitude and heading system. The analytical basis, system hardware description, and comparison between simulation and flight test results is presented. Techniques for possible system improvements are also described.

3. CONCLUDING REMARKS

The intent of this Lecture Series is to provide an up-to-date overview of strapdown inertial system technology. To that end, lectures on components, algorithms, and systems are presented. The reader has in this one document a set of papers summarizing many of the present interesting applications of strapdown inertial technology. In addition, a detailed bibliography of references published during the last few years appears at the end.

REFERENCE

1. Strap-Down Inertial Systems, NATO AGARD Lecture Series No. 95, June 1978.

ADVANCES IN STRAPDOWN SENSORS

By

Paul G. Savage
President
Strapdown Associates, Inc.
Woodbridge Plaza, Suite 150
10201 Wayzata Blvd.
Minnetonka, Minnesota 55343

SUMMARY

This paper reviews the advances that have taken place in strapdown sensor technology since 1978. It is intended as an update to the paper on Strapdown Sensors presented as part of AGARD Lecture Series 95 in 1978 (1). Principal areas addressed in strapdown gyro technology are the state-of-the-art in mainstream floated rate-integrating and tuned-rotor strapdown gyros, performance advances in laser gyros, special design considerations associated with mechanically dithered laser gyros, the state-of-the-art in magnetic mirror and multioscillator laser gyros, present and projected application areas for laser gyros related to size, performance and cost, the theory of operation and state-of-the-art in fiber-optic rate sensor technology, and the fundamental distinctions between the laser gyro and fiber-optic rate sensor. Basic areas addressed in strapdown accelerometer technology are performance advances in pendulous accelerometers, and the theory of operation and state-of-the-art in vibrating beam accelerometer technology.

1. INTRODUCTION

The state-of-the-art in strapdown sensor technology has advanced considerably since 1978, particulary in the higher accuracy performance categories. Ring laser gyros designed by several manufacturing groups have demonstrated their ability to meet the requirements for 1 nmph inertial navigation. Laser gyros are now in operational use on several major aircraft programs, and have demonstrated reliabilities in the field that are exceeding user goals. Advanced development programs have been initiated to extend the performance capabilities of the ring laser gyro into the class needed for 0.1 nmph navigation.

Conventional floating rate-integrating and tuned-rotor gyro technology has been increasingly applied in the moderate to low performance strapdown areas. These instruments continue to provide a good alternative to the ring laser gyro in applications requiring small size and low cost, where lower performance is acceptable. A new optical rate sensor technology based on the use of fiber-optics has emerged over the past few years as a lower cost/reduced performance alternative to the ring laser gyro. Simultaneously, ring laser gyro development activities have been directed at cost and size reduction to extend its applicability range into the moderate performance areas.

Strapdown accelerometer technology continues to be principally based on the pendulous electrically servoed accelerometer design approach. Design refinements since 1978 have upgraded the performance of this instrument and somewhat reduced its cost. It continues to remain compatible in cost and performance with requirements in most strapdown application areas (in proportion to the cost of the gyro and computing elements that are also contained in a strapdown system). To meet cost targets for the future, a vibrating beam accelerometer technology is being developed as a lower cost alternative to the pendulous accelerometer.

This paper reviews each of the instruments discussed above, with emphasis on the performance capabilites, problem areas, and applications where they have been used or planned for use since 1978. For each instrument, a brief discussion is also included which describes its principal of operation. Analytical descriptions and detailed design considerations for the floated rate-integrating gyro, tuned-rotor gyro, ring laser gyro, and pendulous accelerometer have been provided in the AGARD Lecture Series 95 paper on Strapdown Sensors (1), and are not repeated here. Error characteristics for the fiber-optic rate sensor and vibrating beam accelerometer are presented, but from a qualitative standpoint, because the performance characteristics of these devices have not been sufficiently disclosed in the open literature to allow detailed accurate analytical modeling that accounts for the important critical error sources, particularly those that are environmentally induced and which change over time and operating cycles.

A generalized error budget is also provided for reference at the beginning of the paper which attempts to define typical gyro and accelerometer performance requirements for four types of strapdown inertial systems.

2. SENSOR PERFORMANCE REQUIREMENTS

Table 1 defines typical accuracy requirements for strapdown sensors in four application

areas: the classical 1 nmph inertial navigator, a higher performance advanced 0.1 nmph inertial navigator, a lower performance strapdown attitude heading reference system (AHRS), and a still lower performance tactical missile midcourse guidance system. The performance categories depicted in Table 1 are considered typical for most strapdown sensor applications today and in the immediate future. Table 1 should be used as a reference to categorize typical sensor performance requirements during discussions on individual sensor capabilities.

TABLE 1 - TYPICAL STRAPDOWN SENSOR PERFORMANCE REQUIREMENTS

Performance Parameter	0.1 nmph INS	1.0 nmph INS	AHRS	Tactical Missile Midcourse Guidance
Gyro Bias Uncertainty (deg/hr)	0.001	0.01	1.0(0.1)* to 10	5 to 30
Gyro Random Noise (deg/$hr^{\frac{1}{2}}$)**	0.005	0.002	0.01	0.1
Gyro Scale-Factor Uncertainty (ppm)	1	5	200	1000
Gyro Alignment Uncertainty (arc sec)	1	2	200	300
Accelerometer Bias Uncertainty (μg)	10	40	1000	1000
Accelerometer Scale-Factor Uncertainty (ppm)	50	200	1000	1000
Accelerometer Alignment Uncertainty(sec)	2	7	200	300
Accelerometer Bias Trending (μg/sec)	0.003	0.01	NA(0.1)*	NA

* For AHRS with an earth rate gyro-compass heading determination requirement. Other figure shown is for AHRS with heading slaved to magnetic flux heading detector.

** This error source is a characteristic principally of laser gyros.

3. SINGLE-DEGREE-OF-FREEDOM FLOATED RATE-INTEGRATING GYRO

The floated rate-integrating gyro (1, 4, 5) pictured schematically in Figure 1 is the gyro with the longest production history and is the original high-accuracy gimbaled-platform gyro. The device consists of a cylindrical hermetically sealed momentum-wheel/spinmotor assembly (float) contained in a cylindrical hermetically sealed case. The float is interfaced to the case by a precision suspension assembly that is laterally rigid (normal to the cylinder axis) but allows "frictionless" angular movement of the float relative to the case about the cylinder axis. The cavity between the case and float is filled with a fluid that serves the dual purpose of suspending the float at neutral buoyancy, and providing viscous damping to resist relative float-case angular motion about the suspension axis.

A ball-bearing or gas-bearing synchronous-hysteris spinmotor is utilized in the float to maintain constant rotor spinspeed, hence constant float angular momentum. A signal-generator/pickoff provides an electrical output signal from the gyro proportional to the angular displacement of the float relative to the case. An electrical torque generator provides the capability for applying known torques to the float about the suspension axis proportional to an applied electrical input current. Delicate flex leads are used to transmit electrical signals and power between the case and float.

Under applied angular rates about the input axis, the gyro float develops a precessional rate about the output axis (rotation rate of the angle sensed by the signal-generator/pick-off, see Figure 1). The pickoff-angle rate generates a viscous torque on the float about the output axis (due to the damping fluid) which sums with the electrically applied torque-generator torque to precess the float about the input axis at the gyro input rate. The pickoff-angle rate thereby becomes proportional to the difference between the input rate and the torque-generator precessional rate, hence, the pickoff angle becomes proportional to the integral of the difference between the input and torque-generator rates.

To operate the gyro in a strapdown mode, the pickoff angle is electrically servoed to null by the torque generator which is driven by the signal-generator/pickoff output (through suitable compensation and amplifer electronics). The time integral of the difference between the input and torque-generator precessional rates is thereby maintained at zero, and the integral of the torque-generator rate becomes proportional to the integral of the input rate. Thus, the integral of the torque-generator electrical current provides a measure of the integral of input rate for a rate-gyro strapdown inertial navigation system.

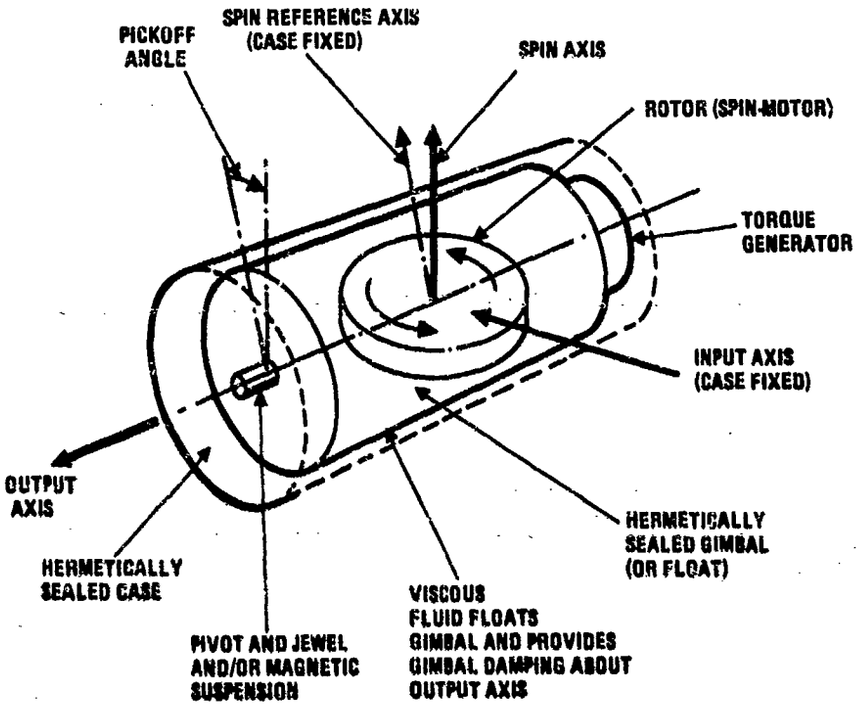

Figure 1 - Single-degree-of-freedom floated rate-integrated gyro concept.

3.1 Performance And Application Areas

Application areas for the strapdown floated rate-integrating gyro (RIG) have been primarily in the lower performance (5 to 30 deg/hr bias accuracy) areas where small-size low angular momentum units meet performance requirements, and costs are competetive with alternative gyro mechanization approaches (e.g., the tuned-rotor gyro). The floatation fluid suspension in the RIG makes the device extremely rugged, hence, provides a natural suitability to those lower performance application areas where high vibrations and shock are prevalent.

Low cost tactical missile midcourse inertial guidance has been a continuing application area for the strapdown RIG. Standard Missile-2, Harpoon, Phoenix, and recently AMRAAM, are examples of tactical missile systems that incorporate strapdown RIG's for midcourse guidance and stabilization/control. Strapdown RIG's have also been used in some applications to implement a short term navigation reference between updates from a higher accuracy navigation device. Examples are motion compensation for airborne radar systems (using the aircraft INS as the "outer-loop" reference), and to generate short term navigation data between precision radio navigation position fixes for aircraft test instrumentation purposes (e.g., ACMR - Air Combat Maneuvering Range).

Higher performance application areas for the strapdown RIG have remained limited due to their higher cost for comparable performance compared to the strapdown tuned-rotor or ring laser gyros.

4. TUNED-ROTOR GYRO

The tuned-rotor gyro (1, 6, 7, 8, 9, 10) is the most advanced gyro in large-scale production today for aircraft 1-nmi/hr gimbaled platforms. Due to its simplicity (compared to the floated rate-integrating gyro), the tuned-rotor gyro is theoretically lower in cost

and more reliable. A drawing of a representative tuned-rotor gyro is presented in Figure 2. Figure 3 is a schematic illustration of the gyro rotor assembly.

The gyro consists of a momentum wheel (rotor) connected by a flexible gimbal to a case-fixed synchronous-hysteresis ball-bearing spinmotor drive shaft. The gimbal is attached to the motor and rotor through members that are torsionally flexible but laterally rigid. A two-axis variable-reluctance signal-generator/pickoff is included that measures the angular deviation of the rotor (in two axes) relative to the case (to which the motor is attached). Also included is a two-axis permanent-magnet torque generator that allows the rotor to be torqued relative to the case on current command. The torquer magnets are attached to the rotor, and the torquer coils are attached to the gyro case.

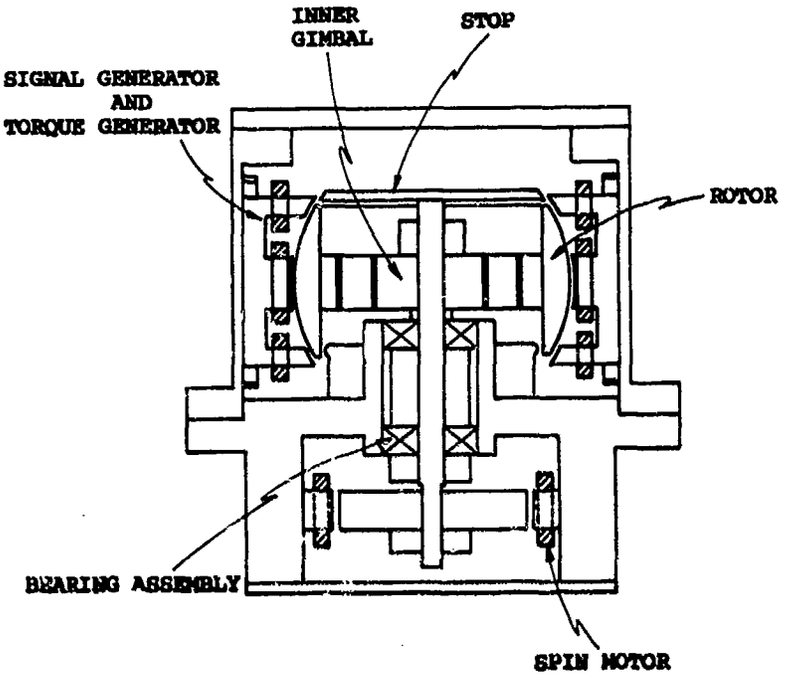

Figure 2 - Typical tuned-rotor gyro configuration.

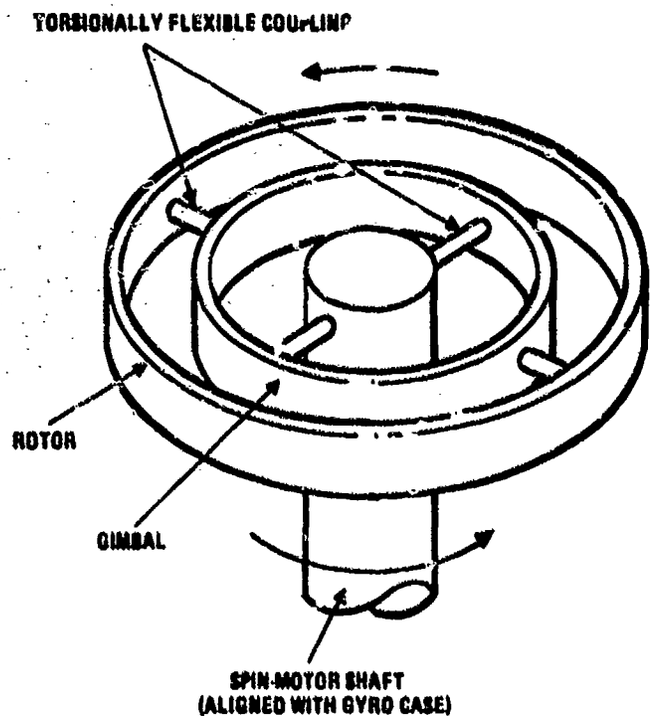

Figure 3 - Tuned-rotor gyro rotor assembly.

As for all angular-momentum-based rate-sensing devices, the key design feature of the gyro is the means by which it can contain the reference momentum (the spinning rotor), without introducing torques (drift rates) in the process. For the tuned-rotor gyro, the method is linked to the dynamic effect of the flexible gimbal attachment between the rotor and the motor. Geometrical reasoning reveals that when the rotor is spinning about an axis that deviates in angle from the motor-shaft axis, the gimbal is driven into a cyclic oscillation in and out of the rotor plane at twice the rotor frequency. Dynamic analysis shows that the reaction torque on the rotor to sustain this motion has a systematic component along the angular-deviation vector that is proportional to the angular displacement, but that acts as a spring with a negative spring constant. The flexible pivots between the rotor and gimbal, on the other hand, provide a similar spring torque to the rotor, but of the opposite sign. Hence, to free the rotor from systematic torques associated with the angular displacement, it is only necessary to design the gimbal pivot springs such that their effect cancels the inverse spring effect of the gimbal. The result (tuning) is a rotor suspension that is insensitive to angular movement of the case.

Use of the tuned-rotor gyro in a strapdown mode parallels the technique used for the floated rate-integrating gyro. Exceptions are that damping must be provided electrically in the caging loop, as there is no fluid, and that the gyro must be caged in two axes simultaneously. The latter effect couples the two caging loops together due to the gyroscopic cross-axis reaction of the rotor to applied torques.

4.1 Performance And Application Areas

Application areas for the strapdown tuned-rotor gyro (TRG) have been primarily in the medium performance areas where small-size low angular momentum units have acceptable accuracy, are lower in cost compared with comparable size/performance ring laser gyro technology, and where bias accuracy compared to equivalent cost RIG units is superior. The inherent simplicity in design of the dry rotor suspension concept for the TRG which lowers its production cost, also limits its usefulness in high vibration/shock environments where rotor resonances can potentially be excited (producing sensor error and, in extreme cases, device failure). Current design improvements for the TRG are being directed at extending its vibration capability while retaining accuracy.

The strapdown AHRS (attitude-heading reference system) has been a primary application area for the strapdown TRG for commercial aircraft, military drones, and most recently, torpedoes. One of the larger potential application areas for the strapdown TRG is for the military aircraft strapdown AHRS where small size and low cost are key requirements, and not yet achievable with ring laser gyro technology.

Two current application areas of interest for the strapdown TRG are for tactical missile midcourse guidance and helicopter or torpedo strapdown AHRS. Small-size low-cost versions of the strapdown TRG have been developed as a competitor to the RIG for the tactical missile midcourse guidance application. Potential vibration/shock susceptability of the TRG is an area of concern for the tactical missile application, but is being addressed by TRG design groups. Shock requirements for torpedo application of the TRG have been handled through use of elastomeric isolators between the TRG sensor assembly and torpedo mounting plate. The helicopter AHRS application imposes a bias stability requirement of 0.1 deg/hr on the TRG which is not achievable today with small size low cost units.

The 0.1 deg per hour helicopter AHRS requirement stems from the need to determine heading prior to takeoff by earth-rate gyro-compassing to an accuracy of 0.5 degrees. This translates into a gyro accuracy requirement of 0.1 deg/hr to detect the direction of horizontal earth rate (at 45 deg latitude) to 0.01 radians (i.e., 0.5 degrees). Typical small-size low-cost TRG's have bias accuracies over long term of 1 to 2 deg/hr. To achieve the 0.1 deg/hr requirement, a turn-table is needed to position the TRG at different orientations relative to the earth rate vector during initial alignment operations. In this way, repeatable gyro biases can be measured and separated from earth rate measurements, and earth rate measurements to the required 0.1 deg per hour accuracy become achievable. The turn-table also provides the means for calibrating the heading gyro scale factor prior to takeoff. The use of such a turn-table as an integral part of a strapdown TRG system for the helicopter AHRS is considered standard practice today.

4.1.1 Design Considerations In A Dynamic Environment

Use of a strapdown TRG (or RIG) in a dynamic vibration environment must address the basic question of wide versus narrow bandwidth for the torque-rebalance loop. If a significant angular vibration environment exists, the loop bandwidth must be broad enough to measure real angular rates that integrate into attitude/heading (33, 34). On the other hand, if the bandwidth is to broad, undesirable high frequency sensor error effects will be amplified and passed as output data to the attitude integration process, generating attitude error. In the case of the tuned-rotor gyro, undamped rotor wobble effects near spin frequency limit the maximum bandwidth that is practically achievable to approximately 80Hz. The minimum torque-rebalance bandwidth is selected so that the gyro rate signal outputs, when integrated, generate attitude data that:

1. Accurately accounts for the accelerometer attitude under combined angular/linear vibration environments (i.e. - sculling (33, 34)).

2. Accurately accounts for multiaxis angular vibration rates that rectify into attitude drift (i.e., coning (33, 34)).

In the case of the TRG, Item 2 is achievable with lower bandwidth than with the RIG because of the inherent nature of the TRG being an attitude sensing instrument (i.e., the pickoff signals measure the true attitude orientation of the gyro case relative to the rotor). As such, attitude errors in the TRG generated by low bandwidth limits, are theoretically recoverable (with a time delay) by proper torque-loop rebalance logic. This contrasts with the RIG torque-loop because the pickoff signal in the RIG represents the integrated input rate (not attitude). As such, the RIG bandwidth must be broad enough to accurately measure all significant multiaxis angular vibrations so that the true attitude can be properly constructed in the attitude integration process. Both the RIG and TRG bandwidths have comparable requirements to satisy Item 1.

One of the principal error mechanisms for torque-rebalance gyros under dynamic environments is torquer heating effects. In addition to producing scale factor errors in the gyro output, bias errors can be produced by associated thermal gradient effects across the instrument. In the case of the gyro scale factor error, much of the temperature induced effect can be eliminated by temperature measurement and modeling correction in the strapdown computer. Unfortunately, for the tuned-rotor gyro, because the torquer magnet is attached to the spinning rotor, direct temperature measurements are difficult to achieve due to the problem of making electrical measurements across the spinning rotor bearings (without resorting to slip-rings and attendent potential reliability problems).

In order to reduce the scale factor error variation with temperature, TRG manufacturers have developed new magnet materials (e.g., doped sumarium cobalt) which has a lower scale factor error as a function of temperature. The penalty is reduced magnet strength, hence, a larger magnet to generate the same torque capability. Note, that the torquer heating effect under angular vibration can also be reduced by lowering the bandwidth of the torque-rebalance loop. In the case of the TRG, this technique has been used in helicopter applications as a compromise between sensor error amplification versus output signal attenuation error. Because the TRG is more tolerant of low bandwidth operation (see previous discussion on Item 2 requirements), a reasonable compromise can usually be found. However, the bandwidth selection then becomes sensitive to vehicle installation and operating condition. In general, no true optimum solution is possible.

Scale factor errors in strapdown gyros under maneuvering flight conditions can rectify into attitude drift in the strapdown system computer (2, 34). The classical effect is through continuous turning in one direction that generates a net attitude error proportional to the product of the scale factor error with the net angle traversed. Cyclic maneuvers can also produce net attitude error buildup; asymmetrical scale factor errors rectify under oscillatory rates about the gyro input axis, symmetrical scale factor errors rectify under multiaxis rates that are phased ninety degrees apart (between axes). The classical case of the latter effect is the "jinking maneuver" which consists of cyclic patterns of roll right, turn right, roll left, turn left. In the case of the tuned-rotor gyro, the scale factor error effect must be assessed to assure compliance to accuracy requirements for the particular application being considered. Reduction of the gyro torquer scale factor temperature coefficient in future versions should broaden the areas of applicability for the instrument in a dynamic environment.

5. RING LASER GYRO

Unlike the gyros that utilize rotating mass for angular-measurement reference, the laser gyro operating principal is based on the relativistic properties of light (1, 11, 12, 14). The device has no moving parts; hence, it has the potential for extremely high reliability.

Figure 4 depicts the basic operating elements in a laser gyro: a closed optical cavity containing two beams of correlated (single-frequency) light. The beams travel continuously between the reflecting surface of the cavity in a closed optical-path; one beam travels in the clockwise direction, the other ih the counterclockwise direction, each occupying the same physical space in the cavity. The light beams are generated from the lasing action of a helium-neon gas discharge within the optical cavity. The reflecting surfaces are dielectric mirrors designed to selectively reflect the frequency associated with the heluim-neon transition being used.

To understand the operation of the laser gyro, consider the effect of cavity rotation on an observer rotating with the cavity. Relative to the observer, it takes longer for a photon of light to traverse the distance around the optical path in the direction of rotation than in the direction opposite to the rotation. This effect is interpreted by the observer as a lengthening of the net optical path length in the direction of rotation, and a shortening of the path length in the opposite direction. Because the laser beam is self-resonating, it is a continuous beam that propagates around the cavity, closing on itself without discontinuity. As a result, the effect of the self-resonance is to maintain a fixed integral number of light wave lengths around the cavity. Under input angular rate, the increase in optical path length experienced by the beam traveling in the direction of rotation, must therefore

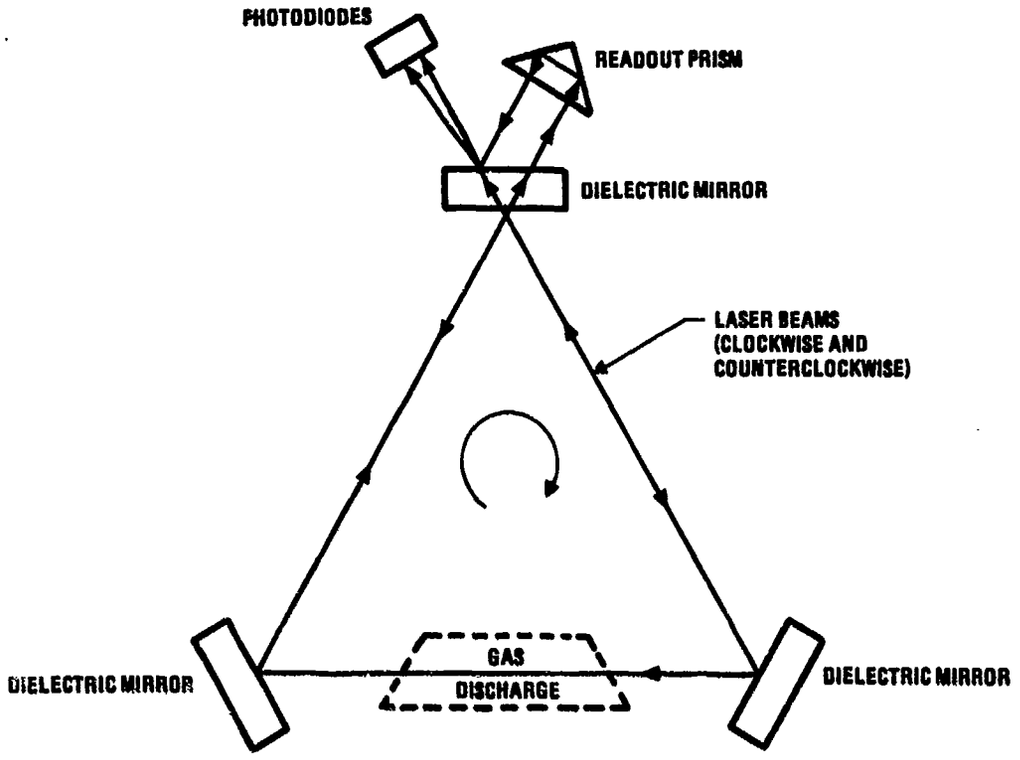

Figure 4 - Laser gyro operating elements.

be accompanied by a proportional increase in wavelength to maintain the same integral number of waves around the lengthened cavity. The converse is true for the beam traveling opposite to the direction of rotation. Thus, a wavelength difference is established between the oppositely directed beams proportional to the optical path length change, hence, proportional to the input angular rate. Because the speed of light is constant, the wavelength difference is accompanied by a frequency difference between the two beams in the opposite sense. Hence, a frequency difference is generated between the two beams that is proportional to input rotation rate.

The frequency difference is measured in the laser gyro by allowing a small percentage of the laser radiation to escape through one of the mirrors (Figure 4). An optical prism is typically used to reflect one of the beams such that it crosses the other in almost the same direction at a small angle (wedge angle). Due to the finite width of the beams, the effect of the wedge angle is to generate an optical fringe pattern in the readout zone. When the frequencies between the two laser beams are equal (under zero angular rate input conditions), the fringes are stationary relative to the observer. When the frequencies of the two beams are different (under rotational rates), the fringe pattern moves relative to the observer at a rate and direction proportional to the frequency difference (i.e., proportional to the angular rate). More importantly, the passage of each fringe indicates that the integrated frequency difference (integrated input rate) has changed by a specified increment. Hence, each fringe passage is a direct indication of an incremental integrated rate movement, the exact form of the output needed for a rate-gyro strapdown navigation system.

Digital integrated-rate-increment pulses are generated from the laser gyro from the outputs of two photodiodes mounted in the fringe area and spaced 90 degrees apart (in fringe space). As the fringes pass by the diodes, sinusiodal output signals are generated, with each cycle of a sine wave corresponding to the movement of one fringe over the diodes. By observing which diode output is leading the other (by 90 degrees), the direction of rotation is determined. Simple digital-pulse triggering and direction logic operating on the photodiode outputs convert the sinusoidal signal to digital pulses for computer input.

The analytical relationship between the fringe angle change and integrated rate input angle change (11, 12, 34) is given by:

$$\Delta\phi = \frac{8 \pi A}{\lambda L} \Delta\theta \qquad (1)$$

where

$\Delta\phi$ = Gyro fringe angle output change (Note: $\Delta\phi = 2\pi$ for a movement of one fringe across the output photodiode).

A = Area enclosed by the laser beam.

L = Perimeter of the laser beam path.

λ = Laser wavelength (e.g., 0.63 micron).

$\Delta\theta$ = Integrated input rate into the gyro (Note: $\Delta\theta = 2\pi$ for a complete 360 degree input rotation angle).

The "pulse size" for the laser gyro is the value of $\Delta\theta$ for which $\Delta\theta = 2\pi$ (i.e., the input angle which produces a full fringe movement of 2π across the photodiode output detector). It is easily verified that for an equilateral triangle laser gyro with 12.6 inch perimeter (4.2 inches per side), the pulse size for a 0.63 micron laser (typical of today's technology) is 2 arc seconds.

The digital pulse output logic can be mechanized to output a pulse each time a full fringe has passed across the diode (e.g., by triggering on the positive going zero crossing from one of the readout photodiodes). For this approach, the gyro output pulse scaling would equal the "pulse-size" defined above. Alternatively, gyro output pulses can be triggered at the positive and negative-going zero crossings from each of the two photodiodes to achieve an output pulse scaling that is four times finer than the basic full-fringe "pulse-size". Both of the latter approaches are used today.

5.1 Construction

Figure 5 illustrates a typical laser gyro mechanization concept. A single piece structure (typically Zerodur, a ceramic glass material) is used to contain the helium-neon gas, with the lasing mirrors and electrodes forming the seals. High voltage (typically 1500 volts) applied across the electrodes (one cathode and two anodes) maintains the helium-neon gas mixture in an ionized state, thereby providing the required laser pumping action. High-quality optical seals are used to avoid introducing contaminants into the helium-neon mixture, which would degrade performance and ultimately limit life-time.

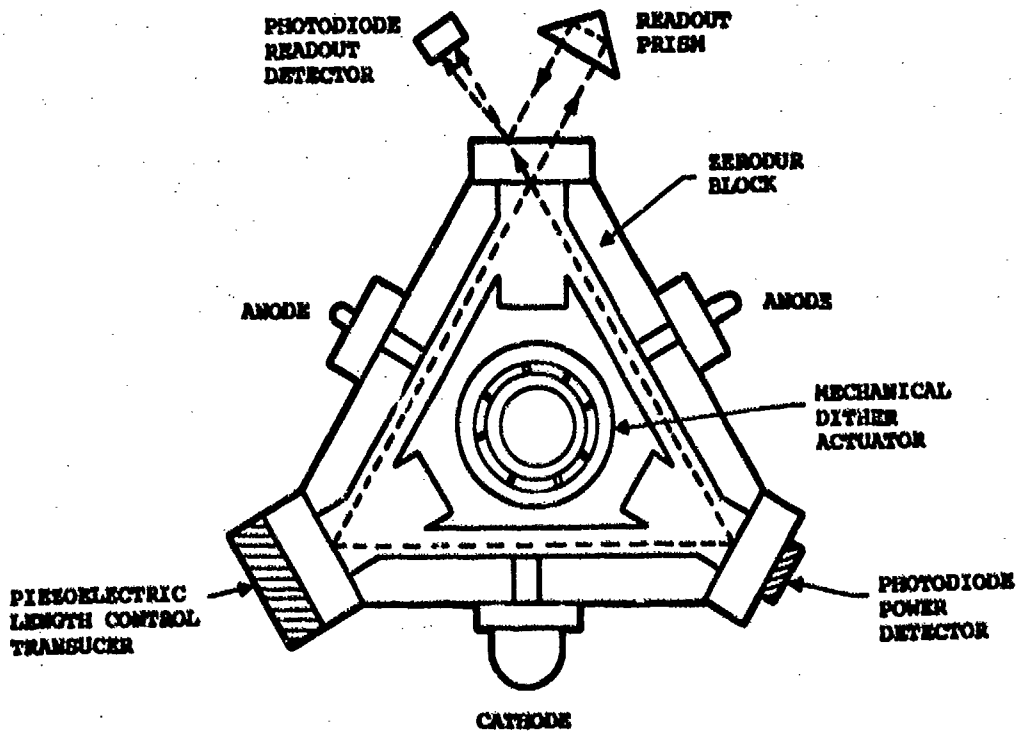

Figure 5 - Laser-gyro block assembly.

The accuracy of the laser gyro depends on the manner in which the laser beams are affected by the influences of the lasing cavity. A key requirement in this regard is that the average of the clockwise and counterclockwise path lengths around the lasing triangle be constant. Many of the error characteristics in the laser gyro vary as a function of average path length (12), hence, stabilizing average path length also implicitly stabilizes performance. Zerodur is used to construct the laser gyro optical cavity due to its low coefficient of thermal expansion, hence, high degree of path-length stability.

To compensate for residual remaining path-length variations, a piezoelectric transducer is mounted on one of the laser gyro mirror substrates (see Figure 5). Actuation of the transducer by a control voltage flexes the mirror substrate to effect a path-length change. The control signal for the transducer is designed to maintain peak average power in the lasing beams. Because average beam power varies cyclically with path-length multiples of laser wavelength, maintaining peak lasing power implicitly controls the average path-length to a constant value. The average beam power is detected in the laser gyro by a photodiode mounted on one of the mirrors that senses a small percentage of the combined radiation from the clockwise and counterclockwise beams.

5.1.1 Square Versus Triangular Ring Laser Gyros

Figure 6 illustrates a square laser gyro geometry utilizing four mirrors (as contrasted with the three-mirror triangular configuration in Figure 5). Both geometries are used today by competing ring laser gyro manufacturers. The rationale espoused by proponents of the triangular versus square geometry can be summarized as follows: Proponents of the triangular geometry point to the three-mirror configuration as having the minimum mirror count to form an enclosed laser ring. As a result mirror costs per gyro are minimized, and lock-in (a performance deficiency in the laser gyro to be discussed in the next section) is reduced due to the minimum number of scatterers (the mirrors) in the laser beam path. From a manufacturing standpoint, the proponents of the triangle point out that alignment of the mirrors on the gyro block is simplified (hence, cost reduced) because the triangle geometry is self-aligning in the lasing plane (through use of one curved mirror), and alignment out of the lasing plane is readily achieved by out-of-plane adjustment of the curved mirror during device assembly.

Proponents of the square laser gyro geometry consider the additional mirror cost a negligible penalty when technology advances are taken into account. The additional alignment requirement for the fourth mirror in a square is identified as a benefit by square gyro proponents due to the added flexibility it affords to adjust beam/cavity positioning, and thereby optimize performance. Another performance advantage identified for the square

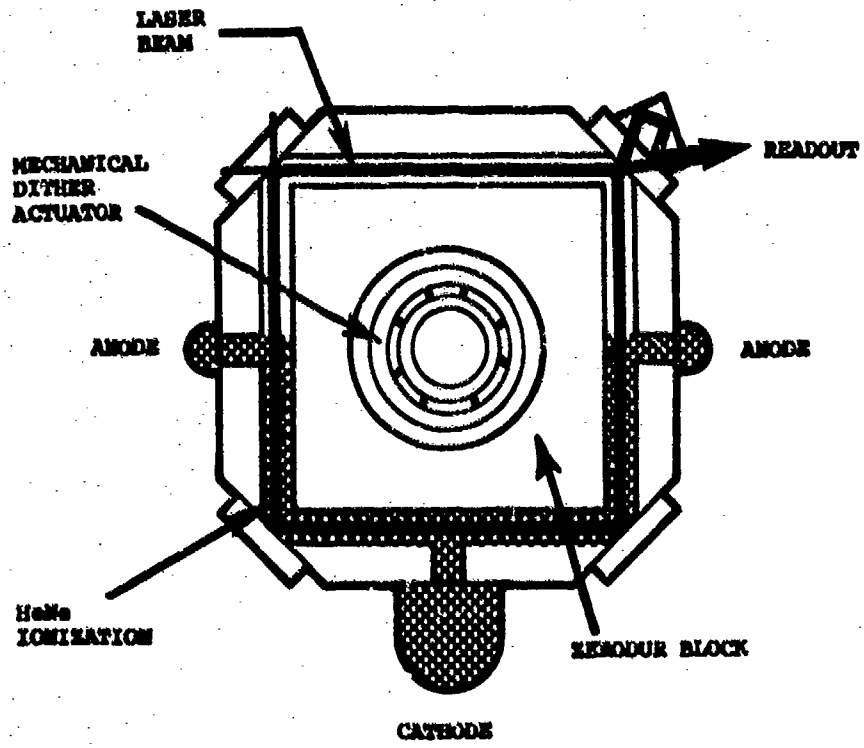

Figure 6 - Square laser gyro configuration.

is its higher area-to-perimeter ratio compared to a triangle of the same size, which directly increases accuracy. The area-to-perimeter ratio (see Equation (1)) is the primary parameter in the device that impacts performance (12, 13, 17). Proponents of the square also point to the lower angle of incidence at the laser beam/mirror interface which reduces back-scattering per mirror. The net result is a combined mirror reduction in back-scattering which more than compensates for the additional mirror scattering, hence, reduces overall gyro lock-in. Finally, from a manufacturing standpoint, square laser gyro enthusiasts claim simpler tooling and machining for square compared to triangular devices, hence, reduced production costs.

Triangular laser gyro proponents acknowledge a performance penalty due to the less favorable area-to-perimeter ratio and beam-incidence geometry. However, they claim that this advantage is minor and will be largely overcome by technology advances. Additionally, triangle proponents argue that when the gyro electrodes (size and geometry) are taken into account, no real size advantage exists for the square gyro configuration. From a machining standpoint, triangle proponents claim no advantage exists for any particular geometry once tooling is complete and experience has been attained.

At this stage in the laser gyro development cycle, it is not clear whether one geometry is superior to another as a general rule.

5.2 Lock-In

The phenomenon of lock-in continues to be the most prominent error source in the laser gyro and the most difficult to handle. The means for compensating lock-in has been the principal factor determining the configuration and performance of laser gyros from different manufacturers.

The phenomenon of laser gyro lock-in arises because of imperfections in the lasing cavity, principally the mirrors, that produce back-scattering from one laser beam into the other (13). The resulting coupling action tends to pull the frequencies of the two beams together at low rates producing a scale-factor error. For slowly changing rates below a threshold known as the lock-in rate, the two beams lock together at the same frequency producing no output (i.e., a dead zone). Figure 7 illustrates the effect of lock-in on the output of the laser gyro as a function of input rate for slowly changing input rate conditions. The magnitude of the lock-in effect depends primarily on the quality of the mirrors. In general, lock-in rates on the order of 0.01 to 0.1 degree-per-second are the lowest levels achievable with today's laser gyro technology (with 0.63-micron laser wavelength). Compared with 0.01 deg/hr navigation requirements, this is a serious error source that must be overcome.

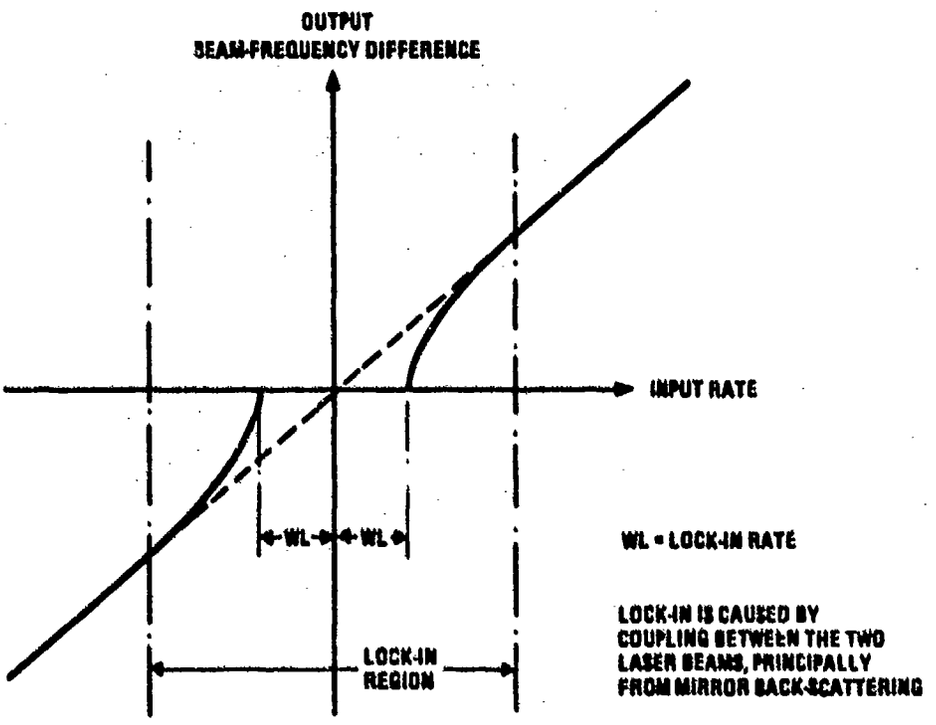

Figure 7 - Laser gyro lock-in.

Under dynamic input rates that rapidly pass through the lock-in region, the effect of lock-in is to introduce a small angle error in the gyro output as the lock-in zone is traversed, but still retaining sensitivity to input rate while in the lock-in region (i.e., no hard dead-zone develops as in Figure 7 (12, 13, 16). The latter effect underlies the basic principal behind adding cyclic high rate bias to the laser gyro as a means for circumventing the lock-in dead-zone effect, and converting it into a random angle error added to the gyro output each time the biased gyro input cycles through the lock-in region. The principal method being used today to generate the oscillating bias in the laser gyro is mechanical dither.

5.2.1 Mechanical Dither

With mechanical dither, the oscillating bias into the laser gyro is achieved by mechanically vibrating the gyro block at high frequency about its input axis through a stiff dither flexure suspension built into the gyro assembly. The spoked-like structures in Figures 5 and 6 conceptually illustrate such a flexure that is attached to the laser block (on the outside) and to the gyro case/mount (on the inside) by metal rings that are connected to each other by flexible metal reeds. Piezoelectric transducers attached to the reeds provide the dither drive mechanism to vibrate the gyro block at its resonant frequency about the input axis. One piezoelectric transducer is mechanized as a dither angle readout detector and used as the control signal to generate voltage into the drive piezo's to sustain a specified dither amplitude. The dither angle amplitude and acceleration are designed so that the dwell time in the lock-in zone is short so that hard lock-in will never develop. The result is a gyro that has continuous resolution over the complete input rate range. The residual effect of lock-in is a small random angle error in the gyro output that is introduced each time the gyro passes through lock-in (at twice the dither frequency). This is the principal source of random noise in mechanically dithered laser gyros. The relationship between laser gyros random noise, lock-in, and dither rate is ideally given by (15):

$$\sigma_R = \frac{\Omega_L}{(\Omega_D K)^{\frac{1}{2}}} \qquad (2)$$

where

σ_R = Gyro random noise (or "random walk") coeffieient ($deg/hr^{\frac{1}{2}}$)

Ω_L = Lock-in rate

Ω_D = Dither rate amplitude

K = Gyro output scale factor in fringes per input revolution (i.e., the reciprocal of the gyro "pulse size" discussed previously, times 2π)

For typical values of σ_R = 0.002 $deg/hr^{\frac{1}{2}}$, Ω_L = 0.03 deg/sec, and K = 648,000 (i.e., 2 arc sec pulse size), equation (2) can be used to show that Ω_D = 72 deg/sec. To achieve sufficient lateral stiffness, the dither spring is designed such that the frequency of the dither motion is on the order of 400 hz. The associated dither cycle amplitude (corresponding to 72 deg/sec dither rate) is 103 arc sec (or 206 arc sec peak-to-peak). Equation (2) is based on the assumption that the angle error generated in the gyro output is uncorrelated from dither cycle to cycle. In practice this is not perfectly achievable, and somewhat larger dither amplitudes are required than predicted by equation (2). Nevorthe-less, the figures presented previously are generally representative of typical mechanical dither requirements.

Once mechanical dither is incorporated for lock-in compensation, means must be provided to remove the oscillating bias signal from the gyro output (so the that the gyro output represents the motion of the sensor assembly to which the gyro is mounted). Figure 5 illustrates the "case mounted readout" method of optically cancelling the dither from the output. By mounting the readout reflecting prism and photodiodes on the gyro case (i.e., off the gyro block) the translational movement of the gyro block relative tc the case (caused by dither) will generate fringe motion at the photodiodes. This purely geometrical effect can be made tc cancel the fringe movement produced by the laser block sensed dither angular motion through proper selection of the rotational center for the mechanical dither mount. The result is a photodiode output signal that responds to rotation of the gyro case and not relative movement between the dithering gyro relative to the case.

The alternative to "case-mounted readout" is "block-mounted readout" as illustrated in Figure 6. With this approach the gyro readout optics are mounted directly to the gyro block. Relative movement between the block and case is removed by measurement and substraction, or by filtering. In the measurement/substraction approach, a transducer (typically electromagnetic) is used to electrically measure the instantaneous angle between the gyro block and case. The electrical signal is then digitized and subtracted from the gyro pulse output for dither motion compensation. With the filter approach, a digital filter is used to filter signals near and above the dither frequency from the gyro output.

The result is a cancellation of the unwanted dither rate between the gyro block and case. The penalty is attenuation of real oscillating rates of the gyro case which, if significant, must be accurately measured for processing in the strapdown computer. Use of the filter approach is only valid for relatively benign environment applications where it can be assured that the only angular rate signals that need to be measured have frequency content well below the dither frequency.

5.2.1.1 Mechanical Dither Design Complications - Orginally touted as a simple solution to the lock-in problem with no deleterious side effects, the mechanical dither concept applied in practice has been found to be the source of several subtle mechanical coupling error mechanisms that must be designed for at the three-gyro system level for solution (19, 34). It must be realized at the onset, however, that these complications are directly proportional to the magnitude of dither motion required for lock-in compensation. As lock-in rates are reduced, dither amplitudes can be reduced proportionally (see equation (2)), and design solutions for the effects described below can be more easily achieved.

The basic problem with mechanical dither stems from a kinematic property of three-axis rotary motion that cyclic rates in two orthogonal axes, if at the same frequency but phase shifted by ninety degrees, will produce a real constant attitude rate about the third axis (33, 34). The effect, known as "coning", if present, must be measured as cyclic rate signals by the strapdown gyros, and delivered to the strapdown computer so that the true drift about the third axis will be properly calculated. The problem arises when gyro output errors are also being generated at the same frequency as the real rates to be measured. Cyclic error signals from the gyro in one axis, in combination with errors or real cyclic rates from the gyro in one of the other orthogonal axes, will produce a vector rate profile which appears as coning, but is false ("pseudo-coning" is the nonmenclature typically used to describe this phenonemon). Since the composite gyro output signals (real plus error) are processed in the same computer used to measure real coning motion, a pseudo-coning error will be created in the strapdown computer as a false drift rate about the "third" axis. Filtering the gyro signals to remove the output error oscillations is not acceptable if real cyclic motion is present, since the true drift caused by the real cyclic coning motion will not be properly measured and accounted for.

In the case of mechanically dithered laser gyros, a potential source of real high frequency coning in a strapdown system is the reaction torque of the gyro dither drives into the sensor assembly (the sensor assembly typically consists of a metal casting to which the gyros and accelerometers are mounted). To minimize dither reaction torque resonance effects, and to provide compliance for thermal expansion, most RLG sensor assemblies are mechanically isolated from the system chassis by elastomeric isolators (34). To generate coning motion, equal angular rate vibration frequencies must exist simultaneously in two orthogonal axes. Dither induced vibrations from nominally orthogonal laser gyros into the sensor assembly can become frequency correlated between axes if mechanical coupling exists between the axes (e.g., principal moment-of-inertia axes of the sensor assembly not parallel to gyro input axes). The mechanical coupling mechanisms tend to pull the dither frequencies in orthogonal axes together, thereby creating real coning at dither frequency. Hence, even if single gyro dither frequencies are separate, the mechanical coupling can shift the frequencies toward each other, thereby creating correlated frequency components between axes, or coning. Another source of real high frequency coning is linear random vibrations into the strapdown system that produce correlated frequency rotary sensor assembly motion in orthogonal axes due to sensor assembly/elastomeric mount asymmetries.

The real coning motion effects described above would not be a problem in themselves, since laser gyros have the bandwidth and sensitivity required for accurate measurement of these effects. The problem arises from pseudo-coning created at dither frequency, also due to dither mechanical interraction. A classical example is sensor assembly bending induced by the dither reaction torque which produces false gyro outputs at dither frequency (e.g., due to bending in the mechanism used to measure and remove gyro block/case relative angular dither motion from the gyro output, or gyro mount twisting about the gyro input axis).

Exacting and sophisticated mechanical design techniques must be used in the overall sensor, sensor assembly, and sensor assembly mount to assure that pseudo-coning effects are negligible below the frequencies where real coning exists and has to be measured (33, 34). The coning computation algorithm in the strapdown computer (33) can then be run at an iteration rate that is only high enough to measure the real coning motion frequency effects (i.e., so that high frequency pseudo-coning effects are attenuated). Classical techniques utilized to minumize pseudo-coning effects are to design for stiffness in the sensor assembly, design for mechanical symmetry in the sensor assembly to minimize mechanical dither cross-coupling between gyro axes, and to assure sufficient gyro dither frequency separation so that the tendency for frequency pulling together is minimized. If performed properly, a total design can be acheived that meets overall system requirements under external vibration. Proper design is more easily achieved for benign vibration environments (e.g., commerical aircraft).

5.2.2 Magnetic Mirror Bias

The magnetic-mirror concept is a nonmechanical biasing technique based on the transverse

magneto-optic Kerr effect (14, 18, 21). A special inner coating (e.g., ferromagnetic metal) is applied to one of the laser gyro mirrors which, when magnetized normal to the plane of incidence by an applied magnetic field, imparts a nonreciprocal (i.e., opposite) phase shift between the clockwise and counterclockwise laser beams. This produces an apparant differential path-length shift between the laser beams which generates a frequency difference or output rate. The result is a bias imposed on the gyro output that is controllable by the applied magnetic field. Bias uncertainties are compensated through use of alternating bias control (i.e., square-wave dithering of the applied magnetic field). The magnetic field intensity is set at a high enough level to operate the magnetic mirror in a saturated state. In this way, bias shifts generated by stray magnetic fields are minimized.

The advantage of the magnetic mirror is the elimination of the need for mechanical dither, its associated design complications, and size/weight penalties. A problem area for the magnetic mirror has been difficulties in generating a large enough bias for the 0.63 micron laser gyro due to low reflectance of the ferromagnetic coating (14, 20). The resulting loss must be compensated by higher gain in the laser helium-neon discharge. For the 0.63 micron laser, high gain cannot be tolerated because the laser begins to resonate unwanted mode shapes that deteriorate performance. The net result is that the magnetic mirror biasing capability must be diluted by appropriate layering of dielectric coatings on the mirror to recover reflectance. The net bias levels achieved with this approach have not been sufficient to adequately compensate lock-in. (It should be noted that ferromagnetic magnetic mirror technology has been successfully applied to the lesser accurate 1.15 micron laser gyro which can be operated at a higher gain before multimoding problems develop (24)). Another problem area for magnetic mirror technology has been the introduction of residual nonrecipocal phase shifts between the incident laser beams that are temperature sensitive. The result is a bias instability that is temperature sensitive and which produces turn-on transients.

Recent work on laser gyro magnetic mirror technology has concentrated on the development of a garnet magnetic mirror in which the dielectric layer coatings on the laser mirror are made with a transparent garnet film that produces nonreciprocal phase shift to incident light on application of a magnetic field (20). The result has been that the loss effect (associated with the ferromagnetic magnetic mirror technology) has been significantly reduced so that high bias levels can be achieved with 0.63 micron lasers. Current design work is concentrating on doping the garnet material to reduce the effect of residual nonreciprocal temperature sensitive phase shifts that have remained with the new garnet mirror technolgy. Engineering personnel associated with these developments are predicting a breakthrough within the next year based on experimental results achieved to date on doped garnet coatings.

5.2.3 Multioscillator Laser Gyro

Conventional two-beam (clockwise and counterclockwise) laser gyros are designed to amplify plane polarized laser light (i.e., in which the electric vector normal to the laser beam is either perpendicular to the lasing plane (S-polarization) or in the lasing plane (P-polarization). Triangular lasers typically use the former polarization while square laser gyros typically use the latter. In the case of the multioscillator laser gyro (26, 27), circular polarization is used in which both S and P modes are simultaneously excited, but at one quarter wavelength phase shifted from one another. The result is a combined electric vector polarization that spirals between S and P, denoted as circular polarization. Right circularly polarized (RCP) or left circularly polarized (LCP) light is generated by creating a plus or minus quarter wavelength shift between the S and P waves, thereby creating a right or left sense spiralling electric vector wave.

In the multioscillator, both RCP and LCP laser beams are created in the same cavity, each with clockwise and counterclockwise components (i.e., a four-beam laser gyro). The two polarization states are excited by a reciprocal polarization rotator (e.g., a quartz crystal) in the beam path that imparts an additional spiral rotation to the circularly polarized light, and which operates identically on both the clockwise and counterclockwise components of the RCP or LCP beams (i.e., recriprocal). The additional rotation adds to the spiralling for the RCP beam and retards the spiraling of the LCP beam. The effect of the added rotation on the RCP beam is to resonate the light components with decreased wavelength such that a net spiral angle reduction is acheived around the beam path to match the spiral angle increase across the rotator. As a result, the RCP beam (both the clockwise and counterclockwise components) are up-shifted in frequency (proportional to the wavelength decrease). The opposite effect is created in the LCP light which is down-shifted in frequency by the same amount that the RCP light frequency is up-shifted. As for the two-beam laser gyro, each polarization state (RCP or LCP) contains a clockwise (CW) and a counterclockwise (CCW) beam component. Hence, two sets of CW and CCW beams are established, one RCP and the other LCP, each operating at a different center frequency. Each set is used to generate an independent output signal equal to the frequency difference between the CW and CCW beams. As for the two-beam laser gyro, the frequency difference output from each polarization state is proportional to input rotation rate. Also, as for the two-beam laser gyro, the frequency difference output from the RCP and LCP lasers experience lock-in which pull the CW and CCW frequencies together at low input rates.

In order to overcome lock-in, a nonreciprocal polarization rotator is introduced into the beam path which rotates circularly polarized light in the opposite sense for clockwise

compared to counterclockwise beams. Hence, a frequency shift is imparted between the clockwise and counterclockwise beams (i.e., a bias) for both the RCP and LCP light. The frequency difference is maintained at a high enough level to remain far from the lock-in region under frequency shifts produced by angular rate inputs. The common means for introducing the nonreciprocal bias in the multioscillator laser gyro has been through use of a Faraday rotator consisting of a piece of amporphous glass placed in the beam path with a magnetic field applied across it parallel to the beam. The resulting Faraday effect introduces the desired frequency bias on the circularly polarized light that is in the opposite sense for the LCP compared to the RCP light beams. As a result, the RCP beam output (i.e., the difference between the clockwise and counterclockwise RCP beam frequencies) is positively biased, while the LCP beam frequency difference output is negatively biased by an equal amount.

By summing the outputs from the RCP and LCP beam sets, the input rate sensitivity is doubled, while the Faraday bias effect is cancelled. The cancelling of the bias by summing both outputs eliminates the need for alternating bias to compensate for Faraday rotator gain uncertainties. Elimination of the oscillating bias eliminates a main source of laser gyro random noise (i.e., dithering through the lock-in region). Hence, the random noise in the multioscillator is lower, and closer to the theroretical limit created by random gain and loss of photons from the laser beams (25, 26).

5.2.3.1 Principal Error Sources - The basic principal behind lock-in compensation in the multioscillator laser gyro relies on the Faraday bias (and Faraday bias uncertainties) being equal between the two laser beam sets so that they cancel one another. In practice, this is not totally true, to a large degree because the operating frequencies of the left and right circularly polarized laser sets are different by design. This frequency difference causes each to behave slightly differently to the Faraday bias, producing a net residual error when combined. The error is both temperature and magnetically sensitive, requiring some degree of magnetic shielding and temperature measurement compensation.

Another source of bias error in the multioscillator is variations in the lock-in characteristic between the right and left circularly polarized beams. Even through the Faraday bias keeps the lasers well outside of the lock-in region, small scale factor nonlinearities still exist at the bias point caused by lock-in. Because the lock-in rates for the two beam sets differ, when the gyro outputs are summed, the residual lock-in error effects at the bias point do not cancel. The resulting bias error created is temperature sensitive and can have unpredictable varations over time.

Multioscillator design groups claim that the above effects are for the most part, predictable and can be compensated sufficiently for satisfactory operation in high accuracy applications.

Two areas where serious errors can develop and are not easily compensated arise from anisotropic and birefringence effects introduced in the light beams as they pass through a quartz crystal reciprocal polarization rotator and Faraday nonreciprocal rotator. The net effect is to introduce unpredictable nonreciprocal path length variation between all four beams which are temperature, acceleration and magnetically sensitive.

Recent advances in multioscillator design techniques have replaced the quartz crystal reciprocal polarization rotator with an out-of-plane beam path geometry that rotates the laser beam by optical reflection at the mirrors (thereby, mimicking the rotational effect of the quartz crystal) (27). The result is elimination of birefringence effects originally created by the presence of the quartz crystal in the beam path. Current work on the multioscillator is addressing improved methods for providing nonreciprocal polarization rotation that have small and more predictable error characteristics than were achieved with original Faraday rotator design configurations.

5.3 Laser Gyro Performance And Application Areas

Over the past 6 years, the ring laser gyro (RLG) has progressed from advanced development into full scale production in 1-nmph strapdown inertial navigation applications. The successful 1-nmph laser gyro system programs to date have utilized the 0.63 micron transition with mechanical dither. Systems in the 1-nmph range have been developed by several competing manufacturing groups for both commerical and military application.

Performance advances in RLG technology have been rapid. Continuing advances in laser gyro mirror technology has reduced lock-in (and random noise) by more than an order of magnitude over the past eight years. Lock-in rates lower than 0.0003 deg/hr$^{\frac{1}{2}}$ have been reported. Advanced development programs are now in progress to design laser gyros with performance capabilities required for 0.1 nmph navigation applications.

Principal problems remaining with RLG technology are size and weight for the high performance applications, and size, weight and cost for the lower accuracy applications. For the higher performance applications, the total weight of an RLG strapdown inertial navigation system is typically 30% higher than its comparable gimbaled system counterpart. Significant cost, reliability, and reaction time benefits for the RLG system, however, make

it an attractive alternative to the traditional gimbaled system. It is generally conceded that laser gyro performance in the lower accuracy AHRS and tactical missile midcourse guidance application areas is superior to the competing strapdown RIG or TRG strapdown technologies, however, size, weight, and cost advantages for the RIG or TRG with acceptable performance are prevailing factors today that continue to restrict entry of the RLG into the lower performance application areas.

Performance advances in future RLG's may make it possible to build smaller, lighter weight laser gyro systems for the lower performance market. Advances in nonmechanically dithered RLG technology may make it possible in the future to build a a small size cost/performance competetive integrated 3-axis laser gyro sensor assembly (1, 24) in a single Zerodur structure using interleaved laser paths to reduce net size/weight. If advances in mirror technology continue to reduce lock-in rates and associated dither amplitude requirements, mechanically dithered RLG system size/weight will also be reduced in the future. Production learning is expected to be the determining factor that will decide the degree to which laser gyro production costs will be reduced in the future to be competitive with the lower performance RIG and TRG strapdown sensors. For the higher performance strapdown applications areas, strapdown RIG and TRG manufacturer's generally conceed that the ring laser gyro is now the industry standard, and not a viable competition area for higher performance but more expensive versions of strapdown TRG or RIG technology.

6. FIBER-OPTIC ROTATION RATE SENSOR

One of the newer rate sensor technologies that has emerged over the past few years is the fiber-optic rotation rate sensor (28). The concept for the device is illustrated in Figure 8. Light generated from a suitable light source at a specified design frequency is transmitted through a fiber-optic coil. The light beam is first split by a beam-splitter so that half the radiation traverses the coil in the clockwise (CW) direction, and half in the counterclockwise (CCW) direction. The emerging light from both ends of the coil are then recombined at the beam splitter, and transmitted onto a photodetector. The photodetector output power is proportional to the average intensity of the recombined light.

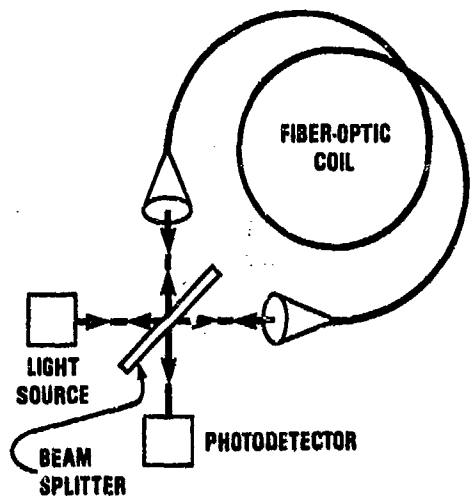

Figure 8 - Basic fiber-optic rotation rate sensor concept

Under rotation of the device about an axis normal to the plane of the fiber-optic coil, the effective optical path length is changed for the CW compared to the CCW beams in a manner similar to the ring laser gyro. In the direction of rotation, the path length increases (i.e., a photon of light has to traverse the length of the coil plus the distance that the coil has been rotated during the traversal period). In the direction opposite to the rotation, the light traverses the length of the coil, minus the distance that the coil has been rotated during the traversal period. The difference between the CCW and CW optical path lengths, then, is twice the distance of rotation, or:

$$\Delta L = 2 \frac{L}{C} \frac{D}{2} \omega = \frac{L D}{C} \omega$$

where

L = Total fiber length

D = Diameter of coil (assumed circular)

ΔL = Difference between CW and CCW optical path-lengths

ω = Input angular rate

C = Speed of light

This corresponds to a phase shift between the CW and CCW light beams emerging from the coil given by :

$$\Delta\phi = 2\pi \frac{\Delta L}{\lambda} = 2\pi \frac{L D}{C \lambda} \omega \qquad (3)$$

where

λ = Wavelength of light source

Thus, the phase angle between the emerging light beams becomes proportional to the input angular rate. This contrasts with the ring laser gyro resonator for which the phase angle change is proportional to the integral of the input rate (see Equation (1)). Hence, the fiber-optic rotation sensor is a "rate gyro" while the laser gyro is a "rate integrating gyro". The other difference between the two sensors is that the laser gyro CW and CCW beam frequencies are shifted from each other proportional to the input rotation rate (due to the self-resonance of the laser); the frequencies for the CW and CCW beams in the fiber-optic rate sensor remain equal under rotation rates.

The photodetector in Figure 8 is used to sense the phase shift between the CW and CCW beams. The amplitude of the combined beams at the photodiode equals the sum of the individual beam amplitudes, including the phase shift factor. The result is a combined beam intensity which is maximum for $\Delta\phi = 0$ and minimum (zero) for $\Delta\phi = \pi$ (i.e., varies as $\cos^2(\Delta\phi/2)$). The photodetector output is proportional to the light intensity, hence, also varies approximately as $\cos^2(\Delta\phi/2)$.

In order to achieve high sensitivity (high scale factor), the length L of the fiber coil is large. A typical value of L = 400 meters with D = 0.1 meters and λ = 0.82 microns produces a $\Delta\phi$ from equation (3) of approximately one radian at 1 rad/sec input rate.

6.1 Practical Design Refinements

As depicted in Figure 8, the fiber-optic rotation rate sensor has fundamental error mechanisms that make it impractical to implement. Among these are large scale factor errors associated with photodetector scale factor uncertainties, light source intensity variations, and light amplitude losses in the fiber; loss of rate sensitivity around zero input rate (due to the $\cos^2(\Delta\phi/2)$ output characteristic of the photodetector; phase angle variations due to mechanical movement between the beam splitter and fiber that produce changes in path length between the CW and CCW beams; and polarization state differences between the CW and CCW beams that produce phase shifts due to nonreciprocal birrefringence and anisotropic effects in the fiber material that are aggravated by environmental exposure. To overcome these fundamental problems, recent fiber-optic rotation sensor configurations (28) have adopted refined interface and control elements such as those depicted in Figure 9.

In Figure 9, the discrete component beam-splitter in Figure 8 is replaced by fiber-optic couplers which consist of integrated fiber-optic junctions that split entering beams 50% to the left and 50% to the right. A polarizer (28) is included to suppress unwanted polarization states in the light. The fiber itself is specifically manufactured to preserve a single polarization state (28) ("polarization preserving fiber"). In this manner, nonreciprocal fiber-beam interractions are suppressed.

A light source (typically a super-luminiscent diode such as Galium Arsenide) transmits narrow frequency bandwidth light* into the fiber that splits into CW and CCW components at the coupler junction. Acousto-optic shifters (A/O) (such as Bragg cells**) at the end of

---

*Note - Original fiber-optic sensors used laser light. One of the major technological break-throughs for the fiber-optic sensor was replacement of the coherent laser light with a broader spectrum source. The result was a significant reduction in nonreciprocal beam/fiber interraction error mechanisms due to the shorter correlation distance for the broader spectrum light (28, 29).

**Note - A Bragg cell (28) is typically mechanized as a piezoelectric device that imparts an acoustical vibration transverse to the light beam at its input drive frequency. The result is a bending of the light (by the "Bragg angle") with an accompanying frequency shift in the light passing through the cell equal to the Bragg cell drive frequency.

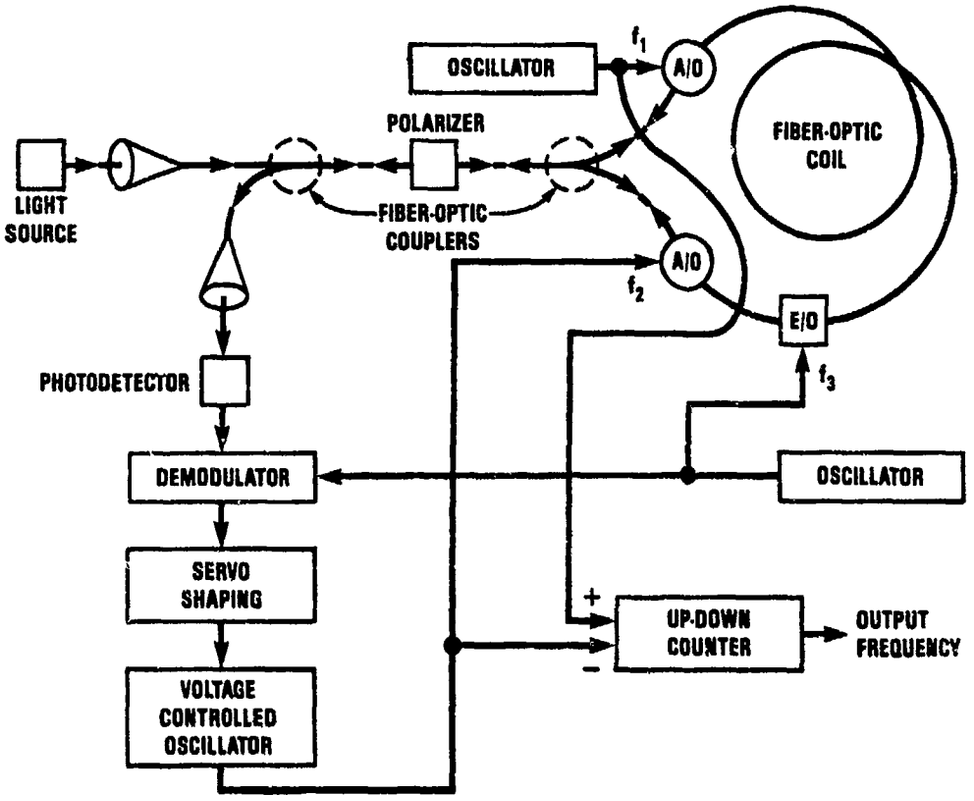

Figure 9 - Improved fiber-optic rotation rate sensor configuration.

the fiber coil are then used to generate a controlled phase shift in the light illuminating the photodector.

To function properly, each Bragg cell in Figure 9 must be biased at a large offset frequency F_1 (typically 20 MH_z). A Bragg cell mounted at one end of the coil is driven directly at the bias frequency F_1 (see Figure 9) which up-shifts the light leaving the cell by F_1 from the light entering the cell. The light entering from the left (the clockwise CW beam in Figure 9) must traverse the length of the coil at the up-shifted frequency before it leaves the coil and illuminates the photodetector. The beam entering from the right (the counterclockwise CCW beam in Figure 9), on the other hand, immediately leaves the coil and illuminates the detector after it is frequency up-shifted. The net result is that the CW beam travels a further distance at the up-shifted frequency than the CCW beam, thereby generating a net phase shift between the CW and CCW beams at the photodetector proportional to F_1 and the coil length.

The Bragg cell at the opposite end of the coil is driven at F_2 which generates a phase shift at the photodiode in the opposite sense to that created by the F_1 Bragg cell. The F_2 frequency is controlled in servo fashion to maintain the photodetector output at peak power (i.e., zero net phase angle). Under zero input angular rate, the F_2 servo drives F_2 to equal F_1 (i.e., so that equal and opposite phase shifts are created that cancel one-another). Under input angular rate, the servo creates a frequency difference between F_2 and F_1, the device output in Figure 9, proportional to the input angular rate (that generates an equivalent phase shift at the readout to null the phase shift created by input rotation). It is easily demononstrated that the frequency difference generated to achieve a net zero phase angle is given by:

$$F_2 - F_1 = \frac{4A}{\lambda I}\,\omega \qquad (5)$$

where

ℓ = Length around one coil of the fiber (which typically consists of several coils).

If equation (5) is compared with equation (1) for the laser gyro resonator, it should be clear that they are identical on an integral basis (i.e., the frequency difference pulse count cycles from equation (5) times 2π radians/cycle is proportional to the input angle by the same factor that, in equation (1), relates RLG output fringe angle change to input angle change.

Figure 9 also includes an electro-optic phase shifter (E/O) driven at frequency F_3 at one end of the fiber, which imparts an oscillating path length change to the CW and CCW beams passing through (Note: The E/O is typically mechanized as a piezoelectric actuated "stretcher" which physically changes the length of the fiber by introducing stresses in the fiber proportional to applied voltage (28, 29). This induces an equivalent phase shift in the light). Because the E/O driver is at one end of the coil, the light beam passing out of the coil delivers the phase shift effect first to the photodetector. The beam traveling in the opposite direction has to traverse a longer length of fiber to the photodetector, hence, delivers its phase shift, by an equal amount, later. The delay creates an alternating phase bias at the photodiode mixed beam output, generating an oscillation of the output about the peak power point. By comparing the positive half cycle output decrease with the negative cycle decrease, a linear signal can be generated proportional to the average deviation of the input light phase angle difference from zero. The linear signal is generated in the phase sensitive demodulator shown in Figure 9 driven by F_3. The result is a signal out of the demodulator that is linearly proportional to the $\Delta\phi$ phase deviation from zero, thereby eliminating the $\cos^2(\Delta\phi/2)$ sensitivity problem around $\Delta\phi = 0$ that exists without the E/O device.

The basic advantages for the Figure 9 compared to the Figure 8 mechanization approach are the elimination of the discrete light/beam-splitter/fiber junctions, thereby reducing phase shift errors caused by mechanical movement; elimination of the photodetector zero-phase angle sensitivity problem through use of the E/O demodulator; and, through the closed-loop servo operation that maintains the phase angle signal at null, elimination of scale factor errors associated with light source intensity, optical intensity losses in the fiber and beam-splitters, and photodetector scale factor uncertainties.

6.2 Development Status And Application Areas

The basic motivation behind the development of the fiber-optic rate sensor was to design a low cost alternative to the ring laser gyro that was inherently void of lock-in problems. The resonant characteristic of the laser gyro which regenerates its light source by stimulated emission, is the transfer mechanism that couples the CW and CCW beams together from back-scatter, producing lock-in. For the fiber-optic rate sensor, the light source is external to the sensing ring, hence, does not amplify the effects of back-scatter. As a result, the lock-in phenomenon associated with the laser gyro is absent in the fiber-optic sensor. This has been proven experimentally (29). The rationale behind the projected low cost of the fiber-optic sensor is that use of fiber-optics and integrated-optics technologies should reduce labor hours associated with device manufacture. It also assumes continuing reductions in the cost of high quality optical fiber which has been occuring over the past few years. From a performance standpoint, the fiber-optic rotation sensor is not expected to compete with the high performance laser gyro for accuracy, but is envisioned as a competitor to the lower cost autopilot, and eventually tactical missile and AHRS quality gyros.

Much has been accomplished since 1976 when the fiber-optic rotation sensor concept was originally conceived. To a large degree, these accomplishments are summarized by the evolution of the concept from its original form (in Figure 8) to its more refined practical form (in Figure 9). Nevertheless, much remains to be accomplished before this device can be considered a serious competitor with mature low cost conventional spinning wheel gyro technology or new lower cost/medium performance laser gyro technology. The device has still to be designed into a practical form that is producible at low cost, and which achieves overall performance goals over opertional environments in a reasonable form factor. To a large extent the development status reflects the level of funding committment assigned by individual groups toward device development. Although many small funded activities have existed over the past 8 years, few dedicated programs have been heavily funded. From another standpoint, the funding limits could reflect lack of confidence by funding agencies in the new technology, or a lack of available funds to pursue new technologies after completing heavy investments in recent technologies that are only now entering large scale production (e.g., the laser gyro).

Some of the technical problems that remain for the fiber-optic rotation rate sensor (28) include larger than desired size (2 to 4 inches in diameter) for the fiber-optic ring to avoid introducing beam interractions with the fiber walls under tight fiber turns; scale factor errors due to photodiode output frequency variations with temperature; bias errors associated with photodiode output frequency side-bands creating phase offsets at the photodetector; bias errors created from large required Bragg cell drive frequency offsets coupled with variations in the CW and CCW Bragg biased coil lengths due to off-nominal

variations between the Bragg cell distances to the fiber-optic coupler (see Figure 9); bias errors associated with the E/O demodulator electronics loop; bandwidth limits associated with the closed-loop operation in Figure 9; and increasing complexity of the sensor configuration to resolve problem areas. Virtually no data has been published on the performance of the fiber-optic rate sensor under dynamic environments. One of the principal potentional error mechanisms for the device (as for all angular rate sensing instruments) is bias error created under dynamic temperature, mechanical vibration, acoustic vibration, acceleration, and magnetic enviroments. Fiber-optic rate sensor enthusiasts remain confident that these problems can be resolved, given time and funding. For evidence they point to the significant performance advances made over the past eight years, where the fiber-optic rate sensor has progressed from an original concept that could barely detect earth's rate, to current technology versions that have demonstrated milli-earth-rate sensitivities (29).

7. PENDULOUS ACCELEROMETER

The pendulous accelerometer (Figure 10) (1) consists of a hinged pendulum assembly, a moving-coil signal-generator/pickoff that senses angular movement of the pendulum from a nominally null position, and a permanent-magnet torque-generator that enables the pendulum to be torqued by electrical input. The torquer magnet is fixed to the accelerometer case, and the coil assembly is mounted to the pendulum. Delicate flex leads provide electrical access to the coil across the pendulum/case hinge junction. Electronics are included for pickoff readout and for generating current to the torquer.

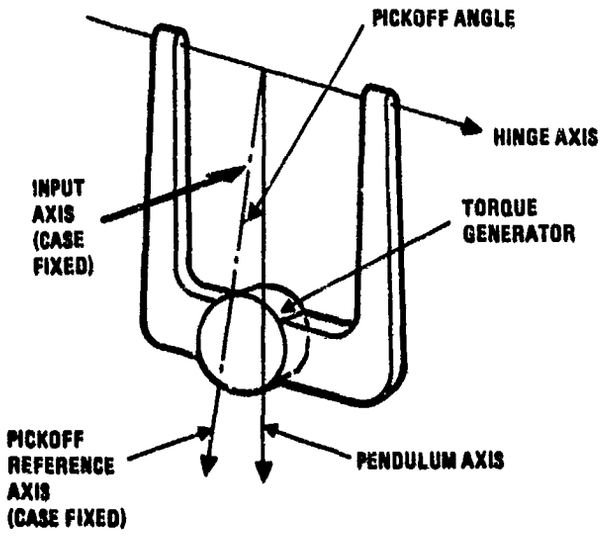

Figure 10 - Electrically servoed pendulous accelerometer concept.

The device is operated in the captured mode by applying electrical current to the torquer at the proper magnitude and phasing to maintain the pickoff at null. Under these conditions, the electrically generated torque on the pendulum balances the dynamic torque generated by input acceleration normal to the pendulum plane. Hence, the electrical current through the torquer becomes proportional to input acceleration, and is the output signal for the device.

Mechanization approaches for the pendulous accelerometer (1) vary between manufacturers but generally fall into two categories: fluid filled and dry units. Fluid-filled devices utilize a viscous fluid in the cavity between the pendulum and case for damping and partial floatation. The dry units use dry air, nitrogen, or electromagnetic damping.

The hinge element for the pendulous accelerometer is a flexible member that is stiff normal to the hinge line to maintain mechanical stability of the hinge axis relative to the case under dynamic loading, but flexible about the hinge line to minimize unpredictable spring restraint torques that cannot be distinguished from acceleration inputs. Materials selected for the hinge are chosen for low mechanical hysteresis to minimize unpredictable spring-torque errors. To minimize hysteresis effects, the hinge dimensions are selected to assure that hinge stresses under dynamic inputs and pendulum movement are well below the yield-stress for the hinge material. Beryllium-copper has been a commonly used pendulum-hinge material due to its high ratio of yield-stress to Young's modulus (i.e., the ability to provide large flexures without exceeding material yield-stress). Another successful

design approach for dry accelerometers has utilized fused quartz for both the hinge and pendulum by etching the complete assembly from a single-piece quartz substrate (1).

7.1 Performance And Application Areas

The pendulous accelerometer continues to be the primary mechanization approach being used for almost all strapdown applications. Design refinements over the past 6 years now provide units from several manufacturers that meet 1.0 nmph strapdown inertial navigation requirements in heaterless configurations. The heaterless configuration operates without temperature controls and achieves its accuracy through thermal modeling of the sensor errors in the strapdown system computer based on temperature measurements taken with temperature probes mounted within the sensing unit. The heaterless accelerometer configuration has been perfected within recent years for operation with ring laser gyros which are also operated heaterless using direct path-length control to stabilize performance (Note: Use of heaters to control temperature and stabilize performance with the ring laser gyro is impractical due to the long thermal time constant of the Zerodur material from which it is constructed, and the associated reaction time penalty that would be introduced from turn-on until temperature/performance stabilization. Laser gyro performance variations with temperature are also compensated by thermal modeling). It is highly fortunate that pendulous accelerometer designs originally developed for heated operation (to stabilize performance), have been predictable enough thermally, to allow accurate characterization over their complete temperature range by analytical modeling using temperature measurements. Hence, major design refinements for heaterless operation have not been necessary.

Most accelerometers today are of the dry pendulous metal flexure hinge variety (1). Design refinements in quartz hinge design configurations (1) (most notably in the plating technology used to conduct current across the hinge into the pendulum-mounted torquer coil to minimize hysteresis) have provided a rugged unit that meets 1.0 nmph strapdown inertial navigation accuracy requirements.

Experimental pendulous accelerometers have recently provided indications that identifiable futher design refinements will make it possible to achieve the accuracy improvements needed for the advanced 0.1 nmph INS applications. Advanced engineering develoment programs are currently being funded (at a fairly modest level) to develop and evaluate these performance improvements.

Unit costs for the pendulous accelerometer, although acceptable, still remain higher than desirable, particularly in the higher accuracy applications. Competitive sourcing in some applications has created the environment needed to reduce costs to some extent through design, manufacturing, and test improvements. Increased production volume has added to cost reduction through learning and improved tooling/automation techniques. However, the production volume has not been sufficient to develop the automatic manufacturing technologies needed to make major in-roads in cost reduction. Nevertheless, the pendulous accelerometer cost is acceptable for most applications, compared to the cost of other strapdown system elements.

8. TORQUE-LOOP MECHANIZATION APPROACHES FOR TORQUE REBALANCE INSTRUMENTS

The implementation of the torque loop for the torque-to-balance instruments (e.g., floated rate-integrating gyro, tuned-rotor gyro, pendulous accelerometer) continue to be mechanized using different approaches, depending on manufacter: digital pulse-rebalance or analog-rebalance with follow-up pulse-rebalance logic, using pulse-on-demand or pulse-width-modulated forced limit-cycle techniques (1). Little data has been published on the performance of these electrical circuits, an unfortunate circumstance, particulary since their accuracy is a key contributor to the overall performance of the intrument they are designed to operate with. Performance data advertized as representative of particular sensors does not always include the effect of the digital pulse-rebalance circuity (i.e., the data was taken on an analog basis at the basic instrument level). This becomes of greater concern when one considers the more demanding application areas that can require dynamic ranges (maximum input versus bias accuracy) in the 10^6 to 10^7 category.

9. THE VIBRATING BEAM ACCELEROMETER

Much of the cost for conventional pendulous electrically-servoed accelerometers is associated with the torque-generator and electronics needed to close-the-loop on the instrument and generate precision pulse outputs representing quantized increments of integrated input acceleration (1). The vibrating beam accelerometer replaces the torque-rebalance mechanism with an open-loop direct-digital-output transducer based on quartz-crystal oscillator technology (30, 31, 32). The concept is depicted in Figure 11.

In Figure 11, two quartz-crystal beams are mounted symmetrically back-to-back so that each axially supports a proof mass pendulum. Each beam is vibrated at its resonant frequency by an electronics loop in a manner similar to the method used to sustain amplitude in quartz-crytal oscillator clock references. In the absence of acceleration along the

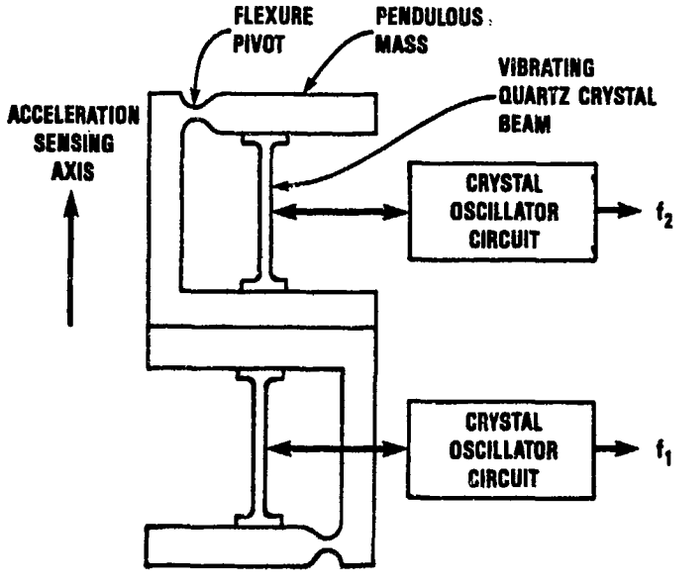

Figure 11 - Vibrating beam accelerometer concept.

acceleration sensing axis, both beams are selected to nominally resonate at the same frequency. Under applied acceleration, one beam is placed in compression and the other in tension by the inertial reaction of the pendulous proof masses. This produces an increase in frequency for the beam in tension, and a decrease in frequency for the beam in compression. The frequency difference ($F_2 - F_1$ in Figure (11)) is a direct digital output proportional to the input acceleration.

The symmetrical arrangement of the beams produces a cancellation of several error effects that would exist for one beam mounted individually. Error effects that are nominally cancelled include nominal beam frequency variations with temperature and aging, asymmetrical scale factor nonlinearities, anisoinertia errors (1), and vibropendulous errors (1) that are common between the individual beam assemblies.

9.1 Design Considerations And Application Areas

The vibrating beam accelerometer is being designed as a lower cost alternative to the conventional pendulous electrically-servoed accelerometer for strapdown applications. Cost reductions are expected to be achieved through elimination of the complex electro-mechanical assembly associated with the pendulous accelerometer torque-generator, and elimination of complex torque-to-balance and pulse quantizer readout electronics.

The ultimate success of the vibrating beam accelerometer will depend on whether its accuracy capabilities will approach those of mature technology pendulous accelerometers at a competetive price. Error mechanisms in the vibrating beam accelerometer arise from unpredictable variations between the two beam assemblies that are temperature, vibration sensitive and which vary over time. One of the more important error mechanisms that must be dealt with in the design of the unit is the potentional problem of mechanical coupling between the beam assemblies that pull the frequencies together under low input acceleration (an effect similar to lock-in for laser gyros). The result is a detection threshold for the unit that is a function of the strength of the mechanical coupling. The key to the design of an accurate vibrating beam accelerometer lies in the ability to isolate one crytsal beam from the other. One approach being used to achieve isolation is through application of a dual-beam construction (32) for each of the crystal beam assemblies as illustrated in Figure 12.

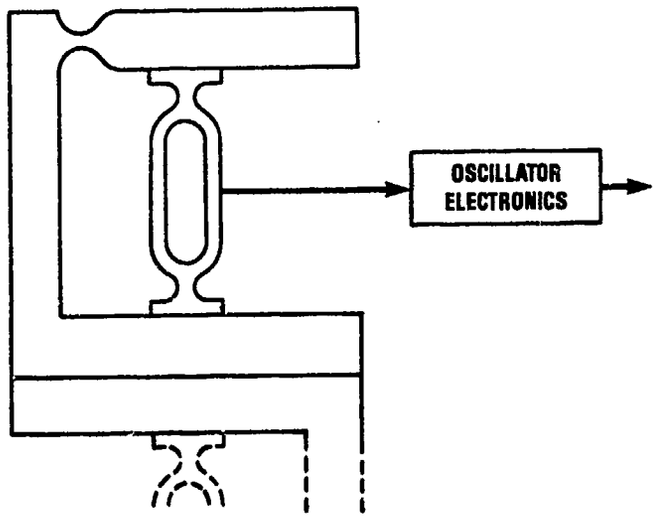

Figure 12 - Dual-beam crystal oscillator concept.

In Figure 12, each beam assembly is composed of an integral dual-beam arrangement in which the beam elements vibrate in opposition (180 degrees out of phase). The resulting counter-vibration allows each beam movement to be counter-acted mechanically by the other such that no net vibration is transmitted into the mount (i.e., similar to a tuning fork). The result is that mechanical coupling mechanisms between the independent dual-beam assemblies are minimized.

A problem area being addressed in the design of the vibrating beam accelerometer is the output resolution. Typical mechanizations are based on using crystals with a 40 KHz center frequency (zero input acceleration) with 10% variation over the design acceleration range. Hence, the inherent maximum frequency output of the device (beam frequency difference) under maximum input acceleration is typically 5 to 10 KHz. For the higher accuracy applications, this resolution is generally too coarse (by at least an order of magnitude under certain conditions). In order to enhance the basic resolution, design techniques being investigated include using time measurement between frequency difference pulses as the output, or use of digital phase-lock loop external circuity to generate higher frequency waveforms whose integral tracks the frequency difference output signal.

The vibrating beam accelerometer is still in its development stage with units becoming available for evaluation by test groups this year. Developmental test results reported to date have been encouraging. It is too early at this time to predict what the ultimate cost/performance of the device will be compared to mature pendulous accelerometer technology.

10. CONCLUDING REMARKS

Over the past six years, the laser gyro has emerged as the rate sensor most suitable for the high performance strapdown applications. Floated rate-integrating and tuned-rotor gyro technologies continue to be the most suitable rate sensors for the low-to-medium performance/low-cost application areas where small size is also important. It is expected that cost and size reductions for the laser gyro will broaden its applicability range in the future so that it will eventually dominate the medium accuracy performance areas as well. It is too early to predict whether the laser gyro will ever be of a low enough cost to successfully compete in the lower accuracy tactical missile application areas.

Pendulous accelerometer technology continues to be the main stay for strapdown applications. Performance advances and some cost reductions over the past few years have enabled this instrument to remain compatible with overall strapdown system cost/performance goals. To generate a significant cost reduction for strapdown accelerometers, the vibrating beam accelerometer is receiving attention by some development groups. Time will tell whether the cost/performance of this instrument will successfully compete with pendulous accelerometers in the future.

11. ACKNOWLEDGEMENTS

I would like to express my appreciation to engineering personnel in the following organizations who participated in valuable technical discussions on strapdown sensor technology during the preparation of this paper. These discussions provided the primary source of technical information for the paper.

Honeywell Avionics Division, Minneapolis, MN
Litton Guidance & Control Systems, Woodland Hills, CA
Naval Research Laboratory, Washington, DC
Raytheon Equipment Development Laboratories, Sudbury, MA
Rockwell Autonetics, Anaheim, CA
Singer Kearfott, Wayne, NJ
Sperry Gyroscope, Great Neck, NY
Sundstrand Data Control, Redmond, WA
Sundstrand Optical Technologies, Newbury Park, CA

REFERENCES

1. Savage, Paul G., "Strapdown Sensors", "AGARD Lecture Series No. 95: Strapdown Inertial Systems - Theory And Applications", June 1978.

2. Savage, Paul G., "Laser Gyros In Strapdown Inertial Navigation Systems", IEEE PLANS, Hilton Inn, San Diego, CA, November 1 - 3, 1976

3. Dynamic Errors in Strapdown Inertial Navigation Systems, NASA Report CR-1962, December 1971.

4. Wrigley, W., Hollister, W.M., and Denhard, W.G.,"Gyroscopic Theory, Design, and Instrumentation", M.I.T. Press, 1969.

5. Macomber, George R., and Fernandes, Manuel, Inertial Guidance Engineering, Prentice-Hall, Englewood Cliffs, New Jersey, 1962.

6. Howe, Edwin W., "A Free Rotor Gyro", Symposium on Unconventional Inertial Sensors, Farmingdale, New York, 1963.

7. Savet, Paul H., "New Trends in Non-floated Precision Gyroscopes", Grumman Research Department Memorandum RM-247J, October 1964.

8. Craig, Robert J.G., "Theory of Operation of Elastically Supported Tuned Gyroscope", IEEE Transactions on Aerospace and Electronic Systems, Vol. AES-8, No. 3, May 1972.

9. Craig, Robert J.G., "Theory of Errors of a Multigimbal, Elastically Supported, Tuned Gyroscope", IEEE Transactions on Aerospace and Electronic Systems, Vol. AES-8, No. 3, May 1972.

10. Craig, Robert J.G., Dynamically Tuned Gyros in Strapdown Systems", AGARD Conference Proceedings No. 116 on Inertial Navigation Components and Systems, AD-758 127, Paris, France, February 1973.

11. Killpatrick, Joseph, "The Laser Gyro", IEEE Spectrum, October 1967.

12. Aronowitz, Frederick, "The Laser Gyro", Laser Applications, Vol. 1, Academic Press, New York, 1971.

13. Aronowitz, Frederick, and Collins R.J., "Mode Coupling Due to Back Scattering in a HeNe Traveling Wave Ring Laser", Applied Physics Letters, Vol. 9, No. 1, 1 July 1966.

14. Dewar, Dr. D., "The Laser Gyroscope", Royal Aeronautical Society, London, 12 January 1977.

15. Hammons, Seridan W., and Ashby, Val J., "Mechanically Dithered RLG At The Quantum Limit", 0547-3578/82/0000-0388 Copyright 1982 IEEE.

16. Hutchings, T.J., and Stjern, D.C., "Scale Factor Non-Linearity of a Body Dithered Laser gyro", IEEE NAECON, 1978, Vol. 2, Pg. 549.

17. Hutchings, T., "Development And Test of A Small Body Dithered Laser Gyro", Electro-Optics/Laser 77 Conference & Exposition, Anaheim, CA, Oct. 25-27, 1977.

18. Henery, R.D., Whitcomb, E.C., and Vescial, F., "Ferrimagnetic Garnets As Laser Gyro Faraday Elements", Electro-Optics/Laser 77 Conference & Exposition, Anaheim, CA, Oct. 25-27, 1977.

19. Mark, John G., Ebner, Robert E., and Brown, Alison K., "Design of RLG Inertial Systems For High Vibration", IEEE PLANS, Atlantic City, NJ, December 6-9, 1982.

20. McClure, R.E., and Vaher E., "An Improved Ring Laser Bias Element", CH1336-7/78/0000-0544 Copyright 1978 IEEE.

21. McClure, R.E., "An Electrical Equivalent Circuit For The Tranverse Mangeto-Optic Effect In Thin Magnetic Films", International Magnetics Conference, Boston, MA, April 24, 1980.

22. Freiser, M.J., "A Survey of Magneto-Optics Effects", IEEE Transactions on Magnetics MAG-4, 152, 1968.

23. Dillon, Jr., J.F., "Magneto-Optical Properties of Magnetic Garnets", Physics of Magnetic Garnets, pp 379-415, A. Paoletti, ed; North Holland, 1978.

24. Morrison, R.F., Levinson, Dr. E., and Bryant Jr., B.L., "The SLIC-7 Laser Gyro, Inertial Guidance System", NAECON, Dayton, Ohio, 1977.

25. Dorshner, Terry A., Hermann, A. Haus, Holz, Michael, Smith, Irl W., and Statz, Hermann, "Laser Gyro At Quantum Limit", IEEE Journal of Quantum Electronics, Vol QE-16, No. 12, December 1980.

26. Mathews, James B., Gneses, Morris I., and Berg, Dennis S., "A High Resolution Laser Gyro", NAECON May 16-18, 1978, Dayton, Ohio.

27. Statz, H., Dorschner, Terry A., Holz, M., and Smith, Irl W., The Multioscillator Ring Laser Gyroscope, Raytheon Research Division Technical Report T-1096, January, 1983.

28. Ezekiel, S., and Arditty, H.J., ed. Fiber-Optic Rotation Sensors, Proceedings of the First International Conference, M.I.T., Cambridge, MA, November 9-11, 1932; Published in Springer Series in Optical Sciences, Vol. 32, Schawlow, Arthur L., ed., Springer-Verlag Berlin Heidelberg New York 1982.

29. Burns, W.K., Moeller, R.P., Villarruel, C.A., and Abebe, M., "Fiber-Optic Gyroscope with Polarization-Holding Fiber", Optics Letters, Vol. 8, No. 10, October 1983.

30. Albert, William C., and Weber Raymond E., "Vibrating Beam Accelerometer For Strapdown Applications", IEEE PLANS, Atlantic City, NJ, December 6-9, 1982.

31. Albert, William C., "Vibrating Quartz Crystal Beam Accelerometer", Copyright ISA, 1982, ISBN: 0-87664-689-5.

32. Gogic, A.M., and Peters, R.B., "Description And Test Methods For A Frequency Output Accelerometer", Inertial Navigation Test Symposium, Holloman AFB, 1983.

33. Savage, P.G., "Strapdown System Algorithms", AGARD Lecture Series No. 133: Advances In Strapdown Inertial Systems", May 1984.

34. Savage, P.G., Introduction To Strapdown Inertial Systems, June 1, 1983 (Third Printing), and Introduction To Strapdown Inertial Navigation Systems - Supplemental Material, November 14, 1983; Third Strapdown Associates Open Seminar On Strapdown Inertial Navigation Systems, Marquette Inn, Minneapolis, MN, Nov. 14-18, 1983.

STRAPDOWN SYSTEM ALGORITHMS

By

Paul G. Savage
President
Strapdown Associates, Inc.
Woodbridge Plaza, Suite 150
10201 Wayzata Blvd.
Minnetonka, Minnesota 55343

SUMMARY

This paper addresses the attitude determination, acceleration transformation, and attitude/heading output computational operations performed in modern-day strapdown inertial navigation systems. Contemporary algorithms are described for implementing these operations in real-time computers. The attitude determination and acceleration transformation algorithm discussions are based on the two-speed approach in which high frequency coning and sculling effects are calculated with simplified high speed algorithms, with results fed into lower speed higher order algorithms. This is the approach that is typically used in most modern-day strapdown systems. Design equations are included for evaluating the performance of the strapdown computer algorithms as a function of computer execution speed and sensor assembly vibration amplitude/frequency/phase environment.

Both direction cosine and quaternion based attitude algorithms are described and compared in light of modern-day algorithm accuracy capabilities. Orthogonality and normalization operations are addressed for potential attitude algorithm accuracy enhancement. The section on attitude data output algorithms includes a discussion on roll/yaw Euler angle singularities near high/low pitch angle conditions.

1. INTRODUCTION

The concept of strapdown inertial navigation was originated more than thirty years ago, largely from an analytical standpoint. The theoretical analytical expressions for processing strapdown inertial sensor data to develop attitude, velocity, and position information were reasonably well understood in the form of continuous matrix operations and differential equations. The implementation of these equations in a digitial computer, however, was invariably keyed to severe throughput limitations of original airborne digitial computer technology. As a result, many of the strapdown computational algorithms originated during these early periods were inherently limited in accuracy, particulary under high frequency dynamic motion. A classical test for algorithm accuracy during this early period was how well the algorithm computed attitude under cyclic coning motion as the coning frequency approached the computer update cycle frequency.

In the late 1960's and early 1970's, several analytical efforts addressed the problem of splitting the strapdown computation process into low and high speed sections (7, 8, 10). The low speed section contained the bulk of the computational equations, and was designed to accurately account for low frequency large amplitude dynamic motion effects (e.g., vehicle maneuvering). The high speed computation section was designed with a small set of simple algorithms that would accurately account for high frequency small amplitude dynamic motion (e.g., vehicle vibrations). Splitting the computational process in this manner allowed the bulk of the strapdown algorithms to be iterated at reasonable speeds compatible with computer throughput limitations. The high speed algorithms were simple enough that they could be mechanized individually with special purpose electronics, or as a minor high speed loop in the main processor.

Over the past ten years, the structure of most strapdown algorithms has evolved into this two speed structure. The techniques have been refined today so that fairly straight-forward analytical design methods can be used to define algorithm analytical forms and computational rates to achieve required levels of performance in specified dynamic environments.

This paper describes the algorithms used today in most modern-day strapdown inertial navigation systems to calculate attitude and transform acceleration vector measurements from sensor to navigation axes. The algorithms for integrating the transformed accelerations into velocity and position data are not addressed because it is believed that these operations are generic to inertial navigation in general, not only strapdown inertial navigation.

For the algorithms discussed, the analytical basis is presented together with a discussion on general design methodology used to develop the algorithms for compatibility with particular user accuracy and environmental requirements.

2. STRAPDOWN COMPUTATION OPERATIONS

Figure 1 depicts the computational elements implemented by software algorithms in typical strapdown inertial navigation systems. Input data to the algorithms is provided from a triad of strapdown gyros and accelerometers. The gyros provide precision measurements of strapdown sensor coordinate frame ("body axes") angular rotation rate relative to nonrotating inertial space. The accelerometers provide precision measurements of 3-axis orthogonal specific force acceleration along body axes.

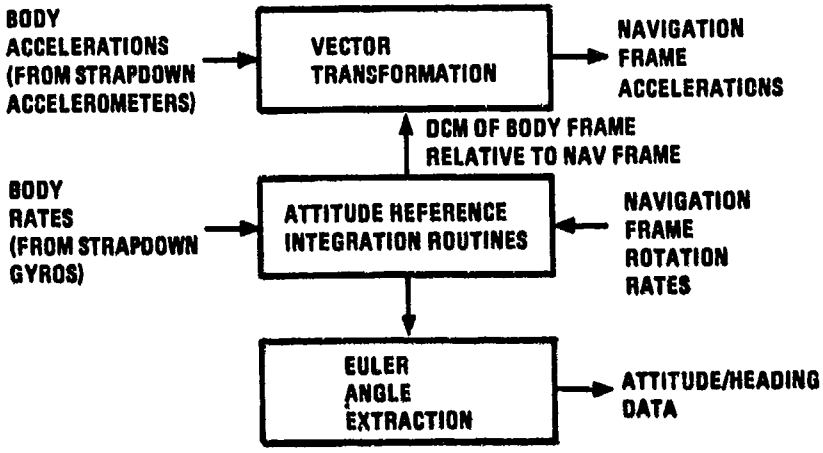

FIGURE 1 - STRAPDOWN ATTITUDE REFERENCE OPERATIONS

The strapdown gyro data is processed on an iterative basis by suitable integration algorithms to calculate the attitude of the body frame relative to navigation coordinates. The rotation rate of the navigation frame is an input to the calculation from the navigation section of the overall computation software. Typical navigation coordinate frames are oriented with the z-axis vertical and the x, y, axes horizontal.

The attitude information calculated from the gyro and navigation frame rate data is used to transform the accelerometer specific force vector measurements in body axes to their equivalent form in navigation coordinates. The navigation frame specific force accelerations are then integrated in the navigation software section to calculate velocity and position. The velocity/position computational algorithms are not unique to the strapdown mechanization concept, hence, are not treated in this paper. Several texts treat the velocity/position integration algorithms in detail (1, 2, 3, 4, 12).

Figure 1 also shows an Euler Angle Extraction function as part of the strapdown attitude reference operations. This algorithm is used to convert the calculated attitude data into an output format that is more compatible with typical user requirements (e.g., roll, pitch, heading Euler angles).

3. STRAPDOWN ATTITUDE INTEGRATION ALGORITHMS

The attitude information in strapdown inertial navigation systems is typically calculated in the form of a direction cosine matrix or as an attitude quaternion. The direction cosine matrix is a three-by-three matrix whose rows represent unit vectors in navigation axes projected along body axes. As such, the element in the i^{th} row and j^{th} column represents the cosine of the angle between the navigation frame i-axis and body frame j-axis. The quaternion is a four-vector whose elements are defined analytically (5, 9) as follows:

$$\begin{aligned} a &= (\alpha_x/\alpha) \sin(\alpha/2) \\ b &= (\alpha_y/\alpha) \sin(\alpha/2) \\ c &= (\alpha_z/\alpha) \sin(\alpha/2) \\ d &= \cos(\alpha/2) \end{aligned} \qquad (1)$$

where

$\alpha_x, \alpha_y, \alpha_z$ = Components of an angle vector $\underline{\alpha}$.
α = Magnitude of $\underline{\alpha}$.

The $\underline{\alpha}$ vector is defined to have direction and magnitude such that if the navigation frame was rotated about $\underline{\alpha}$ through an angle α, it would be rotated into alignment with the body frame. The $\underline{\alpha}$ rotation angle vector and its quaternion equivalent (a, b, c, d, from equations (1)), or the direction cosine matrix, uniquely define the attitude of the body axes relative to navigation axes.

3.1 Direction Cosine Updating Algorithms

3.1.1 Direction Cosine Updating Algorithm For Body Rotations

The direction cosine matrix can be updated for body frame gyro sensed motion in the strapdown computer by executing the following classical direction cosine matrix chain rule algorithm on a repetative basis:

$$C(m+1) = C(m)\, A(m) \tag{2}$$

where

C(m) = Direction cosine matrix relating body to navigation axes at the m^{th} computer cycle time

A(m) = Direction cosine martix that transforms vectors from body coordinates at the $(m+1)^{th}$ computer cycle to body coordinates at the m^{th} computer cycle.

It is well known (9) that:

$$A(m) = I + f_1(\underline{\phi}x) + f_2(\underline{\phi}x)^2 \tag{3}$$

where

$$f_1 = \frac{\sin \phi}{\phi} = 1 - \phi^2/3! + \phi^4/4! - \cdots$$

$$f_2 = \frac{1 - \cos \phi}{\phi^2} = 1/2! - \phi^2/4! + \phi^4/6! - \cdots$$

$$\phi^2 = \phi_x^2 + \phi_y^2 + \phi_z^2 \tag{4}$$

$$(\underline{\phi}x) \triangleq \begin{bmatrix} 0 & -\phi_z & \phi_y \\ \phi_z & 0 & -\phi_x \\ -\phi_y & \phi_x & 0 \end{bmatrix}$$

I = 3 x 3 unity matrix

ϕ_x, ϕ_y, ϕ_z = Components of $\underline{\phi}$.

$\underline{\phi}$ = Angle vector with direction and magnitude such that a rotation of the body frame about $\underline{\phi}$ through an angle equal to the magnitude of $\underline{\phi}$ will rotate the body frame from its orientation at computer cycle m to its orientation at computer cycle m+1. The $\underline{\phi}$ vector is computed for each computer cycle m by processing the data from the strapdown gyros. The algorithm for computing $\underline{\phi}$ will be described subsequently.

The "order" of the algorithm defined by equations (2) through (4) is determined by the number of terms carried in the f_1, f_2 expansions. A fifth order algorithm, for example, retains sufficient terms in f_1 and f_2 such that A(m) contains all $\underline{\phi}$ term products out to fifth order. Hence, f_1 would be truncated after the ϕ^4 term and f_2 would be truncated after the ϕ^2 term to retain fifth order accuracy in A(m). The order of accuracy required is determined by system accuracy requirements under maximum rate input conditions when $\underline{\phi}$ is a maximum. The computation iteration rate is typically selected to assure that $\underline{\phi}$ remains small at maximum rate (e.g., 0.1 radians). This assures that the number of terms required for accuracy in the f_1, f_2 expansions will be reasonable.

3.1.2 Direction Cosine Updating Algorithm For Navigation Frame Rotations

Equation (2) is used to update the direction cosine matrix for gyro sensed body frame motion. In order to update the direction cosines for rotation of the navigation coordinate frame, the following classical direction cosine matrix chain rule algorithm is used:

$$C(n+1) = B(n)\, C(n) \tag{5}$$

where

B(n) = Direction cosine matrix that transforms vectors from navigation axes at computer cycle n to navigation axes at computer cycle (n+1).

The equation for B(n) parallels equation (3):

$$B(n) = I - (\underline{\theta}x) + 0.5(\underline{\theta}x)^2 \tag{6}$$

with

$$(\underline{\theta}x) \triangleq \begin{bmatrix} 0 & -\theta_z & \theta_y \\ \theta_z & 0 & -\theta_x \\ -\theta_y & \theta_x & 0 \end{bmatrix} \tag{7}$$

where

$\theta_x, \theta_y, \theta_z$ = Components of $\underline{\theta}$.

$\underline{\theta}$ = Angle vector with direction and magnitude such that a rotation of the navigation frame about $\underline{\theta}$ through an angle equal to the magnitude of $\underline{\theta}$ will rotate the navigation frame from its orientation at computer cycle n to its orientation at computer cycle n+1. The $\underline{\theta}$ vector is computed for each computer cycle n by processing the navigation frame rotation rate data from the navigation software section (12).

It is important to note that the n cycle (for navigation frame rotation) and m cycle (for body frame rotation) are generally different, n typically being executed at a lower iteration rate than m. This is permissable because the navigation frame rotation rates are considerably smaller than the body rates, hence, high execution rates are not needed to maintain $\underline{\theta}$ small to reduce the order of the iteration algorithm. The algorithm represented by equations (5) and (6) is second order in $\underline{\theta}$. Generally, first order is of sufficient accuracy, and the $(\underline{\theta}x)^2$ term need not be carried in the actual software implementation.

3.2 Quaternion Updating Algorithms

3.2.1 Quaternion Transformation Properties

The updating algorithms for the attitude quaternion can be developed through an investigation of its vector transformation properties (5, 9). We first introduce nomenclature that is useful for describing quaternion algebraic operations. Referring to equation (1), the quaternion with components a, b, c, d, can be described as:

$$u = ai + bj + ck + d \tag{8}$$

where

a,b,c = Components of the "vector" part of the quaternion.

i,j,k = Quaternion vector operators analagous to unit vectors along orthogonal coordinate axes.

d = "Scalar" part of the quaternion.

We also define rules for quaternion vector operator products as:

$$\begin{array}{lll} ii = -1 & ij = k & ji = -k \\ jj = -1 & jk = i & kj = -i \\ kk = -1 & ki = j & ik = -j \end{array}$$

With the above definitions, the product w of two quaternions (u and v) becomes:

$$w = uv = (ai + bj + ck + d)(ei + fj + gk + h)$$

$$\begin{aligned} &= aeii + afij + agik + ahi \\ &\quad + beji + bfjj + bgjk + bhj \\ &\quad + ceki + cfkj + cgkk + chk \\ &\quad + dei + dfj + dgk + dh \end{aligned}$$

$$\begin{aligned} &= (ah + de + bg - cf)i \\ &\quad + (bh + df + ce - ag)j \\ &\quad + (ch + dg + af - be)k \\ &\quad + (dh - ae - bf - cg) \end{aligned}$$

or in "Four-vector" matrix form:

$$w \triangleq \begin{vmatrix} e' \\ f' \\ g' \\ h' \end{vmatrix} = \begin{bmatrix} d & -c & b & a \\ c & d & -a & b \\ -b & a & d & c \\ -a & -b & -c & d \end{bmatrix} \begin{vmatrix} e \\ f \\ g \\ h \end{vmatrix}$$

We also define the "complex conjugate" of the general quaternion u in equation (8) as:

$$u^* \triangleq -ai - bj - ck + d$$

We now define a quaternion operator h(m) for the body angle change $\underline{\phi}$ over computer cycle m as:

$$h(m) = \begin{matrix} (\phi_x/\phi) \sin(\phi/2) \\ (\phi_y/\phi) \sin(\phi/2) \\ (\phi_z/\phi) \sin(\phi/2) \\ \cos(\phi/2) \end{matrix} \qquad (9)$$

where the elements in the above column matrix refer to the i, j, k, and scalar components of h. We also define a general vector $\underline{v}$ with commponents v_x, v_y, v_z, and a corresponding quaternion v having the same vector components with a zero scalar component:

$$v = \begin{vmatrix} v_x \\ v_y \\ v_z \\ 0 \end{vmatrix}$$

Using the above definitions and the general rules for quaternion algebra, it is readily demonstrated by substitution and trigonometric manipulation that:

$$v' \triangleq h(m)\, v\, h(m)^* = A'(m)\, v \qquad (10)$$

where

$$A'(m) \triangleq \begin{bmatrix} A(m) & 0 \\ 0 & 0 \end{bmatrix}$$

$$v' \triangleq \begin{vmatrix} v_x' \\ v_y' \\ v_z' \\ 0 \end{vmatrix}$$

A(m) = As defined in (3).

Equation (10), therefore, is the quaternion form of the vector transformation equation that transforms a vector from body coordinates at computer cycle (m+1) to body coordinates at computer cycle m:

$$\underline{v}' = A(m)\ \underline{v} \qquad (11)$$

where

$\underline{v}', \underline{v}$ = "Three-vector" form of v' and v (i.e., with components v_x', v_y', v_z' and v_x, v_y, v_z).

$\underline{v}$ = The general vector $\underline{v}$ in body coordinates at computer cycle (m+1).

$\underline{v}'$ = The general vector $\underline{v}$ in body coordinates at computer cycle m.

3.2.2 Quaternion Updating Algorithm For Body Motion

Equation (10) with its equation (11) dual can be used to define analagous vector transformation operations between body coordinates and navigation coordinates at computer cycle m as:

$$\begin{aligned} v'' &= q(m)\ v'\ q(m)^* \\ \underline{v}'' &= C(m)\ \underline{v}' \end{aligned} \qquad (12)$$

where

q(m) = Quaternion relating body axes to navigation axes at computer cycle m.

$\underline{v}'$ = The vector $\underline{v}$ in navigation coordinates.

$\underline{v}''$ = The vector $\underline{v}$ in body coordinates at computer cycle m.

v', v'' = Quaternion ("Four vector") form of $\underline{v}'$, $\underline{v}''$.

The q quaternion has four elements (i.e., a, b, c, d) that are updated for body motion at each computer cycle m. The updating equation is easily derived by substituting equation (10) into (12):

$$v'' = q(m)\ h(m)\ v\ h(m)^*\ q(m)^*$$

Using the definition for the quaternion complex conjugate, it is readily demonstrated that:

$$h(m)^*\ q(m)^* = (q(m)\ h(m))^*$$

Thus,

$$v'' = q(m)\ h(m)\ v\ (h(m)\ q(m))^*$$

But we can also write the direct expression:

$$v'' = q(m+1)\ v\ q(m+1)^*$$

Therefore, by direct comparison of the latter two equations:

$$q(m+1) = q(m)\ h(m) \qquad (13)$$

Equation (13) is the quaternion equivalent to direction cosine updating equation (2). For computational purposes, h(m) as defined in equations (9) is equivalently:

$$h(m) = \begin{vmatrix} f_3\,\phi_x \\ f_3\,\phi_y \\ f_3\,\phi_z \\ f_4 \end{vmatrix}$$

$$f_3 = \frac{\sin(\phi/2)}{\phi} = 0.5\left(1 - (0.5\phi)^2/3! + (0.5\phi)^4/5! - \cdots\right) \qquad (14)$$

$$f_4 = \cos(\phi/2) = 1 - (0.5\phi)^2/2! + (0.5\phi)^4/4! - \cdots)$$

$$(0.5\phi)^2 = 0.25\,(\phi_x^2 + \phi_y^2 + \phi_z^2)$$

The "order" of the equation (13) and (14) updating algorithm depends on the order of ϕ terms carried in h which depends on the truncation point used in f_3 and f_4. The rationale for selecting the algorithm order and associated algorithm iteration rate is directly analagous to selection of the direction cosine updating algorithm order (discussed previously).

3.2.3 Quaternion Updating Algorithm For Navigation Frame Rotation

Equation (13) with (14) is used to update the quaternion for body frame motion sensed by gyros. In order to update the quaternion for rotation of the navigation coordinate frame, an algorithm analagous to equation (5) (for the direction cosine matrix) is used with a navigation frame rotation quaternion r:

$$q(n+1) = r(n)\,q(n)$$

$$r(n) = \begin{vmatrix} -0.5\,\theta_x \\ -0.5\,\theta_y \\ -0.5\,\theta_z \\ 1-0.5(\theta/2)^2 \end{vmatrix} \qquad (15)$$

$$(\theta/2)^2 = 0.25\,(\theta_x^2 + \theta_y^2 + \theta_z^2)$$

where

$\theta_x, \theta_y, \theta_z$ = Components of $\underline{\theta}$ as defined previously for equations (6) and (7).

The development of equation (15) parallels the development of (13). The equation for r(n) is a truncated form of the theoretical exact analytical expression (analagous to the second order truncated form of equation (14)). The θ^2 term in equation (15) generally is not required for accuracy (due to the smallness of $\underline{\theta}$ in typical applications).

As for the direction cosine updating algorithm for navigation frame motion, the equivalent quaternion updating algorithm (equation (15)) updating cycle n need not be processed as fast as the body rate cycle m to maintain equivalent accuracy. This is due to the considerably smaller navigation frame rotation rates compared to body rotation rates.

3.2.4 Equivalencies Between Direction Cosine And Quaternion Elements

The analytical equivalency between the elements of the direction cosine matrix and the attitude quaternion can be derived by direct expansion of equations (12). If we define the elements of q as:

$$q = \begin{vmatrix} a \\ b \\ c \\ d \end{vmatrix}$$

equation (12) becomes after expansion, factorization of v', and neglecting the scalar part of the v" and v' quaternion vectors (i.e., carrying only the vector components $\underline{v}$" and $\underline{v}$'):

$$\underline{v}'' = \begin{bmatrix} (d^2 + a^2 - b^2 - c^2) & 2(ab - cd) & 2(ac + bd) \\ 2(ab + cd) & (d^2 + b^2 - c^2 - a^2) & 2(bc - ad) \\ 2(ac - bd) & 2(bc + ad) & (d^2 + c^2 - a^2 - b^2) \end{bmatrix} \underline{v}' \qquad (16)$$

Defining C in equation (12) as:

$$C = \begin{bmatrix} C_{11} & C_{12} & C_{13} \\ C_{21} & C_{22} & C_{23} \\ C_{31} & C_{32} & C_{33} \end{bmatrix}$$

equation (16) when compared with (12) shows that:

$$\begin{aligned} C_{11} &= d^2 + a^2 - b^2 - c^2 \\ C_{12} &= 2(ab - cd) \\ C_{13} &= 2(ac + bd) \\ C_{21} &= 2(ab + cd) \\ C_{22} &= d^2 + b^2 - c^2 - a^2 \\ C_{23} &= 2(bc - ad) \\ C_{31} &= 2(ac - bd) \\ C_{32} &= 2(bc + ad) \\ C_{33} &= d^2 + c^2 - a^2 - b^2 \end{aligned} \qquad (17)$$

The converse of equation (17) is somewhat more complicated. Using the property (from equation (1)) that :

$$a^2 + b^2 + c^2 + d^2 = 1$$

the converse of equation (17) can be shown (11) to be computable from the following sequence of operations:

$$\begin{aligned} T_r &= C_{11} + C_{22} + C_{33} \\ P_1 &= 1 + 2C_{11} - T_r \\ P_2 &= 1 + 2C_{22} - T_r \\ P_3 &= 1 + 2C_{33} - T_r \\ P_o &= 1 + T_r \end{aligned}$$

If $P_1 = \max(P_1, P_2, P_3, P_o)$, then:

$$\begin{aligned} a &= 0.5\, P_1 1/2\, \text{sign}(a_{previous}) \\ b &= (C_{21} + C_{12})/4a \\ c &= (C_{13} + C_{31})/4a \\ d &= (C_{32} - C_{23})/4a \end{aligned}$$

If $P_2 = \max(P_1, P_2, P_3, P_o)$, then:

$$\begin{aligned} b &= 0.5\, P_2 1/2\, \text{sign}(b_{previous}) \\ c &= (C_{32} + C_{23})/4b \\ d &= (C_{13} - C_{31})/4b \\ a &= (C_{21} + C_{12})/4b \end{aligned} \qquad (18)$$

If $P_3 = \max(P_1, P_2, P_3, P_o)$, then:

$$\begin{aligned} c &= 0.5\, P_3 1/2\, \text{sign}(c_{previous}) \\ d &= (C_{21} - C_{12})/4c \\ a &= (C_{13} + C_{31})/4c \\ b &= (C_{32} + C_{23})/4c \end{aligned}$$

If $P_o = \max(P_1, P_2, P_3, P_o)$, then:

$$\begin{aligned} d &= 0.5\, P_4 1/2\, \text{sign}(d_{previous}) \\ a &= (C_{32} - C_{23})/4d \\ b &= (C_{13} - C_{31})/4d \\ c &= (C_{21} - C_{12})/4d \end{aligned}$$

3.3 The Computation Of $\underline{\phi}$

3.3.1 Continous Form

The $\underline{\phi}$ "body attitude change" vector is calculated by processing data from the strapdown gyros. Under situations where the angular rotation rate vector (sensed by the gyros) lies along a fixed direction (i.e., is nonrotating in inertial space), the $\underline{\phi}$ vector is equal to the simple integral of the angular rate vector over the time interval from computer cycle m to computer cycle (m+1):

$$\underline{\phi} = \int_{t_m}^{t_{m+1}} \underline{\omega}\, dt \qquad \text{for cases when } \underline{\omega} \text{ is nonrotating.} \tag{19}$$

where

$\underline{\omega}$ = Angular rate vector sensed by the strapdown gyros.

Under general motion conditions (when $\underline{\omega}$ may be rotating), equation (19) has the more complex form (as derived in (10) or alternatively, in Appendix A):

$$\underline{\alpha}(t) = \int_{t_m}^{t} (\underline{\omega} + 1/2\ \underline{\alpha} \times \underline{\omega} + \frac{1}{\alpha^2}\left(1 - \frac{\alpha \sin \alpha}{(1-\sin\alpha)}\right) \underline{\alpha} \times (\underline{\alpha} \times \underline{\omega}))dt$$

$$\underline{\phi} = \underline{\alpha}(t=t_{m+1}) \tag{20}$$

It can verified by power series expansion that to first order,

$$(1/\alpha^2)\left(1 - \frac{\alpha \sin \alpha}{(1-\cos\alpha)}\right) \approx \frac{1}{12}$$

Hence, $\alpha(t)$ in equation (20), to third order accuracy in α can be approximated by:

$$\underline{\alpha}(t) \approx \int_{t_m}^{t} (\underline{\omega} + 1/2\ \underline{\alpha} \times \underline{\omega} + \frac{1}{12}\ \underline{\alpha} \times (\underline{\alpha} \times \underline{\omega}))dt \tag{21}$$

A second order expression for $\underline{\alpha}(t)$ can be obtained from (21) by dropping the 1/12 term. An even simpler expression for $\underline{\alpha}(t)$ is obtained by dropping the 1/12 term, and approximating the $\underline{\alpha}$ term in the integral by the direct integral of $\underline{\omega}$:

$$\underline{\beta}(t) = \int_{t_m}^{t} \underline{\omega}\, dt$$

$$\delta\underline{\beta}(t) = 1/2 \int_{t_m}^{t} \underline{\beta} \times \underline{\omega}\, dt \tag{22}$$

$$\underline{\phi} = \underline{\beta}(t=t_{m+1}) + \delta\underline{\beta}(t=t_{m+1})$$

An interesting characteristic about equation (22) is that its accuracy is in fact comparable to that of third order equation (21). In other words, the simplifying assumption of replacing α with β in the $1/2\ \underline{\alpha} \times \underline{\omega}$ term is in fact equivalent to introducing an error in equation (21) that to third order, equals the $1/12\ \underline{\alpha} \times (\underline{\alpha} \times \underline{\omega})$ term. This property can be verified by simulation as well as analytical expansion under hypothesized angular motion conditions.

Equation (22) is the equation that is mechanized in software in most modern-day strapdown inertial navigation systems to calcuate $\underline{\phi}$. It can be demonstrated analytically and by simulation that for representative vehicle angular motion and vibration, equation (22) faithfully calculates $\underline{\phi}$ to accuracy levels that are compatible with high performance strapdown inertial navigation system requirements.

For situations where $\underline{\omega}$ is nonrotating, the $\delta\underline{\beta}$ term in (22) is zero and $\underline{\phi}$ equals the simple time integral or $\underline{\omega}$ over the computer interval m (i.e., the equation (19) approximation). For situations where $\underline{\omega}$ is rotating (a situation defined analytically as

"coning"), the $\underline{\delta\beta}$ term is nonzero and must be calculated and used as a correction to the $\underline{\omega}$ integral to properly calculate $\underline{\phi}$.

It is important to note that the accuracy by which equation (22) approximates (20) is dependent on $\underline{\phi}$ being small (e.g., less than 0.1 radian). In order to protect the accuracy of this approximation, the computer iteration rate must be high enough that $\underline{\phi}$ remains small under maximum vehicle rotation rate conditions.

3.3.2 Recursive Algorithm Form

The implementation of equation (22) in a digital computer implies that a higher speed integration summing operation be performed during each body motion attitude update cycle. A computational algorithm for the integration function can be derived by first rewriting equation (22) in the equivalent incremental updating form:

$$\underline{\beta}(t) = \underline{\beta}(\ell) + \int_{t_\ell}^{t} \underline{\omega}\, dt$$

$$\underline{\delta\beta}(\ell+1) = \underline{\delta\beta}(\ell) + 1/2 \int_{t_\ell}^{t_{\ell+1}} \underline{\beta}(t) \times \underline{\omega}\, dt \qquad (23)$$

$$\underline{\beta}(\ell+1) = \underline{\beta}(t=t_{\ell+1})$$

$$\underline{\phi} = \underline{\beta}(t=t_{m+1}) + \underline{\delta\beta}(t=t_{m+1})$$

with initial conditions:

$$\underline{\beta}(t=t_m) = 0$$
$$\underline{\delta\beta}(t=t_m) = 0 \qquad (24)$$

where

ℓ = High speed computer cycle within the m body rate update cycle.

The integrals in (23) can be replaced by analytical forms that are compatible with gyro input data processing if $\underline{\omega}$ is replaced by a generalized time series expansion. For equations (23), it is sufficient to approximate $\underline{\omega}$ over the ℓ to $\ell+1$ time interval as a constant plus a linear ramp:

$$\underline{\omega} \approx \underline{A} + \underline{B}\,(t - t_\ell) \qquad (25)$$

where

$\underline{A}$, $\underline{B}$ = Constant vectors.

Substituting (25) in (23), and recognizing with the equation (25) approximation that:

$$\underline{A}(t_{\ell+1} - t_\ell) \approx 1/2\,(\underline{\Delta\theta}(\ell) + \underline{\Delta\theta}(\ell-1))$$

$$1/2\,\underline{B}(t_{\ell+1} - t_\ell)^2 \approx 1/2\,(\underline{\Delta\theta}(\ell) - \underline{\Delta\theta}(\ell-1))$$

where by definition:

$$\underline{\Delta\theta}(\ell) \triangleq \int_{t_\ell}^{t_{\ell+1}} \underline{\omega}\, dt$$

yields the desired final form for the $\underline{\phi}$ updating algorithm:

$$\underline{\delta\beta}(\ell+1) = \underline{\delta\beta}(\ell) + 1/2\ (\underline{\beta}(\ell) + 1/6\ \underline{\Delta\theta}(\ell-1)) \times \underline{\Delta\theta}(\ell)$$

$$\underline{\Delta\theta}(\ell) = \int_{t_\ell}^{t_{\ell+1}} \underline{\omega}\ dt = \sum_{t_\ell}^{t_{\ell+1}} \underline{d\theta} \qquad (26)$$

$$\underline{\beta}(\ell+1) = \underline{\beta}(\ell) + \underline{\Delta\theta}(\ell)$$

$$\underline{\phi} = \underline{\beta}(t=t_{m+1}) + \underline{\delta\beta}(t=t_{m+1})$$

with initial conditions:

$$\underline{\beta}(t=t_m) \triangleq \underline{\beta}(\ell=0) = 0$$

$$\underline{\delta\beta}(t=t_m) \triangleq \underline{\delta\beta}(\ell=0) = 0$$

where

$\underline{d\theta}$ = Gyro output pulse vector. Each component (x,y,z) represents the occurance of a rotation through a specified fixed angle increment about the gyro input axis.

$\underline{\Delta\theta}$ = Gyro output pulse vector count from ℓ to $\ell+1$.

The computational algorithm described by equation (26) is used on a recursive basis to calculate $\underline{\phi}$ once each m cycle. After $\underline{\phi}$ is calculated, the $\underline{\beta}$ and $\underline{\delta\beta}$ functions are reset for the next m cycle $\underline{\phi}$ calculation. The iteration rate for ℓ within m is maintained at a high enough rate to properly account for anticipated dynamic $\underline{\omega}$ motion effects. Section 6. describes analytical techniques that can be used to assess the adequacy of the ℓ iteration rate under dynamic angular rate conditions.

3.4 The Computation Of $\underline{\theta}$

The $\underline{\theta}$ vector in equations (6) and (15) is computed as a simple integral of navigation frame angular rate over the n cycle iteration period:

$$\underline{\theta} = \int_{t_n}^{t_{n+1}} \underline{\Omega}\ dt \qquad (27)$$

where

$\underline{\Omega}$ = Navigation frame rotation rate as calculated in the navigation software section (12).

Standard recursive integration algorithms can be used to calculate $\underline{\theta}$ in equation (27) (e.g., trapezoidal) over the time interval from n to n+1. The update rate for the integration algorithm is selected to be compatible with software accuracy requirements in the anticipated dynamic maneuver environment for the user vehicle.

3.5 Orthogonality And Normalization Algorithms

Most strapdown attitude computation techniques periodically employ self-consistancy correction algorithms as an outer-loop function for accuracy enhancement. If the basic attitude data is computed in the form of a direction cosine matrix, the self-consistancy check is that the rows should be orthogonal to each other and equal to unity in magnitude. This condition is based on the fact that the rows of the direction cosine matrix represent unit vectors along orthogonal navigation coordinate frame axes as projected in body axes. For the quaternion, the self-consistancy check is that the sum of the squares of the quaternion elements be unity (this can be verified by operation on equation (1)).

3.5.1 Direction Cosine Orthogonalization And Normalization

The test for orthogonality between two direction cosine rows is that the dot product be zero. The error condition, then is:

$$E_{ij} = C_i C_j^T \tag{28}$$

where

C_i = i^{th} row of C

C_j = j^{th} row of C

T = Transpose

A calculated orhogonality error E_{ij} can be corrected by rotating C_i and C_j relative to each other about an axis perpendicular to both by the error angle E_{ij}. Since it is not known whether C_i or C_j is in error, it is assumed that each are equally likely to be generating the error, and each is rotated by half of E_{ij} to correct the error. Hence, the orthogonality correction algorithm is:

$$\begin{aligned} C_i(n+1) &= C_i(n) - 1/2\ E_{ij}\ C_j(n) \\ C_j(n+1) &= C_j(n) - 1/2\ E_{ij}\ C_i(n) \end{aligned} \tag{29}$$

It is easily verified using (29) that an orthogonality error E_{ij} originally present in $C_i(n)$ and $C_j(n)$ is no longer present in $C_i(n+1)$ and $C_j(n+1)$ after application of equation (29).

The unity condition on C_i (i.e., normality) can be tested by comparing the magnitude squared of C_i with unity:

$$E_{ii} = 1 - C_i C_i^T \tag{30}$$

A measured normality error E_{ii} can be corrected with:

$$C_i(n+1) = C_i(n) - 1/2\ E_{ii}\ C_i\ (n) \tag{31}$$

Equations (28) through (31) can be used to measure and correct orthogonality and normalization errors in the direction cosine matrix. In combined matrix form, the overall measurement/correction operation is sometimes written as:

$$C_{n+1} = C_{n+1/2}\ (I - C_n\ C_n^T)\ C_n \tag{32}$$

3.5.1.1 Rows or Columns - The previous discussion addressed the problem of orthogonalizing and nomalizing the rows of a direction cosine matrix C. In combined form, equation (32) shows that the correction is:

$$\delta C = 1/2\ (I - CC^T)\ C \tag{33}$$

Equation (33) can be operated upon by premultiplication with C postmultiplication by C^T, and combining terms. The result is:

$$\delta C = 1/2\ C\ (I - C^TC) \tag{34}$$

The $(I - C^TC)$ term in (34) is the error matrix based on testing orthogonality and normality of the columns of C. Thus, if the rows of C are orthonormalized (i.e., δC is nulled), the columns of C will also be implicitly orthonormalized. The inverse applies if the columns are directly orthonormalized with (34). The question that remains is, which is preferred? The answer is related to the real time computing problem associated with the calculation and correction of orthogonalization and normalization errors.

Ideally, the orthogonalization and normalization operations are performed as an outer loop function in a strapdown navigation computer so as not to impact computer throughput requirements. A computational organization that facilities such an approach divides the orthonormalization operations into submodules that are executed on successive passes in the outer-loop software path. A logical division of the orthonormalization operations into submodules is as defined by equations (28), (29), (30), and (31).

This implies that measurement and correction of orthogonalization and normalization effects are performed at different times in the computing cycle. Such an approach is only valid if the orthogonality and normalizations errors (i.e., E_{ij} and E_{ii}) remain reasonably stable as a function of time.

To assess the time stability of the orthogonality/normalization error is to investigate

the rate of change of the bracketed terms in equations (33) and (34). For convenience, these will be defined as:

$$E_R \triangleq (I - CC^T)$$
$$E_C \triangleq (I - C^TC) \tag{35}$$

The time derivative of (35) is:

$$\dot{E}_R = - \dot{C}C^T - C\dot{C}^T$$
$$\dot{E}_C = - \dot{C}^TC - C^T\dot{C} \tag{36}$$

Expressions for $\dot{C}$ and $\dot{C}^T$ can be developed by returning to equations (2), (3), (5), and (6). These equations can be rearranged to show that over a given time interval, the change in C is given by:

$$\Delta C = C(A - I) + (B - I)C$$

which with (3) and (4) becomes to first order:

$$\Delta C = C(\underline{\phi}x) - (\underline{\theta}x)C \tag{37}$$

Dividing by the time interval for the change in C, recognizing that $\underline{\phi}$ and $\underline{\theta}$ are approximately integrals of $\underline{\omega}$ and $\underline{\Omega}$ over the time interval, and letting the time interval go to zero in the limit, yields the classical equation for the rate of change of C:

$$\dot{C} = C(\underline{\omega}x) - (\underline{\Omega}x)C \tag{38}$$

where

$(\underline{\omega}x)$, $(\underline{\Omega}x)$ = Skew symmetric matrix form of vectors $\underline{\omega}$, $\underline{\Omega}$.

The transpose of (38) is :

$$\dot{C}^T = - (\underline{\omega}x)\, C^T + C^T\, (\underline{\Omega}x) \tag{39}$$

We now substitute (38) and (39) into (36). After combining terms and applying equations (35), the final result is:

$$\dot{E}_R = E_R\, (\underline{\Omega}x) - (\underline{\Omega}x)\, E_R$$
$$\dot{E}_C = E_C\, (\underline{\omega}x) - (\underline{\omega}x)\, E_C \tag{40}$$

Equations (40) show that the rate of change of E_R is proportional to E_R and the navigation frame rotation rate $\underline{\Omega}$, whereas the rate of change of E_C is proportional to E_C and the body rotation rate $\underline{\omega}$. Since $\underline{\omega}$ is generally much larger than $\underline{\Omega}$, $\dot{E}_C$ is generally larger than $\dot{E}_R$. It can be concluded that E_R is more stable over time, hence, orthonormalizing the direction cosine matrix rows (based on the E_R measurement) is the preferred computational approach if the real time computing problem is taken into account.

3.5.2 Quaternion Normalization

The quaternion is normalized by measuring its magnitude squared compared to unity, and adjusting each element proportionally to correct the normalization error. The normalization error is given by:

$$E_q = q\, q^* - 1 \tag{41}$$

It is easily verified using the rules for quaternion algebric that E_q equals the sum of the squares of the elements of q minus 1. The correction algorithm is given by:

$$q(n+1) = q(n) - 1/2\, E_q\, q(n) \tag{42}$$

3.6 Direction Cosine Versus The Quaternion For Body Attitude Referencing

The tradeoff between direction cosine versus quaternion parameters as the primary attitude reference data in strapdown inertial systems has been a popular area of debate between strapdown analysts over the past three decades. In its original form, the tradeoff centered on the relative accuracy between the two methods in accounting for body angular motion. These tradeoffs invariably evolved from the differential equation form of the direction cosine and quaternion updating equations and investigated the accuracy of equivalent algorithms for integrating these equations in a digital computer under hypothesized body angular motion. Invariably, the body motion investigated was coning motion at various frequencies relative to the computer update frequency. For these early studies, the tradeoffs generally demonstrated that for comparable integration algorithms, the quaternion approach generated solutions that more accurately replicated the true coning motion for situations where the coning frequency was within a decade of the computer update frequency.

As presented in this paper, both the quaternion and direction cosine updating algorithms have been based on processing of a body angle motion vector $\underline{\phi}$ which accounts for all dynamiic motion effects including coning. These updating algorithms (equation (2) and (3) for direction cosines and (13) and (14) for the quaternion) represent exact solutions for the attitude updating process for a given input angle vector $\underline{\phi}$. Consequently, the question of accuracy for different body motion can no longer be considered a viable tradeoff area. The principle tradeoffs that remain between the two approaches are the computer memory and throughput requirements associated with each in a strapdown navigation system.

In order to assess the relative computer memory and throughput requirements for quaternion parameters versus direction cosines, the composite of all computer requirements for each must be assessed. In general, these can be grouped into three major computional areas:

1. Basic updating algorithm
2. Normalization and orthogonalization algorithms
3. Algorithms for conversion to the direction cosine matrix form needed for acceleration transformation and Euler angle extraction

Basic Updating Algorithms - The basic updating algorithm for the quaternion parameters is somewhat simpler than for direction cosines as expansion of equations (2) and (3) compared with (13) and (14) would reveal. This results in both a throughput and memory advantage for the quaternion approach. Part of this advantage arises because only four quaternion elements have to be updated compared to nine for direction cosines. The advantage is somewhat diminished if it is recognized that only two rows of direction cosines (i.e., 6 elements) need actually be updated since the third row can then be easily derived from the other two by a cross-product operation (i.e., the third row represents a unit vector along the z-axis of the navigation frame as projected in body axes. The first two rows represent unit vectors along x and y navigation frame axes. The cross-product of unit vectors along x and y navigation axes equals the unit vector along the z-navigation axis).

Normalization And Orthogonalization Algorithms - The normalization and orthogonalization operations associated with direction cosines are given by equation (28) through (31). The quaternion normalization equation is given by equations (41) and (42).

The normalization equation for the quaternion is generally simpler to implement than the orthogonalization and normalization equations for the direction cosines. If only two rows of the direction cosine matrix are updated (as described in the previous paragraph) the direction cosine orthogonalization and normalization operations required are half that dictated by (28) through (31), but are still more than required by (41) and (42) for the quaternion. Since the orthonormalization operations would in general be iterated at low rate, no throughput advantage results for the quaternion. Some memory savings may be realized, however.

A key factor that must be addressed relative to orthonormalization tradeoffs is whether or not orthonormalization is actually needed at all. Clearly, if the direction cosine or quaternion updating algorithms were implemented perfectly, orthonormalization would not be required. It is the author's contention that, in fact, the accuracy requirements for strapdown systems dictate that strapdown attitude updating software cannot tolerate any errors whatsoever (compared to sensor error effects). Therefore, if the attitude updating software is designed for negligible drift and scale factor error (compared to sensor errors) it will also implicity exhibit negligible orthogonalization and/or normalization errors.

The above argument is valid if the effect of orthonormalization errors in strapdown attitude data is no more detrimental to system performance than other software attitude error effects. This is in fact the case, as detailed error analyses would reveal. Since modern-day general purpose computers used in today's strapdown inertial navigation systems have the capability to implement attitude updating algorithms essentially perfectly within a reasonable throughput and memory requirement, it is the author's opinion that orthonormalization error correction should not be needed, hence, is not a viable tradeoff area relative to the use of quaternion parameters versus direction cosines.

Algorithms For Conversion To The Direction Cosine Matrix - If the basic calculated

attitude data is direction cosines directly, no conversion process is required. For cases where only two rows of direction cosines are updated, the third row must be generated by the cross-product between the two rows calculated. For example:

$$\begin{aligned} C_{31} &= C_{12}\,C_{23} - C_{13}\,C_{22} \\ C_{32} &= C_{13}\,C_{21} - C_{11}\,C_{23} \\ C_{33} &= C_{11}\,C_{22} - C_{12}\,C_{21} \end{aligned} \qquad (43)$$

For quaternion parameters, equation (17) must be implemented to develop the direction cosine matrix, a significantly more complex operation compared with (43) for the two row direction cosine approach. Since direction cosine elements are generally required at high rate (for acceleration transformation and Euler angle output extraction) both a throughput and memory penalty is accrued for the quaternion approach. The penalty is compounded if the calculated direction cosine outputs are required to greater than single precision accuracy (including computational round-off error). For noise-free acceleration transformation operations (such as may be needed to effect an accurate system calibration) double-precision accuracy is needed. The result is that equation (17) for the quaternion versus (43) for direction cosines would have to be implemented in double-precision imposing a significant penalty for the more complex quaternion conversion process.

Tradeoff Conclusions - From the above qualitative discussion, it is difficult to draw hard conclusions regarding a preference for direction cosines versus quaternion parameters for attitude referencing in strapdown inertial systems. Pros and cons exist for each in the different tradeoff areas. Quantitative comparisons based on actual software sizing and computer loading studies have led to similar inconclusive results. Fortunately, today's computer technology is such that the slight advantage one attitude parameter approach may have over the other in any particular application is insignificant compared with composite total strapdown inertial system throughput and memory software requirements. Hence, ultimate selection of the attitude approach can be safely made based on "analyst's choice".

4. STRAPDOWN ACCELERATION TRANSFORMATION ALGORITHMS

The acceleration vector measurement from the accelerometers in a strapdown inertial system is transformed from body to navigation axes through a mechanization of the classical vector tranformation equation:

$$\underline{a}^N = C\,\underline{a} \qquad (44)$$

where

$\underline{a}$ = Specific force acceleration measured in body axes by the strapdown accelerometers

$\underline{a}^N$ = Specific force acceleration with components evaluated along navigation axes.

The implementation of equation (44) is accomplished on a repetative basis as a recursive algorithm in a digital computer such that its integral properties are preserved at the computer cycle times. In this manner, the velocity which is formed from the integral of (44) will be accurate under dynamic conditions in which $\underline{a}^N$ may have erratic high frequency components. The recursive algorithm for (44) must account for the effects of body rotation (and secondarily, rotation of the navigation coordinate frame) as well as variations in $\underline{a}$ over the computer iteration period.

4.1 Acceleration Transformation Algorithm That Accounts For Body Rotation Effects

To develop an algorithm for equation (44) that preserves its integral properties, we begin with its integral over a computer cycle:

$$\underline{u}^N = \int_{t_m}^{t_{m+1}} C\,\underline{a}\,dt \qquad (45)$$

where

$\underline{u}^N$ = Change in the integral of equation (44) (or specific force velocity change) over a computer cycle m

The velocity vector in the navigation computer is generated by summing the $\underline{u}^N$'s corrected for Coriolis and gravity effects.

The C matrix in (45) is a continuous function of time in the interval from t_m to t_{m+1}. An equivalent form for C in terms of its value at the computer update time (m) is:

$$C = C(m)\,A(t) \qquad (46)$$

where

C(m) = Value of C at t_m

A(t) = Direction cosine matrix that transform vectors from body axes at time t to the body attitude at the start time for the computation interval t_m.

Equation (46) with the definition for A(t) above accounts for the effect of gyro sensed body motion over the computer interval. The next section will discuss the correction used to account for the small rotation of the navigation frame over the computer interval.

Substituting (46) in (45) and expanding:

$$\underline{u}^N = C(m) \int_{t_m}^{t_{m+1}} A(t)\, \underline{a}\, dt$$

We now use a first order approximation for A(t) as given by equation (3), with $\underline{\phi}$ treated as a function of time in the interval as defined to first order in equation (22):

$$\underline{\phi}(t) \approx \underline{\beta}(t) = \int_{t_m}^{t} \underline{\omega}\, dt$$

Thus,

$$A(t) \approx I + (\underline{\beta}(t)x) \qquad (47)$$

and

$$\underline{u}^N \approx C(m) \int_{t_m}^{t_{m+1}} (I + (\underline{\beta}(t)x))\, \underline{a}\, dt$$

$$= C(m) \left(\int_{t_m}^{t_{m+1}} \underline{a}\, dt + \int_{t_m}^{t_{m+1}} (\underline{\beta}(t) \times \underline{a})\, dt\right)$$

We now define

$$\underline{u} \overset{\Delta}{=} \int_{t_m}^{t_{m+1}} \underline{a}\, dt$$

Hence,

$$\underline{u}^N \approx C(m) \left(\underline{u} + \int_{t_m}^{t_{m+1}} (\underline{\beta}(t) \times \underline{a})\, dt\right) \qquad (48)$$

with

$$\underline{\beta}(t) = \int_{t_m}^{t} \underline{\omega}\, dt$$

$$\underline{u} = \int_{t_m}^{t_{m+1}} \underline{a}\, dt$$

An alternative form of (48) can also be derived through direct application of the integration by parts rule to the integral term in the equation (48) $\underline{u}^N$ expression.:

$$\underline{u}^N = C(m) \left(\underline{u} + 1/2\, \underline{\beta} \times \underline{u} + 1/2 \int_{t_m}^{t} (\underline{\beta}(t) \times \underline{a} + \underline{u}(t) \times \underline{\omega})\, dt\right) \qquad (49)$$

with

$$\underline{\beta}(t) = \int_{t_m}^{t} \underline{\omega}\, dt$$

$$\underline{u}(t) = \int_{t_m}^{t} \underline{a}\, dt$$

$$\underline{\beta} = \underline{\beta}(t=t_{m+1})$$

$$\underline{u} = \underline{u}(t=t_{m+1})$$

Equations (48) and (49) are algorithmic forms of equation (44) that can be used to calculate $\underline{u}^N$ in the strapdown computer exactly (within the approximation of equation (47)). These equations show that the specific force velocity change in navigation coordinates is approximately equal to the integrated output from the strapdown accelerometer ($\underline{u}$) over the computer cycle, times the direction cosine matrix which was valid at the previous computer update time. Correction terms are applied to account for body rotation. In general, the correction terms involve an integral of the interractive effects of angular $\underline{\omega}$ and linear $\underline{a}$ motion over the update cycle. The integral terms have been coined "sculling" effects.

The equation (49) form of the $\underline{u}^N$ equation includes a $1/2\ \underline{\beta} \times \underline{u}$ term which can be evaluated at t_{m+1} as the simple cross-product of integrated gyro and accelerometer measurements (i.e., without a dynamic integral operation). Furthermore, it is easily demonstrated that for approximately constant angular rates and accelerations over the computer cycle, the integral term in (49) is identically zero. This forms the basis for an approximate form of (49) which is valid under benign flight conditions (i.e., using equation (49) without including the integral term). The $1/2\ \underline{\beta} \times \underline{u}$ term in (49) is sometimes denoted as "rotation compensation".

4.1.1 Incremental Form of Transformation Operations and Sculling Terms

In a severe dynamic environment, equations (48) or (49) would be implemented explicitly with the integral terms mechanized as a high speed digital algorithmic operation within the t_m to t_{m+1} update cycle. The integral terms we are dealing with are from (48) and (49):

$$\underline{S}_1 \triangleq \int_{t_m}^{t_{m+1}} (\underline{\beta}(t) \times \underline{a})\, dt$$

$$\underline{S}_2 \triangleq 1/2 \int_{t_m}^{t_{m+1}} (\underline{\beta}(t) \times \underline{a} + \underline{u}(t) \times \underline{\omega})\, dt \qquad (50)$$

With the equation (50) definitions, (48) and (49) become:

$$\underline{u}^N = C(m)\ (\underline{u} + \underline{S}_1) \qquad (51)$$

or

$$\underline{u}^N = C(m)\ (\underline{u} + 1/2\ \underline{\beta} \times \underline{u} + \underline{S}_2) \qquad (52)$$

Recursive algorithms for $\underline{S}_1$ or $\underline{S}_2$ can be derived by first rewriting (50) in the equivalent form:

$$\underline{\beta}(t) = \underline{\beta}(i) + \int_{t_i}^{t} \underline{\omega}\, dt$$

$$\underline{u}(t) = \underline{u}(i) + \int_{t_i}^{t} \underline{a}\, dt$$

$$\underline{x}_1(i+1) = \underline{x}_1(i) + \int_{t_i}^{t_{i+1}} (\underline{\beta}(t) \times \underline{\omega})\, dt$$

$$\underline{x}_2(i+1) = \underline{x}_2(i) + 1/2 \int_{t_i}^{t_{i+1}} (\underline{\beta}(t) \times \underline{a} + \underline{u}(t) \times \underline{\omega})\, dt \qquad (53)$$

$$\underline{\beta}(i+1) = \underline{\beta}(t=t_{i+1})$$

$$\underline{u}(i+1) = \underline{u}(t=t_{i+1})$$

$$\underline{S}_1 = \underline{x}_1(t=t_{m+1})$$

$$\underline{S}_2 = \underline{x}_2(t=t_{m+1})$$

with initial conditions

$$\underline{\beta}(t=t_m) = 0$$
$$\underline{u}(t=t_m) = 0$$
$$\underline{\gamma}_1(t=t_m) = 0$$
$$\underline{\gamma}_2(t=t_m) = 0 \qquad (54)$$

where

ℓ = High speed computer cycle within m lower speed computation cycle.

The integrals in (53) can be replaced by analytical forms that are compatible with gyro and accelerometer input data processing if $\underline{\omega}$ and $\underline{a}$ are replaced by a generalized time series expansion. For equations (53), it is sufficient to approximate $\underline{\omega}$ and $\underline{a}$ over the ℓ to $\ell+1$ time interval as constants. Using this approximation in (53) yields the final algorithm forms. For $\underline{S}_1$, the companion to equation (51), the algorithm is:

$$\underline{\gamma}_1(\ell+1) = \underline{\gamma}_1(\ell) + \left(\underline{\beta}(\ell) + 1/2\ \underline{\Delta\theta}(\ell)\right) \times \underline{\Delta v}(\ell)$$

$$\underline{\beta}(\ell+1) = \underline{\beta}(\ell) + \underline{\Delta\theta}(\ell)$$

where

$$\underline{\Delta\theta}(\ell) = \int_{t_\ell}^{t_{\ell+1}} \underline{\omega}\, dt = \sum_{t_\ell}^{t_{\ell+1}} \underline{d\theta}$$

$$\underline{\Delta v}(\ell) = \int_{t_\ell}^{t_{\ell+1}} \underline{a}\, dt = \sum_{t_\ell}^{t_{\ell+1}} \underline{dv}$$

and

$$\underline{S}_1 = \underline{\gamma}_1(t=t_{m+1}) \qquad (55)$$

For equation (51):

$$\underline{u}(\ell+1) = \underline{u}(\ell) + \underline{\Delta v}(\ell)$$

$$\underline{u} \triangleq \underline{u}(t=t_{m+1})$$

with initial conditions:

$$\underline{\beta}(t=t_m) \triangleq \underline{\beta}(\ell=0) = 0$$

$$\underline{\gamma}_1(t=t_m) \triangleq \underline{\gamma}_1(\ell=0) = 0$$

where

$\underline{d\theta}$, $\underline{dv}$, = Gyro and accelerometer output pulse vectors. Each component (x, y, z) represents the occurance of a rotation through a specified angle about the gyro input axis (for $\underline{d\theta}$ components) or an acceleration through a specific force velocity change along the accelerometer input axis (for $\underline{dv}$ components).

$\underline{\Delta\theta}$, $\underline{\Delta v}$, = Gyro and accelerometer pulse vector counts from ℓ to $\ell+1$.

For the alternative $\underline{S}_2$ form, the companion to equation (52), the algorithm is:

$$\underline{\gamma}_2(\ell+1) = \underline{\gamma}_2(\ell) + 1/2\ (\underline{\beta}(\ell) \times \underline{\Delta v}(\ell) + \underline{u}(\ell) \times \underline{\Delta\theta}(\ell))$$

$$\underline{\beta}(\ell+1) = \underline{\beta}(\ell) + \Delta\theta(\ell)$$

$$\underline{u}(\ell+1) = \underline{u}(\ell) + \underline{\Delta v}(\ell)$$

where

$$\underline{\Delta\theta}(\ell) = \int_{t_\ell}^{t_{\ell+1}} \underline{\omega}\ dt = \sum_{t_\ell}^{t_{\ell+1}} \underline{d\theta}$$

$$\underline{\Delta u}(\ell) = \int_{t_\ell}^{t_{\ell+1}} \underline{a}\ dt = \sum_{t_\ell}^{t_{\ell+1}} \underline{dv}$$

and (56)

$$\underline{S}_2 = \underline{\gamma}_2(t=t_{m+1})$$

For equations (52):

$$\underline{\beta} = \underline{\beta}(t=t_{m+1})$$

$$\underline{u} = \underline{u}(t=t_{m+1})$$

with initial conditions:

$$\underline{\beta}(t=t_m) \triangleq \underline{\beta}(\ell=0) = 0$$

$$\underline{u}(t=t_m) \triangleq \underline{u}(\ell=0) = 0$$

$$\underline{\gamma}_2(t=t_m) \triangleq \underline{\gamma}_2(\ell=0) = 0$$

Equations (51) with (55), or (52) with (56) are computational algorithms that can be used to calculate the navigation frame specific force velocity changes. Two iteration rates are implied: a basic m cycle rate, and a higher speed ℓ cycle rate within each m cycle.

The m cycle rate is selected to be high enough to protect the approximation of neglecting the $(\underline{\beta}(t)x)^2$ term in A(t) (contrast equation (47) with the equation (3) exact form for A). This design condition is typically evaluated under maximum expected linear acceleration/angular rate envelope conditions for the particular application. Typically, the m cycle rate required for accuracy in the attitude updating algorithms is also sufficient for accuracy requirements in the m cycle of the acceleration transformation algorithms.

The ℓ cycle rate within m is set high enough to properly account for anticipated composite dynamic $\underline{\omega}$, $\underline{a}$ effects. Section 6. describes analytical techniques that can be used to assess the adequacy of the $\underline{S}$ iteration rate for the sculling computation under dynamic input conditions.

4.1.3 Acceleration Transformation Algorithms Based on Quaternion Attitude Data

Equations (51) or (52) were based on the use of direction cosine data (C) in the strapdown computer. If the basic attitude data is calculated in the form of a quaternion, the equivalent C matrix for transformation can be calculated using equations (17). Alternatively, the quaternion data can be applied directly in the implementation of the tranformation operation through application of equation (12) to equations (51) and (52):

$$u^N = q(m)\ (u + S_1)\ q(m)^* \tag{57}$$

or

$$u^N = q(m)\ (u + S_2')\ q(m)^* \tag{58}$$

$$\underline{S}_2' \triangleq 1/2\ \underline{\beta} \times \underline{u} + \underline{S}_2$$

where u and the terms in the middle brackets are the quaternion form of the vector of the same nonmenclature defined as having the first three terms (i.e., vector components) equal to the vector elements, and the fourth scalar term equal to zero. The $\underline{S}_1$ and $\underline{S}_2$ terms are calculated as defined by equations (55) and (56).

4.2 Acceleration Transformation Algorithm Correction For Navigation Frame Rotations

The acceleration transformation algorithms represented by equation (51), (52) or (57), (58) with (55), (56) neglects the effect of navigation frame rotation. In general, this is a minor correction term that can be easily accounted for at the n cycle update rate (i.e., the computer cycle rate used to update the attitude data for the effect of navigation frame rotations). It can be shown through a development similar to that leading to equation (52), that the correction algorithm for local navigation frame motion is given to first order by:

$$\underline{\Delta u}^N(n) = -1/2\ \underline{\theta} \times \underline{v}(n) \tag{59}$$

where

$\underline{\Delta u}^N(n)$ = Correction to the value of $\underline{u}^N$ computed in the m cycle that occurs at the current n cycle time. (Note: the m cycle is within the lower speed n cycle time frame).

$\underline{v}(n)$ = Summation of $\underline{u}(m)$ over the n cycle update period.

$\underline{\theta}$ = Integral of the navigation frame angular rotation rate over the n cycle period (as described in Sections 3.1.2 and 3.4)

5. EULER ANGLE EXTRACTION ALGORITHMS

If the body attitude relative to navigation axes is defined in terms of three successive Euler angle rotations ϕ, θ, ψ about axes z, y, x respectively (from navigation to body axes), it can be readily demonstrated (9) that the relationship between the direction cosine elements and Euler angles is given by:

$$\begin{aligned}
C_{11} &= \cos\theta\cos\psi \\
C_{12} &= -\cos\phi\sin\psi + \sin\phi\sin\theta\cos\psi \\
C_{13} &= \sin\phi\sin\psi + \cos\phi\sin\theta\cos\psi \\
C_{21} &= \cos\theta\sin\psi \\
C_{22} &= \cos\phi\cos\psi + \sin\phi\sin\theta\sin\psi \\
C_{23} &= -\sin\phi\cos\psi + \cos\phi\sin\theta\sin\psi \\
C_{31} &= -\sin\theta \\
C_{32} &= \sin\phi\cos\theta \\
C_{33} &= \cos\phi\cos\theta
\end{aligned} \tag{60}$$

For conditions where $|\theta| \neq \pi/2$ the inverse of equations (60) can be used to evaluate the Euler angles from the direction cosines:

$$\begin{aligned}
\phi &= \tan^{-1}\frac{C_{32}}{C_{33}} \\
\theta &= -\tan^{-1}\frac{C_{31}}{\sqrt{(1-C_{31}^2)}} \\
\psi &= \tan^{-1}\frac{C_{21}}{C_{11}}
\end{aligned} \tag{61}$$

For situations where $|\theta|$ approaches $\pi/2$, the ϕ and ψ equations in (61) become indeterminate because the numerator and denominator approach zero simultaneously (see

equations (60)). Under these conditions, an alternative equation for ϕ, ψ can be developed by first applying trigonometric algebra to equations (61) to obtain:

$$\begin{aligned} C_{23} + C_{12} &= (\sin\theta - 1)\sin(\psi + \phi) \\ C_{13} - C_{22} &= (\sin\theta - 1)\cos(\psi + \phi) \\ C_{23} - C_{12} &= (\sin\theta + 1)\sin(\psi - \phi) \\ C_{13} + C_{22} &= (\sin\theta + 1)\cos(\psi - \phi) \end{aligned} \tag{62}$$

Taking appropriate reciprocals of sine, cosine terms in (62) and applying the inverse tangent function:

For θ near $+\pi/2$

$$\psi - \phi = \tan^{-1}\frac{C_{23} - C_{12}}{C_{13} + C_{22}}$$

(63)

For θ near $-\pi/2$

$$\psi + \phi = \tan^{-1}\frac{C_{23} + C_{12}}{C_{13} - C_{22}}$$

Equations (63) can be used to obtain expressions for the sum or difference of ψ and ϕ under conditions where $|\theta|$ is near $\pi/2$. Explicit separate solutions for ψ and ϕ cannot be found under the $|\theta| = \pi/2$ condition because ψ and ϕ both become angle measures about parallel axes (about vertical), hence, measure the same angle (i.e., a degree of rotational freedom is lost, and only two Euler angles, $\theta = \pm\pi/2$ and ψ or ϕ define the body to navigation frame attitude). Under $|\theta|$ near $\pi/2$ conditions, θ or ψ can be arbitrarily selected to satisfy another condition, with the unspecified variable calculated from (63). As an example, ψ might be set to a constant at the value it had from equations (61) when the $|\theta|$ near $\pi/2$ region was entered. This selection avoids jumps in ψ as the solution equation is transitioned from the (61) to the (63) form.

6. ALGORITHM PERFORMANCE ASSESSMENT

The division of the attitude updating and acceleration transformation algorithms into high and low speed loops for body motion effects (λ and m rates) provides for flexibility in selection of the iteration rates to maintain overall algorithm accuracy at system specified performance levels. The λ and m rate algorithms have been designed such that the high rate λ loop consists of simple computations that can be iterated at the high rate needed to properly account for high frequency vibration effects. The m rate loop algorithms, on the other are more complicated, based on computationally exact solutions.

Iteration rates for the m loop are selected to maintain accuracy under maximum maneuver induced motion conditions. The m loop iteration rate to maintain accuracy under maximum maneuver conditions can be easily evaluated analytically, or by simulation, through comparision of the actual algorithm solution with the Taylor series truncated forms selected for system mechanization. Iteration rates for the λ loop are selected to maintain accuracy under anticipated vibratory environmental conditions.

6.1 Vibration Environment Assessment

A fundamental calculation that should be performed prior to the analysis of λ loop algorithm iteration rate requirements is an assessment of the dynamic inputs that must be measured by the algorithms. In essence, this consists of an evaluation of the continuous (i.e., infinitely fast iteration rate) form of the algorithms in question under dynamic input conditions. The specific continuous form equations of interest are equations (22) for $\underline{\delta\beta}$ and (50) for $\underline{S}_1$ or $\underline{S}_2$.

6.1.1 $\underline{\delta\beta}$ Dynamic Environment Assessment (Coning)

We repeat equations (22) for $\underline{\delta\beta}$ evaluated at $t = t_{m+1}$:

$$\underline{\beta}(t) = \int_{t_m}^{t} \underline{\omega}\, dt$$

$$\underline{\delta\beta}(t=t_{m+1}) = 1/2 \int_{t_m}^{t_{m+1}} \underline{\beta}(t) \times \underline{\omega}\, dt \qquad (64)$$

and analyse the solution for $\underline{\delta\beta}(t=t_{m+1})$ under general cyclic motion at frequency f in axes x and y with angular amplitudes θ_x, θ_y and relative phase angle ϕ such that:

$$\int_0^t \underline{\omega}\, dt = (\theta_x \sin(2\pi ft),\ \theta_y \sin(2\pi ft+\phi),\ 0)^T$$

$$\underline{\omega} = 2\pi f\ (\theta_x \cos(2\pi ft),\ \theta_y \cos(2\pi ft+\phi),\ 0)^T \qquad (65)$$

Substituting (65) in (64), expanding through application of appropriate trigonometric identities, and carrying out the indicated integrals analytically between the assigned limits, yields zero for the x, y components and the following for the z component of $\underline{\delta\beta}(t=t_{m+1})$:

$$\delta\beta_z(t=t_{m+1}) = \pi\, \theta_x\, \theta_y\, (\sin\phi)\, f\, \left((t_{m+1} - t_m) - \frac{\sin 2\pi f(t_{m+1} - t_m)}{2\pi f}\right)$$

Defining the m cycle time interval as T_m, the latter exression is equivalently:

$$\delta\beta_z = \pi\, \theta_x\, \theta_y\, (\sin\phi)\, f\, T_m \left(1 - \frac{\sin 2\pi fT_m}{2\pi fT_m}\right) \qquad (66)$$

Hence, even though the $\underline{\omega}$ rate is cyclic in two axes as defined by equation (65) in x and y, the value for $\delta\beta_z$ is a constant proportional to the sine of the phase angle between the x, y angular vibrations. Under conditions where $\phi = 0$ (defined as "rocking" motion), $\delta\beta_z$ is zero. Under conditions where $\phi = \pi/2$, $\delta\beta_z$ is maximum. The equation (65) rate when $\phi = \pi/2$ has been termed "coning motion" due to the characteristic response of the z axis under this motion which describes a cone in inertial space.

Equation (66) can be put into a "drift rate" form by dividing the $\delta\beta_z$ angle by the time interval T_m over which it was evaluated:

$$\dot{\delta\beta}_z = \pi\, \theta_x\, \theta_y\, (\sin\phi)\, f\, \left(1 - \frac{\sin 2\pi fT_m}{2\pi fT_m}\right) \qquad (67)$$

Equation (67) is a fundamental equation that can be used to assess the magnitude of $\dot{\delta\beta}_z$ that must be accounted for by the $\delta\beta$ computer algorithm under discrete frequency input conditions. If $\dot{\delta\beta}_z$ is small relative to system performance requirements, it can be neglected, and the $\delta\beta$ loop algorithm for $\delta\beta$ need not be implemented.

Equation (67) describes how $\dot{\delta\beta}_z$ can be calculated for a discrete input vibration frequency f. In a more general case, the input rate is composed of a mixture of frequencies in x and y at different phase angles ϕ for each. If the source of the gereralized angular vibration is random input noise to the strapdown system, the x, y motion is colored by the transmission characteristics of the noise input to the x, y angular response. A more general development of equation (67) that accounts for the latter effects shows that the comparable equation for $\dot{\delta\beta}_z$ is given by:

$$\dot{\delta\beta}_z = \int_0^{\infty} \omega\, A_x(\omega)\, A_y(\omega) \sin(\phi_{Ay}(\omega) - \phi_{Ax}(\omega)) \left(1 - \frac{\sin\omega T_m}{\omega T_m}\right) P_{nn}(j\omega)\, d\omega \qquad (68)$$

where

$A_x(\omega)$, $A_y(\omega)$ = Amplitude of transfer function relating system input vibration noise to angular attitude response of sensor assembly about x, y axes.

$\phi_{Ax}(\omega)$, $\phi_{Ay}(\omega)$ = Phase of transfer function relating system input vibration noise to angular attitude response of sensor assembly about x, y axes.

$P_{nn}(j\omega)$ = Power spectral density of input vibration noise.

ω = Fourier frequency (rad/sec)

Note: Mean squared vibration energy = $\int_0^\infty P_{nn}(j\omega)\, d\omega$

Equation (68) can be used to assess the extent of random spectrum dynamic angular environment to be measured by the $\delta\beta$ computational algorithm. The $\delta\beta_z$ value calculated by (68) measures the composite correlated coning drift in the sensor assembly that must be calcuated to accurately account for the actual motion present. If the $\delta\beta_z$ magnitude calculated from (68) is small compared to other systems error budget effects, the mechanization of an algorithm to calculate $\delta\beta$ is not needed (i.e., can be approximated by zero).

The extension of equations (67) and (68) to y, z or z, x axis angular vibration motion should be obvious.

6.1.2 $\underline{S}_1$, $\underline{S}_2$ Dynamic Environment Assessment (Sculling)

We repeat equations (50) with $\underline{u}$ and $\underline{\beta}$ from (48) and (49):

$$\underline{\beta}(t) = \int_{t_m}^{t} \underline{\omega}\, dt$$

$$\underline{u}(t) = \int_{t_m}^{t} \underline{a}\, dt$$

$$\underline{S}_1 = \int_{t_m}^{t_{m+1}} (\underline{\beta}(t) \times \underline{a})dt \qquad (69)$$

$$\underline{S}_2 = 1/2 \int_{t_m}^{t_{m+1}} (\underline{\beta}(t) \times \underline{a} + \underline{u}(t) \times \underline{\omega})dt$$

and analyse the $\underline{S}_1$, $\underline{S}_2$ solutions under general cycle motion at frequency f in axes x, y with angular amplitude θ_x about axis x and acceleration amplitude D_y along axis y at relative phase ϕ such that:

$$\int_0^t \underline{\omega}\, dt = (\theta_x \sin(2\pi ft),\ 0,\ 0)^T$$

$$\underline{\omega} = (2\pi f\, \theta_x \cos(2\pi ft),\ 0,\ 0)^T \qquad (70)$$

$$\underline{a} = (0,\ D_y \sin(2\pi ft+\phi),\ 0)^T$$

Substituting (70) in (69), expanding through application of appropriate trigonometric identities, and carrying out the indicated integrals analytically between the assigned limits, yields zero for the x, y components and the following for the z component of $\underline{S}_1$ and $\underline{S}_2$:

$$S_{2z} = 1/2\ T_m\, \theta_x\, D_y\, (\cos\phi)\, \left(1 - \frac{\sin \pi f T_m}{2\pi f T_m}\right) \qquad (71)$$

$$S_{1z} = 1/2\ (\underline{\beta} \times \underline{u})_z + S_{2z} \qquad (72)$$

where

$(\underline{\beta} \times \underline{u})_z$ = z - component of $\underline{\beta} \times \underline{u}$ evalulated at $t = t_{m+1}$.

Hence, even though the $\underline{\omega}$ and $\underline{a}$ inputs are cyclic in two axes as defined in equations (70), the value for S_{2z} is a constant proportional to the cosine of the phase angle between

the x angular vibration and y linear acceleration vibration. Under conditions where $\phi=\pi/2$, S_{2z} is zero. Under conditions where $\phi=0$, S_{2z} is a maximum. Equation (70) motion when $\phi=0$ has been termed "sculling motion" due to the analogy with the characteristic angular movement and acceleration forces imparted to an oar used to propel a boat from the stern. Note also that S_{1z} is equal to S_{2z} plus the correction term (rotation compensation) measured as the cross-product of the simple angular rate and linear acceleration integrals taken over the m computation cycle. (See equations (48) and (49) for definitions).

Equation (71) for S_{2z} can be put into an "acceleration bias" form by dividing the velocity change correction S_{2z} by the time interval T_m over which it was evaluated:

$$\dot{S}_{2z} = 1/2\ \theta_x\ D_y\ (\cos\phi)\ \left(1 - \frac{\sin 2\pi f T_m}{2\pi f T_m}\right) \tag{73}$$

Equation (73) (with (72) for S_{1z}) is a fundamental equation that can be used to assess the magnitude of $\dot{S}_{2z}$ that must be accounted for by the S_1 or S_2 computer algorithm under discrete frequency input conditions. If S_{2z} is small relative to system performance requirements, it can be neglected, and the $\hat{A}$ loop algorithm for calculating S_1 or S_2 need not be implemented. Under the latter conditions, S_1 would be set equal to the cross-product term in (72) which makes the basic equation (51) and (52) transformation algorithms identical.

Equation (73) describes how $\dot{S}_{2z}$ can be calculated with a discrete input vibration frequency f for angular motion about x and linear motion along y. In a more general case, the input rates and accelerations are composed of mixtures of angular and linear motion about x and y at different frequencies and relative phase angles. If the source of the generalized vibration motion is random input noise to the strapdown system, the x, y angular and linear motion is colored by the transmission characteristics of the noise input to the x, y angular and linear response. A more general development of equation (73) that accounts for the latter effects show that the comparable equation for $\dot{S}_{2z}$ is given by:

$$\dot{S}_{2z} = \int_0^\infty \left(A_y(\omega)\ B_x(\omega)\ \cos\left(\phi_{Ay}(\omega) - \phi_{Bx}(\omega)\right) - A_x(\omega)\ B_y(\omega)\ \cos\left(\phi_{Ax}(\omega) - \phi_{By}(\omega)\right)\right)\ \left(1 - \frac{\sin\omega T_m}{\omega T_m}\right)\ P_{nn}(j\omega)\ d\omega \tag{74}$$

where

$A_x(\omega)$, $A_y(\omega)$, $\phi_{Ax}(\omega)$, $\phi_{Ay}(\omega)$, $P_{nn}(j\omega)$, ω = As defined previously.

$B_x(\omega)$, $B_y(\omega)$, $\phi_{Bx}(\omega)$, $\phi_{By}(\omega)$ = x, y, amplitude/phase linear acceleration response of the sensor assembly to the input vibration.

Equation (74) can be used to assess the extent of random spectrum dynamic motion environment to be measured by the S_1 or S_2 computational algorithms. The $\dot{S}_{2z}$ value calculated by (74) measures the composite correlated sculling acceleration bias in the sensor assembly that must be calculated to accurately account for the actual motion present. If the $\dot{S}_{2z}$ magnitude calculated from (74) is small compared to other system error budget effects, the mechanization of an algorithm to calculate S_1 or S_2 in the high rate $\hat{A}$ loop is not needed (i.e., S_2 can be approximated by zero in (52) or S_1 can be set equal to the cross-product term in (52)).

The extension of equations (73) and (74) for y, z or z, x axis vibration motion should be obvious.

6.2 Algorithm Accuracy Assessment

The accuracy of the computation algorithm for $\delta\beta$ or S_1, S_2 can be assessed by comparing their solutions to the comparable continuous form solutions developed in Section 6.1 under identical input conditions.

6.2.1 $\delta\beta$ Coning Algorithm Error Assessment

The computational algorithm for calculating $\delta\beta$ in a strapdown system is given by equation (26). A measure of the accuracy of the equation (26) algorithm can be obtained by analytically calculating the solution generated from (26) under assumed cyclic motion and

comparing this result to the equivalent solution obtained from the idealized continuous algorithm described in Section 6.1. For a discrete frequency vibration input, the equation (65) motion can be used analytically in equation (26) to calculate the algorithm solution for $\underline{\delta\beta}$ at $t = t_{m+1}$ (i.e., analagous to the equation (67) solution for the continuous (infinitely fast) algorithm. After much algebraic manipulation, it can be demonstrated that the algorithm solution for $\underline{\delta\beta}$ as calculated from equation (26) under equation (65) input motion, has zero x, y components, with a z component rate given by:

$$\dot{\delta\beta}_{zALG} = \pi\, \theta_x\, \theta_y\, (\sin\phi)\, \left((1 + 1/3\,(1 - \cos 2\pi f T_\ell))\, \frac{\sin 2\pi f T_\ell}{2\pi f T_\ell} - \frac{\sin 2\pi f T_m}{2\pi f T_m}\right) \tag{75}$$

where

$\dot{\delta\beta}_{zALG}$ = Recursive algorithm solution for $\delta\beta_z$ rate

T_ℓ = Time interval for high speed ℓ computer iteration cycle

Equation (75) for the $\underline{\delta\beta}$ discrete recursive algorithm solution of equation (26) is directly analagous to the equation (67) solution of the equation (22) continuous $\underline{\delta\beta}$ algorithm. It is easily verified that (75) reduces to (67) as T_ℓ approaches zero.

The error in the $\underline{\delta\beta}$ algorithm is measured by the difference between (67) and (75); i.e.:

$$e(\dot{\delta\beta}_z) = \pi\, f\, \theta_x\, \theta_y\, (\sin\phi)\left((1 + 1/3\,(1 - \cos 2\pi f T_\ell))\, \frac{\sin 2\pi f T_\ell}{2\pi f T_\ell} - 1\right) \tag{76}$$

where

$e(\dot{\delta\beta}_z)$ = Error rate in the equation (26) algorithm.

Equation (76) can be used to assess the error in the equation (26) $\underline{\delta\beta}$ algorithm caused by finite iteration rate (i.e., the effect of T_ℓ) under discrete frequency input conditions.

Under random vibration input conditions, the equation (26) algorithm can be analysed to obtain the more general solution for the $\dot{\delta\beta}_{zALG}$ rate:

$$\dot{\delta\beta}_{zALG} = \int_0^\infty \omega\, A_x(\omega)\, A_y(\omega)\, \sin(\phi_{Ay}(\omega) - \phi_{Ax}(\omega))\, \left((1 + 1/3\,(1 - \cos\omega T_\ell)\, \frac{\sin \omega T_\ell}{\omega T_\ell} - \frac{\sin \omega T_m}{\omega T_m}\right) P_{nn}(j\omega)\, d\omega \tag{77}$$

The $\delta\beta$ algorithm error under random inputs is the difference between the equation (77) discrete solution and the equivalent continuous equation (68) solution form. The result is:

$$e(\dot{\delta\beta}_z) = \int_0^\infty \omega\, A_x(\omega)\, A_y(\omega)\, \sin(\phi_{Ay}(\omega) - \phi_{Ax}(\omega))\, \left((1 + 1/3\,(1 - \cos\omega T_\ell)\, \frac{\sin \omega T_\ell}{\omega T_\ell} - 1\right) P_{nn}(j\omega)\, d\omega \tag{78}$$

Equations (76) and (78) can be used to assess the error in the equation (26) $\underline{\delta\beta}$ algorithm caused by finite iteration rate under discrete or random vibration input conditions. The extension of equations (76) and (78) to y, z or z, x axis effects should be obvious.

6.2.2 $\underline{S}$ Sculling Algorithm Error Assessment

The computational algorithm for calculating $\underline{S}_1$ or $\underline{S}_2$ is given by equations (55) and (56). A measure of the accuracy of these algorithms can be obtained by analytically

calculating the solution generated from (55) or (56) under assumed cyclic motion and comparing the result to the equivalent solution obtained from the continuous algorithm as described in Section 6.1.2. For a discrete frequency vibration input, the equation (70) motion can be used analytically in equation (55) and (56) to calculate the algorithm solution for $\underline{S}_1$, $\underline{S}_2$ (i.e., analogous to the equation (72) and (73) solution for the continuous (infinitely fast) algorithm). After much algabraic manipulation, it can be demonstrated that the algorithm solution for $\underline{S}_1$ and $\underline{S}_2$ as calculated from equations (55) and (56) under equation (70) input motion, has zero x, y components, with a z component rate given by:

$$\dot{S}_{2zALG} = 1/2\ \theta_x\ D_y\ (\cos\phi)\ \left(\frac{\sin 2\pi f T_\ell}{2\pi f T_\ell} - \frac{\sin 2\pi f T_m}{2\pi f T_m}\right) \tag{79}$$

$$S_{1zALG} = 1/2\ (\underline{\beta} \times \underline{u})_z + S_{2zALG} \tag{80}$$

where

S_{1zALG}, S_{2zALG} = Recursive algorithm solutions for S_{1z}, S_{2z}.

Equations (79) and (80) for the $\underline{S}_1$, $\underline{S}_2$ discrete recursive algorithm solution is directly analogous to the equations (73) and (72) solution to the continuous $\underline{S}_1$, $\underline{S}_2$ algorithm. It is easily verified that (79) and (80) reduce to (73) and (72) as T_ℓ approaches zero.

The error in the $\underline{S}_1$, $\underline{S}_2$ algorithm is measured by the difference between (79), (80) and (73), (72) ; i.e.,

$$e(\dot{S}_{1z}) = e(\dot{S}_{2z}) = 1/2\ \theta_x\ D_y\ (\cos\phi)\ \left(1 - \frac{\sin 2\pi f T_\ell}{2\pi f T_\ell}\right) \tag{81}$$

where

$e(\dot{S}_{1z})$, $e(\dot{S}_{2z})$ = Error rate in the equation (55) and (56) algorithm solutions.

Equation (81) can be used to assess the error in the equation (55) and (56) algorithms caused by finite iteration rate (i.e., the effect of T_ℓ) under discrete frequency input conditions.

Under random vibration input conditions, the equation (55) and (56) algorithms can be analysed to obtain the more general solution for S_{1z}, S_{2z}:

$$\dot{S}_{2z} = \int_o^\infty (A_y(\omega)\ B_x(\omega) \cos(\phi_{Ay}(\omega) - \phi_{Bx}(\omega)) - A_x(\omega)\ B_y(\omega) \cos(\phi_{Ax}(\omega) - \phi_{By}(\omega)))\ \left(\frac{\sin \omega T_\ell}{\omega T_\ell} - \frac{\sin \omega T_m}{\omega T_m}\right) P_{nn}(j\omega)\ d\omega \tag{82}$$

$$S_{1z} = 1/2\ (\underline{\beta} \times \underline{u})_z + S_{2z}$$

The S_{1z}, S_{2z} algorithm error under vibration is the difference between the equation (82) discrete solutions and the equivalent continuous equation (74) with (72) forms:

$$e(\dot{S}_{1z}) = e(\dot{S}_{2z}) = \int_o^\infty (A_y(\omega)\ B_x(\omega) \cos(\phi_{Ay}(\omega) - \phi_{Bx}(\omega)) - A_x(\omega)\ B_y(\omega) \cos(\phi_{Ax}(\omega) - \phi_{By}(\omega)))\ \left(1 - \frac{\sin \omega T_\ell}{\omega T_\ell}\right) P_{nn}(j\omega)\ d\omega \tag{83}$$

Equation (82) and (83) can be used to assess the error in the equation (55) and (56) algorithms caused by finite iteration rate under discrete or random vibration input conditions. The extension of equation (83) to y, z or z, x axis effects should be obvious.

7. CONCLUDING REMARKS

The strapdown computational algorithms and associated design considerations presented in this paper are representative of the algorithms being used in most modern-day strapdown inertial navigation systems. The unique characteristic of the attitude and transformation algorithms presented is the separation of each into a complex low speed and simple high speed computation section. Due to the simplicity of the high speed calculations they can be executed at the high rates necessary to properly account for high frequecy but generally low amplitude vibratory effects without posing an insurmountable throughput burden on the computer. The lower speed calculations which contain the bulk of the computational equations can then be executed at a fairly modest update rate selected to properly account for lower frequency but larger magnitude maneuver induced motion effects. Perhaps the principal advantage of the algorithm forms presented, is their ability to be analyzed for accuracy using straight-forward analytical techniques. This allows the algorithms to be easily tailored and evaluated for given applications as a function of anticipated dynamic environments and user accuracy requirements.

REFERENCES

1. Pitman, George R. Jr., ed., Inertial Guidance, John Wiley and Sons, New York, 1962.

2. Leondes, Cornelius T., ed., Guidance and Control of Aerospace Vehicles, McGraw-Hill, 1963.

3. Macomber, George R. and Fernandes, Manuel, Inertial Guidance Engineering, Prentice-Hall Englewood Cliffs, New Jersey, 1962.

4. Britting, Kenneth R., Inertial Navigation System Analysis, John Wiley and Sons, New York, 1971.

5. Morse, Philip M. and Feshback, Herman, Methods of Theoretical Physics, McGraw-Hill, 1953.

6. A Study of Critical Computational Problems Associated with Strapdown Inertial Navigation Systems, NASA Report CR-968, April 1968.

7. Savage, P.G., "A New Second-Order Solution for Strapped-Down Attitude Computation", AIAA/JACC Guidance & Control Conference, Seattle, Washington, August 15 - 17, 1966.

8. Jordan, J.W., "An Accurate Strapdown Direction Cosine Algorithm", NASA TN D-5384, September 1969.

9. Mckern, Richard A., A Study of Transformation Algorithms For Use In A Digital Computer, Massachusetts Institute of Technology Master's Thesis, Department of Aeronautics and Astronatics, January 1968.

10. Bortz J.E., "A New Mathematical Formulation for Strapdown Inertial Navigation, "IEEE Transactions on Aerospace and Electronic Systems, Volume AES-7, No. 1, January 1971.

11. Shepperd, Stanley W., "Quaternion from Rotation Matrix", AIAA Journal of Guidance and Control, Vol. 1, No. 3, May-June 1978.

12. Savage, P.G., Introduction To Strapdown Inertial Navigation Systems, June 1, 1983 (Third Printing); Third Strapdown Associates Open Seminar On Strapdown Inertial Navigation Systems, Marquette Inn, Minneapolis, Minnesota, November 14 - 18, 1983.

APPENDIX A

DERIVATION OF $\dot{\underline{\phi}}$ EQUATION

A differential equation for the rate of change of the $\underline{\phi}$ vector can be derived from the equivalent quaternion rate equation. The quaternion h in equations (13) and (14) is the quaternion equivalent to the $\underline{\phi}$ rotation angle vector. A differential equation for h can be derived from the incremental equivalent to (13) that describes how h changes over a short time period Δt (from t_i to t_{i+1}) within the larger time interval from t_m to t_{m+1}:

$$h(i+1) = h(i)\, p(i) \qquad \text{(A1)}$$

where

$$p = \begin{vmatrix} g_3 \alpha_x \\ g_3 \alpha_y \\ g_3 \alpha_z \\ g_4 \end{vmatrix}$$

$$g_3 = \frac{\sin(\alpha/2)}{\alpha} \qquad g_4 = \cos(\alpha/2) \tag{A2}$$

$\underline{\alpha}$ = Rotation angle vector associated with the small rotation of the body over the short computer time interval from ℓ to $\ell+1$ within the larger interval from m to m+1.

$\alpha_x, \alpha_y, \alpha_z, \alpha$ = Components and magnitude of $\underline{\alpha}$.

Equation (A1) is equivalently:

$$\frac{h(\ell+1) - h(\ell)}{\Delta t} = h(\ell) \frac{p(\ell)-1}{\Delta t} \tag{A3}$$

$$\Delta t \overset{\Delta}{=} t_{\ell+1} - t_\ell$$

The basic definition of angular rate states that for small Δt,

$$\underline{\alpha} \approx \underline{\omega}\, \Delta t$$
$$\alpha \approx \omega\, \Delta t \tag{A4}$$

Hence, for small Δt, $\underline{\alpha}$ is small, and therefore, from (A2),

$$g_3 \approx 1/2$$
$$g_4 \approx 1 - \frac{\alpha^2}{2} \approx 1 - \frac{\omega^2 \Delta t^2}{2} \tag{A5}$$

Using mixed vector/scalar notation, substitution of (A4) and (A5) in (A2) yields:

$$p = g_3 \underline{\alpha} + g_4$$
$$\approx 1/2\, \underline{\omega}\, \Delta t + 1 - \frac{\omega^2 \Delta t^2}{2}$$

Substituting in (A3) obtains:

$$\frac{h(\ell+1) - h(\ell)}{\Delta t} \approx h(\ell) \left(1/2\, \underline{\omega} + 1/2\, \omega^2 \Delta t\right)$$

In the limit as $\Delta t \to 0$, the latter reduce to the derivative form:

$$\dot{h} = 1/2\, h\, \underline{\omega} \tag{A6}$$

We now return to (14) and express h as a function of $\underline{\phi}$ in mixed vector/scaler notation:

$$h = f_3 \underline{\phi} + f_4$$
$$f_3 = \frac{\sin(\phi/2)}{\phi} \tag{A7}$$
$$f_4 = \cos(\phi/2)$$

Substituting in (A6),

$$\dot{h} = 1/2\, f_3\, \underline{\phi}\, \underline{\omega} + 1/2\, f_4\, \underline{\omega} \tag{A8}$$

It is readily demonstrated by algebraic expansion and using the rules of quaternion algebra that $\underline{\phi}\, \underline{\omega}$ in (A8) is equivalently:

$$\underline{\phi}\,\underline{\omega} = \underline{\phi} \times \underline{\omega} - \underline{\phi} \cdot \underline{\omega}$$

Differentiation of (A7) shows that:

$$\dot{h} = \dot{f}_3\,\underline{\phi} + f_3\,\dot{\underline{\phi}} + \dot{f}_4$$

$$\dot{f}_3 = 1/2\,\frac{\cos\phi/2}{\phi}\,\dot{\phi} - \frac{\sin\phi/2}{\phi^2}\,\dot{\phi}$$

$$= \frac{\dot{\phi}}{\phi}\,(1/2\,f_4 - f_3)$$

$$\dot{f}_4 = -1/2\,(\sin\phi/2)\,\dot{\phi} = -1/2\,\phi\,\dot{\phi}\,f_3$$

Hence, with (A8),

$$\dot{h} = f_3\,\dot{\underline{\phi}} + \frac{\dot{\phi}}{\phi}\,(1/2\,f_4 - f_3)\,\underline{\phi} - 1/2\,\phi\,\dot{\phi}\,f_3$$

$$= 1/2\,f_3\,(\underline{\phi} \times \underline{\omega}) - 1/2\,f_3\,\underline{\phi} \cdot \underline{\omega} + 1/2\,f_4\,\omega$$

Dividing by f_3 and solving for $\dot{\underline{\phi}}$:

$$\dot{\underline{\phi}} = 1/2\,\frac{f_4}{f_3}\,\underline{\omega} + 1/2\,(\underline{\phi} \times \underline{\omega}) - \frac{\dot{\phi}}{\phi}\,(1/2\,\frac{f_4}{f_3} - 1)\,\underline{\phi} + 1/2\,\phi\,\dot{\phi} - 1/2\,\underline{\phi} \cdot \underline{\omega} \qquad \text{(A9)}$$

Equation (A9) is now separated into its vector and scalar components:

$$\dot{\underline{\phi}} = 1/2\,\frac{f_4}{f_3}\,\underline{\omega} + 1/2\,(\underline{\phi} \times \underline{\omega}) - \frac{\dot{\phi}}{\phi}\,(1/2\,\frac{f_4}{f_3} - 1)\,\underline{\phi} \qquad \text{(A10)}$$

$$1/2\,\phi\,\dot{\phi} = 1/2\,\underline{\phi} \cdot \underline{\omega}$$

The scalar equation is equivalently:

$$\frac{\dot{\phi}}{\phi} = \frac{1}{\phi^2}\,\underline{\phi} \cdot \underline{\omega}$$

Substituting in the vector part of (A10) yields:

$$\dot{\underline{\phi}} = 1/2\,\frac{f_4}{f_3}\,\omega + 1/2\,(\underline{\phi} \times \underline{\omega}) - \frac{1}{\phi^2}\,(1/2\,\frac{f_4}{f_3} - 1)\,(\underline{\phi} \cdot \underline{\omega})\,\underline{\phi}$$

Using the vector triple product rule, it is easily demonstrated that:

$$(\underline{\phi} \cdot \underline{\omega})\,\underline{\phi} = \underline{\phi} \times (\underline{\phi} \times \underline{\omega}) + \phi^2\,\underline{\omega}$$

Substituting,

$$\dot{\underline{\phi}} = 1/2\,\frac{f_4}{f_3}\,\underline{\omega} + 1/2\,\underline{\phi} \times \underline{\omega} - (1/2\,\frac{f_4}{f_3} - 1)\,\underline{\omega} + \frac{1}{\phi^2}\,(1 - \frac{f_4}{2f_3})\,\underline{\phi} \times (\underline{\phi} \times \underline{\omega})$$

Combining terms:

$$\dot{\underline{\phi}} = \underline{\omega} + 1/2\,\underline{\phi} \times \underline{\omega} + \frac{1}{\phi^2}\,(1 - \frac{f_4}{2f_3})\,\underline{\phi} \times (\underline{\phi} \times \underline{\omega})$$

Using the definition for f_4 and f_3 from (A7), it can be shown by trigonometric manipulation that the bracketed coefficient in the latter expression is equivalently:

$$1 - \frac{f_4}{2f_3} = \frac{1}{\phi^2}\,(1 - \frac{\phi \sin\phi}{2(1-\cos\phi)})$$

Substitution yields the final expression for $\dot{\underline{\phi}}$:

$$\dot{\underline{\phi}} = \underline{\omega} + 1/2\ \underline{\phi} \times \underline{\omega} + \frac{1}{\phi^2}\left(1 - \frac{\phi \sin \phi}{2(1-\cos\phi)}\right) \underline{\phi} \times (\underline{\phi} \times \underline{\omega}) \qquad \text{(A11)}$$

Equation (20) in the main text is the integral from of (A11) over a computer cycle (from t_m to t_{m+1}).

REQUIREMENTS, APPLICATIONS, AND RESULTS OF STRAPDOWN INERTIAL TECHNOLOGY TO COMMERCIAL AIRPLANES

Phillip J. Fenner
Manager, Navigation Sensors/Displays
737/757/767 Flight Systems Technology
Boeing Commercial Airplane Company
Box 3707
Seattle, WA 98124-2207

SUMMARY

The basis for selection of a strapdown inertial system for short to medium range jet transports is discussed. Inertial data requirements and associated performance requirements are shown for commercial airplanes. Good performance at low cost and high reliability are key requirements of inertial technology application to commercial airplanes which do not have a long range navigation need. The Honeywell laser inertial reference system (IRS) selected by Boeing for the 757/767/737 airplanes is described, along with airplane installation and interface details. Test programs instituted to validate the design and reduce program risk are described. Performance and reliability experience data from Boeing flight tests, and over the first year of airline service, are shown to exceed expectations.

INTRODUCTION

Boeing has recently introduced inertial navigation technology as the basic airplane system component for primary attitude and heading data in the medium range, two engine airplanes, the 757 and 767. The short to medium range 737-300 airplane will also have the same inertial navigation technology as basic equipment when delivered in late 1984.

The question is often raised, "Why inertial for short to medium range airplanes?", because navigation is usually the primary purpose of installing inertial systems in commercial airplanes.

One of the goals of the new airplane development programs (757/767) at Boeing was the following: "Any new airplane should include in the basic configuration, automatic navigation/guidance computing and control systems having the capability and flexibility to operate in the forecast ATC environment and be relatively unlimited in its application without the necessity for future expensive modifications to the avionic systems."

During the preliminary design phase of the new technology transports at Boeing, which ultimately, turned out to be the 757 and 767 airplanes, the airplane attitude system design specification was at a cross-roads. Do we continue with 20-30 year old technology systems or is this the proper time to select new technology systems at potentially higher risk and cost, but which provide the data needed to improve the airplane operational capability?

Boeing has long recognized, through its research programs that inertial navigation systems are a very desirable attribute to any type of commercial airplane.

The experience base started with the 747 in 1957 as shown in figure 1, continued with the American SST program, which was followed by Boeing research activities using inertial data for various airplane functions including autoland, advanced displays, and 4D navigation and guidance. A key Boeing research activity was the program to design, build and fly a strapdown inertial system to meet airplane systems requirements, but at a cost that was viable for short to medium range aircraft. This program success was the stimulus to study the applicability of strapdown technology on new airplane programs.

This report is organized first with discussion of inertial data requirements for commercial airplanes, followed by the candidate systems considered, and system performance requirements development. The strapdown inertial development work at Boeing is then covered and finally, a description of the system and test experience with the laser strapdown system on the 757 and 767 airplanes, is provided which is the primary focus of the report.

INERTIAL DATA REQUIREMENTS

An examination of the functional requirements for inertial data on commercial airplanes shows that significant improvements in airplane-operating capability are gained from using attitude data that are insensitive to airplane maneuvers, and ground referenced velocity vector data. These airplane-system functions and their required inertial data are shown in Table 1. To satisfy all of these requirements, an inertial quality attitude system, and specifcally a strapdown configuration, must be specified. Gravity erected attitude systems do not provide the range of data nor the quality of data desired, and gimballed inertial systems are too costly, and not all the desired data are available.

With a strapdown inertial reference system, a commercial airplane has for the first time a self-contained data system that completely determines the airplane's state - a desirable feature for airplane applications now and for improvements in the future.

A description of the key applications of inertial data to the airplane systems which can significantly improve as commercial transport's operability is given in the following paragraphs.

Navigation/Guidance

Continuous, very low noise, acceleration, velocity and position data, from an inertial reference system can be used to improve the accuracy and response characteristics of a radio based (e.g., VOR/DME) navigation system. Excellent ground referenced high frequency data from this type of attitude system complements the noisy, lower data rate from RF navigation aids whose performance is dependent on station geometry and

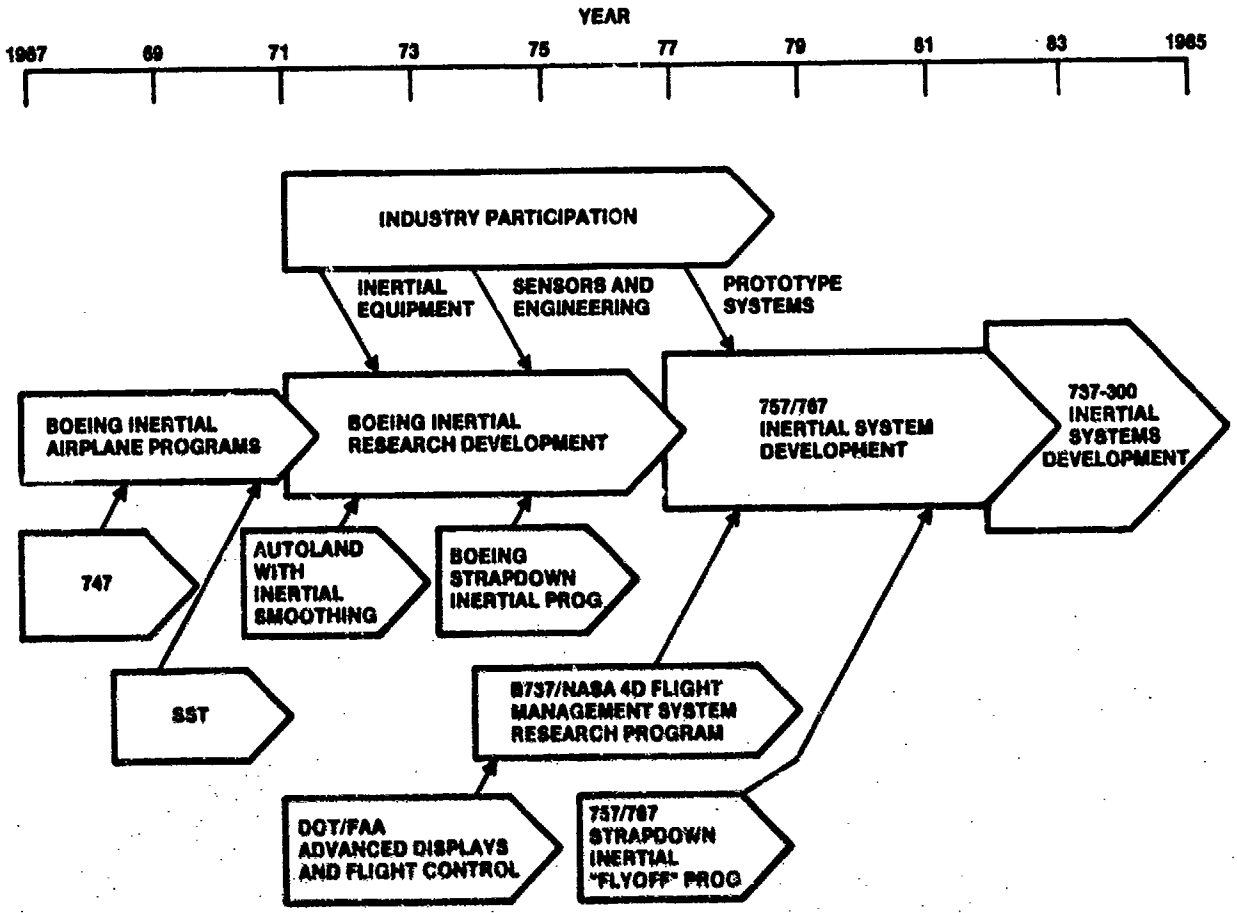

Figure 1. Inertial Technology Evolution in Boeing Commercial Airplanes

distance and are also interrupted periodically for station changing. Navigation accuracy and flight path capture and tracking are improved with an inertial data aided system. This will be particularly important in high density terminal areas where congestion will require tighter path control. For growth to time navigation which is expected to be employed in the high density terminal areas of the 1980's, the ground referenced data available from an inertial quality attitude system is required. Boeing achieved a 5-second average 4D error using this type of system on the NASA Terminal Configured Vehicle (TCV) program using a 737 airplane. This performance satisfies the time Nav requirements predicted by many air traffic control analyses.

Long range navigation requirements usually require installation of an additional system that is certified as sole means of navigation. If an inertial reference system was installed as the basic attitude system, the long range navigation requirements could be satisfied automatically, assuming the navigation performance is adequate for overwater navigation.

Fuel Economy Computations

Investigations indicate that the optimum Mach for maximum ground nautical miles/pound of fuel in wind are shifted from the handbook (still-air) values. Knowledge of ground speed would therefore be beneficial in selecting the optimum Mach under headwind/tailwind conditions. High quality estimates of ground speed are available from inertial navigation systems, for this function.

Displays

It is very desirable to display basic airplane attitude and heading accurately at all times. Gravity erected systems exhibit several degrees of error due to airplane accelerations, e.g., takeoff, banking maneuvers, large thrust changes. For maximum crew confidence, and less nuisance warnings from instrument comparators, attitude and heading are desired from a source that is insensitive to airplane maneuvers. These data are only available from an inertial reference system. Advanced display (CRT type) research by Boeing, both flight and simulation, has shown that properly displayed flight path acceleration and velocity provides improved thrust management capability and more precise airplane control. These data are only available from an inertial attitude reference system.

Current pneumatic vertical speed indicators indicate false rates in roll maneuvers due to the seismic mass in the instrument sensing the centripetal accelerations. Electric instruments will eliminate this problem, but several seconds of filtering on the noisy air data computer altitude rate signal is required to generate acceptable display characteristics. This filtering adds lag to the data and hardware to the display. All these problems can be obviated by providing instantaneous, low noise vertical speed from an inertial attitude reference system, which is insensitive to maneuvers, and atmospheric noise.

Table 1. New Airplane Functions Requiring Inertial Data

Function	Data Required	Comments
Navigation/guidance, precise path control, improved NAV accuracy	Low noise, high frequency, earth referenced acceleration, velocity and position	Improves accuracy/response. Allows paths without VORTAC reception
Time NAV (4D)	Ground reference velocity and acceleration	More efficient control for those terminals with time controlled flow
Long range NAV	Self-contained, accurate present position	Provide overwater navigation where needed
Energy management	Ground speed	Need to know wind continuously to determine optimum Mach for maximum ground nm/lb of fuel
Displays		
Accurate attitude	Attitude insensitive to environment	Improved weather radar stabilization and crew confidence
Accurate vertical speed	Inertial vertical velocity	Improved high frequency response and vertical wind shear detection
Takeoff acceleration, flight path angle	Longitudinal acceleration, ground reference velocity vector	Engine thrust monitor. Allows better thrust management and airplane control
Flight path acceleration	Ground reference acceleration vectors	Allows predicted path to be displayed on map display
Automatic Flight Control		
Autoland	Attitude insensitive to environment. Ground referenced velocity vector, body rates	Improves control performance required for Cat. III and offers performance gains for poor ILS facilities and wind shear conditions
Rollout	Ground speed, track, track rate, body rates	Longitudinal guidance needs to know distance traveled and track deviations
Response/Performance improvements in other modes	Along track acceleration, vertical velocity, vertical acceleration, track, ground speed, stable attitude, heading, body rates	Better response characteristics with accurate attitude and earth referenced acceleration and velocity data
Wind shear detection	Ground reference velocity acceleration	Allows comparison of airspeed and ground speed for shear indication
Over rotation	Pitch, pitch rate	Allows precise calculation of predicted pitch angle
Anti-skid	Ground speed	Improves performance under hydroplaning conditions
Autobrake	Ground speed/acceleration	Provides improved control and repeatability
Nose gear steering	Ground speed	More accurate than airspeed at low speeds for gain scheduling
Auto thrust reversal	Ground speed	Ground speed will allow more precise scheduling
Taxi speed monitor	Ground speed	Provide information for better control in restricted areas and reduce wear on gear and tires

Autopilot/Autoland

The classic autoland problem is to derive a signal proportional to cross-track velocity for damping in the approach mode. This is difficult to achieve because of beam noise, bends, wind shear, turbulence, and inaccurate roll attitude data. A common method to obtain X-track velocity is called lagged roll which depends heavily on roll attitude accuracy because the dominant damping signal is derived from the term, $g\sin\phi$, where ϕ is roll angle. A lateral body mounted accelerometer is also used in this damping scheme (747 type) and its use restricts approaches to constant speed because of errors developing from longitudinal acceleration during decelerating approaches coupling into the lateral accelerometer during crabbed (crosswind) approaches.

An IRS system provides the accurate, unperturbed roll attitude signal plus true cross-track acceleration and velocity independent of wind or airplane deceleration conditions. No maneuver restrictions are required. The inertial cross-track velocity information (drift angle, track angle, track angle rate) in addition to the required roll attitude accuracy, have been shown by Boeing to aid significantly during transient conditions such as large beam bends, overflights, winds, and landing aid faults.

Other autopilot modes, such as autothrottle and altitude hold, can provide better performance with true along-track and vertical acceleration data, rather than attitude compensated longitudinal and normal acceleration sensor data.

Control damping requires body angular rate and linear acceleration data. Contemporary flight control systems have utilized body mounted sensors to satisfy this requirement. Strapdown attitude systems, either inertial or non-inertial, can now provide this data, thus eliminating the need for 16 sensors in a 3-channel fail-op system and 12 sensors in a dual fail-passive system.

Autobrake/Antiskid

Most antiskid systems rely on measurement of wheel rotation for determining airplane ground velocity and wheel lockup (skid) to control braking forces. Unsatisfactory operation occurs when wheel speed is not a true measure of airplane ground velocity. This is especially sensitive during hydroplane conditions. Therefore, some external measurement of ground speed is considered essential to improve modern antiskid systems.

The autobrake systems currently average several wheelspeed signals and differentiate the average to obtain a measurement of airplane deceleration. This has provided to be less than satisfactory and often results in excessive or insufficient braking. Acceleration data from the inertial reference system would eliminate these current braking inefficiencies.

INERTIAL DATA SYSTEM CANDIDATES

Airplane attitude reference systems may be partitioned into two generic types: Schuler-tuned (inertial) and gravity erected vertical references. A primary difference between the two types is the quality of the attitude and heading data. A Schuler-tuned system is capable of providing accurate attitude (< .05°) and heading unperturbed by airplane maneuvers, which can cause errors of several degrees in the gravity erected systems. There are, in addition, other data available from an inertial system which are not present in any gravity erected system. These are navigation data (latitude/longitude), flight path velocity vector, drift angle, flight path acceleration vector, true heading, and synthesized magnetic heading (no magnetic sensor required).

Boeing research studies for the new airplane programs included in depth reviews of new attitude system technology which could be considered candidates for the new airplane programs, meeting most or all the requirements shown in Table 1. These candidates included strapdown attitude/heading reference system (AHRS) as well as strapdown inertial navigation systems.

The AHRS systems are basically gravity referenced systems, and gave the desired, improved verticality, but did not provide the inertial navigation quality velocity and other related parameters felt to be needed in a good inertial sensing system. For example, the AHRS needed radio data combined with the system acceleration data to develope reasonable velocity information. This system also depended on air data and magnetic field sensors to obtain the verticality during maneuvers and for stabilized magnetic heading. Thus, a rather complex system was required to obtain the basic inertial data and still had limited information capability and very limited growth potential. In addition, it was not clear from an in-house system design synthesis of each system type that a significant cost advantage was held by AHRS over strapdown inertial systems. A review of table 2 shows the limitations of this type of system and other candidate attitude systems when compared against the requirements. The strapdown inertial navigation system is shown to fulfill the requirements for inertial data.

Cost has been a problem that prevented wide application of this kind of system. Long-range airplane applications have been economically viable because the human navigator may be eliminated. Boeing studies in 1973 indicated the economy of strapdown inertial systems, if the functions provided by the conventional attitude and heading reference systems and the body-mounted inertial sensors used for flight control are replaced by the inertial system.

Cost of ownership studies were performed to substantiate the viability of this technology as a basic sensing system to Boeing airplanes for applications other than long range navigation. A summary of this activity is shown in Table 3. The difference between installed cost and unit cost is the incurred expense for test and calibration after airplane installation. The greatest differential in this category is for the conventional vertical gyro based system because of its large number of components. From this cost trade study, it was concluded that, although the inertial reference system was somewhat more expensive than other non-inertial quality candidates, the system capability warranted the extra investment.

In summary two basic questions had to be answered by Boeing engineering to satisfy the Boeing and airline management teams for new airplane development: "Why inertial", and how do you justify the probable increase in unit (black box) cost?

The answers to these two questions are summarized in Table 4 and 5. To satisfy the criteria of Table 5 required a break through in inertial system technology from that used in the high cost gimballed systems which could be used on a cost effective basis only on long range transports. The technology most promising at the time was the strapdown inertial mechanization which is summarized in Table 6.

Table 2. Attitude Systems Performance Comparison

757/767 Study Configurations						
Function	Require. For New Airplane	Existing Fleet Capabilities	Strapdown Inertial	Gimbal INS (Low Cost)	Gimbal Att/Hdg System	Strapdown Att/Hdg System
Attitude	0.1° under all conditions	0.5° 2-5° under maneuvers	0.05°	0.2°	0.5° 2° (transient)	0.25° 1° (transient)
Magnetic heading	2° under all conditions	2°, 5° under maneuvers	2°	2°	2° 5° (transient)	2° <5° (transient)
True heading	<0.4°	Not available	<0.25°	<0.25°	Not available	Not available
Ground speed	<10 kn	Not available	8-10 Kn	6-8 Kn	Not available	Requires VOR/DME true airspeed data
Track ref. accel.	0.01g	Not available	0.001g	0.001g	Not available	Requires VOR/DME true airspeed data
Track angle	<3°	Not available	<3°	<3°	Not available	Requires VOR/DME true airspeed data
Flight path angle	0.4°	Not available	<0.4°	<0.4°	Not available	Requires VOR/DME true airspeed data
Track angle rate	0.25°/sec	Not available	<0.25°/sec	<0.25°/sec	Not available	Requires VOR/DME true airspeed data
Body angular rate	0.1°/sec	Not available	0.015°/sec	Not available	Not available	0.01°/sec
Present position	<2 nm/hr	Not available	<2 nm/hr	<2 nm/hr	Not available	Not available
Vertical velocity	<1 ft/sec	Not available	<1 ft/sec	<1 ft/sec	Not available	3-4 ft/sec
Body ref. accel.	0.01g	Not available	0.001g	Not available	Not available	0.01g
Interfaces	Digital	Analog	Digital	Analog/digital	Digital	Digital
Flyaway cost/channel	≤$33K	$33K	$37	$90K	$27K	$27K
Risk	Low-medium	Low	Medium	Medium-high	Low-medium	Medium-high

Table 3. Cost of Ownership Summary for Inertial Data Alternatives, Brickwall

Cost Parameter ($/FL Hr/Channel)	Inertial Systems		Heading/Attitude Systems	
	ARINC 581 (747) Gimballed (Actual Cost Data)	Strapdown IRS	(2nd Order AHRS) Digital Interfaces	VG/DG (1st Order Leveling) (Actual Cost Data)
Direct maintenance cost (shop)	1.54	0.65	0.51	0.57
Direct operating cost (shop, burden, fuel, delay)	4.08	1.7	1.61	1.73
Amortized equipment cost	4.72	1.2	0.82	0.82
Installed cost (unit cost)	>$100K/(84K)	$37K/(36K)	$27K/(24K)	$33K/(23K)

Table 4. Why Inertial?

- Attitude/Heading Unperturbed by Airplane Dynamics
  - Attitude displays without errors
  - Eliminates cockpit nuisance warnings during maneuvers
  - Improved autoland performance
  - Weather radar stabilization problems eliminated
- Ground Referenced Data
  - Wind vector
  - Improved displays
  - Wind shear detection
  - Improved autoland performance and capability
  - Improved path control
  - Time navigation improvements
  - Enhance energy management computations
- Improved Navigation Performance and Operation
  - Smooth vortac navigation
  - Allows paths without vortac reception
  - Inherent over water navigation and direct route operation
- Growth
  - Self-contained data system to completely determine airplane's state
    - Taxi speed monitor
    - Overweight landing monitor
    - T/O accel monitor
    - Auto thrust reversal
    - Nose wheel steering

Table 5. How Do We Justify Inertial for 757/767?

- Cost Competitive (Fly Away Cost)
- Cost-of-Ownership Acceptable
- Replaces Equipment on the Airplane
- Functional Integration

Table 6. Why Strapdown?

- Low Cost Potential
  - Initial
  - Cost-of-ownership
- High Reliability Potential
- Functional Integration Capability
- Inherently Digital

Confidence in this technology was achieved with the Boeing strapdown research program described in the next section. The results of this internal IR&D spawned an industry "fly-off" competition which is described in the section after next, and confirmed that industry had the technology with acceptable risk for a commercial airplane venture.

BOEING STRAPDOWN RESEARCH PROGRAM

The airplane equipment replacement study results and the attributes of high-quality inertial data led to the design, build, and flight test of a strapdown inertial system by the Boeing research staff. The program had three objectives:

- To demonstrate technical feasibility of a potentially low cost strapdown inertial system
- To gather sufficient knowledge to write a realistic procurement specification for future Boeing airplanes
- To encourage industry in the development of a low-cost strapdown inertial system.

Boeing reserach engineering developed a strapdown inertial system "working" specification for internal use and from this document designed and built a strapdown inertial system which performed better than the requirements. Lab and flight testing occurred in 1975-76, and 8 minute alignments and 2 nmi/hr navigation performance were demonstrated with a system without any temperature controlled sensors. This system used two degree-of-freedom tuned rotor gyros from Teledyne, Systron-Donner force-rebalanced accelerometers and a Boeing designed digital computer and strapdown algorithms. Typical performance exhibited by this sytem is shown in Figure 2.

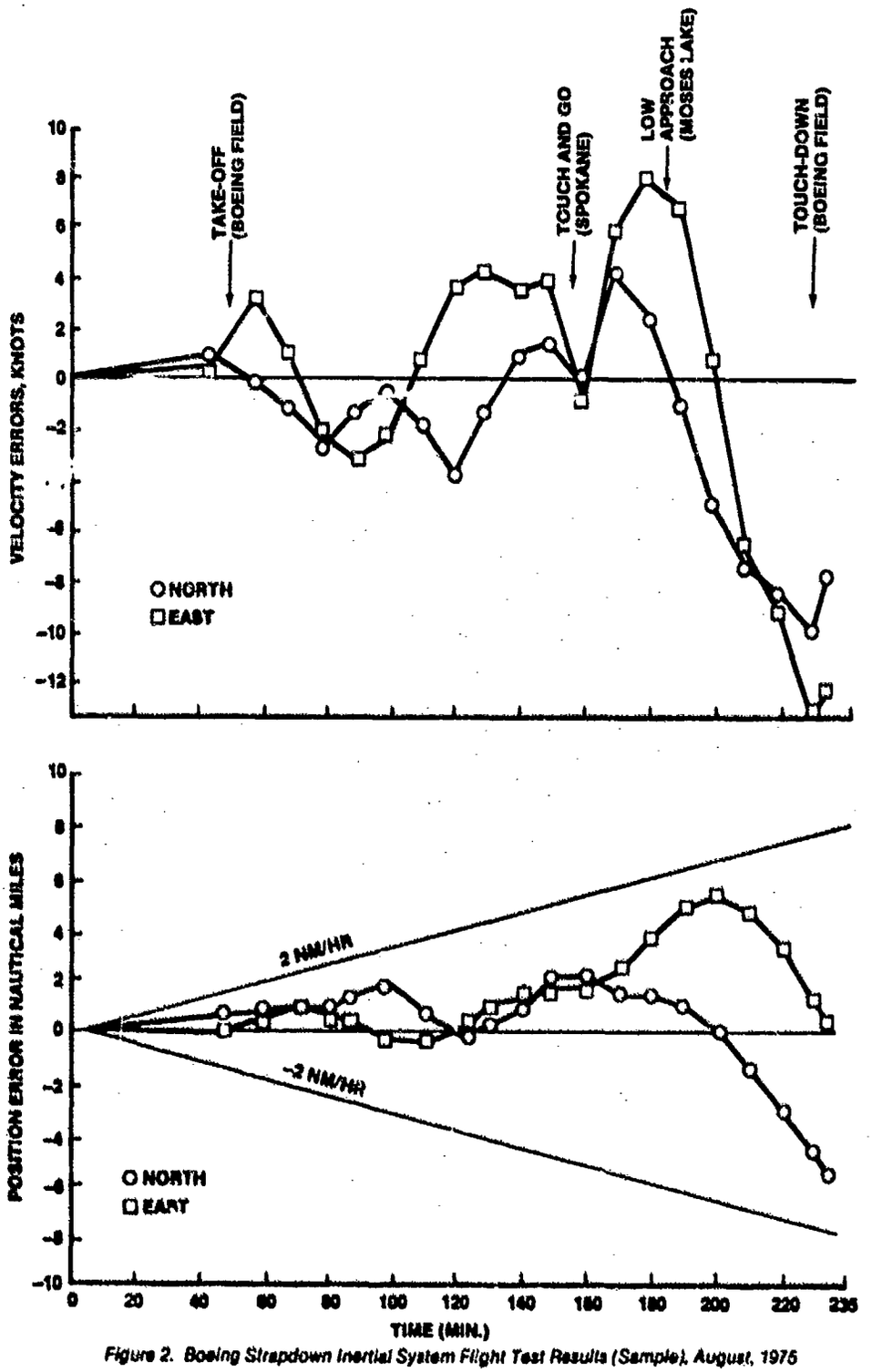

Figure 2. Boeing Strapdown Inertial System Flight Test Results (Sample), August, 1975

This program success provided the necessary confidence for Boeing management to pursue a strapdown inertial system for the new airplane programs being developed. This research effort in strapdown inertial technology at Boeing is summarized in Table 7. (Ref. 1, 2)

Table 7. Boeing Strapdown Research Program

- Objectives
  - Determine feasibility of low cost strapdown inertial system
  - Stimulate industry to develop low cost system on their funds for commercial applications
  - Develop a specification for procurement
- Results
  - Boeing designed and built a low cost strapdown system (1973-75)
    - Teledyne gyro
    - Systron-Donner accel
    - Boeing computer
  - Lab and flight tested successfully (1975-76)
    - Demonstrated 8 minute alignments
    - No heaters used
    - Flight tested with 2 nmi/hr NAV performance and 8 kn velocity performance
    - Laser gyro lab test
  - Stimulated 767 program to pursue strapdown inertial technology

NEW AIRPLANE STRAPDOWN INERTIAL "FLY-OFF" PROGRAM

To support the new airplane programs, Boeing established an inertial development program with the objectives and vendor participation shown in Table 8.

The key to reduce the risk of introducing new technology on a commercial airplane was to stimulate a "fly-before-buy" competition between potential suppliers of strapdown inertial systems. As shown in Table 8, three manufacturers participated in varying degrees.

Table 8. 767 Inertial Reference System Development Program

- Objectives
  - Promote the development of an inertial reference system which is cost competitive with a conventional attitude/heading/body/rate/body acceleration sensor system
  - Reduce the risk of introducing new technology (strapdown inertial) into commercial aircraft
    - Evaluate pre-production digital strapdown inertial system performance
    - Investigate technical design problems
    - Produce detailed system design specifications
    - Validate cost goals
  - Promote an ARINC specification (704)
- Vendor Participation
  - Joint development program to produce flight test hardware with 3 vendors
    - Teledyne — flyable equipment delivered April 1978
    - Honeywell — flyable equipment delivered April 1978
    - Litton — lab test demo of gyro/electronics June 1978

The basic requirements of the system design which manufacturers needed to satisfy during this evaluation phase are listed in Table 9. These systems provided by the potential vendors were prototype configurations for commercial airplanes. The system described in this paper, a laser inertial system, had its heritage in the protoype system developed for a Boeing 727 test airplane flight evaluation, where over 70 hours of flight time and 200 hours of laboratory test time were accumulated. This system met all test objectives and operated without any failures - all factors which provided a strong technical basis for its ultimate selection on the 757-767 airplane program. The manufacturers Litton and Teledyne participated with tuned-rotor gyro technology with only Teledyne meeting the flight test schedule. These tuned rotor gyro based systems did not exhibit the maturity needed for a commercial airplane program at the time (1978) of their evaluation.

Table 9. Low Cost Inertial Reference Requirements

• Provide Airplane Heading, Attitude, Body Axis Rates and Acceleration, and Ground Referenced Position and Velocity Information Unperturbed by Airplane Maneuvers
• Cost Competitive With Conventional Systems Replaced
• Unrestricted Airplane Attitude and World-Wide NAV Capability
• Performance • Alignment — <10 minutes • Radial position — <4 nmi/hr • Attitude — <2 arc-minutes • Magnetic heading — <1° synthesized • Radial velocity — <8 knots • Vertical velocity — <1 ft/sec

A summary of the Honeywell laser inertial system test results of this competition is given in Table 10. Summaries of this test program for the lab and flight phases are shown in Tables 11 and 12. Detailed performance characteristics exhibited by the system in position and velocity are shown in Figure 3 through 6.

The performance data and the integrity of the system during the evaluation at Boeing and by other evaluators such as the Central Inertial Guidance Test Facility of the US Air Force, led to the conclusion that this technology was viable. The key question that remained was "could the supplier provide laser gyros with the performance and reliability required from a production facility at a cost acceptable for airline operations.

An in-depth review of the laser gyro technology, the manufacturing processes required, design changes planned for producibility reasons, and company commitment to the product were conducted at the supplier's facilities. This review showed the risks were acceptable in the technology, the production facility was well along in construction, and the company's commitment and funding sources were very strong. Consequently, the strong technical status, with the favorable cost proposal and strong company commitment, led to the selection of the Honeywell laser gyro-based inertial reference system for the 757/767 airplane programs.

Table 10. Boeing Prototype Honeywell Laser Inertial System Test Summary

Test Period	April 18 - July 12, 1978
Aircraft Type	727-100
Laboratory Tests	180 hours • EMI • Scoreby • Vibration • Temperature • Heading/alignment • Navigation
Flight Tests	70 hours • Air work — Emergency descent — 360° turns at 40° bank — Approach to stalls — Instrument approaches • Touch and go landings
Position Error Rate	• 2.0 nm/hr 95% prob
Velocity Error	• 7.22 kts 95% prob
System Turn-ons	• 50
System Alignments	• 65
System Failures	• 0

Table 11. Honeywell Laboratory Test Ensemble Performance

Total Lab Test Series	Radial Position Error Rates, 95 Percentile, nm/hr		Radial Velocity Errors 95 Percentile, ft/sec (knots)	
12	With Scorsby runs 1.67	Without Scorsby runs 1.29	With Scorsby 7.22 (4.3)	Without Scorsby 7.39 (4.4)

Table 12. Honeywell Individual Laboratory Test Results

Laboratory Test Description	NAV Time, hr	Pos Error Rate 95 Percentile, nm/hr	Ground Speed Error 95 Percentile, ft/sec (knots)
Static NAV baseline	4.00	1.46	5.7 (3.4)
Static NAV with azimuth rotation	4.00	0.98	6.1 (3.6)
High temperature static NAV	3.00	1.50	4.6 (2.7)
Cold temperature static NAV	3.46	1.23	8.6 (5.1)
Static NAV with 45° heading and 5° tilt in each axis	1.53	1.89	6.4 (3.8)
Scorsby Motion @ ±7° tilt	3.00	2.18	6.8 (4.0)
Scorsby Motion @ ±2-3° tilt	2.83	0.49	3.6 (2.1)
Scorsby Motion @ ±7.5° tilt	2.16	1.64	6.1 (3.6)
Scorsby Motion @ ±4° tilt	2.16	2.75	6.5 (3.8)
First long term static NAV	6.83	0.65	4.8 (2.7)
Second long term static NAV	10.00	1.26	9.8 (5.8)
Third long term static NAV	8.32	0.88	8.1 (4.8)

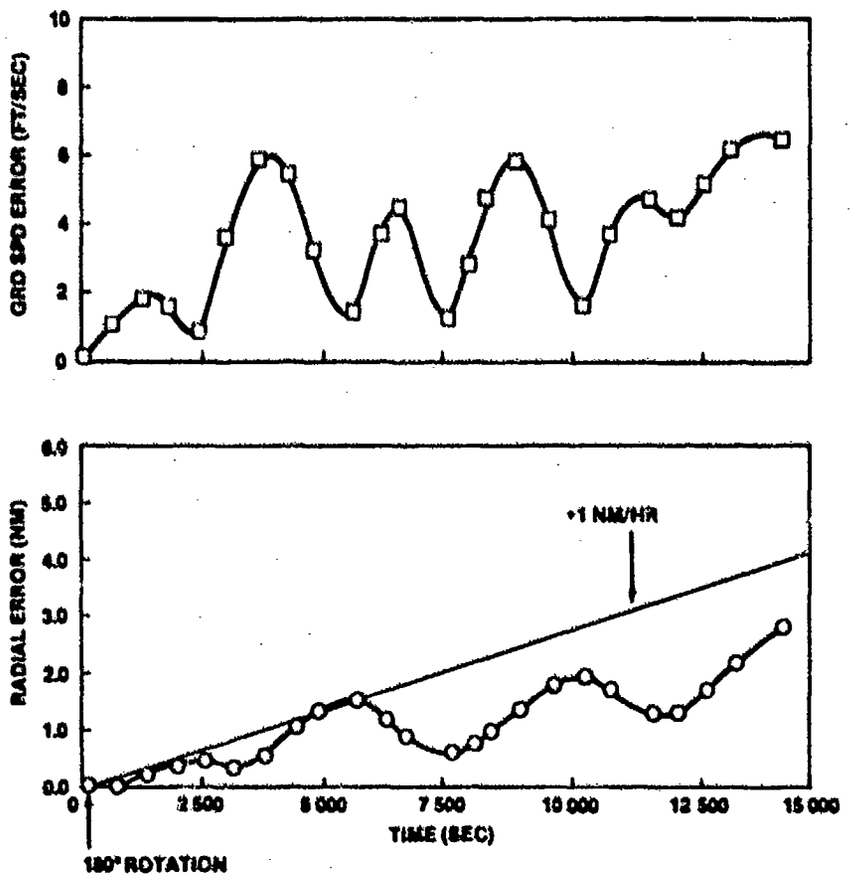

Figure 3. Sample Lab Navigation Performance Test Results by Boeing of the Honeywell Prototype Laser Inertial System

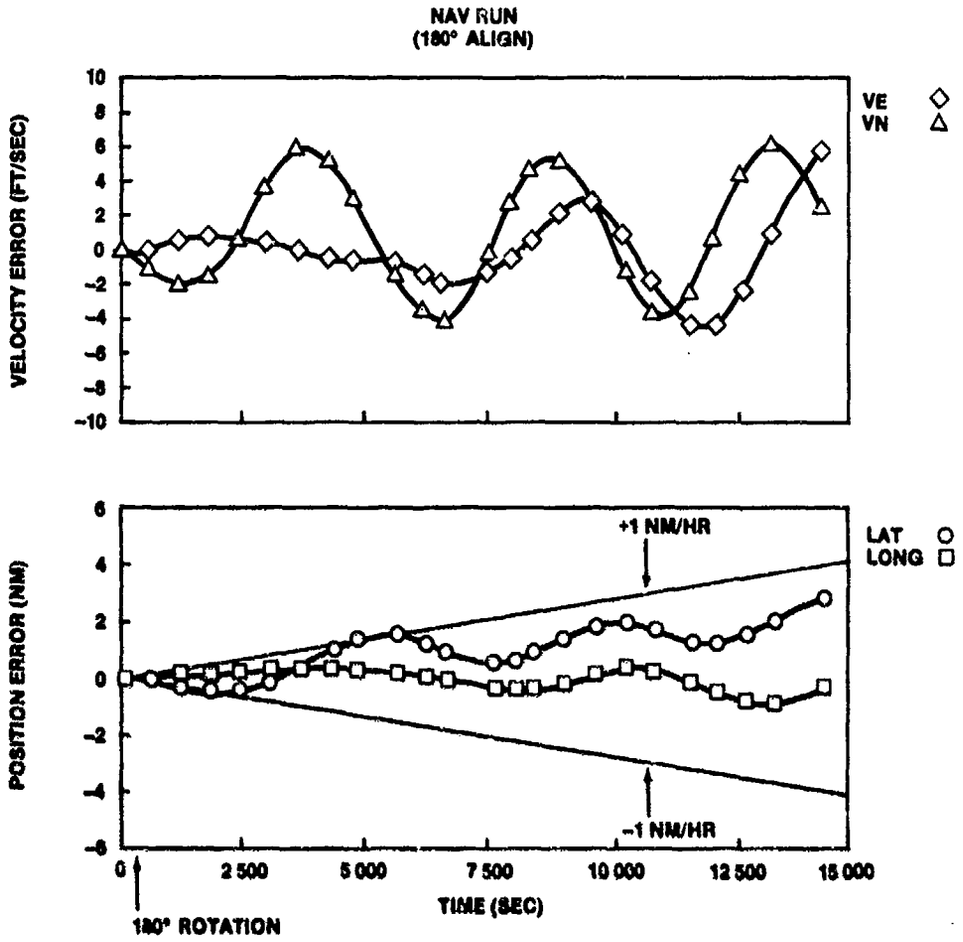

Figure 4. Sample Lab Navigation Performance Test Results by Boeing of the Honeywell Prototype Laser Inertial System

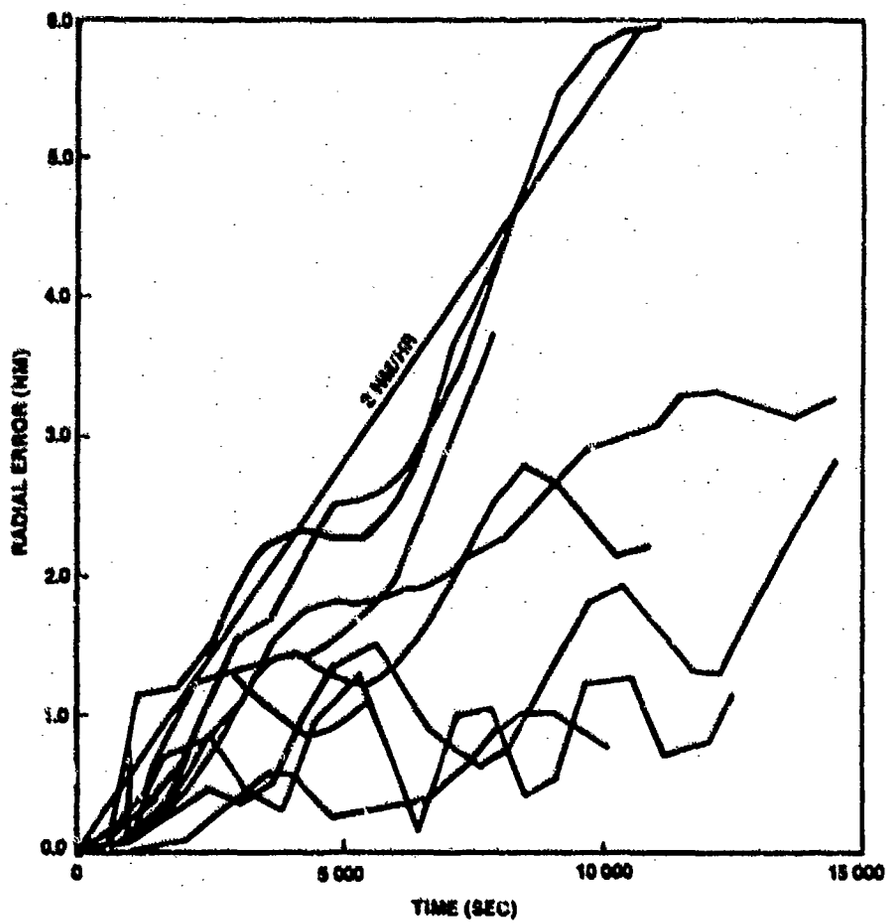

Figure 5. Composite Errors of Lab Tests of the Honeywell Prototype Laser Inertial System

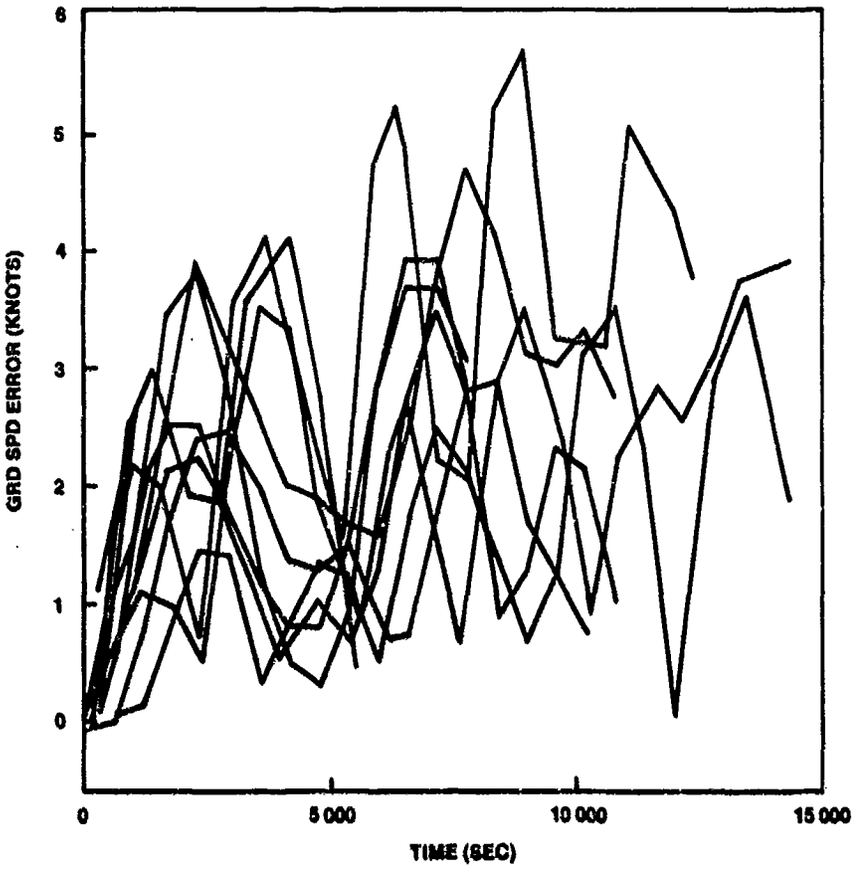

Figure 6. Composite Velocity Errors of Lab Tests on the Honeywell Prototype Laser Inertial System

SYSTEM PERFORMANCE REQUIREMENTS DEVELOPMENT

Parameter Performance

The performance requirements for a commercial inertial navigation system used for purposes other than just navigation are driven primarily from the equipment using inertial information.

For example, track angle (a velocity based parameter) is desired for control and display purposes with a strong desire to maintain its accuracy in the 2-3° range during low speed operations. Track angle is defined as $\tan^{-1} V_e/V_n$. Using partial derivatives, $\delta\psi_{tk}/\delta V_e$ and $\delta\psi_{tk}/\delta V_n$ to develop error contributions due to each velocity component and then combining to develop the total error in ψ_{tk} due to inertial velocity error yields the following equation for estimating track angle error:

$$\Delta\psi_{tk} = \frac{\sqrt{V_n^2 \cdot cV_e^2 + V_e^2 \cdot cV_n^2}}{V_n^2 + V_e^2}$$

For $\Delta\psi_{tk}$ of 2-3°, the velocity errors must be less than 6 knots per axis.

Since, we felt this velocity performance requirement could result in an unacceptable system cost, the requirement was reluctantly changed to 4°, requiring errors in the 8 knot per axis range.

This process was essentially followed for the other inertial parameters of flight path angle, track referenced accelerations, track angle rate, etc. The final specification requirements had to be balanced between the user requirements (usually too tight) and what could be achieved with a system of acceptable cost. The judgment for the latter was based considerably on the experience Boeing gained in the strapdown inertial research program previously discussed.

Navigation/Magnetic Heading

Exceptions to the requirements process described above were navigation performance and magnetic heading. These are controlled, in the US, by the Federal Air regulations.

Navigation performance for inertial systems in civil transport use is specified in FAR 121, Appendix G to be: "For flights up to 10 hours duration, no greater than 2 nautical miles per hour of circular error on 95% of system flights completed is permitted".

Magnetic heading performance requirements are less clear in the regulations, but 2° is the generally acceptable value by flight crews and regulatory agencies. Magnetic heading was specified to be synthesized using a stored worldwide magnetic field model for magnetic variation computation. This would eliminate the magnetic field sensing hardware components used in the current commercial fleet.

However, Boeing did not have a requirement for long range navigation performance at the time of launching the 757/767 two engine medium range airplanes. Therefore, to keep the expected system costs to acceptable, the navigation performance was specified to be 4 nm/hr, 95%. This performance was still expected to provide velocity performance that was acceptable for flight control, guidance, and display purposes. Fortunately, the 767/757 airplane contract competition resulted in obtaining a system with the navigation performance required for lony range navigation. The 757/767 airplane suddenly had long range navigation capability that could be offered to customers at no extra cost. It turns out that this capability had more demand by airlines than ever anticipated, especially the foreign carriers who have routes over regions without radio navigation coverage.

Alignment

The alignment time requirement of 10 minutes is about 1/2 that of commerical gimbal inertial navigation systems and stems from the desire of the airlines to minimize align times during the small turn around time operations that short to medium range operations have at through-stops. It also is the time felt to be achievable with sensors without temperature control and still provide sufficient alignment accuracy needed for good navigation. Boeing demonstrated 8 minutes in its strapdown research program.

Vertical Velocity

Vertical velocity is specified to be output from the 757/767 inertial systems as the primary source of airplane vertical speed, an industry first. No air data computer derived vertical speed is used on the airplane as is normally done.

A baro-inertial velocity and altitude filter was specified to be implemented to provide low noise, wide bandwidth signals with no lags in response to airplane maneuvers or configuration changes and optimized for autopilot control laws. This feature also allows the vertical speed indicator to be less complex and error free in turns due to the elimination of a seismic mass used for damping noisy air data computed vertical speed, which is differentiated altitude. This feature has been particularly applauded by flight crews. The basic accuracy is specified to be the same as that for commercial airplane air data computers vertical speed, 30 ft/minute.

Output Data Filter Characteristics

To prevent data aliasing effects in using digital systems which operate generally at a lower sample rate than the inertial reference system, anti-aliasing pre-sample filters were specified for the output parameters with special emphasis on the body rate and acceleration data. The final choices of sample rate and pre-sampling filter depend upon the input signal and noise spectra, maximum allowable signal-to-noise ratio degradation due to aliasing, maximum allowable transport delay, available computational resources, and the bandwidth of the system which uses the data. A practical way to make these choices is to analyze the system for various sample rates and filters. This was done with the aid of a computer program which computes the effect of each combination of sample rate and filter characteristic on the output signal-to-noise ratio for the defined input signal and noise spectra.

Transport delay or equivalent phase shift in the data to the different control systems was the primary design constraint used to develop acceptable filter characteristics, although there are three interrelated parameters that must be specified to assure dynamic interface signal compatibility. These are maximum bandwidth, maximum transport delay and minimum sample rate. Examination of airplane structural vibration power spectral densities were used as the assumed noise source in determining the filter characteristics required. The results of the analyses indicated that second order Butterworth filters with a 3 dB bandwidth of 3.2Hz were needed to provide acceptable anti-aliasing characteristics (-20 dB at the autopilot foldover frequency, 10Hz) for both body rates and acceleration data, and still have transport delays which were satisfactory to the control system designs. Analog or digital filtering may be used depending on sensor signal characteristics. For example, the laser gyro output is essentially digital in nature and the body rate filters could be implemented in software. The accelerometers are analog devices and the anti-aliasing filters were implemented with analog circuitry prior to sampling with an A/D multiplexer to develop the acceleration data for the control system users. These anti-aliasing filters are not in the data flow to the attitude and navigation solutions.

Reliability

Reliability requirements were daveloped based on the predicted MTBFs provided by the competing suppliers in their proposals and the results of in-house strapdown system synthesis studies, which permitted a paper design to sufficient detail that a reliability estimate could be made from the parts count. Reliability estimates of 4000 to 5000 hours MTBF were predicted to be achievable. Compliance with certification regulations require in-flight MTBFs to be in the range of 1000 to 2000 hours MTBF. This requirement is developed from the US Federal Air regulation FAR 25.1309(b) which is a general failure requirement for all airplane systems. When specifically applied to the inertial reference system, the regulation has been interpreted by the FAA to require that the total loss of the airplane's primary attitude systems be "improbable". Improbable has been quantified by the FAA to be an event with a probability of occurrence of approximately 10^{-5} - 10^{-6}.

Consequently, dual independent attitude systems with reliabilities of about 1000 hours MTBF each will satisfy the regulation. However, when adding in other attitude data dependent components such as displays, requires raising the inertial system reliability requirment above 1000 hours to satisfy the availability requirement for the entire attitude data "chain".

Warranty/Component Reliability (MTBUR/MTBF) Programs

The airframe manufacturer, Boeing in this case, is contractually obligated to obtain the best possible product assurance package for the customer airline as is possible with the supplier. This package is passed on to the customer, who may elect to negotiate their own specific package, including warranty terms and MTBF (mean time before failure) and MTBUR (mean time before unscheduled removals) targets that may be somewhat better than those obtained by Boeing. Leverage is high, of course, for the airline and Boeing in the competitive phase of a new airplane program. The warranty period typically is three years for electronic systems including the inertial reference system, starting with delivery of each aircraft. Remedies under the supplier's warranty involve repairing, modifying or replacing the defective part.

The reliability "guarantee" program is also a controlling mechanism for determining which party (airline or supplier) pays for maintenance. This is commonly termed, "Supplier Component Reliability (MTBUR/MTBF) Program" and establishes MTBF and MTBUR contractual targets or "guarantees." Remedies include technical assistance, redesign and additional spare parts at no charge. This program runs for a period of five years, starting with the introduction of the new airplane into revenue service (September 8, 1982 for 767). The program concept is based on obtaining mature level values (MTBF and MTBUR contractual targets) during the introductory period of each new airplane program, however, in the case of electronics/avionics suppliers, many have insisted on introductory values only or "guarantee" steps at several time intervals during the five year program. For the IRS, these "guarantee" MTBF/MTBUR steps are the following in flight hours:

YEAR	1	3	5
MTBF	1600	2000	2400
MTBUR	800	1000	1200

As one will see later in this paper, these goals have been surpassed by more than five times for the first year of service. They represent the conservatism expected for the introduction of such a new, sophisticated technology.

BOEING AIRPLANE IRS CONFIGURATIONS

Figure 7 shows the 757/767 IRS configuration. The basic installation has three Inertial Reference Units (IRU) and a single, common Inertial Reference Mode Panel (IRMP) for initializing and displaying data from any of the three IRUs. The triple system is required to support the fail-operational auto-land system, a basic feature in the 757/767 airplanes. However, only dual systems are required for airplane dispatch. To maintain the inertial reference during power interrupts and transients, the IRUs are connected to the airplane Hot Battery bus, a non-interruptible backup power source. This was possible because of the low power (100 watt) requirements of the IRU. Because of their large power requirements, INS in commercial service (e.g. 747) require their own independent battery. Additionally, the IRS was specifically designed for installation in a commercial jet transport in accordance with the ARINC 704 airline standard specification. (Ref. 3, 4)

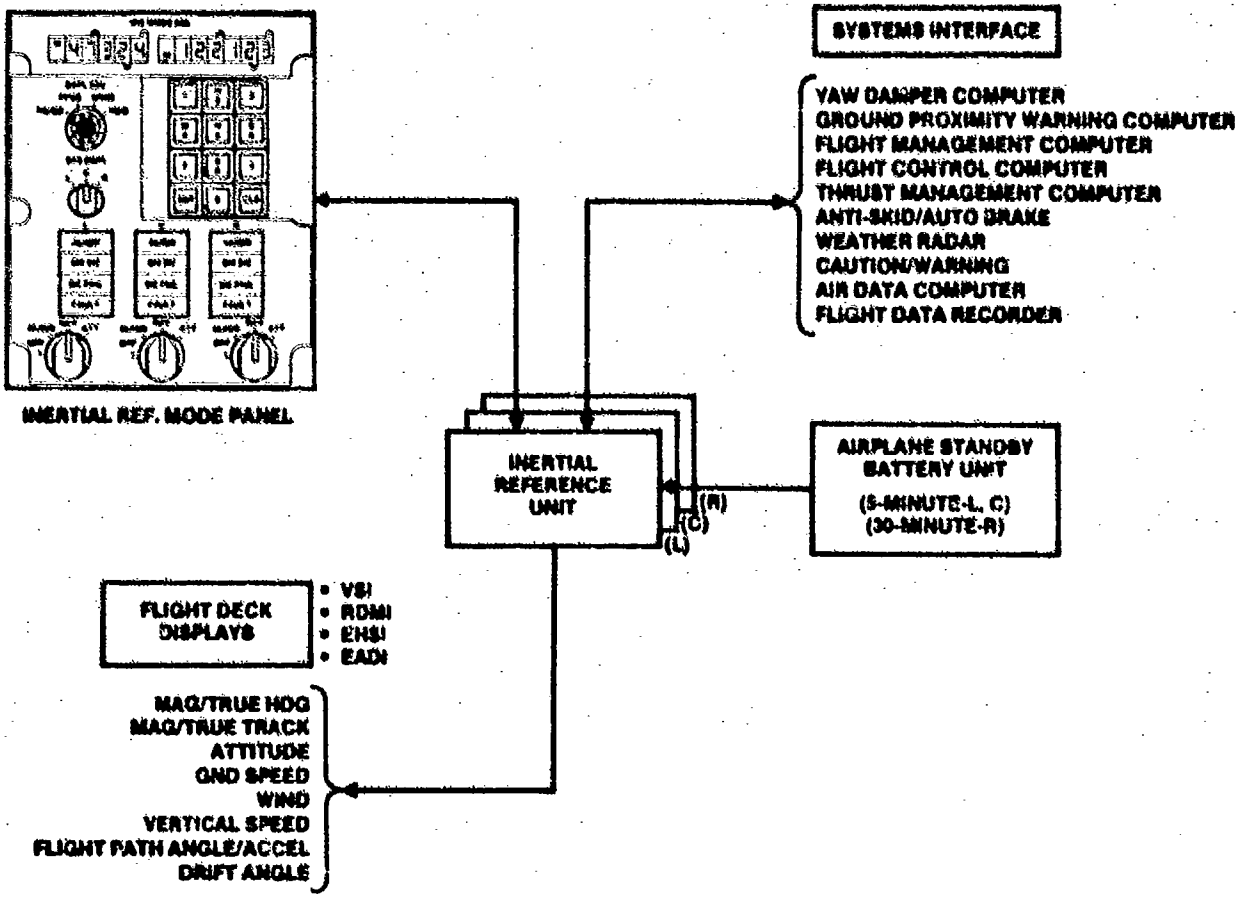

Figure 7. 757/767 Inertial Reference System

Figure 8 shows the 737-300 IRS configuration which differs from the 757/767 configuration because of the analog interfaces in the 737 derivative airplane. A digital to analog adapter unit had to be designed to handle the conversion requirements of the IRUs and Flight Management Computer which are built to the 757/767 specifications, for these systems. A dual IRU configuration is utilized on the 737 because the autoland system requirements are less stringent than the 757/767, being fail-passive as opposed to fail-operational.

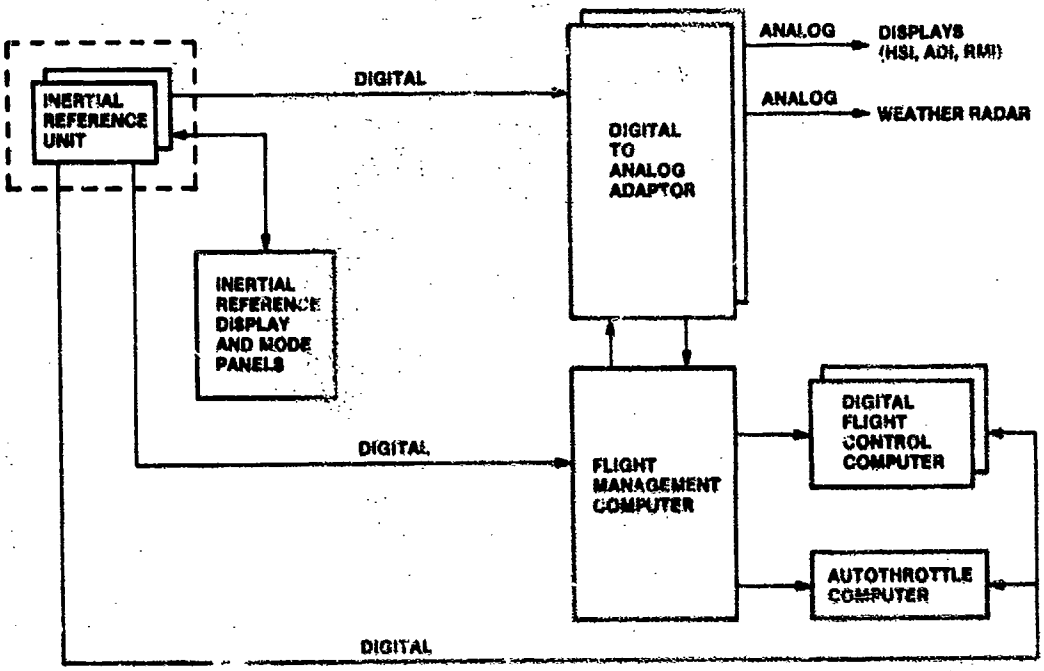

Figure 8. 737-300 Inertial Navigation System

The 757/767 IRS fulfills a wide variety of airplane system requirements, as shown in the Figure 9 system interface diagram. From this diagram, one can see the degree of integration and systems' dependence on inertially derived data to satisfy their respective functional and performance requirements. The 737-300 IRU integration is significantly less because of the airplane interfacing systems' design maturity.

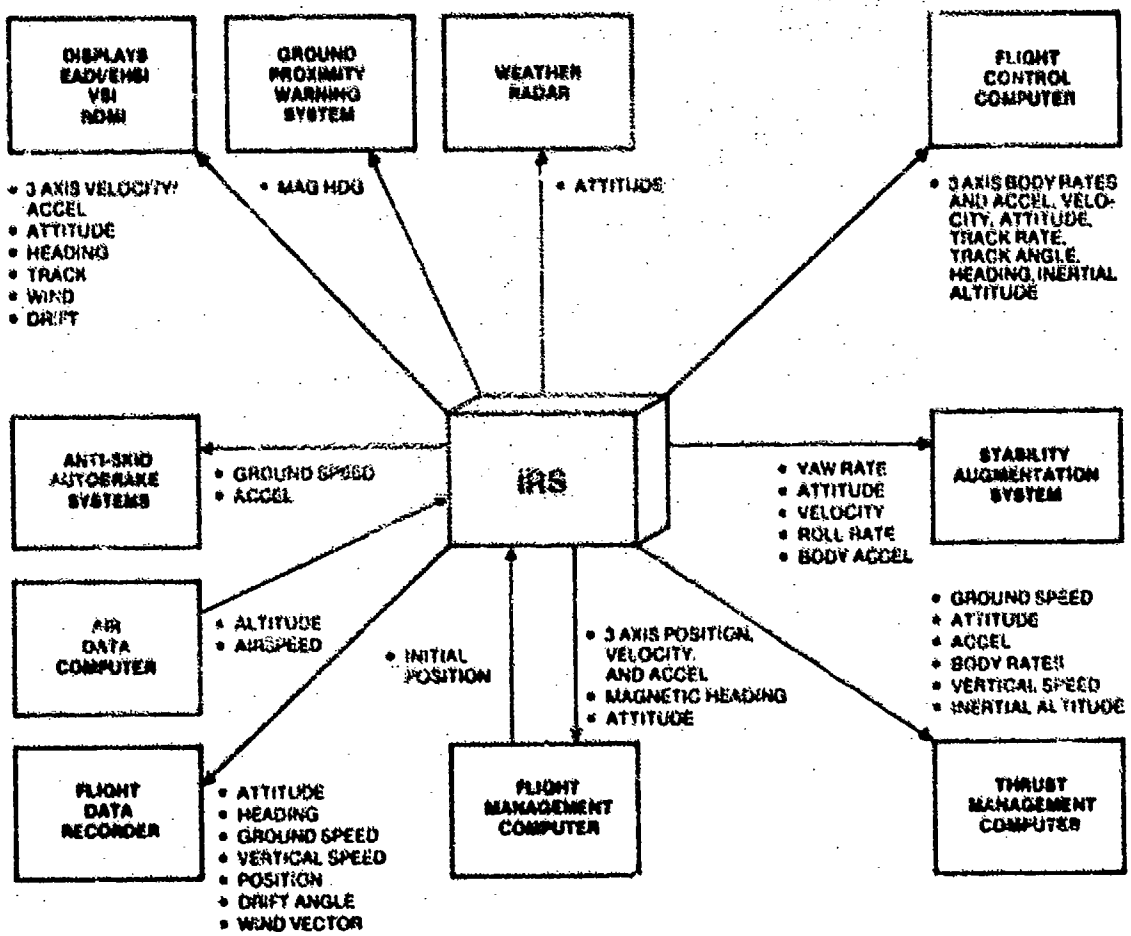

Figure 9. 757/767 IRS Interface Diagram

The original goal to eliminate all the separate inertial sensors utilized in flight control systems has been realized on the strapdown inertial equipped airplanes. It is believed that the 757/767 airplanes represent the first occurrences in aviation history of this long sought objective. The only independent inertial sensor remaining is the normal accelerometer for the flight data recorder which is required by Federal regulation to be mounted in the vicinity of the airplane center of gravity.

The inputs the IRS requires are latitude and longitude for initialization and air data altitude and true airspeed for the baro-inertial filter and wind vector calculations, respectively.

The airplane's Flight Management Computer (FMC) provides the guidance function; therefore, the only navigation data provided by the IRS are position, velocity, track and heading. The FMC has knowledge of waypoint and route data requested by the flight crew and computes guidance commands from this desired route data and actual position data which varies from radio (VOR-DME) updated inertial information to pure inertial information. Figure 10 shows an overview of the entire 757/767 navigation and guidance system.

Each IRU produces digital data according to the ARINC 429 serial digital data bus format on three identical independent broadcast data buses to the airplane systems. The effect of a bus fault is isolated to only one output bus, and therefore only one of the three classes of using equipment, critical, essential, non-essential is affected. Two busses are dedicated to flight control and displays systems, and all other less critical systems are connected to the remaining bus.

The data bus architecture is shown in Figure 11. This bus distribution was designed to prevent any single point failure from causing the loss of IRU data to any flight critical system.

Figure 12 shows the location of the IRUs in either the 757, 767 or 737-300 in the basic electronics bay of the airplane. The units are hard mounted in a special alignment mounting tray designed to maintain the redundant systems' relative alignment to each other. The mounting tray is hardmounted to the airplane floor for rigidity and is aligned to the airplane reference axes during the factory build process. All alignment tolerances, relative and absolute (tray to airplane) are 12 minutes of arc.

The IRU, shown in Figure 13, is packaged in a 10 MCU size box, as required in ARINC 600, "Air Transport Avionics Interface", which includes the inertial sensors and various supporting electronic assemblies. The dimensions of the unit are 7.6 inches high X 12.7 inches wide X 14.5 inches long. Unit weight is approximately 44 pounds. This installation is in accordance with that specified in ARINC 704. The units are being installed in any of four possible orientations (fore, aft, and athwartship) in Boeing airplanes. Installation wiring (pin logic) is used to specify each orientation and no internal modification to IRU hardware or software are required.

Forced air cooling is provided in accordance with ARINC 600 Level 2 and adequately supports the power dissipation (approximately 100 watts) requirements for each unit. No active control of internal thermal state is required. The IRU utilizes strategically mounted thermal transducers to generate data for inertial sensor corrections due to variations in internal temperature.

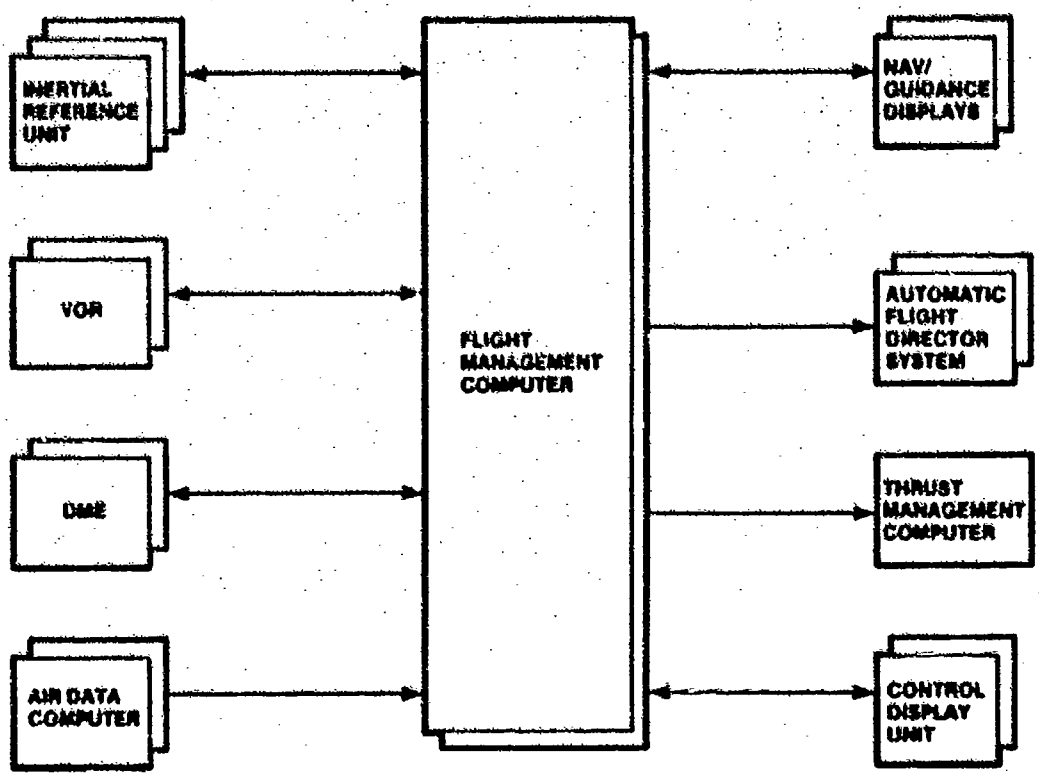

Figure 10. 757/767 Navigation System

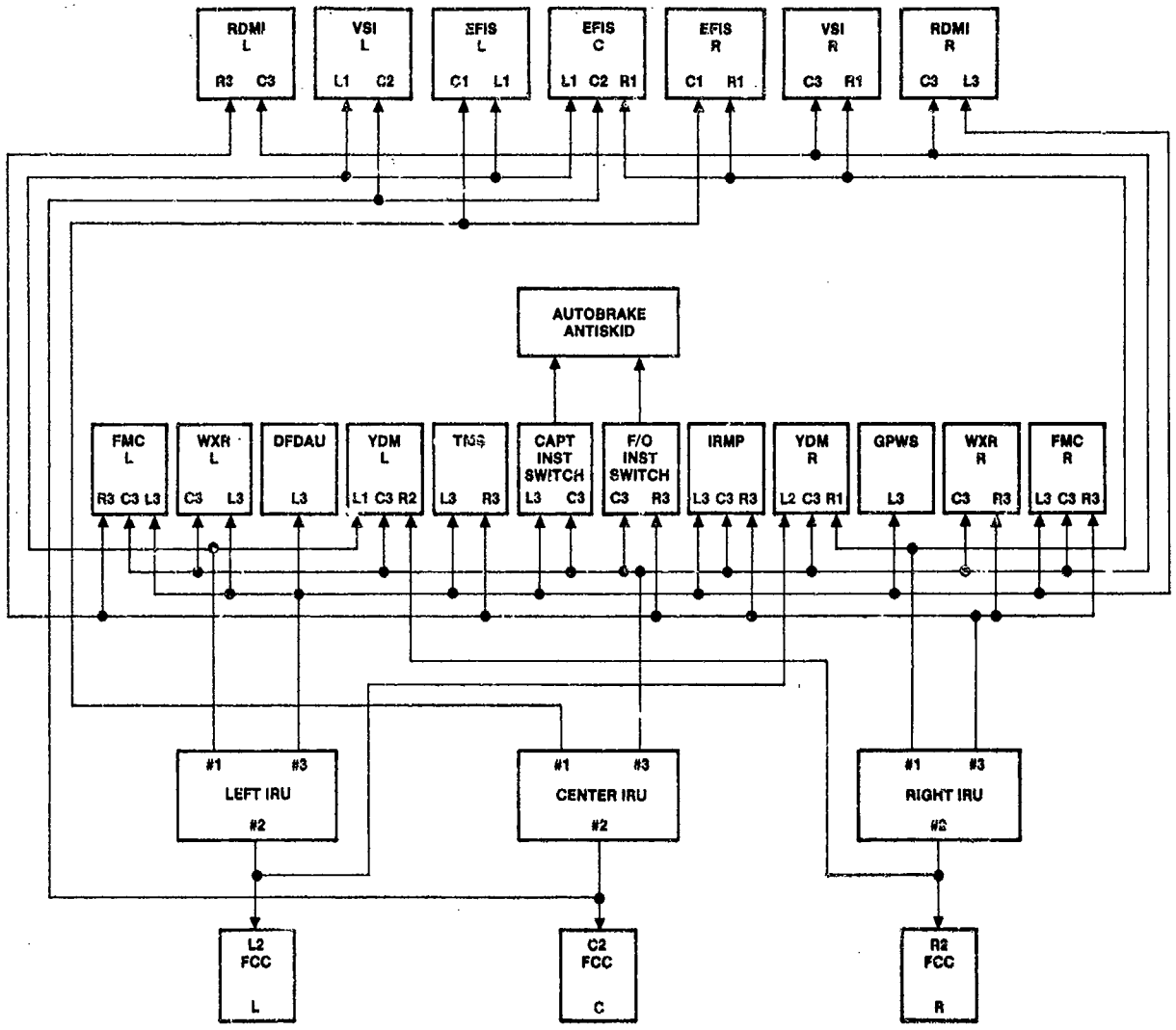

L1, L2, L3 — LEFT IRU DATA BUSES

C1, C2, C3 — CENTER IRU DATA BUSES

R1, R2, R3 — RIGHT IRU DATA BUSES

Figure 11. IRS Data Bus Distribution Diagram

Power is supplied from normal airplane AC power systems with abnormal transient protection provided by the airplane standby battery. Two IRUs are capable of being powered 5 minutes and the right IRU for a minimum of 30 minutes from this battery. The power organization is shown in Figure 14. The airplane main battery is protected from the full 3 IRU load during a total A-C power loss by limiting the L & C units to 5 minutes.

The remaining unit is maintained to provide heading information to the pilot displays for this flight condition, as long as is necessary.

757/767/737 IRU DESIGN FEATURES

The functions in the specific strapdown IRU for Boeing airplanes are divided between hardware and software as shown in Figure 15. Laser gyros and conventional pendulous forces rebalanced accelerometers provide the inertial data required for the attitude reference computation and the inertial navigation computation. These inputs are conditioned and accumulated by the sensor input electronics. The digital computer performs the software functions of sensor systematic error compensation of bias, scale factor, misalignment, and temperature effects. The compensated gyro signals are used in a three-axis attitude algorithm to compute aircraft attitude relative to the local level navigation coordinates. The compensated acceleration signals are transformed into the local-level coordinate frame and are used to compute the velocity and position navigation data. The software function of output calculation and parallel data formatting is followed by the hardware functions of parallel to serial conversion, data bus timing, and electrical signal isolation and transmission. Body rate and acceleration data are passed through anti-aliasing filters as shown, prior to outputting these data on the data bus.

Two features or functions are provided by the IRU which prior to the 757/767 application had never been certified on commercial aircraft as sole source of these functions. These functions are vertical velocity and synthesized magnetic heading.

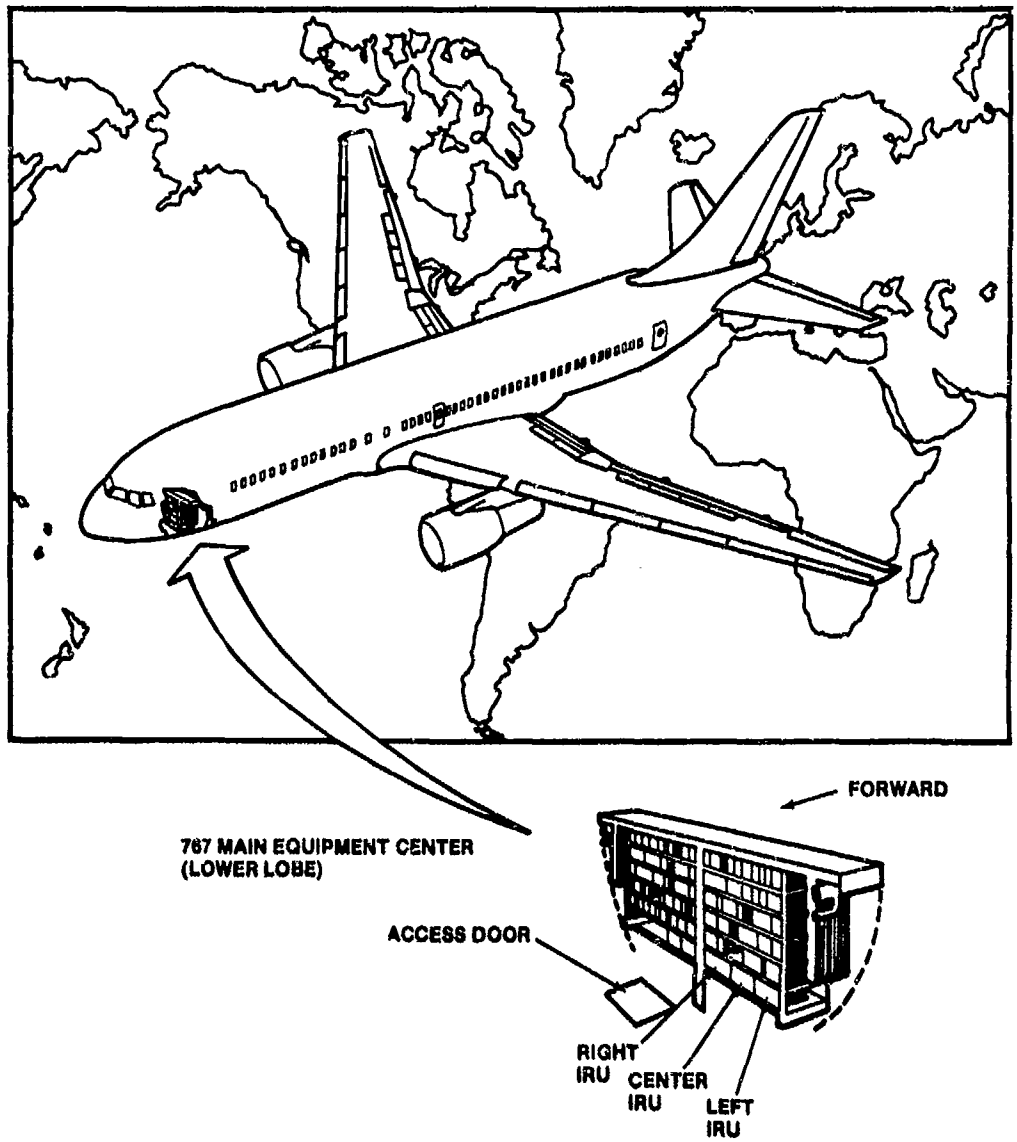

Figure 12. IRU Airplane Installation Location

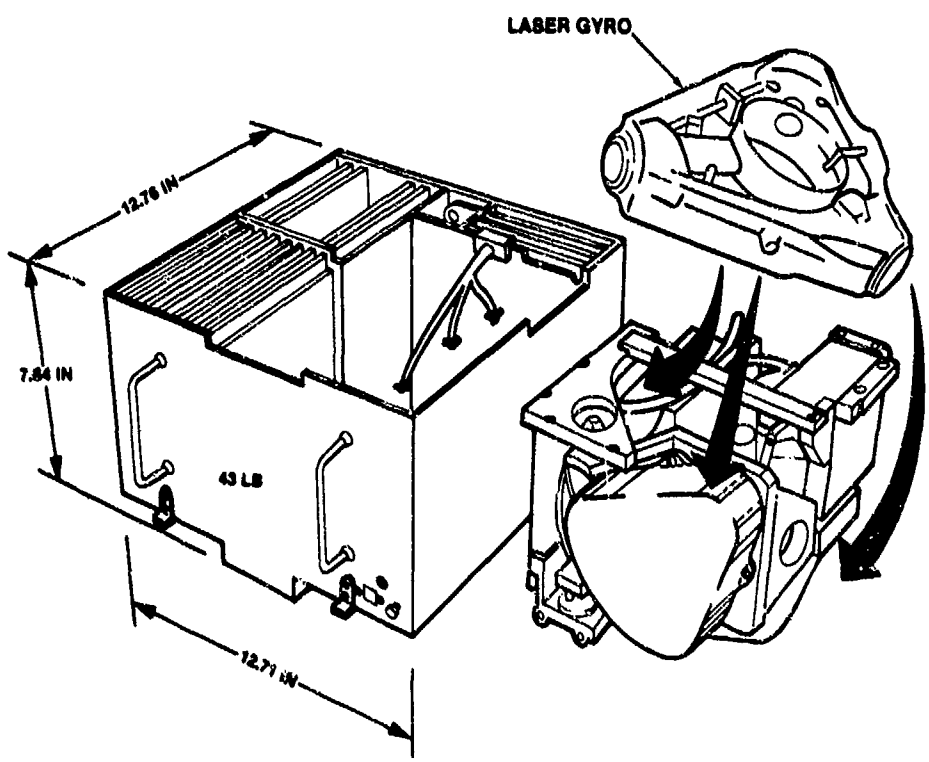

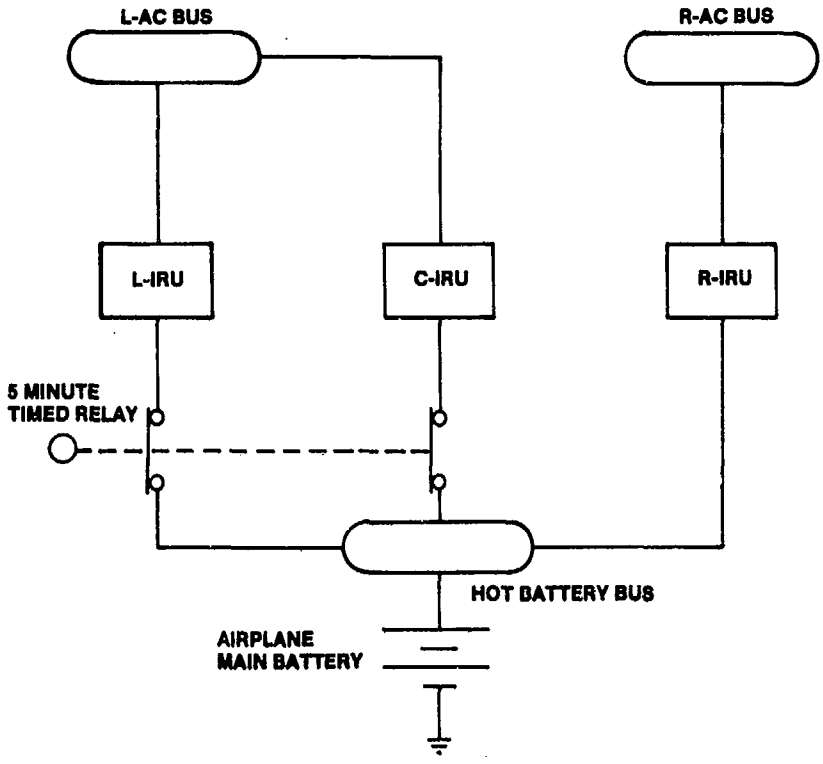

Figure 14. 757/767 IRS Power Sources

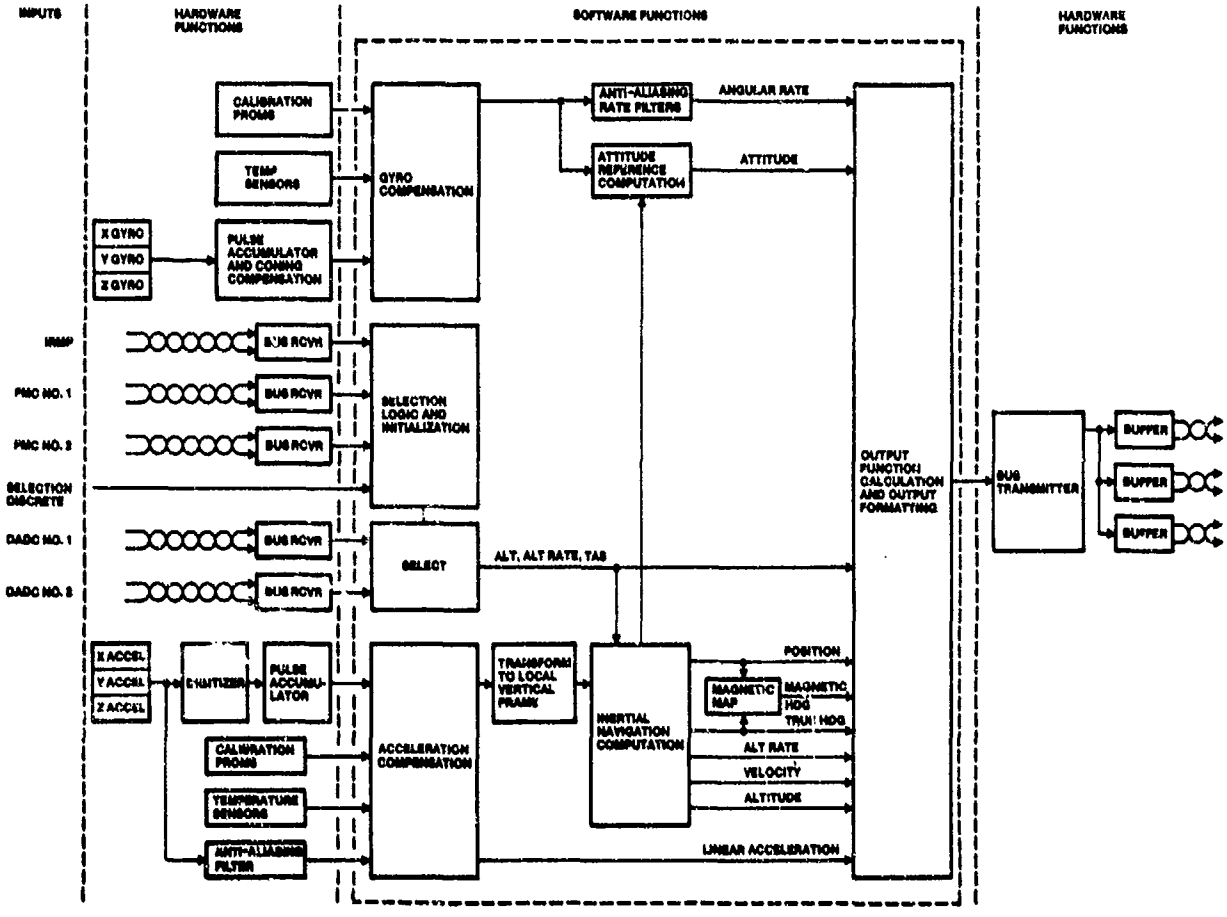

Figure 15. IRU Signal Flow Diagram

Complementary Baro-Inertial Filter. The altitude input from the air data computer is used to stabilize the vertical channel in a complementary filter with inertial vertical acceleration as shown in Figure 16. This mechanization provides a wide bandwidth, inertially smoothed output of altitude and altitude rate. The altitude rate, vertical speed, is used to drive the pilots' vertical speed indicator and is used by the autopilot and flight management computer for various control functions, as is inertial altitude.

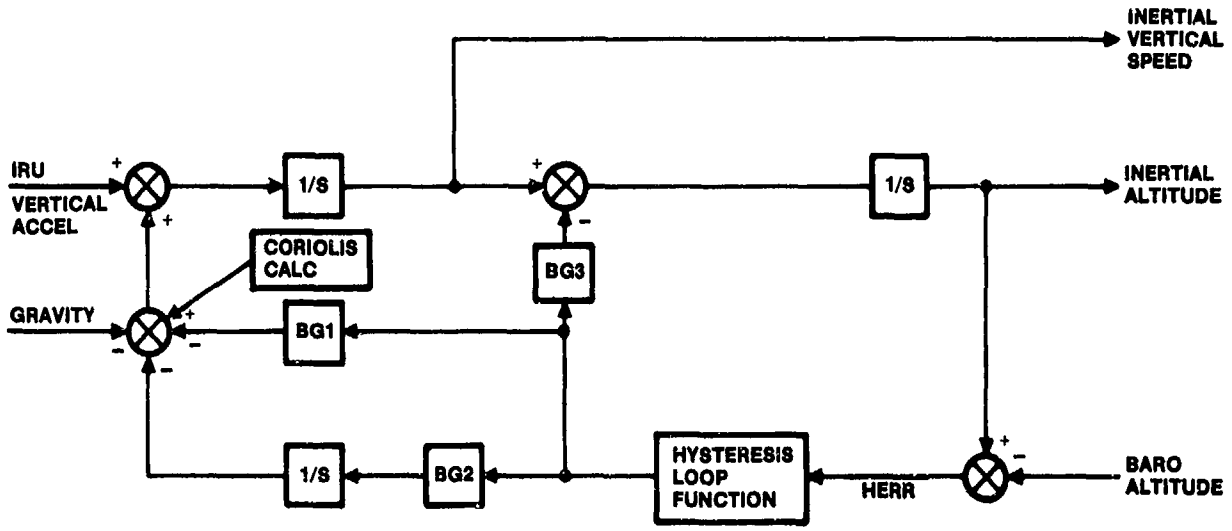

Figure 16. Complementary Baro-Inertial Filter

This implementation is designed to utilize the high frequency response characteristics of the accelerometers to reduce the normal lag in air data parameters which occurs during altitude changes. The hysteresis loop provides dampening of feedback loops to limit overshoots and minimize settling times with large step inputs of altitude. These steps can occur during ADC source switching and during periods of no ADC data.

This feature has provided very low noise vertical speed data to the crew displays without any lags or maneuver induced-errors and has been very well received by flight crews.

Synthesized Magnetic Heading. Magnetic heading output from the IRS is derived from a lookup table of magnetic variations stored in memory. This stored table forms a grid of points which is used in an interpolation scheme based on known latitude and longitude. The table of grid points is generated from a twelfth order spherical harmonic equation using the most up-to-date world magnetic field model being used for aeronautical charting and cartography. The current model available is for 1980 (AWC80). To compute magnetic heading, four grid points are chosen which surround the aircraft and a linear interpolation is performed using the variations at these grid points. A description of this technique is shown in Figure 17. This interpolated variation is then added to true heading to get magnetic heading. To minimize data storage with this approach, the latitude data was limited to an operational area encompassing all the magnetic north referenced ground navigation aids, in the latitude range of N73° to S60° where large transport service is available. This approach uses the same magnetic field model reference for the IRU as that used for aeronautic facilities and charts, insuring compatibility. This is shown pictorially by Figure 18.

There are two sub-modes to the Boeing specification for strapdown inertial that should be explained. One is new to commercial operations, and the other is similar to that mechanized in gimbal INS. These are downmode align and attitude modes.

Downmode Align

A provision is made for re-entry of the align mode from a prior navigation mode condition without turning the system off. When the mode switch is rotated from the NAV to the ALIGN position and ground speed is less than 20 knots in this situation, the course alignment function is bypassed and the attitude reference vertical data, available from the navigate mode calculations, is transferred over as initial conditions for the alignment mode operations. For this situation, the alignment filter is reconfigured to perform its computation optimally from the more accurate initial conditions derived from the navigate mode data to achieve a more rapid alignment sequence.

This action should normally be performed on intermediate short stops when the IRS is left operating and insufficient time is available to perform a complete 10 minute alignment to correct existing alignment errors. The procedure can also be used to trim errors during extended waiting periods for takeoff or during delays prior to departure.

The result of this action is to remove the velocity errors (set groundspeed to zero) and to re-erect the navigation reference coordinate frame to level (remove pitch/roll attitude errors). Errors in position can also be corrected if the option to re-enter ramp latitude and longitude is also exercised. This is normally done when the flight plan is loaded into the FMC.

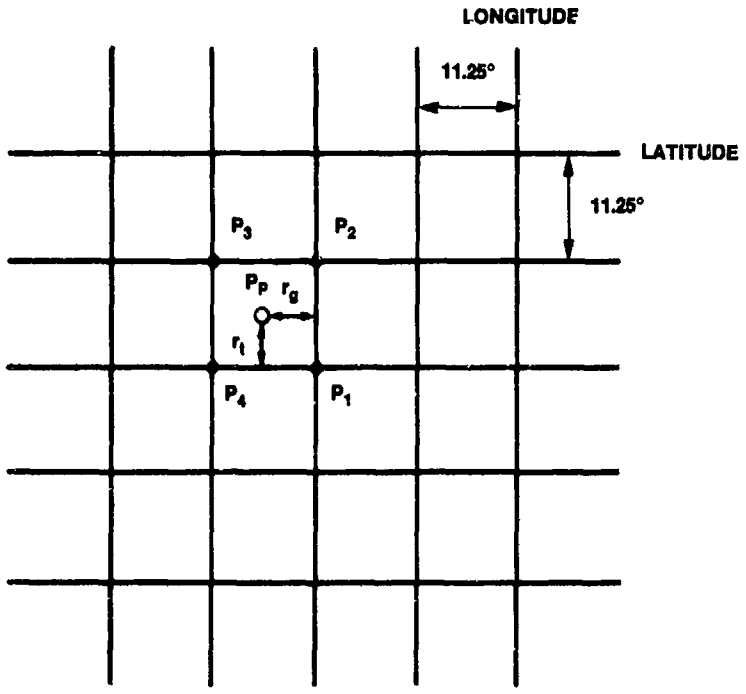

$$MV_P = MV_{P1} + r_l\left[(MV_{P2} - MV_{P1}) + r_g\,(MV_{P1} + MV_{P3} - MV_{P2} - MV_{P4})\right] + r_g\,(MV_{P4} - MV_{P1})$$

Figure 17. Magnetic Variation Model

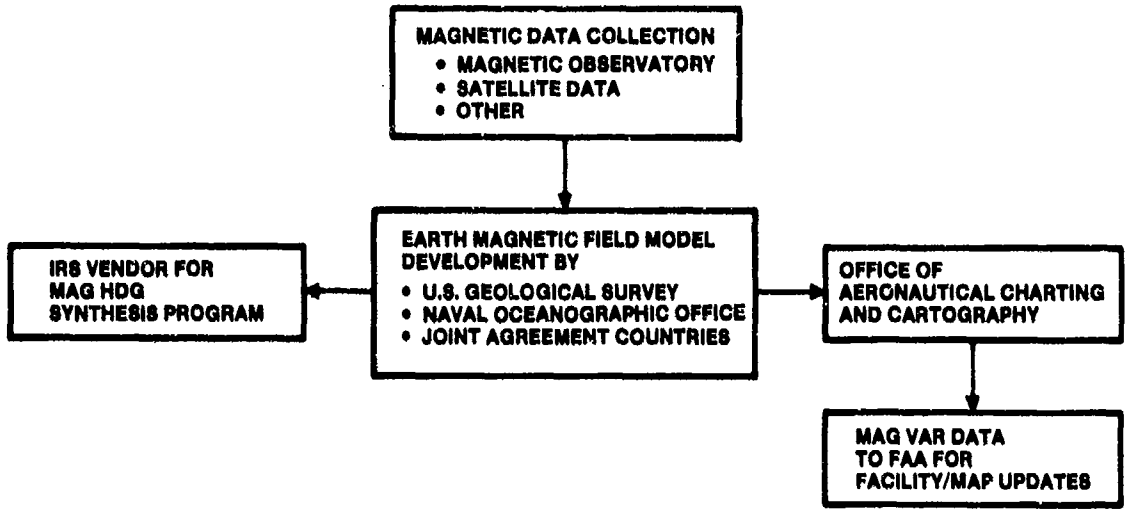

Figure 18. Magnetic Variation Development Process

The duration of the align downmode is 30 seconds following activation, or whenever the mode select switch is rotated to the NAV position, whichever is greater.

If the IRU is allowed to remain in the align mode for a period greater than 30 seconds, the alignment filter will begin to correct aircraft heading. However, the difference between this procedure and the normal align is that NAV mode can be entered at any time and the normal 10 minute waiting period is not required. In this situation the degree of refinement of the prior NAV mode heading will be a function of the operating time in the align mode.

Attitude Mode

The attitude mode provides a backup reversionary capability to allow restoration of IRU attitude operation during flight for the potential condition of total power loss and then power restoration after a period of time that exceeds the battery or inertial system energy storage capability.

The primary function of the attitude mode is to provide a minimal set of flight critical outputs sufficient to support aircraft operation.

The basic attitude mode operating elements (Figure 19) consist of two integration functions (attitude and velocity) driven by strapdown gyro and accelerometer sensor data and interconnected through appropriate feed-forward and feed-back elements to execute the attitude mode functions. Outputs of these elements when appropriately operated upon, provide the signals required for IRU output.

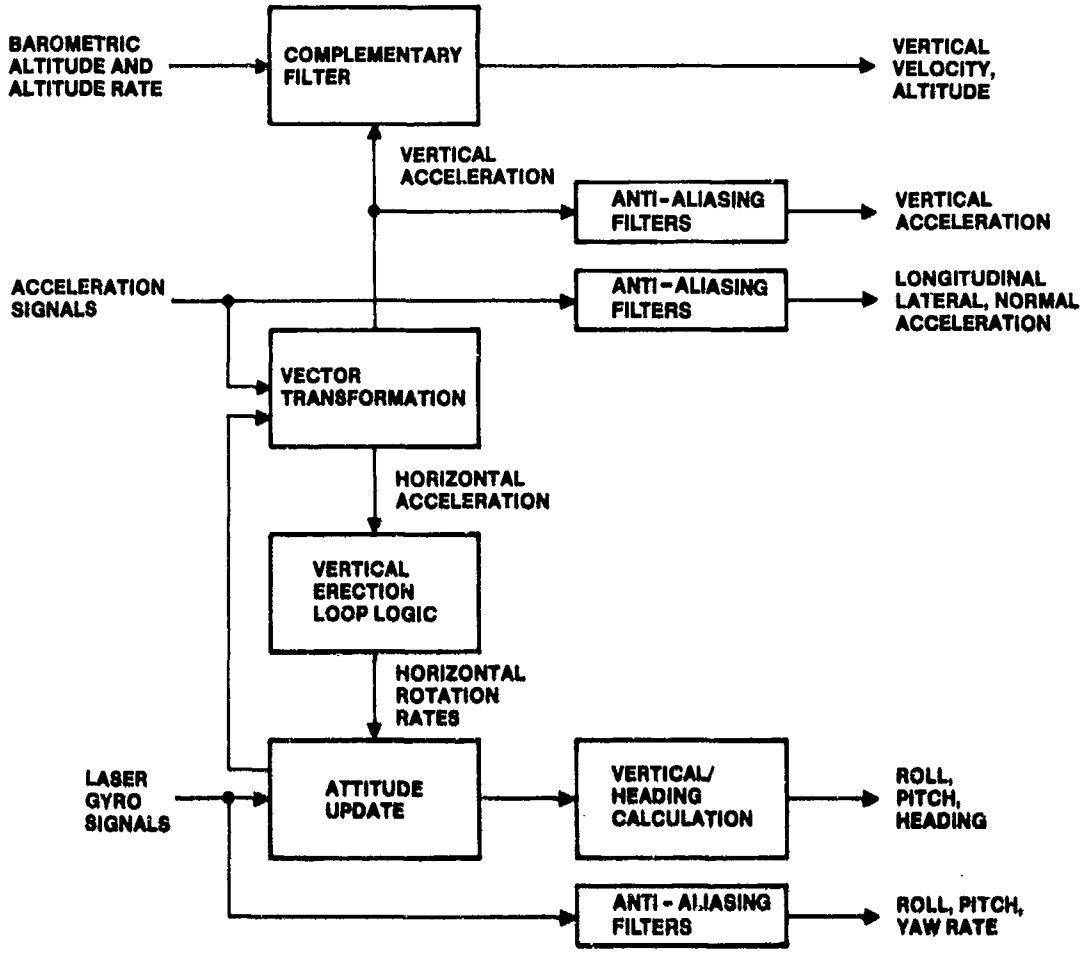

Figure 19. IRS Attitude Mode

The attitude function is identical to that performed in the navigate mode, except for heading which is space stabilized, but set to zero at attitude mode entry and not output until initialized with a reference heading. The IRU design provides the capability of entering a "set heading" input, via either the FMC CDU or the inertial mode panel to align IRU magnetic heading output to actual aircraft magnetic heading.

The velocity function is implemented in a manner different from the navigate mode and is used to maintain erection of the reference coordinate frame to the local level attitude. The attitude output is affected, in this mode, by horizontal components of acceleration due to aircraft turns and erection cutout logic is implemented to minimize attitude errors resulting from this cause. This mode provides attitude and heading analogous to a conventional vertical and directional gyro in current aircraft.

Inertial Reference Mode Panel (IRMP) Configuration

The IRMP contains the manual input and display functions necessary to control and to initiate the three (or two) IRUs contained in the IRS. To maintain the multi-channel redundancy concept, the mode control and annunciation-and-warning functions are completely separate for each channel. The initialization and display functions are common for all channels, with the exception of the IRU signal interfaces that maintain complete electrical signal isolation - so that a fault in the IRMP on one of the IRU interfaces will affect only one IRU.

The functions are partitioned between hardware and software as shown in Figure 20 for the 757/767 panel. The mode select and data input are hardware functions that convert manual entries into electrical signals. The ARINC 429 serial digital data input and output data bus interfaces are also contained in hardware. The input data processing, the display format processing, and the output data process and format are provided by the IRMP software. The 737 control panel is very similar with the primary difference of only handling 2 IRUs rather than 3.

The panel as viewed from the pilot is shown in Figure 21, again for the 757/767 unit.

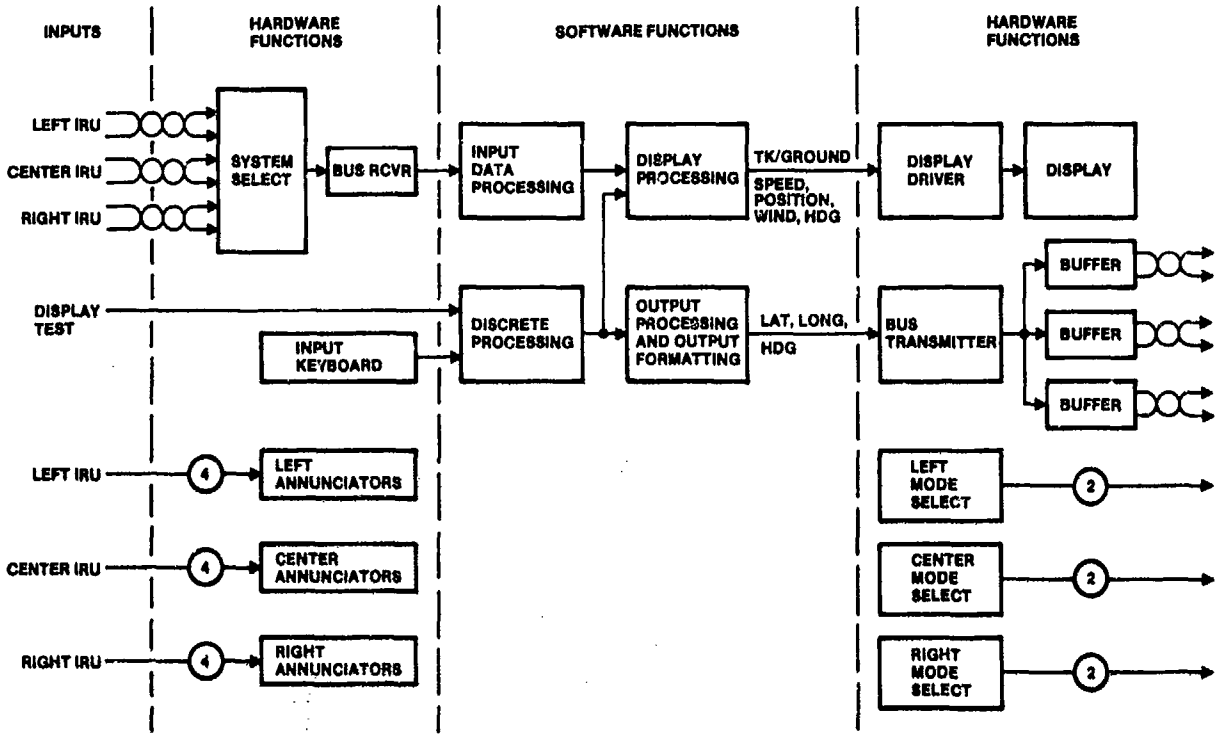

Figure 20. Inertial Reference Model Panel Signal Flow Diagram

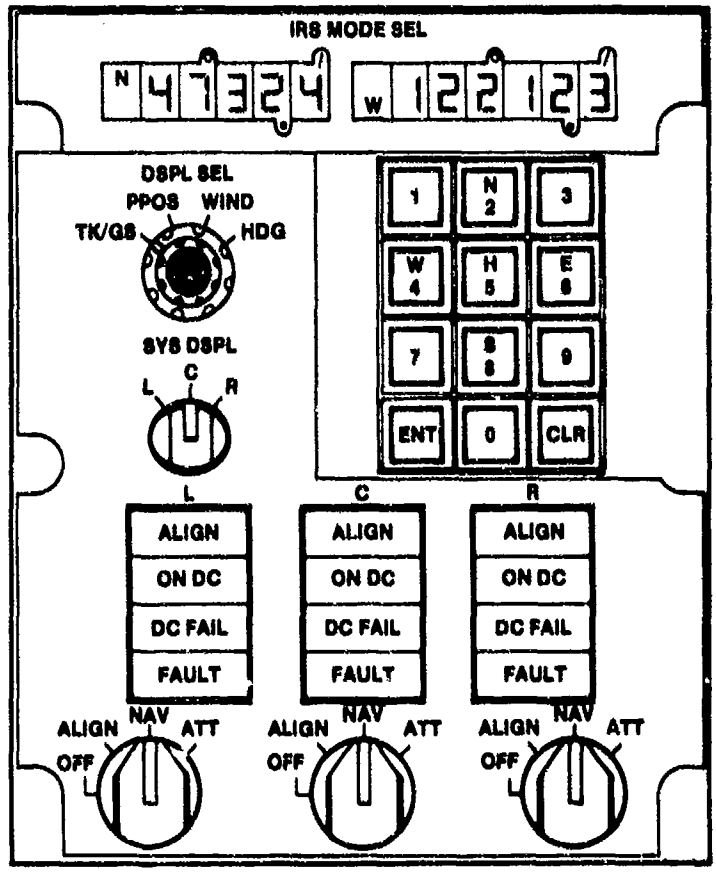

Figure 21. Inertial Reference Mode Panel, 757/767 Airplane

IRS Operation

The IRS provides all the strapdown, inertial reference outputs required for the avionics system in the serial digital format defined by ARINC 429. These outputs are shown in Table 13.

The data is computed in a multi-rate structure in accordance with the software design and is interrupt driven at 50Hz. Attitude, accelerations, and most rate parameters are output at 50 samples/second. Velocity, heading, and related terms are output between 10 and 25 samples/second depending on user requirements. Position data is output at 5 samples/second.

Data Computation Description

Navigation

In the strapdown inertial system accelerometers and gyros are "fixed" to the airplane structure. The angular rates and linear accelerations as measured by the body mounted sensors are sent to the digital computer which continuously computes the airplane attitudes of roll, pitch and true heading and maintains the navigation coordinate system (stable platform) from the information obtained by the angular rate sensors (gyros). This data and computation flow is shown in Figure 22.

Table 13. IRS Output Data

Function	Range	Accuracy (2 Sigma)
Attitude		
Roll	Unlimited	0.1°
Pitch	Unlimited	0.1°
Heading		
True	Unlimited	0.4°
Magnetic	73°N - 60°S	2.0°
Body		
Linear accelerations	4.0g	0.01g
Lateral	4.0g	0.01g
Normal	4.0g	0.01g
Longitudinal	4.0g	0.01g
Body angular rates (P, Q, R)	128°/sec	0.1°/sec
Inertial velocity		
V_N	4 096 kn	12 kn
V_E	4 096 kn	12 kn
V_G	4 096 kn	12 kn
V_Z	32 000 ft/min	30 ft/min
Track related data		
Track angle	Unlimited	5° (low speed)
Drift angle	60°	5° (low speed)
Flight path angle	Unlimited	0.4° (low speed)
Flight path acceleration	0.5g	0.01g
Along track acceleration	0.5g	0.01g
Cross track acceleration	0.5g	0.01g
Vertical acceleration	4.0g	0.01g
Track angle rate	32°/sec	0.25°/sec
Present position (lat/long)	Unlimited	2 nm/hr
Inertial altitude	131,000	5 ft

The gyro data, taken into the IRU computer from the three orthogonal IRU laser gyros, is used to compute three orthogonal body inertial rotation rate signals. Compensations are included in the body rate calculations to correct the input data for known fixed and temperature sensitive error effects. These temperature compensations are calculated using measurements obtained from gyro-mounted temperature transducers.

The orthogonal body rate data is used in a three-axis integration algorithm to compute the attitude of the IRU sensor axes ("body axes") relative to a locally level navigation coordinate frame. The navigation frame is the "wander azimuth" type whereby the z-axis is vertical and the orientation of the horizontal X, Y axes about Z is inertially stabilized. In order to maintain reference of the computed attitude to the locally level navigation frame, angular rates are applied to the attitude integration algorithm to account for the inertial rotation rate of the navigation coordinate axes. The navigation frame inertial angular rates account for aircraft transport rate over the earth as well as earth's rotation rate (the latter being a function of computed aircraft position).

The computed attitude data is used to transform a calculated set of three-axis orthogonal body acceleration data from body axes into navigation coordinate frame axes. The three-axis body accelerations are computed from inputs from the three axis orthogonal accelerometer data. Appropriate compensations are applied to the body acceleration signals to correct for known fixed and temperature sensitive errors. The temperature compensations utilize measurements obtained from sensor-mounted thermal transducers.

The transformed body acceleration data are integrated to derive measurements of aircraft velocity components in navigation coordinate axes. Prior to integration, corrections are first applied to the transformed accelerations signals for Coriolis acceleration effects and to compensate for gravitational acceleration along the vertical axis. The gravitational acceleration compensation is based on calculated aircraft altitude and position. To prevent vertical channel divergence under sensor error conditions, Air Data barometric altitude is mixed with inertial velocity for the vertical channel computation elements through a complementary filter. Inertial vertical speed and aircraft altitude are derived from this filter.

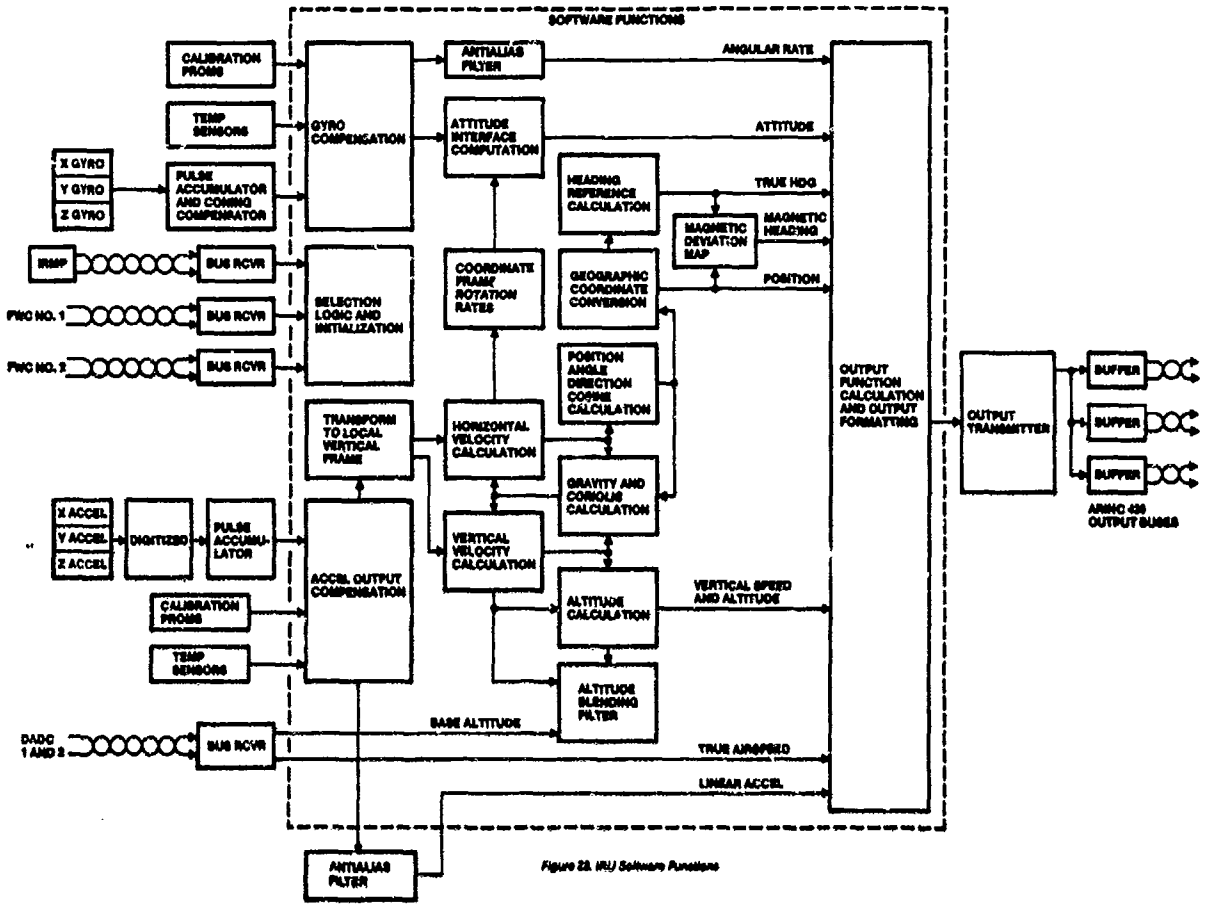

Figure 22. IRU Software Functions

The computed aircraft velocity in navigation frame coordinates is operated upon to calculate the instantaneous horizontal angular rotation rate of the locally level navigation coordinate frame relative to earth fixed coordinates. These rates are then integrated using direction cosines to compute aircraft position over the earth in the form of the orientation of the navigation frame relative to earth fixed coordinates. The navigation frame Z-axis angular orientation relative to earth fixed coordinates defines the aircraft position. The X, Y navigation axes orientation data relative to the earth fixed coordinates (i.e. wander angle) defines the true north reference for navigation output data. The aircraft orientation relative to earth coordinates requires an additional transformation from body to navigation axes using the body axis direction cosine matrix, derived from gyro data.

The IRU output functions during the navigation mode are derived from the body rate, body acceleration, attitude, velocity, and position data developed during the above described navigation operations. Additionally, the output function calculations incorporate a magnetic variation computation for use in referencing output data to magnetic north rather than true north. The magnetic variation data is a computed, as a function of calculated aircraft position, based on a stored data table.

Alignment

The basic equations utilized in the alignment initialization process are similar to those for navigation. In this case, the assumption that the vehicle carrying the inertial system is stationary so that sensed acceleration is due to the effects of gravity inputs on the sensors (i.e. vehicle disturbances are transitory and can be filtered out). Establishing the orientation of the systems with respect to vertical, therefore, is accomplished by measurement of the direction of the sensed acceleration vector (gravity) relative to body axes. The initial heading is established in a similar fashion by the assumption that the rate input to the system is due to earth rotation. Since the horizontal component of the earth rate vector is directed north, the components of this measured vector in the leveled reference coordinate frame are used to compute the system heading relative to true north.

The fine alignment implementation uses a seven state Kalman filter with a pre-set gain schedule to perform the alignment function.

Attitude Mode

The basic equations implemented in the attitude mode are similar to those used for the attitude portion of the navigation function. The major differences are that the earth rate and transport rate terms are deleted (due to the absence of position and velocity data) and a special vertical erection loop is added. The absence of earth rate compensation causes the azimuth to be space stabilized resulting in apparent low magnitude heading drift due to earth rotation.

Erection of the attitude matrix with respect to the apparent vertical is accomplished with a second order control loop. Since erection is in the direction of the apparent vertical (i.e. in the direction of gravity minus vehicle acceleration), "down" for a coordinated turn is in the plane normal to the wings. Because of this, the vertical reference will be offset during turns and erection cutout logic is employed when a heading rate threshold is exceeded to limit this error in the vertical.

Initialization of the attitude mode, prior to engagement of the closed-loop second order dynamics, is accomplished by proportional torquing.

In addition to the attitude function, the complementary baro-inertial filter remains operative in the attitude mode to provide altitude and altitude rate outputs.

IRS Selectable Modes

The IRS has four modes selectable from the IRMP as shown in Figure 21; OFF, ALIGN, NAV, and ATT. Primary modes of operation are the ALIGN and NAV modes, with the ATT mode selected as a reversionary mode should a failure cause the NAV mode to be inoperable, or should a total loss of power cause the reference attitude and position data to be lost.

- OFF Mode - The OFF mode removes power from the IRU and IRMP with the exception of the circuits required to initiate the operating modes.

- ALIGN Mode - The ALIGN mode provides leveling and heading determination required to initiate the NAV mode. This mode requires 10 seconds of initialization during which the initial BITE is completed and ten minutes of alignment characterized by a Kalman filter. The filter gains are predetermined functions of align time developed for an optimum final alignment error that considers the sensor noise characteristics and the aircraft disturbances that may occur during alignment, such as wind gusts, refueling and passenger-loading.

  The mode requires initial latitude and longitude inputs from either the IRMP or one of the two flight management computers (FMC). The IRS estimates latitude as well as heading; however, the input values for both latitude and longitude are used as the navigation initial conditions because the input position values are more accurately known.

  The IRS alignment concepts allow the latitude input to be entered any time during the process without compromising either alignment time or accuracy. For example, the conventional process requires that latitude be entered before the alignment process begins because it is used to calculate the vertical component of earth rate during the process. However, the IRS proceeds with the alignment process and corrects the introduced error at the end of the alignment - after the latitude has been inserted.

- NAV Mode - The NAV mode provides a worldwide, all-attitude, inertial navigation mode. The mode provides all navigation and body-referenced parameters to various avionics systems on the airplane.

- ATT Mode - The ATT mode is a back-up mode selected by the pilot. If the inertial reference is ever lost due to power interrupts, the pilot selects the ATT mode, which provides attitude output, with full performance in 20 seconds. Heading is initialized by the crew member with a reference heading input via the IRMP or FMC. Once initialized, the IRU provides valid heading as well as attitude in this mode.

Selectable Mode Sequence

The IRS operation is also controlled by the mode selection sequence that provides additional capability. The mode sequences are controlled by the pilot from the IRMP, with each of the IRUs controlled by their separate mode control knobs.

- OFF to ALIGN - The IRU remains in the ALIGN mode as long as the mode is selected and continues the fine leveling an earth rate estimation. This allows the pilot to control when the NAV mode is entered, with the potential of improving the navigation performance if delays prolong the time at the gate, since navigation performance is a function of the time in the NAV mode.

- OFF to NAV - The NAV mode may be selected immediately. It results in an alignment time of 10 minutes, after which the IRU automatically enters the NAV mode. This mode sequence requires the minimum of pilot interaction, mode selection, and latitude/longitude initialization input.

- OFF to ATT - The attitude mode has priority over all selectable modes and is entered immedately upon selection. The ATT mode is deselected only by the OFF mode since operational entry of the NAV or ALIGN mode is not possible because of the loss of the navigation reference data in the ATT mode.

- NAV to ALIGN - After the NAV mode has been entered, the ALIGN mode may be reentered if the indicated ground speed is less than 20 knots. This feature provides increased accuracy for a route that includes several takeoff/landings, since the ALIGN mode may be entered while the aircraft is stationary. The velocities are reset to zero, and the alignment process is initiated, which rapidly determines the approximate level and continues to refine the leveling and heading determination as long as the ALIGN mode is selected. Inputs of latitude or longitude or both may be entered but are not required. When initial data is entered, the information updates the present position and increases the position accuracy.

- NAV to ALIGN to NAV - When ALIGN mode is momentarily selected and the IRS returns to the NAV mode, velocities are set to zero and within 30 seconds the level attitude is determined. The IRS automatically remains in the ALIGN mode for the required 30 seconds, even though the mode control is prematurely returned to the NAV mode.

These selectable modes and sequences are summarized in table 14.

Table 14. IRS Selectable Modes

Normal Alignment	10 minute self alignment, leveling and gyrocompass
NAV	Provides full system performance
Attitude	Backup, gravity erected mechanism to provide attitude and heading data — full performance in 20 seconds
Down Mode Alignment	Sets residual velocities to zero and re-levels the "platform" in 30 seconds

Operation Monitoring

The IRS includes a comprehensive monitoring and fault isolation system provided by built-in test equipment (BITE). The BITE provides fault isolation to the IRS line replaceable unit (LRU) with a 95 percent success rate through tests automatically performed when the IRS power is applied, through ALIGN mode completion criteria, and through in-flight monitors and tests. This detection and isolation is achieved without IRU-to-IRU communication, since IRU-to-IRU interfaces have the potential of compromising the system redundancy integrity through single-point faults. Each IRU contains a nonvolatile fault-storage memory used for recording detailed fault status of IRU subassemblies that aid in fault isolation to the LRU subassembly in the maintenance shop. In addition, upon command by a remote switch or a switch on the IRU, the IRU establishes fixed values of the output parameters on the ARINC 429 serial digital output data bus for testing the interface between the IRS and the recipient avionics equipment. This test mode does not interrupt the internal updating process and may be activated at any time during the ALIGN or NAV modes if the ground speed is below 20 knots.

IRU Hardware Features.

Laser Gyro - The laser gyro is an instant-on, large dynamic range, wide-bandwidth-rate sensor with extremely stable performance parameters and input axis alignment. The laser gyro detects and measures angular rates by measuring the frequency difference between two counter-rotating laser beams enclosed in an optical path. (See Figure 23). The two laser beams coexist in the same path enclosed by three mirror surfaces. The resonant frequency of each beam is a function of the path length seen by the beam. At rest, with no angular rate input, the clockwise and counter-clockwise apparent path lengths are the same. However, when the gyro is rotated about the input axis, defined to be perpendicular to the plane as defined by the path of the laser beams, one beam experiences an increased path length and the other, a decreased path length, which results in two distinct resonant frequencies, wherein the frequency differential is directly proportional to the angular rate. The frequency difference is measured by optical means that results in a digital output. Each pulse output represents a fixed angle of rotation with the pulse rate proportional to the angular rate input.

Accelerometer - The inertial grade, force rebalance accelerometers used in the IRU are heaterless analog output devices. The analog output signal is digitized by a precise electronic circuit, the output of which represents a fixed increment of velocity. Accelerometers from three manufacturers were certified both in a mixed and matched configuration as they are interchangeable at the IRU level.

IRU Electronics - The IRU uses two microprocessors structured in an internal parallel bus system, with primarily serial digital external interfaces in ARINC 429 format. (See Figure 24.) The Honeywell Inc. HDP 5301 main processor is a sixteen bit, four bit slice micro-processor based on the 2901 integrated circuit incorporating double-precision numerical processing-and-data handling modes that provide thirty-two bit capability, where necessary. A second eight-bit micro-processor (Intel 8048) is used as an input data processor. The electronics are functionally partitioned to minimize intercard wiring and to simplify fault isolation.

IRU Packaging - The IRU packaging is an optimum combination of Large Scale Integrated Circuits (LSIC), and commercially-standard integrated circuits and discrete components. The IRU incorporates flow-through cooling and careful thermal design to eliminate hot spots, and to reduce average component junction temperature thereby increasing the IRU reliability. This thermal design has been verified by thermal analysis and thermal testing. (Ref. 3)

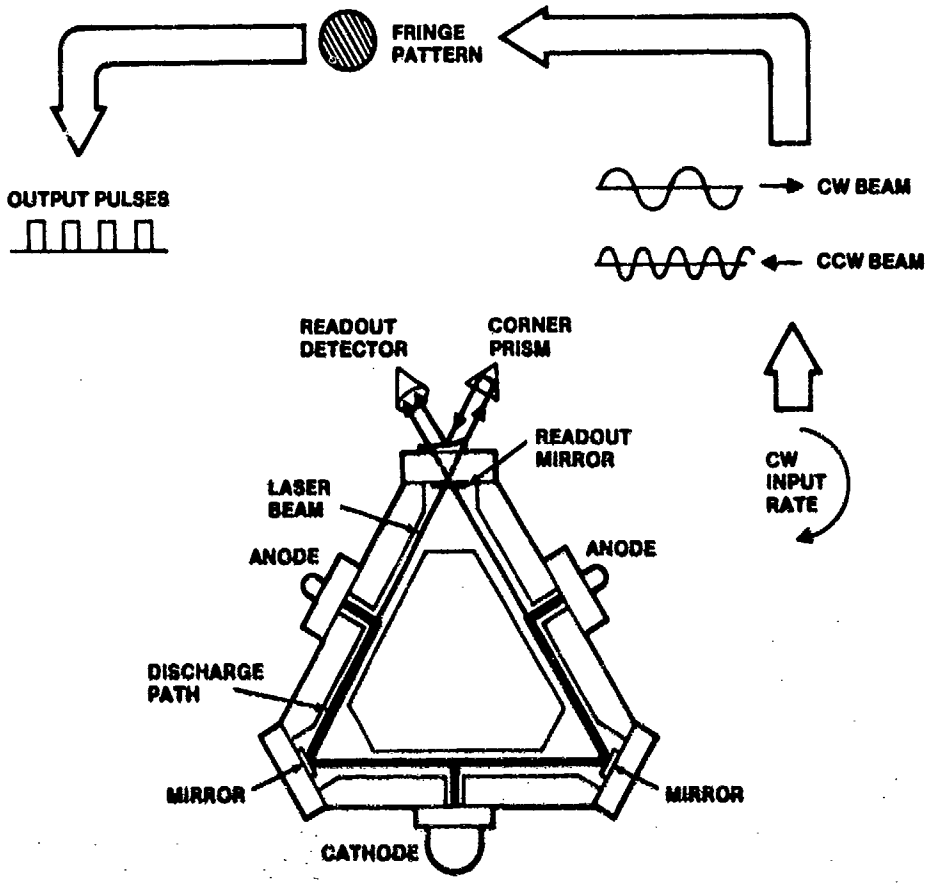

Figure 23. Laser Gyro Schematic

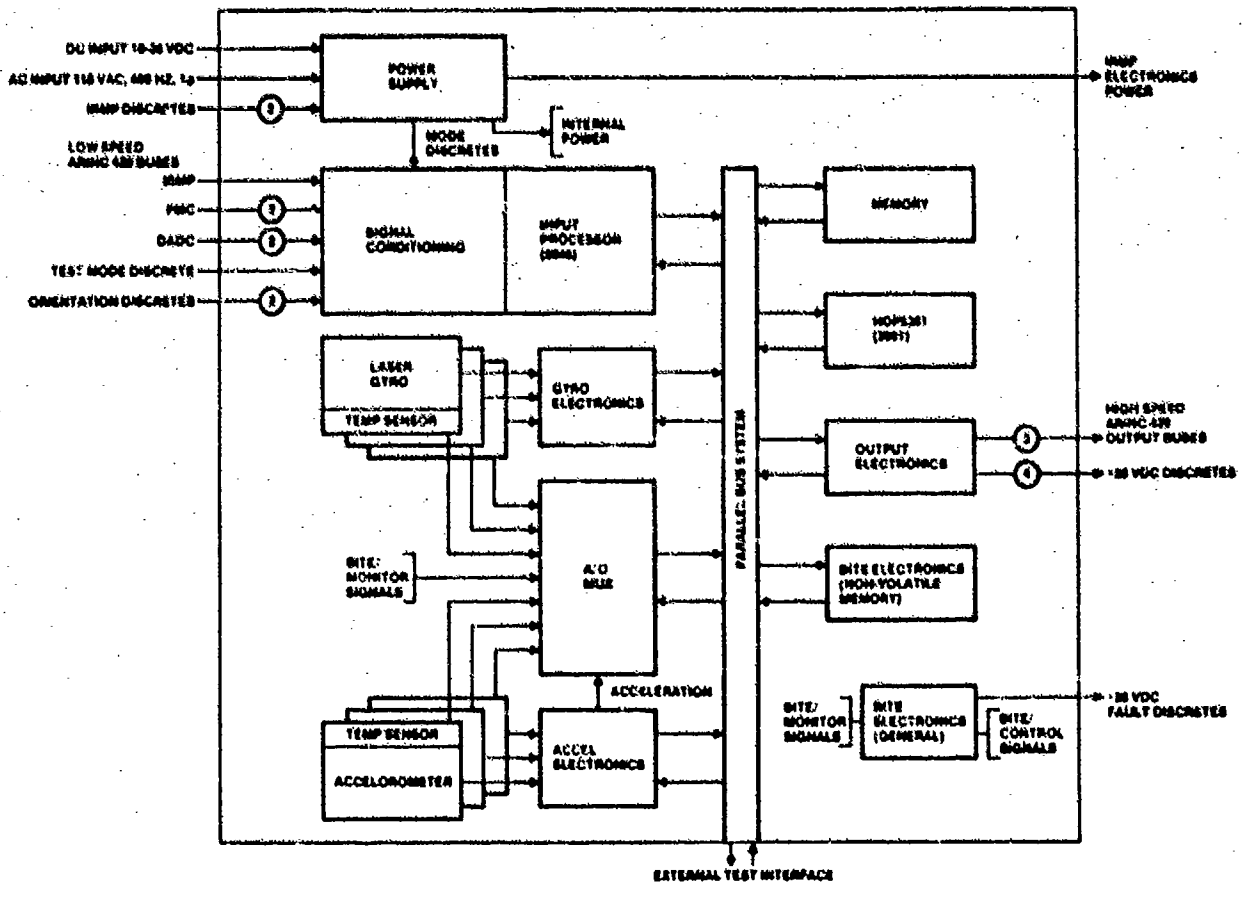

Figure 24. IRU Block Diagram

AIRPLANE SYSTEM REQUIREMENTS

The basic IRS data requirements for the 737/757/767 airplanes are compared in Table 15 with current INS systems in commercial service. The basic performance of these two differing technologies are the same because the application requirements are essentially the same. The primary differences are the body axis data availability in the strapdown configuration. The alignment time of 10 minutes for the strapdown system must be completed satisfactorily over the temperature range of -15°C to +70°C for latitudes of ±73°. This is to be accomplished without heaters and the power to the IRU is limited to 125 watts compared to 1200 watts used by INS during warmup and 400 watts continuous after warm-up cycle is complete. The IRU used in the Boeing 757/767/737 airplanes dissipates under 100 watts and has been qualified to give full performance over a 90 minute no cooling air environment to satisfy the regulatory agency of the United Kingdom, the BCAA.

Table 15. IRS/INS Performance Specification Comparison

Function	IRS	INS (747 Type)
Align time	10 minutes	15-20 minutes
Attitude	0.1°	0.2° (analog)
Magnetic heading	2°	Not provided
True heading	0.4°	Not specified but similar
Navigation	2 nm/hr, world wide	2 nm/hr, world wide
Ground speed	12 knots (4-5 typical)	Not specified, but typically 4-8 knots
Vertical velocity	0.5 ft/sec	Not provided
Body angular rates	0.1°/sec	Not provided
Body accelerations	0.01g	Not provided
Flight path accelerations	0.01g	Not provided
Track angle true	5°	Not specified, but similar
Track angle magnetic	6°	Not provided
Flight path angle	0.4°	Not provided
Track angle rate	0.25°/sec	Not provided
Inertial altitude	5 ft	Not provided

The system redundancy requirements for the 757/767 airplanes are three separate, isolated inertial data channels to satisfy the requirements of the fail operational autopilot. For the 737-300 airplane, dual, independent channels of inertial data are provided to satisfy the basic airplane attitude requirements in accordance with the air regulations. This configuration also satisfies the fail-passive autopilot design of the 737-300 airplanes.

The single inertial mode panel is designed so that no single failure can cause the loss of more than one IRU. The display function of the mode panel is common to all redundant IRUs, but is not required for in-flight operations.

LASER STRAPDOWN INERTIAL REFERENCE SYSTEM CERTIFICATION ISSUES

After reviewing the IRS design and applications to the 757/767 airplane, the US Federal Aviation Administration primary certification issues were the following:

- Reliability and Failure Modes
- Synthesized Magnetic Heading
- Navigation Performance
- Software Verification and Validation

The test programs and results described in the next sections were designed to answer the FAA's (and Boeing's) concerns and were successful in accomplishment.

IRS TEST PROGRAM DESCRIPTION AND RESULTS

The IRS test program at Boeing for the 757/767 program consisted of three phases. The first phase, called "Blue Label", involved the full engineering evaluation of an engineering model of the production system. This unit was completely packaged in a production configuration, but was built in engineering model shops. The second phase, called "Red Label", were pre-production units built by production shops but were the systems used and evaluated during the 757/767 airp ane flight test program over a 1-½ year period leading to certification. The last phase called "Black Label" or full production built and controlled units were evaluated only for any changes from the "Red Label" configuration used for type certification demonstration of the basic airpane. An overview of the test program required for certification is shown in Figure 25 and

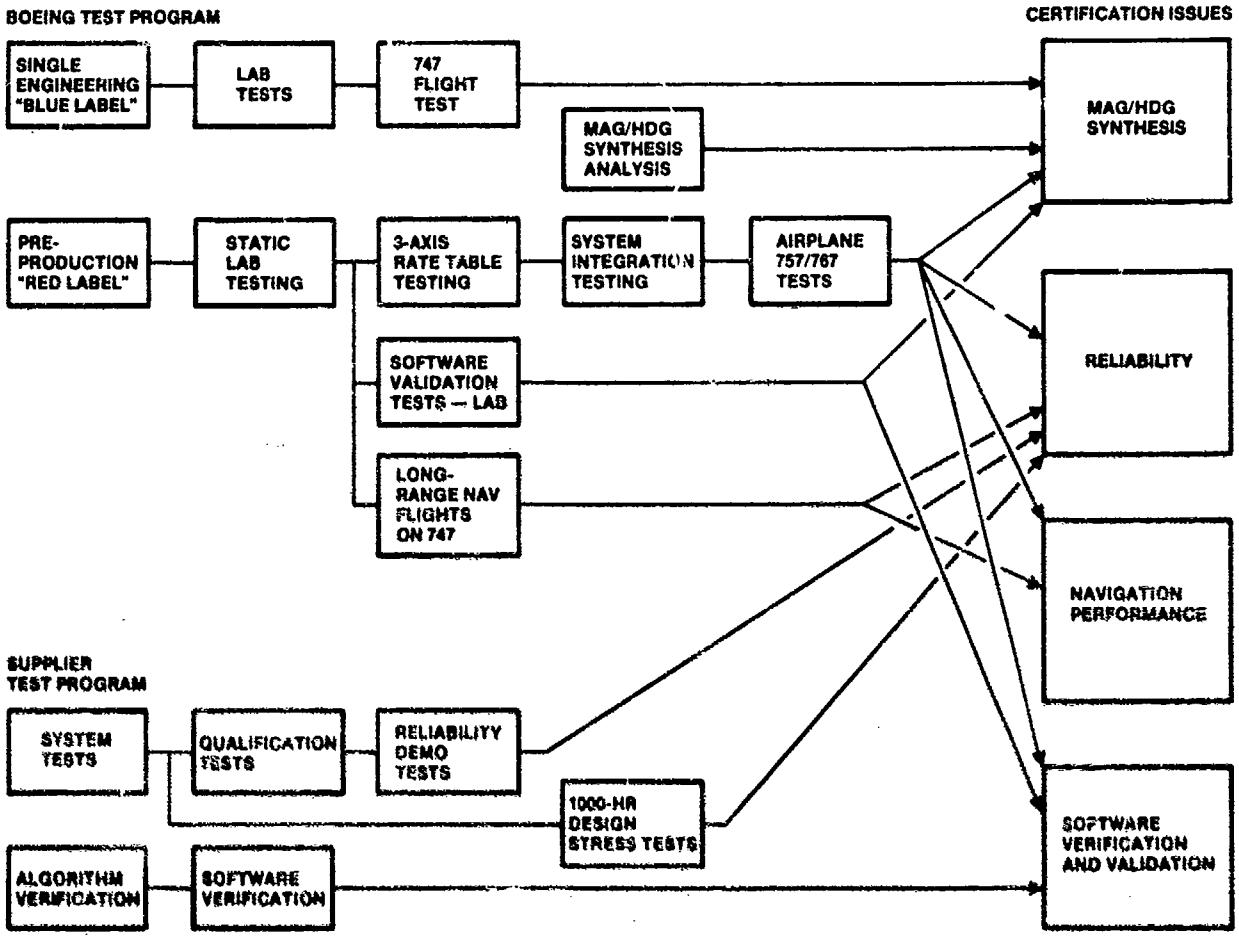

Figure 25. 757/767 IRS Test Program For Certification

Boeing System Laboratory Tests

All laboratory configurations were evaluated independently at Boeing to validate the Boeing design requirements and supplier changes to his requirements. Performance, functional, environmental, and software testing were performed at this level. Integration testing was a key test with all interfacing equipment to insure data bus and function compatibility.

A series of laboratory tests were performed, using single-axis and 3-axis position/rate tables to evaluate the system's attitude, heading, angular rate, alignment, and navigation performance. Alignments and navigation runs were performed under a limited range of thermal and vibration environments to evaluate the thermal and vibration sensitivity and stability of the sensors. Navigation runs ranged from 2 to 10 hours in length. Interface tests were performed to evaluate the ARINC 429 digital data bus electrical performance and functional compatibility with using airplane systems. Additional tests included EMI and power transient and power variation tests. The systems performed well within specifications, with only minor hardware and software anomalies. The laboratory test configuration is shown in Figure 26. There were no failures of any IRUs during the three year lab test program of all three system configurations, (Blue, Red, Black). A summary of the scope of the lab test program is given in Table 16.

Two unique sets of tests, at least for commercial inertial systems, were performed on the IRUs at Boeing. These were 3-axis Rate Table Tests and system level software tests.

3-Axis Rate Table Tests

To evaluate the system's attitude algorithm, rate sensitivity, and total performance under dynamic conditions, an IRU was mounted in a 3-axis rate table which allowed simultaneous application of various pitch, roll, and yaw rates, both linear and oscillatory. For example, the maximum specified angular rates of 70°/second were applied about all three axes simultaneously for periods of up to an hour. The appropriate output parameters were recorded and examined over this test period with no anomalous behavior indicated, which fully validated the attitude/rate computations, under worst case test conditions, and demonstrated the all-attitude capability of the system. This test allowed evaluation of attitude and rate accuracy by comparing IRU outputs with the table parameters. Of special interest were conditions which could have singularity problems such as 90° pitch angles. These test series provided excellent confidence in the attitude algorithms under a wide range of dynamic conditions.

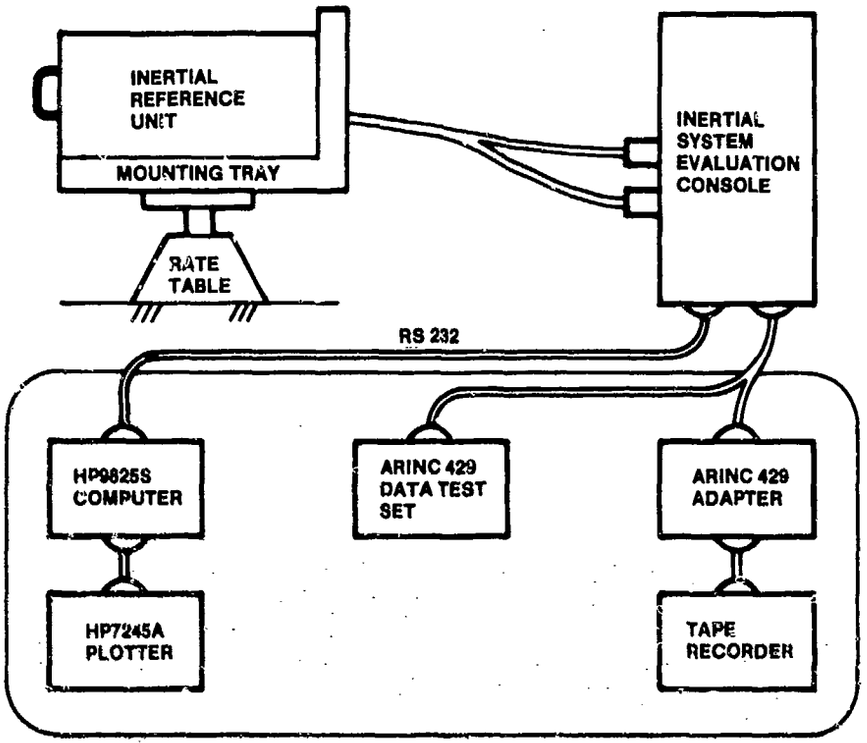

Figure 26. 757/767 IRS Laboratory Test Configuration

Software Validation

The other unique test was software validation. This test was performed at the system level with the software being executed as designed in the system except for the test input points. The test consisted of "opening up" (software patch) the gyro and accelerometer inputs to the software and inserting simulated accelerometer and gyro "pulse count" data. This would allow testing under controlled flight path conditions to evaluate conditions difficult to achieve during flight test. It also allows very repeatible testing to be performed, a necessary condition for evaluating software. This test configuration is shown in Figure 27. The test driver, resident in a Harris computer, consists of an independently derived strapdown IRU model. This model operates on data files which define the dynamic flight profile and generates outputs consisting of body axis components of inertially referenced rates and accelerations in the form of gyro and accelerometer "counts". The input data files are used to define flight profiles for specific test cases such as climbs, turns, specific flight paths, and combinations of each. This test driver is shown in Figure 28.

The IRS Test Driver (IRSTD) provides a mechanism for dynamic testing of the IRS computer and software by application of simulated sensor inputs. These inputs are generated by the laboratory simulation computer (HARRIS) and transmitted (via RS-232) to the IRS test equipment. The IRS test equipment decodes the Harris inputs and relays the data to the IRS computer utilizing DMA to transmit the inputs to assigned buffers in the IRU computer memory. Special patches are utilized in the IRU operational software to disable the normal sensor interface and replace these inputs with the simulated data. The IRU computer is "slaved" to the Harris input, so that a single computer cycle is executed following receipt of each data block (i.e. set of simulated inputs) from the Harris computer.

In addition to the simulated sensor inputs, the IRU also receives simulated air data and flight management computer inputs via an ARINC 429 bus from the Harris computer.

The Harris computer system also provides an ARINC 429 receiver, which is used to read and record IRS digital output parameters. Test data is obtained from dynamic CRT displays available at the simulation operation console and printout of specified ARINC labels by post-processing the recorded data tape.

A summary of these tests and resulting benefits are listed in Table 17.

Supplier Software Verification

The software verification program required by Boeing resulted in a very exhaustive test process at the supplier, Honeywell (Reference 5).

Prior to beginning the verification of the target computer software, the basic attitude and navigation algorithms implemented were required to be verified.

The method used for verification provides a comparison of IRU navigation and attitude response with results obtained from known classical solutions.

Table 16. IRS Lab Test Description Summary

Test	Description
Functional	Verify functions are present and mechanized per specification
Moding	Verify all possible mode sequences via the operator are acceptable to system operation
Alignment	
Basic stability (day-to-day) Heading sensitivity Thermal sensitivity Attitude orientation sensitivity Time sensitivity Base motion sensitivity EMI/power (variations and interrupts)	Perform repeated alignments under various heading, attitude, and environmental conditions to evaluate basic performance and sensitivities to these conditions
Navigation	
Basic stability (day-to-day) Heading sensitivity Thermal sensitivity Attitude orientation sensitivity Time sensitivity Base motion sensitivity EMI/power (variations and interrupts)	Perform repeated navigation drift runs under various unit orientations and environmental conditions and time to evaluate basic performance and sensitivities
Interfaces	
Digital data bus electrical characteristics and performance	Evaluate basic signal performance (rise time, threshold) under various load and external fault conditions
Digital data	Verify data format and rates
Interface airplane systems	Validate communication and response is acceptable under various loads, modes, and fault conditions when connected to interfacing system
Attitude algorithm	
Sensitivity to maximum angular rates around all 3-axes	Validate attitude data performance is acceptable under any attitude orientation and rotation sequence
Software Validation	
Magnetic heading synthesis	Evaluate synthesis program limits and performance on worldwide basis
Baro-inertial filter	Evaluate performance, response and logic with step and dynamic air data inputs
Align/attitude/navigation	Evaluate algorithms under simulated airplane flight profiles (e.g. align at southern latitudes and navigate over the pole)
Attitude mode	Evaluate attitude mode performance under various airplane dynamics
BIT	Evaluate BIT response to simulated failures

The basic Navigation algorithm is verified using a computer program (Global Simulator) which generates gyro and accelerometer pulse counts by numerical integration of dynamic equations of a point moving on a great circle orbit in inertial space. The derived gyro and accelerometer pulse counts are in turn entered into the IRS strapdown navigation equations and the resulting navigation solution is compared to that used to define the inertial orbit. The errors derived by comparison of the navigation equation integral with the inertial orbit are the basic Schuler and Focault inaccuracies of the strapdown navigation algorithms. The process utilized is shown in Figure 29.

The IRS attitude algorithm simulation (IRS C Matrix Spin Simulator) is a Fortran Computer Program which generates a closed form analytic solution of the IRS attitude differential equations. This solution is then compared to an integral of the IRS attitude integration algorithms for evaluation of truncation and drift characteristics of the algorithms.

Once the algorithms themselves were correct and implemented with sufficient accuracy, the target software verification process was started.

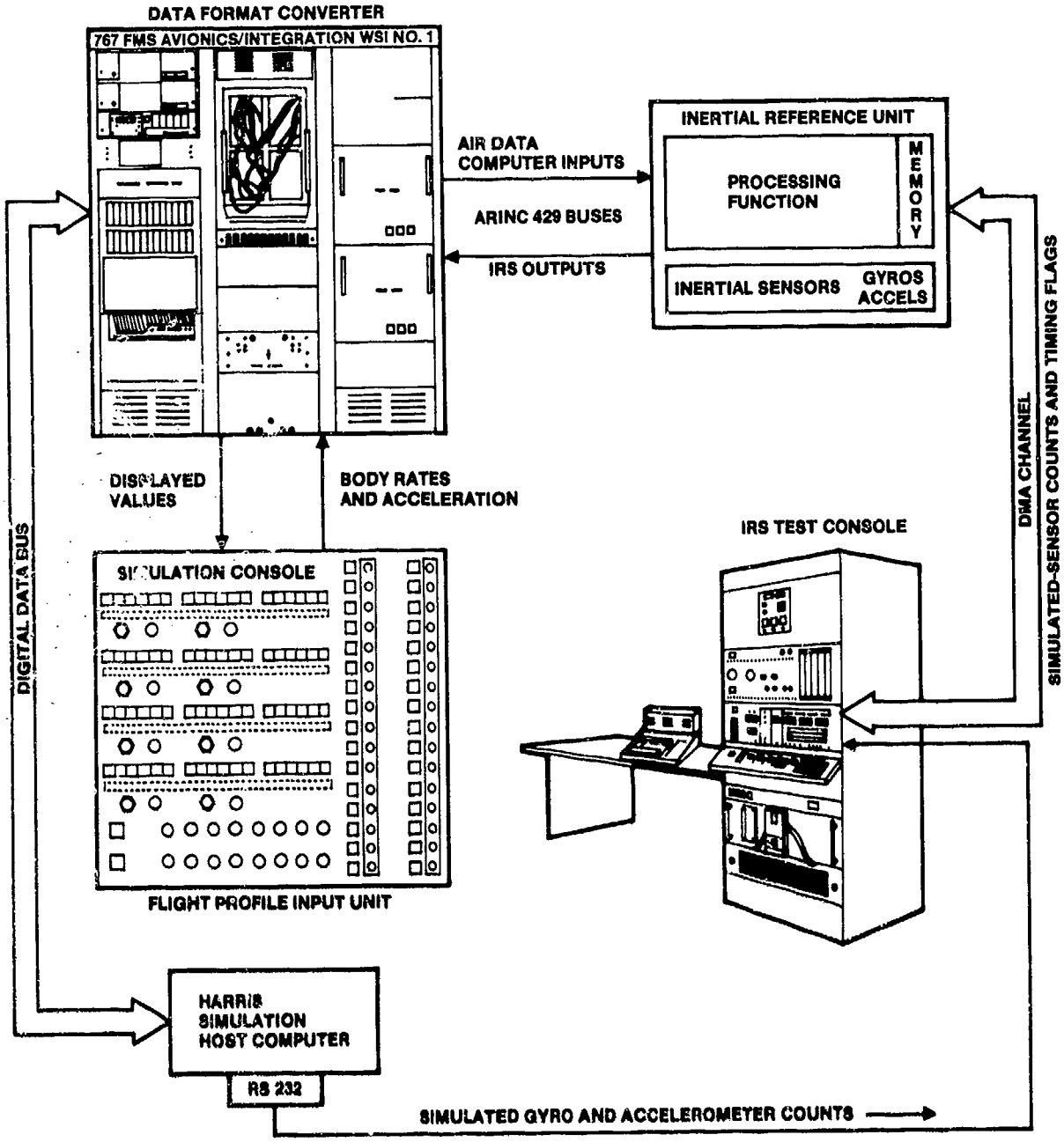

Figure 27. IRS Software Validation Test Configuration

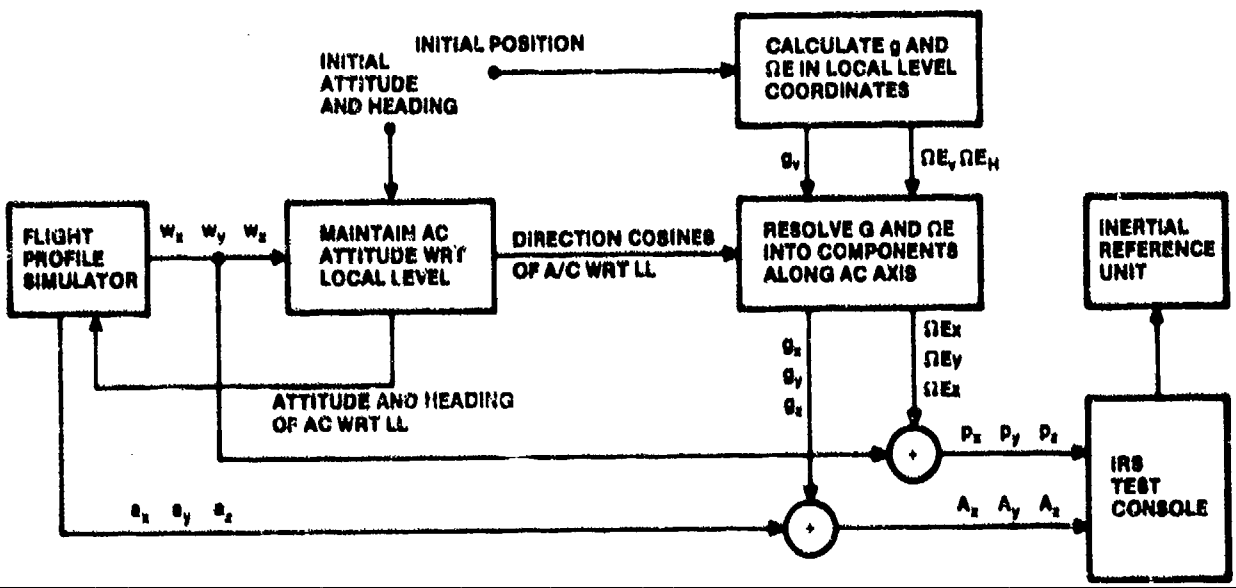

Table 17. Boeing S/W Validation Test Summary

• **Test Coverage**	
Computational accuracy	— Correlate IRS outputs with known flight path (e.g. great circle, constant radius turn)
Special cases/singularities	— Run special cases (such as polar crossings) where flight testing is either difficult or impractical
Dynamic range	— Allows verification of IRU transfer function through complete range of inputs
Bite evaluation	— Provides complete control of external interface and computer operation for evaluation of response to fault conditions
• **Test Experience**	— Software was thoroughly verified by vendor previously. As a result, few problems were identified, and none critical. Evaluation of various flight conditions results in eliminating airplane flight test conditions to verify system performance which resulted in large cost savings.

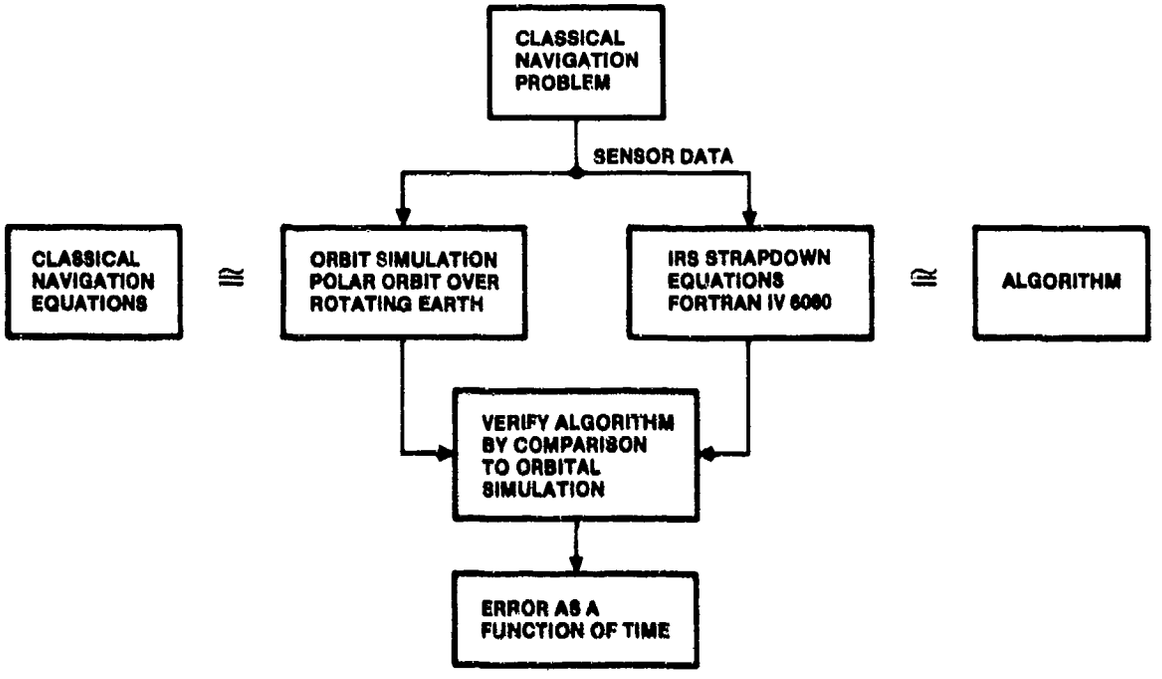

Figure 29. Algorithm Verification — Navigation

Fundamental to a good verification program is a straightforward, structured, modular design which lends itself to complete and visible testing. This was established by Boeing and Honeywell early in the program, with the Software Design Standards used by Boeing for all suppliers.

The supplier established an independent test team from the software design group and both the design and verification test procedures were reviewed and approved by the inertial systems engineering personnel who had established the design requirements. In addition to the testing, walk through reviews were held for the design, test procedures, and test cases used.

Boeing added another check to this process by performing an independent review and approval of the test procedures. This process was also used for any retesting required due to changes in the code.

A very tightly controlled change process was used to insure all changes were implemented and tested properly. For consistency and accuracy, the change process was also applied to software documentation from requirements to test procedures.

The tests included individual module verification tests, module integration tests, hardware/software integration, and end-to-end tests of total software/ hardware elements. As an example of the latter testing, a trajectory generator was used to "drive" the system align/navigation/attitude solutions and logic under various initial conditions and flight paths. These solutions were compared to the "standard" high level language simulation on a host computer for acceptance.

The results of this total software development, test and change tracking process were very successful when considering the complexity of the problem being solved by the IRU. Only 38 software problem reports were issued at Boeing as a result of Boeing tests over 1-1/2 years of lab and flight testing. Of these, 12 were found as a result of flight test and only 3 of these were viewed as significant to certification. Even more interesting is the fact that only 15 of the 38 were true software design or code errors. The majority of the errors were incorrect design requirements provded by the systems engineers to the software designers. The distrubtion of S/W errors over the test program life is shown in Figure 30.

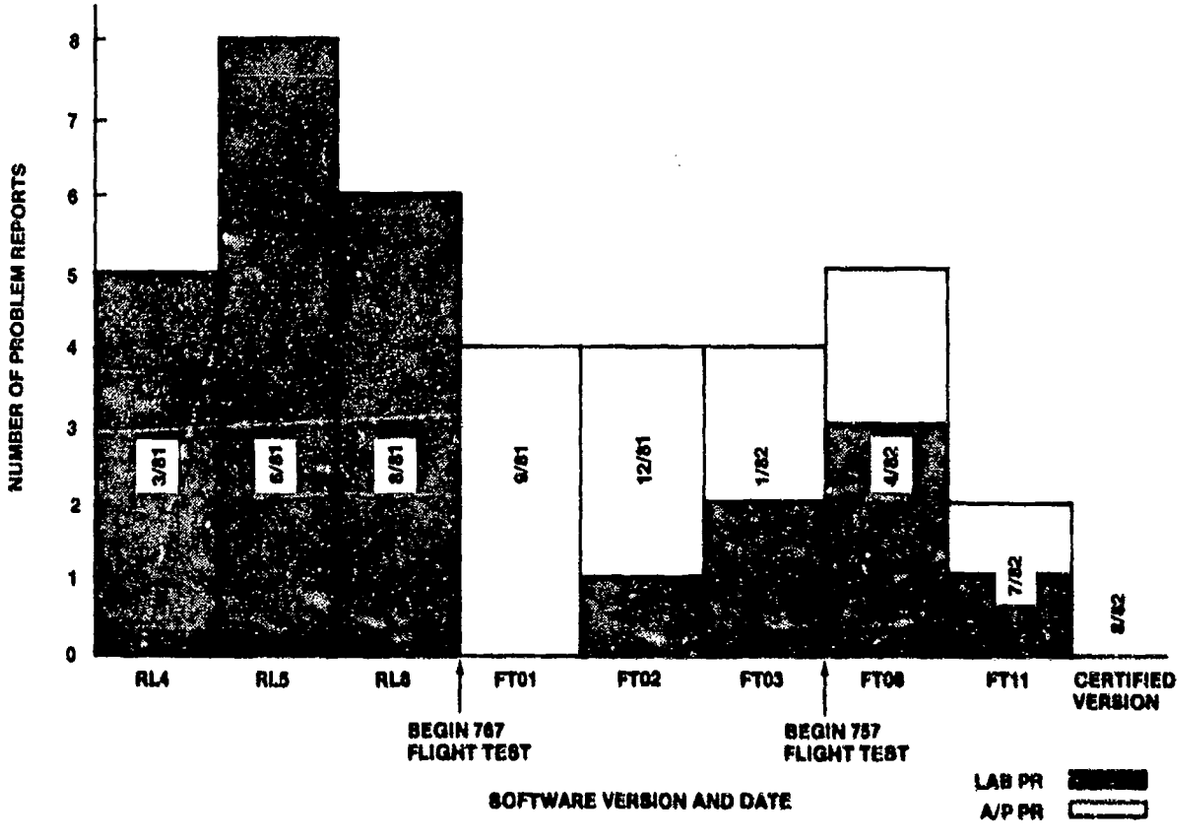

Figure 30. IRU Software Problem Reports During 757/767 Test Program at Boeing

IRU FLIGHT TEST PROGRAM DESCRIPTIONS AND RESULTS

757/767 Flight Test Performance Results.

Extensive flight testing by Boeing was performed to validate and certify the IRS functions.

The "Blue Label" or engineering system was initially flight tested on 747 and 737 test airplanes to verify the system would operate satisfactorily in the airplane dynamic and electrical environment. This test was very successful with excellent navigation performance exhibited and no problems experienced in the airplane environment.

Flight testing of the IRUs during the 757/767 test program accumulated over 94,000 unit operating hours on nine aircraft using a total of 91 IRUs.

The data summarized in Tables 18, 19, and 20 are the IRS navigation performance resulting from 757/767 flight test activity. These data were obtained from a total of nine aircraft (five 757's and four 767's) comprising the Boeing flight test fleet. The source of data is the IRS operation log which was completed for each flight after landing and included final position and velocity data with time in nav and flight. The data base consists of 2800 757 system flight hours and 5100 767 system flight test hours.

These data show that the IRS navigation performance demonstrated in the 757 and 767 airplanes is in compliance with the requirements of FAR 121 Appendix G and AC 25-4 and therefore is satisfactory as sole source of navigation data for long range navigation routes.

Table 18. IRS Navigation Performance Summary Combined 757/767 Airplane Tests

Data Category	Flight Hours	Number IRU Flights	IRU's Used	Radial Error Rate (95%) (nmi/hr)
All flight test data	7 691	2 240	91	1.85
All flight test data — exclude flights where ground time >50% of flight time	7 490	2 014	91	1.69
All flight test data use NAV time instead of flight time to compute RPE rate	9 331	2 240	91	1.56
Certification configuration IRU's — exclude flights where ground time >50% of flight time	3 584	971	44	1.47

Table 19. IRS Navigation Performance Summary 757 Airplane Tests

Data Category	Flight Hours	Number IRU Flights	IRU's Used	Radial Error Rate (95%) (nmi/hr)
All flight test data	2 794	806	63	1.84
All flight test data — exclude flights where ground time >50% of flight time	2 604	767	63	1.66
All flight test data use NAV time instead of flight time to compute RPE rate	3 328	806	63	1.54
Certification configuration IRU's — exclude flights where ground time >50% of flight time	1 913	561	40	1.44

Table 20. IRS Navigation Performance Summary 767 Airplane Tests

Data Category	Flight Hours	Number IRU Flights	IRU's Used	Radial Error Rate (95%) (nmi/hr)
All flight test data	5 087	1 374	67	1.86
All flight test data — exclude flights where ground time >50% of flight time	4 886	1 247	67	1.71
All flight test data use NAV time instead of flight time to compute RPE rate	6 004	1 374	67	1.58
Certification configuration IRU's — exclude flights where ground time >50% of flight time	1 671	410	27	1.51

The overall 95% radial error rate for all flights (2240 system flights) is shown to be 1.85 nm/hr, which is within the 2.0 nm/hr specification. This is a very conservative estimate of the IRS performance because flight time and not time in NAV mode was used to compute the radial error rate. The radial position error is determined by computing the distance between the indicated position displayed on each IRU and the known true position of the parked aircraft at the completion of flight. The 95% radial position error rate is established by utilizing the following equation to process the ensemble of radial errors:

$$R_{95} = 2.45 \left[\frac{\sum_{i=1}^{n} (RPEi/T_i)^2}{2n} \right]^{1/2}$$

Where n = number of data samples

RPE_i = radial position error, i^{th} data sample

T_i = flight time, i^{th} data sample

These three tables provide a summary of IRS navigation performance in each airplane and for the combined data sets. Data is also provided for comparison to show the differences in performance due to the relatively substantial operating time on the ground in the flight test environment. One category excludes all flights where the operating time in navigate mode prior to flight is excessive (exceeds 50% of flight time). The result of segregating these flights is to reduce the measured radial error ratio by 9% (1.85 to 1.69 nm/hr).

The data was further evaluated to show the relationship of radial position error rate as a function of flight time. The Figure 31 plot was obtained by successively removing data below a specified minimum flight duration threshold. The intent of this plot is to show the relative improvement of radial error rate as a function of increasing flight duration. For example, an improvement of approximately 45% is evident in Figure 31 if the computed radial error rate for all flights is compared to the subset which includes only those flights in excess of 6 hours flight duration. This was done to show the regulatory agencies that radial error rate for short flight periods is misleading as an indicator for over all navigation performance.

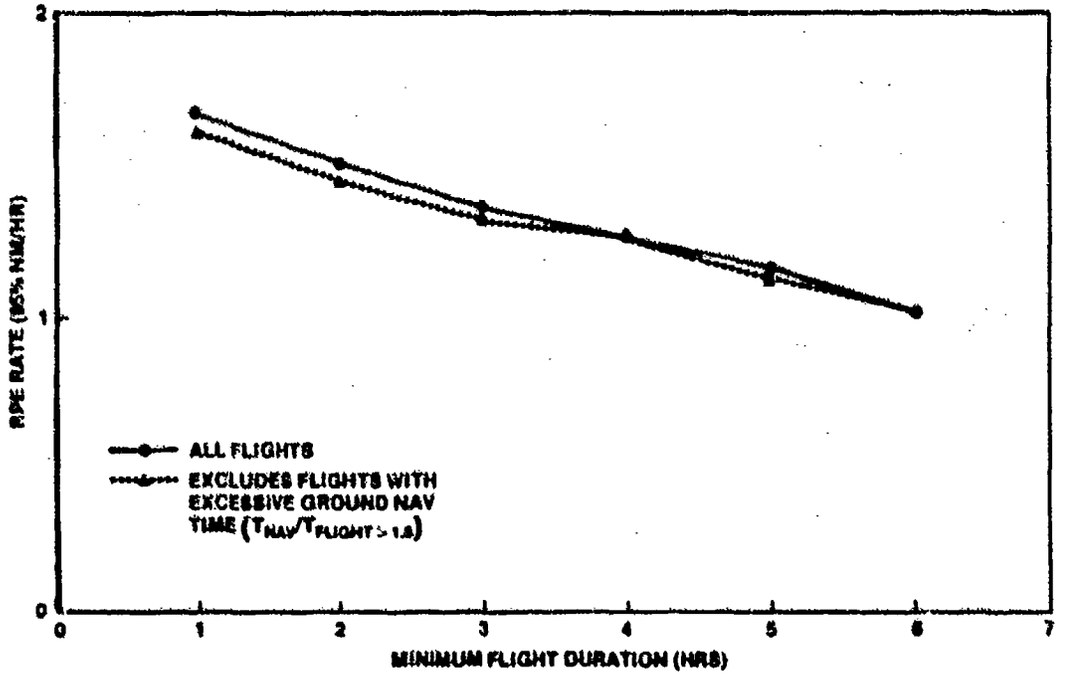

Figure 31. RPE Rate vs. Minimum Flight Duration

An evaluation of the flight test data was also performed to determine the velocity performance being demonstrated. A total of 2320 IRU flights (3 IRUs/flight) represented the population for this analysis. Only terminal (after landing) data were available, but because of the large population which covered a wide range of flight times, profiles, and units, the estimate was felt to be valid. The flight data analysis showed the velocity (ground speed) performance to be less than 8 kn, 95% basis.

Flight Test Events, Operations and Problems of Interest

Performance Problems

As previously inferred and as shown with the navigation test data, very few problems were encountered during flight test. Those that did can be categorized as BITE, Baro-inertial/Vertical acceleration loop, anti-aliasing filtering, and Schuler "pumping".

The BITE problems resulted from tolerances set too tight or the test turned out to be impractical. One such test was cross-track velocity which was designed in an attempt to automatically detect unacceptable navigation performance at the end of the flight by calculating what the cross-track velocity (velocity error) was when the airpane was in rollout on the runway (i.e. when actual cross-track velocity was zero). Early in the program, large velocity errors were being induced by a gyro connector problem (unknown at the time) and when the airplane was turning during taxi on or off the runway, this error would often be in a direction to add to the actual cross-track velocity created by the lever arm action on the IRU which can be 100 to 150 feet from the turn center depending on nosewheel angle. This event is depicted in the kinematic diagram of Figure 32 and the parametric analysis shown in Figure 33. This figure indicates the BITE test sensitivity to the turn maneuver during taxi operations when a 10 knot error exists in the cross track direction. The result was the cross-track velocity error threshold was exceeded and the IRU would fault. The frequency of this event became unacceptable and the test was removed. The gyro connector problem causing the larger than normal velocity error was eliminated also, but the test was not reinstated. The decision was made to let the crew determine the out-of-tolerance navigation or velocity performance, as is done with the gimbal INS in commercial service.

The baro-inertial/vertical acceleration problems stemmed from interface incompatibilities with the autopilot and were due to output filter instability under small altitude changes from the air data input, and undesireable response to air data failure conditions. These were not difficult to resolve, but it took the 1-¼ years flight period to discover them all.

Based on the anti-aliasing filter analyses performed in support of the system specification, the body rate and acceleration data were specified to have an 8Hz bandwidth. Because of design constraints and compromises made during the development of the digital autopilot and autothrottle systems, it was discovered during the flight test that this "wide" bandwidth was causing some instability in the control loops. These automatic control systems were undersampling (20Hz) the data (50Hz) and the high level of vibration noise in the 5-8Hz region at the inertial system location was getting folded over or "aliased" into the control system bandwidth (1-2Hz) by virtue of their low sample rate processing. Changing the second order Butterworth filter bandwidth from 8Hz to 3.2Hz resolved the problem.

The last category, "Schuler pumping", is not unique to strapdown systems, but because of the strapdown mechanization this phenomenon occurs more easily and one must be aware of this system sensitivity for strapdown applications.

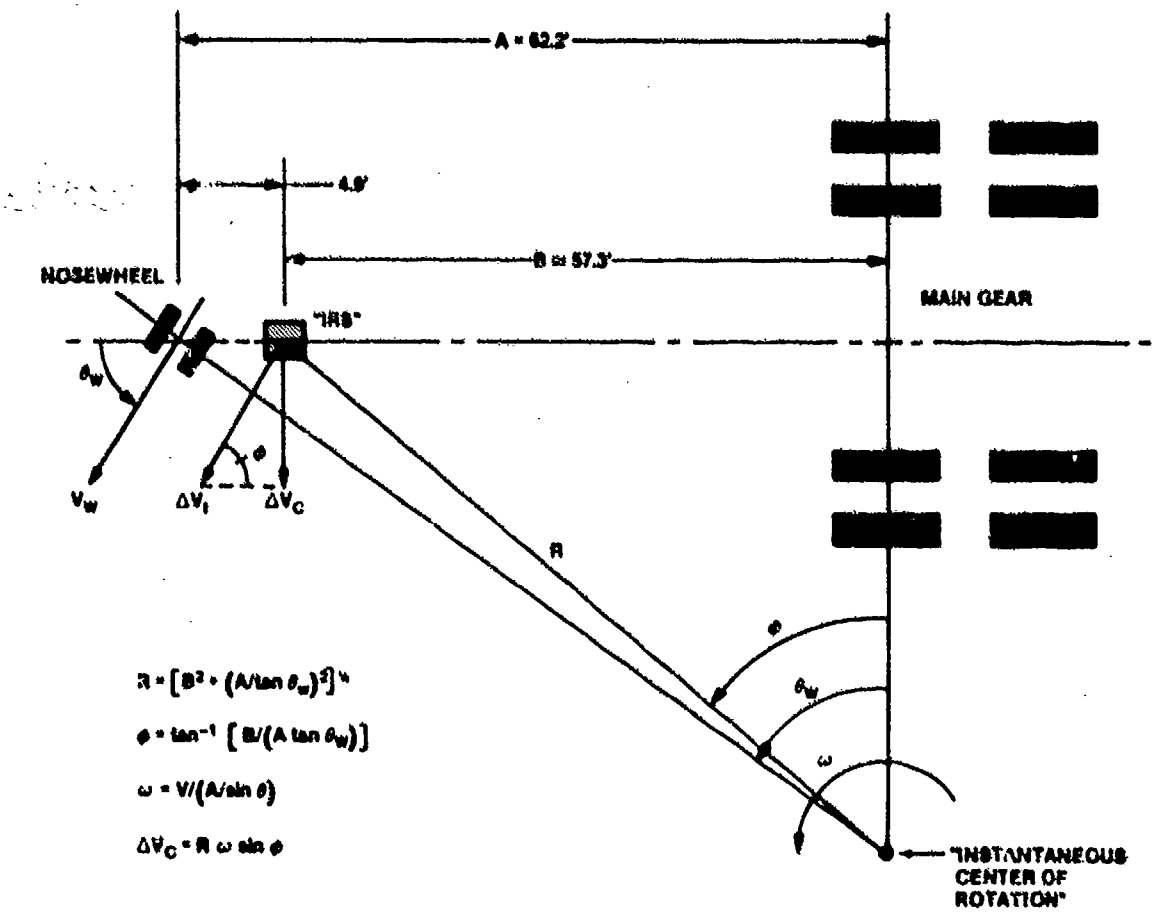

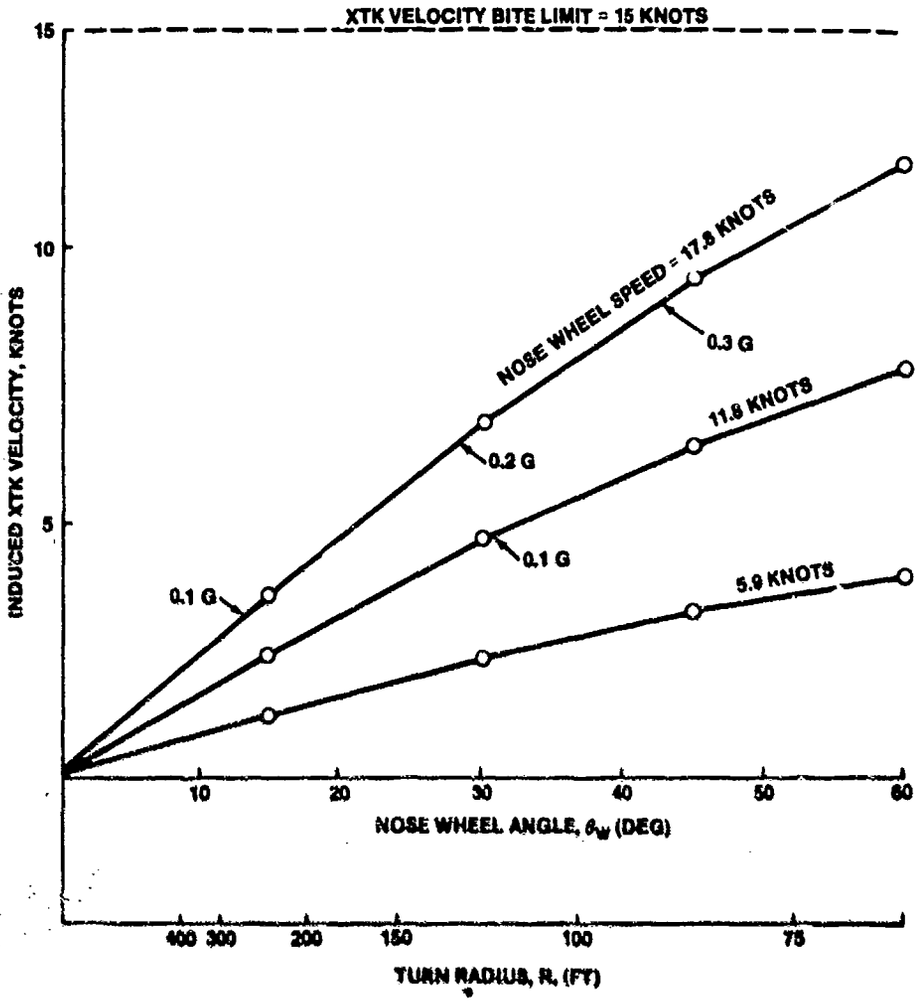

Figure 33. Induced XTK Velocity Increment vs. Turn Conditions (Taxi)

The strapdown operating characteristic is such that the align solution compensates for any accelerometer bias by providing an attitude error or tilt with respect to the level plane which results in exact cancellation. For an ideal system, with no heading change, the groundspeed would remain constant (zero).

The effect of a 180° heading change at align completion (T=10 minutes) would result in a step input to the IRU of twice the accelerometer bias (-2X bias) (i.e. accel bias vector reverses direction). This would cause the sinusoidal response shown in Figure 34.

If another 180° heading change is attempted at, for example 40 minutes, the effect would be to introduce an additional step input of +2 X bias. The response to this input would be a sinusoid of opposite sign, as shown in Figure 34. The net IRU response would then be represented by the linear sum of the response to the initial rotation and the response to the 40 minute rotation, as shown in Figure 34.

Inspection of Figure 34 indicates that subsequent heading changes can either increase or decrease the amplitude of the IRU Schuler oscillation, depending on the heading angle change and the phasing of the existing Schuler oscillation at the time that the heading change is made.
This cause of occasional high ground speeds was verified by examining flight test profiles which had a large ground speed at the end of the flight, and correlating the velocity errors with heading changes. A vivid example is shown in Figure 35. The systems exhibiting these large "Schulers" had accelerometers from one vender exhibiting relatively large bias errors (since fixed) which magnified the "pumping" action of the flight profile. A verification of this error source was performed by simulating a large accelerometer bias error and comparing the error analysis results which was run using the same heading change profile as the actual flight, against the actual flight test data. Good correlation is shown in Figure 36.

This strapdown sensitivity was not expected to be excited during the relatively benign commercial flight profiles and this seems to be a correct assumption, based on limited velocity data taken during in-service observations and the lack of removals or customer complaints on ground speed performance. In addition, the early accelerometer performance problem has been resolved so that any "pumping" action would result in much smaller errors.

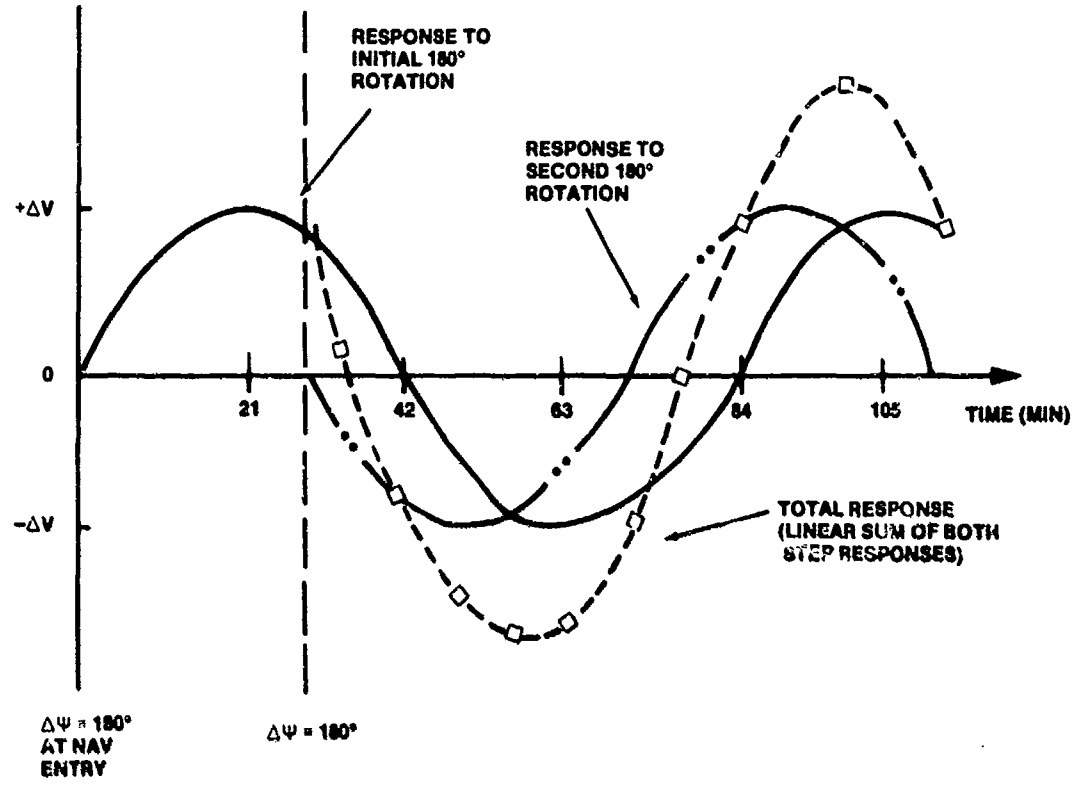

Figure 34. Example of IRU Velocity Error Response to Heading Changes

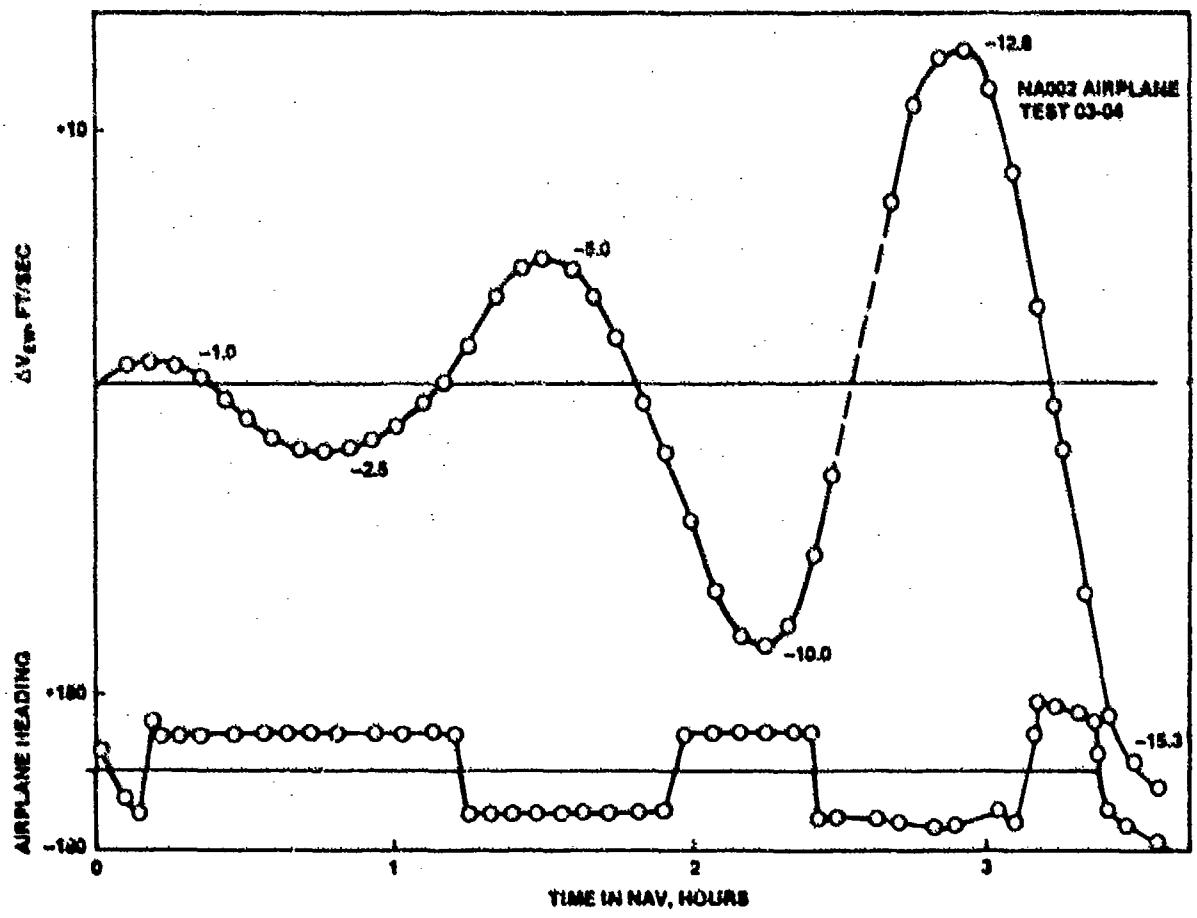

Figure 35. Flight Test "Schuler Pumping" Example

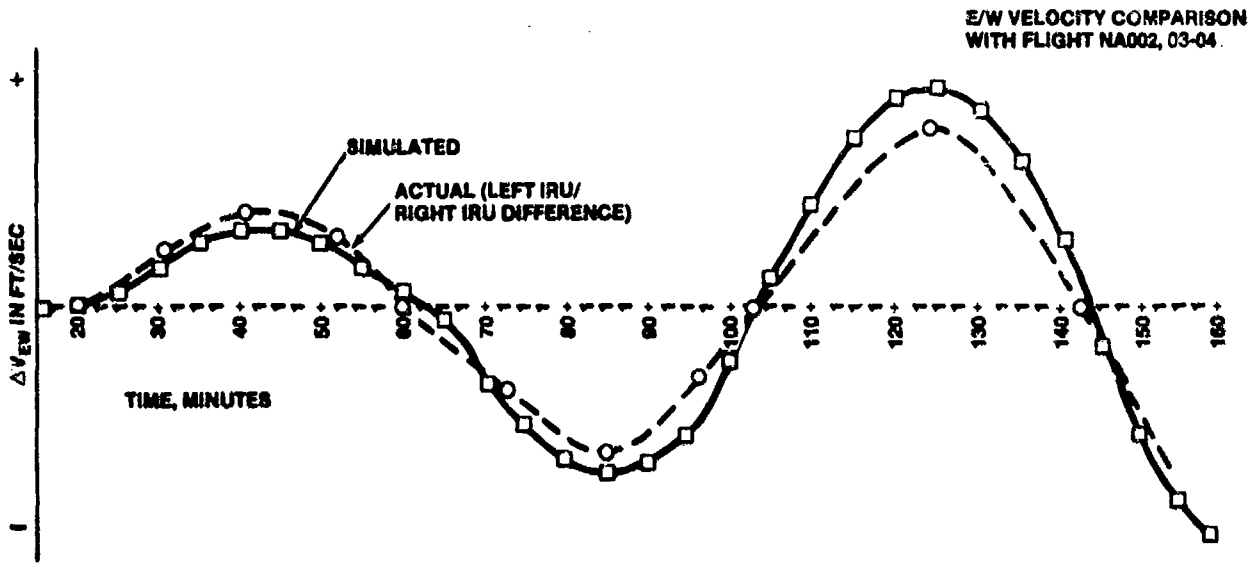

Figure 36. Comparison of Simulated "Schuler Pumping" Error With Actual

Operational Problem

When specifying the design of the magnetic field model for the inertial reference system, consideration was given to the effect of long term earth magnetic field "drift" on maintenance or updates to the stored model over the life of the system.

A great deal of study and analysis of historical magnetic field behavior was performed by Boeing. It was concluded that the magnetic field model could be safely "pushed" 10 years into the future such that as time passed, the magnetic variation data in the IRU became more accurate until the 10 year point was reached. After that the data was expected to degrade assuming the earth's magnetic field continued to exhibit it's "westward drift", as it generally has over the last 60 years of observation.

Our clever scheme, then, was to use a 1990 model based on the 1980 (latest available) model which has the 1st time derivative included.

During flight testing, the pilots complained they were seeing 2-3° errors at takeoff at certain airports, and found this to be unacceptable. An investigation revealed that the magnetic reference data used for airfields and NAV aids (VORs) by the FAA were as much as 15-20 years out-of-date. This fact when coupled with the 1990 model in the IRU produced errors which appeared worse than they really were by the high resolution CRT heading displays. This "error magnification" is shown in Figure 37. The numeric data in the heading window also contributed to this magnification.

The pilot unacceptability came as a surprise and was disappointing, because we had to go back to the 1980 magnetic field model to develop display data compatible with the "old" facilities reference information. It is doubtful the FAA will update their reference information, except incrementally, as operations show a need. European facility reference data did not show this "aging" problem and appears to be relatively current (< 10 years old). However, even with this change in approach, the field model appears compatible with a 20 year system life.

IRU Airplane Instrumentation Utility

One interesting aspect of the flight test program that was not a problem, occurred because of the IRS attributes. Enough confidence in this system had been generated through the "fly-off" competition and the engineering model (blue label) testing on a 737 and 747 that the IRU was designated to be used as basic airplane instrumentation during the 757/767 flight test program for other testing such as aero, brakes, anti-skid, stability and control, etc. The quality and reliability of the rate, acceleration, attitude, heading, and velocity data satisfied all of the instrumentation requirements for these parameters. Thus, no further instrumentation system needed to be installed to provide these data measurements, a great savings to the test program.

Long Range Navigation Data Flight Test

In addition to the Boeing-conducted flight tests, a long range certification exercise was conducted on an American Airlines 747 freighter in revenue service to collect reliability and performance demonstration leading to long range navigation certification. This test accumulated over 1200 hours on four IRUs. A triple IRU pallet was installed as shown in Figure 38 and flown on the routes shown in Figure 39. Only flight paths which had flight times greater than three hours were counted as data flights.

A summary of the overall test program is given in Table 21, with a navigation performance for the data flights by city-pairs shown in Table 22.

A series of comparative analyses of the test data were made to establish any correlation of IRU performance with flight path. Inspection of the results shown in Table 22 shows that no flight path dependency or

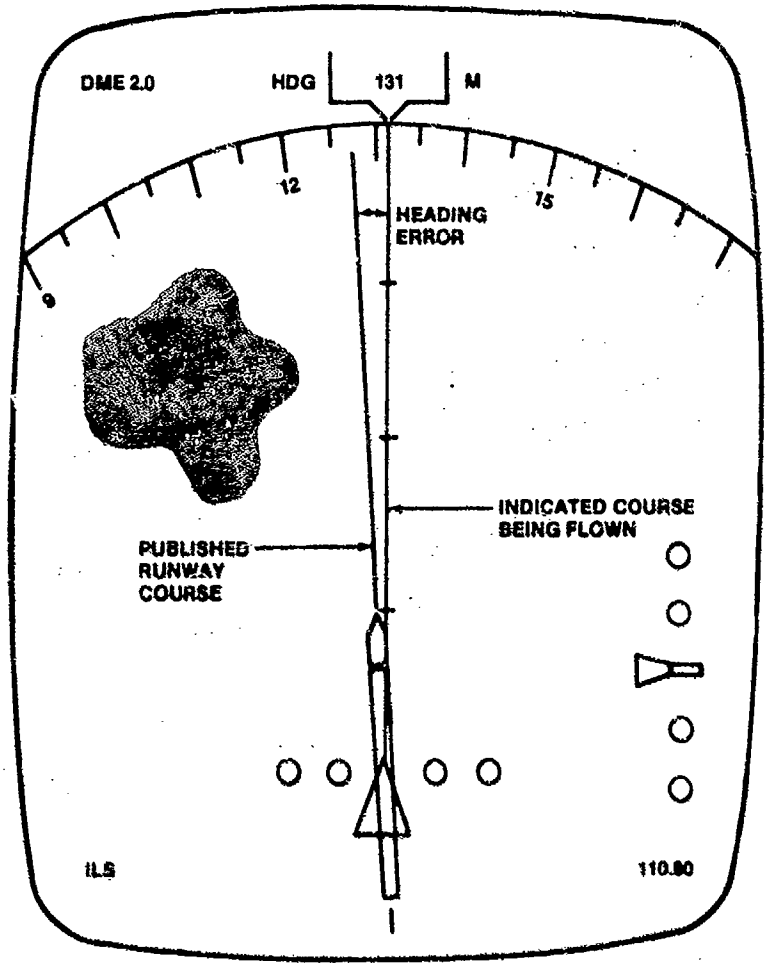

Figure 37. Mag Var Model Error During Approach

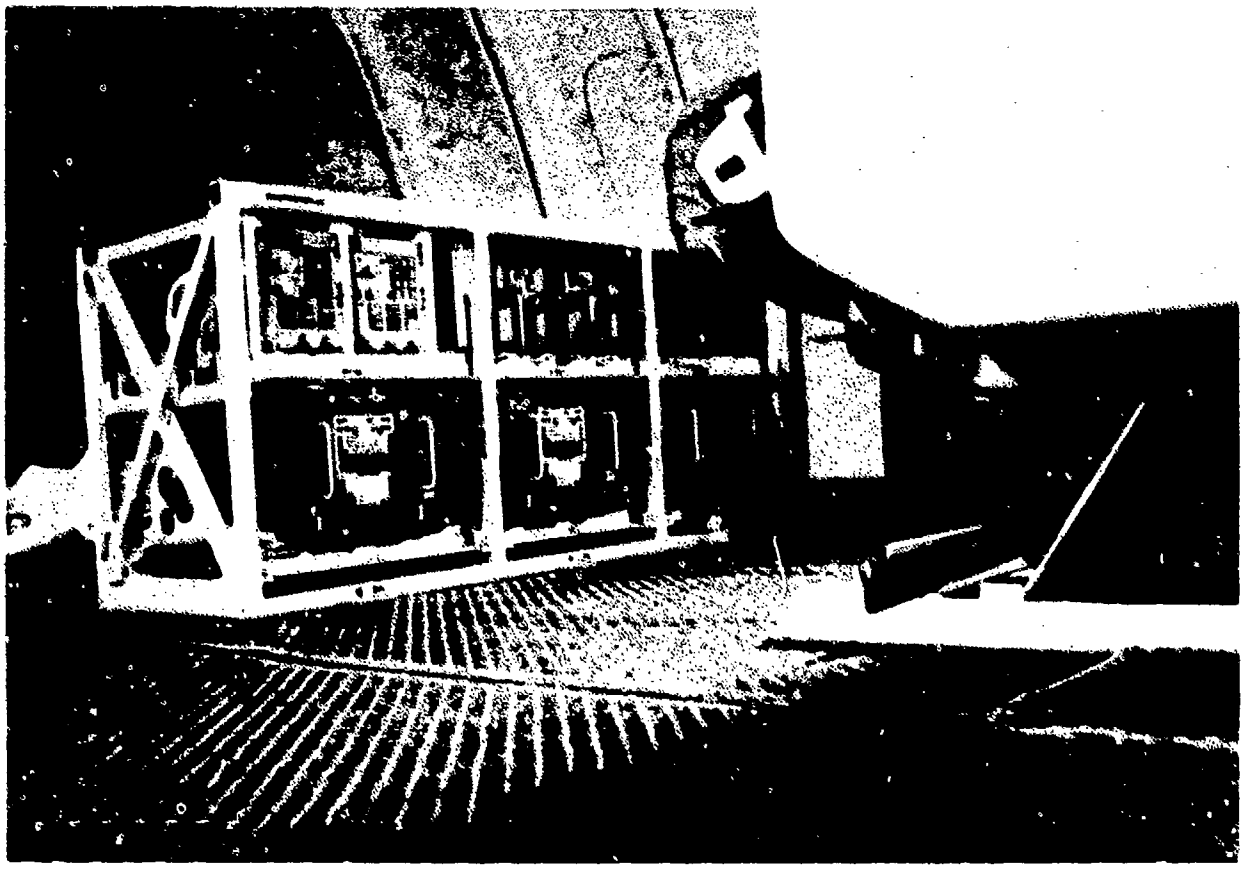

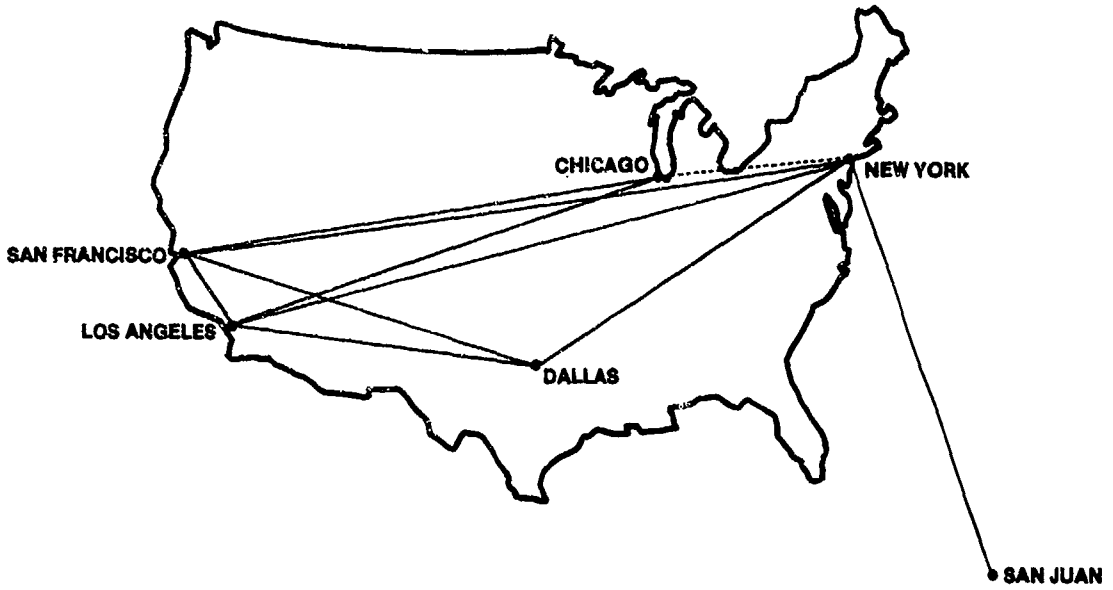

Figure 39. IRS Long Range Navigation Data Flights

Table 21. IRS Long Range Navigation Flight Test Results

Total Operating Time	1 236 hours
Total Flight Time	1 077 hours
Total System Flights	278
Total System Data Flights	165
Number of IRU's	4
Navigation Performance (Data Flights)	1.65 nm/hr (95%)
Navigation Performance (All Flights)	1.63 nm/hr (95%)
Terminal Along Track Error Rate	0.76 nm/hr (95%)
Terminal Cross-Track Error Rate	1.50 nm/hr (95%)
% IRU Flights Within Specification	99.64%
Failures	1 (false)

Table 22. Long Range Navigation Data Flight Route Summary

Route	Number of Flights		Approximate Great Circle Distance (nmi)	General Direction of Travel	Average Flight Time (hr)	Average RPER (nmi/hr)
	A/P	System				
1. JFK-DFW	2	6	1 200	SW	3.42	0.59
2. DFW-JFK	1	3	1 200	NE	3.03	0.61
3. DFW-LAX	5	15	1 070	W	3.15	0.47
4. SFO-ORD	8	24	1 600	E	3.97	1.07
5. JFK-SJU	5	15	1 390	SE	3.55	1.10
6. SJU-JFK	5	15	1 390	NE	3.74	0.77
7. JFK-LAX	5	15	2 140	SW	5.49	0.65
8. SFO-JFK	4	12	2 240	E	5.59	0.96
9. LAX-ORD	4	12	1 510	NE	3.88	0.88
10. DFW-SFO	4	12	1 270	W	3.68	0.56
11. LAX-JFK	5	15	2 140	NE	5.39	0.79
12. ORD-LAX	6	18	1 510	SW	4.20	0.83
13. JFK-ORD	1	3	640	NE	3.60	0.48
Total	55	165			4.18 (average)	

JFK = Kennedy (New York City) SFO = San Francisco
DFW = Dallas/Fort Worth ORD = O'Hare (Chicago)
LAX = Los Angeles SJU = San Juan

The method used for computing the 95% Radial Position Error rate involves ordering the data by error magnitude, then establishing the error limit which includes 95% of the data samples.

The cross-track and a long-track error rates were obtained by resolving the terminal position error into along-approach heading and cross-approach heading components, based on an assumed great circle flight path between departure and destination airports, then dividing the result by block time for each flight. The method to establish the 95% limits is the same as that used for radial error rate.

As a result of the data presented in the above summary, the applicable FAA requirements are satisfied. The radial position error rate, 1.65 nm/hr, is significantly less than the FAA requirement (FAR 121, Appendix G) of 2 nm/hr.

North Atlantic Navigation Performance Analysis

Analyses were performed on the data obtained in the American Airlines 747 flight test program to show that the IRS performance meets the specification parameters in AC120-33 as well as meeting the requirements of FAR 121 Appendix G, the basic FAA requirement for long range navigation using inertial systems. AC 120-33, North Atlantic Minimum Navigation Performacne Specification, is an FAA requirement for navigation systems used in the North Atlantic track system.

The cross track errors were computed for each data flight and successively added and plotted against the criteria in AC120-33. It is shown in Figure 40 that approximately 30 independent observations were required before reaching the "pass" region in the AC120-33 test requirements. For the remainder of the data flights, the cross track errors remained in the "pass" region. It is concluded the Honeywell IRS has shown acceptable performance for operation in the North Atlantic track system.

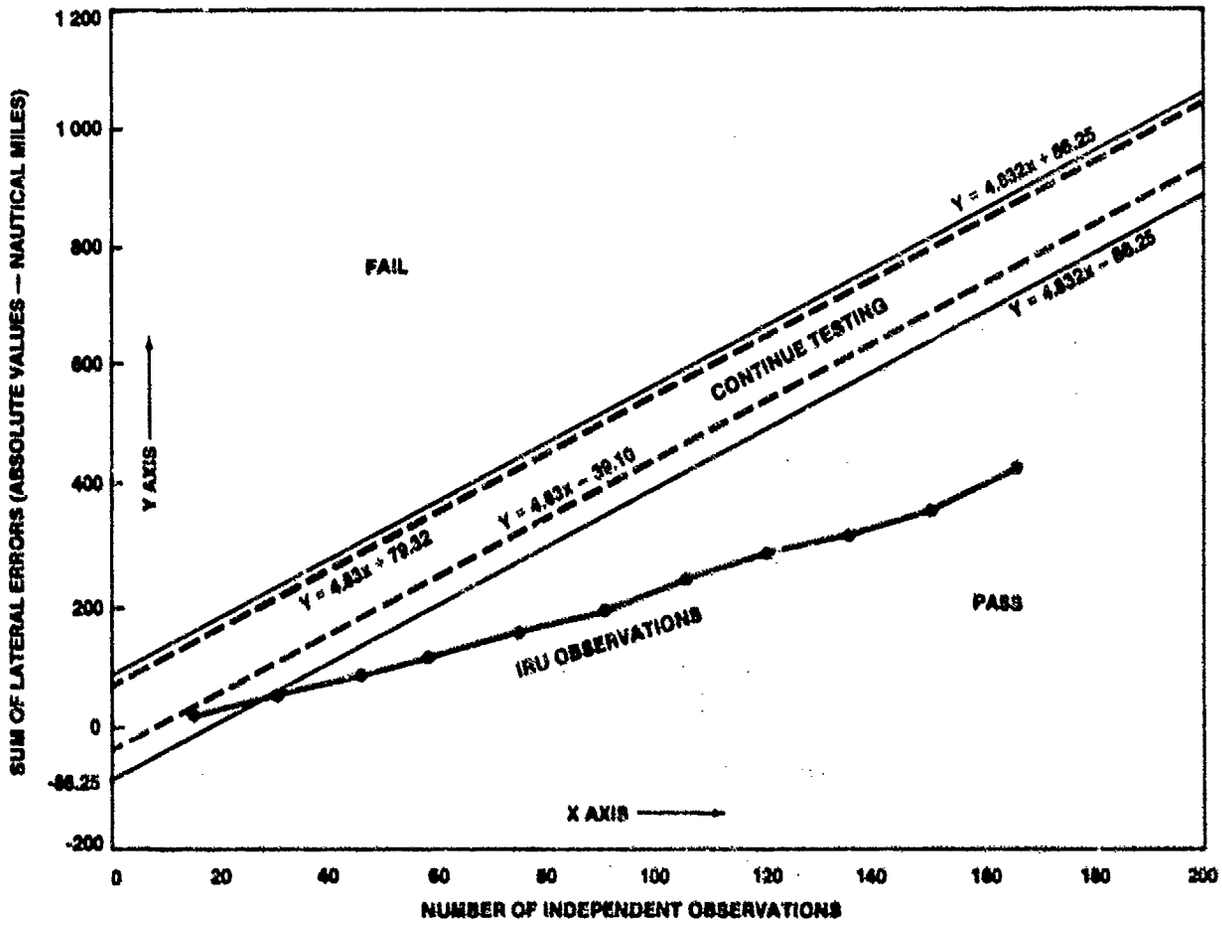

Figure 40. North Atlantic MNPS Analysis Results Using Long Range Nav Data

High Latitude Flight Test

In addition to the flight tests described a special flight was made to Deadhorse, Alasks to demonstrate high latitude alignment performance for certification. This test demonstrated a successful alignment at N70.2° latitude and the subsequent flight to Minneapolis indicated no significant effect on navigation performance, being less than 1 nm/hr after the 6 hr. flight.

RELIABILITY ASSURANCE PROGRAM

General

Reliability of the laser strapdown inertial system for commercial airplane application was a key certification issue. To reduce this risk, a series of test programs were instituted by Boeing and Honeywell to augment the experience gained in the laboratory and flight test fleet. The Boeing required tests were a 1000 hr. design stress test and reliability demonstration tests. In addition, Honeywell established their own in-house reliability development testing which augmented the Boeing test requirement.

Design Stress Test

The 1000 hour (minimum) design stress test, in accordance with Boeing specified procedures, was performed to uncover any reliability weaknesses and to accelerate maturity of the design. This test operates the equipment under electrical and thermal cycling, and vibration environments which approach but do not exceed the design margin levels. The intent is to exercise the system under extreme environmental conditions, but within its design stress limits. The test environment is much more severe than the normal airplane environment in order to accelerate design maturity. The test was performed on a single red label unit over an approximate three month period.

Reliability Demonstration

The objective of the Reliability Demonstration Test was to obtain a numerical assessment of the MTBF at the time of certification with respect to the certification requirements on IRS attitude/heading reference outputs. The following summarizes individual test conditions:

a. Temperature Cycling/Environment - One cycle per day, of which 20 hours is conducted at a chamber temperature which simulates "Normal Flight Operation" and four hours at a temperature which simulates "Low Operating Temperature" per Boeing Specification.

b. Powercycling - Power is cycled on during "Normal Flight Operation" and cycled off at "Low Operating Temperature".

c. Once every two weeks, an acceptance test is performed on each IRU and IRMP.

The first test hardware consisted of three IRU's with the initial flight test Red Label configuration. An additional six units, with the certification configuration were later included. The total accumulated test time was 2700 hours on the original test units and 10,000 hours on the six certification units. The 6 certification units exhibited only 3 relevant failures over the test period.

This reliability demonstration test was designed to simulate the normal airplane environment and the failure experience is very similar to that experienced on the flight test fleet. (3300 hrs. vs. 4250 hrs. MTBF) of the certification configuration.

Reliability Development Testing

There tests were established by the supplier to accelerate any reliability weaknesses in the system and were similar to the Boeing 1000 hr design stress test, but was extended to 10,000 hours to insure that a problem did not exist that took longer to occur that would effect warranty claims over the long term. Eighteen (18) systems were used for these tests which consisted primarily of wide thermal cycles (+65C to -40°C) high temperature operation, random vibration and power cycles at the extreme temperature conditions. The results of these tests provided excellent correlation with early failures in the flight test program and led to the determination of the cause and design corrections. In addition, several previously unidentified failure modes in the field were exposed and corrected before production units were delivered. (Ref. 6)

Production Burn-In Tests

A production burn test is required on every unit by Boeing and the current test is 168 hours long, which requires several thermal cycles between +65°C and -40°C with power cycling at these extremes. Operational vibration levels are also run several times during this test sequence. In addition, sensor burn-in tests are utilized for screening prior to installation in the IRU. These tests include 240 hours of thermal cycling for each gyro and 24 to 72 hours, depending on vendor, for accelerometers. (Ref. 6)

Boeing Flight Test Reliability Experience

Experience from the 757/767 flight test program was provided by 9 test aircraft and 91 different IRUs. A series of failures occurred in the first several months of the 767 flight test program due to improper BITE design and thresholds, and one major hardware deficiency. After these problems were identified and corrected, the system provided excellent reliability and performance. A summary of the reliability performance is given in Table 23. The significance of the early problems is to be noted with a 3 to 1 improvement of MTBF after corrective action was taken.

757/767 IRS In-Service Reliability Experience

As of December, 1983 a total of 15 airlines were flying 99 757 and 767 airplanes in revenue service. A total of 515,000 IRU flight hours and 772,500 unit operating hours had been accumulated with an overall MTBF average of 8200 flight hours and 12,000 op-hrs being experienced with 174 removals. This excellent performance compares to a mature (15 years) inertial technology of gimballed systems with about 2500-3000 hrs MTBF, in commercial service. The three month running averages in December, 1983 were 9600 flight hours, and 14,000 op hours, MTBF. The MTBF 3-month running average history is shown in Figure 41.

Table 23. IRS Reliability Experience During Flight Test of 757/767

Before Corrective Action	
Total removals	44
In-flight failures	4
Unit operation hours	60 000
Unit flight hours	4 600
MTBF operation hours	1 360
MTBF flight hours	1 150
After Corrective Actions	
Total removals	8
In-flight failures	1
Unit operation hours	34 000
Unit flight hours	3 400
MTBF operation hours	4 250
MTBF flight hours	3 400 (1 failure)

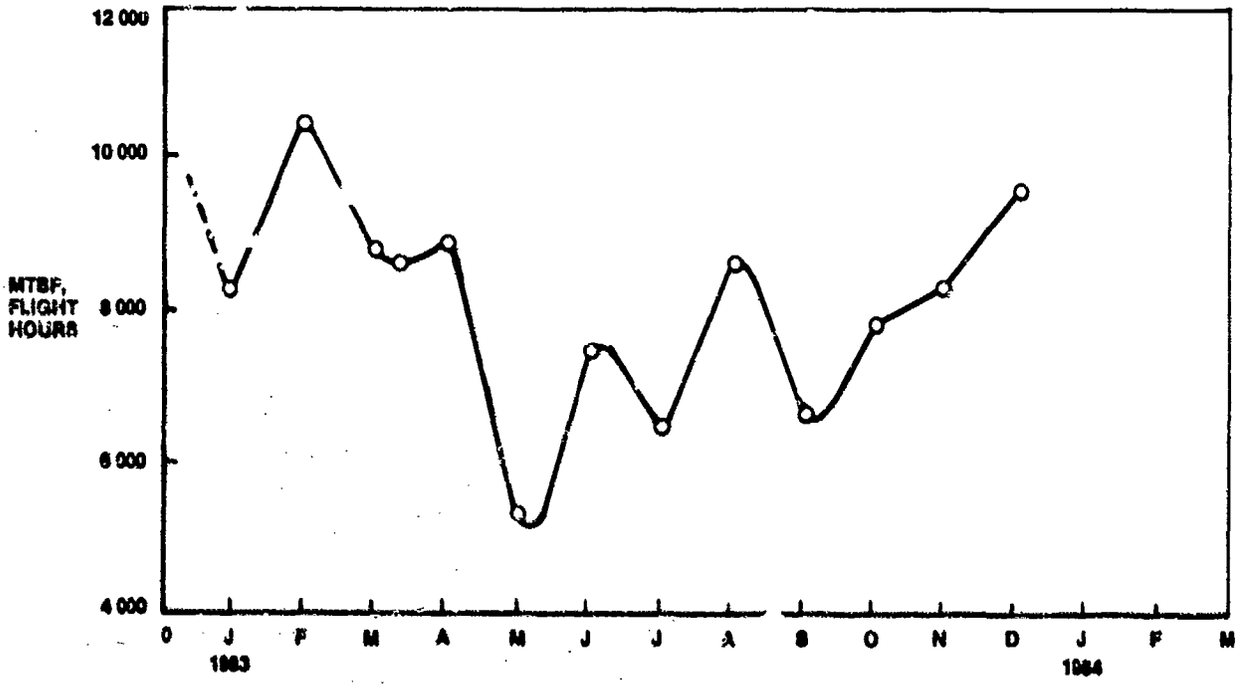

Figure 41. IRU Airline Fleet MTBF — 3 Month Moving Average

The distribution of the 63 confirmed failures from the removals during this period are the following:

- electronics - 34
- accel - 5
- gyro - 24

estimate of gyro reliability - 100,000 op-hrs
accel reliability - 425,000 op-hrs

Navigation performance data has not been available except through failure reports of unacceptable NAV performance. Limited data has been taken on one airline for a month in the summer of 1983 and showed performance similar to that exhibited during flight test with the velocity data being significantly better. The latter was expected because airline flight profiles do not have heading changes to "pump" the Schuler as occured in Boeing flight test.

This in-service experience is five times better than the vendor or Boeing ever expected, for the first year of use, and certainly demonstrates the "payoff" predicted for strapdown inertial and digital technology.

CONCLUSIONS

The recent successful introduction of the laser gyro strapdown inertial system into commercial airplane service with the Boeing 757 and 767 airplanes has proven that this technology is a very viable product. The reliability demonstrated has been five times the predicted value at this point in service and is three times better than the mature gimbal inertial technology. This has been achieved without any sacrifice in performance which has been more than adequate for commercial operations. For the first time ever, a system is now available to completely determine the airplane state and at a very reasonable cost. It is believed that this complete inertial data system has contributed significantly to the success of the 757/767 airplane operation and systems acceptance. Inertial technology is no longer economical only on long range airplanes, but is now available at a cost acceptable for short to medium range aircraft, especially those that take advantage of the inertial data available to enhance the airplane's operational capacity. A summary of the primary achievements of the Boeing/Honeywell laser gyro strapdown application is given in Table 24.

Table 24. Honeywell Laser Gyro IRS/Boeing 737/757/767 Industry "Firsts"

- "First" application of inertial system technology to short to medium range airplanes as basic equipment for attitude and heading-navigation considered to be a secondary function
- "First" application of production laser gyro based strapdown inertial system
- "First" application of all digital inertial system to commercial airplanes
- "First" application of a strapdown inertial system to meet all vehicle inertial data requirements for navigation, guidance, and control — eliminated all body mounted rate gyros and accelerometers
- "First" commercial airplane to use "synthesized" magnetic heading as primary airplane heading
- "First" commercial airplane to use inertial vertical velocity for primary vertical speed indication

REFERENCES

1) D6-47029, Boeing Document, "AGCS Strapdown Sensor Working Specification", J. Gilbert/N. McIntyre/G. Olbrechts/J. C. Shaw

2) J. C. H. Shaw, "Benefits of Strapdown Over Gimbal Inertial Systems for Aircraft Application", Boeing Commercial Airplane Company, Naecon Conference, May, 1976, Dayton, Ohio, USA.

3) P. J. Fenner and C. R. McClary, "The 757/767 Inertial Reference System (IRS)", Fourteenth Joint Service Data Exchange for Inertial Systems, 18-20 Nov. 1980, Clearwater, Florida, USA.

4) P. J. Fenner, "Application of Laser Inertial Technology to Commercial Airplanes", AIAA/IEEE Digital Electronics Conference, Nov. 1983, Seattle, Washington, USA.

5) T. H. Friddell, "Software Verification - A Case Study of The 757/767 Inertial Reference System", AIAA/IEEE Digital Electronics Conference, November, 1983, Seattle, Washington, USA.

6) R. R. Shoquist, "The ARINC 704 Ring Laser Gyro Inertial Reference System", National Technical Meeting of the Institute of Navigation (ION), January 17-19, 1984, San Diego, California.

SYSTEMES INERTIELS LIES A GYROMETRES BALOURDES POUR MISSILES TACTIQUES

par

J.L.Michelin
Responsable des Etudes "Systèmes Inertiels Liés"
Société de Fabrication d'Instruments de Mesure (SFIM)
13 Avenue Marcel Ramolfo Garnier
91301 Massy, France

et

P.Masson
Ingénieur d'Essais Composants Inertiels
Laboratoire de Recherches Balistiques et Aérodynamiques (LRBA)
27207 Vernon, France

0 - RESUME

Depuis 1974, SFIM a lancé des études sur les systèmes inertiels liés à base de gyros secs ; après les premières études de faisabilité (74) - Voir AGARD LS n° 95 - SFIM développe depuis 1979 des matériels pour un grand nombre d'applications parmi lesquelles les applications missile tactique sont les plus importantes.

Tous les développements actuels sont basés sur quelques concepts - gyros balourdés - numérisation complète de l'électronique - qui conduisent à une famille de systèmes - SIL 1 - ou les contraintes de volume et de coût sont les plus importantes. L'exposé qui suit décrit ces concepts de base, quelques exemples d'utilisation et les résultats d'essai obtenus par SFIM et surtout par le LRBA sur quelques matériels maquettes et prototypes.

PREMIERE PARTIE : SFIM

1 - HISTORIQUE

Depuis 1972, SFIM fabrique des gyroscopes accordés miniatures - GAM - pour des applications diverses - gyromètres ; stabilisation optique. En 1974, SFIM a été retenue par les services officiels français (STET) pour les premières études de faisabilité sur les systèmes inertiels liés ; l'étude portait sur l'application missile tactique, au moment où peu de missiliers n'imaginaient encore le besoin.

Cette étude de faisabilité, suivi d'autres concernant les applications hélicoptères, torpille, s'est conclue avec livraison aux centres d'essai officiels, de plusieurs matériels ; SFIM présentait en 1978, une conférence dans le cadre AGARD (LS 95), où on décrivait un matériel prototype - SIL 3 - qui a depuis été testé par le Centre d'Essais en Vol (CEV) de Brétigny, et le LRBA, avec des résultats très encourageants :

- stabilité : $0{,}5^{\circ}/h$ 1σ sur une gamme de 100°/sec et sur 1 an.
- CEP $<$ 100 mètres sur un vol de 2 minutes.

A partir de 1979, le développement de matériels prototypes associés à des programmes a débuté, pour des applications diverses, avec une forte demande sur les missiles tactiques : air-air - mer-mer - air-sol - sol-air, et autres. SFIM s'est alors attaché à développer une famille cohérente de références inertielles liées de 2 types :

* SIL 2 : à base de 2 gyromètres 2 axes GAM et 3 accéléromètres
* SIL 1 : à base de 3 gyromètres GAM balourdés

Ces références inertielles liées, peuvent être ensuite intégrées, comme module, dans des systèmes inertiels plus complets (applications hélicoptère et torpille par exemple).

La famille SIL 1, utilisée sur la presque totalité des matériels en développement ou en étude, est l'objet de cet exposé.

2 - BESOINS MISSILES TACTIQUES

Les applications sur missiles tactiques ont mis en évidence des besoins particuliers :

- Référence inertielle multirôle

Les objectifs de volume et de coût au niveau missile ont conduit les missiliers à définir la référence inertielle pour réaliser souvent 3 fonctions différentes :

- guidage inertiel

La référence inertielle doit fournir au calculateur missile des informations de déplacement angulaire et linéaire précises pour assurer un bon préguidage inertiel avant accrochage autodirecteur.

- Pilotage

Les capteurs liés de la R.I. sont utilisés en gyromètres et accéléromètres de pilotage (ensemble gyroaccélérométrique 3 axes).

- Stabilisation

De plus en plus, les informations RI sont utilisées pour la stabilisation autodirecteur (mécanique ou électronique).

Le premier besoin demande de la précision moyenne, alors que les deux autres font appel à une bonne qualité des fonctions de transfert et de niveau de bruit. Il s'agit classiquement de performances difficiles

On peut citer les valeurs suivantes, recouvrant l'ensemble des applications missiles tactiques.

- 1 à 100°/h (1 σ)
- 1.10^{4} à 1.10^{-2}g (1 σ)
- 1.10^{-4} à 1.10^{-3} err. fact. ech. (1 σ)
- bande passante $>$ 100 Hz
- bruit $<$ 0,1% gamme

Les concepts mis en place à la SFIM répondent à ces besoins particuliers :

- Dynamique élevée

La dynamique du missile augmente en fonction de la diminution des inerties, de l'efficacité des gouvernes et du pilotage, en fonction surtout des capacités opérationnelles désirées.

On cite couramment, comme valeurs maximales possibles :

. 50.000°/s^2
. 2000°/s
. 100 g

Cette demande de "haute dynamique" se combine bien entendu difficilement avec le besoin de performances en guidage.

- Volume et coût

Il s'agit d'un objectif prioritaire. La diminution du volume et du coût missile entraîne une contrainte équivalente au niveau référence inertielle ; encore faut-il évaluer le coût RI dans son aspect multifonction (à comparer avec le coût d'une solution classique capteurs de guidage + capteurs de pilotage + capteurs pour la stabilisation auto-directeur).

La solution SFIM SIL 1 est résolument orientée vers ces objectifs de volume et de coût, on peut citer :

- volume 1,5 litres
- prix 150 KF (1982 HT)

3 - CONCEPTS PARTICULIERS

Tous les systèmes inertiels liés SFIM sont basés sur la famille de gyroscopes GAM 1G ; les caractéristiques générales en sont les suivantes :

- encombrement typique : Ø 31 x 35 mm
- cardan à lames croisées
- moteur d'entraînement synchrone,
- moteur couple à aimant samarium cobalt (mono/bicouronne suivant les applications).

Voir figure 1.

Ce gyroscope est utilisé en gyromètre associé à une boucle d'asservissement, et une commande ternaire modulée en largeur, qui est apparue le meilleur compromis simplicité-performances (statique et dynamique).

Ce gyromètre est utilisée avec des accéléromètres Qflex dans le système SIL 2.

Dans les systèmes type SIL 1, il est intégré dans une structure faisant appels à quelques concepts particuliers développés à la SFIM depuis plusieurs années.

3.1. Gyromètre balourdé

Les premières études sur le gyro balourdé et ses applications ont débuté à la SFIM en 1977.

Si le centre de gravité du volant - G - n'est plus confondu avec le centre de suspensions - S - (balourdage), le gyro devient sensible à des accélérations horizontales (voir figure 2).

Un modèle simplifié du fonctionnement est :

$Mx = \omega y - B.\ \gamma y$
$My = -\omega x + B.\ \gamma x$

. ωx, ωy : vitesse angulaire boîtier (deg/sec)
. γx, γy : accélération linéaire boîtier (g)
. Mx , My : couples appliqués par les moteurs (deg/sec) ; mesures effectuées par le capteur
. B : balourd, proportionnel à la masse du volant et à la distance GS (deg/sec/g).

Un modèle plus complet fait apparaître l'expression des couples en fonction des mesures Sx, Sy (facteurs d'échelle directe et croisée K), l'erreur de positionnement moyenne du spin γx, γy, les dérives Dx, Dy, les termes de non linéarités, les autres termes du modèle en accélération, le terme d'anisoinertie, et les termes dynamiques (inertie, oscillations moteur, débattement,...) nuls à vitesse ω, constante ∂x, ∂y, avec un résidu Rx, Ry.

$Kxx\ .\ \ + Kxy\ .\ Sy + NL\ (Sx, Sy) + Dx + Bx.\ \gamma y + P\ .\ \gamma x$
$\quad \omega y + \gamma x\ .\ \omega z + Cai\ .\ \omega y\ .\ \omega z + \partial x + Rx$

$Kyx\ .\ Sx + Kyy\ .\ Sy + NL\ (Sx, Sy) - Dx - By.\ \gamma x + P\ .\ \gamma y$
$\quad = -\omega x + \gamma y\ .\ \omega z - Cai\ .\ \omega x\ .\ \omega z + \partial y + Ry$

Le gyromètre mesure donc une combinaison de vitesses angulaires et d'accélérations ; avec deux mesures par gyro, il suffira de 3 gyromètres pour obtenir 6 mesures, d'où on tirera les 6 informations utiles : ωXM, ωYM, ωZM et γxM, γyM, γzM (axes missile). Pour celà, il faut faire un choix convenable pour les balourds et le positionnement des axes capteurs ; ce choix dépend de l'application, il apparaît cependant que la meilleure séparation ω, γ s'obtient en positionnant les 3 spins gyros suivant un trièdre, et en maximisant les écarts de balourds $|B2 - B3|$, $|B3 - B1|$, $|B1 - B2|$, ce qui conduit à l'organisation typique suivante :

- gyro 1 non balourdé, spin suivant Xm,
- gyro 2 balourdé > 0, spin suivant Ym,
- gyro 3 balourdé < 0, spin suivant Zm.

avec $|B2| = |B3|$
Voir figure 3.

On trouve (même notation que précédemment) :

$Mx2 = \omega z$
$My1 = -\omega y$

$Mx2 = \omega x - B.\gamma x$
$My2 = -\omega z + B.\gamma z$

$Mx3 = \omega y + B.\gamma y$
$My3 = -\omega x - B.\gamma x$

Ce qui donne :

$\omega x = \frac{1}{2}(Mx2 - My3)$

$\omega y = -My1$

$\omega z = Mx1$

$\gamma x = -\frac{1}{2B}(Mx2 + My3)$

$\gamma y = (Mx3 + My1) / B$

$\gamma z = (My2 + Mx1) / B$

On peut faire un certain nombre de remarques :

- Il n'y a qu'un seul type de capteur ; le balourdage d'un gyro correspond à un réglage possible de l'écrou de balourd ; l'obtention d'un balourd inverse s'obtient en faisant tourner le gyro en sens inverse.

- La capacité de mesure accélérométrique n'est pas limitée par elle même ; on choisit la valeur de balourd utilisé B en fonction des trajectoires de vol ; valeur typique de 1°/s/g à 10°/s/g.

- La mesure accélérométrique bénéficie des performances gyro :

  par exemple, biais accéléro = D/B
  ou D est la dérive gyro.

  (5°/h (1 σ) et 5°/s/g $\longrightarrow 3.10^{-4}$ g (1 σ))

- la solution à gyro balourdé entraîne un effet secondaire :
  sensibilité des mesures accélérométriques en fonction des vitesses angulaires, à travers les erreurs de facteur d'échelle essentiellement.

Un modèle d'erreur simplifié du SIL 1 a la forme matricielle suivante :

$$\left|\frac{\delta\omega}{\delta\gamma}\right| = \left[Sij\right] \cdot \left|\frac{\omega}{\gamma}\right| + \left|\frac{D}{b}\right|$$

où, $\delta\omega$ est l'erreur de mesure de ω
$= [\delta\omega x, \delta\omega y, \delta\omega z]'$
. $\delta\gamma$ est l'erreur de mesure de γ
. $D = [Dx, Dy, Dz]'$ dérives système
. $b = [bx, by, bz]'$ biais système.

Les coefficients Sij sont des termes de sensibilités ;on fait apparaître des termes croisés

$$\delta\omega = S.\omega$$

où S contient des termes de la forme

$$S = \varepsilon k/B$$

où k est l'erreur de facteur d'échelle gyro, B le balourd.

L'effet de ce terme de couplage doit être examiné en fonction de l'application ; dans le cas des missiles tactiques, l'accélération mesurée (facteur de charge) est largement orthogonale à la vitesse angulaire, ce qui tend à annuler l'effet de couplage.

Dans le cas de l'application missile, il reste l'accélération initiale souvent associée à un mouvement en roulis (missile non piloté) :

Valeurs typiques : - 360° en roulis
- $\varepsilon k : 5.10^{-4}$
- B = 5. deg/sec/g

$\longrightarrow$ erreur de vitesse de 0,4 m/sec en fin de phase initiale, due à l'effet de couplage.

Voir figure 4.

Une analyse fine de cet effet de couplage est faite pour chaque application, sur un ensemble de trajectoires type (analyse avec matrice de covariance) ; il apparaît que dans la plupart des cas, ce terme ne grève pas nettement le budget d'erreur.

La figure 5 présente les performances comparées de systèmes SIL 1 et SIL 2 typiques sur une trajectoire typique d'une application missile tactique courte portée ; les spécifications des composants sont semblables.

	SIL 1	SIL 2
Dérive	18°/h (1 σ)	18°/h (1 σ)
Balourd	5°/s/g	/
δB	9°/h/g (1 σ)	9°/h/g (1 σ)
δKg	1.10^{-3} (1 σ)	1.10^{-3} (1 σ)
δKa	/	1.10^{-3} (1 σ)
δba	/	$1.10^{-3}g$ (1 σ)

3.2. Numérisation de l'électronique

Les systèmes inertiels liés n'ont pu être développés qu'avec l'apparition des microcalculateurs, une partie importante des fonctions spécifiques d'une plateforme à cardans (stabilisation) étant faite par logiciel.

Compte tenu de l'évolution technc gique rapide de la microinformatique, SFIM a orienté dès 1977 ses études dans deux directions complémentaires :

- effectuer le plus grand nombre de tâches système par logiciel,
- numérisation la plus complète de l'électronique, utilisant la technologie actuelle.

Ce sont des moyens pour atteindre à terme les objectifs principaux :

- diminution du volume et du prix,
- souplesse de conception et d'évolution du matériel,
- augmentation des performances.

On examine successivement les aspects logiciel et matériel.

3.2.1. Logiciel

L'option logiciel choisie par SFIM va au delà de ce qui est couramment pratiqué :

- Tous les signaux sont numérisés le plus près possible des capteurs : angles d'écart, sondes de températures, commandes moteurs-couple,....
- Un seul microprocesseur 16 bits se charge de toutes les fonctions système, pour les 3 gyros (multiplexage) :

  . acquisition des informations (analogiques, discrets....),
  . bouclage (3 gyros),
  . sorties internes ou système (commandes moteurs-couple, discrets....),
  . traitement dynamique (voir § 3.3.2.),
  . séparation des informations ω / γ
  . sortie sur bus numérique externe,
  . compensations
  . autotests,
  . séquencement.

Comme on le voit, la fonction bouclage est ici réalisée par logiciel.

Les angles d'écart sont codés (12 bits) et envoyés au microprocesseur 16 bits, après un traitement préliminaire (mise à l'échelle, décalage, réjection de bruit - voir § 3.3.3). On exécute par logiciel les fonctions classiques - action proportionnelle et intégrale, avance de phase, correcteur spécifique - ce qui fournit une valeur de précession sur 16 bits, qui est ensuite quantifiée en 8 ou 12 bits (suivant les applications) pour la transformation numérique - modulation effectuée par hardware (codeur N/A spécifique) ; voir figure 6.

Les axes gyros sont traités ensemble (multiplexage).

La solution logicielle offre un grand nombre d'avantages, sans aucun inconvénient :

- élimination du matériel correspondant à la fonction bouclage,
- grande souplesse de conception et d'évolution du matériel,
- réalisation de fonctions impossibles à faire au niveau matériel,
- le microprocesseur possède par principe, toutes les informations nécessaires pour la mesure, et des traitements sophistiqués (voir § 3.3.).

Bien entendu, pour réaliser toutes ces fonctions dans 1 seul microprocesseur, il est nécessaire d'écrire un logiciel avec un grand soin, directement en assembleur, le problème principal étant de minimiser l'occupance sans nuire à la modularité du logiciel.

Implanté sur un microprocesseur 16 bits puissant (INTEL 8086/186/286 ou MOTOROLA 68000), on obtient, avec une organisation synchrone du logiciel, 3 niveaux d'interruptions cycliques, une occupance de 80 à 90%; une répartition typique des tâches est présentée dans ce document.

3.2.2. Matériel

Les contraintes de volume nécessitent l'utilisation de technologies électroniques très intégrées, on peut citer :

- hybridation des fonctions analogiques (précision, puissance), et de quelques fonctions numériques,
- développement de fonctions numériques spécifiques avec composants prédiffusés ou précaractérisés (bipolaires ou CMOS),
- montage "chip carrier" directement sur circuit,
- circuits multicouche flex. rigide monobloc (pour éliminer les connecteurs).

Le gain de volume total de l'électronique est dans un rapport 5 à 10, par rapport à une électronique équivalente en composants discrets.

Le gain en prix est sensible (50%) sur les fonctions numériques et analogiques bas niveau ; l'hybridation des fonctions analogiques de puissance ou de précision reste chère.

La figure 7 montre une carte flex.rigide avec des fonctions analogiques et puissance hybridées.

3.3. Performances dynamiques

Les applications missiles tactiques, en particulier les petits missiles (air-air, sol-air....) demandent des performances dynamiques spécifiques, parmi lesquelles :

- tenue en accélération angulaire élevée ($> 50.000°/s^2$),
- sortie vitesse angulaire à haute cadence (>1 KHz), retard faible ($<$ 1 m sec), bande passante élevée ($>$ 150 Hz),
- niveau de bruit faible ($<$ 0,1% étendue de mesure).

Les possibilités offertes par la numérisation complète des signaux et la microinformatique permettent de résoudre la totalité de ces problèmes, sans matériel supplémentaire, et souvent sans solution de remplacement matérielle convenable pour une fonction équivalente.

3.3.1. Tenue en accélération angulaire

Un des problèmes à prendre en compte pour la tenue en accélération angulaire concerne le moteur d'entraînement synchrone (à hystérésis ou à aimants permanents).

Il est connu qu'un moteur synchrone :

- peut décrocher sous forte accélération angulaire le long de son axe de rotation (effet d'inertie de l'ensemble tournant),
- oscille naturellement sous l'effet de couples parasites, de perturbations dynamiques.

Une électronique de commande numérique de champ tournant, gérée par microprocesseur permet de répondre au problème, elle réalise l'asservissement de phase du champ tournant, ramenant un amortissement électronique.

On utilise une information de position toupie (1 top par tour) ; cet asservissement, fait par logiciel, commande le champ tournant (à travers correcteur, filtrage) en prenant en compte les informations d'accélérations angulaires mesurées par les autres capteurs (voir figure 8), d'où une avance de phase physique améliorant largement la tenue en accélération angulaire.

Associé à une commande discrète de surtension (gérée aussi par logiciel), on atteint $100.000°/s^2$ avant décrochage, pour une consommation statique autour de 1W ; voir exemple de réponse dynamique figure 9.

3.3.2. Bande passante élevée

Le microprocesseur 16 bits effectue par logiciel le bouclage des 3 gyromètres, il possède donc pour chaque gyro, les informations utiles pour reconstituer l'entrée gyro (vitesse angulaire boîtier) : commandes moteur-couple, angles d'écart, variables internes.

SFIM a mis au point un algorithme d'observation (issu de la théorie des observateurs, en automatique avancée), qui reconstitue l'entrée $\underline{\omega}e = [\omega ex, \omega ey]'$ en $\underline{\hat{\omega}}e$ avec une fonction de transfert $\underline{D}$ e $/\underline{\omega}e$ proche d'un retard pur ; voir figure 10.

Il apparaît en effet que le vecteur d'état représentant l'ensemble du gyroscope et de sa boucle est mesurable (soit directement, soit par observation d'état).

L'ensemble bouclage + algorithme d'observation d'estimation est optimisé pour donner un algorithme implantable sur le microprocesseur.

On montre que la reconstitution est utilisable pour toute fréquence, hors d'une zone entourant la fréquence de nutation (fn $\pm$ 10%) ; voir figure 11.

On découple ainsi complètement :

- la fonction de transfert du bouclage proprement dit, qui donne la limitation en dynamique et joue sur les performances.
- La fonction de transfert de la sortie numérique, qui est le résultat d'un algorithme d'observation (traitement numérique par le logiciel).

Pratiquement, il est possible d'abaisser la vitesse de rotation de la toupie, afin d'obtenir une forte capacité de précession sans pour autant limiter la boucle passante de l'information numérique fournie.

Il est évident qu'un tel concept ne peut être mis en oeuvre qu'avec un bouclage gyro entièrement réalisé par logiciel.

3.3.3. Niveau de bruit

L'algorithme d'observation a l'inconvénient d'augmenter le niveau de bruit ; de nombreuses précautions sont donc prises au niveau logiciel et matériel pour atteindre l'objectif de 0,1% de l'étendue de mesure :

- résolution 12 bits sur l'entrée (angles d'écart) et la sortie (commande moteur couple),

- précautions nombreuses sur les erreurs de quantification,
- réjection des bruits No + harmoniques, caractéristiques du gyro sec, type GAM 1G.

Ce dernier point utilise :

- la nature déterministe du signal (modélisation temporelle),
- l'information de position toupie, déjà utilisée pour l'asservissement du moteur d'entraînement.

Il apparait que le bruit résiduel sur la sortie numérique $\widehat{\omega}$, est approximativement une dérivée de bruit blanc numérique filtré, de la forme.

$$b_{\omega\, n} = \lambda * b_{\omega\, n-1} + (1 - \lambda).\, b'_{\omega\, n}$$

$$b'_{\omega\, n} = bb_n - bb_{n-1}$$

bb bruit blanc.

4 - SYNTHESE

Comme annoncé dans l'introduction, la totalité des systèmes inertiels SFIM sont organisés autour des 2 types de références inertielles :

- SIL 2 : 2 gyromètres GAM 1 G non balourdés et 3 accéléromètres Qflex.
- SIL 1 : 3 gyromètres GAM 1 G balourdés en mettant en oeuvre les concepts décrits précédemment.

La référence inertielle SIL 1 est utilisée dans 80% des applications en études ou en développement chez SFIM.

On peut décrire très généralement une référence inertielle SIL 1 typique, pour missile air-air, en effectuant une synthèse des études et développement en cours (confidentiels) :

- classe 10°/h ; 1.10^{-3}g. (1σ),
- 500°/sec (X) ; 150°/s (Y, Z) ; 40 g XYZ ; 50.000°/s^2 (X),
- volume $< 1{,}5$ l,
- sorties numériques sur bus MIL 1553 B (cadence $>$500 Hz) communes pour les 3 fonctions : guidage, pilotage, stabilisation.

Voir fig. 12 l'ensemble simplifié des caractéristiques.
Voir figures 13 et 14 les encombrements.

Cette référence contient :

- 3 gyromètres GAM 1 G (description plus haut), montés sur un support mécanique,
- un microprocesseur monopuce 80186 avec 8 K PROM, 2 K EEPROM et 2 K RAM,
- 8 hybrides (4 différents) pour les fonctions analogiques de puissance ou de précision,
- quelques prédiffusés ou précaractérisés pour les fonctions numériques spécifiques (horloges) et quelques fonctions standard, montés en "chip carrier" directement sur le circuit,
- les circuits liaison E/S type MIL 1553 B,
- les circuits de réchauffage,
- une alimentation, à partir d'une tension 27V non régulée,
- un boîtier mécanique contenant l'ensemble.

La figure 15 donne le positionnement des axes gyros. La figure 16 donne le synoptique de principe, avec les diverses informations.

La figure 17 précise l'organisation "temps réel" du logiciel.

Remarques :

- on visualise sur la figure l'asservissement gyro par microprocesseur, ainsi que la commande numérique des moteurs d'entraînement,
- la commande des moteurs couples est ternaire modulée en largeur,
- le positionnement à 45° des axes capteurs permet une dynamique agrandie sur l'axe de roulis, toujours particulier sur un missile,
- la répartition des tâches logiciel (avec l'échantillonnage des angles d'écart présenté) est optimisée pour le bouclage gyro, et une sortie numérique avec faible retard.

Le volume de cette référence inertielle type est de 1,5 litres, avec la décomposition suivante :

. capteurs + support : 0,3 litres
. électronique : 0,5 litres
. alimentation : 0,5 litres
. mécanique : 0,2 litres

5 - CONCLUSION

La référence inertielle SIL 1 présentée est le coeur de la plupart des systèmes inertiels liés en étude ou en développement à la SFIM ; de 1977 à 1983, SFIM s'est attachée avant tout à la diminution des volumes et des coûts, il apparaît que dès à présent, la réalisation d'une référence inertielle de classe 10°/h, 1.10^{-3}g, 500°/sec, dans une valeur de 1,5 litres est obtenue sans difficultés ; cette référence inertielle, complètement numérisée, a une capacité multifonction.

L'extension à des systèmes plus complets est immédiate :

- système de guidage/pilotage autonome (attitude, vitesse, position) : pas d'augmentation de volume (fonctions logiciel).
- système de navigation hybride pour hélicoptère (avec doppler, baro, référence magnétique) : système STIRS, en cours de développement.
- système de guidage/pilotage pour torpille.

La SFIM a été retenue en 1981 pour le développement de tout le système de guidage/pilotage/gestion de la nouvelle torpille développée en FRANCE : système CAPITOLE ; la référence inertielle retenue utilise des gyros balourdés et une électronique entièrement numérique.

La figure 18 donne les principaux matériels, à base de SIL, en cours d'étude ou de développement à la SFIM, on met en évidence la décroissance de volume obtenue en quelques années.

Il apparaît que le gyroscope sec type GAM est une voie à poursuivre plus que jamais ; sa sensibilité aux accélérations, bien utilisée, est en fait un avantage évident.

Cet avantage apparaît aussi lorsqu'on recherche une redondance, le gyro balourdé permettant de l'obtenir indifféremment pour les informations gyrométriques et accélérométriques.

Les progrès dans cette technologie se feront par une diminution de l'inertie des parties tournantes, ce qui entraîne une diminution des puissances consommées ; un gain très important sur l'alimentation et les électroniques de puissance est alors attendu, ainsi qu'une numérisation encore plus poussée.

SFIM développe de nouveaux capteurs mettant en oeuvre ces quelques idées générales ; affaire à suivre...

SECONDE PARTIE : LRBA

1 - INTRODUCTION

Dans le cadre des études générales de guidage des missiles futurs, le LRBA a été conduit à évaluer la première maquette de référence inertielle à gyromètres balourdés étudiée pour le pré-guidage inertiel, le pilotage et la stabilisation de l'auto-directeur du missile.

Le système proposé représente une solution nouvelle au problème posé en ce sens qu'il fournit simultanément les informations nécessaires au guidage, pilotage et stabilisation et qu'il utilise pour ce faire une référence à composants inertiels liés (R.I.) dans laquelle la fonction accélérométrique est obtenue par balourdage axial de la toupie de 2 ou 3 gyromètres à suspension dynamique accordée constituant le bloc capteur.

Le concept du gyromètre devait normalement conduire à ré-examiner les différentes méthodes et modèles utilisés pour l'évaluation des matériels. De plus, le domaine de variation des entrées ayant tendance à s'élargir vers les hautes vitesses et accélérations angulaires et linéaires, le problème de l'adaptation des moyens existants s'est posé et reste en partie non résolu.

Ce problème de l'évaluation est abordé ici sous le simple aspect de caractérisation statique du capteur et de la référence inertielle, c'est-à-dire celui de la modélisation et de l'estimation des coefficients des modèles pour des entrées en vitesse angulaire et accélération linéaire constantes. De plus, cette caractérisation s'applique à des matériels préliminaires n'intégrant pas l'ensemble des résultats des études passées et en cours. L'accent est mis naturellement sur les aspects de l'expérimentation liés au principe du gyromètre balourdé.

2 - MATERIELS EVALUES

Les essais ont été conduits tout d'abord sur un gyromètre balourdé à suspension accordée SFIM GAM 1G3 représentatif sur le plan gyroscope seul de ce que pourrait être le gyromètre prototype et donc à l'exclusion du bouclage gyrométrique et autres dispositifs spécifiques liés à sa mise en oeuvre dans la R.I., tels que chauffage et alimentations, ainsi que de l'interface mécanique et environnement thermique.

L'asservissement du gyromètre est assuré par une boucle de laboratoire à commande continue en courant.

Ces essais ont été poursuivis sur une maquette de référence inertielle SFIM SIL IN-M02 censée être représentative du niveau des performances visées à l'exclusion des points suivants :

- encombrement (seul le bloc capteur est représentatif du prototype),
- tenue en température (limitation à 20°C ± 2°C),
- tenue en vibration,
- certaines conditions d'emploi,
- interfaces électriques et mécaniques,
- performances dynamiques : fonction de transfert et bruit sur les sorties.

La maquette utilise un préchauffage de durée minimum 12 mn qui est maintenu pendant les essais.

Toutes les mesures sont réalisées en mode "dégradé" ou "opérationnel" (au plus tôt 10s après la mise sous tension) sur les sorties fonctionnelles vitesses angulaires et accélérations linéaires fournies en numérique dans un trièdre de référence lié au boîtier de la R.I. par l'intermédiaire d'une sortie BUS.

Le niveau de performance atteint par un système à composants liés dépend pour une large part de la connaissance des modèles d'erreur et des compensations d'erreurs réalisées.

La stabilité des termes du modèle d'erreur reflète donc la performance ultime du matériel, performance qui ne pourra cependant être atteinte qu'après études et calibrations plus ou moins complexes. Il importe donc de préciser la nature des compensations réalisées, qui sont pour cette maquette les suivantes :

- compensation d'erreur des facteurs d'échelles des moteurs-couples,
- compensation des désalignements moteurs-couples et axe de spin,
- compensation de dérive d'aniso-inertie,

- compensation thermique statique des facteurs d'échelles moteurs-couples
- compensation des termes de dérives : couples indépendants de g et proportionnels à g et à g^2,
- compensations thermiques statiques du couple indépendant de g et du balourd axial des gyromètres balourdés,
- compensation d'erreur de linéarité des moteurs-couples.

Ces compensations sont réalisées à la fréquence maximum de 93 Hz uniquement pour la fonction navigation nécessaire au guidage.

3 - MOYENS UTILISES

Les conditions restrictives d'emploi de la maquette évaluée ont limité les essais à ceux réalisables en laboratoire en ambiance régulée (20°C ± 1°C) sur un simulateur 2 axes type GOERZ 52 M2 piloté par un calculateur du commerce assurant les fonctions acquisition d'attitude du simulateur et des sorties des matériels, commande des axes et traitement.

Les sorties analogiques des boucles gyrométriques du gyromètre sont converties à l'aide de convertisseurs tension/fréquence en impulsions comptées par le calculateur.

Les sorties numériques incrémentales de la R.I. sont lues par le calculateur à la fréquence typique de $\frac{1}{36}\ s^{-1}$.

Les paragraphes suivants donnent les modèles représentatifs des matériels, avec les symboles suivants :

X : scalaire
$\underline{X}$: vecteur
$|\overline{X}|$: matrice
$|X|^t$: matrice transposée de X
$\underline{\Omega}$: vecteur vitesses appliquée $= (\omega x, \omega y, \omega z)^t$
$\underline{A}$: vecteur accélération appliquée $= (ax, ay, az)^t$
$\underline{\hat{\Omega}}$: vecteur vitesse estimée
$\underline{\hat{A}}$: vecteur accélération estimée
$\underline{\Delta\Omega}$: vecteur erreur vitesse estimée $= \underline{\hat{\Omega}} - \underline{\Omega}$
$\underline{\Delta A}$: vecteur erreur accélération estimée $= \underline{\hat{A}} - \underline{A}$
δXij : erreur résiduelle de compensation du terme d'erreur $\underline{X}$, axe i (i = x, y ou z), gyro j (j = 1, 2 ou 3)
δSij : erreur résiduelle de calibration du facteur d'échelle moteur couple axe i (i = x,y ou z)
var (X) : variance du paramètre X
var $(\underline{X})$: matrice de covariance du vecteur $\underline{X}$
$\underline{H}$: moment cinétique
$\frac{C-A}{H}$: terme d'aniso-inertie noté également J
B : balourd axial toupie
P, V : balourds tranverses
E, D : aniso élasticité
Γ : couple fixe
ζ : mésalignement des lignes d'action moteur-couple
$\varkappa$: mésalignement de spin.

4 - MODELE D'ERREUR DETERMINISTE

4.1. Modèle statique du gyromètre balourdé

L'équation ci-dessous exprime les couples des moteurs-couples en fonction des vitesses et accélérations appliquées au gyromètre dans les axes x, y, z du gyromètre :

$$-\frac{My}{H} = (1 + \delta Sx).(\omega x + B.\ ax) + \frac{C-A}{H}.\omega x.\omega z - \varkappa y.(\omega z + B.az) + \zeta x.(\omega y + B.ay) + \Gamma y$$

$$\frac{Mx}{H} = (1 + \delta Sy).(\omega y + B.ay) + \frac{C-A}{H}.\omega y.\omega z + \varkappa x.(\omega z + B.az) - \zeta y.(\omega x + B.ax) - \Gamma x$$

Eq. 4.1.

équation dans laquelle les couples Γ sont fonctions de l'accélération appliquée :

$$\left.\begin{aligned}\Gamma x &= \Gamma bx + Vx.az + P.ax - (D.ay - E.ax).az\\ \Gamma y &= \Gamma by + Vx.az + P.ay - (D.ax + E.ay).az\end{aligned}\right\}\ \text{Eq. 4.2}$$

(les termes utilisés sont définis dans la liste des symboles).

La particularité du gyromètre balourdé apparait dans les termes d'erreur suivants :

* $\delta Sx.B.ax$, $\delta Sy.B.ay$: erreurs dues aux facteurs d'échelle des moteurs-couples.

* $\zeta x.B.ay$, $\zeta y.B.ax$ et $\varkappa y.B.az$, $\varkappa x.B.az$: erreurs dues aux mésalignements.

Après compensation, les équations précédentes sont modifiées de façon à traduire les erreurs résiduelles de compensation. Le symbole δ désigne les erreurs résiduelles de compensation des termes d'erreurs ou de calibration des facteurs d'échelle :

$$\begin{vmatrix} -My/H \\ Mz/H \end{vmatrix} = \begin{vmatrix} \omega x + B.a_x \\ \omega y + B.a_y \end{vmatrix} +$$

$$+\begin{vmatrix} \delta S_x & \delta \xi_x & -\delta \alpha_y \\ -\delta \xi_y & \delta S_y & \delta \alpha_x \end{vmatrix} \cdot \begin{vmatrix} \omega_x \\ \omega_y \\ \omega_z \end{vmatrix} + \begin{vmatrix} \delta J & 0 \\ 0 & \delta J \end{vmatrix} \cdot \begin{vmatrix} \omega_x . \omega_z \\ \omega_y . \omega_z \end{vmatrix}$$

$$+\begin{vmatrix} \delta S_x . B + \delta B & \delta P + \delta \xi_x . B & \delta V_y - \delta \alpha_y . B \\ -\delta P - \delta \xi_y . B & \delta S_y . B + \delta B & -\delta V_x + \delta \alpha_x . B \end{vmatrix} \cdot \begin{vmatrix} a_x \\ a_y \\ a_z \end{vmatrix}$$

$$+\begin{vmatrix} \delta D & \delta E \\ -\delta E & \delta D \end{vmatrix} \cdot \begin{vmatrix} a_x . a_z \\ a_y . a_z \end{vmatrix} + \begin{vmatrix} \delta \Gamma_{by} \\ \delta \Gamma_{bx} \end{vmatrix}$$

où B est la valeur nominale du balourd touple.

posant $\underline{M} = \begin{vmatrix} -M_y/H \\ M_x/H \end{vmatrix} = \begin{vmatrix} m_x \\ m_y \end{vmatrix}$

l'équation 4.3. devient :

$$\begin{vmatrix} m_x \\ m_y \end{vmatrix} = \begin{vmatrix} \omega_x + B.a_x \\ \omega_y + B.a_y \end{vmatrix} + \begin{vmatrix} \delta_x \\ \delta_y \end{vmatrix}$$

ou $\underline{M} = \underline{\Omega} + B.\underline{A} + \underline{\Delta}$ } Eq. 4.4.

$\underline{M}$: sorties du gyromètre
$\underline{\Omega}$ et $\underline{A}$: entrées
B : balourd nominal
$\underline{\Delta}$: vecteur erreur

L'équation 4.4. est celle du gyromètre balourdé après compensation d'erreur. L'erreur résiduelle $\underline{\Delta}$ contient l'évolution des coefficients par rapport à leurs valeurs de calibration, évolution fonction du temps et des conditions de mise en oeuvre, d'utilisation et d'environnement.

La principale erreur liée à l'environnement est celle due à la température ambiante T et à son influence sur les termes Γ , B et δS :

. $\delta \Gamma_T = \Gamma_T$ (T)
. $\delta B_T = B_T$ (T)
. $\delta S_T = S_T$ (T)

Γ_T , B_T et S_T étant les sensibilités en température réduites en première approximation à des fonctions linéaires de T.

Après compensation thermique, l'erreur résiduelle en température est en principe aléatoire et est incluse dans les termes $\delta\Gamma$, δB et δS.

L'équation du gyromètre non balourdé après compensation d'erreur est obtenue en annulant le terme B dans l'équation 4.4 :

$$\underline{M} = \underline{\Omega} + \underline{\Delta} \qquad \text{Eq. 4.6}$$

4.2. Modèle statique de la référence inertielle à gyromètres balourds

La disposition des 3 gyromètres dans la référence inertielle (R.I.) est définie figure19. Les rotations en tangage et lacet sont mesurées par un gyromètre non balourdé d'axe de spin parallèle à l'axe de roulis. Les 4 autres paramètres (la rotation en roulis et les 3 accélérations) sont mesurés par 2 gyromètres balourdés d'axes de spin orientés en tangage et lacet.

La séparation des informations est obtenue par résolution du système d'équations ci-dessous obtenus par application de l'équation 4.4 aux 3 gyromètres indicés 1, 2 et 3 respectivement en roulis, lacet et tangage :

$$\left.\begin{aligned}
m_{x1} &= -\frac{\sqrt{2}}{2}.(\omega_y + \omega_z) + \delta_{x1} \\
m_{y1} &= -\frac{\sqrt{2}}{2}.(\omega_y - \omega_z) + \delta_{y1} \\
m_{x2} &= \frac{\sqrt{2}}{2}.(\omega_x - \omega_y) + \frac{\sqrt{2}}{2}.B.(a_x - a_y) + \delta_{x2} \\
m_{y2} &= -\frac{\sqrt{2}}{2}.(\omega_x + \omega_y) - \frac{\sqrt{2}}{2}.B.(a_x + a_y) + \delta_{y2} \\
m_{x3} &= -\frac{\sqrt{2}}{2}.(\omega_x - \omega_z) + \frac{\sqrt{2}}{2}.B.(a_z - a_z) + \delta_{x3} \\
m_{y3} &= \frac{\sqrt{2}}{2}.(\omega_x + \omega_z) - \frac{\sqrt{2}}{2}.B.(a_x + a_z) + \delta_{y3}
\end{aligned}\right\} \quad \text{Eq. 4.7}$$

Nota : . B1 = 0 ; B2 = - B3 = B > 0
. Xi, Yi, Zi : trièdre lié au gyromètre i = 1 à 3
. X, Y, Z : trièdre lié à la R.I.

La solution unique du système 4.7 permet de définir les erreurs ($\Delta\underline{\Omega}$ et $\Delta\underline{A}$) sur les sorties par :

$$\Delta\underline{\Omega} = \hat{\underline{\Omega}} - \underline{\Omega}$$

$$\Delta\underline{A} = \hat{\underline{A}} - \underline{A}$$

$$\underline{\Delta\Omega} = \begin{vmatrix} \delta\omega_x = \frac{\sqrt{2}}{4}\cdot\left[(\delta X_2 - \delta y_2) - (\delta X_3 - \delta y_3)\right] \\ \delta\omega_y = \frac{\sqrt{2}}{2}\cdot\left[-\delta y_1 - \delta X_1\right] \\ \delta\omega_z = \frac{\sqrt{2}}{2}\cdot\left[\delta y_1 - \delta X_1\right] \end{vmatrix}$$

$$\underline{\Delta A} = \begin{vmatrix} \delta a_x = \frac{\sqrt{2}}{4.B}\cdot\left[(\delta X_2 - \delta y_2) + (\delta X_3 - \delta y_3)\right] \\ \delta a_y = \frac{\sqrt{2}}{2.B}\cdot\left[(\delta X_1 + \delta y_1) - (\delta X_2 + \delta y_2)\right] \\ \delta a_z = \frac{\sqrt{2}}{2B}\cdot\left[(\delta y_1 - \delta X_1) - (\delta X_3 + \delta y_3)\right] \end{vmatrix}$$

Eq. 4.8

L'équation 4.8 montre que les erreurs en vitesse et en accélération sont homogènes. La figure 20 fournit l'expression des vecteurs erreur $\underline{\Delta\Omega}$ et $\underline{\Delta A}$ en fonction des erreurs résiduelles de compensation des termes de chaque gyromètre définies par l'équation 4.3.

L'expression générale de ces vecteurs erreur est la suivante :

$$\underline{\Delta\Omega} = \underline{D_o} + |K|\cdot\underline{\Omega} + |J|\cdot|\Omega|\cdot\underline{\Omega} + |B|\cdot\underline{A} + |E|\cdot|A|\cdot\underline{A}$$

$$\underline{\Delta A} = \underline{A_o} + |G|\cdot\underline{\Omega} + |H|\cdot|\Omega|\cdot\underline{\Omega} + |M|\cdot\underline{A} + |N|\cdot|A|\cdot\underline{A}$$

Eq. 4.9

expression dans laquelle :

$$|\Omega| = \begin{vmatrix} 0 & \omega_z & 0 \\ 0 & 0 & \omega_x \\ \omega_y & 0 & 0 \end{vmatrix} \quad ; \quad |A| = \begin{vmatrix} 0 & a_z & 0 \\ 0 & 0 & a_x \\ a_y & 0 & 0 \end{vmatrix}$$

la forme générale des matrices

$$|K|\ ,\ |J|\ ,\ |B|\ ,\ |E|\ ;\ |G|\ ,\ |H|\ ,\ |M|\ ,\ |N|$$

est donnée figure 20 et l'origine des termes de ces matrices est la suivante :

Modèle d'erreur de la P.I. (Eq.4.9)	Erreur de compensation gyro (Eq. 4.4)
Kii : facteur d'échelle en vitesse	* δSYi + δSXi : facteur d'échelle des moteurs-couples (variation de l'induction magnétique de la couronne d'aimants de la toupie) * $\delta\zeta$yi - $\delta\zeta$xi : octhogonalité des lignes d'action des moteurs-couples
Mii : facteur d'échelle en accélération	* idem Kii plus : * δBi - δBj : erreur de compensation des balourds toupie
Kij : facteur d'échelle transverse i ≠ j en vitesse	* δSYi - δSXi : erreur d'anisotropie des facteurs d'échelles des moteurs-couples (principalement liée à l'électronique) * $\delta\zeta$Yi + $\delta\zeta$Xi : mesalignement du gyro autour de l'axe de spin * $\delta\alpha$: mésalignement de l'axe de spin
Mij : facteur d'échelle transverse i ≠ j en accélération	* idem Kij (i ≠ j) plus : * $\delta P/B$; $\delta V/B$ termes P et V réduits
B i , j Couplage statique E i , j vitesse x/accélération i = 1	* $\frac{B}{4}\delta$S : facteurs d'échelle des moteurs couples * $\frac{B}{4}\delta\zeta$: mésalignement des lignes d'action des moteurs couples * $\frac{B}{4}\delta\alpha$: mésalignement de l'axe de spin * δB, δP, δV, δE, δD : termes des 2 gyros balourdés
B i , j E i , j couplage statique i = 2 et 3 vitesse y et z/ accélération	* δB_1 , δP_1, δV_1 , δE_1 , δD_1 termes du gyro non balourdé
Gij : couplage statique Hij : accélération/vitesse	* $\frac{\delta S}{B}$, $\frac{\delta\zeta}{B}$ et $\frac{\delta\alpha}{B}$ * $\frac{\delta J}{B}$: anisoinertie
Jij : dérive proportionnelle à ω^2	* δJ : anisoinertie
Doi et Aoi : dérive et biais constants	* $\delta\Gamma_b$: couples fixes
Nij : biais proportionnal à a^2	* D : anisoélasticité

Cette répartition des erreurs montre que par rapport à un bloc capteur gyrométrique classique, la sortie vitesse comporte des termes supplémentaires de couplage statique (sur l'axe uniquement), ce qui ne constitue pas une modification de structure du modèle.

5 - MODELE D'ERREUR STATISTIQUE

Une fois les paramètres du modèle statique déterminés par des essais appropriés décrits au chapitre suivant, il est déduit :

- le résidu de modélisation dans chaque essai,
- les variations des paramètres du modèle.

A partir du modèle de l'équation 4.9 et de sa composition donnée figure 20, il ressort que :

$$Var(\underline{\Delta}\,\underline{\Omega}) = \begin{vmatrix} Var(\delta\omega_x) & 0 & 0 \\ 0 & Var(\delta\omega_y) & cov(\delta\omega_y, \delta\omega_z) \\ 0 & cov(\delta\omega_z, \delta\omega_y) & Var(\delta\omega_z) \end{vmatrix} \quad \text{Eq. 5.1}$$

avec en particulier pour $\underline{\Omega}$ et $\underline{A}$ constants :

$$\begin{aligned} Var(\delta\omega_j) = {} & \omega_x^2 . Var(K_{jx}) + \omega_y^2 . Var(K_{jy}) + \omega_z^2 . Var(K_{jz}) \\ & + a_x^2 . Var(B_{jx}) + a_y^2 . Var(B_{jy}) + a_z^2 . Var(B_{jz}) \\ & + \omega_z . \omega_x . Var(J_{jy}) + \omega_x . \omega_y . Var(J_{jz}) \\ & + a_y . a_z . Var(E_{jx}) + a_z . a_x . Var(E_{jy}) \\ & + a_x . a_y . Var(E_{jz}) + Var(D_j) \end{aligned} \quad \text{Eq. 5.2}$$

l'expression de la variance en accélération est, par contre, générale :

$$Var(\underline{\Delta A}) = \begin{vmatrix} Var(\delta a_x) & cov(\delta a_x, \delta a_y) & cov(\delta a_x, \delta a_z) \\ cov(\delta a_y, \delta a_x) & Var(\delta a_y) & cov(\delta a_y, \delta a_z) \\ cov(\delta a_z, \delta a_x) & cov(\delta a_z, \delta a_y) & Var(\delta a_z) \end{vmatrix} \quad \text{Eq. 5.3}$$

La variance de chaque paramètre est composée des variances fonction du temps et de la température selon les variances élémentaires suivants :

σ_a^2 : variance en fonctionnement continu en fonction du temps.
σ_r^2 : variance caractérisant la répétabilité à court terme entre arrêt-démarrage.
σ_l^2 : variance à long terme.
σ_T^2 : variance fonction de la température ambiante T.
σ_w^2 : variance induite par la mise en température au démarrage
σ_b^2 : bruit de mesure (résidu de modélisation).

La variance totale, toutes conditions de fonctionnement incluses, est la somme :

$$\sigma^2 = \sigma_a^2 + \sigma_r^2 + \sigma_l^2 + \sigma_T^2 + \sigma_w^2 + \sigma_b^2 \quad \text{Eq. 5.4}$$

ce qui signifie l'indépendance des erreurs ainsi définies. La liste des variances élémentaires n'est pas limitative.

6 - IDENTIFICATION DU MODELE

6.1. Type d'essais

Deux types d'essais sont utilisés :

- des essais à l'arrêt : essais de mise en température et essais multipositions. Ces essais sensibilisent les termes constants et les termes fonction de l'accélération.

- des essais en rotation pour sensibiliser les termes fonction de la vitesse.

Les essais en laboratoire limités à $\pm$ 1g ne permettent pas d'identifier le modèle en accélération avec suffisamment de précision.

D'autres essais sont alors nécessaires pour valider les résultats obtenus sous 1 g

- essais sur centrifugeuse
- essais sur table sinusoïdale
- essais en vibration.

6.2. Essais à l'arrêt

6.2.1. Essais de mise en température (MET)

Cet essai consiste à mesurer les sorties lors du régime en fonctionnement transitoire (R.T.) obtenu par la mise en route du matériel. Pour l'application missile Air-Air, cette phase transitoire est la phase de fonctionnement opérationnel. Compte tenu du caractère non stationnaire de cette phase, il n'est pas possible de conduire l'ensemble des essais nécessaires à l'identification pendant cette phase. Aussi est-il uniquement mesuré l'évolution des sorties $\underline{M}$ (mx et my) du gyromètre ou $\underline{\Omega}$ et $\underline{\hat{x}}$ de la référence inertielle pour des entrées constantes dans les 3 positions fixes suivantes :

POSITION

X vertical - Zenith
Y vertical - Nadir
Z vertical - Zenith

Ces positions sensibilisent :

- les termes constants
- les termes proportionnels à l'accélération
- pour une très faible part, les termes proportionnels à $\underline{\Omega}$ ($\underline{\Omega} = \underline{\Omega}$terre)

et ne sensibilisent pas les termes d'anisoélasticité et l'aniso-inertie.

Parallèlement aux mesures gyrométriques mx et my, la température interne du gyromètre est enregistrée.

On présente figure 21, un exemple de dérive obtenue (M01, Z vertical).

a) Gyromètre

- les évolutions à la mise en route sont relativement importantes sur ce type de gyromètre (jusqu'à 60°/h) mais en aucun cas agravées par la présence d'un balourd axial toupie.
- les évolutions ne sont pas efficacement compensées par une correction thermique statique ce qui confirment la nécessité d'une compensation dynamique. Les phénomènes sont à titre d'exemple de la forme :

  Posx vertical

$$\delta\omega_x = 15^\circ/hr \cdot \left(1 - e^{-t/\tau_x}\right) \qquad \tau_x = 180\ sec$$
$$\delta\omega_y = 60^\circ/hr \cdot \left(1 - e^{-t/\tau_y}\right) \qquad \tau_y = 210\ sec$$

- le régime transitoire dépend de l'interface mécanique du gyromètre. Deux types de montage mécanique ont été utilisés.

b) R.I.

Les performances en régime permanent (R.P.) obtenues sur une période d'essai intervenant 6 mois après la calibration de la R.I. sont les suivantes :

Performances en R.P. (1 σ)	Unités		Erreurs élémentaires
	o/h	10^{-4} g	
Dérive aléatoire en fonctionnement continu sur 1 heure après stabilisation	0,75	1,3	σ_a
Répétabilité à court terme entre arrêt-démarrage (dérive stabilisée)	4	8	$\left(\sigma_r^2 + \sigma_T^2\right)^{1/2}$
Répétabilité à long terme (6 mois)	39	52	$\left(\sigma_r^2 + \sigma_T^2 + \sigma_\rho^2\right)^{1/2}$

Le régime transitoire (R.T.) sur les sorties de la R.I. est caractérisé par :

Performances en R.I.	Unités		Erreurs élémentaires
	o/h	10^{-4} g	
Variation entre la 1ère mesure et après 30 mn (Valeur crête)	60	90	$\delta\omega_m$, δa_m
Répétabilité à court terme sur la 1ère mesure ($t = 10s$ à $t = 10 + 36s$) (1 σ)	5	12	$\left(\sigma_r^2 + \sigma_T^2 + \sigma_a^2\right)^{1/2}$

Un exemple de mise en température sur les 6 sorties est présenté fig. 22

6.2.2. Essais - Multiposition

Ces essais ont pour but de déterminer les valeurs des coefficients du modèle d'erreur composé des termes suivants :

- termes indépendants de g
- termes proportionnels à g et à g^2
- la sensibilité thermique de ces coefficients définis dans les équations 4.6 et 4.9 respectivement pour le gyromètre et la R.I.

La sensibilité thermique des coefficients n'a pu être évaluée sur le gyromètre seul, c'est-à-dire sur des coefficients non compensés en température.

La procédure consiste à mesurer les sorties ($\underline{N}$ ou $\underline{\Delta\Omega}$ et $\underline{\Delta A}$) dans 20 positions en régime permanent, estimer les valeurs des coefficients des modèles et leurs incertitudes par la méthode des moindres carrés généralisés :

$$\underline{\Delta} = |a_{ij}| \cdot \underline{X} + \underline{\varepsilon} \qquad \text{Eq. 6.1}$$

où $\underline{\Delta}$ = vecteur erreur a) gyromètre (Eq. 4.6) : $\underline{\Delta} = \underline{N} - \underline{\Omega}$

b) R.I. (Eq. 4.9) : $\underline{\Delta} = \underline{\Delta\Omega}$ et $\underline{\Delta A}$

$|a_{ij}|$ = matrice des accélérations
$\underline{X}$ = vecteur inconnu
$\underline{\varepsilon}$ = bruit

La solution de l'équation 6.1 étant :

$$\underline{X} = \left[|a_{ij}|^t \cdot |a_{ij}|\right]^{-1} \cdot |a_{ij}|^t \cdot \underline{\Delta}$$

$$\text{Var}(\underline{X}) = \sigma^2 \left[|a_{ij}|^t \cdot |a_{ij}|\right]^{-1}$$

ou σ^2 est la variance du bruit de mesure estimée à partir du résidu de modélisation

a) Gyromètre

$$\underline{X} = \left[\Gamma_{bx}, \Gamma_{by}, \delta S_x \cdot B + B, \delta S_y \cdot B + B, P + \xi_x \cdot B, P - \xi_y \cdot B, V_y - \alpha_y \cdot B, -V_x + \alpha_x \cdot B, E, D\right]^t \quad \text{Eq. 6.4}$$

La sensibilité en température est obtenue par la détermination de $\underline{X}$ (Eq. 6.4) à 20, 40 et 60°C de température ambiante.

Les termes αx, αy, ξx, ξy, δSx, δSy étant déterminés par les essais en rotation, l'équation 6.4 peut se réduire à :

$$\underline{X} = \left[\Gamma_{bx}, \Gamma_{by}, B, P, V_x, V_y, E, D\right]^t \quad \text{Eq. 6.7}$$

b) R.I.

vitesse :

$$\underline{X} = \left[D_{x0}, B_{xx}, B_{xy}, B_{xz}, E_{xx}, E_{xy}, E_{xz}, D_{y0}, B_{yx}, B_{yy}, B_{yz}, E_{yy}, E_{yz}, D_{z0}, B_{zx}\right]^t \quad \text{Eq. 6.5}$$

accélération :

$$\underline{X} = \left[A_{x0}, M_{xx}, M_{xy}, M_{xz}, N_{xx}, N_{xy}, N_{xz}, A_{y0}, M_{yx}, M_{yy}, M_{yz}, N_{yy}, N_{yz}, A_{z0}, M_{zx}, M_{zy}, M_{zz}, N_{zz}\right]^t \quad \text{Eq. 6.6}$$

résultats :

a) Gyromètre :

Coefficient	Valeur moyenne	Incertitude	Sensibilité en température (20 - 60°C)
Γ_{bx}	- 64°/h	0,7°/h	2,25°/h/°C
Γ_{by}	- 39°/h	0,7°/h	- 1,45°/h/°C
P	- 4°/h/g	1,0°/h/g	0,05°/h/g/°C
B	5038°/h/g	1,0°/h/g	0,09°/h/g/°C
$Vx - \alpha x.B$	- 13°/h/g	0,9°/h/g	0,05°/h/g/°C
$Vy - \alpha y.B$	- 27°/h/g	0,9°/h/g	0,05°/h/g/°C
E	- 0,2°/h/g²	2,1°/h/g²	0,01°/h/g²/°C
D	- 0,6°/h/g²	2,1°/h/g²	

Coefficient	Répétabilité à court terme (T = 20°C ± 1°C
Γ_b	8°/h
B	1,7°/h/g
P	0,4°/h/g
V	1,3°/h/g
E	0,2°/h/g²
D	0,2°/h/g²

erreurs élémentaires :

* erreur statistique : σ_r

* erreur déterministe : influence de la température T (non compensée)

Les termes Γ, P, B, et V sont déterminés avec suffisamment de précision pour que les valeurs obtenues soient significatives et constituent une validation du modèle dans le domaine ± 1g.

Les termes E et D ne sont pas estimés avec une précision suffisantes. Des essais en vibration sont habituellement utilisés pour estimer ces paramètres avec plus de précision.

La répétabilité à court terme inclut les variations des coefficients dues à la température ambiante par l'intermédiaire :

- de la sensibilité des termes eux-mêmes à la température : Γ_{bx}, Γ_{by} et dans une moindre part B.
- de la sensibilité du facteur d'échelle des moteurs-couples à la température (4.10^{-4}/°C) : erreur d'estimation du terme B (cf § 6.3.).

b) Référence inertielle

Les résultats d'identification du modèle en vitesse (équation 6.5) et en accélération (équation 6.6) sont illustrés par l'exemple donné figure 23 où figurent sous forme matricielle

- le modèle
- les valeurs estimées des coefficients du modèle
- l'incertitude des coefficients ainsi que le résidu de modélisation "Sigma".

Les termes en vitesse sont exprimés en °/h , °/h/g et °/h/g².

Les termes en accélération en 10^{-4}g, 10^{-4} g/g et 10^{-4} g/g².

NOTA : Le symbole * masquant les paramètres Ex2 et Nzz signifie que ces paramètres n'ont pas été sensibilisés par les 20 positions choisies. Ultérieurement 24 positions seront utilisées.

Coefficients	Répétabilité à court terme	Répétabilité à long terme (6 mois)	Unités
Doi	0,9	34	°/h
Bij	0,9	10	°/h/g
Eij	1,3	1,8	°/h/g²
Aoi	1,9	32	10^{-4}g
Mij	4,3	28	10^{-4}g/g
Nij	2,3	3,3	10^{-4}g/g²
Erreurs élémentaires	$(\sigma_r^2 + \sigma_T^2)^{1/2}$	$(\sigma_r^2 + \sigma_T^2 + \sigma_\rho^2)^{1/2}$	

Performances en essais multiposition à ± 1 g

Coefficients	Répétabilité à court terme	Répétabilité à long terme (6mois)	Unités
$\delta\omega$	1,2	35	°/h
δ a	2,3	40	10^{-4} g
Erreurs élémentaires	$(\sigma_{\delta r}^2 + \sigma_{\delta T}^2)^{1/2}$	$(\sigma_{\delta r}^2 + \sigma_{\delta\rho}^2 + \sigma_{\delta T}^2)^{1/2}$	

6.3. Essais en rotation

6.3.1. But des essais

Ces essais ont pour but de déterminer

a) sur le gyromètre

- les facteurs d'échelle des moteurs-couples Kx et Ky
- les mésalignements : γx, γy, αx et αy
- le terme d'aniso-inertie : (C - A) / H

Les précessions électriques définies dans l'équation 4.4 s'expriment par :

$$Mx/H = Kx \cdot Ix$$
$$My/H = Ky \cdot Iy \qquad \text{Eq. 6.1}$$

b) sur la R.I

- les erreurs de facteurs d'échelle : matrice |K|
- les termes de couplage statique accélération/vitesse : matrice |G|
- les termes d'aniso-inertie : matrice |J| et |H|

6.3.2. Modèle d'erreur du facteur d'échelle

Les facteurs d'échelle Kx , Ky sont fonctions de la vitesse appliquée au gyromètre et du temps t :

$$K_x(\omega,t) = K_{xo} \cdot [1 + U_x(\omega,t) + V_x(\omega,t)]$$
$$K_y(\omega,t) = K_{yo} \cdot [1 + U_y(\omega,t) + V_y(\omega,t)] \qquad \text{Eq. 6.2}$$

équation dans laquelle :

- Kxo et Kyo sont les valeurs des facteurs d'échelle nominales, mesurées pour des conditions initiales nulles, aux vitesses ± ωYo et ± ωXo.
- u (ω , t) est une fonction paire de ω :
$$u(\omega) = k_0 + k_1 \cdot \text{signe}(\omega) + k_2\omega^2 + \ldots \qquad \text{Eq. 6.3}$$
- V (ω , t) est une fonction impaire de ω :
$$v(\omega) = l_1 \cdot \omega + l_2 \cdot \omega^2 \text{ signe } (\omega) + \ldots \qquad \text{Eq. 6.4}$$

Voir définition pratique des termes figure 24.

Le modèle d'erreur correspondant dans la R.I. : δSx et δSy est fourni par les relations suivantes :

$$\delta S_x = -\delta K_{yo}/K_y - \delta u_y - \delta v_y$$
$$\delta S_y = -\delta K_{xo}/K_x - \delta u_x - \delta v_x \qquad \text{Eq. 6.5}$$

6.3.3. Procédure appliquée

Les essais réalisés sont limités à l'application de vitesse angulaires sur les axes canoniques X , Y, Z du gyromètre ou de la R.I. (les termes d'aniso-inertie n'étant excités que pour des rotations appliquées autour d'axes non canoniques, ne seront pas évalués par cet essai).

La gamme des vitesses $\pm\omega o$, $\pm\omega max$ appliquées en régime permanent (R.P.) est :

	ω o	ω max
gyromètre	10°/s	200°/s
R.I.	10°/s	100°/s

Le cycle des vitesses appliquées est du type :

$+\omega o, -\omega o, \ldots +\omega i, -\omega i, \ldots +\omega max, -\omega max.$

Pour chaque vitesse appliquée, les mesures sont réalisées sur des évolutions complètes de l'axe de la table pour moyenner les dérives proportionnelles à g et pendant un temps de 360s.

L'évolution en fonction du temps est mesurée pour $\omega \geqslant 40°/s$ à intervalle de 9s (40 mesures successives sont réalisées pendant 360s pour chaque vitesse, chacune de ces 40 mesures étant intégrées sur 9s).

Après chaque vitesse appliquée, le système est maintenu à l'arrêt pendant 9mn pour rétablir les conditions thermiques initiales.

6.3.4. Résultats

a) Gyromètre

Le modèle identifié est le suivant :

$$\left.\begin{aligned} V_x(\omega,t) &= k(t).\ \omega_y{}^2 \\ V_y(\omega,t) &= k(t).\ \omega_x{}^2 \end{aligned}\right\} \quad \text{Eq. 6.6}$$

$$V_x(\omega,t) = o\ ;\ V_y(\omega,t) = o \qquad \text{Eq. 6.7}$$

Ce résultat est illustré figure 25 représentant

par le symbole ◇ : V (ω, t) pour t = 9s

par les symboles ← : u (ω, t) pour t = 90s
↓ " " " t = 180s
→ " " " t = 270s
↑ " " " t = 360s

dans la gamme ± 10°/s ; ± 200°/s .

L'axe des abscisses représente la fonction U (ω, t = 9s).

La fonction u (ω, t) traduit l'échauffement par effet JOULE de la couronne d'aimant des moteurs-couples.

Pour ω fixé, u (t) est solution de :

$$U(t) + \tau.\ \frac{\partial u(t)}{\partial t} = U\ (\infty) \qquad \text{Eq. 6.7}$$

Les valeurs typiques obtenues sont :

$k\ (\infty) = -2{,}6\ 10^{-4}\ /\ (rd/s)^2$

$\tau = 150s$

La forme générale du modèle de l'équation 6.6 pour des entrées en vitesse simultanées sur les 2 axes x et y est donc :

$$Ux\ (\omega, t) = Uy\ (\omega, t) = K\ (t)\ .\ (\omega x^2 + \omega y^2)$$

soit $U(t) = k(t)\ .\ (\omega x^2 + \omega y^2)$ Eq. 6.8

où $k(t) + \tau.\ \frac{\partial k(t)}{\partial t} = k(\infty)$ Eq. 6.9

Ces équations pourraient être utilisées comme modèle de compensation d'échauffement des moteurs-couples.

La sensibilité thermique du coefficient Kxo est évaluée à $\omega = \pm 10°/s$ dans la gamme de température ambiante T = 20 à 60°C :

$$\frac{\partial K_o}{K_o.\partial T} = 4.10^{-4}/°C$$

b) R.I.

L'estimation des coefficients des matrices |K| et |C| est conduite de la même façon sur la R.I.

Une illustration des résultats est donnée sur les termes ωy et ay :

$$\omega y = Kyx.\ \omega x + Kyy.\ \omega y + Kyz.\ \omega z$$
$$ay = Gyx.\ \omega x + Gyy.\ \omega y + Gyg.\ \omega z$$

Les termes Kyx, Ky ou Gy , Gy sont les termes de couplage thermique inférieure à 2.10^{-3} (o/h) / (°/h) ou (10^{-4}g) (°/h) et indépendants de ω et du temps t.

La fonction Kyy (ω, t) est représentée figure 26 dans la gamme ± 10, ± 100°/s pour t = 36 à 360s.

Le résultat obtenu est cohérent avec le modèle d'échauffement identifié sur le gyromètre.

L'erreur de linéarité est inférieure dans ces conditions à 4.10^{-4} :

$$Kyy\ (\omega, t) = Kyyo\ .\ \left[1 + u(\omega, t)\right]$$
$$u\ (\omega, t) < 4.10^{-4}$$

Kyo : déterminé par $\omega = \pm 10°/s$

7 - CONCLUSION

Les premiers essais des matériels mettant en oeuvre le concept de gyromètre balourdé réalisés dans les conditions d'emploi de laboratoire ($\pm$ 1g, $\pm$ 100°/s, 20°C $\pm$ 2°C) et pour des entrées en vitesses et accélérations constantes montrent que ce principe est applicable au système de guidage visant les ordres de grandeurs suivantes :

Dérive $<$ 100°/h ou 10^{-2} g

erreur de facteur d'échelle $<10^{-3}$

Il apparaît en particulier :

- Que le modèle du gyromètre balourdé n'est pas différent du gyro non balourdé et qu'aucune caractéristique statique n'est affectée par le balourdage axial de la toupie.
- Que les erreurs en accélération se déduisent sensiblement des erreurs en vitesse à partir du rapport défini par la valeur du balourd axial (ici 1°/h $\simeq$ 1, 1. 10^{-4}g).
- Que les performances actuelles sont améliorables par une modélisation dynamique des effets thermiques (transitoire à la mise sous tension et échauffements internes des moteurs-couples).

Les études se poursuivent actuellement sur des prototypes de R.I. qui seront évalués au L.R.B.A. en 1984. Le modèle bien connu du gyromètre à suspension accordé va servir de base à l'élaboration des essais futurs. Ces essais permettront une évaluation des performances et des erreurs dynamiques ainsi que la validation des modèles dans les domaines de vitesses et accélérations linéaires et angulaires plus élevés.

Des études sont conduites dans ce sens sur des moyens spécifiques du L.R.B.A tels que la table sinusoïdale 20 g et la centrifugeuse 80 g.

STRAPDOWN INERTIAL SYSTEMS FOR TACTICAL MISSILES USING MASS UNBALANCED TWO-AXIS RATE GYROS

by

J.L.Michelin
Strapdown Systems Engineering Group Manager
Société de Fabrication d'Instruments de Mesure (SFIM)
13 Avenue Marcel Ramolfo Garnier
91301 Massy, France

and

P.Masson
Inertial Components Manager
Laboratoire de Recherches Balistiques et Aérodynamiques
27207 Vernon, France

0 - SUMMARY

In 1979, SFIM began work on strapdown inertial systems using two axis dry tuned gyros (DTG). Since the first feasibility developments (74-79 - see reference AGARD LS n° 95) SFIM has worked on a large number of applications, the most important being for tactical missiles.

All our current developments are based on the same concepts - mass unbalanced gyros (M.U.G.) - fully digitized electronics - leading to a systems family - SIL 1 ("Systèmes Inertiels Liés") - in which the cost and volume requirements are the essential points.

The following paper describes the basic ideas, some examples of utilization and the test results obtained on some functional models and prototypes by SFIM and essentially by LRBA.

FIRST PART S.F.I.M.

1 - BACKGROUND

SFIM has produced GAM ("Gyroscopes Accordés Miniatures") dry tuned gyros since 1972 for various applications : rate gyros, optical stabilization, ... In 1974, SFIM has contracted by the French Governmental Department (STET, "Service Technique des Engins Tactiques") for the first feasibilit studies on strapdown inertial systems. This development was based on tactical missile applications, at a time when very few missile designers could imagine this requirement.

This feasibility development, together with others covering helicopter and torpedo applications, was completed by the delivery of some systems to government ground test or flight test laboratories. In 1978, SFIM gave a lecture (AGARD n° 95) and described the SIL 3 prototype, which has since been tested in French Flight Test Center (Bretigny) and by LRBA, with very encouraging results :

- stability $< 0.5°/hr$ (1σ) (1 year) over a range of 100°/sec.
- CEP $<$ 100 meters for a 2-minute flight.

These tests are continuing, with an improved version, on a drone (C 22 SNIAS ; 1984).

Since 1979, prototype developments have been carried out for various programs and application, with a strong demand for tactical missiles : air-to-air ; sea-to-sea ; air-to-ground ; ground-to-air and others. SFIM devoted their efforts to develop a coherent Strapdown Inertial References family, with two standards :

- SIL 2 : based on 2 two-axis GAM rate gyros and 3 accelerometers.
- SIL 1 : based on 3 two-axis GAM mass unbalanced rate gyros.

These strapdown inertial reference system (INU) can then be integrated, as a module, into more complex inertial systems (for missile, helicopter or torpedo applications).

The SIL 1 family, which is used in almost all the systems under development, is the main topic of this lecture.

2 - TACTICAL MISSILE REQUIREMENTS

Tactical missile applications stress special requirements :

- Multifunction inertial reference

  The cost and volume objectives led missile manufacturers to define inertial reference (I.R.) for 3 different purposes :

  - inertial guidance

    Inertial reference must provide precise angular and linear rate data to the missile computer in order to achieve quality inertial guidance before autopilot target homing.

- missile control

  The strapdown inertial sensors are used as flight control accelerometers and rate gyros (3-axis gyro and accelerometer package).

- stabilization

  Frequently, the I.R. are used for stabilization of homing heads (mechanical or electronic stabilization).

The first function requires average accuracy, with the other two need high quality transfer functions and low noise levels. These parameters are often not easily obtainable at the same time on a single sensor.

The following values, covering all tactical missile applications, can be noted :

- 1 to 100 °/hr drift (1 σ)
- 1.10^{-4} to 1.10^{-2}g bias (1 σ)
- 1.10^{-4} to 1.10^{-3} scale factor error (1 σ)
- $>$ 100 Hz bandwith
- $<$ 0,1 % range noise.

- High dynamics

  Missile dynamics increase in inverse proportion to inertia, the efficacity of control surfaces and flight control systems, and above all the new operational requirements.

  The following maximum values are usually quoted :

  . 50.000 °/sec^2

  . 2000 °/sec

  . 100 g

  It is difficult to combine this high dynamics requirement with accurate guidance.

- Volume and cost

  This is a high priority objective. The decrease of missile volume and cost induces a similar constraint for the inertial reference. It is of course necessary to evaluate I.R. cost in relation to the multifunction aspect, to compare with a standard solution : guidance system + control sensors + aerial stabilization sensors .

  The SFIM solution - SIL 1 - is resolutely directed toward cost and volume objectives, which can now be quoted as :

  . volume $<$ 1.5 liters

  . cost $<$ 150 KF (1983 HT).

3 - SPECIFIC CONCEPTS

All the strapdown inertial systems at SFIM are based on a gyroscope family - GAM 1 G - which has the following general characteristics :

- typical size : Ø 31 x 35 mm,
- gimbal using crossed blades flexure,
- synchronous drive motor,
- samarium cobalt magnet torquers (1 or 2 rings according to application) ; see figure 1.

This gyroscope is used as a rate gyro with an electronic servo loop and a ternary pulse width modulated torquer control, which has proved be the best simplicity/performance (static and dynamic) ratio.

This rate gyro is implemented together with Qflex accelerometers in SIL 2 systems.

In SIL 1 systems, the GAM 1 G is integrated in a new design calling for special conception developed at SFIM over a last few years.

3.1. Mass unbalanced gyros (M.U.G.)

The first work on mass unbalanced gyros and applications began at SFIM in 1977.

If the center of gravity of the spin wheel (G) is not identical with the suspension center (S) - unbalancing - the gyro becomes sensitive to accelerations in the torquers plane (see figure 2).

A simplified operating model is :

$Mx = \omega y - B.\gamma y$
$Mx = -\omega x + B.\gamma x$

. ωx, ωy : case angular rate (deg/sec)

. γx, γy : acceleration (g)

. Mx, My : torque applied by gyro torquers (deg/sec) ; measurements provided by sensor.

. B : mass unbalance, proportional to wheel mass and the GS distance (deg/sec/g).

In a more complex model, the torques Mx, My can be expressed with respect to real measurements Sx, Sy (direct and crossed scale factors K) ; spin position mean value γx, γy ; drift Dx, Dy; no linearity terms, the other model terms in acceleration, anisoinertia term, and dynamic terms $\partial x, \partial y$ (inertia, spin motor hunting, dynamic spin offset, ...) zeroed with a constant angular rate ωx, ωy, with residue Rx, Ry.

$$Kxx \cdot Sx + Kxy \cdot Sy + NL(Sx, Sy) + Dx + Bx \cdot \gamma y + P \cdot \gamma x = \omega y + \eta x \cdot \omega z + Cai \cdot \omega y \cdot \omega z + \partial x + Rx$$

$$Kyx \cdot Sx + Kyy \cdot Sy + NL(Sx, Sy) - Dx - By \cdot \gamma x + P \cdot \gamma y = -\omega x + \eta y \cdot \omega z - Cai \cdot \omega x \cdot \omega z + \partial y + Ry$$

The rate gyro therefore measures a combination of angular rates and accelerations ; with two measurements for one gyro, 3 sensors will provide 6 values, from which the 6 required parameters will be calculated : ω XM, ω YM, ω ZM and γ XM, γ YM, γ ZM (missile axis). Of course, it is necessary to choose mass unbalance and sensor axis positioning correctly ; the optimal choice depends on application ; but it seems that the ω / γ seperation is obtained by placing the gyro axis along the trihedral axis, and by maximizing mass unbalance differences $|B2 - B3|$, $|B3 - B1|$, $|B1 - B2|$, leading to the typical following implementation :

- gyro 1 : non-mass unbalanced ; spin Xm,
- gyro 2 : unbalanced > 0 ; spin Ym,
- gyro 3 : unbalanced < 0 ; spin Zm, with $|B2| = |B3|$; see figure 3.

Hence (same notations as above) :

$$Mx1 = \omega z$$
$$My1 = -\omega y$$
$$Mx2 = \omega x - B \cdot \gamma x$$
$$My2 = -\omega z + B \cdot \gamma z$$
$$Mx3 = \omega y + B \cdot \gamma y$$
$$My3 = -\omega x - B \cdot \gamma x$$

These equations yield :

$$\omega x = (Mx2 - My3)/2$$
$$\omega y = -My1$$
$$\omega z = Mx1$$
$$\gamma x = -(Mx2 + My3)/2.B$$
$$\gamma y = (Mx3 + My1)/B$$
$$\gamma z = (My2 + Mx1)/B$$

Several notes can be made :

- <u>there is only one kind of sensor</u> : the unbalancing of a gyro corresponds to possible adjustment of an unbalance screw ; the opposite unbalance is obtained by rotating the spin motor in the opposite direction.
- <u>the accelerometer range capability is not limited by itself</u> : the unbalance value B is choosen in relation to the flight trajectories ; typical value from 1 deg/sec/g to 10 deg/sec/g.
- <u>the accelerometric measurement benefits from gyro accuracy</u> : for example, the induced accelerometer bias is D/B where D is the gyro drift.

  (5 deg/hr (1 σ) and 5 deg/sec/g $\longrightarrow 3.10^{-4}$g (1 σ))
- the mass unbalanced gyro induces a secondary effect :

  <u>accelerometric measurements sensitivity versus angular rates</u>, through gyro scale factors errors essentially.

  A SIL 1 simplified error model has the following matrix form :

$$\begin{vmatrix} \delta\omega \\ \delta\gamma \end{vmatrix} = [Sij] \cdot \begin{vmatrix} \omega \\ \gamma \end{vmatrix} + \begin{vmatrix} D \\ b \end{vmatrix}$$

  where :

  . $\delta\omega$ is the measurement error of ω = $[\delta\omega x, \delta\omega y, \delta\omega z]$ '

  . $\delta\gamma$ is the measurement error of γ

  . $D = [Dx, Dy, Dz]$ ' system drift

  . $b = [bx, by, bz]$ ' system accelerometric bias.

  Coefficients Sij are sensitivity terms. The following crossed terms appear : $\delta\omega = S \cdot \omega$

  where S has the form

$$S = \varepsilon k/B$$

  with εk the scale factor error, and B the unbalance.

  The coupling term effect must be examined in relation to the application ; in the case of tactical missiles, the resulting acceleration (load factor) is clearly orthogonal to the angular rate, tending to cancel the coupling effect.

  For missile applications, the initial acceleration, often associated with a rolling turn (non-controlled missile) remains :

  tYpical values : - 360° roll turn

$$- 5.10^{-4} (1\ \sigma)\ \varepsilon k$$

- 5 deg/sec/g B

⟶ coupling induced velocity error ≃ 0,4 m/sec at the end of initial phase ; see figure 4.

For each application the coupling effect is analysed accurately with a typical set of trajectories (matrix covariance analysis). In most of cases it appears that this coupling term does not degrades the system error by much.

Figure 5 compares typical SIL 1 and SIL 2 system performances, with a typical short range tactical missile trajectory (matrix covariance analysis) ; the accuracies of components are similar :

	SIL 1	SIL 2
Drift	18 deg/hr (1 σ)	18 deg/hr (1 σ)
Unbalance	5 deg/sec/g	-
δB	9 deg/hr/g (1 σ)	9 deg/hr/g (1 σ)
δKg	1.10^{-3} (1 σ)	1.10^{-3} (1 σ)
δKa	-	1.10^{-3} (1 σ)
δba	-	1.10^{-3} g (1 σ)

3.2. Digitization of electronics

Strapdown inertial systems could only be developed when microcomputers appeared on the market as a large part of gimballed platform specific tasks (stabilization) are performed by software.

Given the fast technological evolution of microelectronics, SFIM began to orient development in two complementary direction as from 1977 :

- to perform the maximum number of system tasks by software,
- to digitize electronics as far as possible using state of the art technology.

These methods tend to achieve the following main objectives :

- reductions in volume and cost,
- flexible system design and evolution,
- improvement in performances.

Both software and hardware aspects are examined successively.

3.2.1. - Software

The software option chosen by SFIM reaches beyond standard concepts :

- all the data are digitized as closely as possible to the sensors : gyro offsets, temperatures, torquer inputs, ...
- a single 16-bit microprocessor organizes all the system functions, for all 3 gyros (multiplexing) :

  . data acquisition (analog, discrete, ...)
  . all 3 gyro servo loops
  . internal system outputs
  . dynamic behaviour software (see § 3.3.2.)
  . separation of measurements ω / δ
  . digital bus external output
  . compensations
  . build-in-tests
  . monitoring, ...

As quoted above, the gyro servo loop is produced by software.

The gyro angular offsets are coded (12 bits) and fed into the 16-bit microprocessor ; after preliminary processing (scaling, bias, noise filtering, see § 3.3.3.) standard servo functions are performed - integral and proportional action, phase lead, specific compensator - yielding a 16-bit precession value to be quantizised (8 or 12 bits according to application) before hardware digital/ternary modulation decoding ; see figure 6.

The gyro axes are processed at the same time (multiplexing).

The software solution offers a lot a advantages, without any tangible draw-back :

- elimination of gyro servo loop hardware
- high adaptability of design and evolution
- capability of functions that is impossible using hardware technology
- the microprocessor is designed to process all the data used for measurements and sophisticated processing (see § 3.3.).

Of course, in order to implement all these functions in only one microprocessor, designers must write the software with great care, directly in assembler language. The most crucial problem is to minimize occupancy without cancelling good software modularity (for reliability and software quality).

Typical task distribution is presented in figure. The software is implemented on a powerful 16-bit microprocessor (INTEL 8086/186/286 or MOTOROLA 68000) with synchronous organization (3 cyclic interrupt levels) and 80 - 90 % occupancy.

3.2.2. - Hardware

Volume constraints demande utilization of highly integrated electronics technology including :

- Hybridization of analog electronics (precision, power) and source digital functions,
- development of specific digital functions with gate array circuits (bipolar or CMOS),
- 'chip carrier' mounting directly on board,
- multi-layer flex-rigid-'one piece' - boards (no connectors).

The total electronics volume is about 5 to 10 times less than the same functions with discrete components.

The cost gain is noticeable (50 %) for low-level digital or analog circuits ; hybridization of ahalog electronics for precision or power remains expensive.

The figure 7 shows a flex-rigid board with hybrid analog and power circuits.

3.3. Dynamic performances

Tactical missile applications (especially short range : air-to-air ; ground-to-air, ...) require specific dynamic performances :

- high angular acceleration (> 50.000°/s^2),
- high frequency angular rate output (>1 KHz) ; small lag (<1 msec) ; high bandwith (>150 Hz).
- low noise level (< 0.1 % range).

The capabilities offered by total digitization of data, and by computerization of the system, solve these problems without any supplementary hardware and often without solution suitable for an equivalent function).

3.3.1. Sustained angular acceleration

One problem to be taken into account concerns the synchronous spin motor (hysteresis or permanent maquet). It is well known that a synchronous motor :

- can lose running speed under the effect of strong angular acceleration along the rotation axis (inertial effet of the rotating mass),
- oscillate naturally under the effect of unwanted torques or dynamic perturbations.

Digital control electronics for the rotating magnetic field, which are monitored by the microprocessor, servo the phase of the rotating field, thus providing electronic damping.

A wheel angular position signal is used (1 pulse per cycle, together with angular acceleration data from the other gyros, providing a physical phase lead which strongly improves the angular acceleration capability.

This system, associated with a discrete overvoltage control (also managed by software), achieves 100.000°/s^2 before running speed loss, for static con umption of approximatively 1 W ; see dynamic response example firure 9.

3.3.2. High bandwith

The 16-bit microprocessor loops all 3 gyros by software ; it therefore has available all the data required to estimate angular rate input to each gyro : torquer outputs, gyro offset, internal states.

SFIM has completed an observation algorithm (resulting from the observer theory in advanced automatics), which restores the input $\omega e = [\omega ex, \omega ey, \omega ez]^t$ as $\hat{\omega} e$, with a transfer function $\hat{\omega} e / \omega e$, close to a pure delay ; see figure 10.

Indeed, it appears that the state vector representig both frequency, out of an area around nutation frequency (f_N ± 10 %) ; see figure 11.

The loop together with the restoration algorithm is optimised to give an algorithm usable by a microprocessor.

In this way the following two functions are completely disconnected :

- the gyro loop transfer function, which gives dynamic limitations and affects accuracy,
- the digital output transfer function, resulting from a software restoration algorithm.

From a practical point of view, it is possible to lower the spin motor speed, in order to sustain a higher precession rate capability at the same time limiting the output data bandwith.

It is obvious that such a concept can only be achieved with a software gyro loop.

3.3.3. Noise level

One drawback of observation algorithm is the increase in noise level : much care is therefore taken at hardware and software levels to achieve the 0.1 % range objective :

- 12 bits resolution on input (gyro angle offset) and on output (torquers),
- many precautions on software quantization errors,
- 1 N + harmonics noise rejection (typical noise of DTG, as GAM 1 G).

The last point uses :

- the deterministic nature of this noise (leading to a time modelization),
- the wheel position pulse, already used for the phase loop for the spin motor magnetic field.
- It appears that the residual noise on the digital output $\hat{\omega} e$ is approximated by the derivative of filtered white noise, as :

$$b\omega_n = \lambda \cdot {}^b\omega_{n-1} + (1 - \lambda).b'\omega_n$$

$$b'\omega_n = bb_n - bb_{n-1}$$

bb = digital white noise.

4 - RESULTS

As announced in the introduction, all SFIM strapdown inertial systems are designed around 2 inertial reference models :

- SIL 2 : 2 non-unbalanced GAM 1 gyros and 3 Qflex accelerometers.
- SIL 1 : 3 non-unbalanced GAM 1 G, utilizing the general concepts described above.

The SIL 1 strapdown -inertial reference system is used in 80 % of applications currently being researched or developed at SFIM.

A typical SIL 1 inertial reference system for air-to-air tactical missiles can be described by synthesizing current research and development :

- 10°/hr class ; 1.10^{-3} g (1 σ),
- 500°/sec (X) ; 150°/sec (YZ),
  50.000°/s^2 (X) ; 40 g (XYZ),
- volume $<$1.5 liters,

  digital outputs on MIL 1553 B bus
  ($>$500 Hz output frequency), common to all 3 functions : guidance, control, stabilization.

See figure 12 (simplified technical data sheet), and figures 13 an 14(dimensions).

This system contains :

- 3 GAM 1 G rate gyros (see description above), mounted on a mechanical block.
- a single -chip 80186 microprocessor, with 8K PROM, 2K EEPROM and 2K RAM.
- some 'gate arrays' circuits for specific digital functions (such as clocks) and some standard functions mounted with chip carriers, directly on the board.
- I/O MIL 1553 B bus circuits.
- heating circuits.
- power supply, using a non-regulated 27 V DC supply.
- a mechanical case.

Figure 15 shows the positioning of the gyro axis.
Figure 16 is a schematic diagram showing the various data.
Figure 17 shows the real time organisation of software tasks.

Notes :

- On figure 16, the microprocessor-multiplexed gyro loop, together with the digital spin motor control, can be seen,
- the torquer control is ternary pulse width modulation.
- the 45 degrees gyro axis positioning provides improved dynamics along the roll axis which is always distinctive on a missile.
- real-time software organization (with sampling of the presented gyro offset angles) is optimized for the gyro loops and to reduce the delay on the digital output.

The volume of this typical inertial reference system is 1.5 liters, distributed as follows :

- sensors + block : 0.3 l.
- electronics : 0.6. l.
- power supply : 0.4. l.
- case + connections : 0.2. l.

5 - CONCLUSION

The SIL 1 strapdown inertial reference system presented in this paper is the center of most SFIM systems currently undergoing development.

Since 1977, SFIM has devoted all its efforts to decreasing cost and volume ; and by now, an inertial reference system -class 10°/hr, 1.10^{-3}, 500°/sec - in a typical 1.5 liters volume is obtained without difficulties.

This fully digitized job-oriented inertial reference system has a multifunction capability.

Extension to more complex systems is easy :

-systems for short term self-contained guidance and control (attitude,velocity, position) ;no volume increase (use of software functions).

- attitude and heading reference, with external heading reference ; no volume increase (supplementary software functions).

-hybrid navigation system for helicopters (with doppler, baro, magnetic reference) : STIRS system, presently under development.

- guidance, control and monitoring system for torpedoes.

In 1981, SFIM won a contract to the entire guidance, control and monitoring system for the new French light torpedo : CAPITULE system ; the inertial reference system ordered uses mass-unbalanced gyros and fully digitized electronics.

Figure 18 presents the main systems in current development at SFIM ; the reduction in volume obtained over a few years is outlined.

It appears that the mechanical gyro - such as the SFIM GAM DTG - is a increasingly important path to follow, because the sensitivity to acceleration - when correctly utilized - is an obious advantage.

The advantage is also apparent as a mass-unbalanced gyro provides redundancy for both rate-gyro an accelerometer data.

Progress in this technology will be made by reducing the volume of the rotatinf parts, thus decreasing consumption ; a very large gain in power supply and electronics is then expected, together with even more highly digitized electronics.

SECOND PART : LRBA

1 - INTRODUCTION

In the context of the general guidance developments ofr future missiles, functional model LRBA has been led to evaluate the first inertial reference using mass-unbalance rate gyros developed for inertial pre-guidance, flight control, and stabilization of a missile homing head.

The proposed system represents a new solution to the problem posed by supplying simultaneously the data required for guidance, flight control and stabilization, and by using for this purpose a reference with strap-down inertial components (inertial reference) in which the accelerometer function is obtained by axial mass-unbalancing of this spin wheel of 3 tuned dynamic suspension gyros which make up the sensor block.

The concept of a mass-unbalanced rate gyro should normally have led to a re-examination of the various methods and models used to evaluate these systems. In addition, as the range within which input values vary tends to widen for higher speeds and angular and linear accelerations, the problem of adapting test systems is presented and has remained partially unsolved.

This problem of evaluation is approached here simply as the aspect of the static characterization of the sensor and the inertial reference, i.e. the aspect of modelization and estimation of the coefficients of models for inputs with constant angular speed and linear acceleration. In addition, this characterization applies to preliminary equipments which do not include all the results of past and present development. Of course stress is placed on aspects of testing associated with the principle of the mass-unbalanced rate gyro.

2 - SYSTEMS EVALUATED

The tests were performed initially on a SFIM GAM 1 G3 tuned suspension mass-unbalanced rate gyro which, as far as the gyroscope only is concerned, is representative of what the prototype rate gyro could be, i.e. excluding the rate-gyro loop and other specific devices associated with implementation in the inertial reference system, such as heating and power supplies, and the mechanical interface and thermal environment.

The rate gyro is servoed by a laboratory d.c. control loop.

Then tests were undertaken on a SFIM IN-M02 inertial reference which is supposed to be representative for the intended performances, except for the following points :

- dimensions (only the sensor block is representative of the prototype)
- resistance to temperature (limited to 20°C ± 2°C)
- resistance to vibrations
- certain utilization conditions
- electrical and mechanical interfaces
- dynamic performances : transfer function and noise on the outputs.

The functional model uses pre-heating for a minimum period of 12 minutes. This temperature is maintained during the tests.

All the measurements are made in "degraded" or "operational" mode (at earliest 10 sec. after switch-on) on the angular velocity and linear accelerations functional outputs which are supplied through a bus line in a digital form in a reference trihedral related to the Inertial Reference unit.

The performance level achieved by a strap-down system largely depends on knowledge of the error models and the error compensations made.

The stability of the terms in the error model thus reflects the ultimate performances of the system, which can however only be achieved after more or less complex research and calibrations. It is therefore important to specify the type of compensation made. For this model there are the following possibilites:

- compensation of scale factor error on the torquers,
- compensation of misalignment between torquers and spin axis,
- compensation of anisoinertial drift,
- thermal compensation of torquer scale factors,
- compensation of drift terms : torques independent of g and proportional to g and g^2,
- thermal compensations of torque independent of g and of the axial mass-unbalance on the mass-unbalanced rate gyros,
- compensation of linearity error on the torquers.

These compensations are made at a maximum frequency of 93 Hz for the both guidance and control functions.

3 - MEASUREMENT SYSTEMS USED

The restrictive operating conditions on the functional model under evaluation limit the tests to those that can be performed in the laboratory in a regulated environment (20°C ± 1°C) on a CORYS 52 M2 2-axis simulator driven by a commercial computer which performs the simulator attitude and system output acquisition functions, controls the axes, and performs processing.

The analog outputs from the rate gyro loops are converted using voltage/frequency converters working on pulses counted by the computer.

The incremental digital outputs from the inertial reference system are read out by the computer at a typical frequency of $1/36\ S^{-1}$.

The next paragraphs give systems representative models, with the following symbols :

X : scalor
$\underline{X}$: vector
$|\overline{X}|$: matrix
$|X|$: transposed matrix of X
$\underline{\Omega}$: applied angular rate vector, $(\omega x, \omega y, \omega z)^t$
$\underline{A}$: applied acceleration vector ; $(ax, ay, az)^t$
$\underline{\hat{\Omega}}$: estimated angular rate vector
$\underline{\hat{A}}$: estimated acceleration vector
$\underline{\Delta\Omega}$: estimated angular rate error vector ; $\underline{\hat{\Omega}} - \underline{\Omega}$
$\underline{\Delta A}$: estimated acceleration error vector ; $\underline{\hat{A}} - \underline{A}$
δXij : residual compensation error for the error terme X, i (X, Y or Z) axis, j (1,2 or 3) gyro
δSij : residual calibration error for the torquer scale factor
Var (X) : X parameter variance
Var ($\underline{X}$) : $\underline{X}$ vector covariance matrix
H : angular momentum
(C-A)/H : anisoinertia terms (also noted J)
B : wheel axial mass unbalance
P,V : crossed unbalence terms
E,D : anisoelasticity
Γ : unwanted, fixed torque
ξ : torquers axis misalignment
α : spin misalignment

4 - DETERMINISTIC ERROR MODEL

4.1. Static model of the mass-unbalanced rate gyro

The equation below expresses the torques according to the angular rates and accelerations applied to the rate gyro along axies X, Y and Z :

$$-\frac{MY}{H} = (1 + \delta Sx).(\omega x + B.ax) + \frac{C-A}{H}.\omega x.\omega z - \alpha y.(\omega z + B.az) + \xi x.(\omega y + B.ay) + \Gamma y$$

$$-\frac{MX}{H} = (1 + \delta Sy).(\omega y + B.ay) + \frac{C-A}{H}.\omega y.\omega z + \alpha x.(\omega z + B.az) - \xi y.(\omega x + B.ax) - \Gamma x \qquad \text{Eq. 4.1.}$$

In this equation the torques Γ are a function of the acceleration applied :

$$\Gamma x = \Gamma bx + Vx.az + P.ay - (D.ay - E.ax).az$$
$$\Gamma y = \Gamma by + Vz.az + P.ay - (D.ax + E.ay).az \qquad \text{Eq. 4.2}$$

(the terms used are defined in the list of symbols)

The special features of the mass-unbalanced rate gyro appear in the following error terms :

* $\delta Sx.B.ax$, $\delta Sy.B.ay$: error due to torquers scale factors
* $\delta.B.ay$, $\xi y.B.ax$ and $\alpha y.B.az$ $\alpha x.B.az$: errors due to misalignments.

After compensation, the precedings equations are modified to represent residual compensation errors. The symbol δ designates the residual compensation errors for error terms.

$$\begin{vmatrix} -My/H \\ Mx/H \end{vmatrix} = \begin{vmatrix} \omega x + B.ax \\ \omega y + B.ay \end{vmatrix} + \begin{vmatrix} \delta Sx & \delta\xi x - \delta\alpha y \\ -\delta\xi y & \delta Sy \quad \delta\alpha x \end{vmatrix} \cdot \begin{vmatrix} \omega x \\ \omega y \\ \omega z \end{vmatrix} + \begin{vmatrix} \delta J & 0 \\ 0 & \delta J \end{vmatrix} \cdot \begin{vmatrix} \omega x.\omega z \\ \omega y.\omega z \end{vmatrix}$$

$$+ \begin{vmatrix} \delta Sx.B + \delta B & \delta P + \delta\xi x.B & \delta V y - \delta\alpha y.B \\ -\delta P - \delta\xi y.B & \delta Sy. & \delta B \quad -\delta Vx + \delta\alpha x.B \end{vmatrix} \begin{vmatrix} ax \\ ay \\ az \end{vmatrix} + \begin{vmatrix} \delta D & \delta E \\ -\delta E & \delta D \end{vmatrix} \begin{vmatrix} ax.az \\ ay\ az \end{vmatrix} + \begin{vmatrix} \delta\Gamma bx \\ \delta\Gamma by \end{vmatrix}$$

Eq. 4.3.

where B is the nominal value of the spinwheel unbalance.

If we take $\underline{M} = \begin{vmatrix} -My/H \\ Mx/H \end{vmatrix} = \begin{vmatrix} mx \\ my \end{vmatrix}$

Equation 4.3. becomes :

$$\begin{vmatrix} mx \\ my \end{vmatrix} = \begin{vmatrix} \omega x + B.ax \\ \omega y + B.ay \end{vmatrix} + \begin{vmatrix} \delta x \\ \delta y \end{vmatrix} \qquad \text{or} \quad \underline{M} = \underline{\Omega} + B.\underline{A} + \underline{\Delta} \qquad \text{Eq. 4.4.}$$

$\underline{M}$: rate gyro outputs
$\underline{\Omega}$ and $\underline{A}$: inputs
$\overline{B}$: nominal mass unbalance
$\underline{\Delta}$: error vector

Equation 4.4. is that for the mass-unbalance rate gyro after error compensation. The residual error $\underline{\Delta}$ contains the changes on coefficients with respect to their calibration values.

These changes depend on time and on operating, utilization, and environmental conditions.

The main error caused by environment is that due to ambient temperature T and to its influence on terms Γ , B and δS :

- $\delta\Gamma_T = \Gamma_T(T)$
- $\delta B_T = B_T(T)$
- $\delta S_T = S_T(T)$

where Γ_T, B_T and S_T are the sensitivities to temperature, reduced as a first appromisation to linear functions of T.

After thermal compensation, the residual temperature error is theoretically random and is included in terms $\delta\Gamma$ δB, and δS.

The non-unbalanced rate gyro equation, after error compensation, is obtained by cancelling term B in equation 4.4. :

$$\underline{M} = \underline{\Omega} + \underline{\Delta} \qquad \text{Eq. 4.6.}$$

4.2. Static model of the inertial reference with the mass-unbalanced rate gyros

The two rate gyros are arranged in an Inertial Reference system as defined in figure 19 Rotations in pitch and yaw are measured by a non-unbalanced rate gyro with its spin axis parallel to the roll axis. The other 4 parameters (rotation in roll and 3 accelerations) are measured by 2 mass-unbalanced rate gyros on the spin axes which are oriented in pitch and yaw).

Data are separated by resolving the system of equations obtained below, applying equation 4.4. to the 3 rate gyros (indexed 1, 2 and 3 for roll, yaw, and pitch respectively) :

$$\left.\begin{aligned}
m_{x1} &= -\sqrt{2}/2 \cdot (\omega_y + \omega_z) + \delta x_1 \\
m_{y1} &= -\sqrt{2}/2 \cdot (\omega_y - \omega_z) + \delta y_1 \\
m_{x2} &= \sqrt{2}/2 \cdot (\omega_x - \omega_y) + \sqrt{2}/2 \cdot B \cdot (a_x - a_y) + \delta x_2 \\
m_{y2} &= -\sqrt{2}/2 \cdot (\omega_x + \omega_y) - \sqrt{2}/2 \cdot B \cdot (a_x + a_y) + \delta y_2 \\
m_{x3} &= -\sqrt{2}/2 \cdot (\omega_x - \omega_z) + \sqrt{2}/2 \cdot B \cdot (a_x - a_z) + \delta x_3 \\
m_{y3} &= \sqrt{2}/2 \cdot (\omega_x + \omega_z) - \sqrt{2}/2 \cdot B \cdot (a_x + a_z) + \delta y_3
\end{aligned}\right\} \qquad \text{Eq. 4.8.}$$

Nota : . B1 = 0 ; B2 = - B3 = B > 0
. Xi, Yi, Zi : trihedral related to rate gyro i = 1 to 3
. X, Y, Z : trihedral related to inertial reference.

. The single solution to system 4.7 is used to define the errors ($\underline{\Delta\Omega}$ and $\underline{\Delta A}$) on the outputs by : $\underline{\Delta\Omega} = \underline{\hat{\Omega}} - \underline{\Omega}$. $\underline{\Delta A} = \underline{\hat{A}} - \underline{A}$

$$\underline{\Delta\Omega} = \left|\begin{aligned}
\delta\omega_x &= \sqrt{2}/4 \cdot [(\delta x_2 - \delta y_2) - (\delta x_3 - \delta y_3)] \\
\delta\omega_y &= \sqrt{2}/2 \cdot [-\delta y_1 - \delta x_1] \\
\delta\omega_z &= \sqrt{2}/2 \cdot [\delta y_1 - \delta x_1]
\end{aligned}\right.$$

$$\underline{\Delta A} = \left|\begin{aligned}
\delta a_x &= \sqrt{2}/4.B \cdot [(\delta x_2 - \delta y_2) + (\delta x_3 - \delta y_3)] \\
\delta a_y &= \sqrt{2}/2.B \cdot [(\delta x_1 + \delta y_1) - (\delta x_2 + \delta y_2)] \\
\delta a_z &= \sqrt{2}/2.B \cdot [(\delta y_1 - \delta x_1) - (\delta x_3 + \delta y_3)]
\end{aligned}\right. \qquad \text{Eq. 4.8}$$

Equation 4.8 shows that the angular rate and acceleration errors are of the same type.
The figure 20 gives the expression of error vectors $\underline{\Delta\Omega}$ and $\underline{\Delta A}$ according to residual compensation errors for the terms of each rate gyro defined in equation 4.3.

The general expression for these error vectors is as follows :

$$\underline{\Delta\Omega} = \underline{D_0} + |K| \cdot \underline{\Omega} + |J| \cdot |\Omega| \cdot \underline{\Omega} + |B| \cdot \underline{A} + |E| \cdot |A| \cdot \underline{A}$$

$$\underline{\Delta A} = \underline{A_0} + |G| \cdot \underline{\Omega} + |H| \cdot |\Omega| \cdot \underline{\Omega} + |M| \cdot \underline{A} + |N| \cdot |A| \cdot \underline{A} \qquad \text{Eq. 4.9.}$$

In the expression :

$$|\Omega| = \begin{vmatrix} 0 & \omega_z & 0 \\ 0 & 0 & \omega_x \\ \omega_y & 0 & 0 \end{vmatrix} \qquad |A| = \begin{vmatrix} 0 & a_z & 0 \\ 0 & 0 & a_x \\ a_y & 0 & 0 \end{vmatrix}$$

The general form of matrices $|K|, |J|, |B|, |E|, |G|, |H|, |M|, |N|$
is given in figure 20 and the physical origin of there matrices is as follows :

Error model of the inertial reference (eq. 4.9.)	Gyro compensation error (eq. 4.4.)
Kii : angular rate direct scale factor	• δSY_i + δSX_i : scale factor torquers (variation in the magnetic induction of the ring of magnets in the spinwheel) • $\delta\zeta y_i$ - $\delta\zeta x_i$: orthogonality of the torquers action lines
Mii : acceleration scale factor	• as above (Kii) ; plus

	* $\delta B_i - \delta B_j$: compensation error on the spinwheel unbalance masses.
Kij : angular rate transverse scale factor $i \neq j$	* $\delta Sy_i - \delta Sx_i$: error in the torquer scale factors (mainly connected with electronics) * $\delta\xi Y_i + \delta\xi X_i$: misalignment of the gyro around the spin axis * $\delta\alpha$: misalignment of the spin axis.
Mij acceleration transverse scale factor	* as above (Kij ($i \neq j$)) plus * $\frac{\delta P}{B}$ and $\frac{\delta V}{B}$: normalized terms P and V
B_1, j static coupling E_1, j angular rate x/acceleration	* $\frac{B}{4} \cdot \delta S$: torquer scale-factors * $\frac{B}{4} \cdot \delta\xi$: misalignment of the torquers action lines * $\frac{B}{4} \cdot \delta\alpha$: misalignment of the spin axis * δB, δP, δV, δE and δD : terms for the 2 mass-unbalanced gyros.
Bi, j static coupling Ei,j i = 2 and 3 angular rate Y and Z/acceleration	* δB_1, δP_1, δV_1, δE_1 and δD_1 terms for gyro with no mass unbalance
Gij static coupling acceleration/angular rate Hij	* $\frac{\delta S}{B}$, $\frac{\delta\xi}{B}$ and $\frac{\delta\alpha}{B}$ * $\frac{\delta J}{B}$ aniso-inertia
Jij : drift proportional to ω^2	* δJ : aniso-inertia
Nij : bias proportional to a^2	* δD : anisoelasticity
DOi and AOi : constant drift and bias	* $\delta\Gamma b$: fixed torques

The distribution of errors shows that - with respect to a standard rate-gyro sensor block - the speed output includes extra static coupling terms (on the X axis only) which does not really modify the structure of the model.

5 - STATISTICAL ERROR MODEL

When the state model parameters have been determined by the appropriate tests as described in the previous chapter, the following deduction can be made :

- the modelization residual in each test,
- the variations in the model parameters.

Using the model from equation 4.9. and the compensation given on the figure 20, we can deduce that :

$$Var(\underline{\Delta\Omega}) = \begin{vmatrix} var(\delta\omega_x) & cov(\delta\omega_x, \delta\omega_y) & cov(\delta\omega_x, \delta\omega_z) \\ cov(\delta\omega_z, \delta\omega_y) & var(\delta\omega_y) & cov(\delta\omega_y, \delta\omega_z) \\ cov(\delta\omega_z, \delta\omega_x) & cov(\delta\omega_y, \delta\omega_x) & var(\delta\omega_z) \end{vmatrix}$$

In particular, for constant $\underline{\Omega}$ and $\underline{A}$ this gives : Eq. 5.1.

$$\begin{aligned} var(\delta\omega_j) = {} & \omega_x^2 \cdot var(K_{jx}) + \omega_y^2 \cdot var(K_{jy}) + \omega_z^2 \cdot var(K_{jz}) \\ & + a_x^2 \cdot var(B_{jx}) + a_y^2 \cdot var(B_{jy}) + a_z^2 \cdot var(B_{jz}) \\ & + \omega_z \cdot \omega_x \cdot var(J_{jy}) + \omega_x \cdot \omega_y \cdot var(J_{jz}) \\ & + a_y \cdot a_z \cdot var(E_{jx}) + a_z \cdot a_x \cdot var(E_{jy}) + a_x \cdot a_y \cdot var(E_{jz}) + var(D_j) \end{aligned}$$ Eq. 5.2.

On theother hand the expression for variance of acceleration in general :

$$Var(\underline{\Delta A}) = \begin{vmatrix} var(\delta a_x) & cov(\delta a_x, \delta a_y) & cov(\delta a_x, \delta a_z) \\ cov(\delta a_y, \delta a_x) & var(\delta a_y) & cov(\delta a_y, \delta a_z) \\ cov(\delta a_z, \delta a_x) & cov(\delta a_z, \delta a_y) & var(\delta a_z) \end{vmatrix}$$ Eq. 5.3.

The variance of each parameter is composed of variances depending on time and temperature according to the basic variances defined below :

σ_a^2 : variance during continuous operation, as a function of time
σ_r^2 : variance characterizing the short-term "run-to-run" repeatibility
σ_l^2 : long-term variance
σ_T^2 : variance as a function of ambient temperature T
σ_w^2 : variance induced by warming up on starting
σ_b^2 : noise on the measurement (modelization residual)

Total variance, including all operating conditions, is the following sum :

$$\sigma^2 = \sigma_a^2 + \sigma_r^2 + \sigma_l^2 + \sigma_T^2 + \sigma_w^2 + \sigma_b^2$$ Eq. 5.4.

which means the errors defined in this way are independent.

The list of basic variances is not limitative.

6 - IDENTIFICATION OF THE MODEL

6.1. Types of tests

Two types of tests are used :

- tests at rest, warming-up tests, and multi-position tests. These tests are sensitive to the constant terms and to the terms depending on acceleration.
- rotation tests, which are sensitive to terms depending on angular rate. Laboratory tests limited to $\pm$ 1 g cannot identify the acceleration model accurately enough.
  Other tests are then required to validate the results obtained on 1 g :
  - . centrifuge tests
  - . tests on sinusoidal table
  - . vibration tests.

6.2. Tests at rest

6.2.1. Warming up-tests

These tests consist in measuring the outputs during the transitory operating mode obtained by setting the system into operation. For the air-to-air missile application this transitory phase is the functional operating phase. Given the non-stationary character of this phase, it is not possible to conduct all the tests required for identification during this phase. Therefore the only measurements made are on the changes in outputs $\underset{\sim}{M}$ (mx and my, from the rate gyro) or $\underset{\sim}{\Omega}$ and $\underset{\sim}{A}$ (from the inertial reference system) for constant inputs obtained in the following 3 fixed positions :

POSITION

X Vertical - Zenith
Y Vertical - Nadir
Z Vertical - Zenith

These functions are sensitive to :

- the constant terms
- the terms that are proportional to acceleration
- for a very small part the terms that are proportional to $\underset{\sim}{\Omega} = \underset{\sim}{\Omega}$ earth)

and are not sensitive to terms of aniso-elasticity and aniso-inertia.

In parallel to the rate gyro measurements mx and my, the internal temperature of the rate gyro is recorded.

The figure 21 presents an example of the resulting drift (SIL 1 M MO1 Z nadir).

a) Rate gyro

- Drift variations during the run-up of this type of rate are relatively large (up to 60°/h) but is never worsened by the presence of an axial spinwheel unbalance.
- Drift variations are not effectively compensated by static thermal compensation, which confirms the requirement for dynamic comepnsation. Transient phenomenoms have, for example, the following form :

  Pos. X vertical

$$\delta\omega x = 15°/h.(1 - e^{-t/\tau x}) \qquad \tau x = 180 \text{ s}$$
$$\delta\omega y = 60°/h.(1 - e^{-t/\tau y}) \qquad \tau y = 210 \text{ s}$$

- The transient thermal dynamics depend on the mechanical interface with the rate gyro. Two types of mechanical mount have been used.

b) Inertial reference system

- The performances in continous operating mode over a test period occuring 6 months after calibration of the inertial reference system are as follows :

Performances in continuous operating mode (1 σ)	Units °/h	10^{-4}g	Basic errors (1 σ)
Random drift during continuous operation over 1 hour after stabilization Filtering : 36 s	0.75	1.3	σ_a
Short-term repeatibility betwen startings (stabilized drift)	4	8	$(\sigma_v^2 + \sigma_T^2)^{1/2}$
Long-term repeatibility	39	52	$(\sigma_v^2 + \sigma_T^2 + \sigma_t^2)$

The transient operating mode on the inertial reference system outputs is characterized by :

Performances in thermal transient	UNITS °/h	UNITS 10^{-4} g	Basic errors
Variation between the 1st measurement and after 30 mins (peak value)	60	90	$\delta\omega_m$, δa_m
Short-term repeatability on the first measurement (t = 10 s to t = 10 + 36s) (1 σ)	5	12	$(\sigma_F^2 + \sigma_T^2 + \sigma_a^2)^{1/2}$

One example of warm-up showing the 6 outputs is presented figure 22.

6.2.2. Multiposition tests

The purpose of these tests is to determine the values of the coefficients of the error model composed of the following terms :

- terms independent of g
- terms proportional to g and to g^2
- thermal sensitivity of these coefficients defined in equations 4.6 and 4.9 for the rate gyro adn the inertial reference system respectively.

The thermal sensitivity could only be evaluated on the rate gyro, i.e. on coefficients without temperature compensation.

The procedure consists in measuring the outputs ($\underline{M}$ or $\underline{\Delta\Omega}$ and $\underline{\Delta A}$) in 20 positions in continuous operating mode, and in estimating the values of the model coefficients, and their uncertainties, by the generalized least squares method :

$$\underline{\Delta} = |aij| \cdot \underline{X} + \underline{\mathcal{E}} \qquad \text{Eq. 6.1.}$$

where $\underline{\Delta}$ = error vector

a) rate gyro (eq. 4.6.) = $\underline{\Delta} = \underline{M} - \underline{\Omega}$

b) inertial ref. (eq. 4.9.) = $\underline{\Delta} = \underline{\Delta\Omega}$ and $\underline{\Delta A}$

$|aij|$ = accelerations matrix
$\underline{X}$ = unknown vector
$\underline{\mathcal{E}}$ = noise

The solution to eq. 1 is :

$$\underline{X} = \left[|aij|^t \cdot |aij|\right]^{-1} \qquad \text{Eq. 6.2.}$$

$$\text{vax}(\underline{X}) = \sigma^2 \cdot \left[|aij|^t \cdot |aij|\right]^{-1} \qquad \text{Eq. 6.3.}$$

where σ^2 is the variance of the measurement noise, estimated from the modelization residual.

a) Rate gyro

$$\underline{X} = \left[\Gamma bx,\ \Gamma by,\ \delta Sx \cdot B + B,\ \delta Sy \cdot B + B,\ P + \xi x \cdot B,\ P - \xi y \cdot B,\ Vy - \alpha y \cdot B,\ -Vx + \alpha x \cdot B,\ E,\ D\right]^t \qquad \text{Eq. 6.4.}$$

The sensitivity with respect to temperature is obtained by determining $\underline{X}$ (eq. 6.4.) at 20, 40 and 60° C ambient temperature (T).

As terms αx, αy, ξ_x, ξ_y, δS_x, δSy are determined by rotation tests, equation 6.4. can be reduced to :

$$\underline{X} = \left[\Gamma bX,\ \Gamma bY,\ B,\ P,\ Vx,\ Vy,\ E,\ D\right]^t \qquad \text{Eq. 6.7.}$$

b) R.I.

Angular rate :

$$\underline{X} = \left[Dxo,\ Bxx,\ Bxy,\ Bxz,\ Exx,\ Exy,\ Exz,\ Dyo,\ Byx,\ Byz,\ Byy,\ Eyz,\ Dzo,\ Dxx\right]^t \qquad \text{Eq. 6.5.}$$

Acceleration :

$$\underline{X} = \left[Axo,\ Mxx,\ Mxy,\ Mxz,\ Nxx,\ Nxy,\ Ayo,\ Myx,\ Myy,\ Myz,\ Nyy,\ Nyz,\ Azo,\ Mxx,\ Mzy,\ Nzz\right]^t \qquad \text{Eq. 6.6.}$$

Results :

a) Rate gyro (without compensation)

Coefficient	Mean value	uncertainty	Sensitivity to temperature T (20 - 80° C)
Γbx	- 64°/h	0.7 °/h	2.25 °/k/°C
Γby	- 39 °/h	0.7 °/h	- 1.48 °/k/°C
P	- 4 °/h/g	1.0 °/h/g	0.05 °/k/g/°C
B	5038 °/h/g	1.0 °/h/g	0.09 °/k/g/°C
$V_x - \alpha x.B$	- 13 °/h/g	0.9 °/h/g	0.05 °/k/g/°C
Vy - y.B	- 27 °/h/g	0.9 °/h/g	0.05 °/k/g/°C
E	- 0.2 °/h/g^2	2.1 °/h/g^2	0.01 °/h/g^2/°C
D	- 0.6 °/h/g^2	2.1. °/h/g^2	0.01 °/h/g^2/°C

Coefficient	Short-term repeatability	(T = 20° C ± 1° C)
Γ_b	8°/h	
B	1.7 °/h/g	basic errors
P	0.4 °/h/g	
V	1.3 °/h/g_2	* statistical error σ_r
E	0.2 °/h/g_2	* deterministic error : influence of temperature T (without compensation
D	0.2 °/h/g^2	

Terms Γ , P, B and V are determined with sufficient accuracy for the values obtained to be significant, and consitute a validation of the model in the ± 1 g range. Terms E and D are not estimated with sufficient accuracy. Vibration tests are normally used in order to estimate these parameters more accurately.
Short-term repeatability includes variations on coefficients due to ambient temperature, caused by :

- the sensitivity of the actual terms to temperature Γ_{bx} , Γ_{by} and for a lesser part B
- the sensitivity to temperature (4.10^{-4}/°C) of the torquers scale factor : estimation error of term B (cf. § 6.3.).

b) Inertial Reference

The results of identification of angular rate model (equation 6.5.) and the acceleration model (equation 6.6.) are illustrated by the example given in figure which provide a matricial representation of the following :

- the model
- the estimated values of the coefficients of the model
- the uncertainty of the coefficients

and the "sigma" modelization residual.

The angular rate terms are expressed as °/h , °/h/g, and °/h/g^2.

The acceleration terms are expressed in 10^{-4}g . 10^{-4}g/g and 10^{-4}/g/g^2.

Note : The symbol * marking parameters Exz and Nzz, this signifies that the parameters hare not been sensed by the selected positions. In future 24 positions will be used.

Coefficients	Short-term repeatability	Long-term repeatability (6 months)	Units
Doi	0.9	34	°/h
Bij	0.9	10	°/h/g_2
Eij	1.3	1.8	°/h/g^2
Aoi	1.9	32	10^{-4}g
Mij	4.3	28	10^{-4}g/g_2
Nij	2.3	3.3	10^{-4}g/g^2
Basic errors	$(\sigma_r^2 + \sigma_T^2)^{1/2}$	$(\sigma_{sr}^2 + \sigma_H^2 + \sigma_{tr}^2)^{1/2}$	

Performances in multiposition tests ± 1g

Coefficients	Short-term repeatability	Long-term repeatability (6 months	Units
	1.2	35	°/h
	2.3	40	10^{-4}g
Basic errors	$(\sigma_{sr}^2 + \sigma_{st}^2)^{1/2}$	$(\sigma_{sv}^2 + \sigma_{st}^2 + \sigma_{sr}^2)^{1/2}$	

6.3. Rotation tests

6.3.1. Purpose of the tests

The purpose of these tests is to determine

a) on the rate gyro

. the scale factors of the torque motors Kx and Ky
. the misalignments $\int x$, $\int y$, αx, αy
. the anisoinertial term (C - A)/H

The "electrical" precessions defined in equation 4.4 are expressed by :

$\frac{Nx}{H}$ = Kx . Ix Eq. 6.1.

$\frac{My}{H}$ = Ky . Iy

b) on the inertial reference system

- the scale factor errors : matrix |K|
- the static coupling acceleration/angular rate : matrix |G|
- the anisoinertial terms : matrices |J| and |H|

6.3.2. Error model of the scale factor

Scale factors Kx, Ky are functions of the angular rate applied to the rate gyro and of time t :

$$Kx(\omega, t) = Kyo.[1 + Ux(\omega, t) + Vx(\omega, t)]$$
$$Ky(\omega, t) = Kyo.[1 + Uy(\omega, t) + Vy(\omega, t)] \quad \text{Eq. 6.2.}$$

In this equation :

- Kxo and Kyo are the values of the nominal scale factors measured for zero initial conditions, at rates $\pm\omega yo$ and $\pm\omega xo$.
- $U(\omega, t)$ is an even function of ω :
  $U(\omega) = Ko + K1 \cdot \text{sign}(\omega) + K2\,\omega^2 + \ldots$ Eq. 6.3.
- $v(\omega, t)$ is an old function of ω :
  $v(\omega) = \ell 1.\omega + \ell 2.\omega^2 \text{ sign}(\omega) + \ldots$ Eq. 6.4.

The figure 24 presents the terms definition.

The corresponding error model in the inertial reference system : δSx and δSy is supplied by the following relations :

$$\delta Sx = -\frac{\delta KYo}{Ky} - \delta uy - \delta vy \quad \text{Eq. 6.5.}$$
$$\delta Sy = -\frac{\delta KXo}{Kx} - \delta ux - \delta vx$$

6.3.3. Procedure

The tests performed are limited to applying angular rates to the standard axes X, Y, Z ot the rate gyro or the inertial reference system (the anisoinertial terms which are only excited for rotations applied about the non-standard axes will not be evaluated for these tests. The range of rates $\pm\omega o$, $\pm\omega max$ applied in continous operating mode is :

	ω_o	ω_{max}
rate gyro	10°/s	200°/s
inertial reference	10°/s	100°/s

The cycle of angular rates applied is of the type $+\omega o, -\omega o, \ldots, +\omega 1, -\omega \ldots +\omega max, -\omega max$. For each rate applied, measurements are made on complete turns of the table axis in order to average the drifts proportional to g, for a period of 360 s.

Changes as a function of time are measured for $\omega \geq 40°/s$ at 9-second intervals (40 successive measurements are made over 360 s for each rate. Each of these 40 measurements is integrated over 9 s).

When each rate has been applied, the system is maintened at rest for 9 mins to re-establish the initial thermal conditions.

6.3.4. Results

The model identified is as follows

$$Ux(\omega, t) = k(t).\omega y^2 \quad \text{Eq. 6.6.}$$
$$Uy(\omega, t) = k(t).\omega x^2$$

$$Vx(\omega, t) = 0 \quad \text{Eq. 6.7.}$$
$$Vy(\omega, t) = 0$$

The result is illustrated in figure 25 in which symbol ◇ represents : $V(\omega, t)$ for t = 9 s.

and symbols → represent $u(\omega, t)$ for t = 90 s
↓ represent " " " t = 180 s
← represent " " " t = 270 s
↑ represent " " " t = 360 s

in the range 10°/s to ± 200°/s
(function $U(\omega, t = 9\ s)$ represents axis)

The function $u(\omega, t)$ describes heating, by the Joule effect, of the torquer magnet ring. For fixed ω, $U(t)$ is the solution to

$$u(t) + \tau . \frac{\partial u(t)}{\partial t} = k(\omega) \quad \text{Eq. 6.7.}$$

Typical values obtained are :

$$k(\omega) = -2.6 \cdot 10^{-4}/(rd/s)^2$$
$$= 150\ s.$$

The general form of the model is equation 6.6. for the simultaneous rate inputs on axes X and Y, therefore : $Ux(\omega, t) = Uy(\omega, t) = k(t).(\omega x^2 + \omega y^2)$

i.e. $u(t) = k(t) \cdot (\omega x^2 + \omega y^2)$ Eq. 6.8.
where $k(t) + \tau . \frac{\partial k(t)}{\partial t} = k(\omega)$ Eq. 6.9.

These equations could be used as a compensation model for heating of the torquers.
The thermal sensitivity of coefficient Kxo is evaluated at $\omega = \pm 10°/s$ in the ambient temperature range T = 20 to 60°C.

$$\frac{\partial Ko}{Ko.\partial T} = 4.10^{-4}/°C$$

b) Inertial Reference

The matrix coefficients $|K|$ and $|G|$ are estimated in the same way on the Inertial Reference system. An illustration of the results is given by terms ωy and ay.

$$\omega y = Kyx.\omega x + Kyy.\omega y + Kyz.\omega z$$
$$ay = Gyx.\omega x + Gyy.\omega y + Gyz.\omega z$$

Terms Kyx, Kyz - or Gyx, Gyy, Gyz are static coupling terms less than 2.10^{-3} (°/h)/(°/h) or $(10^{-4}g)/(°/h)$ and are independent of time t.

The function Kyy (ω, t) is represented by figure 11 in the range $\pm$ 10, $\pm$ 100°/s for t = 36 to 360 s.
The result obtained is coherent with the heating model identified on the rate gyro.
The linearity error remains less than 4.10^{-4} in these conditions :

$$Kyy(\omega, t) = Kyyo_{-4}.\left[1 + u(\omega, t)\right]$$
$$u(\omega, t) < 4.10^{-4}$$
Kyyo : determined by $\omega = \pm$ 10°/s.

7 - CONCLUSION

The first tests have been performed on equipments utilizing the mass-unbalance gyro concept in laboratory operating conditions ($\pm$ 1g, $\pm$ 100°/s, 20°C $\pm$ 2°C) and for constant angular rate and acceleration inputs. These tests demonstrate that this principle is applicable to the guidance using the following typical values :
drift $<$ 100°/h or 10^{-2}
scale factor error $< 10^{-3}$

In particular the following factors appear :

- the model of the mass unbalance gyro is not different from the non-unbalanced gyro, and no static characteristics are affected by axial unbalancing of the spinwheel.
- the errors in acceleration are largely deducible from the angular rate errors using the ratio defined by the value of the axial unbalance (here $1°/h \simeq 1 \times 10^{-4}$ g).
- the current performances can be improved by dynamic modelization of thermal effects (transient on switch-on and internal heating of the torquers).

Research is currently being made on the inertial reference prototypes which will be evaluated at LRBA in 1984. The well-known model of a tuned suspension rate gyro will be basis for elaboration of future tests, which will evaluate performances and dynamic errors, and validate models in the fields of high angular and linear rates and accelerations. Research is currently being made in this direction on LRBA job-oriented test systems such as the 20 g sinusoidal table and the 80 g centrifuge.

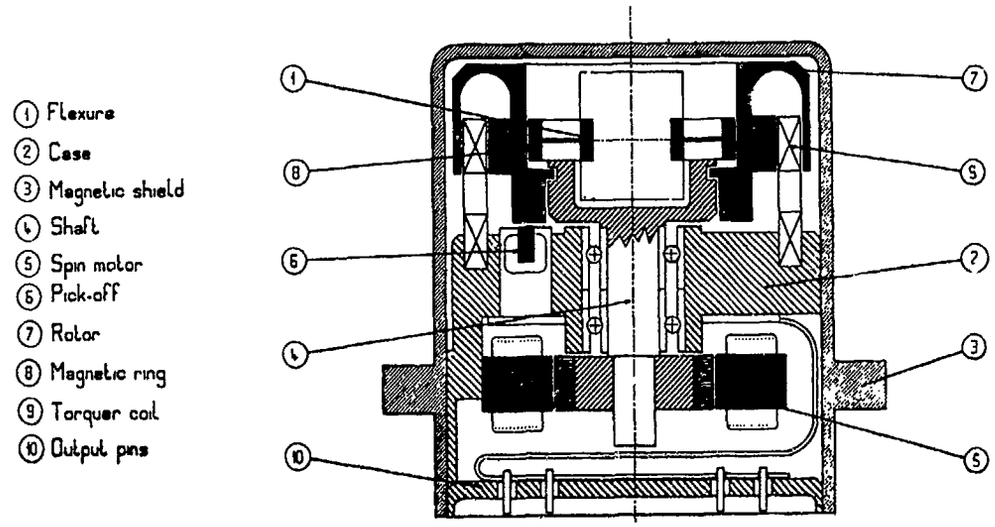

Fig. 1 . GAM 1 G

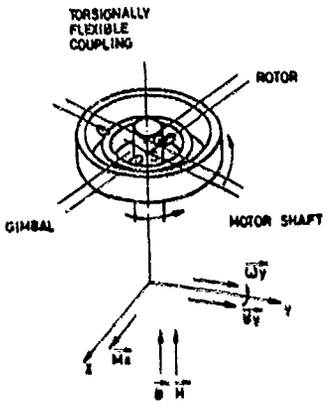

$$\vec{M} = \vec{B} \wedge \vec{\beta} + \vec{\omega} \wedge \vec{H}$$

$$\Rightarrow \begin{cases} Mx = \omega y \cdot \beta y \\ My = -\omega x \cdot \beta x \end{cases}$$

Fig. 2 . MASS UNBALANCED GYRO (MUG)

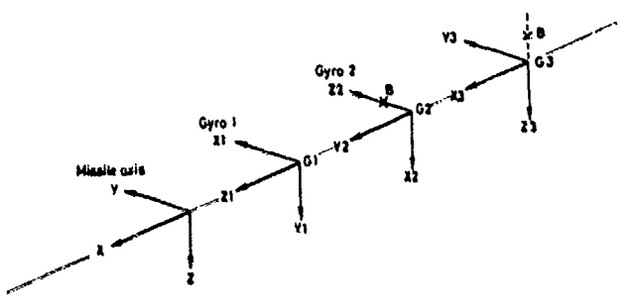

Fig 3 . SIL 1 . MASS UNBALANCED GYRO MEASUREMENTS UTILIZATION

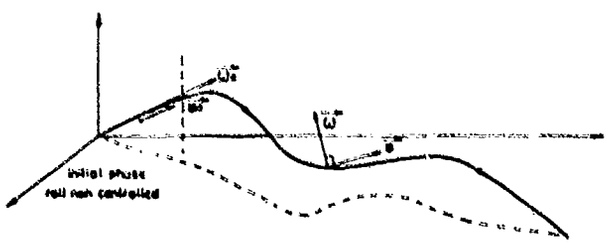

$$\delta\theta = \frac{\varepsilon_b}{\beta} \cdot \omega \quad \Rightarrow \quad \Delta V = \frac{\varepsilon_b}{\beta} \cdot \Delta\varphi$$

with $\varepsilon_b = 5.10^{-4}$ (1°/h), $\beta = 5^{\circ}/h/g$, $\Delta\varphi = 360°$

$\Rightarrow$ $\Delta V = 0.6$ m/sec after initial phase

and $\Delta P = 8$ meters for a 30 sec flight time

Fig 4 . SIL 1 . CROSS COUPLING GYRO ACCELERO EFFECT.

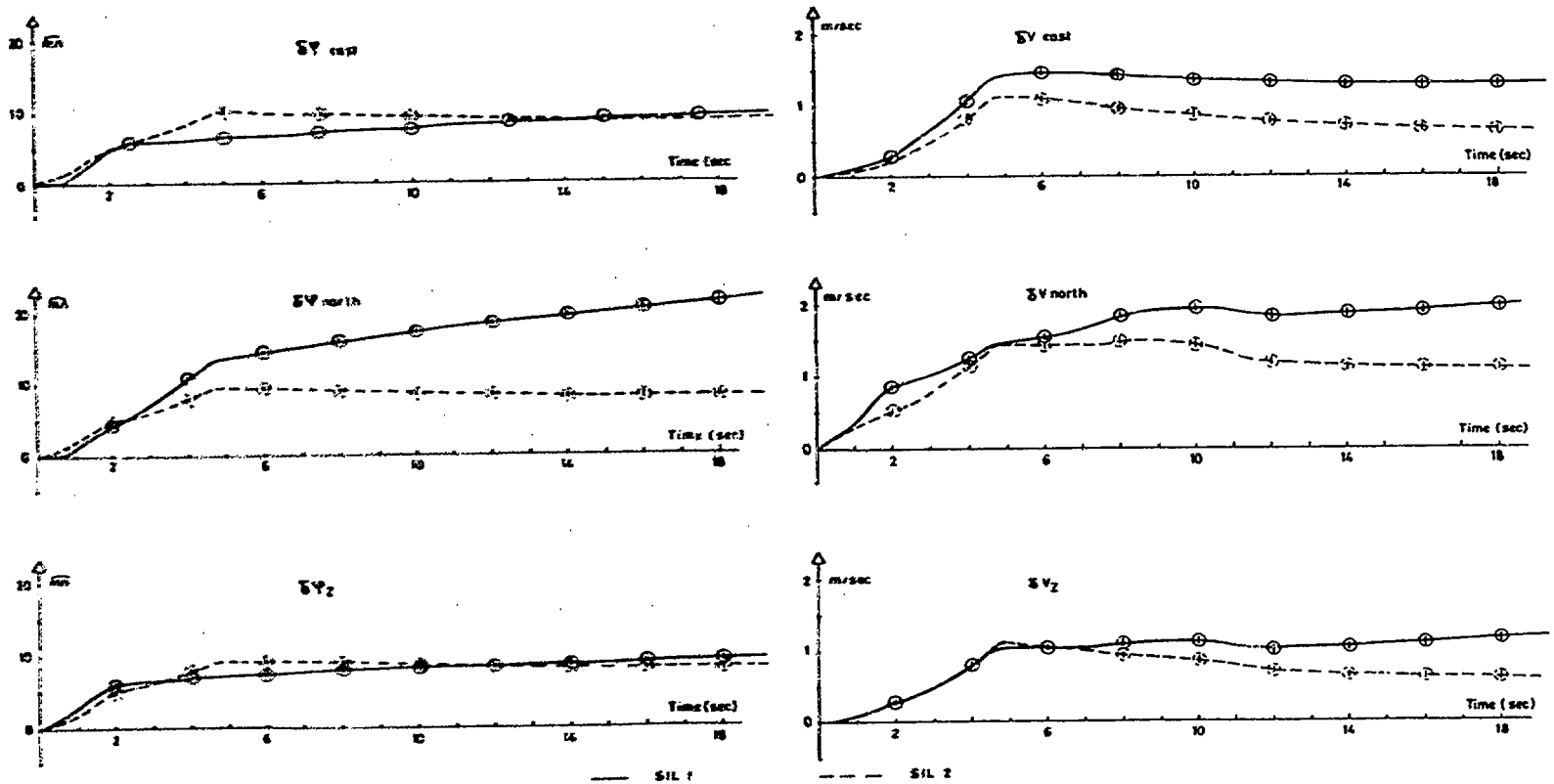

Fig. 5 - SIL 1, SIL 2 - ATTITUDE ERROR COMPARISON; VELOCITY

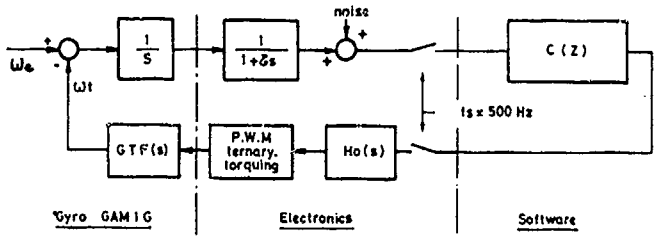

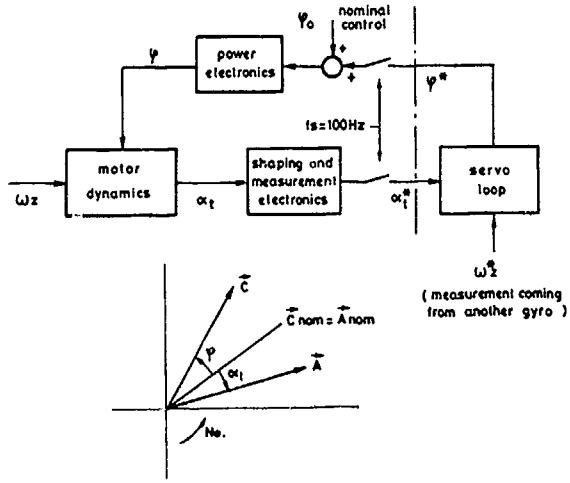

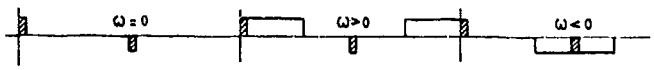

Fig. 6 - SIL 1 - SOFTWARE GYRO LOOP AND PWM TERNARY TORQUING

Fig. 8 - SIL 1 - SPIN MOTOR SERVO LOOP

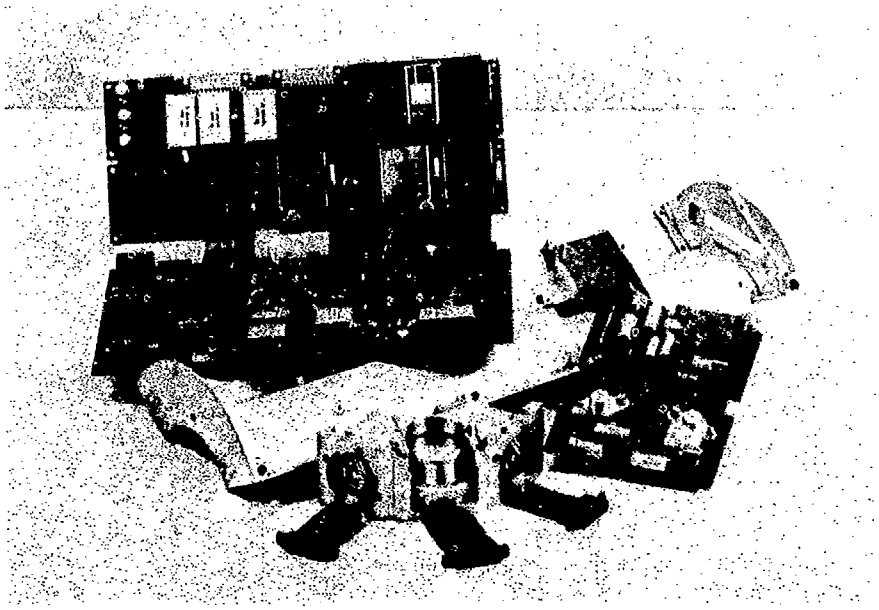

Fig. 7 SIL 1 MECHANICS AND ELECTRONICS

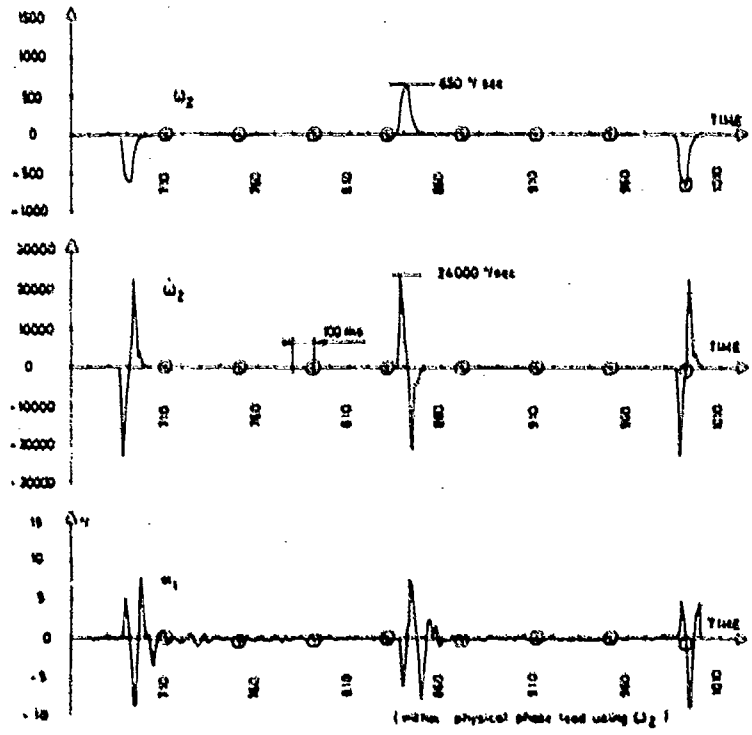

Fig 9 - SIL 1 - SPIN MOTOR SERVO LOOP TEST

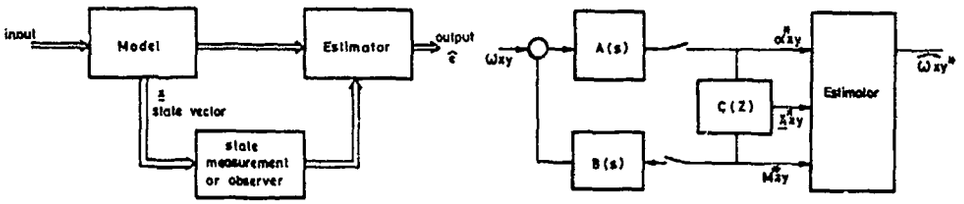

$$\widehat{\omega xy}^{*} = \frac{1}{T}\int_{-\frac{T}{2}}^{+\frac{T}{2}} \omega xy \; dt \qquad \widehat{\omega xy}^{*} = D(Z).\overset{n}{M}xy + E(Z).\overset{n}{\alpha}xy + F(Z).\overset{n}{\underline{x}}xy$$

Fig.10 - SIL 1 - OPTIMAL ESTIMATION $\widehat{\omega xy}^{*}$

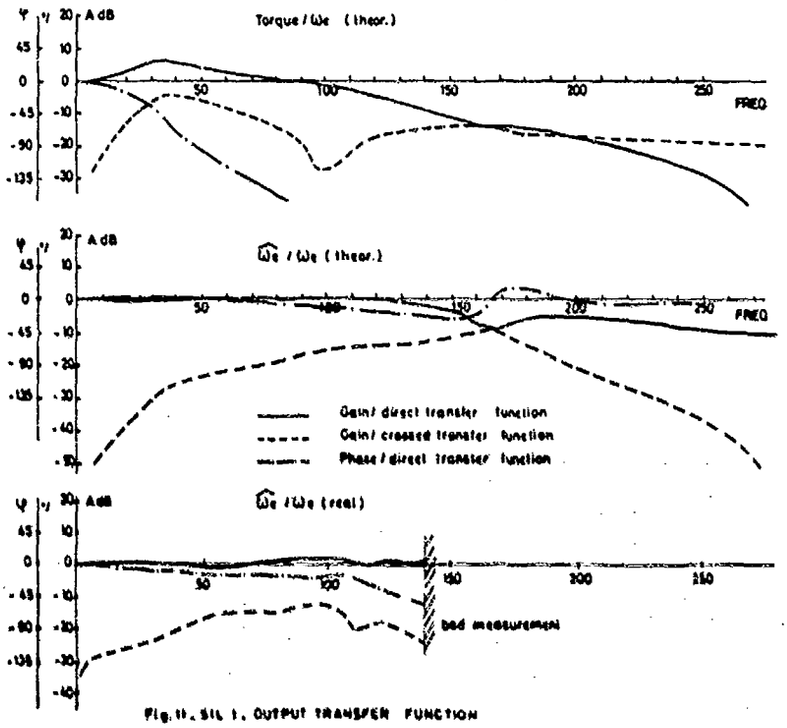

Fig.11 - SIL 1 - OUTPUT TRANSFER FUNCTION

Tactical missile / typical short-range application

Volume	≤ 1.5 liters
Power supply	27 V / ≤ 70 W
Pre-launch heating	≤ 80 W / 3 minutes
Run up time	≤ 2 sec
Multifunction (UM)	: Guidance / control / stabilization
Interface	: MIL 1553 B
Output	: Angular and velocity increments > 500 Hz
Cost (Fr 1982)	: ≤ 150 kF

Dynamic range

- 40 g (3 σ)
- 500 °/sec (4), 150 °/sec (3 σ)
- 20 000 °/s² (4)

Typical accuracy and performances

- Drift : 1 to 100 °/h (1 σ)
- Bias : 1.10^{-4} to 1.10^{-2} g (1 σ)
- Scale factor (accel and gyro) 1.10^{-4} to 1.10^{-3} (1 σ)
- Bandwidth : > 100 Hz
- Noise : ≤ 0.1 % range

Fig 12 - IMU - SIL 1

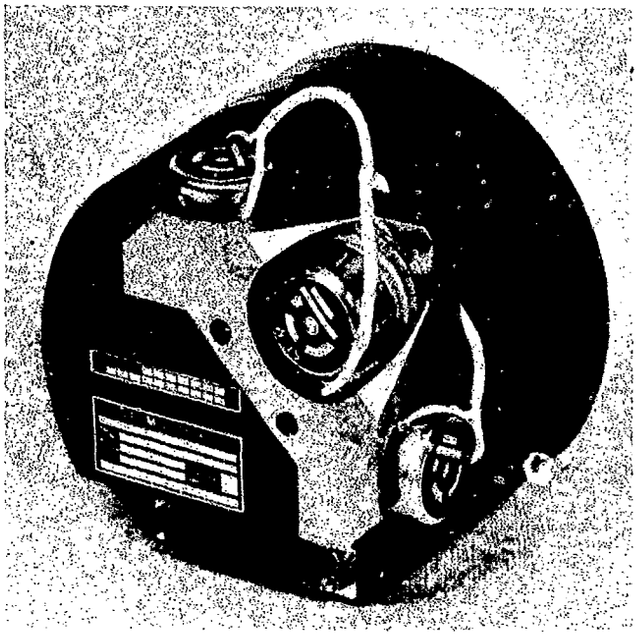

Fig. 13 SIL 1. GENERAL SIZE

Fig. 14 SIL 1. SENSOR BLOCK

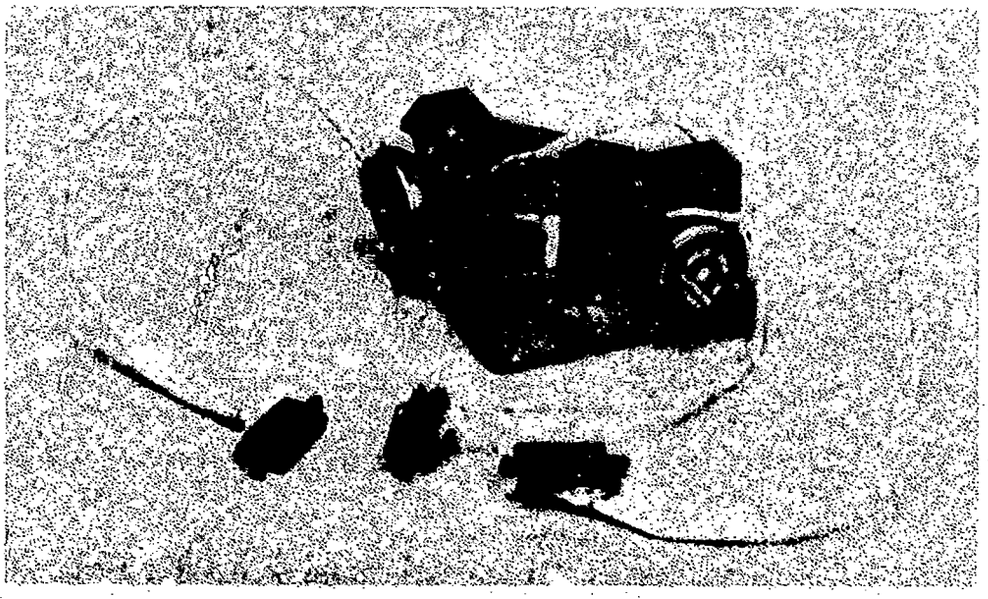

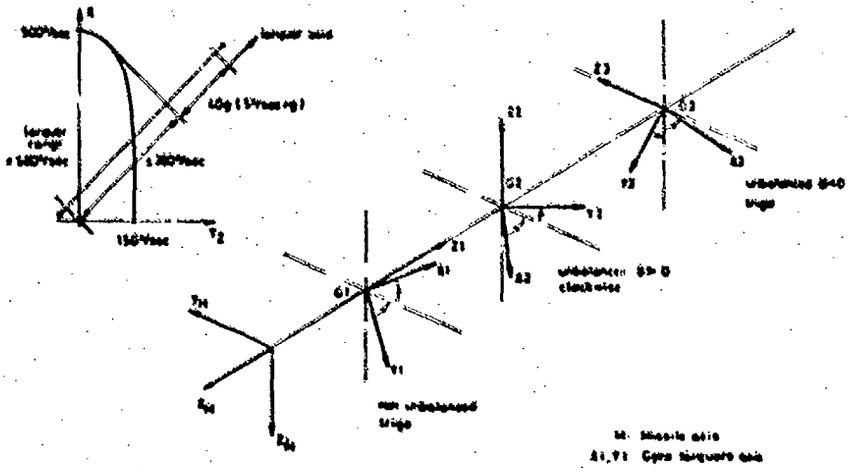

Fig 15 . SIL 1 . MISSILE / GYRO AXIS ; RATE DIAGRAM

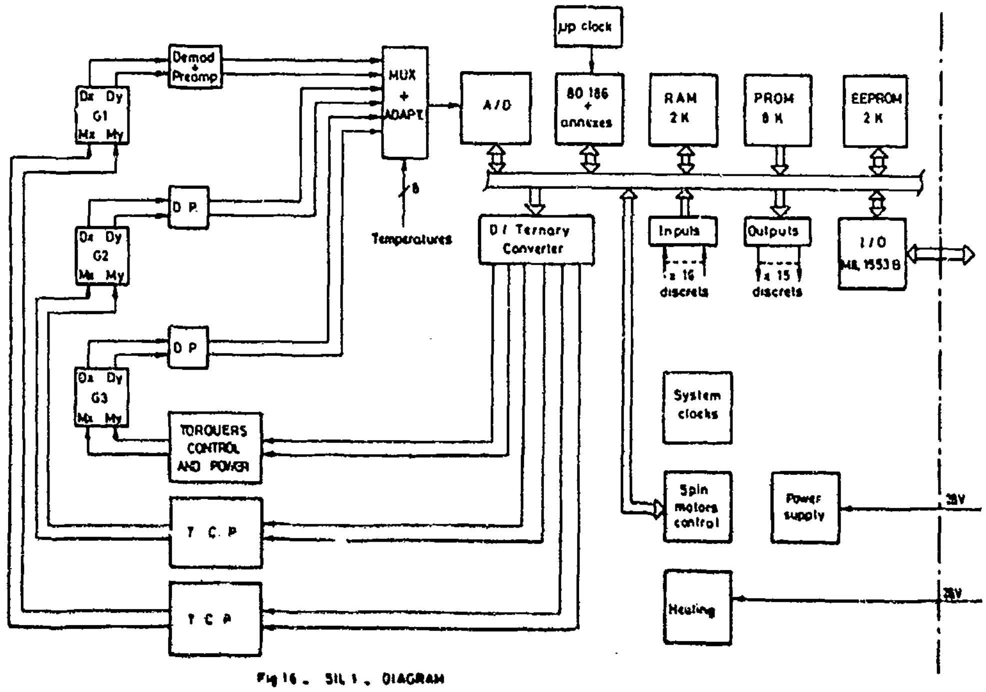

Fig 16 - SIL 1 - DIAGRAM

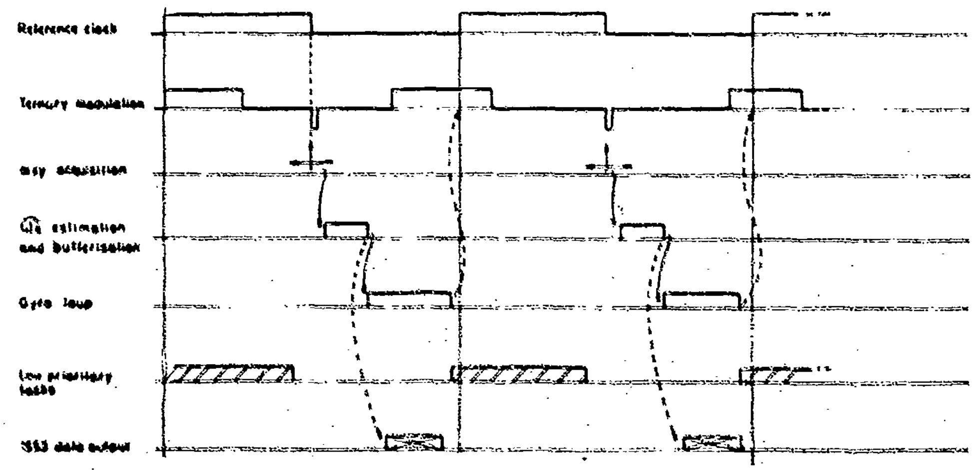

Fig 17. SIL 1. SOFTWARE TASKS IMPLEMENTATION

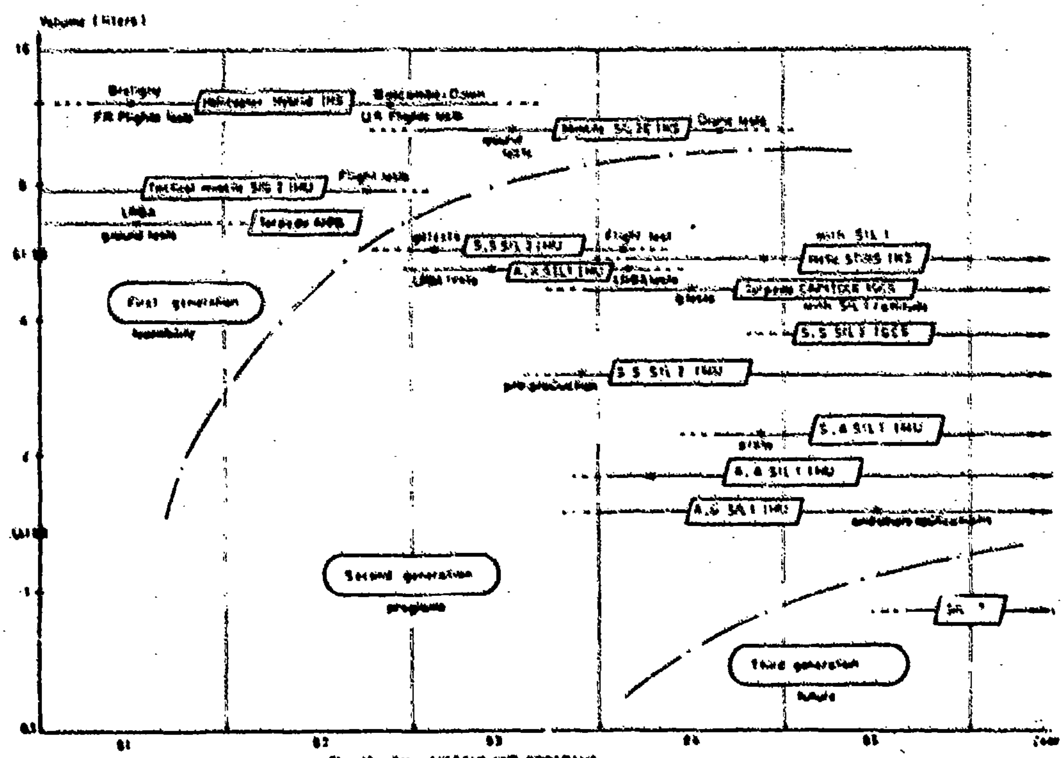

Fig 18 - SIL SYSTEMS AND PROGRAMS

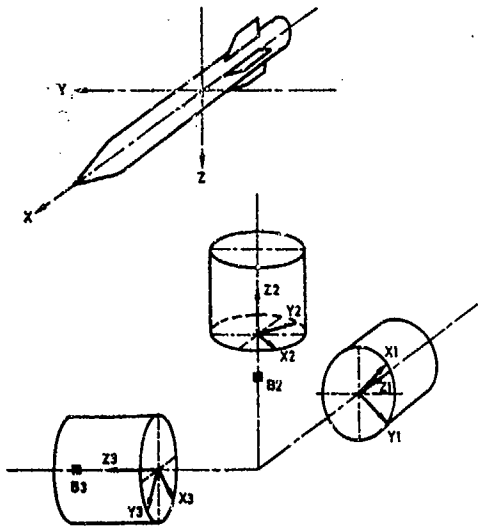

Fig.18 - M02(IMU) RATE GYROS AND MISSILE AXIS POSITIONING
MASS UNBALANCES VALUES
B2 = -B3 = B
B1 = 0

$$\begin{vmatrix} \delta\omega X \\ \delta\omega Y \\ \delta\omega Z \end{vmatrix} = \begin{vmatrix} DXO \\ DYO \\ DZO \end{vmatrix} + \begin{vmatrix} KXX & KXY & KXZ \\ KYX & KYY & KYZ \\ KZX & KZY & KZZ \end{vmatrix} \cdot \begin{vmatrix} \omega X \\ \omega Y \\ \omega Z \end{vmatrix} + \begin{vmatrix} 0 & JXY & JXZ \\ 0 & 0 & JYZ \\ 0 & JZY & 0 \end{vmatrix} \cdot \begin{vmatrix} \omega Y\,\omega Z \\ \omega Z\,\omega X \\ \omega X\,\omega Y \end{vmatrix} + \begin{vmatrix} EXX & EXY & EXZ \\ BYX & BYY & BYZ \\ BZX & BYZ & BYY \end{vmatrix} \cdot \begin{vmatrix} aX \\ aY \\ aZ \end{vmatrix} + \begin{vmatrix} EXX & EXY & EXZ \\ 0 & EYY & EYZ \\ 0 & EYZ & EYY \end{vmatrix} \cdot \begin{vmatrix} aY\,aZ \\ aZ\,aX \\ aX\,aY \end{vmatrix}$$

$$\begin{vmatrix} \delta a X \\ \delta a Y \\ \delta a Z \end{vmatrix} = \begin{vmatrix} AXO \\ AYO \\ AZO \end{vmatrix} + \begin{vmatrix} GXX & GXY & GXZ \\ GYX & GYY & GYZ \\ GZX & GZY & GZZ \end{vmatrix} \cdot \begin{vmatrix} \omega X \\ \omega Y \\ \omega Z \end{vmatrix} + \begin{vmatrix} 0 & HXY & HXZ \\ 2HXY & 0 & HYZ \\ 2HXZ & -HYZ & 0 \end{vmatrix} \cdot \begin{vmatrix} \omega Y\,\omega Z \\ \omega Z\,\omega X \\ \omega X\,\omega Y \end{vmatrix} + \begin{vmatrix} MXX & MXY & MXZ \\ MYX & MYY & MYZ \\ MZX & MZY & MZZ \end{vmatrix} \cdot \begin{vmatrix} aX \\ aY \\ aZ \end{vmatrix} + \begin{vmatrix} MXX & MXY & MXZ \\ 2MXY & MYY & MYZ \\ 2MXZ & -MYZ & MZZ \end{vmatrix} \cdot \begin{vmatrix} aY\,aZ \\ aZ\,aX \\ aX\,aY \end{vmatrix}$$

STATIC ERRORS GENERAL EXPRESSION

Fig. 20 - M02 MODELIZATION

$$\begin{vmatrix} \delta\omega x \\ \delta\omega y \\ \delta\omega z \end{vmatrix} = \begin{bmatrix} \begin{vmatrix} \frac{1}{2}(S2^{+}-S3^{+}) & \frac{1}{2}S2 & \frac{1}{2}S3^{-} \\ 0 & S1^{+} & -S(^{-} \\ 0 & -S1^{-} & S1^{+} \end{vmatrix} + \begin{vmatrix} \frac{1}{2}(\epsilon 2^{+}-\epsilon 3^{+}) & -\frac{1}{2}\epsilon 3^{+} & -\frac{1}{2}\epsilon 2^{+} \\ 0 & -\epsilon 1^{-} & -\epsilon 1^{+} \\ 0 & +\epsilon 1^{+} & \epsilon 1^{-} \end{vmatrix} + \begin{vmatrix} 0 & \frac{1}{2}\alpha 3^{+} & \frac{1}{2}\alpha 2^{+} \\ -\alpha 1^{-} & 0 & 0 \\ -\alpha 1^{+} & 0 & 0 \end{vmatrix} \end{bmatrix} \cdot \begin{vmatrix} \omega X \\ \omega Y \\ \omega Z \end{vmatrix}$$

$$+ \begin{bmatrix} \begin{vmatrix} \frac{B}{2}(S2^{+}-S3^{+}) & \frac{B}{2}S2^{-} & \frac{B}{2}S3^{-} \\ 0 & 0 & 0 \\ 0 & 0 & 0 \end{vmatrix} + \begin{vmatrix} \frac{B}{2}(\epsilon 2^{+}-\epsilon 3^{+}) & -\frac{B}{2}\epsilon 2^{+} & -\frac{B}{2}\epsilon 3^{+} \\ 0 & 0 & 0 \\ 0 & 0 & 0 \end{vmatrix} + \begin{vmatrix} 0 & \frac{B}{2}\alpha 3^{+} & \frac{B}{2}\alpha 2^{+} \\ 0 & 0 & 0 \\ 0 & 0 & 0 \end{vmatrix} \end{bmatrix} + \begin{vmatrix} \delta\omega x \\ \delta\omega y \\ \delta\omega z \end{vmatrix} = \begin{vmatrix} \frac{1}{2}(\Gamma 2^{+}-\Gamma 3^{+}) \\ -\Gamma 1^{-} \\ -\Gamma 1^{+} \end{vmatrix} + \begin{vmatrix} 0 & -\frac{1}{2}SJ2 & \frac{1}{2}SJ3 \\ 0 & 0 & -SJ1 \\ 0 & -SJ1 & 0 \end{vmatrix} \cdot \begin{vmatrix} \omega Y\,\omega Z \\ \omega Z\,\omega X \\ \omega X\,\omega Y \end{vmatrix} + \begin{vmatrix} \frac{1}{2}(SE2-SE3) & -\frac{1}{2}SD2 & \frac{1}{2}SD3 \\ 0 & SE1 & -SD1 \\ 0 & -SD1 & -SE1 \end{vmatrix} \cdot \begin{vmatrix} aY\,aZ \\ aZ\,aX \\ aX\,aY \end{vmatrix}$$

ANGULAR RATE ERROR (terms VS $\underline{\Omega}$ and $\underline{A}$)

$$\begin{vmatrix} \delta ax \\ \delta ay \\ \delta az \end{vmatrix} = \begin{vmatrix} \frac{1}{2B}(\Gamma 2^{+}+\Gamma 3^{+}) \\ \frac{1}{B}(\Gamma 1^{-}-\Gamma 2^{-}) \\ \frac{1}{B}(-\Gamma 1^{+}-\Gamma 3^{-}) \end{vmatrix} + \begin{vmatrix} 0 & -\frac{1}{2B}SJ2 & -\frac{1}{2B}SJ3 \\ -\frac{1}{B}SJ2 & 0 & \frac{1}{B}SJ1 \\ -\frac{1}{B}SJ3 & -\frac{1}{B}SJ1 & 0 \end{vmatrix} \cdot \begin{vmatrix} \omega Y\,\omega Z \\ \omega Z\,\omega X \\ \omega X\,\omega Y \end{vmatrix} + \begin{vmatrix} \frac{1}{2B}(SE2+SE3)-\frac{1}{B}SD2 & -\frac{1}{2B}SD3 \\ -\frac{1}{B}SD2-\frac{1}{B}(SE1+SE2) & \frac{1}{B}SD1 \\ -\frac{1}{B}SD3 & -\frac{1}{B}SD1-\frac{1}{B}(SE1-SE3) \end{vmatrix} \cdot \begin{vmatrix} aY\,aZ \\ aZ\,aX \\ aX\,aY \end{vmatrix}$$

ACCELERATION ERRORS (terms VS $\underline{\Omega}$ and $\underline{A}$)

$$\begin{vmatrix} \delta ax \\ \delta ay \\ \delta az \end{vmatrix} = \begin{bmatrix} \frac{1}{B} \begin{vmatrix} \frac{1}{2}(S2^{+}-S3^{+}) & \frac{1}{2}S2^{-} & -\frac{1}{2}S3^{-} \\ -S2^{-} & S2^{+}-S1^{+} & S1^{-} \\ -S3^{-} & -S1^{-} & S1^{+}-S3^{+} \end{vmatrix} + \frac{1}{B} \begin{vmatrix} \frac{1}{2}(\epsilon 2^{+}-\epsilon 3^{+}) & -\frac{1}{2}\epsilon 2^{+} & \frac{1}{2}\epsilon 3^{+} \\ \epsilon 2^{+} & \epsilon 1^{+}-\epsilon 2^{-} & \epsilon 1^{+} \\ -\epsilon 3^{-} & \epsilon 1^{+} & \epsilon 1^{+}-\epsilon 2^{-} \end{vmatrix} + \frac{1}{B} \begin{vmatrix} 0 & -\frac{1}{2}\alpha 3^{+} & \frac{1}{2}\alpha 2^{+} \\ \alpha 1^{-} & 0 & -\alpha 2^{-} \\ -\alpha 1^{+} & \alpha 3^{-} & 0 \end{vmatrix} \end{bmatrix} \cdot \begin{vmatrix} \omega X \\ \omega Y \\ \omega Z \end{vmatrix}$$

$$+ \begin{bmatrix} \begin{vmatrix} \frac{1}{2}(S2^{+}-S3^{+}) & \frac{1}{2}S2^{-} & -\frac{1}{2}S3^{-} \\ S2^{-} & S2^{+} & 0 \\ -S3^{-} & 0 & -S3^{+} \end{vmatrix} + \begin{vmatrix} \frac{1}{2}(\epsilon 2^{+}-\epsilon 3^{+}) & -\frac{1}{2}\epsilon 2^{+} & \frac{1}{2}\epsilon 3^{+} \\ \epsilon 2^{+} & \epsilon 2^{+} & 0 \\ -\epsilon 3^{+} & 0 & \epsilon 3^{+} \end{vmatrix} + \begin{vmatrix} 0 & -\frac{1}{2}\alpha 3^{+} & \frac{1}{2}\alpha 2^{+} \\ 0 & 0 & -\alpha 2^{+} \\ 0 & \alpha 3^{+} & 0 \end{vmatrix} \end{bmatrix}$$

$$+ \frac{1}{B} \begin{vmatrix} \frac{1}{2}(SB2-SB3) & \frac{1}{2}(-SP2+V3^{+}) & \frac{1}{2}(SP3-V2^{+}) \\ SP2-V1^{-} & SB2-SB1 & SP1+V2^{+} \\ -SP2+V1^{+} & SP1-V2^{+} & SB1-SB3 \end{vmatrix} \cdot \begin{vmatrix} \alpha X \\ \alpha Y \\ \alpha Z \end{vmatrix}$$

ACCELERATION ERROR (terms VS $\underline{\Omega}$ and $\underline{A}$)

Gyro		IMU	
Torquers scale factor errors	δSxi	$Si^{+} = \frac{1}{2}(\delta Syi + \delta Sxi)$	Scale factor error (caused principally by magnets)
	δSyi	$Si^{-} = \frac{1}{2}(\delta Syi - \delta Sxi)$	Electrical origin
Torquers misalignment	$\delta\xi xi$	$\xi i^{+} = \frac{1}{2}(\delta\xi yi + \delta\xi xi)$	Position around spin axis
	$\delta\xi yi$	$\xi i^{-} = \frac{1}{2}(\delta\xi yi - \delta\xi xi)$	Orthogonality error (torquers)
Spin misalignment	$\delta\alpha xi$	$\alpha i^{+} = \frac{\sqrt{2}}{2}(\delta\alpha yi + \delta\alpha xi)$	Due to a 45° rotation around spin axis
	$\delta\alpha yi$	$\alpha i^{-} = \frac{\sqrt{2}}{2}(\delta\alpha yi - \delta\alpha xi)$	
Drift error	$\delta\Gamma bxi$	$\Gamma i^{+} = \frac{\sqrt{2}}{2}(\delta\Gamma byi + \delta\Gamma bxi)$	
	$\delta\Gamma byi$	$\Gamma i^{-} = \frac{\sqrt{2}}{2}(\delta\Gamma byi - \delta\Gamma bxi)$	
V term error	δVxi	$Vi^{+} = \frac{\sqrt{2}}{2}(\delta Vxi + \delta Vyi)$	
	δVyi	$Vi^{-} = \frac{\sqrt{2}}{2}(\delta Vyi - \delta Vxi)$	

Fig 20_2 MO2 MODELIZATION

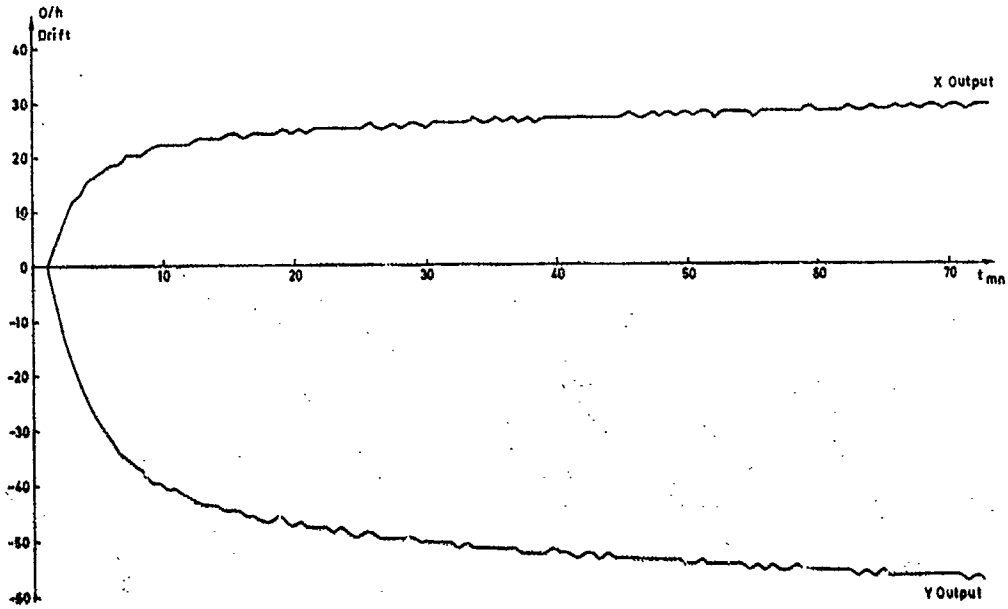

Fig 21 - MOI (6.X0) - WARM UP

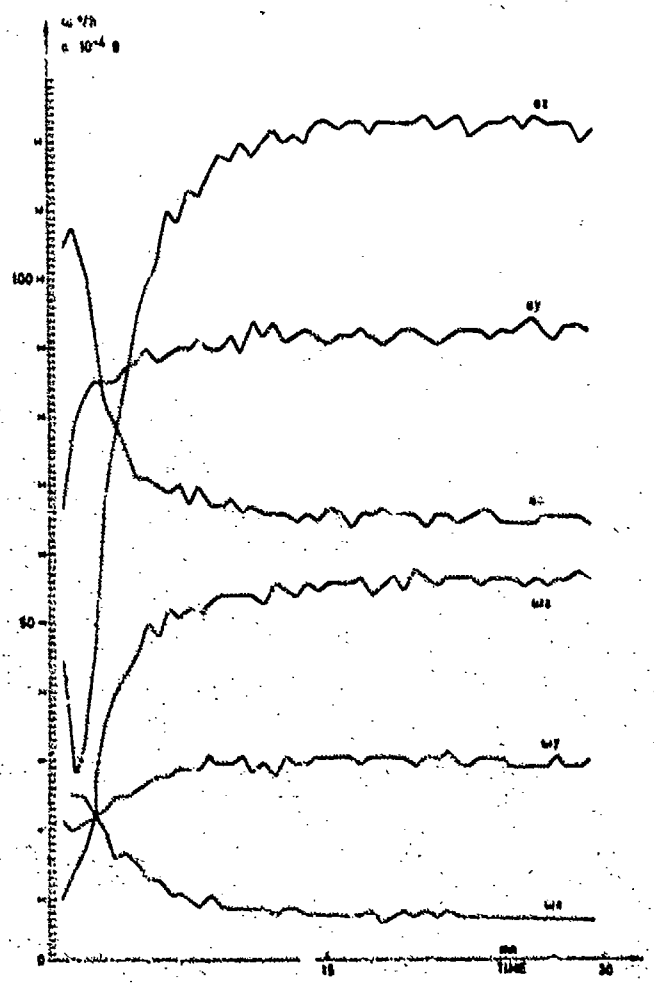

Fig 22 - MOI (IMU) - IMU OUTPUT WARM UP

MODEL

DXO		BXX BXY BXZ		EXX EXY ***	
DYO	(o/hr)	BYX BYY BYZ	(o/hr/g)	0 EYY EYZ	(o/hr/g^2)
DZO		BZX -BYZ BYY		0 EYZ-EYY	

ESTIMATED VALUES

-11.3		17.2 18.9 5.2		-2.9 1.2 *******	
-46.6		2.2 .8 -1.9		.0 .7 -1.9	
33.7		-9.0 1.9 .8		.0 -1.9 -.7	

UNCERTAINTIES

1.01		1.46 1.46 1.60		3.58 3.58 *******	
.80		1.46 .96 .96		.00 3.58 3.58	
.80		1.46 .96 .96		.00 3.58 3.58	

SIGMA = .292•001 ***: non estimated parameter

MODEL: ANGULAR RATES

MODEL

AXO		MXX MXY MXZ		NXX NXY NXZ	
AYO		MYX MYY MYZ		2NXY NYY NYZ	
AZO		MZX MZY MZZ		2NXZ -NYZ ***	

ESTIMATED VALUES

-13.6		47.1 9.8 7.0		-1.5 -6.3 -2.6	
48.8		40.1 44.3 -5.6		-12.6 2.4 1.0	
24.3		-.5 36.4 -5.7		-5.3 -1.0 *******	

UNCERTAINTIES

.91		1.12 1.31 1.44		3.22 1.44 1.61	
.91		1.31 1.27 1.44		2.88 3.22 3.22	
.91		1.31 1.31 1.44		3.22 -3.22 *******	

SIGMA = .263•001

MODEL: ACCELERATIONS

Fig. 23 - M02 (IMU) - MODELIZATION RESULTS

$\omega X = 0$ $\omega Y = \pm \omega Y0$	$KX_0 = \frac{2\omega Y0}{IX(\omega Y0) - IX(-\omega Y0)}$
$\omega X = \pm \omega X0$ $\omega Y = 0$	$KY0 = \frac{-2\omega X0}{IY(\omega X0) - IY(-\omega X0)}$
$\omega X = 0$ $\omega Y = \pm \omega Yi$	$\omega_{Xi} = \frac{2\omega Yi}{KX0\ [IX(\omega Yi) - IX(-\omega Yi)]} - 1$
	$\nu_{Xi} = -\frac{IX(\omega Yi) + IX(-\omega Yi) - [IX(\omega Y0) + IX(-\omega Y0)]}{IX(\omega Yi) - IX(-\omega Yi)}$
$\omega Z = \pm \omega Xi$ $\omega Y = 0$	$\omega_{Yi} = \frac{-2\omega Xi}{KY0\ [IY(\omega Xi) - IY(-\omega Xi)]} - 1$
	$\nu_{Yi} = \frac{-[IY(\omega Xi) + IY(-\omega Xi)] - [IY(\omega X0) + IY(-\omega X0)]}{IY(\omega Xi) - IY(-\omega Xi)}$

Fig.24 - M02 (IMU) . SCALE FACTOR MEASUREMENTS PROCESS

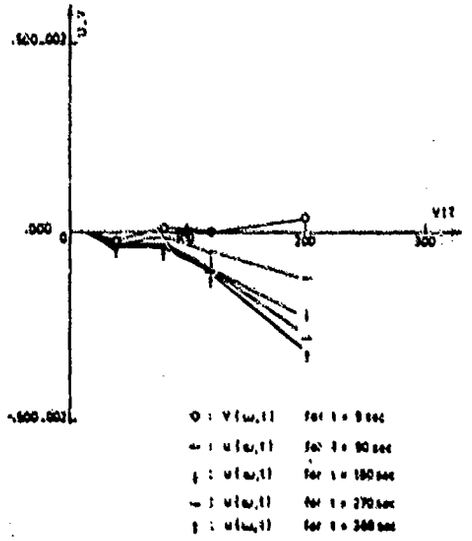

Fig 25. M01 (GYRO) SCALE FACTOR ERROR RESULTS

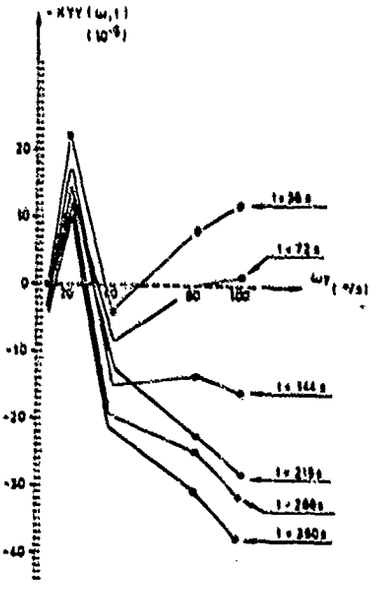

Fig 26. M02 (IMU) SCALE FACTOR ERROR RESULTS

MODULAR STRAPDOWN GUIDANCE UNIT WITH EMBEDDED MICROPROCESSORS

Jerold P. Gilmore
Division Leader, Inertial Subsystem Division
The Charles Stark Draper Laboratory, Inc.
555 Technology Square
Cambridge, Massachusetts 02139

SUMMARY

The Low-Cost Inertial Guidance System (LCIGS) is a modular strapdown design implementation of attitude (gyro) and velocity (accelerometer) axes which permits the interchangeable use of different manufacturer's instruments without affecting the system's electronic or mechanical interfaces or processing software. This design flexibility is made possible by the use of microprocessors for processing and control. The microprocessors are embedded in each module and five are used: one per accelerometer triad, one each per gyro module, and one in the service module. The processors effect on-line digital torque control of the gyros, active instrument error model compensation, including modeling for temperature sensitivity effects, temperature control, self-testing, etc. Adaptation of processing and calibration algorithms to accommodate for instrument changes or sensed environmental variations is achieved through the use of an alterable read-only data base that may be updated by the LCIGS support equipment as required at calibrations or upon an instrument replacement. This data base is accessed by the microprocessors and used to compute coefficient corrections for the processing algorithms. This paper describes the LCIGS modular system architecture, its functions and the corresponding microprocessor software partitioning.

INTRODUCTION

This paper describes a strapdown guidance unit which uses embedded microprocessors for instrument control and data processing. It was designed for use in tactical air-to surface standoff missiles, but is also applicable to a broad spectrum of avionics implementations such as synthetic radar motion compensation.

The name chosen for this development was the Low-Cost Inertial Guidance System (LCIGS).[1] This name underscored one of the program's primary objectives, that is, development of a strapdown inertial reference unit that could be competitively produced at a production unit cost (PUC) target goal of $10,000 in FY1976 dollars in quantities of 2000 systems per buy. To address this goal, the design was configured as a modular implementation of sensing axes, attitude (gyro), and velocity (accelerometers). The axes were configured about mature available single-degree-of-freedom (SDF) instruments. Each sensing axis design is such that different SDF manufacturer's instruments, of the same generic class, could be interchangeably used without affecting the electronic or mechanical interface or processing structure. Thus, if a vendor's proprietary instrument meets a basic normalized specification, it can be interchangeably used in the system by all LCIGS manufacturers.

The modularity is extended within each sensing axis so that the electronics is also functionally partitioned into replaceable electronic modules with corresponding interface specifications. This partitioning was defined to permit graceful modernization and technology growth through the phase-in of new components or modules that meet the common interface design requirements. Thus, performance or reliability improvements, via instrument or electronics changes, can be readily incorporated. Similarly, obsolescent part problems can be circumvented by module upgrades that retain the interfaces. The standardized modular interchangeability feature minimizes system life cycle costs (LCC). This design flexibility is in large measure made possible by the use of microprocessors, embedded within the modules, for data processing and control.

The LCIGS system described was developed by The Charles Stark Draper Laboratory (CSDL) during the period of 1976-1980. Subsequently, the Air Force, as a result of an industry competition, arranged with Lear Siegler, Inc. to validate the CSDL baseline concept and deliver five systems for laboratory and flight testing which has been conducted up to the present time period.[2] Both aircraft and cruise missile implementations have been demonstrated. Furthermore, an LCIGS version using 2 two-degree-of-freedom gyros has also been flight tested and integrated with a low-cost Global Positioning System (GPS) received by the Air Force Armament Laboratory. Although certain design changes have evolved during the 1983-1984 time period, the fundamental embedded microprocessor concept has remained unchanged and is the subject of this Lecture.

A block diagram of the system is shown in Figure 1. Five microprocessors are used: one each per gyro module, one per accelerometer triad (velocity reference module), and one in the service module. The respective microprocessors perform instrument control and error compensation, data processing, and formatting functions. Adaptation of the control and compensation algorithms to the specific instruments is achieved by using coefficient variables that are stored in the service module

processor's data base, an electrically alterable read-only memory (EAROM). The EAROM is loaded using the test support equipment (PSE) and may be altered as required at system calibrations or when instruments are replaced. (Subsequent sections describe the processor architecture and software processing features.)

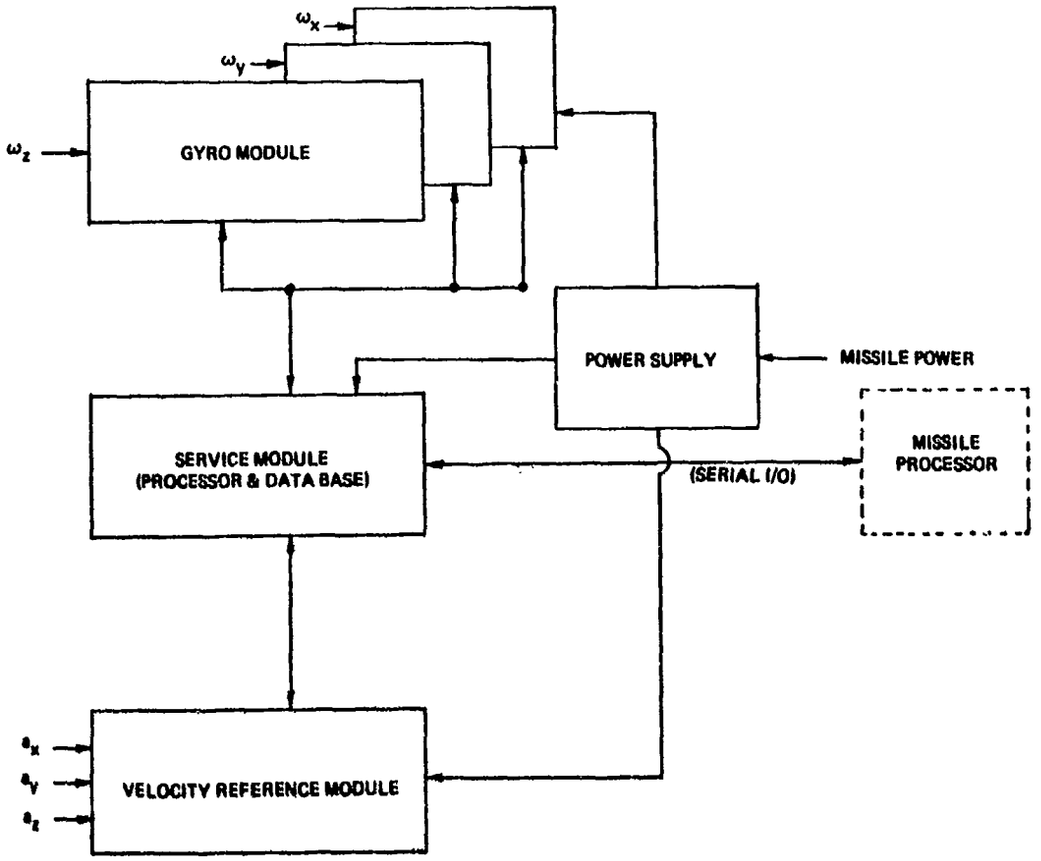

Figure 1. LCIGS block diagram.

LCC and rapid operational deployment goals were major design drivers; a 10-yr inventory life with extended storage periods was specified. Thus, testing requirements were minimized and concepts that permit rapid checkout and calibration were developed. A 30-minute calibration capability was realized. The calibration and checkout technique accommodates large initial bias errors while permitting relatively loose tolerances on test fixturization. The PSE, which includes a minicomputer, effects the calibration processing and also commands the embedded microprocessors to perform self-test diagnostics automatically. The cost of ownership estimate for the 10-yr inventory life based on a once per year retest and an abbreviated readiness functional test before installation corresponded to 10% of the PUC.

DESIGN FEATURES

In the CSDL baseline design, the LCIGS configuration was scoped to be compatible with use in the guidance adapter section of the USAF modular glide bomb/GBU-15 configuration. Angular rate and acceleration dynamic range design requirements of ±150 deg/s and ±10 g, primarily for the preservation of the in-flight alignment while attached to the launch aircraft (i.e., across aircraft evasionary maneuvers), were defined. Data requirements, $\Delta\theta$ and ΔV of ~3 arcsec and 0.03 ft/s per pulse, respectively, with an interface iteration rate of 100/s were selected to be compatible with Global Positioning System, or radiometric correlator aided navigation and autopilot operations. A serial interface with a two-way communication capability was provided.

The GBU-15 physical space envelope limitations necessitated the L-shaped brassboard LCIGS assembly shown in Figure 2. The frame utilizes a low-cost aluminum casting, which requires a minimum of final machining.

The electronic cards are printed circuit assemblies that incorporate integral heat sinks. The instruments are mounted in normalization assemblies. Consistent with the previously stated program intent, as many as four gyros (Timex IG10, Honeywell GG1111, etc.) and two accelerometers (Sundstrand QA 1200 and Systron 4851) were candidates that could be used interchangeably in this system. The brassboard system weight was 23.25 lb.; the volume was 450 in^3. An additional 56 in^3 were required for the cooling fins and blower provisions. The March 1978 PUC estimate for this assembly corresponded to $10,969 in FY76 dollars.[1]

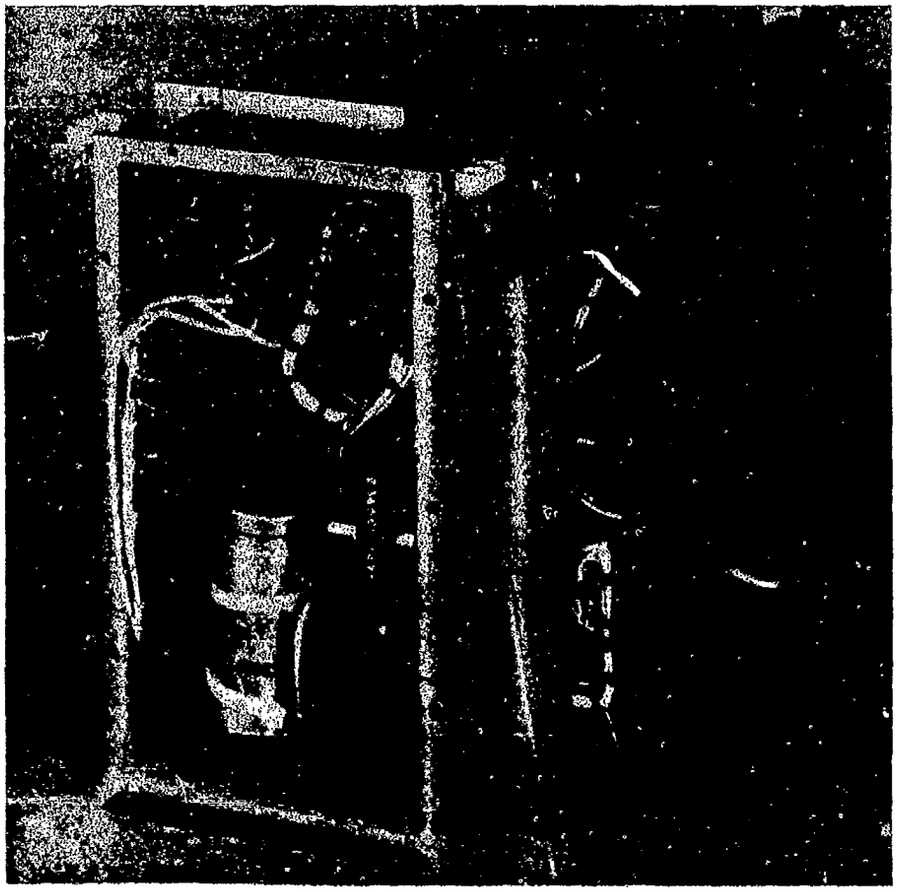

Figure 2. LCIGS system (with covers removed).

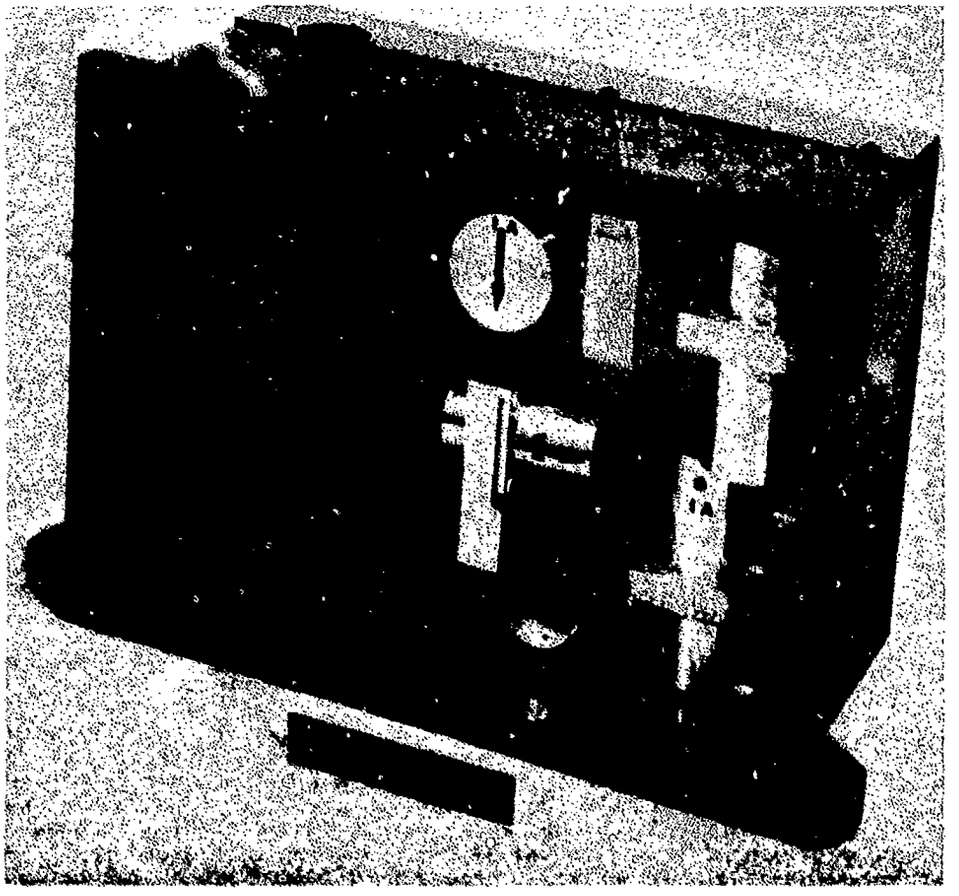

Figure 3. Hybridized model.

An alternate design, based on the use of hybrid electronic packaging, is shown in Figure 3. It preserved all the LCIGS design characteristics and was investigated to provide a sizing basis for this application when space and weight are critical. The corresponding volume and weight are 166 in^3 and 8.7 lb., respectively. If cooling provisions are also needed, an additional 36 in^3 and 1.1 lb. would be required. The corresponding PUC for the hybridized version was estimated at $17,000 in FY76 dollars.

SYSTEM ARCHITECTURE

The detailed system mechanization diagram shown in Figure 4 depicts the LCIGS distributed processing architecture. A microprocessor operates through interfacing conversion electronics with the instrument, in the respective velocity reference module (VRM) and the gyro modules (GM's), and communicates with the system service processor (SP) under its executive control. In the VRM the translational motion sensed by the accelerometers, whose outputs are analog voltages proportional to specific force, is digitized by voltage-to-frequency converters (V/F's). The resultant digitized incremental velocity data (ΔV) is collected, accumulated, compensated for errors (e.g., bias and scale factor), and formatted by the VRM Processor.

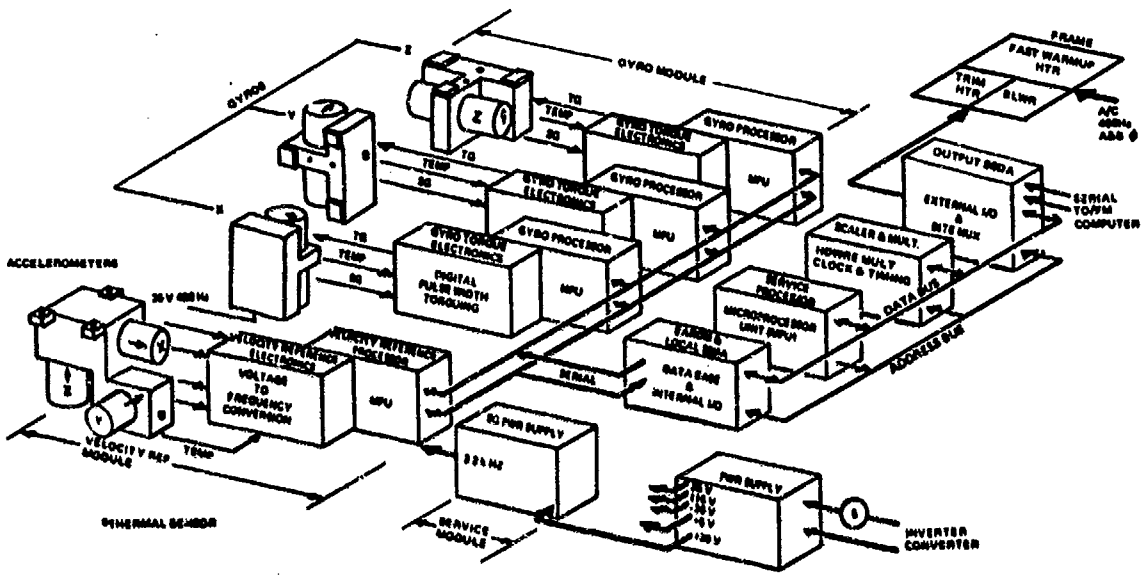

Figure 4. System mechanization.

In the GM, the processor operates in conjunction with the gyro torquing electronics (GTE) to effect closed-loop digital pulse torquing of the gyro. In each control cycle the processing algorithm operates on the basis of the digitized gyro signal generator's output and commands the torquing electronics to issue a net variable current pulse width to the gyro torque generator. (The torque current can be applied in either a ternary or binary mode sequence dependent on the selected microcomputer mode command to the GTE.) The resultant torque commands correspond to an integer number of angular rotational measurement increments (Δθ). The Δθ data across data transmission updates is accumulated in the processor, where it is compensated for scale factor (SF) and bias errors and formatted for transmission to the SP.

The processed Δθ and ΔV data is synchronously transmitted across a two-way serial internal bus structure to the SP where the data is collected and formatted. Data transmission is under SP polling and gating control.

The SP communicates with the instrument processors to initialize and synchronize the system upon turn-ons or system resets. It also provides updates of the SF and bias coefficients that are used in the instrument processor compensation routines. These updates are determined by the SP by accessing the thermal sensitivity data stored in its alterable data base (EAROM) and computing coefficient corrections based on the sensed instrument temperatures. The EAROM also contains variable data, which permits the interchangeable use of different instruments.

The SP communicates with the missile system processor across a two-way serial data interface (500 KHz bit rate). The output I/O structure is shown in Figure 5. A variable length block transfer protocol is used in which "Flag" (a pulse) and "LCIGS Sending" (LCBLOK, a level) signals the missile processor (MP) that the LCIGS output must have priority servicing. The missile processor must respond after each "Flag" by clocking out two LCIGS bytes plus parity with a CTS signal from the transmitter section of the external output I/O serial synchronous data adapter (SSDA) device in the SP module. Block transmissions from the MP are sent to LCIGS by sending "Request to Send" and the "Sending Data Block" levels to the SP module peripheral interface adapter device, used for external I/O handshaking. After each LCIGS "Flag", two bytes may be clocked into LCIGS when accompanied by the Data Carrier Detect (DCD) signal to the SSDA receiver.

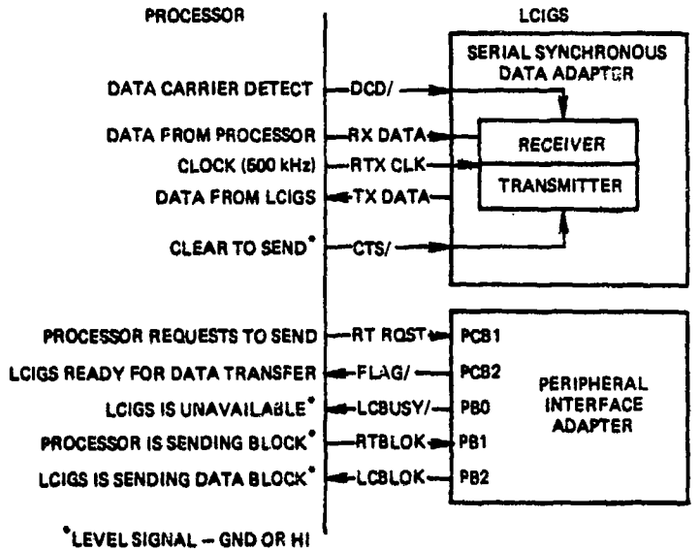

Figure 5. LCIGS/missile I/O.

Output transmissions from LCIGS include the preprocessed and formatted sensor data, $\Delta\theta_{x,y,z}$ and $\Delta V_{x,y,z}$ and other specific LCIGS parameters (e.g., gyro g-sensitive drifts and/or output axis coupling, anisoinertia coefficients, etc.) as required. Status information, such as LCIGS "Ready" or that a reset has occurred, is also sent when applicable. Missile processor messages may request specific LCIGS data (e.g., memory status) and it can initiate a reset. The PSE also functions through this I/O, augmented by additional functions, to alter the EAROM loads and effect diagnostic test, etc.

A summary of the various processing tasks that are allocated to each of the different embedded microprocessors is shown in Figure 6. When compared to a traditional customized digital logic design, this processing implementation provided the flexibility for enhanced automated system testing and eliminated the need for special-purpose built-in test monitors and equipment (BITE). The microprocessor costs are competitive with traditional designs, and their high volume industrial usage is assured.[3] High-volume cost reduction trends are already yielding PUC reductions.

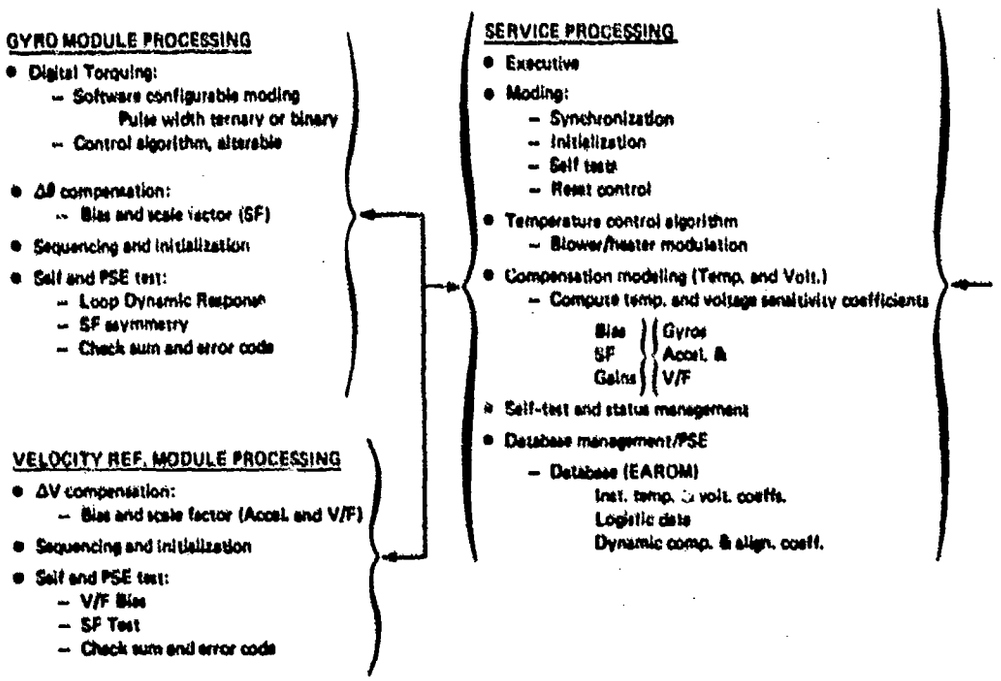

Figure 6. Microprocessor tasks.

PROCESSOR STRUCTURE

All of the processors were configured with the family of Motorola M6800 microcomputer components. High-volume industrial usage, second source availability, and military environmental qualification considerations were major factors in the selection of the M6800 family.[4] Additionally, its system-oriented architectural features were compatible with the hardware interfacing inferred in the mechanization shown in Figure 4 and the software tasks structure of Figure 6.

Although not unique to the M6800 family, the interface functions provided by the peripheral interface adapter (PIA) and the serial synchronous data adapter (SSDA) components facilitated the LCIGS I/O architectural design. These peripherals simply correspond to memory locations on the MPU address and data bus; they are programmable from the bus and their real-time status is accessed through the bus. These provisions simplified interfacing and eliminated the need for I/O instructions. Another highly desirable feature is that the 6800 family buffers are compatible with standard TTL load driving and only a +5V power supply was required.

Figure 7 depicts the processor organization used in the instrument modules. The specific interfacing shown is used in the GM. The VRM processor is identical; interfacing differences are effected by the individual software utilization choices and system interconnection provisions.

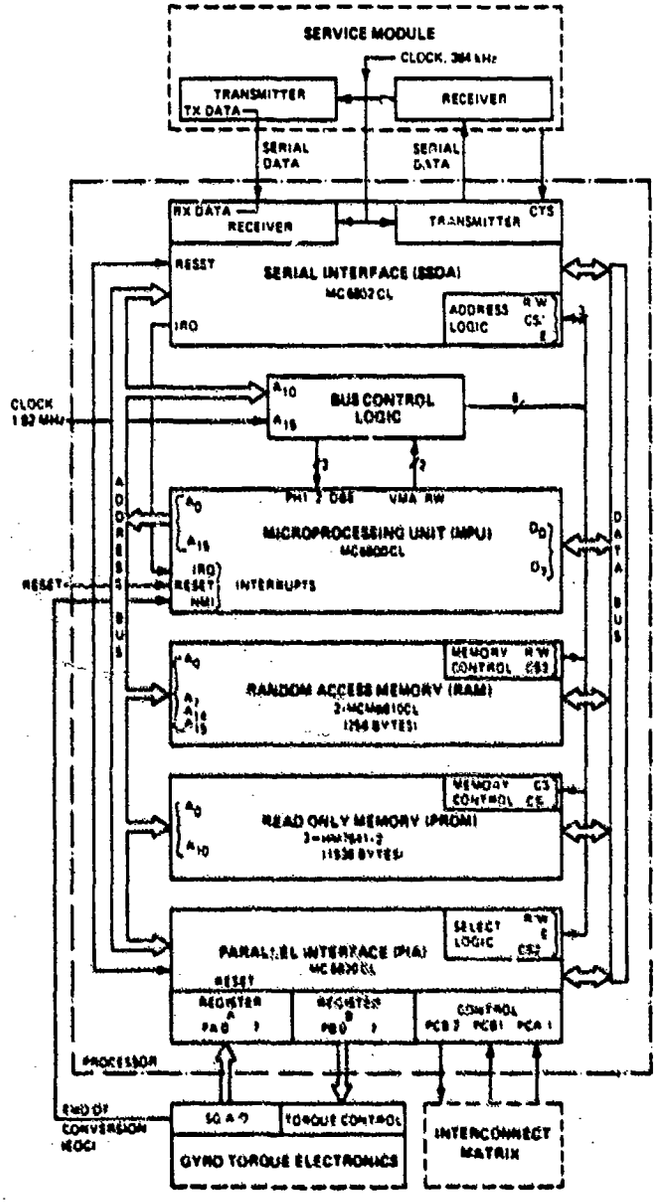

Figure 7. Processor organization.

The MPU, a M6800CL, functions as a bidirectional bus-oriented general purpose processor. Eight-bit parallel processing is implemented and a 16-bit address bus is available (65K bytes of addressing). The processor is capable of directly interfacing with eight peripheral devices and one TTL load to the bus at a 1 MHz cycle clock rate. As shown, seven peripherals (including 2 RAM and 3 PROM components) are used in the instrument processor. The SP bus is buffered since 12 peripheral devices are interfaced with its bus. The MPU contains: an arithmetic logic unit (ALU), two 8-bit accumulato. a 16-bit index register, a 2-byte stack pointer, and a 16-bit program counter.

The minimum execution time for this 1 MHz processor configuration is 2 μs. The instruction set (72) provides a variable length capability that aids in optimizing memory and processing time utilization. Three interrupts are available: reset, nonmaskable (NMI), and peripheral interrupt request (IRQ). The reset, which is software vectored, is used for LCIGS initialization at power turn-ons, or if unacceptable system power excitation conditions occur, or when commanded by the higher-level missile processor. The NMI interrupt is used in the different processors as a basic internal program cycle initiator. It also serves to provide a basis for synchronization of all the processors in the system. The IRQ functions as the input message processing interrupt (SSDA receiver).

Programmable read-only fusible link memory is used. These memory elements are programmed, as applicable, to contain the dedicated routines required for the different VRM and GM functions. The RAM is used for processing task variables. The special-purpose bus control logic shown was added primarily to enable the peripheral expansion capabilities that were required for the service processor configuration. The SSDA provides for serial synchronous communications between the instrument processor and the service module. It permits simultaneous transmission and reception with 3 bytes of FIFO buffering in each direction and includes automatic generation and detection of parity. The PIA provides parallel interfacing capabilities and two 8-bit bidirectional channels in which each bit may be independently configured as either an input or an output. In the GM, the two channels are dedicated to an input (GTE SG A/D data transfers) and an output (GTE torque control commands), respectively. In the VRM, the channels are mixed and 12 bits are allocated for reaching the ΔV accumulators, while the other lines are used for accumulator control.

The service processor configuration Figure 8 corresponds to an expansion of Figure 7 by the addition of several peripheral devices. The RAM and PROM are increased, and an EAROM is added. Two SSDA's are required - one for internal and the other for the external data communications shown in Figure 5. Two PIA's are used. One provides control functions for the EAROM and the polling and gating control of each of the GM and VRM SSDA's. The second PIA is used for data transfer and control of an A/D multiplexer in the service module (temperature monitoring), and provides the external communication control function shown in Figure 5.

It is of interest to note that the modular partitioning concept advantages noted in the introduction section permitted the phase in, during the industrial LCIGS development[2], of the more powerful INTEL 8088 microprocessor (a 16-bit internal architecture with an 8-bit bus structure, same as M6800). This design modification permitted technology growth while preserving the embedded processing architecture.

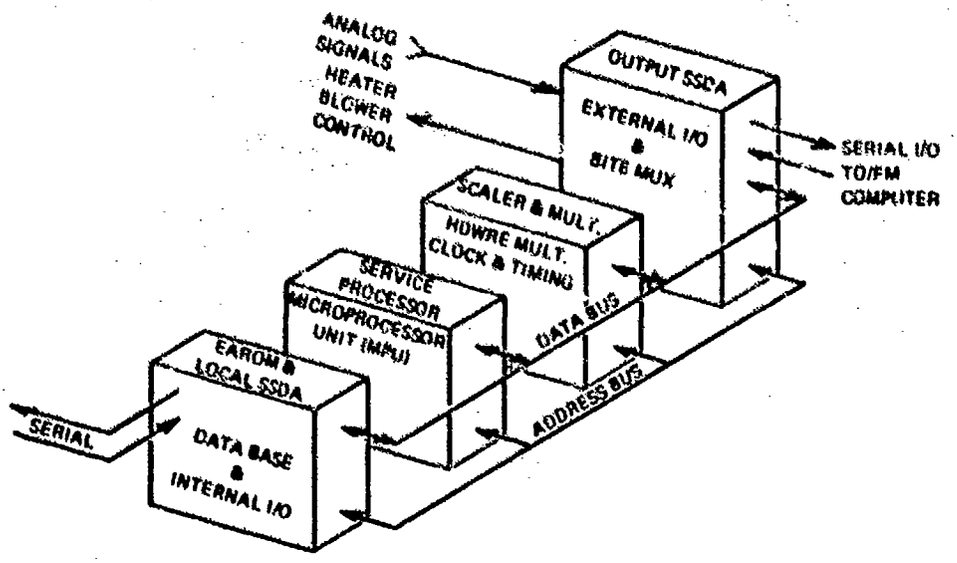

Figure 8. Block diagram of Service Processor configuration.

GYROSCOPE MODULE (GM)

The gyro, installed in an aluminum mounting block, is interconnected to the torque electronics (GTE) card, which interconnects via the system "motherboard" to the instrument processor. The gyro input axis is approximately perpendicular to the plane defined by the pads on the mounting block. These pads mate with surfaces on the LCIGs frame assembly. Three different sets of mating surfaces on the frame define an orthogonal angular rate-sensing triad. A temperature sensor is mounted on the block to provide the temperature measurements used by the temperature compensation processing algorithms. Block mounted electronics also provide an instrument normalization function (i.e., torquer and motor tuning, etc.) so that different instruments once normalized are configured to provide identical loading and signal interfacing with the GTE card.

The GTE, Figure 9, interfaces with the gyro signal and torque generator. It amplifies, filters and digitizes the gyro signal generator (SG) output signal (peak sampling at 3.2 kHz) with an A/D. The A/D output is read by the instrument processor via PIA data register A. The processor computes a torque control command in each sampling cycle which is transmitted via PIA register B to the GTE.

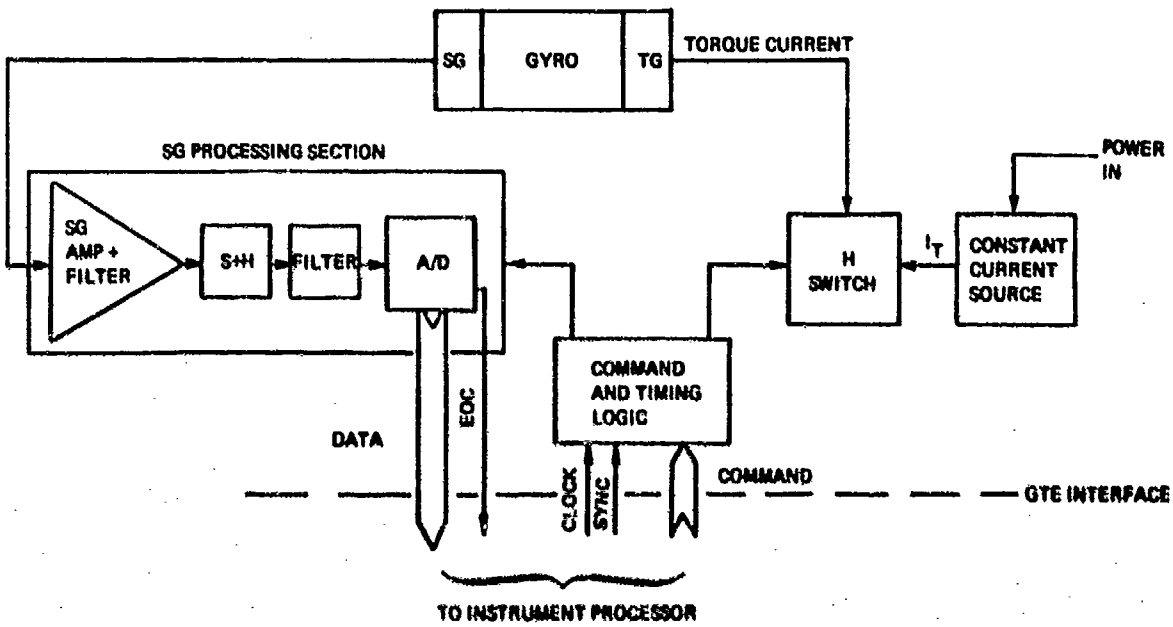

Figure 9. GTE block diagram.

The GTE, in response to the torque command, applies a precise amplitude-controlled current to the gyro permanent magnet torque generator. The decoding logic configures the GTE in ternary (PWT) or binary (PWB) torquing operation and meters the current pulse width and polarity to the gyro torquer in accordance with the processor's moding and $\Delta\theta$ data command. The maximum pulse width in each cycle correspond to approximately 312 μs with an equivalent width resolution of 60 to 1.

The different moding options were provided so that different instruments could be controlled in a manner best suited to their specific design sensitivities. For example, PWB control maintains constant power on the gyro torquer, and scale factor asymmetry (ASF) yields and equivalent bias. However, ASF instability could result in large bias instabilities. PWT avoids the ASF instability problem, but applies variable power, dependent upon the sensed angular rate. The mode that is used by a processor is based on the data stored in the EAROM.

The gyro processor performs the control-loop algorithm and compensates the accumulated $\Delta\theta$ torque count for bias and scale factor errors, including thermal variations, and formats the corrected data for transmission. The compensation processing is similar to the VRM described in the next section, except that independent gyro and electronics modeling is not required since closed-loop operation is used in the GM. The coefficient used in compensation processing are altered in the processor by updates from the service processor (SP). The updates are determined by the SP from stored EAROM data sensitivity coefficients and sensed instrument and electronics temperatures.

The processor functionally implemented a control algorithm of the form

$$T = K_1\theta + K_2\dot{\theta} + K_3\int\theta dt \qquad (1)$$

where T is the torque command to the GTE and corresponds to the SG-sensed gyro motion, and K_1, K_2, and K_3 correspond to proportional, rate, and integral gain coefficients.

respectively. The rate term is used to compensate for the lags associated with the gyro time constants and computational delays of the digital processing. The integrating function was implemented to minimize gyro gimbal offsets with rate inputs, which reduces errors due to cross-axis coupling, etc.

In practice the processor is not called upon to perform the rate function by direct rate taking, derivation of θ, as this would result in a very noisy process or require significant processing complexity. The rate compensation function is implemented in the processor using a feedback approach, wherein the command signal is feedback through an equivalent first-order lag filter implemented in the processor. In an idealized representation, the processor implements the signal flow depicted in Figure 10. The value K_f is given by:

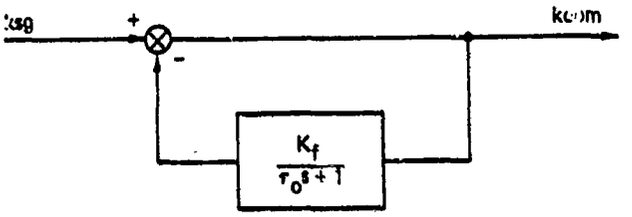

Figure 10. Feedback processing implementation.

$$K_f = \left(\frac{Q_T}{Q_{AD}}\right)\left(\frac{\tau_o}{\Delta t}\right)K_s \qquad (2)$$

where

Q_T = torque pulse quantization, arcsec input-axis angle/pulse
Q_{AD} = A/D quantization, arcsec input axis angle/quanta
τ_o = gyro float time constant, seconds
Δt = interval between samples, seconds (0.0003125 s in LCIGS)

The factor K_s is a "software gain" which scales the number of torque pulses generated per sample cycle to achieve a compromise between speed of response of the T/B loop and required stability margin.

To avoid extraneous pulsing of the gyro torque when the system is initialized, it was decided to implement an equivalent decay in the integrator processing function, a "leak" time constant, τ_i. Thus, when the gyro float is near null the integrator feed forward command also nulls.

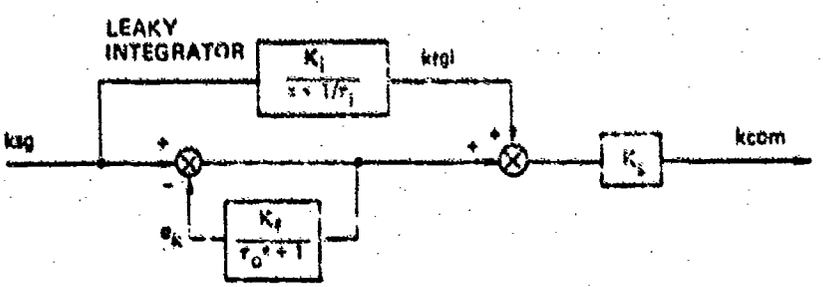

Figure 11. Controller implementation.

Figure 11 depicts the complete processing controller implementation. The sequence of operations performed by the processor corresponding to this analog representation are represented by the following difference equations:

$$\begin{aligned}
e_\phi &= ksg - e_{k(old)} \\
e_k &= e_\phi(C_1) + e_{k(old)}(C_2) \\
ksgi &= ksgi_{(old)} + C_3(ksg) \\
ksgi &= ksgi - K_L(ksgi) \\
kcom &= K_s(e_\phi + ksgi) \\
e_{k(old)} &= e_k \\
ksgi_{(old)} &= ksgi
\end{aligned} \qquad (3)$$

The suffix (old) refers to the value of the quantity of the previous sample period. The following constants are defined, where Δt is the sample period of 0.0003125 second and:

$$C_1 = K_f(1 + \tau_o/\Delta t)$$

$$C_2 = \tau_o \Delta t(1 + \tau_o \Delta t)$$

$$C_3 = K_i \Delta t$$

To simplify processing complexity and timing requirements, the constant multipliers, i.e., C_1, C_2 and C_3 were constrained so that they corresponded to simple combinations of powers of two. Thus, they could be configured by a sequence of add and shift functions which enhanced processing speed.

Because the integrator "leak" was incorporated in the controller, the gyro signal will be slightly offset from null for steady-state input-axis rates. The offset will be proportional to rate, and from breadboard tests it was found that at 150°/second input-axis rate the offset is approximately 44 A/D quanta, or about 350 arcseconds of input-axis angle. The float angle remained within control limits for angular accumulations in excess of 35 radians per second squared.

The design achieved a nominal loop bandwidth of 80 Hz. The step response rise time is approximately 3.75×10^{-3} s, and the overshoot is less than 20%. An average gyrofloat hang-off, 80 arc-sec, exists at an angular acceleration of 5 rad/s^2. Figure 12 is a plot of a GM step response, as obtained from reading the processor A/D register and torque command data at 3.2 kHz. To generate this plot the GM processor was instructed to set the gyro SG control point offset from the normal null condition by 40 A/D bits (240 arcsec) and the control command was then returned to the SG null point. The step response shown corresponds to one of the self-test provisions. Others include SF asymmetry, A/D resolution, processor checksum, and error code testing. These test functions are embodied in the processing software structure.

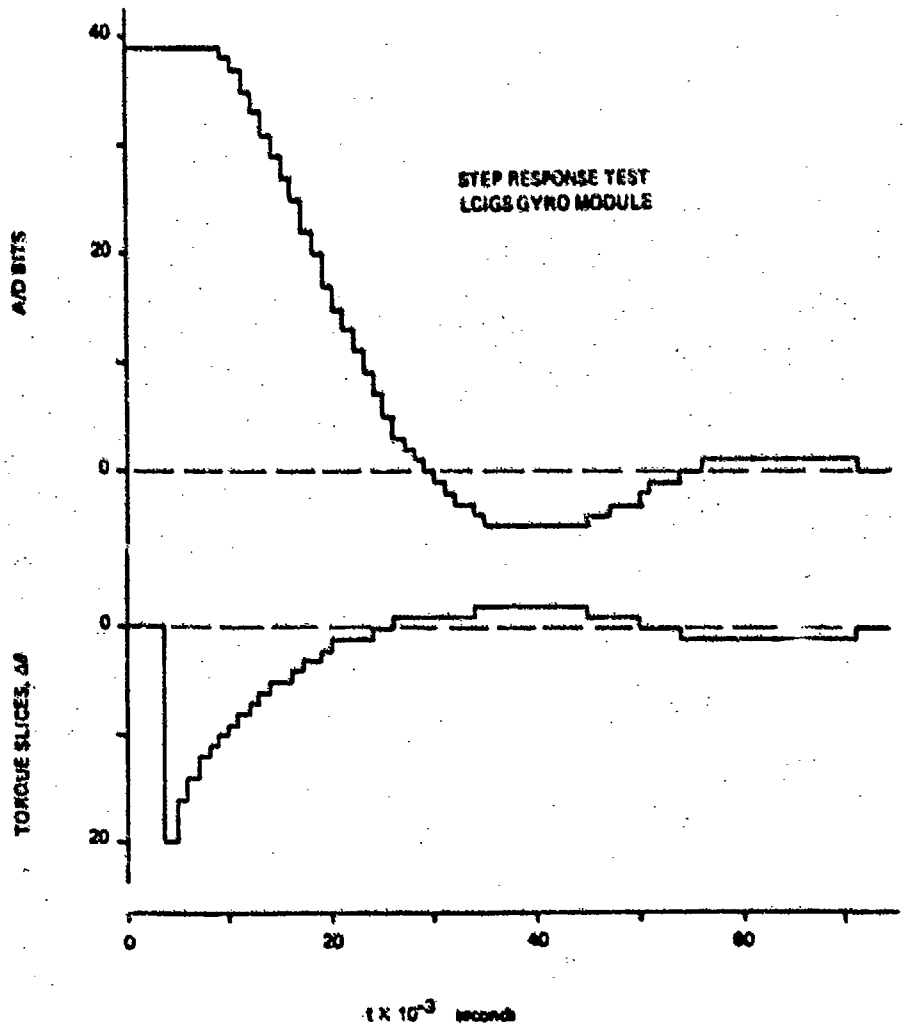

Figure 12. Step response test results.

The use of identical interchangeable microprocessors for the GM requires that they be able to identify their own axis system assignments since communications with the SP is across a "party" line. Similarly, software phasing must be included so that the modules' NMI cycle rate and the SP's data transfer rate can be synchronized. Finally, for transient resets, recovery provisions must assure that the closed loop torquing operations are resumed rapidly. Thus, the gyro processor automatically reverts to a default PWT operating mode until system reinitialization is completed. The GM memory capacity and MPU utilization levels are shown in Table 1.

Table 1. Gyro processor utilization[a].

Memory	Capacity	Utilization
RAM	256	143
ROM	1536	1433

[a]Time available utilized = 85%

The software flow organization implemented in the embedded processor is partitioned so that each function is essentially dedicated to a specific real-time processing task. In a sense the software reverts to a firm-ware allocation in each module and there are no multi-tasked or shared memory functions between module processors. This is consistent with the modularity objective and allows modification of algorithms without a ripple effect.

The instrument module microprocessor program is structured into the three interrupt processing and one background processing routine, as illustrated in Figure 13.

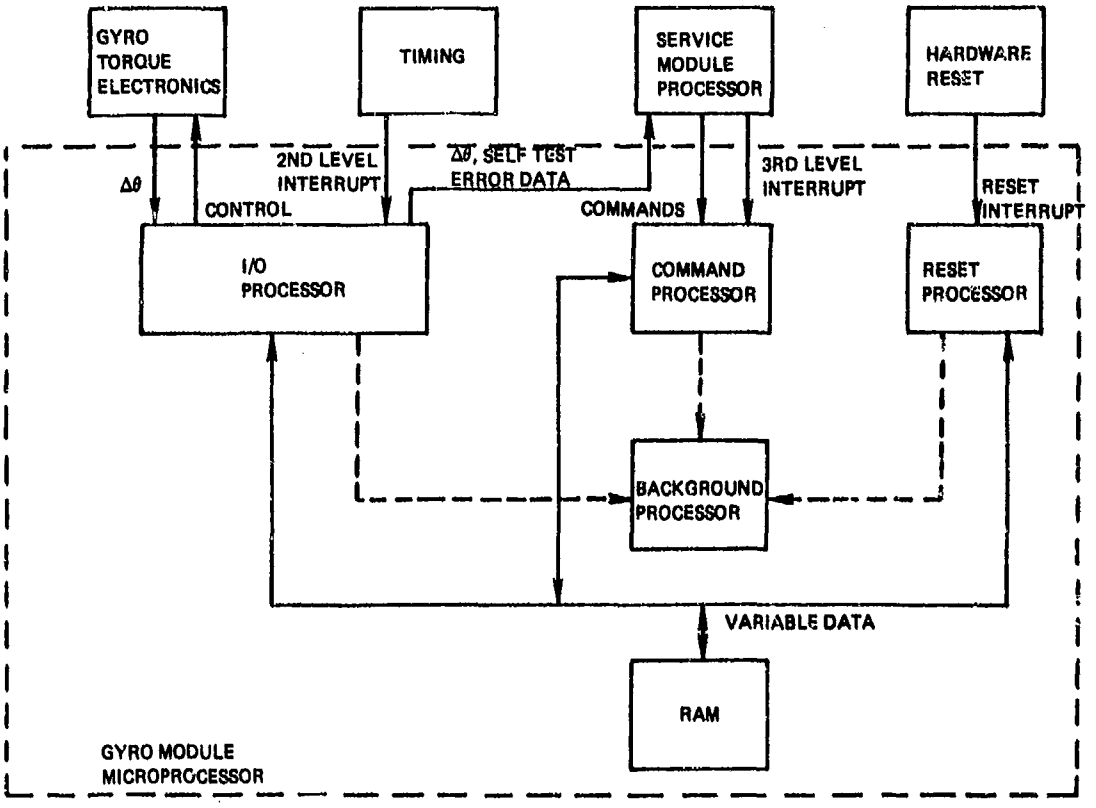

Figure 13. Functional software structure.

In the GM the I/O processing routine is executed upon receipt of the second-level priority interrupt activated by the EOC signal (3200 Hz) from the GTE. The major functions performed are reading and rescaling of the gyro float angle to a signed binary number, computation of the desired gyro torquing command, compensation of accumulated torque pulses ($\Delta\theta$), and transmission of data to the Service Module at the proper rate.

The GTE is configured to operate in either a ternary mode or a binary mode, depending on the mode of operation selected, the required torque command is computed and transmitted to the GTE over the parallel interface. The mode of operation is selected by command transmitted by the service processor to the instrument processor.

These commands function through the GM processor's command processing routine which set the output routine of the I/O processing to various modes, for example: transmission of torque command and A/D readings; or uncompensated torque signals; or gyro ID and memory checksum data; or memory dump data; or internal error counter status data. The various modes permit considerable flexibility in test and diagnostics of each modular function.

The command processor is executed asynchronously upon receipt of the third-level priority interrupt (IRQ) issued by the SSDA on receipt of command data from the SM. Its main function is to interpret and implement the SM commands. The command processor is a low-priority task and may be interrupted by the I/O processor or the Reset processor. Execution of the command processor is delayed pending a I/O processing cycle completion. Commands from the SM are transmitted asynchronously and consist of initialization commands and update commands to set modes, described previously. It also enables input of data variables, i.e., updates of bias, SF, gyro null offset parameters, etc., for use in the I/O processing routines.

The command processing also performs error detection and recovery. Upon receipt of the third-level priority interrupt, the GM/SM interface status is checked to ensure that data is available to be read from the SM. If not, the error counter corresponding to "undefined third-level interrupts" is incremented.

All data received from the SM is checked for parity errors. If a parity error is detected, the error counter corresponding to "serial interface parity errors" is incremented and processing on that command is terminated. Any undefined commands are flagged as errors, and command processing is also terminated.

The reset processing performs RAM initialization and I/O interface setup upon receipt of a hardware reset interrupt which may be generated when power is turned on, when the 5.0 VDC logic excitation drops below an acceptable level (4.45 VDC), and when commanded by the PSE or Missile Computer.

The reset processor has the highest priority and may interrupt any of the other processing tasks.

Initialization performed may be grouped into the following areas:

(1) RAM variables are initially set to zero or their starting value.

(2) The GTE parallel I/O interface is set up to allow input of gyro A/D float angles and output of gyro torque commands at a data rate of 3200 Hz.

(3) The GM/SM serial I/O interface is set up to allow two byte bidirectional transfers between the SM and the GM at a 100 Hz rate.

(4) GM self-identification is accomplished by sending the identification interface. The identification signal is fed back over the parallel interface as two logical bits.

In the instrument modules the background processor operates in the absence of other processor activity and performs the memory self-check (checksum) computation. The self-check corresponds to a summation computation of the ROM ignoring overflow. Its output is a single byte CHKSUM.

VELOCITY REFERENCE MODULE (VRM)

The VRM consists of an accelerometer triad assembly, an electronics assembly, and an instrument processor. Power and timing are provided by the service module.

The accelerometer triad assembly consists of three accelerometers mounted with their axes nominally orthogonal in an aluminum block. A temperature sensor is mounted on the block for use in temperature compensation. The accelerometer is a gas-filled hinged pendulum with an integral analog torque-to-balance loop.

The accelerometer loop output, an analog dc voltage proportional to acceleration, is fed into voltage-to-frequency (V/F) converters in the velocity reference electronics (VRE), scaled to a nominal 0.5 VDC/1000 cm/s^2. The V/F output frequency is proportional to acceleration, and each output frequency pulse corresponds to 1 cm/s.

A bipolar V/F design was configured to achieve the required bias stability. Three V/F converters and their associated data buffers are mounted on the VRE printed circuit card.

The V/F output frequency is defined by

$$f_{out} = (K_{+,-})(V_{out} + V_{0g}) \qquad (4)$$

where the gain, K_{+-}, is dependent on the polarity (a bipolar design characteristic) of the input voltage, $V_{out} + V_{0g}$.

$$V_{out} = K_{1a}(V_{0a} + A_{in}) \qquad (5)$$

where K_{1a} is the accelerometer scale factor, K_{0a} is the accelerometer bias, A_{in} is the sensed acceleration input, and V_{0g} is the offset voltage of the V/F converter. The V/F bias (K_{0VF}) corresponds to

$$K_{0VF} = (K_{+,-})(V_{0g}) \quad (6)$$

The VRM processor accumulates the V/F count in the VRE buffer every 625 μs and compensates this data for bias and scale factor errors. Since the V/F functions as an open-loop digitizer, the processor compensation routines must correct for the V/F bias (V_{0g}) and its plus and minus scale factors, as well as the accelerometer bias and scale factor. All of these terms are temperature sensitive, and the thermal modeling must also include them.

The velocity reference processor computes a corrected velocity, ΔV_{comp}, of the form

$$\Delta V_{comp} = [(1 + \Delta SF_c)\Delta V_r] + B_c\Delta t \quad (7)$$

where ΔV_r is the raw accumulated V/F output velocity change data in an update interval, B_c is the bias correction in velocity during the update interval, ΔSF_c is the scale factor correction, and Δt is the time between updates. The memory capacity and current MPU utilization levels are shown in Table 2. The processing architecture apart from the real-time control function is identical to that of the GM.

Table 2. VRM processor utilization[a].

Memory	Capacity	Utilization
RAM	256	188
ROM	1536	1328

[a]Time available utilized = 58%

SERVICE MODULE PROCESSOR (SP)

A major function of the SP is to effect the thermal compensation modeling. For example, the B_c and SF coefficients in Equation (7) are computed by the SP using the parameters stored in its EAROM and the sensed temperature data that is multiplexed and digitized in the service module. The computations are achieved using the hardware multiply provisions in the service module and are of the form

$$B_c = [K_{0a} + K_{0VF}]$$

$$\Delta SF_c = 1/(1 + \Delta K_1) - 1 \quad (9)$$

where

$$\Delta K_1 = [(1 + \Delta K_{1a})(1 + \Delta \pm K_{1VF})] - 1$$

and $\pm K_{1VF}$ represents the plus and minus V/F scale factors.

The coefficients K_0 and K_1, are corrected for temperature sensitivity using a two-slope characterization, if required. The processor determines the individual K_0 and K_1 terms for the accelerometer and using processing structure of the form

$$K(\ ) = K(\ ) + (K(\ )/\Delta T)(T - T_N) \quad (10)$$

K is the coefficient corresponding to the nominal operating system temperature and $(K(\ )/\Delta T)$ corresponds to the applicable slope segment thermal sensitivity. The B_c and SF_c coefficients are then determined using Equations (8) and (9). The SP computes new correction coefficients for all of the modules, and updates all of the modules once every 20s. These computations also include modeling to account for thermal transients, the thermal lag between sensor readings, and the instrument responses to environment temperature changes.

The bias and scale factor parameters may be determined during module or system level testing. The parameters are loaded into the EAROM via the PSE. The EAROM serves as the data base for the LCIGS system. In addition to instrument parameters, compensation parameters, torque moding (PWT or PWB), control loop gains and dynamic terms (g-sensitive and OA coupling coefficients, etc.), information defining instrument type, serial number, installation date and last test date, etc., may be stored for logistic purposes. Data base management is effected by using the PSE. A magnetic stripe card function is included in the PSE. The stripe card accompanies the LCIGS, and its data duplicates the EAROM load. The card "current data" is used by the PSE to verify the EAROM load. It is updated at each calibration or repair by using the PSE. Card file status may also be compiled for inventory control.

In addition to the compensation processing function, the SP also implements a coarse temperature control function using aircraft power during captive flight. The SP implements a control algorithm using the thermal sensor data and time-modulates the application of power via solid-state relays to either a trim heater or a blower. Since coolant sources are not available and battery power cannot be spared for heating in free fall, thermal modeling is also required. The coarse control provision narrows the thermal variation region which optimizes modeling during captive flight.

In addition to the application tasks just described, the SP performs the major system executive and moding functions decribed in the next section.

The SP memory capacity and current MPU utilization levels are shown in Table 3. The basic elements of the SP were shown in Figure 8.

Table 3. Service processor utilization[a].

Memory	Capacity	Utilization
RAM (8 bit-bytes)	1024	269
ROM (8 bit-bytes)	4096	2361
EAROM (8 bit-bytes)	1024	730

[a]Time available utilized = 70%

SP EXECUTIVE SOFTWARE

The executive is responsible for all I/O procedures and internal task scheduling. As noted previously, the executive functions, in order of priority, correspond to the system rest, nonmaskable interrupt (NMI), and interrupt request processing routine (IRQ).

As noted previously in the instrument processor, the reset routine initializes all variables stored in RAM, and configures I/O devices as required. It leaves the processor in a well-defined default mode that can only be altered by command from the SP. The NMI, common to all processors, provides intrasystem synchronization while the IRQ routine is an input message processor. The SP broadcasts various commands and data to the instrument processor. Some examples of these messages are: send compensated inertial data; send raw inertial data; send self-test data; receive this bias correction; receive this scale factor correction; and perform self-test program. The instrument module IRQ processing routine interprets these messages and configures its executive to perform the requested command.

The SP executive also contains reset, NMI and IRQ programs, and provides for low-priority task schedule control.

The SP reset program must also initialize SP RAM and I/O devices, but it also has the responsibility of insuring that all processors are synchronized correctly. A power-up reset is a special case, where the SP must command all GM processors to torque their associated gyro into a preferred stop.

The most important responsibility of the SP NMI program is that of gathering the inertial data from the four sensor processors and passing this information to the missile processor. The NMI program must also maintain the real-time clocks, index and selected temperature and voltage multiplexed channels, and provide system temperature control.

The IRQ program performs message control functions similar to those described for the instrument processor. The low-priority tasks are initiated either by a message interpreted by the IRQ or from another active low-priority task. The subroutines used to execute task control (Figure 14) are called CMDPRO, ADDJOB, and JOBCTL. The CMDPRO subroutine interprets messages received from IRQ, selects the application task, and adds it to the task queue by using the ADDJOB subroutine. The tasks in the queue are activated in sequence by the JOBCTL program. A listing of the application tasks is also shown in Figure 14. For example, the BITEJB task corresponds to the compensation modeling functions, Equations (8)-(10).

The task "INERT" is initiated on command from the missile processor. The command is interpreted as "Start inertial data processing and transmission." The task performs the transfers of initial compensation coefficients to the instrument processors and the missile processor. The instrument processors are then instructed to transmit compensated inertial data. The final responsibility of INERT is to schedule the BITEJB task.

"PIPELN" transfers, without interpretation, a command message directed to an instrument processor. This feature is primarily used by the PSE during system test. It provides the PSE with flexible control over the instrument modules for test purposes.

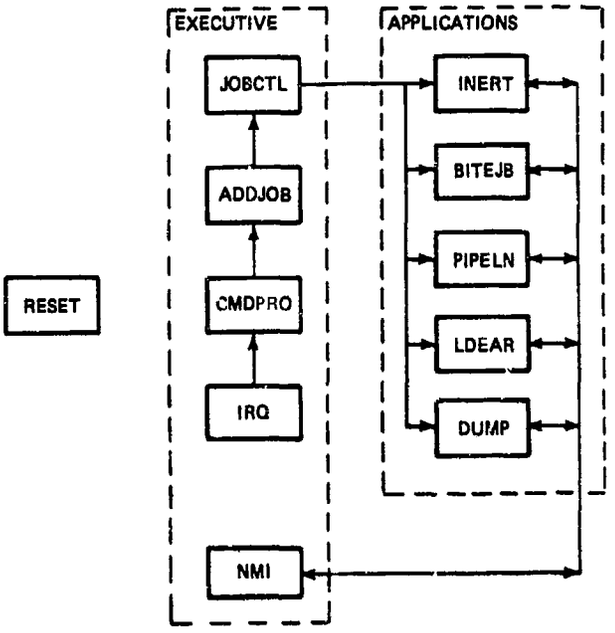

Figure 14. Executive applications.

The electrically alterable read-only memory (EAROM) is updated by the PSE (e.g., after a system calibration). The task "LDEAR" provides the capability of selecting loading blocks of EAROM.

The DUMP task is used by the PSE to selectively interrogate any block of memory, whether it be RAM, ROM, or EAROM. For example, this feature is used with LDEAR to read, update, and restore EAROM after a calibration.

EXPANDED PROCESSING

The expansion of the LCIGS processing capabilities to include cross-axis compensation attitude and velocity algorithms, and navigation functions is feasible. Several alternatives are possible. An additional processor, which is also augmented by a hardware multiply functio' interfaced with the SP output port, can be used to replace the SP, or a more extensive hardware multiply function can be added.

The current SP could be replaced with the M68000, a 16-bit MPU that contains hardware multiply functions, and a control bus that is designed to connect directly to the standard M6800 peripheral chips used in the LCIGS instrument processors.

CONCLUSION

The distributed processing implementation in LCIGS provided a unique level of design and application flexibility. It permitted functional hardware partitioning with instrument interchangeability and enables considerable growth potential. The dedicated processing also allows partitioning of software to manageable subsets of "firmware" that are isolated from mission- or weapon-related changes. Further, the microprocessors have enhanced testing by permitting microscopic checkout capabilities; e.g., the processors perform their own test control and data acquisition.

Microprocessor implementations do present constraints for the software designer. Because of the microcomputer limitations, the designer must effect tradeoffs between duty cycle and memory utilization. Often table-lookups, in lieu of conventional processing, become a required time-saving measure. Similarly, compromises may be required that replace software multiplication with simple shifting operations in order to optimize operating speed.

Finally, program development software for microprocessors has not yet reached the general-purpose computer maturity level. For example, cross-assemblers with provisions for independent relocatable subroutine generation and linking are not universally available. Thus, independent development of programs is practically impossible and intensive coordination between programmers is required.

REFERENCES

1. Gilmore, J.P., "Low Cost Inertial Guidance System Design Concept and Operating Features," The Charles Stark Draper Laboratory, Inc., Cambridge, Mass., C-5072, March 1978.

2. Stob, W.K. and T.K. Wu, "Industry Low Cost Inertial Guidance System Development," AGARD Conference Proceedings #292, October 1980.

3. "Motorola Wins Microprocessor Contract from GM," Electronics, Vol. 50, No. 2, January 1977, p. 31.

4. "M6800 Microcomputer System Design Data," Motorola, Inc., Phoenix, Arizona, 1976.

ACKNOWLEDGMENTS

The work reported in this paper was sponsored in part by the U.S. Air Force Armament Laboratory of the U.S. Air Force Systems Command under Contract F08635-76-C-0306.

The author gratefully acknowledges the assistance of J. Avery, R. Cooper, D. Dunn, D. Mayhew, R. McKern, H. Musoff, T. Schamp, and K. Vincent.

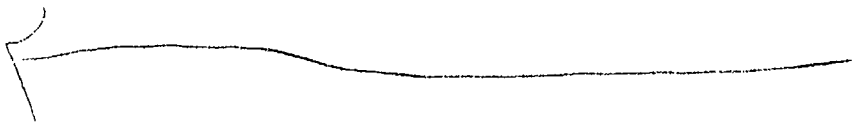

APPLICATION OF MULTIFUNCTION STRAPDOWN INERTIAL SYSTEM

Mr. David L. Sebring, McDonnell Douglas Corporation,
Post Office Box 516, St. Louis, MO 63166

Mr. John M. Perdzock, Air Force Flight
Dynamics Laboratory, AFWAL/FIGL,
Wright-Patterson Air Force Base, OH 45433

Captain John T. Young, Air Force Flight
Dynamics Laboratory, AFWAL/FIGL,
Wright-Patterson Air Force Base, OH 45433

SUMMARY

Reliability, redundancy, and survivability are key issues as integrated requirements for flight control, fire control, propulsion control and navigation are developed. These integrated systems require dependable sources of inertial measurement data. Current inertial sensors, however, are expensive to acquire and maintain, dedicated to specific systems, and are not designed to meet integrated reliability, redundancy, and survivability requirements. The Multifunction Strapdown Inertial System concept uses a minimum number of inertial sensors in a survivable configuration to provide inertial data for flight control, navigation, weapon delivery, cockpit displays, and sensor stabilization. Because of advantages in survivability, life cycle cost, maintainability and performance, the Multifunction Flight Control Reference System (MFCRS) program was initiated to verify, through flight test, on a McDonnell Douglas F-15 Eagle the key issues of redundancy management and flight control. A redundancy management system based on parity equations was designed. The sensors were arranged in two skewed and dispersed clusters. Each cluster was an orthogonal triad of colocated inertial quality ring laser gyros and accelerometers. Six simulation and computer studies were used during the course of the program to develop algorithms and to predict system performance. These studies indicated that a fundamental problem facing the MFCRS concept would be resolution of the conflict between effective compensation of sensor errors and maintenance of the basic F-15 flight control stability and handling qualities. This problem was compounded by the inherent amplification and translation of sensor errors due to the coordinate transformations and moment arm corrections required to develop body axis rates and accelerations using skewed and dispersed sensors. Laboratory testing revealed higher than predicted noise levels. While this noise had little effect on navigation performance special filtering was required for MFCRS to prevent false alarms and high frequency actuator response. This filtering affected the flight control stability and performance, necessitating modification of the flight control design. A key lesson learned is that integration of inertial data for fire control, flight control, navigation and propulsion control will require close coupling and coordination between functional groups to resolve performance conflicts and compromises.

1. BACKGROUND

Improvements currently being developed for advanced fighter/attack aircraft include integration of flight control, fire control, navigation and propulsion control systems. Also, flight control is becoming more sophisticated with advances in trajectory control and automatic terrain following/terrain avoidance techniques. As these advanced developments proceed, formerly mission critical functions are becoming flight critical. The high reliability and redundancy classically associated with flight control must be designed into these integrated systems. Survivability is also a major design factor given the increase of the number and quality of the threat air defense systems.

Inertial data is required for all advanced flight control techniques and is a key component in many of the integrated systems. As shown in Figure 1, most current operational fighters obtain inertial data from a number of different sources such as the Inertial Navigation System (INS), the Attitude Heading and Reference System (AHRS), the Flight Control Gyros and Accelerometers, and the fire control Lead Computing Gyro (LCG). These sensors are dedicated to and optimized for specific functions. Current generation inertial sensors do not, however, meet the reliability and survivability requirements that integrated systems will need. For example, flight control sensors are not considered survivable when the gyros are clustered at a single location near the primary aircraft bending antinode or when the accelerometers are clustered at a node. Mission critical sensors such as the INS or LCG are neither redundant nor survivable. This will become an increasingly important problem as the INS outputs are used to generate inputs to the flight control/flight management system to perform maneuvering attack, automatic terrain following/terrain avoidance, or night, all weather control. For these functions, the inertial sensors are, in essence, part of the flight control/flight management system and should be designed to meet the rigorous flight control safety requirements. Another problem with current inertial sensors is their long reaction time. Gimbaled systems require 4 to 6 minutes for warm-up and alignment. Current inertial systems are also costly to maintain. This is due in part to the fact that they require complex platform electronics to support the electromechanical gimbaled devices. Also, each unique inertial data source requires a dedicated interface which must be maintained through the

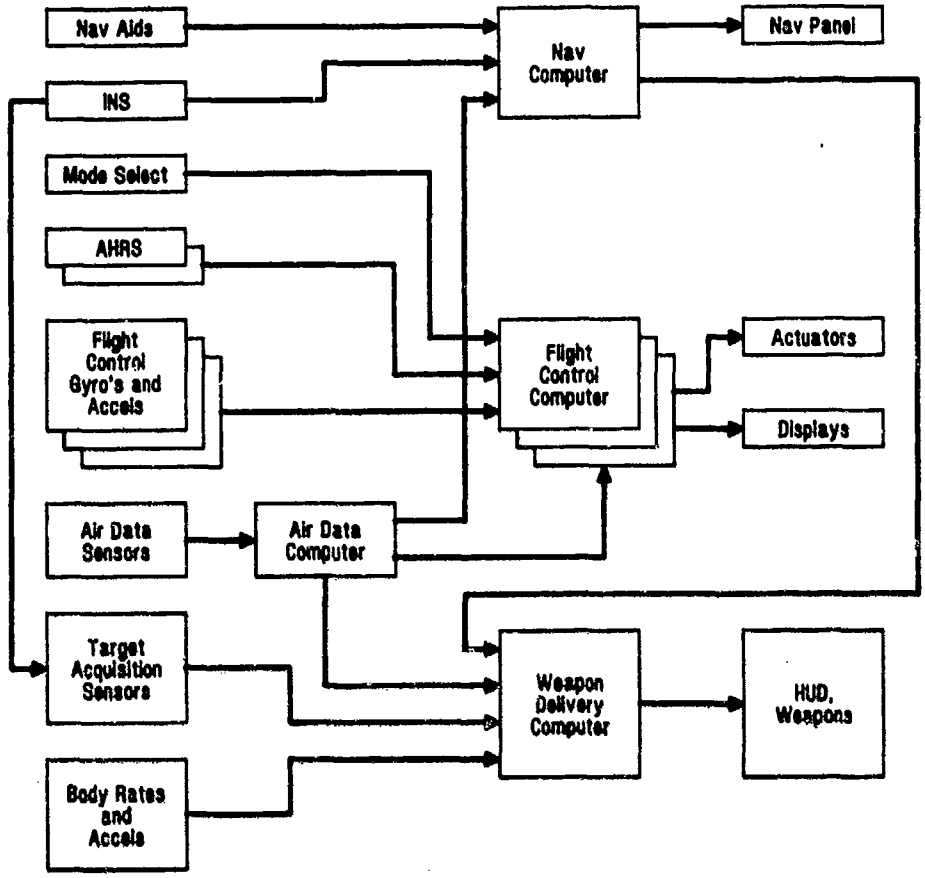

Figure 1. Conventional Approach to Inertial Data Requirements

existence of aircraft intermediate shop support and the training of highly skilled maintenance personnel in each specialty field.

The Multifunction Inertial Reference concept shown in Figure 2 was developed to solve these problems (1,2). This MFCRS concept is an innovative approach that uses a minimum number of inertial sensors in a survivable configuration to satisfy the combined inertial data requirements of flight control, navigation, weapon delivery, cockpit displays, and sensor stabilization. One key element of this concept is the Ring Laser Gyro (RLG). In a strapdown configuration, the RLG has both the accuracy required for navigation and the dynamic bandwidth required for flight control. The strapdown RLG assembly/cluster is also less complex and more rugged than the current four gimbal inertial platform since the RLG is a solid state device. The other key to this concept is the availability of high speed digital microprocessors. Microprocessors allow the wide variety of functions required of the Multifunction System to be calculated in real-time. The processor does fault detection, fault isolation, dynamic reconfiguration, navigation, flight control compensation, and the data management required to interface with other systems.

The Multifunction Strapdown Inertial System concept was initially investigated by the Multifunction Inertial Reference Assembly (MIRA) program (1,2). Jointly sponsored by the Air Force Wright Aeronautical Laboratories Flight Dynamics Laboratory and Avionics Laboratory the MIRA program identified potential benefits and payoffs for a late 1980's production system. First, reliability and mission success probabilities would be increased for all functions. This is due to the fact the system could provide fail-operate, fail-operate flight control data, and fail-operate navigation and weapon delivery data. The MIRA study also estimated a 21% decrease in life cycle cost. This was based on the mean-time between failures increasing from 240 hours to 1,670 hours and the mean-time to repair decreasing from 2.6 hours to 1.4 hours. Weight would also decrease from 120 pounds to 90 pounds and only 2 line replaceable units would be required instead of 7. The RLG has a faster turn on time than the present gimbaled INS and reaction time could be reduced to 1.5 minutes for gyrocompass alignment and to less than 30 seconds for stored heading alignment. MIRA also predicted a 30% improvement in combat survivability when the sensors were dispersed in two clusters. These benefits and payoffs are summarized in Figure 3.

These increases in reliability, survivability and redundancy afford the opportunity to eliminate aircraft intermediate shop (AIS) maintenance support for inertial systems. They are also required to support the operational readiness of advanced weapon system functions such as integrated flight/fire control, terrain following/terrain avoidance, and multimode control laws. When the MIRA program was completed in December 1979,

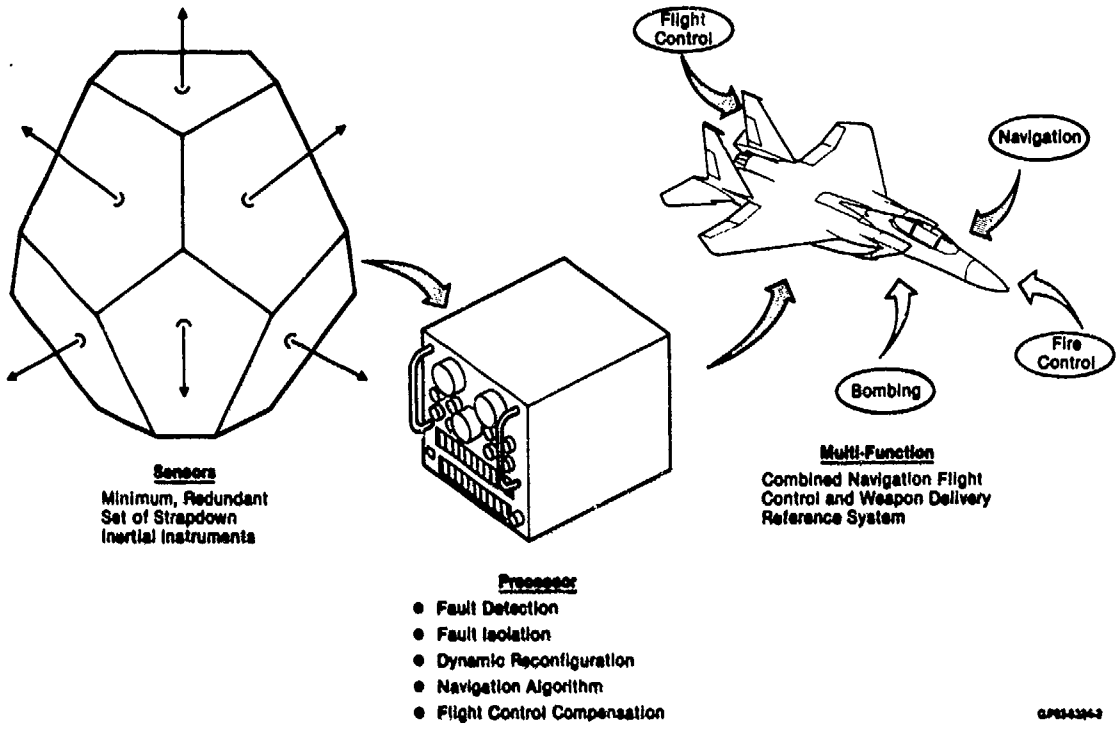

Figure 2. Multifunction Concept

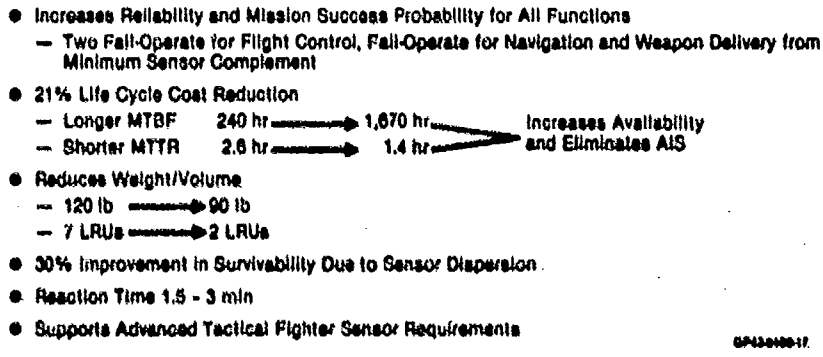

Figure 3. Benefits and Payoffs of MFCRS Concept

several key issues had been identified that could not be resolved in MIRA's limited laboratory demonstrations. The Multifunction Flight Control Reference System (MFCRS) program was initiated in May 1980 to examine, through flight test, the key issues of redundancy management of skewed and dispersed sensors and the compensation required to use navigation quality RLG's and accelerometers for flight control reference in an advanced high performance fighter. A contract was awarded by the Flight Dynamics Laboratory's Flight Control Division (AFWAL/FIG) to McDonnell Aircraft Company (MCAIR) to develop and flight test a multifunction unit.

2. BASELINE DESIGN

The MFCRS program is intended to resolve the two key issues of redundancy management and flight control compensation. To meet these objectives in a cost effective manner, two AV-8B prototype RLG navigation units, the Honeywell Model H421 Laser Inertial Navigation System (Figure 4), were chosen as motion reference units (MRU's) for the MFCRS program. The H421 is a strapdown, Schuler-tuned, inertial navigation system which provides:

- o Navigation position data.
- o True heading.
- o Inertial velocity and acceleration vectors.
- o Inertial attitude.
- o Body linear accelerations and angular rates.
- o BIT.

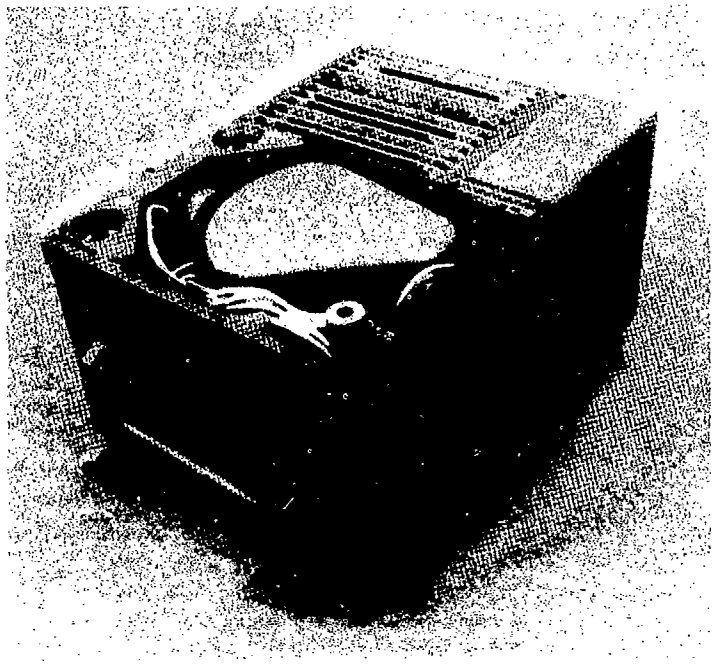

Figure 4. (H421) Laser Inertial Navigation System

The MRU's were modified to allow inter-MRU communication, communication with the aircraft instrumentation, and communication to the flight control computers. A separate MFCRS unit called the Test Management Panel (TMP) was built to serve as an interface between the MRU's and the flight control computers, and as an input/output device for the pilot. Because of safety considerations, a switching unit was also installed to allow selection of either the production aircraft flight control sensors or the MFCRS sensors. The resulting MFCRS design will provide an adequate technology base, validated by flight test, upon which design recommendations for a production multifunction prototype can be made.

Figure 5 shows the components of the MFCRS in the F-15 test aircraft. MRU-A is aligned with the aircraft axes and is located on an avionic shelf in the nose barrel of the aircraft. MRU-B is located 2.8 meters aft and is skewed 60° about its cone axis relative to the aircraft axes. The amount of separation required for survivability was determined in the MIRA program to be at least .76 meters. The limited number of available equipment installation locations on the test aircraft resulted in the large separation for the MFCRS program; however, the compensation developed for this separation will demonstrate a worst case situation. Demonstrating this worst case will provide additional flexibility in locating these components in a new aircraft design. The skewing of MRU B is necessary to provide the redundant inertial information required to perform the two fail-operate redundancy management. The sensor geometry obtained in the installed MFCRS configuration provides a symetrical array which allows rates or accelerations about any axis to be determined using a linear combination of any three of the six sensors of each type available. This geometry is illustrated in Figure 6.

Redundant kinematic information about each sensor axis can also be generated using similar transformations. This ability to replace or duplicate any sensor in the array with a linear combination of any three of the remaining sensors allows the use of parity equations for redundancy management decision making. A parity equation is created by combining two solutions for rate or acceleration about a single axis to form an equation that is equal to zero in the absence of sensor errors.

2.1 REDUNDANCY MANAGEMENT BASELINE DESIGN

A redundancy management system was chosen that compares the sensor outputs using parity equations (3,4). As shown in Figure 7, the results of the sensor comparison, the parity equation residuals, are compared to trip levels and the results used to select the three best sensors based on stored tables. This approach of parity equations and stored tables has a low processing requirement which allows the existing processor to be used at a 50 Hz processing rate. The two key aspects of the redundancy management system are 1) the compensation to allow sensor outputs to be compared and 2) the generation of the stored tables. The sensor differences that act as error sources and methods of compensation are shown in Figure 8.

Moment Arm Effects - The first error source is the moment arm effect caused by the separation of the accelerometers. The sensed acceleration at MRU A is corrected by a set of deterministic equations to the MRU B location so the outputs can be compared.

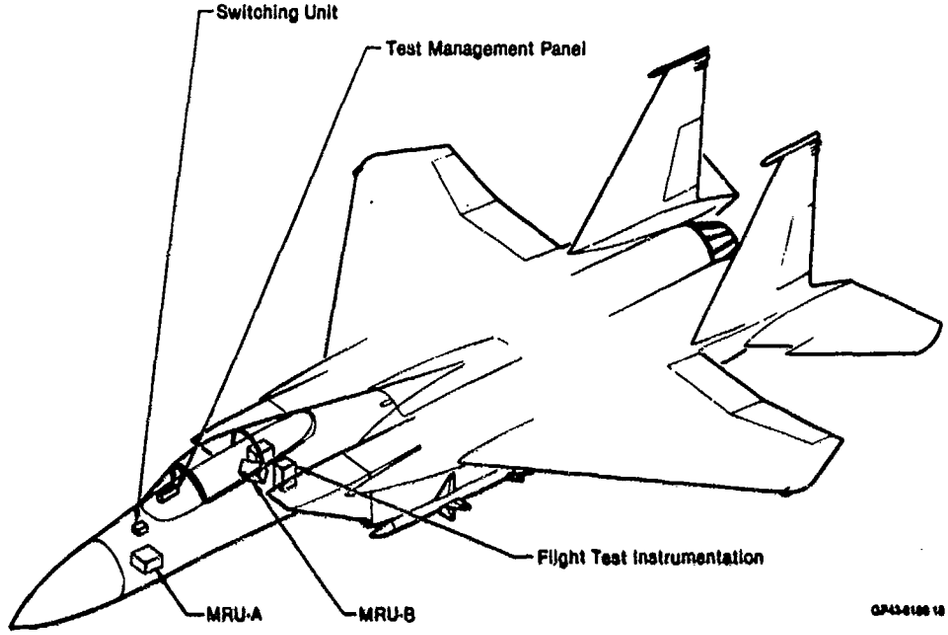

Figure 5. MFCRS Equipment Location - F-15 Eagle

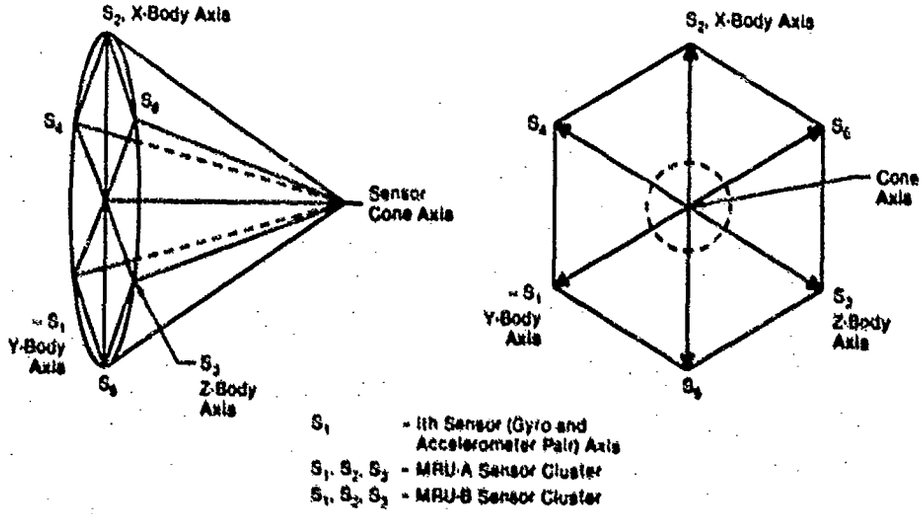

Figure 6. MFCRS Sensor Geometry

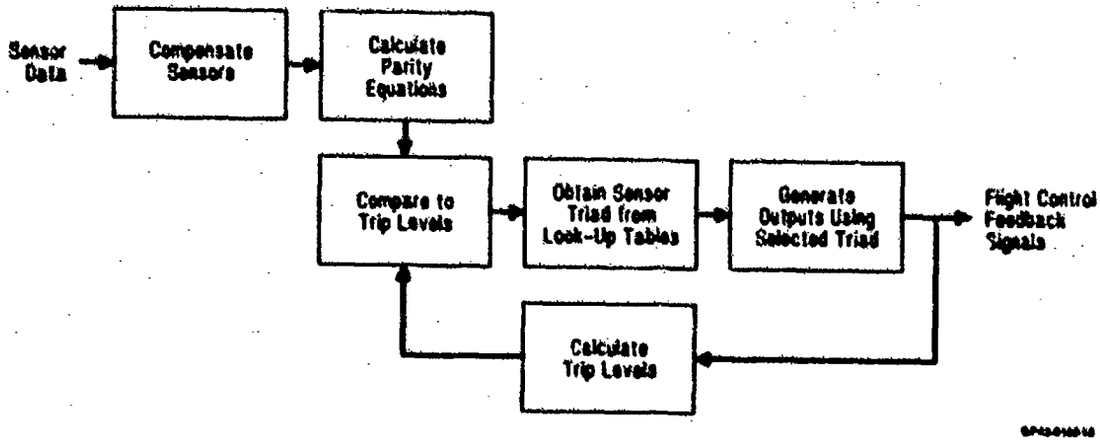

Figure 7. MFCRS Redundancy Management Logic-Simplified Block Diagram

Error Source	Compensation Method
• Moment Arm Effects	• Moment Arm Compensation
• Static Misalignments	• Electronic Alignment
• Dither Noise	• Filtering
• Structural Bending Misalignments	• Trip Level Scheduling
• Bias	• Parity Equation Bias Removal

GP3303264

Figure 8. Redundancy Management Error Compensation

Static Misalignments - Static misalignments are installation errors that are normally corrected by boresighting. Because of limited access, the separation distance between the two MRU's and the complex geometry, boresighting of both boxes proved infeasible. The MFCRS program used a unique approach of boresighting just one box and then using the existing navigation alignment algorithms to calculate the exact installation orientation of each MRU. The results of the navigation alignments were compared and used to calculate the relative orientation of the MRU's to within the required ±1.5 arc-minutes. This method of making corrections for static misalignments is faster, cheaper, and more accurate than conventional boresighting and may have future application in determining the relative orientation of remote installation mounts for other systems.

Mechanical Dithering - The third source of error is noise caused by the mechanical dithering of the RLG's to prevent "lock in" at low angular rates. This dither noise affects both the gyro outputs (by aliasing into the flight control frequencies) and the accelerometer outputs (by causing motion of the sensor block). Dither noise in the gyro channel also couples into the accelerometer channel through the angular rate and angular acceleration terms in the moment arm equations. The gyro outputs require extensive filtering because the differentiation process to get angular acceleration amplifies the dither noise and the long moment arms add further gain. Gain is also added by the coefficients required to transform the MRU B outputs to the aircraft axes. A -60 dB digital notch prefilter at the dither frequencies was placed in the gyro path and a third-order analog lag prefilter was placed in the accelerometer path to attenuate the noise.

Misalignments due to structural bending - The next error source is the misalignment between the two MRU's caused by aircraft bending during high g maneuvering. To account for this misalignment, the trip levels that the parity equation residuals are compared against are scheduled as functions of the sensed rates and accelerations. One major objective of the flight test is to validate the trip level equations and the aircraft bending models upon which they are based.

Bias Errors - Sensor biases are initially accounted for during turn on and warm-up by calculating the parity equation residuals under static conditions and then using these residuals as bias correction factors. Bias correction factors are continually updated during benign flight conditions to account for small changes in sensor outputs over time.

With all of the errors compensated, any miscompares detected by the parity equations should be caused only by incorrect sensor outputs. As mentioned above, the status of the parity equations is used as a pointer in a set of look-up tables to pick the best sensor triad. The look-up table generation was done by an off-line computer program that relates all possible parity equation states to the sensor that is most likely failed. Generation of the redundancy management look-up tables is discussed more fully in Section 3.3.

2.2 FLIGHT CONTROL BASELINE DESIGN

The other key issue to be resolved by MFCRS, the flight control compensation, is shown in Figure 9 and consists of two sets of moment arm compensations and network compensations for the selected gyros and accelerometers (4,5). The first set of moment arm compensations, as discussed above, corrects the sensed acceleration at MRU A to the MRU B location for redundancy management. The second set of equations corrects the selected accelerometer outputs from the MRU B location of the location of the production accelerometers. This second compensation allows switching between the production and MFCRS accelerometers, and avoids any changes in the F-15 flight control computers. The network compensation also avoids changes in the flight control computers by compensating for dynamic bending effects in the feedback loop of the flight control system.

Network compensation is required since the accelerometers are not located at the primary aircraft bending nodes and the gyros are not at the antinodes. Instead, the accelerometers and the gyros are clustered so the system can navigate. In MFCRS this caused flight control system sensitivity to aircraft structural modes resulting in unacceptable stability and handling qualities. Using the baseline F-15 gain and phase margins as design goals, the open loop frequency response was used to determine the network filter requirements to achieve acceptable performance. A 15 dB notch filter was required in the pitch rate and normal acceleration paths and a 30 dB notch was required in the roll path. The yaw path did not require compensation based on the open loop frequency response. To offset the effect of the computational delay, a 3 dB lag-lead network was placed in the pitch rate and yaw rate feedback paths. The 50 Hz computational cycle that was used by the navigation program appeared adequate for both the flight control compensation and the redundancy management.

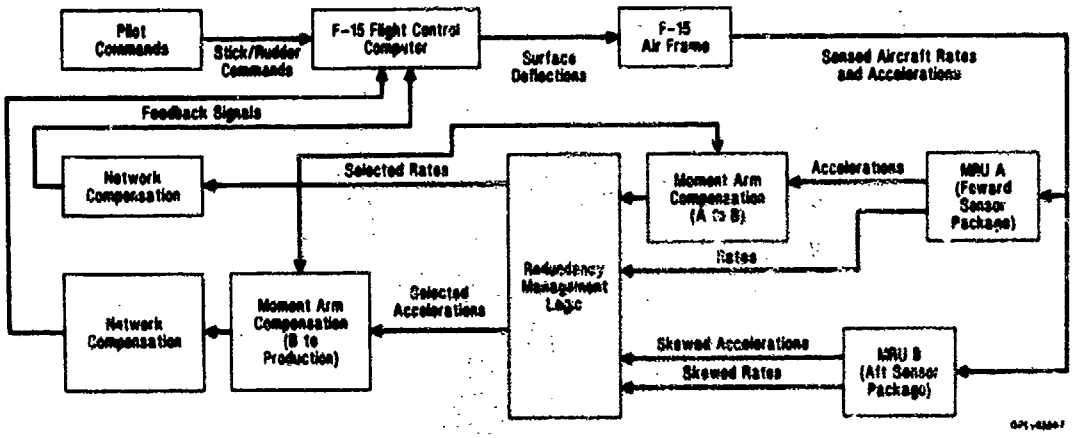

Figure 9. MFCRS Flight Control Compensation-Simplified Block Diagram

3. SIMULATION AND COMPUTER STUDIES

Simulation and computer studies were an essential part of the MFCRS program. They provided a flexible and cost effective means of developing system algorithms and formed the basis, validated by laboratory and flight testing, for evaluating performance. The value of simulations and computer studies becomes apparent when the iterative nature of the design and development process is considered. The simulations and computer studies conducted as part of MFCRS development are summarized in Figure 10.

Computer Program	Role in MFCRS Development
• DIGIKON	• Predict MFCRS Control System Gain and Phase Stability Margins and the Closed-Loop Frequency and Damping of the Aircraft Response Modes
• Continuous System Modeling Program	• Evaluate MFCRS Control System Maneuver Response Characteristics for Command and Disturbance Inputs
• FORTRAN Test Case	• Verify MFCRS Flight Software Code
• Parity Equation Evaluation Program	• Generate the Redundancy Management Look Up Tables
• Man-in-the-Loop Simulation	• Evaluate Closed Loop Handling Qualities
• Monte Carlo Simulation	• Establish a Statistical Basis for Evaluating the MFCRS Redundancy Management Logic

Figure 10. Simulations and Computer Studies

3.1 DIGIKON

The Honeywell developed DIGIKON computer program provides a frequency spectrum analysis of digital and continuous control systems. The stability and performance characteristics of the MFCRS pitch, roll, and yaw flight control systems were determined using DIGIKON at flight conditions that span the range of dynamic pressures likely to be encountered in the F-15 flight envelope. Figure 11, the open loop frequency response of the final MFCRS pitch control system for a high dynamic pressure flight condition was generated using the DIGIKON program. This program was also used to obtain the closed loop frequency and damping characteristics of the predominate rigid and elastic body response modes of the F-15 control system using MFCRS sensors. This analysis provided the information necessary to design the MFCRS flight control compensation networks. The DIGIKON analysis was repeated several times during the iterative design process leading to the final MFCRS configuraiton. The final DIGIKON analysis showed that the basic F-15 flight control system, using MFCRS generated sensor inputs, met the gain and phase stability margin requirments summarized in Figure 12.

3.2 CONTINUOUS SYSTEM MODELING PROGRAM

The IBM developed Continuous System Modeling Program (CSMP) was used to model the MFCRS control system in evaluating time history system performance during closed-loop operation. The program, which included models of the F-15 airframe and flight control system, provided a means of comparison between the time history response of the MFCRS and the basic F-15 control systems. The program was also used to evaluate the performance of the MFCRS redundancy management logic during dynamic, closed-loop operation. Redundancy management performance characteristics evaluated using the CSMP program included the impact of transients induced by sensor reconfiguration on aircraft handling qualities and

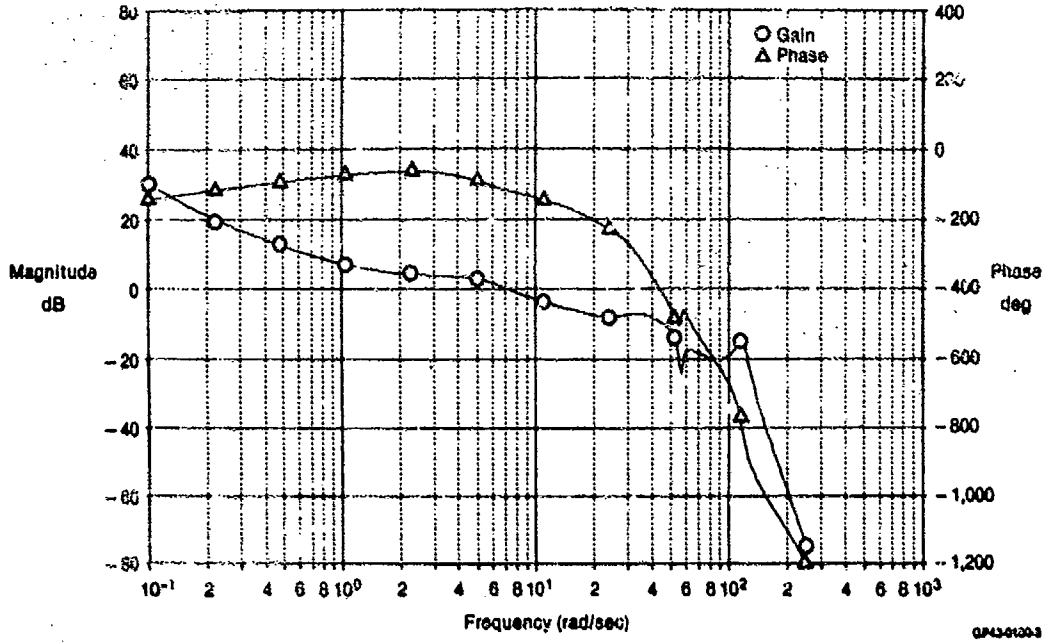

Figure 11. Final MFCRS Pitch Control Loop - High Dynamic Pressure Flight Condition

Summary of Applicable Stability and Performance Requirements from MIL-F-8785B and MIL-F9490D for Class IV Aircraft With Level 1 Flying Qualities in the A, B and C Flight Phase Categories.

Stability Margin Requirements

(a) Rigid Body: 6 dB Gain Margin
± 45° Phase Margin

(b) Elastic Body: 6 dB Gain Margin
± 45° Phase Margin

Performance Requirements

(a) Short Period Frequency:

$$0.28 < \frac{\omega_{sp}^3}{n/\alpha} < 3.6 \text{ and } \omega_{sp} < 1.0 \text{ rad/sec}$$

(b) Short Period Damping:

$0.35 < \zeta_{sp} < 1.3$

(c) Dutch Roll Frequency and Damping:

$0.19 < \zeta_D$ (Damping Ratio)

$1.0 < \omega_d$ (Frequency) and

$0.35 < \zeta_D\omega_D$ (Damping Factor)

(d) Roll Mode Time Constant

$0 < \tau_R < 1.0$ sec

Figure 12. MFCRS Stability and Performance Requirements

safety, and the effect of parametric variations (e.g., sensor noise and sensor misalignments) on redundancy management operation. The scheduled trip levels used in making redundancy management decisions were designed using the information obtained from the CSMP analysis. Information from the CSMP study also led to a restructuring of the MFCRS operational flight program to minimize transport delays and sensor reconfiguration transients and to a simplification of the accelerometer moment arm correction algorithm. The final CSMP analysis showed a close similarity between the time history response characteristics of the basic F-15 and the MFCRS control systems. The analysis also indicated that the redundancy management logic would operate satisfactorily throughout the F-15 operational envelope.

3.3 PARITY EQUATION EVALUATION PROGRAM

As indicated earlier, the MFCRS redundancy management logic compares parity equations to scheduled trip levels in selecting sensors for use in generating the flight control outputs and in detecting failures. The equations that relate sensor failures and parity equation states can be either interpreted geometrically, or derived rigorously using the Greatest Likelihood Ratio test. References 3 and 4 contain a detailed discussion of the redundancy management system.

A computer program developed by the Air Force Wright Aeronautical Laboratories was used to evaluate the MFCRS parity equations and to determine the relative probability of sensor failures for all combinations of parity equation residuals. The number of possible combinations of parity equation residuals was limited by the use of trip levels to establish only two possible parity equation states: 1) residual larger than trip level (failed) or 2) residual smaller than trip level (non failed). The number of possible parity equation statuses was further limited by evaluating only selected subsets of the 15 parity equations available. The subset evaluated at any one time is dependent on the sensor failure status.

The general program flow of the computer program is illustrated in Figure 13.

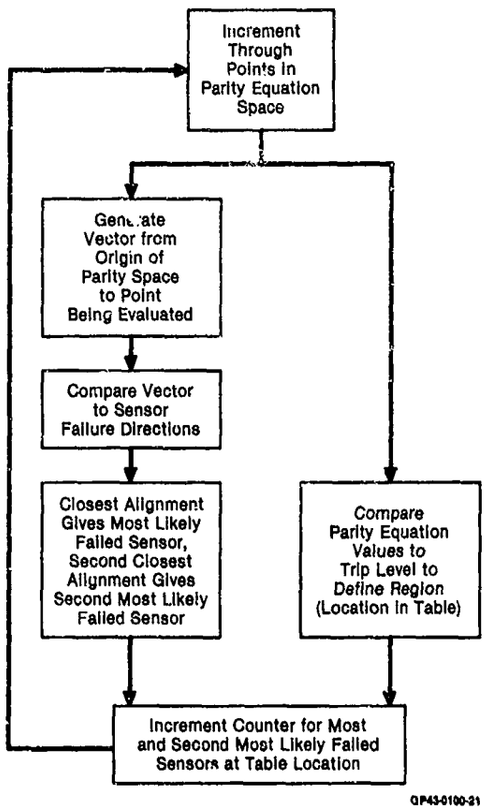

Figure 13. Parity Equation Evaluation Program

The computer program uses the linearily independent parity equations in the selected parity equation set to define a parity equation space (independent parity equations form orthoginal basis). The dependent parity equations and the failure directions of all valid sensors are defined with this space. (Figure 14 and 15) The program then performs a point by point evaluation of the entire space to determine the relative probability of failure for each sensor for all the points in the parity equation space.

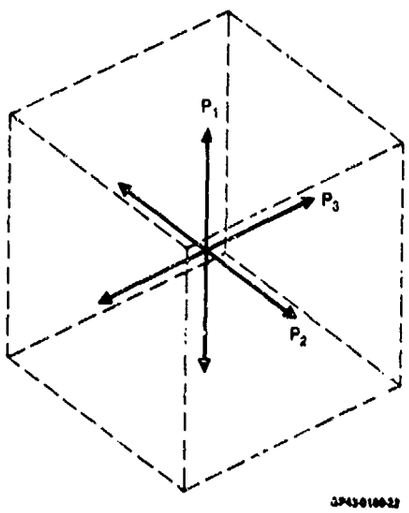

Figure 14. Parity Equation Space

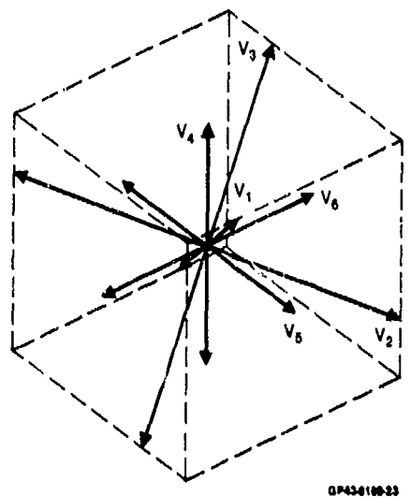

Figure 15. Sensor Failure Directions in Parity Equation Space

The sensor selection tables used in the MFCRS redundancy management approach were generated by selecting the sensors whose failure directions were least aligned with vectors from the origin of the parity equation space to the points in the space that resulted in each particular parity equation status. The fault detection tables were generated by declaring sensors failed when their failure directions were aligned with the test point vectors for a majority of the points that resulted in a particular parity equation status.

The validity of these tables was verified using both the CSMP and Monte Carlo simulations. Exhaustive laboratory testing, over a period of approximately eighteen months, showed that the MFCRS redundancy logic, implemented in the flight hardware, reliably detected and isolated both real and simulated sensor failures.

3.4 FORTRAN TEST CASE

A FORTRAN version of the MFCRS operational flight program was developed and maintained by MCAIR throughout the program. Aircraft motion inputs, obtained from the CSMP simulation for a 7G rolling pull-up maneuver, were applied to the FORTRAN program as a "test case". The same motion inputs were applied to the operational flight program code implemented in the flight hardware. Intermediate and final outputs from the two programs were then compared. This method of testing was instrumental in guarding against coding errors and ensuring a very smooth software development. One of the keys to the success of this approach was the fact that the software for the MCAIR simulation and the operational flight program were generated by different individuals. This check and balance situation ensured design quality. The other key was the absolute requirement that all software changes must be incorporated in both sets of software, a new test case generated, and the results compared to ensure proper coding.

The MFCRS operational flight program underwent six major and numerous minor revisions during the iterative design process leading to the final software configuration. The "test case" approach to software verification proved invaluable in identifying and isolating coding errors. This approach also proved useful in resolving conflicts and clarifying misunderstandings as new requirements evolved.

3.5 MAN-IN-THE-LOOP SIMULATION

The MCAIR Manned-Air-Combat-Simulator (MACS) was used to evaluate MFCRS handling characteristics. MACS is a hybrid facility consisting of several combat domes connected by a large digital computer. Pilots located in the domes, Figure 16, can fly against each other or against realistically structured "canned" target maneuvers. The domes are mechanized with integrated controls and displays and function through the use of an extensive library of computer models. These models reflect both aircraft and weapon characteristics and generate displays which portray the evolving engagement. The F-15 aircraft and flight control system mathematical models used in the MFCRS studies were programmed into the simulation computer. A complete set of large perturbation, nonlinear aerodynamics data, including high angle-of-attack effects for the F-15 aircraft, makes continuous flight possible throughout the flight envelope. The simulation also included a detailed model of the F-15 flight control system providing augmented control in the pitch, yaw, and roll response axes of the aircraft.

The conclusion of the first man-in-the-loop simulation was that the system was stable and controllable for all maneuvers. However, during small amplitude stick raps and rudder kicks, the MFCRS system was slightly less damped than the basic F-15, requiring an extra half-cycle of oscillation to damp. This decrease in damping was traced to the 3 dB lag-lead network. Figure 17 shows the response of the baseline MFCRS control system to half amplitude stick raps at a high dynamic pressure flight condition. To increase the damping and maintain desired stability, this filter was replaced with a 5 dB, second-order, lead-lag network. While this network was adequate to maintain stability and performance, analysis indicated that performance would be better if a computation rate between 80 and 100 Hz was used. This would allow a sharper roll off on the filters. The use of existing hardware with limited processing capability denied this option to the MFCRS program.

A second man-in-the-loop simulation was conducted later in the program following incorporation of these and other changes identified during laboratory testing. The results of the second simulation indicated that the final MFCRS configuration will provide acceptable performance and stability. Figure 18 shows the response of the final MFCRS control system to half amplitude stick raps at a high dynamic pressure flight condition.

3.6 MONTE CARLO SIMULATION

A statistical basis for evaluating the performance of the MFCRS redundancy management logic for various combinations of flight condition, sensor failures and disturbance inputs was obtained using the Monte Carlo simulation. This simulation models both the F-15 flight control system and airframe, including both rigid and elastic body aerodynamics. Closed-loop system response characteristics for both nominal pilot commands and wind disturbance inputs, as well as aircraft response variations due to flight condition, were included in the simulation.

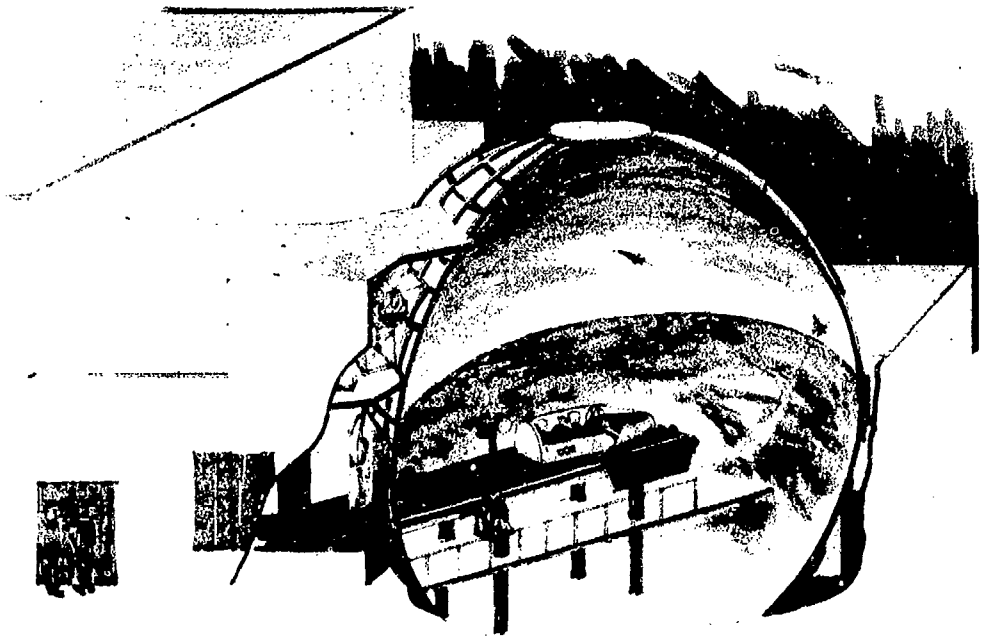

GP43-0100-24

Figure 16. Manned Air Combat Simulator (MACS)

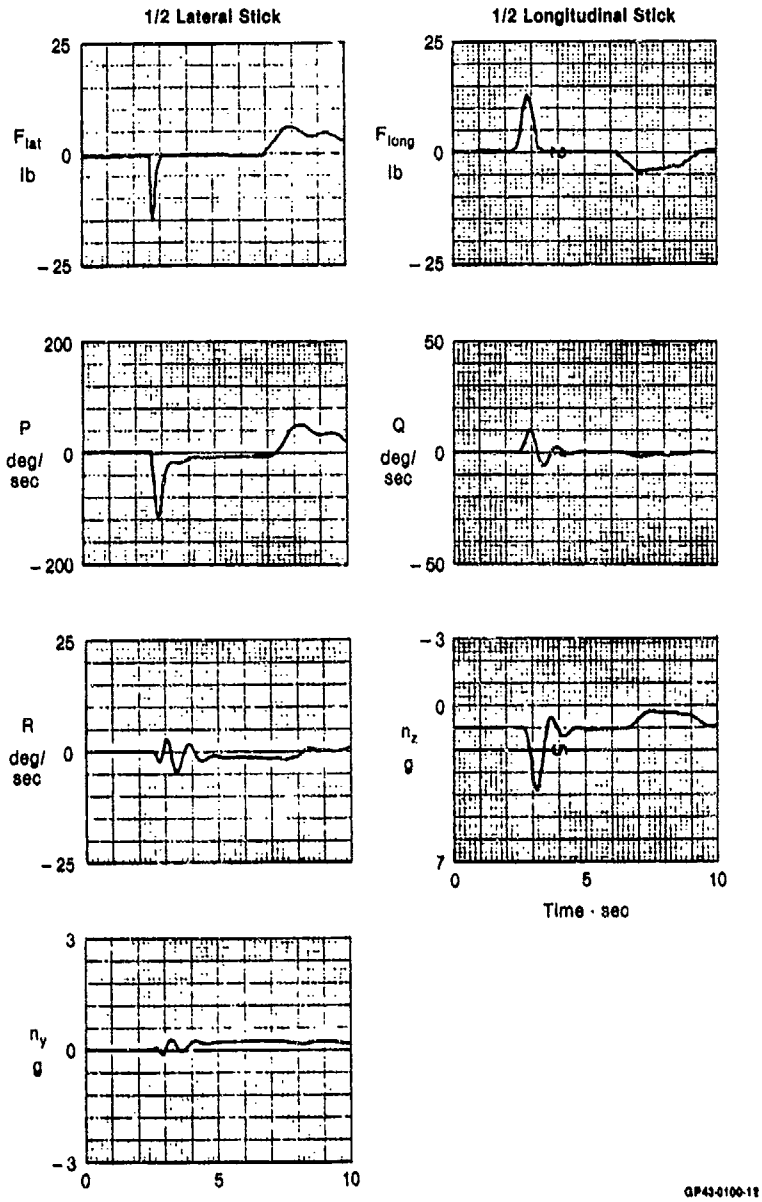

GP43-0100-18

Figure 17. Baseline MFCRS Control System Response to Stick Inputs at a High Dynamic Pressure Flight Condition

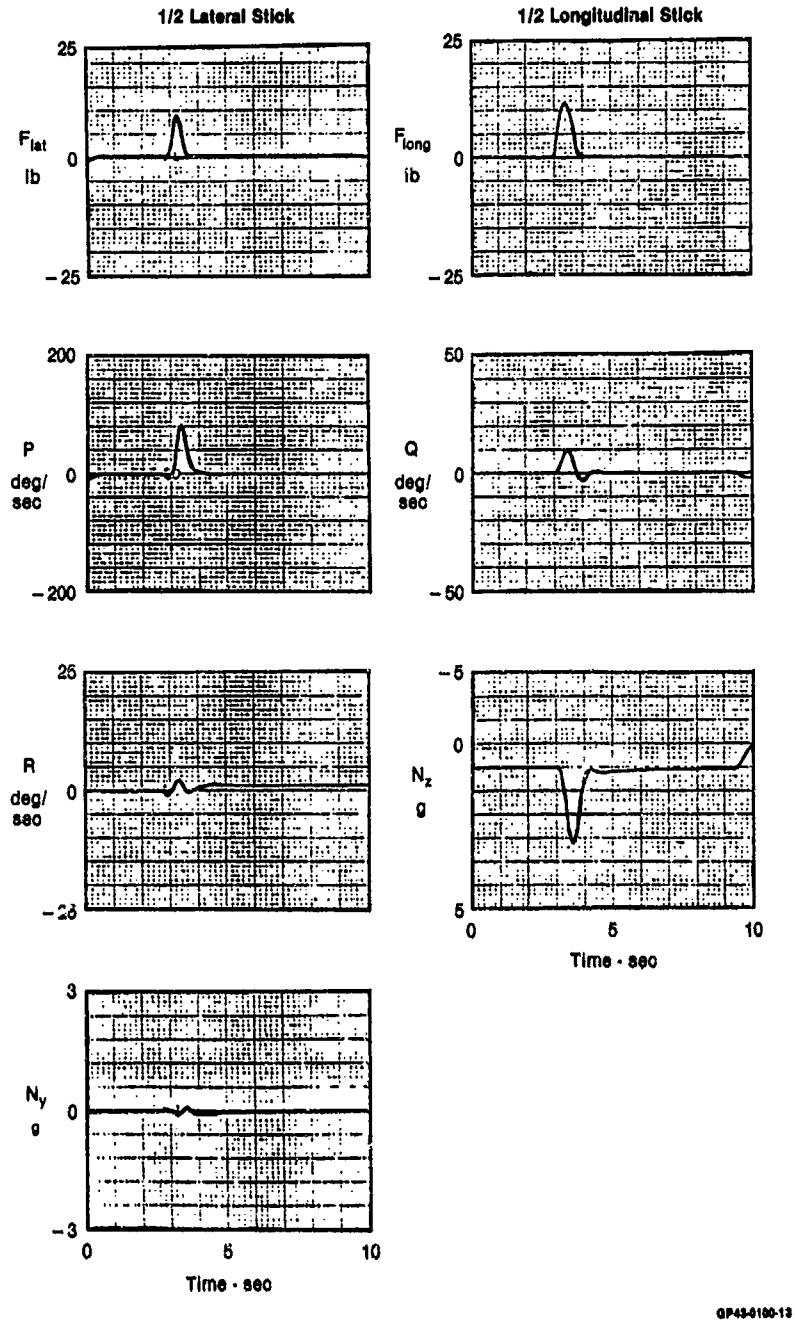

Figure 18. Final MFCRS Control System Response to Stick Inputs at a High Dynamic Pressure Flight Condition

The aircraft motion inputs generated by the simulation include the effects of sensor output variations due to quantization, random noise, ring laser gyro dither and misalignments caused by static bending during aircraft maneuvers. The motion inputs are then modified to include scale factor and bias error terms, which can be varied in a random fashion, singly or in combination, to provide a statistical basis for determining the effectiveness of the MFCRS redundancy management logic in detecting and isolating sensor failures. The generation of the aircraft motion inputs is illustrated in Figure 19.

The simulation runs in an open-loop fashion, applying aircraft motion inputs to the MFCRS logic and providing statistical data on sensors selected, failed sensors detected, failed sensors undetected, false alarms and system status (e.g., parity equation values, trip level values).

A key element of the Monte Carlo simulation, which aided in the analysis of problems and the refinement of the MFCRS algorithms, was the complete emulation of the equations implemented in the flight software. This included the signal selection and fault detection logic, the equations for accelerometer moment-arm compensation and the flight control network compensation.

4. LABORATORY TESTING

Laboratory testing for the MFCRS program was conducted in two phases: 1) environmental testing, hardware/software integration and acceptance testing at Honeywell, and 2)

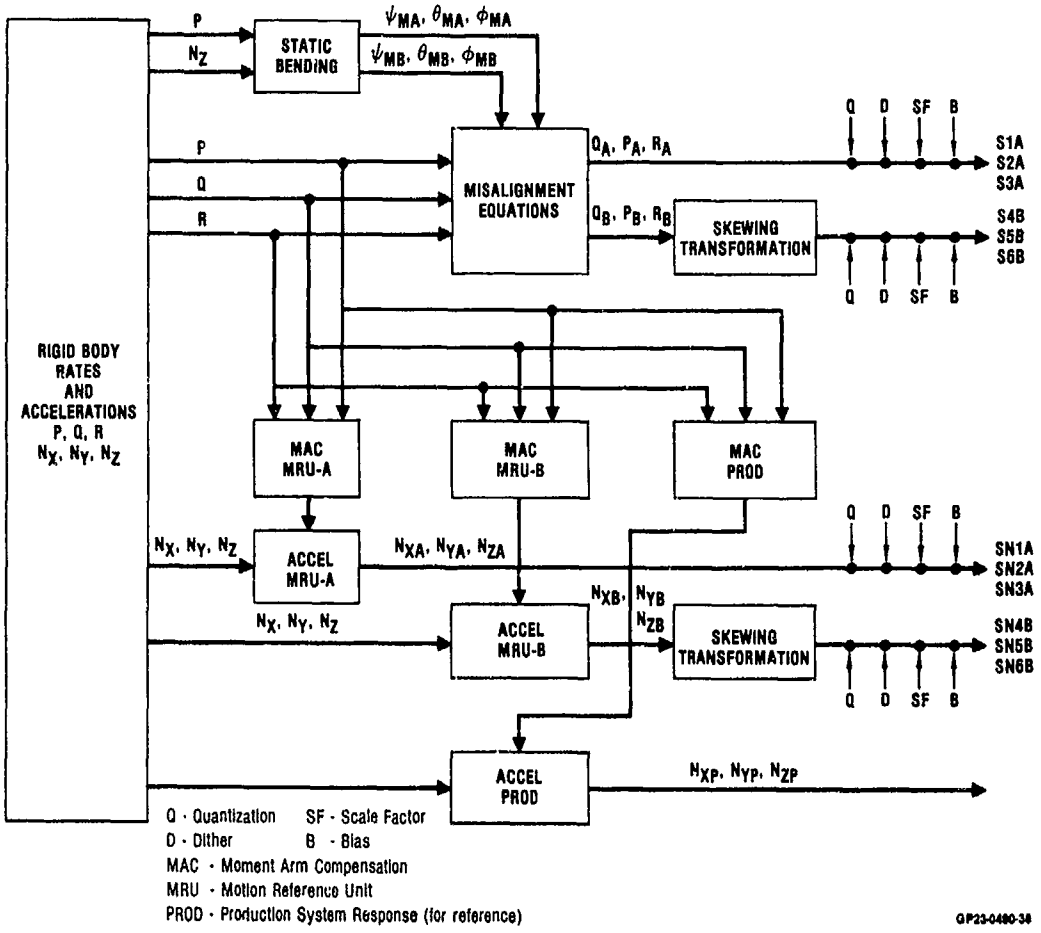

Figure 19. Monte Carlo Simulation-Generation of Sensor Output Signals

integration and performance testing at MCAIR. Some of the major factors that impacted laboratory testing are discussed below.

4.1 ENVIRONMENTAL TESTING

Vibration, temperature/altitude, electromagentic interference and shock tests were performed on the MFCRS hardware to ensure that the equipment would be safe when installed on the F-15 aircraft and to check for abnormal behavior. Design changes were implemented to correct problems uncovered and an abbreviated retest was conducted following equipment delivery to MCAIR. The final MFCRS configuration performed satisfactorily in all areas except for navigation performance in a high vibration environment.

Navigation performance was slightly degraded during random vibration testing in the Y and Z axes. Navigation accuracies were found to degrade rapidly, however, when the MRU's were subjected to sinusoidal vibration near the resonant frequency of the sensor assembly shock mounts. This problem was most apparent in the vertical axis. Preliminary investigations suggested that the problem was associated with the shock mount configuration and the sensor assembly balance. Further investigation was beyond the scope of this program.

4.2 HARDWARE/SOFTWARE INTEGRATION

The first comprehensive estimate of processing spare time (including a walk-through of the actual code) showed that the processing capability of the system had been exceeded by approximately 10%. This problem was initially solved by scrapping the structured navigation software planned for MFCRS in favor of a less structured, more efficient version. This problem reappeared later during hardware/software integration, complicating the design process and limiting the scope of software changes. Figure 20 lists some of the areas where system performance could have been improved had additional processing capability been available.

The final version of the MFCRS operational flight program uses a maximum of 90% of the processing time available. Even though the use of existing hardware with limited processing capability denied many options to the MFCRS program and complicated the development process, the final system was able to meet the performance objectives of the program, thus demonstrating that this technology is feasible using current processors.

Test data obtained during the initial stages of software/hardware integration indicated that the noise due to RLG dither was present on both the accelerometer and gyro

Design Parameter	MFCRS Solution	Preferred Approach
Software	Less Structured Software	Structured Software
Redundancy Management	Table Look-Up Implementation Fault Detection Performed at 25 Hz	Calculate Failure Probabilities in Real Time. Fault Detection Performed at 50 Hz.
Accelerometer Moment-Arm Correction	Include Only Essential Terms	Include All Terms
Flight Control	50 Hz Iteration Rate	80-100 Hz Iteration Rate
Accelerometer Filtering	Analog Prefilter	High-Speed Digital Prefilter

GP43-0100-4

Figure 20. Improvements Possible With Increased Processing Capability

and normal acceleration outputs were slightly above the specification limits when these signals were generated using worst-case sensor combinations. The noise levels in the lateral acceleration outputs (Figure 21), however, were significantly higher than specified maximums for all but the best sensor combinations. This noise was large enough to cause false alarms in the redundancy management system. The trip levels were raised to the point where additional increases would allow sensor failures to cause aircraft transients before they were detected. After the trip levels were raised, the noise in the MFCRS was measured in an end to end test. Results showed that the noise was still outside specification limits, and that the sixth order filter was not providing the expected attenuation. Analysis showed that part of the problem was RLG quantization. The RLG measures angular rotation in discrete increments and accumulates these discrete rotations over a set time period to calculate rate. The increment to which the rotation is quantized creates quantization noise that raises the gyro path noise level to a -30 db value versus the -60 db design goal. The RLG resolution can be changed to reduce the quantization level, but the effort was beyond the scope of this program.

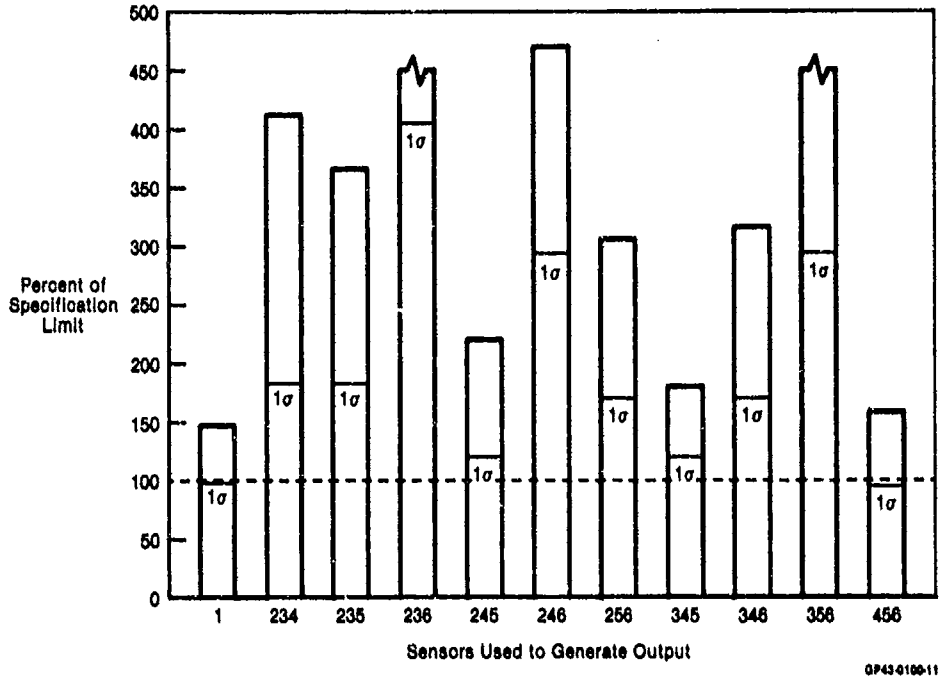

Figure 21. Lateral Acceleration 1σ and Maximum Noise Levels - Initial Laboratory Testing

This problem does not affect navigation since the outputs are integrated over a long period of time and, unlike flight control, any quantization errors average out. Clearly, any future system must consider the flight control requirements in the design of the basic sensors.

In addition to the gyro noise coupled into the accelerometer path by the moment arms, the accelerometer path also had more noise than expected with the third-order lag prefilter. Some of this noise appears to be related to the hardware implementation method rather than any fundamental phenomena. A careful redesign of the electronics with awareness of the noise sensitivity would probably eliminate the problem.

The use of existing hardware and the limited scope of the program did not allow this comprehensive fix. Instead a first-order 0.1 second lag filter was added to the accelerometer path and the parity equation moment arm compensation was changed to do the parity equation comparison at a central location. This last change had the effect of shortening the moment arm and reduced the noise in this path. Minor hardware changes were also made to provide isolation in the accelerometer electronics.

Any future design should attempt to minimize MRU separation in excess of that required for survivability. Another solution that may be available to future systems is the selection of a redundancy management system that is less sensitive to noise. This is a difficult goal to achieve since the sensor reconfiguration must be done quickly enough to prevent transients in the flight control outputs. Some form of weighted averaging may allow a longer time period for decision making.(7)

Analysis indicated that the filtering changes implemented to alleviate sensor noise had reduced the MFCRS control system stability margins to below specified minimums. To maintain stability, the gain in the pitch and yaw control loop had to be scheduled based on dynamic pressure. Analysis also showed the 5 dB lead-lag network provided some gain of the accelerometer noise. The use of gain scheduling allowed elimination of this network. Figure 22 compares pitch axis stability and performance at a high dynamic pressure flight condition for the baseline MFCRS control system and the MFCRS control system configuration following incorporation of changes to alleviate noise. As shown, pitch axis stability and performance have been maintained at this most demanding flight condition.

Flight Condition	Baseline MFCRS					Final MFCRS				
	Stability			Performance		Stability			Performance	
	ω(r/s)	Gain Margin (dB)	Phase Margin (deg)	ω(r/s)	ζ	ω(r/s)	Gain Margin (dB)	Phase Margin (deg)	ω(r/s)	ζ
High Dynamic Pressure	11.19		40.7	11.30	0.84	7.10		63.7	7.60	0.50
	21.38	5.9		15.40	0.35	17.10	7.30		15.20	0.41
	80.52	10.4		29.30	0.22	71.70	14.20		29.70	0.32
	137.80	19.6		56.70	0.08	130.50	19.00		56.90	0.06
				79.80	0.22				121.20	0.05
				123.5	0.07				282.70	0.20

GP43-01460-1

Figure 22. Pitch Axis Performance and Stability - Baseline and Final MFCRS Control Systems at a High Dynamic Pressure Flight Condition

These changes illustrate the difficulty of integrating multifunction sensors with existing systems. Multifunction systems should not be inserted directly into current flight control systems simply as a sensor replacement. The multifunction system is part of the flight control loop and, to derive maximum benefit, the implications of the sensors should be considered in the complete flight control design. The MFCRS was constrained from modifying the flight control hardware so the flight control system could remain compatible with the existing flight sensors. This constraint would be removed in the design of a prototype system.

These problems, solutions and recommendations are summarized in Figure 23.

Problem	MFRCS Solution	Long Term Solution
Gyro Dither Noise	Raise Trip Levels Add - 60 dB Notch Filter	Reduce Gyro Quantization Level Measure Gyro Dither Stiffen Sensor Block Synchronize Dither and Outputs Design Future Gyros Considering Flight Control Requirements
Accelerometer Dither Noise	Raise Trip Levels Add Analog Prefilter Add 0.1 sec Lag Filter Remove Lead Lag Filter Change Moment Arm Compensation Hardware Changes to Increase Channel Isolation	Reduce Moment Arms Reduce Accelerometer Sensitivity to Dither Design Accelerometer Channel Considering Noise Sensitivity Consider Alternate Redundancy Management
Processor Computational Burden	Limit Scope of Software Changes	More Powerful Processor

GP43-01459

Figure 23. MFCRS Noise Problems/Solutions

4.3 ACCEPTANCE TESTING

Acceptance testing at Honeywell was a comprehensive series of performance tests conducted just prior to equipment delivery to MCAIR. Navigation performance using a standard 4 minute and 30 second alignment was consistently better for both MRU-A (normally mounted) and MRU-B (skewed) than that specified for the basic F-15 INS. Figure 24 compares the peak navigation errors during navigation runs conducted at Honeywell with the F-15 specification limit.

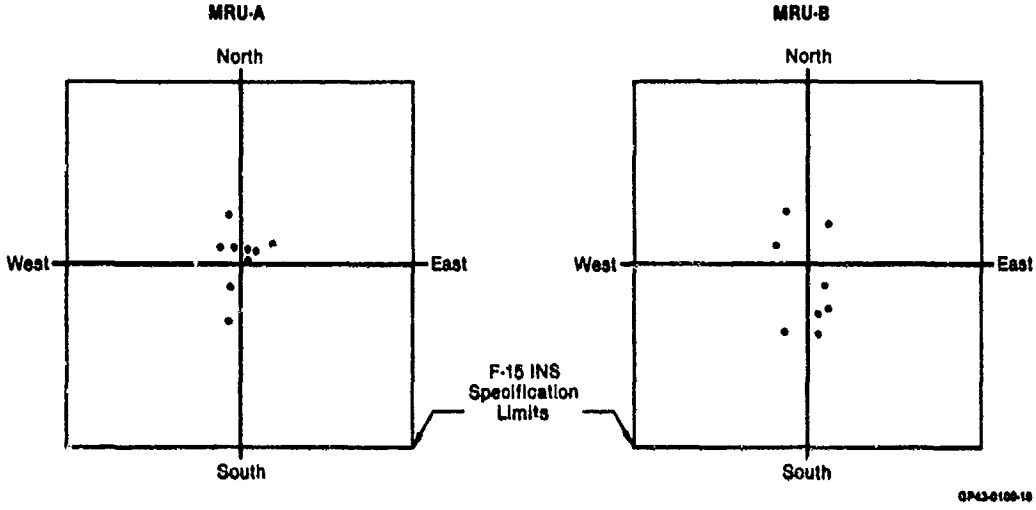

Figure 24. Peak Velocity Errors During 42 Minute Navigation Runs in Honeywell Laboratory

Sensor noise levels were found to be at or near the specification maximums for pitch rate, normal acceleration and lateral acceleration when worst case sensors were selected to generate the outputs. Rate sensor gain and phase measurements, obtained using a two axis rate table and a special MRU mounting fixture, matched expected values. However, several problems were uncovered during this testing. These included electronics alignment performance, synchronization, and transients when simulated faults were applied. All of these problems were traced to implementation errors and were corrected following equipment delivery to MCAIR.

4.4 INTEGRATION TESTING

The MFCRS equipment was interfaced with a production F-15 flight control system (including actuators), a mission computer, a navigation control indicator and an inertial navigation system following delivery to MCAIR.

During static noise testing, it was discovered that significant actuator motion resulted from the noise levels present in the MFCRS outputs, even though these levels were within specified limits and were less than the noise levels present in the basic F-15 sensor assemblies. The problem was traced to the fact that the frequency of the noise in the MFCRS outputs was much lower than that present in the outputs of the basic F-15 analog sensor assemblies. The difference was due to quantization introduced by the MFCRS A/D and D/A converters and the relatively low 50 Hz sample rate. This discovery led to another round of design changes including custom scaling of the accelerometer path to reduce A/D quantization, hardware modifications to reduce ambient noise levels and modifications to network compensation to provide an additional 6 dB of attenuation at frequencies above the notch frequency.

These changes reduced the noise levels on the MFCRS analog outputs to the point where noticable actuator movement occurred only when sensors with worst case geometry (largest coordinate transformation gains) were used to generate the flight control outputs. Figure 25 illustrates the noise levels present in the most sensitive output, lateral acceleration, for the final MFCRS configuration. Ground testing on the testbed aircraft later showed that the actuator motion resulting from MFCRS noise was acceptable and would not be discernable to the pilot. This round of design changes to alleviate noise is another clear indication that noise is a fundamental problem that must be addressed in the basic design of future multifunction systems.

4.5 PERFORMANCE TESTING

Navigation testing at MCAIR, including Scorsby testing, confirmed the excellent results obtained at Honeywell. Figure 26 shows the peak velocity errors during six navigation runs completed at MCAIR.

The electronic alignment procedure, which uses the navigation alignment capability of the MRU's to measure their orientation relative to each other, proved to be more accurate than anticipated. This allowed the procedure to be simplified by reducing the number of alignments required to obtain a solution. Figure 27 shows the variance from

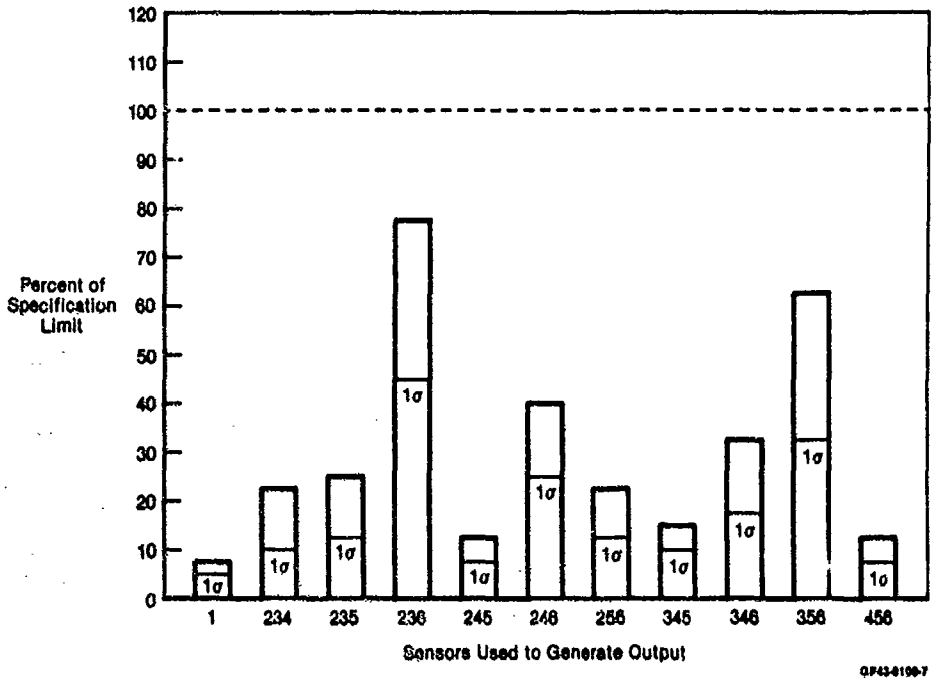

Figure 25. Lateral Acceleration 1σ and Maximum Noise Levels - Final MFCRS Configuration

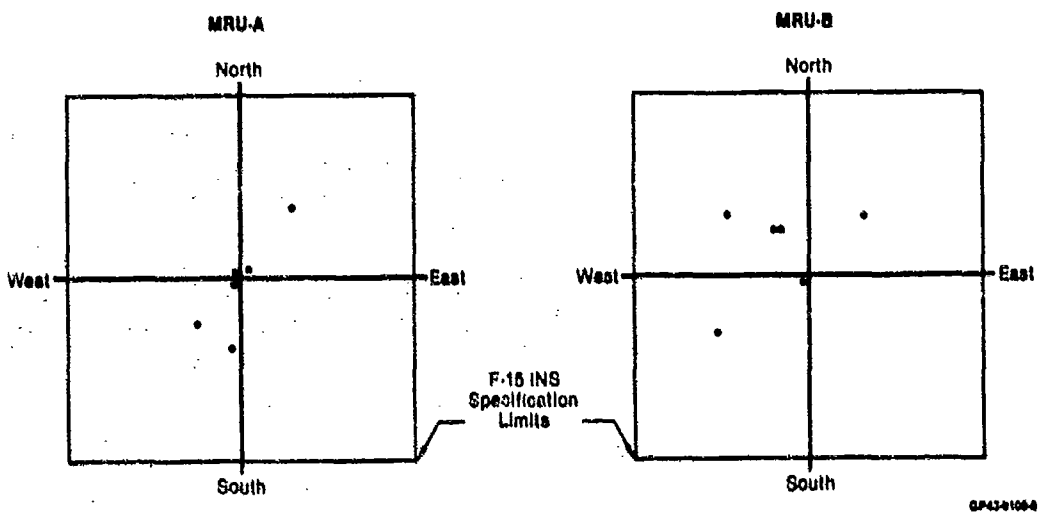

Figure 26. Peak Velocity Errors During Navigation Runs in MCAIR Laboratory

in the MCAIR laboratory. Figure 28 shows the same information for the electronic alignment conducted on the test bed aircraft. These results indicate that the design goal of sensor alignment accuracy to 1.5 arc-minutes can be achieved using eight (or fewer) 10-minute navigation alignments.

Other cricital tests performed at Honeywell during acceptance testing were repeated in the MCAIR laboratory just prior to aircraft installation. This testing served two purposes; 1) verification of Honeywell test results by repeating test with different test personel and test equipment and 2) verification that changes incorporated subsequent to equipment delivery had not invalidated earlier results. Figure 29 summarizes the performance testing conducted at MCAIR.

5. INTEGRATION VS INTERFACING

Taken together, problems discussed above point to a fundamental lesson learned in the design of integrated systems. Currently, systems are designed for specific purposes and are made to interface with other systems. The navigation units available for the MFCRS test demonstration were designed by navigation specialists who did not have any flight control requirements imposed upon them at that time. The flight control specialists who made the initial design modifications to the MRU's were not fully aware of some of the assumptions made in the basic navigation design. True integration, as shown by this program, is more difficult.

In order to minimize integration problems and to take advantage of complementary

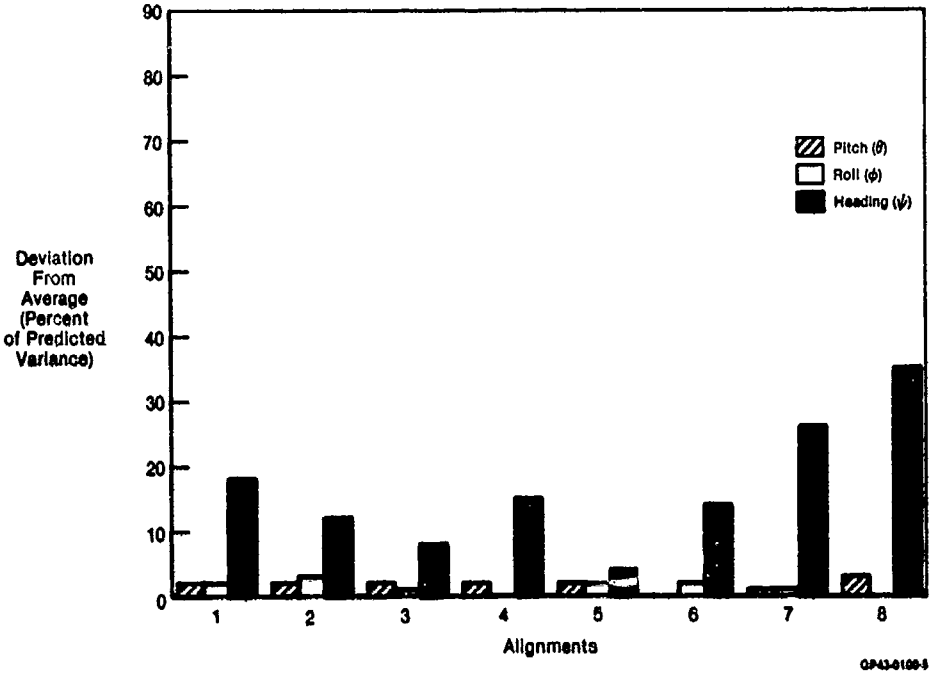

Figure 27. Electronic Alignment in MCAIR Laboratory

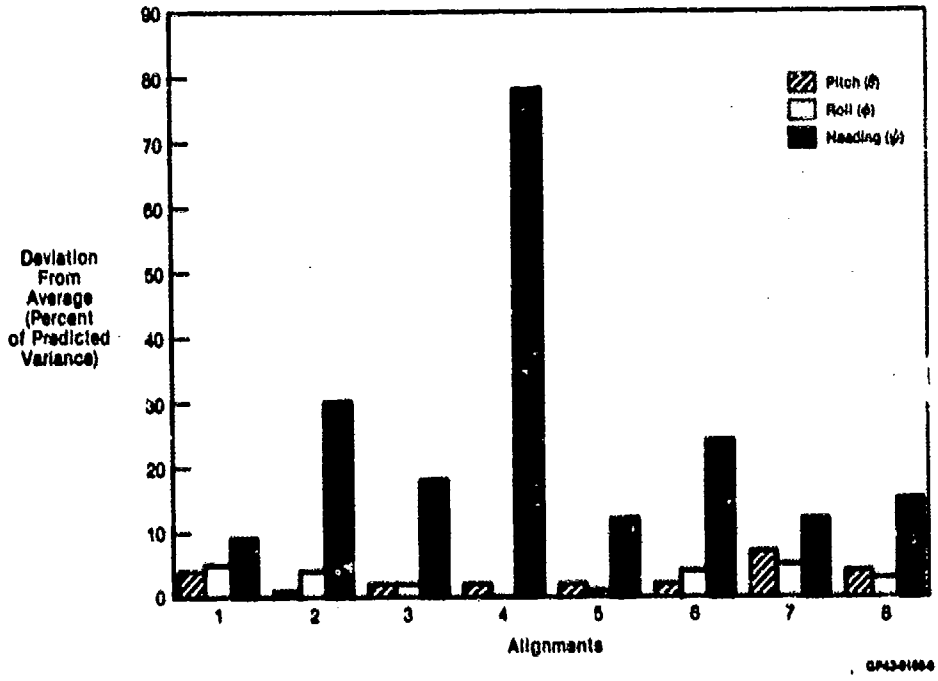

Figure 28. Electronic Alignment on Testbed Aircraft

group. The objective of this group would be to interact with engineers who are specialists in all of the systems being integrated in order to find and resolve conflicting requirements early in the design stage. To carry out this function, excellent communication must exist between the organizational elements responsible for flight control, fire control, navigation and propulsion control, and the coordinated effort must be responsive to the influence exerted by the multifunction integration group. Project organization must facilitate these requirements for communication and coordination.

6. FUTURE PLANS

The testing in the MFCRS program has been instrumental in identifying problem areas and design considerations for future systems. However, there are still questions that cannot be answered by simulation studies or laboratory testing. The MFCRS equipment was installed on a F-15 testbed in late 1983. Following successful ground testing, the MFCRS system will be flown in early 1984 to evaluate aircraft stability and handling qualities.

System Operation
- Pilot Operation
- Intra-System Communications and Synchronization
- Power Tests
- Flight Control Interlock Operation

Flight Control Outputs
- Gain and Phase
- Scale Factor, Linearity, and Null Stability
- Dynamic Range
- Noise

Redundancy Management
- Fault Detection and Isolation
- Reconfiguration Transients
- BIT

Navigation
- Static Navigation
- Scorsby Tests
- Alignment Accuracy
- Electronic Alignment

Figure 29. Performance Tests

focus on two key areas: flight control and redundancy management performance. Stability and handling qualities evaluations will answer the question of how well separated sensors at non-optimal locations can be used for fighter flight control. Fault coverage and reconfiguration transient evaluations will hinge on how well the effects of structural bending and differential vibration have been modeled and compensated for in the redundancy management algorithm.

7. CONCLUSIONS

The Multifunction Flight Control Reference System concept addresses the problems of current systems that require inertial data and provides for the needs of future systems. The MFCRS program uses existing hardware to demonstrate the concept in a cost effective manner.

A redundancy management system using parity equations has been developed for the separated sensors. One key aspect of the redundancy management is the use of an off-line program to relate parity equation status to the most likely failed sensors. This off-line program reduces the real-time processing requirements to allow use of an existing processor. To support the redundancy management system, a one time electronic alignment procedure has been developed and implemented to determine the relative orientation of the two sensor clusters to within ±1.5 arcminutes. This electronic alignment procedure is faster, cheaper, and more accurate than current optical/mechanical boresighting procedures and has potential for application in other programs.

Simulation and computer studies were an essential part of the MFCRS research and development program. The value of simulations and computer studies in providing a flexible and cost effective means of developing system algorithms and evaluating design options becomes apparent when the iterative nature of the design and development process is considered. Simulation and computer studies also formed the basis, validated by laboratory and flight testing, for evaluating MFCRS performance.

Flight control and redundancy management compensation has been developed, implemented and simulated for a worst case sensor separation. The software for the redundancy management and flight control was successfully developed and coded. A key to the successful software development was the use of a test case to validate the original code and all subsequent changes.

The results of testing have shown that noise caused by RLG dither is a severe problem for flight control redundancy management. Noise attenuation should be addressed in the basic system design. Testing has also shown that a multifunction system must be considered as part of the flight control loop and the overall flight control system design must consider issues peculiar to the multifunction system.

The suggested management technique to design future integrated systems will be to use a strong systems integration group to interact with and be part of the design team.

Future testing on an F-15 aircraft will provide data so the key areas of flight control and redundancy management performance can be evaluated.

The design, development, and testing of the MFCRS to date has not shown any basic flaws with the multifunction concept, but has provided valuable insights for future designs of integrated systems.

REFERENCES

1. Perdzock, J., Air Force Flight Dynamics Laboratory; Burns, R.C., McDonnell Douglas Corporation - "Preliminary Feasibility Assessment of Multifunction Inertial Reference Assembly (MIRA)", presented to American Defense Preparedness Association, Avionics Section, Air Armaments Division Technical Symposium, 4 - 5 October 1977 at Naval Surface Weapons Center, White Oak Laboratory.

2. Burns, R.C., McDonnell Douglas Corporation - "Multifunction Inertial Reference Assembly (MIRA)", Final Technical Report, Air Force Flight Dynamics Laboratory Report Nr AFFDL-TR-78-105, September 1978.

3. Sebring, D. L., McDonnell Douglas Corporation, Young, Captain J. T., Air Force Wright Aeronatucial Laboratories, Flight Dynamics Laboratory - "Redundancy Management of Skewed and Dispersed Inertial Sensors", AIAA Paper Nr 81-2296, presented at the Fourth Digital Avionics Systems Conference, 17 - 19 November 1981, St. Louis, MO.

4. Barnard, G., et. al., McDonnell Douglas Corporation - "Multifunction Flight Control Reference System, Volume I - Design and Development", Air Force Flight Dynamics Laboratory Report Nr AFWAI-TR-82-3007, March 1982.

5. Luedde, W. J., McDonnell Douglas Corporation - "The Use of Separated Multifunction Inertial Sensors for Flight Control", AIAA Paper Nr 81-2295, presented at the Fourth Digital Avionics System Conference, 17 - 19 November 1981, St. Louis, MO

6. Young, Captain J.T., Perdzock, J., Air Force Flight Dynamics Laboratory; Sebring, D. L., McDonnell Douglas Corporation; Edinger, L.D., Honeywell Inc. - "Design and Development of the Multifunction Flight Control Reference System", presented to advisory group for Aerospace Research and Development (AGARD), Guidance and Control Panel Technical Symposium, Ensae, Toulouse, France 17 - 20 May 1983.

7. Barnard, G., et. al. McDonnell Douglas Corporation - "Integrated Inertial Reference Assembly (IIRA) Analysis, Trade Studies, System Definition, Test Plan" Air Force Avionics Laboratory Report Number AFWAL-TR-82-1152, February 1983.

INITIAL ALIGNMENT AND AUGMENTATION OF THE ARINC 705 STRAPDOWN AHRS LTR-81

by

W. Hassenpflug, Manager, Systems Design and
Dr. M. Kleinschmidt
LITEF (Litton Technische Werke) der Heflige GmbH,
Loerracher Strasse 18, D 7800 Freiburg

SUMMARY

After systems hardware description the attitude, heading and vertical loops are discussed. System simulation results are compared with flight test results achieved during A 300 B4 FFC flight certification and BMFT/LITEF sponsored flight tests. Techniques for further system improvements are shortly described.

LIST OF SYMBOLS

ε = gyroscope bias
h = altitude
h_r = Reference altitude
V_r = Reference velocity
V = Velocity
R = Radius of earth (6378,388 km)
Ω = Earthrate (0,26253 rad/h)
Φ = Roll angle
Θ = Pitch angle
Ψ = Heading angle
Ψ_m = Heading angle, magnetic
P = Rollrate
Q = Pitchrate
R = Yawrate
$\ddot{Q}$ = Linear Acceleration along the Roll Axis
$\ddot{\Theta}$ = Linear Acceleration along the Pitch Axis
$\ddot{\Psi}$ = Linear Acceleration along the Yaw Axis
ω_s = Schulerfrequency $\sqrt{g/R}$
g = Gravityconstant 9,81 m/sec
∇ = Accelerometer bias

LTR-81 AHRS OVERVIEW

The LTR-81 is a member of the ARINC 705 AHRS LTR-80 Family and consists of an Attitude and Heading Reference Unit (AHRU), a Magnetic Sensor Unit (MSU), an optional Compass Controller Unit (CCU) and an optional Remote Magnetic Compensator Unit (RMCU). Within the AHRU are the inertial instruments, instrument electronics, computer module with associated memory, power supply and the electronic circuitry required for interface of the AHRS with other aircraft avionic systems. The MSU consists of a magnetic flux valve to detect the direction of the earth's magnetic field. The CCU contains controls and annunciators to facilitate manual slaving of the AHRU to the MSU when operating the AHRU in its directional gyro mode (DG). The RMCU contains provisions to power the MSU, resolve its output into sine and cosine components and provide compensation for fixed aircraft installation-related magnetic disturbances. A typical aircraft installation contains three AHRU's, two MSU's and two RMCU's. Typical AHRS outline and mounting requirements are shown in Figure 1.

Characteristic	AHRU	MSU	CCU (Optional)	RMCU (Optional)
Weight	28.6 lb	1.8 lb	0.8 lb	1.2 lb
Dimensions	7.64 in.H	2.5 in.H	1.5 in.H	2.23 in.H
	10.09 in.W	5.0 in.W	5.75 in.W	7.74 in.W
	12.72 in.D (8 MCU)	4.0 in.D	4.432 in.D	4.06 in.D
Power Dissipation	100 W (nominally loaded)			
Cooling	16 CFM @ 1/2" of water pressure drop	none	none	none
Mounting	8 MCU Tray ARINC 600	ARINC 705 Attachm.7	ARINC 705 Attachm.13	ARINC 705 Attachm.12
Input Power	115V, 400Hz, single phase			

Figure 1 AHRS Outline and Mounting Requirements

SYSTEM OPERATION AND INPUTS AND OUTPUTS

The AHRS is mechanized as a fixed gain third order system for the level and vertical channel and as a second order system for heading. A four state kalman filter is implemented to provide ground track, ground speed, horizontal velocity components, drift angle, flight path angle, magnetic track angle, wind speed and direction, provided valid VOR/DME information is available from other aircraft avionics. After turn on, the system will automatically align to the local vertical in pitch and roll, to the output of the MSU in heading and to the barometric altitude in the vertical channel. After 3 min of alignment the system enters the Normal Mode. A System Block Diagram is shown in Figure 2.

Inputs to the system are:

- 115V, 400Hz single phase primary power

- "Standard Ground" control input pins
- True Airspeed (TAS)
- Barometric Altitude
- Very high frequency Omni Range (VOR)
- Distance Measuring Equipment (DME)

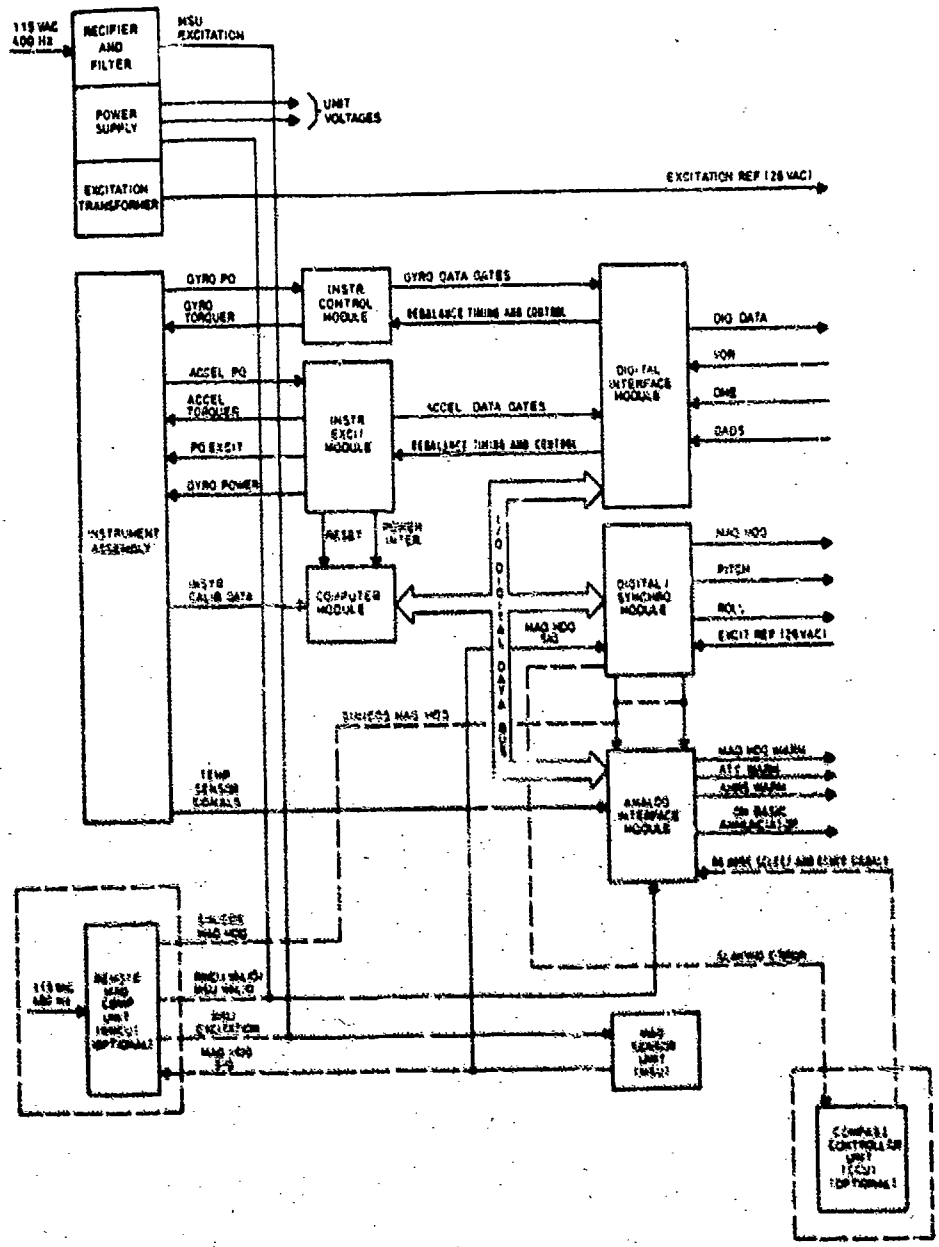

Figure 2 System Block Diagram

The VOR/DME inputs are not required to operate the AHRS in the "Normal Mode" as defined in ARINC 705.

Presently two LTR-81 configurations are in production:
LTR-81 Partnumber 106 704 installed in Airbus A 300 B4 Forward Facing Cockpit (FFC) aircraft and LTR-81-01 Partnumber 113 100-1001 installed in McDonnel Douglas MD-80 aircraft.

In the Airbus version the AHRU interfaces with two ARINC 706 air data systems, two ARINC 709 DME and two ARINC 711 VOR systems, while in the MD-80 version the interface to the two air data systems is made through ARINC 575 busses and the VOR/DME inputs are not provided by the aircraft avionics.

The digital outputs are shown in Table 1. These outputs are in accordance with ARINC 705.

In addition to these digital outputs both AHRS configurations provide analogue two and three wire outputs in accordance with the specific aircraft requirements and ARINC 561.

PARAMETER	OCTAL LABEL	SIGNAL FORMAT	MAXIMUM FILTER BANDWIDTH (HZ)	MAXIMUM TRANSPORT DELAY (MSEC)	MINIMUM UPDATE RATE (SPS)	SIGNIFICANT BITS/FIGURES	BINARY*** RANGE	SENSOR ** RANGE	APPROX RESOLUTION	ACCURACY	UNITS	POSITIVE SENSE	SELF TEST VALUE
ALONG HDG ACCEL	325	BNR	6*	60	50	12	±4	±4	.001	c-3- ±10%	G	FORWARD	.02G
BODY LATERAL ACCEL	332	BNR	6*	60	50	12	±4	±4	.001	±.01	G	RIGHT	.10G
BODY LONGIT ACCEL	331	BNR	6*	60	50	12	±4	±4	.001	±.01	G	FORWARD	.02G
1 BODY NORMAL ACCEL	333	BNR	6*	60	50	12	±4	±4	.001	±.01	G	UP	.10G
BODY PITCH RATE	326	BNR	6*	50	50	13	±128	±128	.015	.1 OR 1%	DEG/SEC	UP	10^{0}/SEC
BODY ROLL RATE	327	BNR	6*	50	50	13	±128	±128	.015	.1 OR 1%	DEG/SEC	RIGHT WING DOWN	10^{0}/SEC
BODY YAW RATE	330	BNR	6*	50	50	13	±128	±128	.015	.1 OR 1%	DEG/SEC	NOSE RIGHT	10^{0}/SEC
CROSS HDG ACCEL	326	BNR	6*	60	50	12	±4	±4	.001	c-3- ±10%	G	RIGHT	.02G
DRIFT ANGLE	321	BNR	2	110	20	11	±180	±90	.09	±5	DEG	RIGHT	-10^{0}(L)
E-W VELOCITY-MAG	324	BNR	2	110	10	15	±4096	±4096	.125	±12	KNOTS	EAST	200 KNOTS (E)
FLIGHT PATH ACCEL	323	BNR	6*	60	50	12	±4	±4	.001	c-3- ±10%	G	FORWARD	.02G
FLIGHT PATH ANGLE	322	BNR	2	110	20	11	±180	±45	.09	±1	DEG	UP	-5^{0}
GROUND SPEED	312	BNR	2	110	10	15	0-4096	0-4096	.125	±12	KNOTS	ALWAYS POSITIVE	200 KNOTS
GROUND SPEED-D	012	BCD			2	4	c-4- 0-7999	0-2000	5		KNOTS	ALWAYS POSITIVE	200 KNOTS
INERTIAL ALTITUDE	361	BNR	6*	65	25	18	±131,072	±131,072	c-3- .5	c-3- ±5 V	FEET	UP	10,000FT
INERTIAL VERT SPD	365	BNR	6*	65	25	c-3- 15	±32,768	±32,768	c-3- 1	30	FT/MIN	UP	-600 FT/MIN
AHRS DISCRETES	270	DIS		500	2	19	N/A	N/A	N/A		N/A	N/A	N/A
AHRS MAINT DISCRETE	350	DIS			2	18	N/A	N/A	N/A		N/A	N/A	N/A
AHRS TEST	277	DIS				18						N/A	
MAGNETIC HEADING	320	BNR	2	110	20	c-3- 15	±180	±180	c-3- .0055	±2	DEG	CW FROM NORTH	15^{0}
MAGNETIC HEADING-D	014	BCD			2	4	c-4- 0-799.9	0-359.9	.1		DEG	CW FROM NORTH	15^{0}
N-S VELOCITY-MAG	323	BNR	2	110	10	15	±4096	±4096	.125	±12	KNOTS	NORTH	200 KNOTS (N)
PITCH ANGLE	324	BNR	8	50	50	14	±180	±90	.011	.5	DEG	UP	5^{0}
PITCH ATT RATE	336	BNR	8*	50	50	13	±128	±128	.015	.1 OR 1%	DEG/SEC	UP	10^{0}/SEC
PLATFORM HEADING	314	BNR	2	110	10	11	±180	±180	.09	c-4- 5	DEG/HR	CW FROM ZERO DEG	22.5^{0}
ROLL ANGLE	325	BNR	8	50	50	14	±180	±180	.01	.5	DEG	RIGHT WING DOWN	45^{0} (R)
ROLL ATT RATE	337	BNR	8*	50	50	13	±128	±128	.015	.1 OR 1%	DEG/SEC	RIGHT WING DOWN	10^{0}/SEC
TRACK ANGLE RATE	335	BNR	8*	40	25	11	±32	±32	.015	.25	DEG/SEC	CW	4^{0}/SEC
TRACK ANGLE-MAG	317	BNR	2	110	20	c-3- 15	±180	±180	c-3- .0055	±6	DEG	CW FROM NORTH	5^{0}
TRACK ANGLE-MAG-D	053	BCD			2	4	c-4- 0-799.9	0-359.9	.1		DEG	CW FROM NORTH	10^{0}
1 VERTICAL ACCEL	364	BNR	8*	60	50	12	±4	±4	.001	±.01	G	UP	0.1G
WIND DIRECT-MAG	272	BNR	2	110	10	8	±180	±180	.7	±10	DEG	CW FROM NORTH	30^{0}
WIND DIRECT-MAG-D	056	BCD			2	3	c-4- 0-799	0-359	1		DEG	CW FROM NORTH	30^{0}
WIND SPEED	315	BNR	2	110	10	8	0-256	0-276	1	±12	KNOTS	ALWAYS POSITIVE	100 KNOTS
WIND SPEED-D	015	BCD			2	3	0-256	0-256	1		KNOTS	ALWAYS POSITIVE	100 KNOTS
POTENTIAL VERT SPD	360	BNR	8*	65	25	13	±32,768	±32,768	4	30	FT/MIN	UP	-600 FT/MIN

1 When aircraft is resting on the ground, output is to be zero.

* SECOND ORDER BUTTERWORTH CHARACTERISTICS OR EQUIVALENT REQUIRED

@ Accuracy specified with constant altitude input and filter at steady state with no error assumed in air data input.

** Accuracy specified refers to the absolute accuracy of the sensor and should not be confused with resolution.

c-4- *** Sensor range is the maximum range of measurement of the sensor. The binary range is the output value at which all bits of the data word are set to "1". Very often the binary range will exceed the measurement range of the sensor.

Table 1 AHRS Digital Outputs

HARDWARE DESCRIPTION

The MSU is a standard magnetic flux valve sensing unit and has so far been provided by the aircraft companies.

The RMCU as installed in the A 300 B 4 FFC is shown in Figure 3.

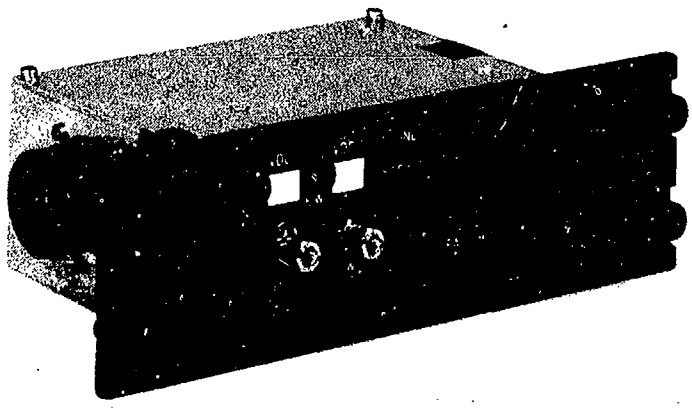

Figure 3 Remote Magnetic Compensation Unit

The MD-80 installation does not require a RMCU and the necessary scott-transformers are incorporated in the LTR-81-01 AHRU. The LTR-81 AHRU is shown in Figure 4.

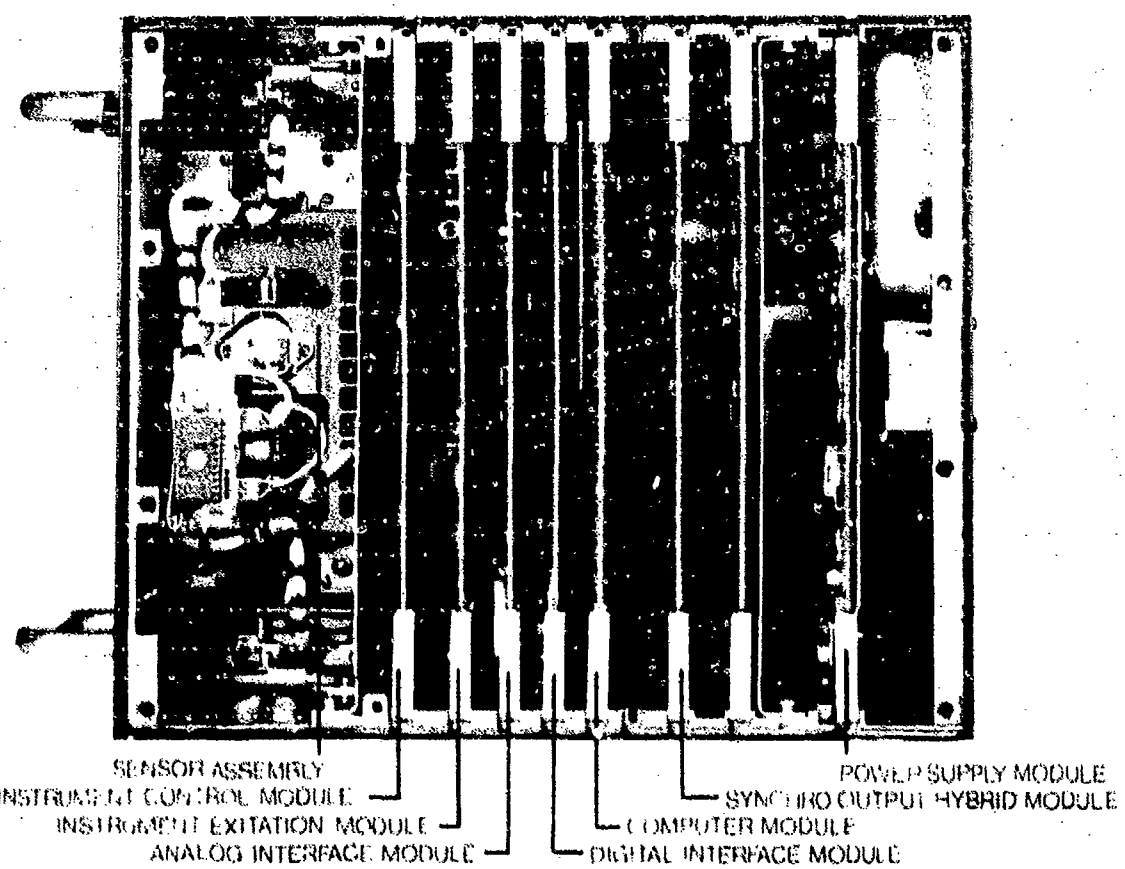

Figure 4 Top View of LTR-81 AHRU

In order to meet the MD-80 requirements, the LTR-81-01 AHRU contains two analogue output boards and additional scott-transformers to accept MSU signals without RMCU's.

The inertial instruments which actually measure the aircraft motion along and around the aircraft principle axis are mounted on the sensor block which is shown in Figure 5.

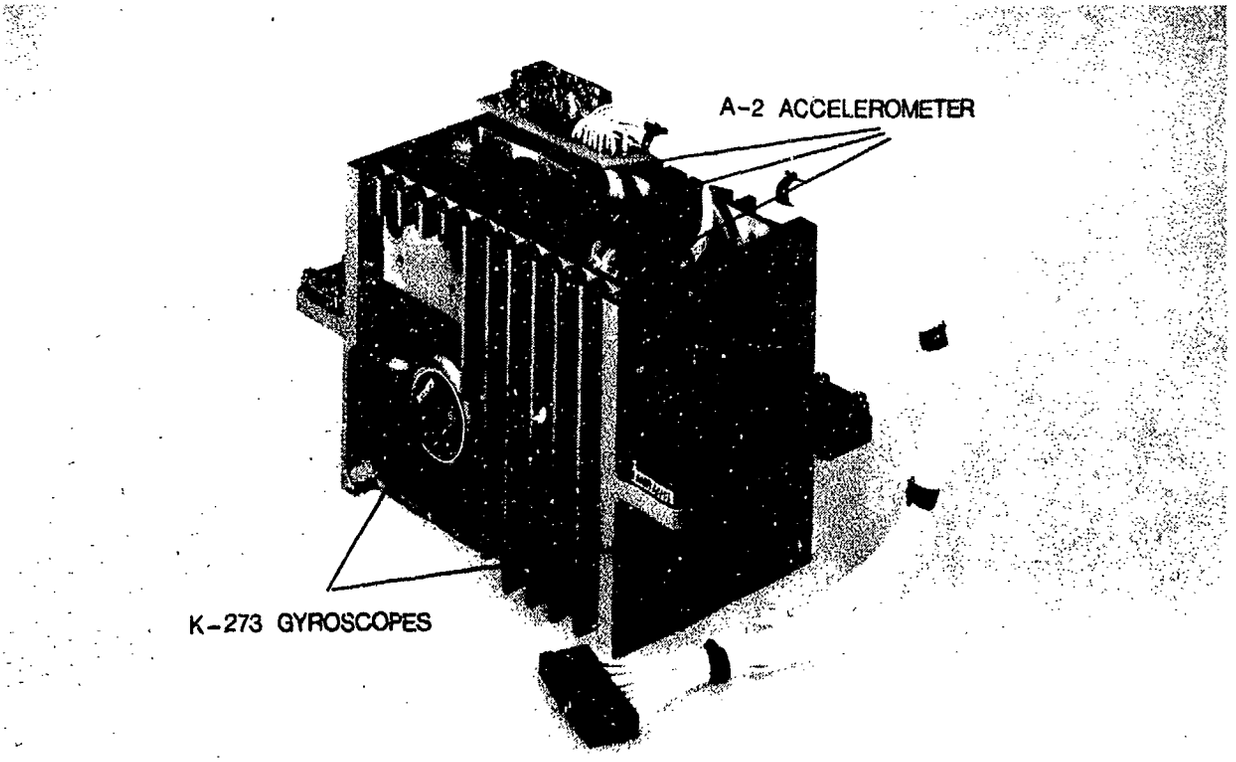

Figure 5 Sensor Assembly

For clarification purposes some harness has been removed for this figure. Together with the inertial instruments an UV E-PROM is located on the sensor block. This memory contains all instruments and systems calibration data as axis misalignment, gyroscope bias, gyro spin frequency, scalefactor temperature coefficient, accelerometer bias etc.

The inertial instruments mounted on the sensor block are:

- two two-degree-of-freedom dry tuned gyroscopes K-273 and
- three pendulous dry accelerometers A-2

The principle of a dry tuned gyroscope is presented in Figure 6.

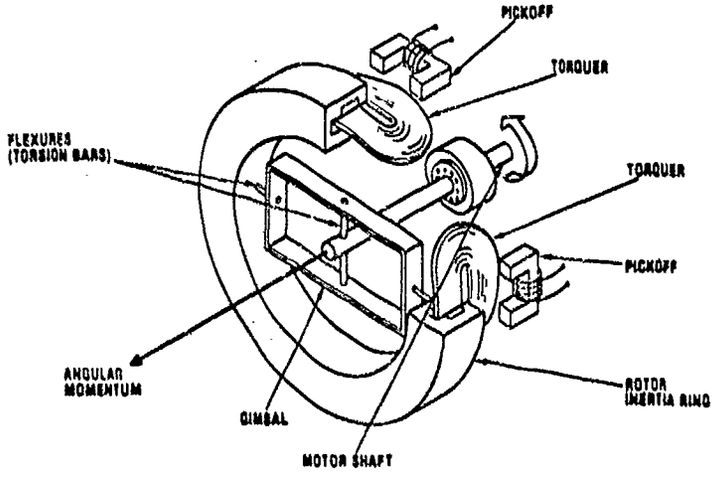

Figure 6 Principle of a Dry Tuned Gyroscope

The actual K-273 cut off view is shown in Figure 7.

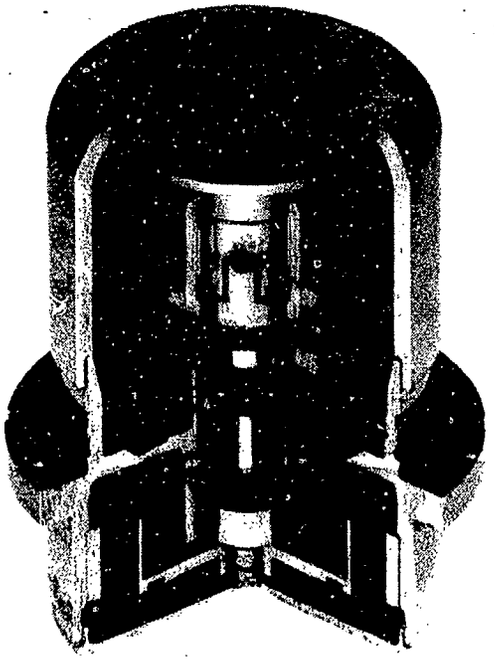

Figure 7 K-273 Dynamically Tuned Twin Axis Gyroscope

K-273 Characteristic figures are presented in Table 2 below.

Type	Two-degree-of-freedom
Weight	250 gms
Size	1.8 in. diameter, 2 in. long
Motor Type	3-phase hysteresis-synchronous
Time Constant	5 seconds
Runup Time	< 30 seconds
Torquer Scalefactor	0.3 ± 0.1 degree/sec/milliampere
Torquer Nonlinearity	±0.2% max
DC Torquing Current	±0.5 A continuous, ±1 A max
Torquer Misalignment	< 1 degree
Spin Exitation Frequency	720 Hz ± 10%
Spin Exitation Voltage	20 V ±0.5 V pp line to neutral
Spin Power	9 watts max
Random Drift	0.3 degrees/hour
"g" Sensitive Drift Repeatability	0.3 degrees/hour/g

Table 2 K-273 Gyroscope Characteristics

As the AHRS uses two two-degree-of-freedom gyroscopes the redundant gyro axis is used to perform a very powerfull test.

It should be mentioned that the sensor block is hard mounted to the AHRU chassis in the A 300 B4 FFC installation and due to higher environmental (shock & vibration) stresses in the MD-80 isolated by means of shockmounts in the LTR-81-01 version. Due to the large usage of the LITTON A-2 accelerometer made in commercial aircraft inertial navigation systems like LTN-72 no specific attention is given to that instrument in this paper.

The Computer Module (CPM) is a self contained general purpose single board computer utilizing two Z-8002 microprocessors. The logic on board provides the clock, control and buffering circuit to enable the two microprocessors to be the system controllers.

The board also contains 20 k x 16 bit of program memory and 3 k x 16 bit of scratch pad area. As illustrated in Figure 8 the module is organised for distributed processing with CPU # 1 being dedicated to computation tasks while CPU # 2 is dedicated to service all input-output functions. Since each computer has its own adress and databus, they may operate asynchronously.

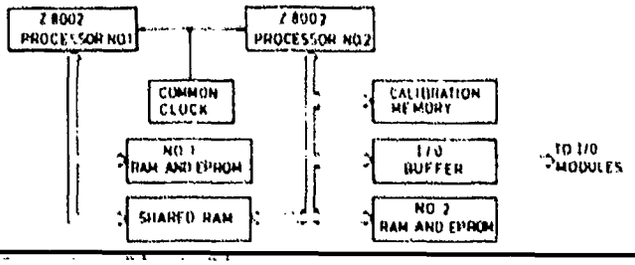

SYSTEM MECHANIZATION

The mechanization schematic is shown in Figure 9.

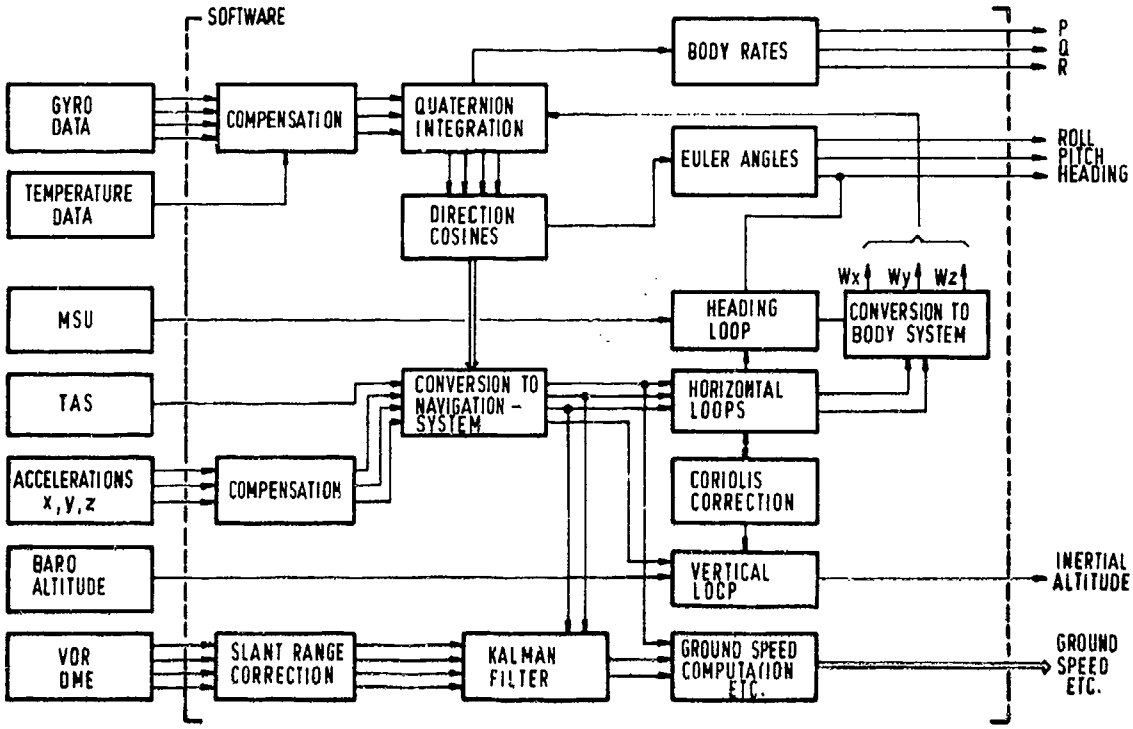

Figure 9 LTR-81 Mechanization Schematic

This mechanization schematic briefly conveys information of the interconnection of the main computational tasks. It can be seen that the instrument outputs are compensated for all errors which can be measured at the system level. It should be noted that instruments always include their appropriate caging electronics when looked at from a systems point of view.

Due to specific caging and digitizing schemes used angular increments and velocity increments are processed. In order to provide body angular rates and body acceleration a division by Δt is performed. As no "Angle of Attack" and "Side Slip Angle" is provided "TAS" could not be resolved exactly in the body coordinate frame but it was found that this shortcoming could be neglected in lieu of the system performance required.

For simplicity the cut-out-logic and the mode switching as contained in the actual LTR-81, LTR-81-01 AHRS will be neglected in the following discussion of the initial alignment and the system augmentation.

Besides the "Initial Alignment" the AHRS performs in the "Normal Mode" with TAS, Magnetic Heading and Barometric Altitude provided. The system will be switched into the "DG-Mode" whenever the Magnetic Heading is not available - either it is cut out intentionally in maneuvers to prevent flux valve errors effecting the output heading or it fails. The system switches into the "Basic Mode" whenever "Air Data" (TAS & Barometric Altitude) is not available.

A hysteresis is implemented to prevent the system from following Air Data transients. For simplicity again the very extensive BITE processing contained in the actual system to provide the required confidence in the software reliability for "CAT III" and "Autoland" procedures will be neglected. As no latitude is provided by the aircraft avionics the system must be able to estimate the respective earthrate components. This requires integrating feedback loops which are used to estimate the respective gyro bias components as well. The choice of time constants is then a compromise between the steady state accuracy and the tolerable transients caused by the aircraft dynamics, because the fixed gain system is always dynamically incorrect but simple.

INITIAL ALIGNMENT

The "Initial Alignment" phase is in principle required to establish the reference coordinate system in the navigation or local horizontal frame and consists of the levelling, the earthrate and gyroscope bias estimation, heading determination and the vertical loop alignment. Levelling is performed during gyroscope run up time.

HORIZONTAL LOOP

Based on the horizontal loop error block diagram /1/ presented in Figure 10,

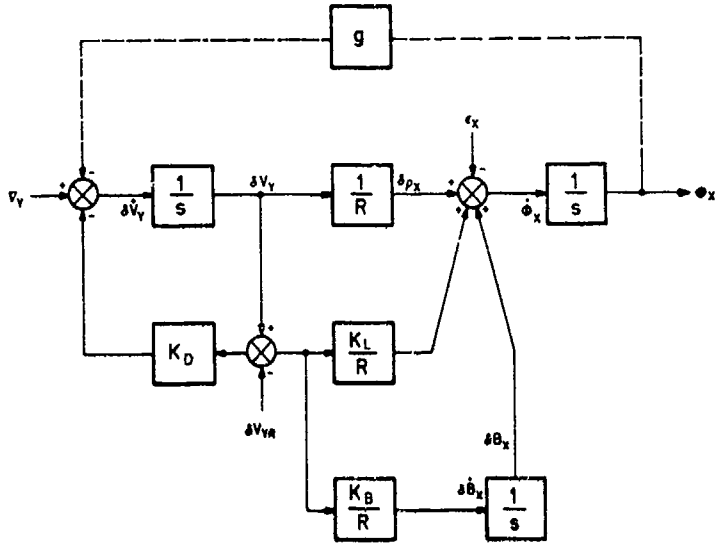

Figure 10 Horizontal Loop Error Block Diagram

It is easily seen that for the steady condition

$$\delta V\ (t\to\infty) = \delta V_{yR} \qquad (1)$$

$$\Phi_x\ (t\to\infty) = \frac{V_y}{g} \qquad (2)$$

$$\delta B\ (t\to\infty) = \Omega_x + \epsilon_x - \frac{\delta V_{yR}}{R} \qquad (3)$$

with $\frac{\delta V_{yR}}{R} \ll \Omega_x + \epsilon_x$

earthrate and gyroscope bias components are estimated.

For the "Initial Alignment" it is required that the aircraft is kept stationary and enough time (180 sec) is available to estimate gyro bias and earthrate components accurately enough. This should be no problem for a transport aircraft.

During the "Initial Alignment" V_R is set to zero and the system time constants are selected to achieve a quick and reliable earthrate and gyroscope bias estimation even in the presence of unavoidable aircraft disturbances due to wind buffeting and / or aircraft loading.

It is well understood that a kalman filter design could have enhanced the system performance but as the required performance could be achieved with a much more simple fixed gain system the simplest possible design was chosen. For the reasoning given above the alignment phase is divided into two parts. Phase I with a system time constant of 5 sec lasts for 30 sec and provides a rapid earthrate and gyroscope bias estimation. This phase is followed by Phase II with a system time constant of 30 sec for the remaining 150 sec of alignment. During this period the earthrate and gyroscope bias estimation is settled to its final value and any aircraft disturbances which might have been occured during Phase I are completely eliminated within the performance requirements limits. Aircraft disturbances which might have been introduced in Phase II are of negligible effect to the system performance. After the 180 sec of alignment have been elapsed the system automatically enters the "Normal Mode".

HEADING LOOP

Based on the Heading Loop Error Block Diagram /1/ presented in Figure 11,

one can find that for the steady state condition

$$\delta\psi\ (t\to\infty) = \delta\psi_m \qquad (4)$$

$$\delta\dot{\psi}\ (t\to\infty) = \Omega_z + \epsilon_z \qquad (5)$$

and therefore the system estimates the vertical earthrate and the appropriate gyroscope bias. As heading rate and earthrate to be estimated could easily be in the same order of magnitude the Phase I and II systems time constant is 40 sec. After the 180 sec of alignment have been elapsed the "Normal Mode" is entered automatically.

With the bias integrator implemented in the heading loop the z-gyro bias will not

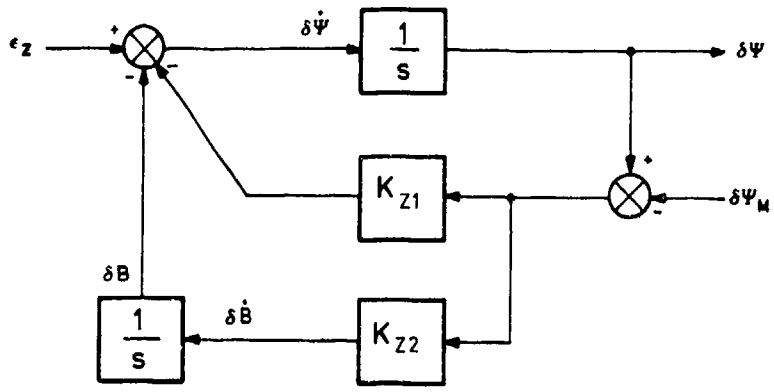

Figure 11 Heading Loop Error Block Diagram

VERTICAL LOOP

Based on the Vertical Loop Error Block Diagram /1/ provided in Figure 12 ,

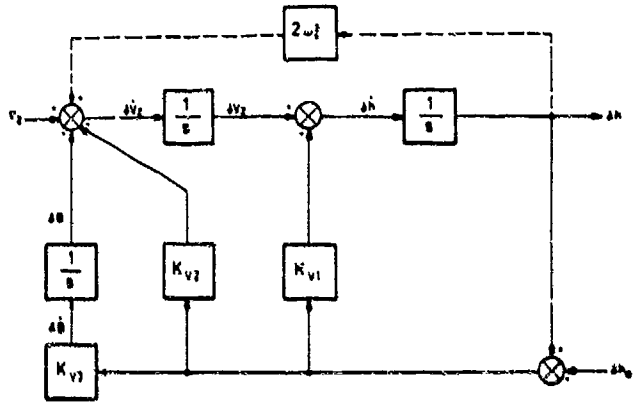

Figure 12 Vertical Loop Error Block Diagram

we get for the steady state condition

$$\delta V_z \ (t\to\infty) = 0 \qquad (6)$$

$$\delta h \ (t\to\infty) = \delta h_R \qquad (7)$$

$$\delta B \ (t\to\infty) \propto V_z + 2\omega_s \cdot \delta h_R \qquad (8)$$

Advantageous in this third order mechanization is the estimation of z-accelerometer bias, the elemination of vertical velocity errors and the altitude errors are the reference altitude errors. During alignment the reference altitude is set to zero and a 30 sec time conscant is implemented. After 180 sec of alignment have been elapsed the loop enters the "Normal Mode" automatically.

NORMAL MODE

For the horizontal loop or level channels the only difference to the alignment mechanization is the system time constant and the appropriate TAS component for augmentation purposes. The proper selection of the system time constants depends very much on the vehicl dynamics and the gyroscopes error figures. Furthermore transient effects during "Take Off" when TAS is made available at approximately 110 knots must be minimized. This all led to a system time constant of 240 sec in the "Normal Mode".

The only difference between alignment and Normal Mode for the heading loop is the system time constant. Again the criteria for the time constant selection are the gyroscope drift figures and the dynamic behavior of the MSU. In addition to this cut-out-levels needed to be defined to prevent MSU-errors effecting output heading performance. Due to the excellent low drift characteristic of the K-273 used a large time constant of 200 sec could be selected and the cut-off-levels could be set that during aircraft maneuvres the system enters the "DG-Mode" most of the time.

In the vertical loop a 50 sec time constant is selected and the barometric altitude is the reference altitude.

It must be pointed out that the selected mechanization depends on the accuracy and quality of the sensors used for system augmentation. On the other hand the mechanization implemented offers the opportunity to achieve considerable good system accuracy with considerable cheap instruments of appropriate accuracy.For example gyro bias tempe-

DG-MODE

As already mentioned this mode is entered automatically whenever the MSU signal is not available.

BASIC MODE

This mode is entered automatically whenever "Air Data" (TAS & Barometric Altitude) is not available for more than 5 minutes. In this mode the horizontal loops are reduced to a critical damped second order loop with a time constant of 15 sec and the vertical loop is reduced to a second order critically damped loop with a 15 sec time constant as well.

SYSTEM MECHANIZATION ENHANCEMENT POSSIBILITIES

During the LTR-81 design phase extensive error simulations were carried out based on a six degree of freedom simulation program developed at LITEF. The flight profile used was comprised from inputs received from various sources including Deutsche Lufthansa and Aeroproducts Division of Litton Industries (ADP). The goal was to design the most realistic profile probable.

Since these early days of LTR-81 design discussions are in progress how the system performance could be enhanced if required. There are several ways how this could be accomplished without increasing inertial instruments performance requirements. First the dynamically incorrect but simple fixed gain system could be replaced by a sophisticated optimal gain system. Second the necessity to use a magnetic heading reference could be eliminated by implementing a multi-position gyrocompassing scheme. This mechanization offers a very good heading determination accuracy with medium to low accurate gyroscopes because the random and day to day drift repeatability of the gyros are compensated for the price of an accurate turn table.

In the meantime a 15 state kalman filter has been rigorously tested in a simulated highly dynamic helicopter environment. Additionally multi-position gyrocompass mechanizations have been designed and they are ready for implementation if required by system performance specifications.

Using the inertial instruments available to LITEF there is presently no need to enhance the LTR-81 mechanization in order to meet the system performance specification presented in Table 1.

SOFTWARE DEVELOPMENT

The software was developed following the TOP-Down-Design Philosophy. This will give the necessary visibility to the approving agencies. The schematic development process is shown in Figure 13. Due to real time requirements, real estate allocated for the CPU, and software verification requirements assembler language with very strict coding rules was used. Software tools have been developed to support design reviews, configuration and change control and visibility from requirements to test and vice versa. A detailed description of the methods used can be found in /2/.

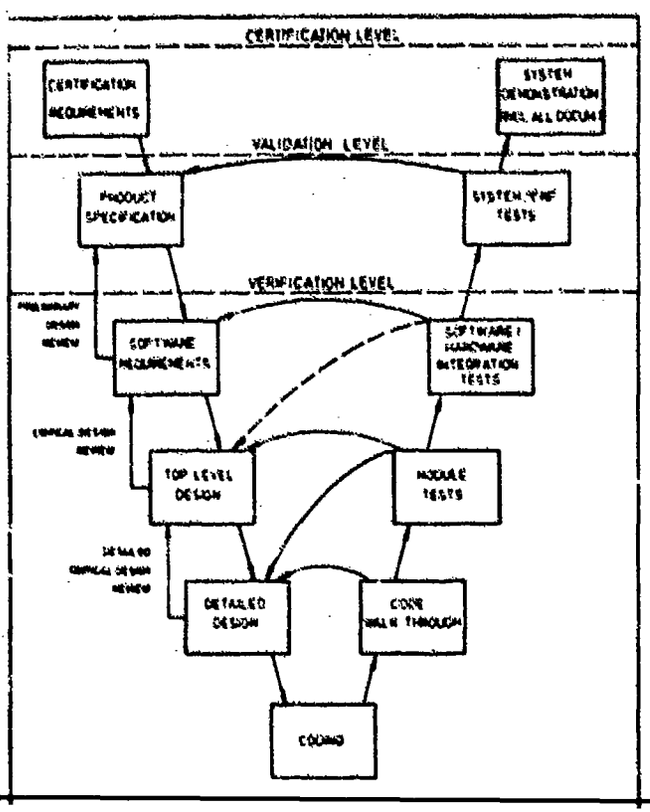

AHRS CERTIFICATION AND FLIGHT TEST RESULTS

The LTR-81 has been certified for installation in the A 300 B 4 FFC aircraft since April 1982 and the LTR-81-01 has been certified for installation in the MD-80 aircraft since December 1983. TSO's for both versions are expected to be granted in the very next future. The equipment has been classified "Flight Critical" and the required rigorous software verification in accordance with RTCA DO-178 has been performed successfully with BOCA (Bureau Officielle de Certification Airbus) and FAA. The Airbus version is in service since April 1982 and has since then accumulated more than 50,000 operating hours and a hardware reliability (MTBF) of more than 5,000 hours has been achieved. The software has not been touched since certification.

The operational integrity of the two AHRS configurations was demonstrated throughout the environmental tests designed in accordance with RTCA DO-160 A and the specific aircraft manufacturers requirements. These environmental tests included shock, vibration (sinosoidal & random), temperature, temperature shock, humidity, pressure drop, EMC and lightning.

The first flight tests were performed during the development phase using a Merlin IV twin turboprop engine aircraft. During these early flight tests the adequate performance of the K-273 gyroscope and the selected system mechanization was verified.

The principle flight test installation included an Inertial Navigator as attitude and heading reference, a tape recorder and the appropriate aircraft avionic to provide the LTR-81 with air data, magnetic heading and VOR/DME signals.

Airbus provided a specifically equipped A 300 B 4 aircraft with the necessary equipment installed for all kinds of flight tests required. As an inertial reference a LTN-72 was used. Before however the system could be installed in the test aircraft (ship 003) extensive laboratory tests at SNIAS were carried out. At this laboratory for example the AHRU could be integrated with actual aircraft avionics like the air data system and actual static and dynamic pressure changes could be exercised. Thus a very good verification of the baro-inertial loop could be performed and software adaptations to specific signal characteristics of the actual aircraft avionics were easily possible. After being installed in ship 003 the AHRS was tested under normal and emergency conditions in the "Normal-DG- and Basic Mode". The system was installed during Pilot Training exercising "Touch and Go's" and other abnormal maneuvres with recordings taken for AHRS evaluation purposes. Typical flight test recordings are presented in Figure 14. More flight test recordings are to be found in /3/.

Following certification for A 300 B 4 FFC installation a flight test campaign was performed in September 1982 at the DFVLR (Deutsche Forschungs- und Versuchsanstalt fuer Luft- und Raumfahrt) in Braunschweig. The flight test was part of a contract with the BMFT (Bundesministerium fuer Forschung und Technologie). The available test bed was a Dornier DO-28 aircraft equipped with a Carousel IV as attitude and heading reference, VOR/DME receivers and air data equipment. Due to flight safety regulations the MSU had to be installed within the aircraft's cabin and therefore no undisturbed location could be found. After calibration the residual north-south error component was smaller than +/- 1 degree but the east-west residual error component was as high as 2.5 degrees. Typical flight test recordings are presented in Figure 15. More recordings to be found in /1/.

It should be noticed that in evaluating INS heading versus AHRS heading one must take the local magnetic variation and time delays caused by output filtering into consideration.

The flight tests carried out with Airbus Industries/SNIAS and DFVLR, the laboratory tests at SNIAS and the environmental tests demonstrated that the LTR-81 meets or exceeds the ARINC 705, DO-178, DO-160 A and Airbus Industries/SNIAS requirements.

Comparing the flight test recordings achieved during A 300 B 4 and DO-28 flight tests with simulation results presented in Figures 16-18 it can be seen that simulation- and flight test results match very well. This gives good confidence in the simulation repertoire developed at LITEF.

Flight tests with McDonnel Douglas started in March 1983 using a DC-9 aircraft (ship 909). Many flight test hours have been accumulated in the DC-9 and Merlin aircraft until the certification flight was performed in a production MD-80 aircraft.

Unfortunately flight test results from McDonnel Douglas are only available in form of listings. Records like the ones from SNIAS and DFVLR are not yet available for publication.

The accuracy of aircraft motion signals (P,Q,R,Ø,Ψ,Θ) could not be evaluated during flight tests due to the lack of appropriate reference systems. These parameters have been extensively tested during the dynamic system performance verification tests carried out at LITEF, SNIAS and APD.

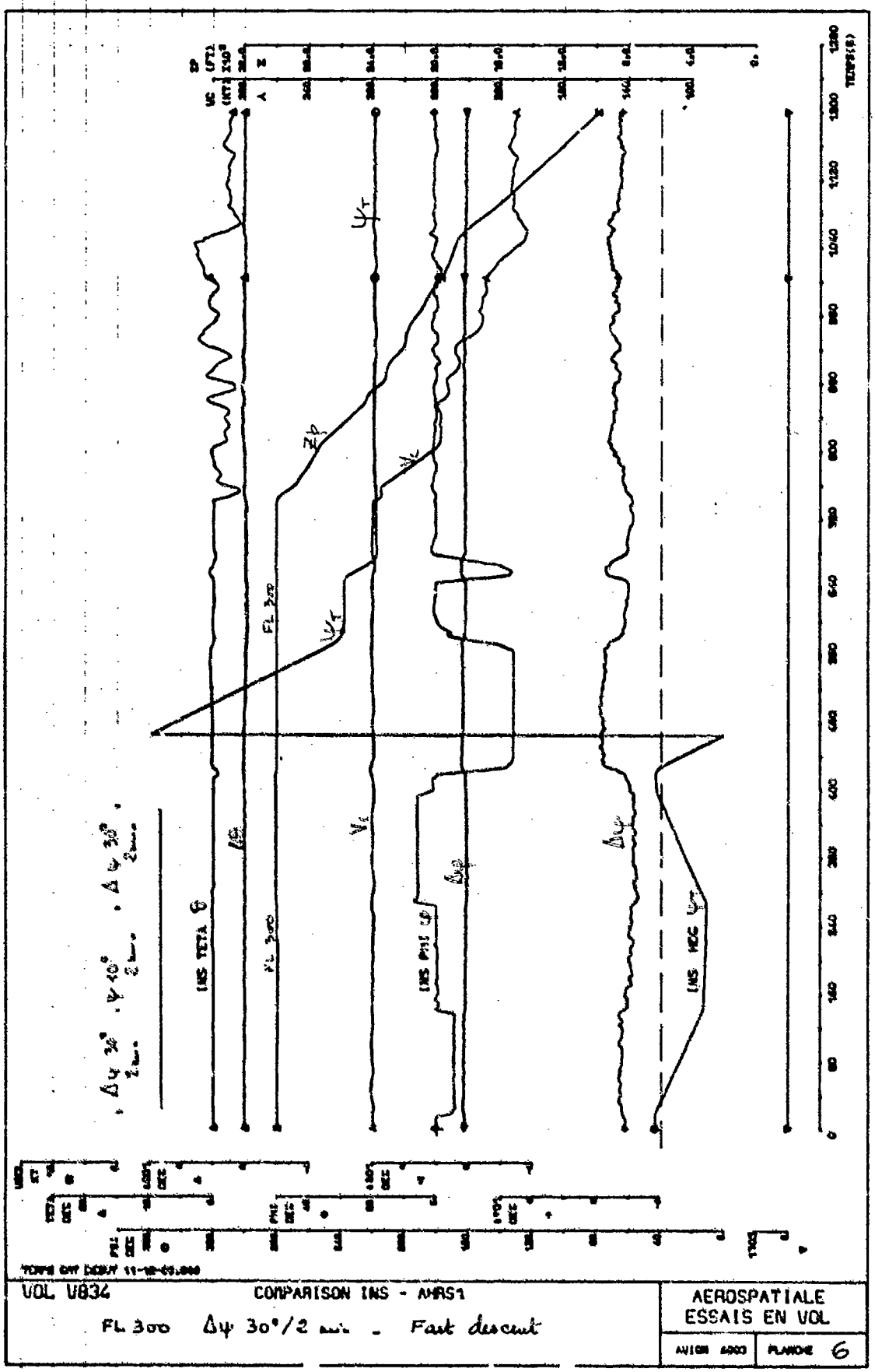
INS TETA θ
INS PHI φ
INS HDG ψ
FL 300
TEMPS(S)
VOL V834
COMPARISON INS - AHRS1
FL 300 Δψ 30°/2 min - Fast descent
AEROSPATIALE
ESSAIS EN VOL
AVION A300
PLANCHE 6

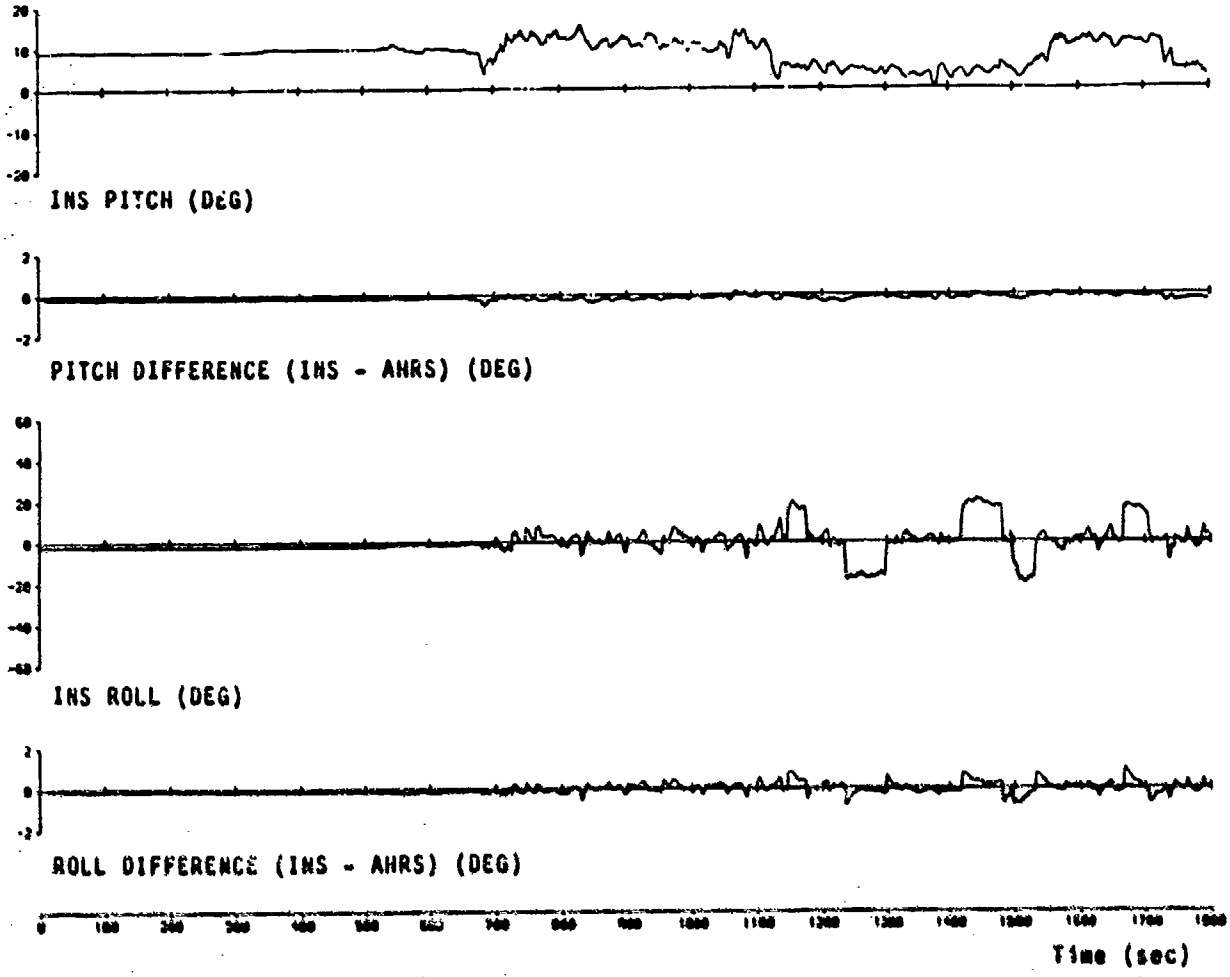

Figure 15 Typical Flight Test Record with Dornier DO-28

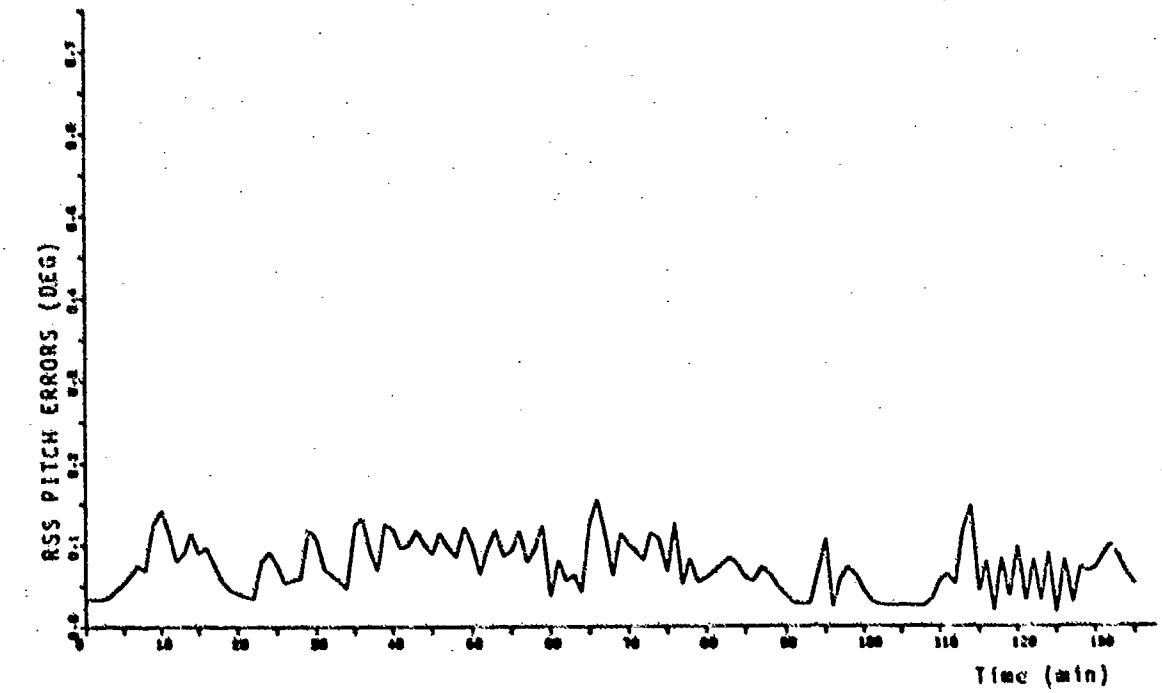

Figure 16 Simulation Results (Pitch Error)

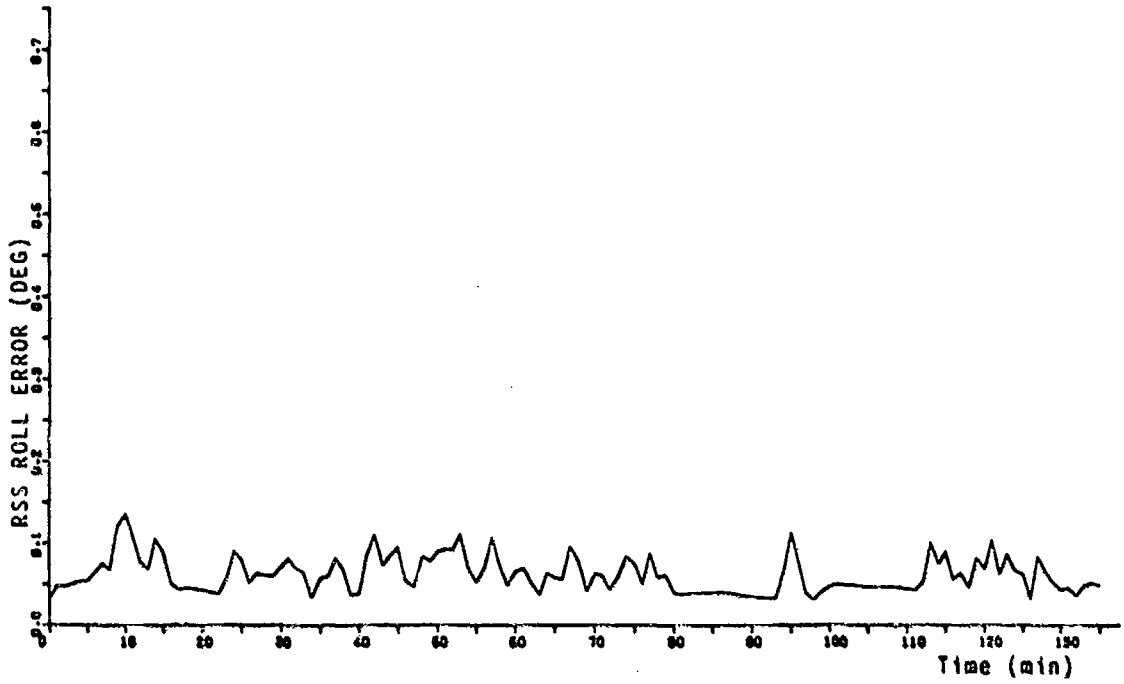

Figure 17 Simulation Results (Roll Error)

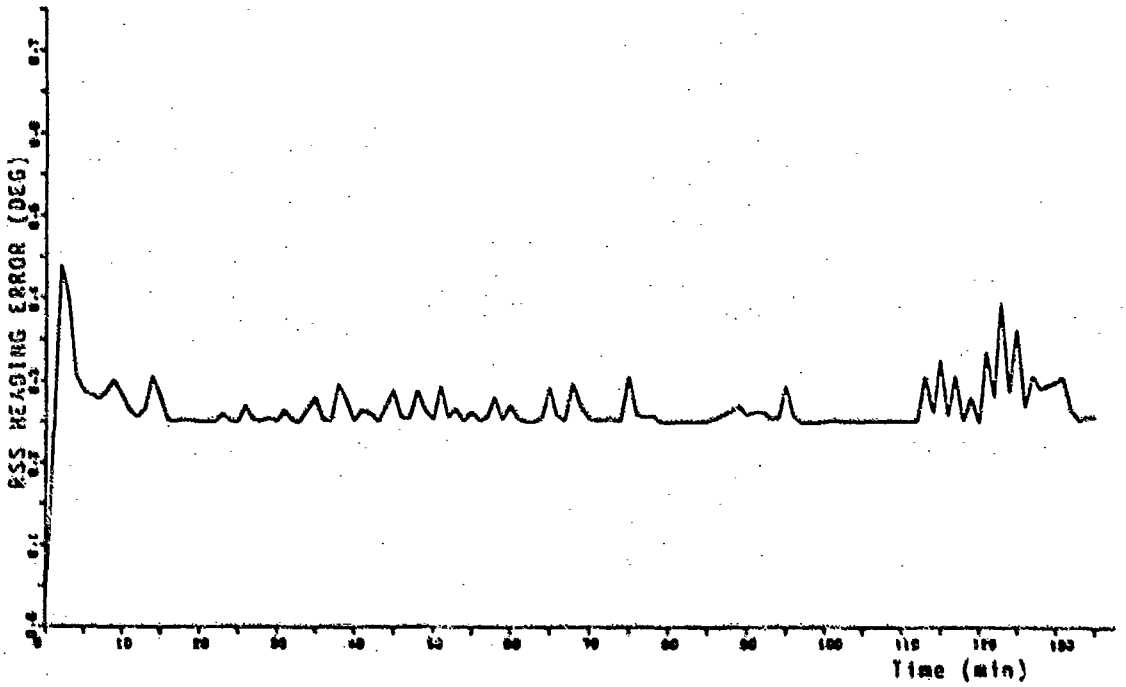

Figure 18 Simulation Results (Heading Error)

REFERENCES

/1/ G. Everett, K. Keller, U. Kirchhoff, D. Ozdes — Bundesministerium fuer Forschung und Technologie Forschungsbericht (LFL 7974) Luftfahrtforschung / -technologie Teil 1: Entwicklung eines standardisierten dreiachsigen Strapdown-Sensors zur inertialen Messwerterfassung fuer zukuenftige Flugregelsysteme

/2/ H. Kleinschmidt, N. Sandner — Software Certification of a Civil Avionic AHR-System AGARD CP 330 Software for Avionics p 31-1 + 31-9

Test und Verifikation der Software von Kurs- und Lagereferenz-Systemen
DGLR Symposium: Test und Verifikation von Software bei digitalen Systemen der Luft- und Raumfahrt 25./26. Oktober 1983

/3/ LTR-81 Design File (internal report)

AGARD Lecture Series No. 133

Advances in Strapdown Inertial Systems

This Bibliography with Abstracts has been prepared to support AGARD Lecture Series No. 133 by the Scientific and Technical Information Branch of the U.S. National Aeronautics and Space Administration, Washington, D.C., in consultation with Dr. G.T. Schmidt of Cambridge, Massachusetts.

UTTL: Unified analysis methods for a fault tolerant redundant strapdown inertial measurement unit
AUTH: A/MORRELL, F. R.; B/MOTYKA, P. PAA: A/(NASA, Langley Research Center, Hampton, VA); B/(Charles Stark Draper Laboratory, Inc., Cambridge, MA) CORP: National Aeronautics and Space Administration, Langley Research Center, Hampton, Va.; Draper (Charles Stark) Lab., Inc., Boston, Mass. Institute of Electrical and Electronics Engineers and American Institute of Aeronautics and Astronautics, Digital Avionics Systems Conference, 5th, Seattle, WA, Oct. 31-Nov. 3, 1983, Paper, 11 p.
ABS: The use of a redundant strapdown inertial measurement unit (RSDIMU) has been considered as a source of sensor information for future aircraft. It is pointed out that failure detection and isolation (FDI) should be accomplished at the sensor level to ensure the accurate transfer of information to elements of the integrated avionics system. The present investigation is concerned with the impact of the FDI algorithm on system reliability and vice versa. A description is given of a technique to identify and assess critical areas of reliability requirements for the RSDIMU. Attention is given to the development of an FDI algorithm to meet these requirements. 83/10/00 84A10670

UTTL: The use of hypercomplex numbers in the algorithms for the operation of a strapdown inertial navigation system
AUTH: A/ONISHCHENKO, S. M. PAA: A/(Akademiia Nauk Ukrainskoi SSR, Institut Matematiki, Kiev, Ukrainian SSR) Mekhaniku Giroskopicheskikh Sistem (ISSN 0203-3771), no. 1, 1982, p. 59-66, In Russian.
ABS: An analysis is made of an algorithm for the ideal operation of strapdown inertial navigation systems. The algorithm is expressed in terms of the geometrical vectors of Euclidian space, Euler parameters, finite rotation vector, quaternions, and matrices of the Rodrigues-Hamilton and Cayley-Klein parameters. The possibility of creating a new type of hybrid computer for the numerical processing of algorithms for the operation of strapdown inertial navigation systems is discussed. 82/00/00 83A44637

UTTL: Design of an integrated strapdown guidance and control system for a tactical missile
AUTH: A/WILLIAMS, D. E.; B/RICHMAN, J.; C/FRIEDLAND, B. PAA: C/(Singer Co., Kearfott Div., Little Falls, NJ) IN: Guidance and Control Conference, Gatlinburg, TN, August 15-17, 1983, Collection of Technical Papers (A83-41659 19-63), New York, American Institute of Aeronautics and Astronautics, 1983, p. 57-66.
ABS: An integrated guidance and control system for tactical missiles is designed using optimum control and estimation theory. Sensors used in this design consist of strapdown accelerometers and rate gyros and a strapdown homing seeker. Error sensitivities and performance characteristics are given for an intercept scenario involving a thrusting bank-to-turn missile against a maneuvering target. For a co-altitude parallel offset (sidestep) maneuver, miss distances with perfect sensors were less than 4 feet. The principal sensor error sources were found to be seeker quantization and gyro scale factor errors. In addition it was found that seeker cutoff prior to impact, i.e., 'blinding' and the seeker sampling interval has an important effect on end-game performance and terminal miss distance.
RPT#: AIAA PAPER 83-2169 83/00/00 83A41665

UTTL: Kalman filter formulations for transfer alignment of strapdown inertial units
AUTH: A/SCHNEIDER, A. M. PAA: A/(California, University, La Jolla, CA) Navigation (ISSN 0028-1522), vol. 30, Spring 1983, p. 72-89.
ABS: Formulations of Kalman filters are obtained which are capable of aligning one strapdown inertial sensor assembly with another by estimating the misalignment angle between them. One strapdown inertial sensor assembly could be in the cockpit of a fighter aircraft and the other could be in a missile on the wing. One formulation treats the case of a fixed misalignment and another formulation treats the case of a dynamic misalignment, caused, for exammple, by bending of the common supporting body. It is shown that measurements can be made by gyros only, or by gyros plus accelerometers. Also examined are filters which estimate inertial sensor error parameters. 83/05/00 83A40303

UTTL: Performance characterization of the dry tuned-gimbal gyro for application to precision spacecraft attitude reference systems
AUTH: A/DONOGHUE, P. J. PAA: A/(Teledyne Systems Co., Northridge, CA) IN: Automatic control in space 1982: Proceedings of the Ninth Symposium, Noordwijkerhout, Netherlands, July 5-9, 1982 (A83-37432 17-18), Oxford, Pergamon Press, 1983, p. 433-442.
ABS: An analytical characterization of the dry-tuned gyro used in strapdown gimballed inertial navigation systems is presented. The dynamic behavior of a gyro is expressed in terms of equations for the case rates.

pickoff rates, misalignments, the angular momentum vector, the time rate of change of the motor torquer angle, and the torques. Static equations are presented for fixed bias errors, the apparent scale factor for relating torque measurements to true rate, the acceleration sensitivities, and misalignments of the gyro case frame from a system-level reference frame. Bandwidth selection for digital sampling of the rate output and aliasing are discussed in terms of tradeoffs. Optimized filtering techniques are required for spacecraft applications in order to achieve high accuracy and low noise. The filtering is carried out through computations of the power spectral density at the rate or angle level, together with autocorrelation functions to detect the random drift of the dry tuned gyro. 83/00/00 83A37476

UTTL: A new strapdown attitude algorithm
AUTH: A/MILLER, R. B. PAA: A/(Department of Defence, Aeronautical Research Laboratories, Melbourne, Australia) Journal of Guidance Control, and Dynamics (ISSN 0731-5090), vol. [illegible], July-Aug. 1983, p. 287-291.
ABS: This paper develops the application to the strapdown attitude problem of the rotation vector concept, in which obtaining a solution for the rotation vector and updating the attitude quaternion are considered entirely separately. A new rotation vector algorithm is derived which takes three samples of gyro data per update, and offers greatly improved coning performance. This is obtained by making the assumption that gyro output varies according to a third-order time relationship, rather than second or first order as in other algorithms. Performance of the three sample algorithm is compared with well-known algorithms in a coning environment and in a random motion environment. The quaternion updating may be performed to whatever degree of accuracy is required: An economical modified fourth-order algorithm is proposed, and its comparative performance shown. This approach to the problem gives versatility in that computing resources use may to some extent be tailored according to the relative extents of coning and of fixed axis rotation in the expected environment. 83/08/00 83A37068

UTTL: Institute of Navigation, Annual Meeting, 38th, U.S. Air Force Academy, Colorado Springs, CO, June 14-17, 1982, Proceedings Washington, DC, Institute of Navigation, 1982, 137 p.
ABS: Topics examined include current U.S. Air Force navigator training, C-141 operations in Operation Bright Star 82, an advanced day/night sight reduction electronic sextant, techniques of VOR area navigation, a STS-1 orbital trajectory reconstruction using unmodeled acceleration estimation, and automated nautical charts. Also discussed are submarine hazard avoidance and piloting equipment, NAVSTAR-GPS at sea, Space Shuttle onboard IMU redundancy management design, the laser gyro as a self-contained inertial navigation aid, and a reverse velocity rocket sled test bed for inertial guidance systems. In addition, other topics considered include the flight testing of a low cost inertial guidance system, a lab test to find the major error sources in a laser strapdown inertial navigator, and advanced single-channel NAVSTAR-GPS multiplex receiver with up to eight pseudochannels, and the benefits of integrating GPS and inertial navigation systems. For individual items see A83-29202 to A83-29214 82/00/00 83A29201

UTTL: National Aerospace Meeting, Moffett Field, CA, March 24, 25, 1982, Proceedings Meeting sponsored by the Institute of Navigation, Washington, DC, Institute of Navigation, 1982, 143 p (For individual items see A83-28777 to A83-28791)
ABS: The present conference topics include Space Shuttle inertial upper stage attitude initialization and update, the evaluation of inertial upper stage navigation algorithms, helicopter guidance and flight control demonstration by means of a laser gyro inertial navigation system, the Nova-1 drag-free navigation satellite, the Conex gyroscope, the performance of a helicopter strapdown ring laser gyro tetrad inertial navigation system, improved accelerometers for high accuracy strapdown inertial navigation systems, and the radar detection of low level wind shear. Also discussed are the timing of a Loran-C navigation system chain, flight demonstrations of the integrated inertial sensor assembly, a trapped readout for an electrostatically supported superconducting gyro, the fault/maneuver tolerance of aided Global Positioning System (GPS) demodulation/navigation processors, and the computer simulation of a differential GPS for civil applications. 82/00/00 83A28776

UTTL: Analysis of the precision of inertial navigation systems
AUTH: A/LOHL, N. Braunschweig, Technische Universitaet, Fakultaet fuer Maschinenbau und Elektrotechnik, Dr.-Ing. Dissertation, 1982, 154 p. In German.
ABS: The present investigation is concerned with a study of the dynamic environment of strapdown sensors, which

are directly exposed to the unsteady environmental conditions on board an aircraft. Environmental effects, such as angular vibrations and linear vibrations, have generally a detrimental effect on the navigational accuracy of the strapdown inertial system. The investigation has, therefore, the objective to use flight test data with a strapdown system as a basis for a characterization of the noise observed in the case of the gyroscope and the acceleration-measuring device of the strapdown system. Statistical analysis methods are used in connection with the data evaluation. The problem of the time dependence of the average value of the sensor signals made it necessary to employ a trend filter for the separation of the measured data into a low-frequency unsteady trend component and a high-frequency steady noise component. 82/00/00 83A26649

UTTL: An azimuth rate inertial navigation system
AUTH: A/REN, S.; B/ZHAO, Y. PAA: A/(Northwestern Polytechnical University, Xian, Shaanxi, People's Republic of China); B/(Baocheng Instrument Factory, People's Republic of China) Acta Aeronautica et Astronautica Sinica, Vol. 3, Dec. 1982, p. 61-70. In Chinese, with abstract in English.
ABS: An inertial navigation system which combines features of the platform type and the strap-down type is described. The azimuth rate is obtained from integrating azimuth rate signals measured with an azimuth gyroscope mounted on a horizontal gimbal. Details of the rate platform, the mechanization equations, the initial alignment techniques, calibration, and drift compensation are discussed. A computer simulation was performed to study error propagation characteristics arising from navigational positioning errors, the velocity errors, and attitude errors. The system offers fast alignment, calibration, and compensation of the horizontal gyroscope through use of an optical system and reference to predefined azimuth angles of land marks and geographical latitudes. The system is intended for transport aircraft and missile guidance. 82/12/00 83A26768

UTTL: Carrier Aircraft Inertial Navigation System /CAINS/ integrated system approach
AUTH: A/BRIENZA, D.; B/BELL, H. In: Integrated navigation: Actual and potential - Sea-air-space: Proceedings of the International Congress, Paris, France, September 21-24, 1982. Volume 1. (A83-24851 09-04) Paris, Institut Francais de Navigation, 1982, p. EU-P4-1-A to EU-P4-16-A.
ABS: By using a ring laser gyro to replace the spinning mass gyro employed in the conventional gimbal systems of the Carrier Aircraft Navigation System (CAINS), it has become possible to design a strapdown inertial navigation device with state-of-the-art technology application. The CAINS system also includes standard alignment/navigation software, and is integrated with the following external reference sensors: the Ship Inertial Navigation System, Doppler radar position fixes, and air data computer. Future integration will add Omega, the Global Positioning System, and attack radar. The same Single Mode Alignment filter is used to process autonomous external reference data for aided navigation, in accordance with the emphasis of the new avionics architecture on distributed microprocessors with the MIL-STD-1553 multiplex data bus. 82/00/00 83A24854

UTTL: Integration of navigation resources in modern avionics systems
AUTH: A/DEYST, J. J., JR. In: Integrated navigation: Actual and potential - Sea-air-space; Proceedings of the International Congress, Paris, France, September 21-24, 1982 Volume 1. (A83-24851 09-04) Paris, Institut Francais de Navigation, 1982, p. EU-P1-1-A to EU-P1-7-A.
ABS: An essential element of next-generation tactical aircraft integrated navigation systems will be inertial sensors capable of serving such multiple functions as flight control, pilot display, and weapon delivery, as well as navigation. In addition, fault tolerance must be an integral part of the inertial sensor design While mechanical gyros have never achieved sufficient scale factor stability to perform adequately as strapdown aircraft navigators, laser gyros are beginning to demonstrate adequate strapdown performance. Attention is given to the role naturally played by a strapdown inertial measurement package as a fault-tolerant system, as well as to gyro geometry and tactical aircraft inertial guidance system integration with such other navigation resources as the Navstar Global Positioning System. 82/00/00 83A24852

UTTL: Inertial navigation and optimal filtering
AUTH: A/KUZOVKOV, N. T.; B/SALYCHEV, O. S. Moscow, Izdatel'stvo Mashinostroenie, 1982. 216 p. In Russian.
ABS: The effect of inaccuracies in the structure and coefficients of an inertial navigation system on the data generated on an object moving on the earth's surface is investigated. The possibility of damping the free vibrations of the inertial navigation system

using the internal connections alone without resorting to the velocity and ballistic corrections is demonstrated. The platform-mounted and strapdown systems are compared in terms of accuracy. Filtering algorithms are discussed with reference to the Kalman filter and suboptimal filters. 82/00/00 83A17123

UTTL: Development of inertial navigation and its employment in measurement technology
AUTH: A/STIELER, B. PAA: A/(Deutsche Forschungs- und Versuchsanstalt fuer Luft- und Raumfahrt, Institut fuer Flugfuehrung, Braunschweig, West Germany)
DFVLR-Nachrichten, vol. 37, Nov. 1982, p. 65-69. In German.
ABS: The origin of inertial navigation can be traced to developments occurring at the turn of the century. Anschuetz-Kaempfe obtained a patent for a gyrocompass in 1905. Investigations conducted in Germany during the Second World War led to a gyrocompass which required only a time of 12 minutes to align itself in the true north-south direction. Developments occurring in Germany in the area of inertial navigation are discussed, taking into account also the utilization and further improvement of the resulting technology in connection with the development of rockets in the U.S. after the Second World War. A description is presented of the evolution of strapdown sensors and systems, giving attention to developments in Germany and the U.S. An investigation is conducted regarding the employment of inertial navigation systems in aviation measurement technology. The concept for a reference system suitable for applications in connection with the DLS microwave landing system is discussed, taking into consideration an integration of the inertial navigation system with radio and optical trajectory measurement systems. 82/11/00 83A16900

UTTL: Integrated optics strapdown inertial system
AUTH: A/WALKER, C. G. PAA: A/(U.S. Army Missile Command, Redstone Arsenal, AL) In: Integrated optics and millimeter and microwave integrated circuits; Proceedings of the Conference, Huntsville, AL, November 16-19, 1981. (A83-13753 03-33) Bellingham, WA, SPIE - The International Society for Optical Engineering, 1982, p. 16-22.
ABS: The use of previous gyro work in the development of a new and better performing strapdown inertial accelerometer is discussed. A block diagram of a common passive ring resonator is shown and discussed, and the proof-mass configuration which provides a highly directional method of measuring acceleration is shown. The theory of the passive laser accelerometer is developed, deriving the basic equation for an accelerometer using a frequency-changing external laser source. The change in optical path length is then related to the change in acceleration, and an expression is found for the acceleration sensitivity of the instrument. The operation of the passive laser gyro is the same as that of the accelerometer except that both beams must be polarized parallel to the stress. Finally, the theory and operation of a phase domain laser accelerometer is summarized, showing that with a system that can maintain polarization, the phase difference between two beams of 0.0001 deg can easily be maintained. 82/00/00 83A13755

UTTL: Unaided tactical guidance flight test results
AUTH: A/RYAN, J. E.; B/PERLMUTTER, L. D.; C/RITLAND, J. T.; D/WATERS, G. R. PAA: A/(USAF, Armament Laboratory, Eglin AFB, FL); D/(McDonnell Douglas Astronautics Co., St. Louis, MO) In: NAECON 1982; Proceedings of the National Aerospace and Electronics Conference, Dayton, OH, May 18-20, 1982, Volume 1. (A83-11083 01-01) New York, Institute of Electrical and Electronics Engineers, Inc., 1982, p. 466-473.
ABS: Results are presented for a captive flight test program, the Unaided Tactical Guidance Validation program, which was conducted using the US Air Force Low-Cost Inertial Guidance Subsystem (LCIGS) as the strapdown inertial reference assembly. The strapdown, navigation, and alignment filter software that were developed for this program are described. The Brassboard LCIGS unit was tested during the first phase of the program, and an engineering model unit was employed during the second phase. The radio-inertial Completely Integrated Range Instrumentation System served as the master navigation reference for transfer alignment and calibration during the Brassboard LCIGS tests, while the pure-inertial Carrier Aircraft Inertial Navigation System was used for the second phase of the program. Ground and flight tests were accomplished using the Central Inertial Guidance Test Facility at Holloman Air Force Base. 82/00/00 83A11140

UTTL: Inflight parity vector compensation for FDI
AUTH: A/HALL, S. R.; B/MOTYKA, P.; C/GAI, E.; D/DEYST, J. J., JR. PAA: D/(Charles Stark Draper Laboratory, Inc., Cambridge, MA) In: NAECON 1982; Proceedings of the National Aerospace and Electronics Conference, Dayton, OH, May 18-20, 1982, Volume 1. (A83-11083 01-01) New York, Institute of Electrical and Electronics Engineers, Inc., 1982, p. 380-387.
ABS: The performance of a failure detection and isolation

(FDI) algorithm applied to a redundant strapdown inertial measurement unit (IMU) is limited by sensor errors such as input axis misalignment, scale factor errors, and biases. This paper presents a technique for improving the performance of FDI algorithms applied to redundant strapdown IMUs. A Kalman filter provides estimates of those linear combinations of sensor errors that affect the parity vector. These estimates are used to form a compensated parity vector which does not include the effects of sensor errors. The compensated parity vector is then used in place of the uncompensated parity vector to make FDI decisions. Simulation results are presented in which the algorithm is tested in a realistic flight environment that includes vehicle maneuvers, the effects of turbulence, and sensor failures. The results show that the algorithm can significantly improve FDI performance, especially during vehicle maneuvers. 82/00/00 83A11129

UTTL: Strapdown inertial performance needed for the 1990s

AUTH: A/ROBINETTE, G. J.; B/SCHWARZ, R. M. PAA: A/(USAF, Avionics Laboratory, Wright-Patterson AFB, OH); B/(McDonnell Aircraft Co., Avionics Engineering Div., St. Louis, MO) In: NAECON 1982; Proceedings of the National Aerospace and Electronics Conference, Dayton, OH, May 18-20, 1982, Volume 1. (A83-11083 01-01) New York, Institute of Electrical and Electronics Engineers, Inc., 1982, p. 364-371.

ABS: A description of the Strapdown Performance Study program is presented. This program is being conducted to determine and quantify the improvements in strapdown inertial technology that will be required to meet the navigation and weapon delivery requirements associated with advanced tactical fighters (ATF) and advanced cruise missiles (ACM) of the 1990s. In addition, the results of an analysis of ATF and ACM performance goals, and the analytical procedure that was used to determine strapdown inertial reference system performance sensitivities, drivers and improvement guidelines are examined. The improvements in strapdown inertial technology that are required for the 1990s are discussed relative to the current state-of-the-art in strapdown ring-laser-gyro inertial system technology, initialization, and gravity modeling. 82/00/00 83A11127

UTTL: Test results of Litton's LN-90 series RLG INS

AUTH: A/EBNER, R. E. PAA: A/(Litton Systems, Inc., Woodland Hills, CA) In: Symposium Gyro Technology 1981; Proceedings of the Symposium, Stuttgart, West Germany, September 23, 24, 1981. (A82-47151 24-35) Duesseldorf, Deutsche Gesellschaft fuer Ortung und Navigation, 1982, p. 12.0-12.16.

ABS: Data from tests on three generations of ring laser gyros (RLGs) are presented, including flight test data and extensive laboratory test results. Gyrocompassing repeatability under laboratory conditions for two different sizes of RLGs is shown, demonstrating an extremely low random walk parameter in recent models. Examples of system performance during static navigation performance, Scorsby motion, and following 180 degree turns are presented. Accuracy is shown to be near 0.5 nm/hr CEP under all conditions with velocity errors at about 2 ft/sec per axis, rms. Block diagrams of the hardware and software are provided. 82/00/00 82A47162

UTTL: Symposium Gyro Technology 1981; Proceedings of the Symposium, Universitaet Stuttgart, Stuttgart, West Germany, September 23, 24, 1981

AUTH: A/SORG, H. PAA: A/(Stuttgart, Universitaet, Stuttgart, West Germany) Symposium sponsored by the Deutsche Gesellschaft fuer Ortung und Navigation Duesseldorf, Deutsche Gesellschaft fuer Ortung und Navigation, 1982, 573 p. In German and English. $22. (For individual items see A82-47152 to A82-47166)

ABS: Various topics on gyro technology are discussed. The subjects addressed include: a coherent optical fiber gyroscope; a fiberoptic rotation sensor with low drift; the fiberoptic rate sensor; advantages of frequency modulators in fiber gyros; investigation of ring laser gyroscope random walk experiments; investigations of magnetooptical bias elements for laser gyros; development of dynamically tuned dry gyro in Japan. Also considered are: test results of digital caged strapdown DTG's; computer automated test and screening of the QA2000 inertial grade accelerometer; line of sight stabilization; a precision roll stable platform for spinning vehicle guidance systems; ball bearings for space applications; simulation of inflight alignment of an inertial platform aided by tracking radar. 82/00/00 82A47151

UTTL: Development of a wave profiling system for the surface effect ship
AUTH: A/RANKIN, T. M.; B/KONIGSBERG, R. L. PAA: B/(Johns Hopkins University, Laurel, MD) In: International Instrumentation Symposium, 27th, Indianapolis, IN, April 27-30, 1981, Proceedings. Part 1. (A82-41776 21-35) Research Triangle Park, NC, Instrument Society of America, 1981, p. 1-8.
ABS: A wave-profiling system that provides an accurate, real-time, on-board electronic signal that is proportional to the profile of encountered waves has been installed and is operating on one of the Navy's high-speed surface effect ships. A bow-mounted altimeter is used to measure the distance from the vehicle to the water's surface, thus providing a signal that contains wave height and vehicle vertical motion. The system computes the vertical motion of the vehicle from strapdown inertial sensor signals (gyros and accelerometers) and removes the vehicle motion from the altimeter signal to yield the real-time wave profile. Details of the system design are presented including results of the at-sea evaluation. 81/00/00 82A41777

UTTL: The adaptation of a strap down formulation for processing inertial platform data
AUTH: A/HECK, M. L.; B/FINDLAY, J. T.; C/KELLY, G. M.; D/COMPTON, H. R. PAA: C/(Analytical Mechanics Associates, Inc., Hampton, VA); D/(NASA, Langley Research Center, Hampton, VA) CORP: Analytical Mechanics Associates, Inc., Hampton, Va.; National Aeronautics and Space Administration, Langley Research Center, Hampton, Va. American Institute of Aeronautics and Astronautics, Atmospheric Flight Mechanics Conference, 9th, San Diego, CA, Aug. 9-11, 1982, 7 p.
ABS: An estimator propagation formulation which ultilizes dynamic data (attitude and sensed acceleration information) from a gimballed inertial platform has been developed to aid in the Shuttle post-flight trajectory reconstruction process and aerodynamic coefficient determination studies. Unlike the classical inertial algorithms, this formulation yields a six degree-of-freedom fully coupled state and attitude estimate. Furthermore, this inertial version is shown to be independent of initial unknown platform misalignments. Results obtained using actual Inertial Measurement Unit (IMU) data and Aerodynamic Coefficient Identification Package (ACIP) strap down data from Shuttle flights are presented.
RPT#: AIAA PAPER 82-1332 82/08/00 82A39108

UTTL: Optimal control and estimation for strapdown seeker guidance of tactical missiles
AUTH: A/VERGEZ, P. L.; B/MCCLENDON, J. R. PAA: B/(USAF, Armament Laboratory, Eglin AFB, FL) Journal of Guidance, Control, and Dynamics, vol. 5, May-June 1982, p. 225, 226.
ABS: An extended Kalman filter is developed that explicitly accounts for the major error sources in a strapdown system and estimates the state information required by an advanced guidance system. The selected guidance law is derived from linear quadratic Gaussian theory, the only assumption being that the missile has instantaneous response and complete control over its acceleration. The filter processes the noise from the strapdown seeker and estimates the information needed by the guidance law referenced to the missile's body-fixed coordinate system. A detailed six-degree-of-freedom simulation of a generic bank-to-turn short range air-to-air missile was used to evaluate the guidance and estimation algorithm developed for the study. 82/06/00 82A31121

UTTL: Accuracy of the solution of kinematic equations. I - The error equation
AUTH: A/BRANETS, V. N. Kosmicheskie Issledovanila, vol. 20, Mar.-Apr. 1982, p. 184-190. In Russian.
ABS: Error equations are derived for the solution of kinematic equations by the quaternion method. It is shown that all the error sources can be reduced to an equivalent error of the primary information. Examples of determining solutions of the kinematic equations and their errors are considered, with particular attention given to the use of angular velocity as the primary information (a case typical for spacecraft attitude measurements). The present study is also pertinent to the formulation of kinematic equations for strapdown inertial navigation. 82/04/00 82A29904

UTTL: Institute of Navigation, Annual Meeting, 37th, U.S. Naval Academy, Annapolis, MD, June 9-11, 1981, Proceedings Washington, DC, Institute of Navigation, 1981, 171 p. (For individual items see A82-24644 to A82-24650)
ABS: The performance of a ring laser strapdown marine gyrocompass is considered along with a brief history of the use of marine radar, a marine NAVSTAR GPS receiver, the application of NAVSTAR differential GPS in the civilian community, the applications of a multiplexed GPS user set, and initial FAA tests on the NAVSTAR GPS Z-set. Attention is given to the Federal Radionavigation Plan, scanning strategies for Air

Traffic Control radars, the View-Nav system, operational and economic benefits deriving from use of loran-C RNAV, loran-C RNAV in mountainous areas, and an analysis of loran-C system reliability for civil aviation. A description is presented of a strapdown configured land navigation system, aspects of marine simulation, bridge simulation, and an empirical INS difference monitoring procedure used to sequence SSBN NAVAID fixes. 81/00/00 82A24643

UTTL: The application of strapdown inertial technology to Attitude and Heading Reference System requirements
AUTH: A/GILSTER, G. W. PAA: A/(Litton Industries, Guidance and Control Systems Div., Woodland Hills, CA) In: Institute of Navigation, Annual Meeting, 36th, Monterey, CA, June 23-26, 1980, Proceedings. (A82-21586 08-04) Washington, DC, Institute of Navigation, 1981, p. 48-56.
ABS: The LR-80 AHRS (Attitude and Heading Reference System) for the YAH-64 advanced attack helicopter is described. The LR-80 offers a unique AHRS solution in that it employs a strapdown inertial navigation mechanization and provides 'dynamically exact' measurement of vehicle maneuvers. A competitive system cost is achieved by the use of automatic self-calibration techniques, Doppler damping, and application of the inherent virtues of a strapdown mechanization which minimizes electromechanical complexity. The system configuration and design features are described, and flight test results for representative helicopter mission conditions are presented, showing the combined Doppler/AHRS navigation results obtained. Also considered are other potential applications for the system, including missiles and other aircraft, and the flexibility for integration with other navigation aids. 81/00/00 82A21590

UTTL: Calibrated and uncalibrated inertial navigation system performance in valid and jammed global positioning system environments
AUTH: A/BROCKSTEIN, A. J.; B/GRETHER, R. J. PAA: B/(Litton Industries, Guidance and Control Systems Div., Woodland Hills, CA) In: Institute of Navigation, Annual Meeting, 36th, Monterey, CA, June 23-26, 1980, Proceedings. (A82-21586 08-04) Washington, DC, Institute of Navigation, 1981, p. 2-10.
ABS: INS performance improvement that can be obtained in a jammed environment after calibration of INS instruments with GPS is compared with uncalibrated INS performance. In addition, gimbaled vs. strapdown INS performance is compared for two trajectories (field test conditions) during jammed and valid operations. It is shown that INS performance can be significantly enhanced during extended periods of GPS outage by prejam INS calibration using GPS. In addition, it is shown that strapdown systems are more difficult to calibrate than gimbaled systems since the major position contributors (gyros) are less observable for a maneuvering trajectory. In addition, the lack of gravity compensation in the strapdown system causes the gyro g-sensitive drift effect to be a major error source. 81/00/00 82A21587

UTTL: A single gimbal/strapdown inertial navigation system for use on spin stabilized flight test vehicles
AUTH: A/WATTS, A. C.; B/ANDREAS, R. D. PAA: B/(Sandia National Laboratory, Albuquerque, NM) In: PLANS '80 - Position Location and Navigation Symposium, Atlantic City, NJ, December 8-11, 1980, Record. (A82-18126 06-04) New York, Institute of Electrical and Electronics Engineers, Inc., 1980, p. 250-256.
ABS: A hybrid strapdown inertial navigation system intended for use on spin stabilized flight test vehicles is described. The configuration consists of three floated rate integrating gyros, one of which is used in conjunction with the gimbal, while the remaining two operate in a rate gyro mode. The navigation algorithms utilize a direction cosine matrix formulation for the attitude computation implemented in the digital computer. An accuracy model and results from a reentry flight test trajectory are presented, and the flight test performance from launch to reentry is discussed. 80/00/00 82A18149

UTTL: System concepts using Ring Laser Gyros
AUTH: A/ENGEBRETSON, H. J. PAA: A/(Rockwell International Corp., Anaheim, CA) In: PLANS '80 - Position Location and Navigation Symposium, Atlantic City, NJ, December 8-11, 1980, Record. (A82-18126 06-04) New York, Institute of Electrical and Electronics Engineers, Inc., 1980, p. 244-249.
ABS: Various system concepts based on the use of Ring Laser Gyros (RLGs) in combination with gimbals are discussed with reference to applications including long-term shipboard inertial navigation, air vehicle navigation and airborne sensor stabilization, ballistic missile guidance, and inertial guidance of space vehicles. Consideration is given to the strapdown approach, the use of gimbals for autocompensation of instrument errors, periodic instrument calibration, performance optimization in various mission phases, and controlled pointing of systems and mission sensors. 80/00/00

82A18148

UTTL: Strapdown attitude algorithms from a geometric viewpoint
AUTH: A/MCKERN, R.; B/MUSOFF, H. PAA: B/(Charles Stark Draper Laboratory, Inc., Cambridge, MA) Journal of Guidance and Control, vol. 4, Nov.-Dec. 1981, p. 657-661.
ABS: This paper derives various well-known strapdown inertial system attitude algorithms using a geometric viewpoint based on the Goodman-Robinson theorem. This theorem describes three-dimensional rotation kinematics of a rigid body. The attitude algorithms derived are the third-order quaternion and direction cosine matrix, the third-order quaternion modified to compute the cross-product term at twice the update rate and the computationally partitioned algorithm using the rotation vector and an associated quaternion. The distinguishing features of these algorithms are readily apparent from the unified derivations. In particular, the assumptions made in the computation of areas on a unit sphere using the Goodman-Robinson theorem illuminates the performance limitations of these algorithms and should be of use in deriving more efficient algorithms. 81/12/00 82A15848

UTTL: A failure detection and isolation system for tactical aircraft with separated IMUs
AUTH: A/MOTYKA, P. PAA: A/(Charles Stark Draper Laboratory, Inc., Cambridge, MA) In: NAECON 1981; Proceedings of the National Aerospace and Electronics Conference, Dayton, OH, May 19-21, 1981, Volume 1. (A82-14576 04-01) New York, Institute of Electrical and Electronics Engineers, Inc., 1981, p. 51-60.
ABS: The development and evaluation of a failure-detection and isolation (FDI) system for tactical aircraft with two physically separated inertial measurement units (IMUs) are described. Each IMU consists of four inertial instruments in a symmetrical conical array. The instrument outputs are used for both navigation and flight control, reflecting the underlying multifunction inertial reference assembly concept. FID is performed using the generalized likelihood test, and the thresholds required for FDI are defined. Digital simulation results are presented which show the operation of the FDI system over a spectrum of sensor failures and indicate the effects of these failures on navigation errors. Results show that it may be feasible to detect and isolate only the first three failures of the dual IMU system. Lever-arm compensation results in the faster detection of accelerometer failures at the expense of increased computer throughput. Finally, failures of a magnitude less than the soft-failure-detection threshold are more 81/00/00 82A14684

UTTL: Performance comparison of a dry tuned gimbal two-degree-of-freedom gyro with laser gyros and gas bearing gyros in precision attitude determination systems
AUTH: A/REDDY, P. B. PAA: A/(Teledyne Systems Co., Northridge, CA) In: NAECON 1981; Proceedings of the National Aerospace and Electronics Conference, Dayton, OH, May 19-21, 1981, Volume 1. (A82-14676 04-01) New York, Institute of Electrical and Electronics Engineers, Inc., 1981, p. 46-50.
ABS: Dynamically tuned two-degree-of-freedom gyros are designed to operate in a strapdown mode, with low gyro noise under maneuvering conditions and a high degree of reliability. A comprehensive noise model of a dry tuned SDG-5 gyro is developed using time series analysis techniques. The model parameters are compared with a recently proposed gas bearing gyro for spacecraft applications; the error magnitudes of the SDG-5 gyro are shown to be smaller. The accuracy of spacecraft attitude determination systems using laser gyros and gas bearing gyros is then compared with that of the SDG-5 gyro based system. Results show that the overall attitude determination accuracy of a dry tuned SDG-5 gyro system is better by a factor of two. 81/00/00 82A14683

UTTL: Size effects in strapdown navigators
AUTH: A/HUNG, J. C.; B/HUNTER, J. S.; C/WHITE, H. V. PAA: A/(Tennessee, University, Knoxville, TN); C/(U.S. Army, Guidance and Control Directorate, Redstone Arsenal, AL) In: National Aerospace Meeting, Trevose, PA, April 8-10, 1981, Proceedings. (A82-12626 02-01) Washington, DC, Institute of Navigation, 1981, p. 179-184.
ABS: Size effects in a strapdown inertial measurement unit (IMU) are not always ignorable. This paper presents results of a study on size effects. It is found that while each individual accelerometer has only one type of size effect, an IMU has two in general, namely, the 'mounting offset size effect' and the 'cluster size effect'. Formulas for determining IMU size effect errors are developed. Numerical examples and flight-simulation result are given to demonstrate the size effects and to reveal their effect on navigation error. It is shown that an optimum orientation for the accelerometer cluster can be chosen to minimize the navigation errors caused by size effects. It is also

shown that, in principal, size effects of an IMU can be compensated using the angular rate information available from the IMU's gyros. A size effect compensation scheme is proposed, and the associated computation algorithm is given. 81/00/00 82A12645

UTTL: Integrated satellite navigation and strapdown attitude and heading reference systems for civil air carriers
AUTH: A/HOPKINS, J. J. PAA: A/(Navigation Development Services, Inc., Northridge, CA) In: National Aerospace Meeting, Trevose, PA, April 8-10, 1981, Proceedings. (A82-12626 02-01) Washington, DC, Institute of Navigation, 1981, p. 163-170.
ABS: The potential of the integrated GPS navigator and the strapdown AHRS as a replacement for several existing avionics systems is investigated. Its application is discussed including the economic impact with regard to acquisition and maintenance. The system components and integration approach are described, and the expectations for favorable performance comparisons with its competition are presented. It is concluded that the economic and performance advantages are unmistakably outstanding. Consequently, to save costs and to safely handle increased traffic there is a strong likelihood that integrated GPS/AHRS will become the standard position, velocity, and attitude reference system for future civil aircraft. 81/00/00 82A12643

UTTL: The integrated inertial sensor assembly /IISA/ - A redundant strapdown system for advanced aircraft navigation and flight control functions
AUTH: A/DIPASQUO, M. S. PAA: A/(U.S. Naval Material Command, Naval Air Development Center, Warminster, PA) In: National Aerospace Meeting, Trevose, PA, April 8-10, 1981, Proceedings. (A82-12626 02-01) Washington, DC, Institute of Navigation, 1981, p. 153-162.
ABS: In order to achieve the benefits of an integrated inertial sensor assembly (IISA) for the next generation aircraft, the U.S. Navy has embarked on an advanced development program to demonstrate the IISA concept. This paper examines the requirements definition, the system concept formulation, and the design definition of the advanced development model (ADM) that will be used for concept validation in a later flight test program. 81/00/00 82A12642

UTTL: Simulation study of a hybrid strapdown attitude and heading reference system
AUTH: A/REID, D. B.; B/MCWILLIAM, B. N.; C/LIANG, D. F. PAA: B/(Philip A. Lapp, Ltd., Toronto, Canada); C/(Defence Research Establishment, Ottawa, Canada) In: National Aerospace Meeting, Trevose, PA, April 8-10, 1981, Proceedings. (A82-12626 02-01) Washington, DC, Institute of Navigation, 1981, p. 139-147.
ABS: The aircraft attitude and heading reference system (AHRS) considered in this paper comprises a low-accuracy strapdown inertial measurement unit (IMU), a strapdown magnetometer triad, which provides reference heading information, and air data sensors from which barometric altitude and true airspeed measurements are derived. A variable-dimension U-D factorized Kalman filter is employed to estimate the AHRS error state from the redundant sensor data. Estimated errors are fed back into the system using a combination of continuous and impulsive control methods to bound the inertial attitude, heading, and velocity errors and reduce the rate of position error growth. A data compression algorithm is employed for smoothing of incoming measurement data to enable high-rate information to be incorporated into the filtering process at minimum computational cost. The system operates in three modes: normal AHRS mode, alignment (erection) mode and magnetics calibration mode, in which the U-D filter is utilized to estimate systematic errors in the sensed magnetic field during a ground 'swing' procedure. Initial results obtained by full-scale simulation indicate that, with a low-accuracy strapdown IMU, the system can achieve roll and pitch accuracies of about 5 arc minutes (RMS) and a heading accuracy of approximately .75 degree (RMS). 81/00/00 82A12641

UTTL: Symposium Gyro Technology 1980; Proceedings of the Symposium, Universitaet Stuttgart, Stuttgart, West Germany, September 24, 25, 1980
AUTH: A/SORG, H. PAA: A/(Stuttgart, Universitaet, Stuttgart, West Germany) Symposium sponsored by the Deutsche Gesellschaft fuer Ortung und Navigation Duesseldorf, Deutsche Gesellschaft fuer Ortung und Navigation, 1981, 336 p. (For individual items see A82-11927 to A82-11933)
ABS: Papers presented include data on a gyrocompass which uses strapdown tuned rotor gyros as a solution to combat helicopter navigational problems, an autonomous, fast-reaction strapdown inertial navigation system, a north-seeking gyro with automatic calibration, and variance-covariance-component estimation of the Helmert type for gyroscopic observations. Other topics covered are the application

of strapdown inertial systems for land vehicle positioning, navigation and pointing, a gyrocompassing precision azimuth and elevation reference unit with land navigation capability, and a low cost gyro heading system for land vehicles. Further consideration is given to the development of military inertial sensor concepts, the interaction of dither and random noise in the testing of mechanically dithered ring laser gyros for inertial navigation, the design of a low cost servocontrolled rate gyro, and design considerations for direct digital control of dry-tuned gyros. 81/00/00 82A11926

UTTL: A comparative study of strapdown algorithms
AUTH: A/GIARDINA, C. R.; B/HECKATHORN, J.; C/KRASNJANSKI, D. PAA: B/(Singer Co., Kearfott Div., Wayne, NJ); C/(U.S. Naval Material Command, Naval Air Development Center, Warminster, PA) (Institute of Navigation, National Aerospace Meeting, Warminster, Pa., Apr. 8-10, 1981.) Navigation, vol. 28, Summer 1981, p. 101-105.
ABS: Four algorithms used computing the attitude matrix in a strapdown navigation system are described: Bortz 9-direction cosine, Bortz-quaternion, Lie algebra, and Cayley transform. A brief historical development of strapdown is given, and an overview of the functions of theoretic strapdown coordinate transformation representations is presented. Each algorithm has a fast cycle in which short term attitude information is computed in a three parameter array; this is then used to compute the attitude matrix in the slow cycle. In the Bortz-quaternion and Lie algebra quaternion algorithms, the attitude information is resident in the quaternion and used to compute the attitude matrix, while in the Bortz 9-direction and Cayley transform algorithms, the attitude matrix is directly updated. The attitude matrix computed from the Bortz 9-direction cosine algorithm is orthonormalized in a separate routine, whereas the Bortz quaternion and Lie algebra quaternion algorithms provide an orthogonal matrix which is normalized by dividing by the length of the quaternion. The attitude matrix computed from the Cayley transform algorithm is inherently orthonormal. For a high frequency fast cycle, the Lie algebra is shown to require minimum CPU time. 81/08/00 82A10647

UTTL: Doppler aided low accuracy strapdown inertial navigation system
AUTH: A/BAR-ITZHACK, I. Y.; B/SERFATY, D. PAA: A/(Technion - Israel Institute of Technology, Haifa, Israel) In: Guidance and Control Conference, Albuquerque, NM, August 19-21, 1981. Collection of Technical Papers. (A81-44076 21-12) New York, American Institute of Aeronautics and Astronautics, Inc., 1981, p. 206-216. Research supported by the Israel Aircraft Industries, Ltd.
ABS: This paper presents a covariance analysis of the performance of a Doppler aided low accuracy, coarsely aligned strapdown inertial navigation system (INS) whose fine alignment takes place automatically in flight. It is shown that the fine alignment in azimuth, which requires turns, consists of in-flight gyro calibration and in-flight gyrocompassing. The spacing of the turns is investigated. The influence of several position fixes is examined and it is shown that they can replace INS turns. It is also shown that the use of magnetic heading reference reduces system errors but is not necessary for the satisfactory performance of the augmented system. Two sub-optimal Kalman filters are designed and evaluated. Their small performance degradation with respect to that exhibited by the optimal filter and their low sensitivity to parameter changes is demonstrated by true covariance simulation runs.
RPT#: AIAA 81-1798 81/00/00 81A44101

UTTL: Repeated trial of guidance in space vehicles
AUTH: A/HE, L. Chinese Society of Astronautics, Journal, no. 2, 1981, p. 66-75. In Chinese, with abstract in English.
ABS: The advantages of the repeated method are discussed and attention is given to applications of the method to strap-down inertial systems. In comparing this method with others, it is noted that it offers improvements not only in reliability but also in accuracy. The proposed method makes is possible to inspect failure by means of range and to derive formulas for calculating accuracy and ineffectiveness. It is noted that the method will make the calculations simple and the operation reliable. 81/00/00 81A42274

UTTL: Fault detection, identification and reconfiguration - An emerging discipline in the development of highly reliable space systems
AUTH: A/DEYST, J. J., JR.; B/HARRISON, J. V.; C/GAI, E.; D/DALY, K. C. PAA: D/(Charles Stark Draper Laboratory, Inc., Cambridge, Mass.) American

Astronautical Society and American Institute of Aeronautics and Astronautics, Annual Meeting on Space Enhancing Technological Leadership, Boston, Mass., Oct. 20-23, 1980, AAS 15 p.

ABS: As spacecraft mission complexities have increased, there has been a trend toward autonomy in spacecraft systems. This paper examines the methodology of fault detection, identification, and reconfiguration, and considers the impact of autonomy on the development of this methodology. The application of these methods to the IUS spacecraft navigation system design is presented as an example. It is concluded that the application of GLT decision rules for FDI, the geometrical interpretation of these rules in parity space, the analytical evaluation of FDI performance, the use of Markov modeling techniques to characterize the random changes in the operational state of the system, the extension of linearized navigation system error analyses to account for the effects of component failures and sensor reconfigurations, and the quantification of performance in terms of scalar figures of merit in order to facilitate sensitivity analysis and threshold selection, represent innovative responses to the problems posed in the design and analysis of fault tolerant systems.

RPT#: AAS PAPER 80-270 80/10/00 81A33527

UTTL: Technology growth in mini-RPV systems

AUTH: A/CHRISTENSEN, G. F.; B/SCHNEELY, F. D.; C/NIEWALD, R. J. PAA: A/(U.S. Army, Aviation Research and Development Command, St. Louis, Mo.); C/(Lockheed Missiles and Space Co., Inc., Sunnyvale, Calif.)

American Institute of Aeronautics and Astronautics, Annual Meeting and Technical Display on Frontiers of Achievement, Long Beach, Calif., May 12-14, 1981, 8 p.

ABS: A review is presented of the technological evolution of the mini-RPVs (weighing 100 to 300 lbs and flying at low subsonic speeds) being developed for the U.S. Army. The initial mini-RPV activities utilized remotely controlled models as a basis for their aerodynamic configuration, engines, and radio link for command and control. The Aequare, developed in 1973-1974, included such technological improvements as an aerodynamic configuration in which the wings were telescoped and rotated to stow in a pod, and the use of elevators and rudders in a rear propeller duct for control. The Acquila target acquisition and reconnaissance system, initiated by the Army in 1974, to determine the feasibility and utility of a mini-RPV system for future Army missions, consisted of a ground control station, an air vehicle, a launcher, and a recovery system. The current Aquila development, begun in September, 1979, is a militarized version of the earlier Aquila system with greater emphasis on mobility, reliability, and maintainability, having additional performance capabilities for meeting mission requirements in target location accuracy, target designation, and enhanced survivability. The impact of technology on air vehicle structure, propulsion system, electrical power requirements, navigation, guidance and flight control system, and payloads is discussed. In the future, the RPV may be used for harassment missions or to carry ECM equipment for radar or communications jamming.

RPT#: AIAA PAPER 81-0936 81/05/00 81A32937

UTTL: High frequency angular vibration measurements in vehicles

AUTH: A/SHER, L.; B/MERRITT, P. PAA: B/(USAF, Weapons Laboratory, Kirtland AFB, N. Mex.)

American Astronautical Society, Annual Rocky Mountain Guidance and Control Conference, Keystone, Colo., Jan. 31-Feb. 4, 1981, 17 p.

ABS: The requirements for accurate and high-frequency response angular sensing in vehicles are examined. It is demonstrated that, in connection with the growth in the size of optical systems, it will not be sufficient any longer to provide devices for wide-bandwidth angular measurements, correlated about each axis. It will be necessary to conduct measurements at several locations of interest and to correlate the measurements from location to location. A description is given of results obtained with angular sensors capable of these measurements. The sensors have been used to measure several aircraft at the Air Force Weapons Laboratory. Attention is given to strapdown sensor errors, strapdown system level errors, the design of angular sensing devices, and information provided by measurements in vehicles.

RPT#: AAS PAPER 81-024 81/01/00 81A32886

UTTL: Description of a dual fail-operational redundant strapdown inertial measurement unit for integrated avionics systems research

AUTH: A/BRYANT, W. H.; B/MORRELL, F. R. PAA: B/(NASA, Langley Research Center, Flight Electronics Div., Hampton, Va.) CORP: National Aeronautics and Space Administration, Langley Research Center, Hampton, Va.

ROLM Computer Users Group Meeting, 4th, San Diego, Calif., Feb. 23-25, 1981, Paper, 10 p.

ABS: Attention is given to a redundant strapdown inertial measurement unit for integrated avionics. The system consists of four two-degree-of-freedom turned rotor gyros and four two-degree-of-freedom accelerometers in

a skewed and separable semi-octahedral array. The unit is coupled through instrument electronics to two flight computers which compensate sensor errors. The flight computers are interfaced to the microprocessors and process failure detection, isolation, redundancy management and flight control/navigation algorithms. The unit provides dual fail-operational performance and has data processing frequencies consistent with integrated avionics concepts presently planned. 81/02/00 81A26934

UTTL: Laser-gyro strapdown inertial navigation
AUTH: A/KERGOAT, M.; B/PERBET, M. PAA: A/(SV2 Crouzet-Sfena, Boulogne-Billancourt, Hauts-de-Seine, France); B/(Societe Francaise d'Equipements pour la Navigation Aerienne, Vellzy-Villacoublay, Yvelines, France) Navigation (Paris), vol. 29, Jan. 1981, p. 11-23. In French.
ABS: After brief reviews of strapdown navigation and the principles of laser gyros, the paper discusses the advantages and applications of laser-gyro strapdown systems. Performance data are given for hybrid systems and civil and military air navigation systems, and the utilization of laser gyros in such programs as Boeing 757 and 767, and Airbus A310 is briefly considered. 81/01/00 81A23868

UTTL: Strap-down inertial systems
AUTH: A/RADIX, J. C. PAA: A/(Ecole Nationale Superieure de l'Aeronautique et de l'Espace, Toulouse; Societe Nationale Industrielle Aerospatiale, Les Mureaux, Yvelines, France) Toulouse, Cepadues Editions, 1980, 367 p. In French.
ABS: The book examines the principles and components of strap-down inertial navigation systems. The general principles of inertial navigation are reviewed, including systems both with and without stabilized platforms, and the theory of attitude determination from strap-down gyroscopic measurements is discussed, with attention given to the quaternion representations of attitudes, the estimation of degradations due to structural motions and various algorithms for attitude determination. The properties of particular strap-down navigation systems on board ballistic missiles and terrestrial vehicles are considered. The design of strap-down inertial systems with redundancy at the gyroscope and accelerometer level is then treated in detail, and examples of one-, two- and three-axis redundant sensor systems are presented. 80/00/00 81A21393

UTTL: A low-noise, high-bandwidth precision gyro for space pointing
AUTH: A/BAUM, R. A.; B/SLABINSKI, R. J.; C/STURNER, B. A. PAA: C/(United Technologies Corp., Hamilton Standard Div., Farmington, Conn.) In: Guidance and control 1980; Proceedings of the Annual Rocky Mountain Conference, Keystone, Colo., February 17-21, 1980. (A81-19351 06-12) San Diego, Calif., Univelt, Inc., 1980, p. 501-550.
ABS: A digital, pulse-width modulated gyro rebalance loop design is described which provides low noise and high bandwidth capability over a single operating rate mode. The basic loop implementation is an adaptation of the existing floated, rate integrating loop mechanization employed in the USAF Inertial Upper Stage (IUS) strapdown Redundant Inertial Measurement Unit (RIMU). A single-axis demonstration unit has been fabricated which provides a single-mode rate range of plus or minus 4.5 deg/sec, a pulse weight of 0.063 arc seconds, and a bandwidth of 30 Hz. Loop noise data are presented in terms of power spectral density and noise equivalent angle traces. Bias and scale factor stability and asymmetry characteristics are also presented. The inherent flexibility of the IUS derivative gyro rebalance loop design is such that a bandwidth of 85 Hz and a pulse weight of 0.008 arc seconds is achievable, over the full plus or minus 4.5 deg/sec rate range, with minimum component modifications. Plans for such a follow-on demonstration unit are described.
RPT#: AAS 80-028 80/00/00 81A19372

UTTL: Asymptotic estimates of errors of methods for computing rigid-body attitude parameters
AUTH: A/PANOV, A. P. PAA: A/(Akademiia Nauk Ukrainskoi SSR, Institut Kibernetiki, Kiev, Ukrainian SSR) Kibernetika i Vychislitel'naia Tekhnika, no. 47, 1980, p. 59-71. In Russian.
ABS: An asymptotic method for determining the integral errors of a strapdown inertial navigation system is developed. Drift and drift rate errors are evaluated for different methods of computing directing cosines and Rodrigues-Hamilton coordinates of the finite-rotation vector. 80/00/00 81A10420

UTTL: Initial leveling of a strapdown inertial navigation system on a fixed base
AUTH: A/TKACHENKO, A. I. PAA: A/(Akademiia Nauk Ukrainskoi SSR, Institut Kibernetiki, Kiev, Ukrainian SSR) Kibernetika i Vychislitel'naia Tekhnika, no. 47, 1980, p. 55-59. In Russian.
ABS: The problem of the initial leveling of a strapdown

system on an oscillating or slowly moving base is treated as a problem of identifying the state of a stationary nonlinear system. A method for compensating the errors of angular-velocity sensors is discussed. 80/00/00 81A10419

UTTL: Reliability and accuracy prediction for a redundant strapdown navigator
AUTH: A/HARRISON, J. V.; B/DALY, K. C.; C/GAI, E. PAA: C/(Charles Stark Draper Laboratory, Inc., Cambridge, Mass.) In: Guidance and Control Conference, Danvers, Mass., August 11-13, 1980, Collection of Technical Papers. (A80-45514 19-17) New York, American Institute of Aeronautics and Astronautics, Inc., 1980, p. 403-413.
ABS: A comprehensive approach to the evaluation of the accuracy and reliability of a redundant strapdown inertial navigation system is described. The operational state of the system changes as system elements fail and as FDI decisions are made. A Markov model of the redundant system and its associated FDI algorithms is used to determine the probabilities of particular operational state time histories. Navigation system accuracies are associated with these state time histories through the use of a modified covariance analysis of the system's navigation errors. Suitable scalar figures-of-merit are used to assess the impact on performance of significant system parameters as well as FDI decision errors. The analysis is applied to a redundant navigator which is used to transfer a payload from launch to geosynchronous orbit.
RPT#: AIAA 80-1788 80/00/00 80A45564

UTTL: Similarities between classical astronomical navigation and navigation by electrostatic gyroscope
AUTH: A/SCHMIDT, J. N. PAA: A/(Rockwell International Corp., Autonetics Strategic Systems Div., Anaheim, Calif.) (Navigation, vol. 26, Autumn 1979.) Navigation (Paris), vol. 28, July 1980, p. 339-354. In French.
ABS: Similarities between classical astronomical navigation and inertial navigation by electrostatic gyroscope (ESG) are developed. Attention is given to the alignment problem and to sources of fundamental errors, such as those attributable to accelerometers, of ESG inertial systems. Cardan and strapdown systems and Kalman filtration are considered. 80/07/00 80A45075

UTTL: Orbital performance evaluation of a precision gyroscopic attitude reference system
AUTH: A/WEINSTEIN, S. P. PAA: A/(Bendix Corp., Guidance Systems Div., Teterboro, N.J.) In: Automatic control in space: Proceedings of the Eighth Symposium, Oxford, England, July 2-6, 1979. (A80-37426 15-12) Oxford, Pergamon Press, Ltd., 1980, p. 267-274.
ABS: The inertial reference assembly (IRA) of the International Ultraviolet Explorer Satellite attitude control system employs a gas bearing gyroscope as the inertial sensor. The gyroscope is operated in a binary (forced-limit-cycle) pulse rebalanced mode which uses quantized pulse-width-modulation of the gyroscope torquing signal. The performance requirements of the IRA are discussed for each operational mode: spacecraft despin, precision pointing, and precision maneuvering. Specific performance parameters include non-g sensitive drift stability, attitude reference, short and long term stability, scale factor stability and linearity, and input axis alignment stability. On-orbit performance data demonstrated an attitude reference error of 0.4 arcsec as compared to 0.5 arcsec demonstrated during laboratory testing; scale factor linearity of 40 ppm and an alignment stability of 10 arcsec demonstrated on-orbit are consistent with the laboratory results. 80/00/00 80A37459

UTTL: A description of a velocity-damped Schuler erected AHRS system
AUTH: A/KLEMES, M. S.; B/BLANCO, J. PAA: B/(Sperry Corp., Sperry Flight Systems, Phoenix, Ariz.) In: Challenge of the '80s: Proceedings of the Third Digital Avionics Systems Conference, Fort Worth, Tex., November 6-8, 1979. (A80-32417 12-06) New York, Institute of Electrical and Electronics Engineers, Inc., 1979, p. 232-239.
ABS: The paper describes the performance and design criteria for a strapdown attitude and heading reference system (AHRS) that uses a velocity-damped Schuler erection system. The design criteria are presented in terms of classical complementary filtering, and optimal statistical evaluation was conducted to assure that the classical system performance was not compromised. The velocity-damped Schuler erection system in a strapdown AHRS was discussed, and the effect of fully implementing an optimal Kalman filter was compared with the use of a suboptimal nonlinear system; it was shown that nonlinear controls must be employed which are external to the optimal linear filter to accommodate the nonstatistical, infrequent disturbances. 79/00/00 80A32449

UTTL: Symposium on Gyro Technology, Universitaet Stuttgart, Stuttgart, West Germany, September 25, 26, 1979, Proceedings

AUTH: A/SORG, H. PAA: A/(Stuttgart, Universitaet, Stuttgart, West Germany) Symposium sponsored by the Deutsche Gesellschaft fuer Ortung und Navigation Duesseldorf, Deutsche Gesellschaft fuer Ortung und Navigation, 1979, 396 p. (For individual items see A80-28212 to A80-28223)

ABS: A collection of papers is presented regarding recent advances in gyro technology. Attention is focused on a detailed discussion of dry tuned gyros. Topics of interest include strapdown gyro development, caging loops for dry tuned gyros, test of strapdown gyros, strapdown dynamically tuned gyroscopes and microprocessors to simplify their applications, error models for strapdown systems, compliant air bearing gyro/seeker, and fluid-filled inertial instruments. The contribution of the late Johannes Gievers to inertial technology is presented. 79/00/00 80A28211

UTTL: Strapdown inertial systems

AUTH: A/RADIX, J.-C. PAA: A/(Ecole Nationale Superieure de l'Aeronautique et de l'Espace, Toulouse, France) Navigation (Paris), vol. 28, Jan. 1980, p. 11-27. In French.

ABS: A basic review of strapdown navigation systems is presented. Attention is given to general principles, coordinate transformations, and the navigation principle for ballistic missiles. Finally some examples of strapdown systems are considered. 80/01/00 80A24381

UTTL: Symposium on Gyroscope Technology, Bochum, West Germany, September 18, 19, 1978, Proceedings Symposium sponsored by the Deutsche Gesellschaft fuer Ortung und Navigation, Duesseldorf, Deutsche Gesellschaft fuer Ortung und Navigation, 1979, 313 p. In German and English. $27.50. (For individual items see A80-17550 to A80-17559)

ABS: The volume consists of the papers which were presented at the Symposium on Gyro Technology 1978 of the German Institute of Navigation (DGON). A strapdown inertial reference system for future commercial airline use in navigation and flight control is presented along with an integrated strapdown guidance and control system for launch vehicle application. Consideration is given to a gyrocompass calibrator, novel gyro hinge design, effects of hinge improvements on design and production cost of a dynamically tuned gyro, and development aspects of a dynamically tuned gyro. Identification procedures for strapdown sensor parameters by system level testing, determination and evaluation of strapdown sensor parameters from system test data, and test facilities and procedures for strapdown systems are described. 79/00/00 80A17549

UTTL: Accuracy and selection of some attitude determination algorithms

AUTH: A/WEINBERGER, M. R.; B/TODMAN, D. C. PAA: A/(ESA, European Space Research and Technology Centre, Noordwijk, Netherlands); B/(British Aircraft Corp., Bristol, England) In: A link between science and applications of automatic control: Proceedings of the Seventh Triennial World Congress, Helsinki, Finland, June 12-16, 1978, Volume 2, (A80-14794 03-63) Oxford and New York, Pergamon Press, 1979, p. 1295-1301.

ABS: This paper deals with algorithms for the numerical integration of the attitude propagation equations when quaternions are used. Algorithms for sensors with rate information and with incremental angle information are studied including sensor error. Various models for local round-off error are discussed in terms of arithmetic and wordlength of the numerical processing. The propagation of attitude error is studied quantitatively, and methods for selecting the best algorithm order and time-step are given. The results presented here provide a rationale for the choice of an algorithm and an a priori estimate of the expected accuracy for given kinds of manoeuvres or pointing modes of a three-axis-controlled spacecraft. 79/00/00 80A14831

UTTL: Calibration of a low cost strapdown inertial guidance system

AUTH: A/MUSOFF, H. PAA: A/(Charles Stark Draper Laboratory, Inc., Cambridge, Mass.) In: International Instrumentation Symposium, 25th, Anaheim, Calif., May 7-10, 1979, Proceedings, Part 2, (A80-12601 02-35) Pittsburgh, Pa., Instrument Society of America, 1979, p. 569-574.

ABS: A set of techniques is presented for calibration of the inertial reference unit of a Low Cost Inertial Guidance Subsystem (LCIGS). Very large instrument error parameters are estimated without the need for external precise knowledge of the system orientation with respect to the earth rate and gravity vectors. This is made possible by utilizing the known nonlinear relations between the components of earth rate and gravity sensed by the instruments and the respective magnitudes of earth rate and gravity at the system test location in addition to the known relations between the error parameters and measurements to allow

solution of the parameters from complete sets of simultaneous equations. 79/00/00 80A12642

UTTL: Flight test results of the strapdown ring laser gyro tetrad inertial navigation system
AUTH: A/CARESTIA, R. A.; B/HRUBY, R. J.; C/BJORKMAN, W. S.
PAA: A/(Univ. of Southern Colorado, Pueblo); C/(Analytical Mechanics Associates, Mountain View, Calif.) CORP: National Aeronautics and Space Administration, Ames Research Center, Moffett Field, Calif.
ABS: A helicopter flight test program undertaken to evaluate the performance of Tetrad (a strap down, laser gyro, inertial navigation system) is described. The results of 34 flights show a mean final navigational velocity error of 5.06 knots, with a standard deviation of 3.84 knots; a corresponding mean final position error of 2.66 n. mi., with a standard deviation of 1.48 n. mi.; and a modeled mean position error growth rate for the 34 tests of 1.96 knots, with a standard deviation of 1.09 knots. No laser gyro or accelerometer failures were detected during the flight tests. Off line parity residual studies used simulated failures with the prerecorded flight test and laboratory test data. The airborne Tetrad system's failure--detection logic, exercised during the tests, successfully demonstrated the detection of simulated ""hard'' failures and the system's ability to continue successfully to navigate by removing the simulated faulted sensor from the computations. Tetrad's four ring laser gyros provided reliable and accurate angular rate sensing during the 4 yr of the test program, and no sensor failures were detected during the evaluation of free inertial navigation performance.
RPT#: NASA-TM-84358 A-9315 NAS 1.15:84358 83/10/00 84N11157

UTTL: Dual-seeker measurement processing for tactical missile guidance
AUTH: A/WESTON, A. C. CORP: Air Force Inst. of Tech., Wright-Patterson AFB, Ohio. CSS: (School of Engineering.)
ABS: The available measurements from a strapdown seeker and a gimballed seeker onboard an air-to-ground anti-radiation missile are analyzed through an extended Kalman filter simulation. Detailed models of both seekers are developed. Only angular measurements are assumed available from the seekers: angle measurements from the strapdown seeker and angle and angle-rate measurements from the gimballed seeker. A 6-state extended Kalman filter model is used to estimate the ground target's position and relative velocity using the seeker's measurements. Four measurement policies are compared to analyze use of the gimballed seeker early in the missile flight and loss of the strapdown seeker in midflight. The results revealed an observability problem in one channel of the filter, that along the range vector. Analyses were made only by comparisons of performance in the other two channels. The comparisons showed insignificant degradation to filter performance through loss of the strapdown seeker at midflight, and substantial benefit from use of the gimballed seeker as early as possible in the flight.
RPT#: AD-A124725 AFIT/GE/EE/82D-70 82/12/00 83N25753

UTTL: Reliability analysis and fault-tolerant system development for a redundant strapdown inertial measurement unit
AUTH: A/MOTYKA, P. CORP: Draper (Charles Stark) Lab., Inc., Cambridge, Mass.
ABS: A methodology is developed and applied for quantitatively analyzing the reliability of a dual, fail-operational redundant strapdown inertial measurement unit (RSDIMU). A Markov evaluation model is defined in terms of the operational states of the RSDIMU to predict system reliability. A 27 state model is defined based upon a candidate redundancy management system which can detect and isolate a spectrum of failure magnitudes. The results of parametric studies are presented which show the effect on reliability of the gyro failure rate, both the gyro and accelerometer failure rates together, false alarms, probability of failure detection, probability of failure isolation, and probability of damage effects and mission time. A technique is developed and evaluated for generating dynamic thresholds for detecting and isolating failures of the dual, separated IMU. Special emphasis is given to the detection of multiple, nonconcurrent failures. Digital simulation time histories are presented which show the thresholds obtained and their effectiveness in detecting and isolating sensor failures.
RPT#: NASA-CR-166050 NAS 1.26:166050 CSDL-R-1588 83/03/00 83N20926

UTTL: Development of low cost multifunction sensors for lightweight fire and forget antitank weapon system
AUTH: A/HUNTER, J. S.; B/HUNG, J. C. PAA: B/(Tennessee Univ.) CORP: Army Missile Command, Redstone Arsenal, Ala. CSS: (Guidance and Control Directorate.) In AGARD Precision Guided Spacecraft, Technol. and Operational Aspects 17 p (SEE N83-18390 08-66)

ABS: The design description, operation, and preliminary evaluation of a multifunction sensing device that is capable of measuring two axes of angular rate and two axes of linear acceleration from a single instrument are discussed. The equations for obtaining three axes of angular rate and three axes of linear acceleration from a single instrument are also developed. Test data is presented that illustrates state-of-the-art performance on available multifunction sensors. Finally, methods of improving the performance of multifunction sensors are discussed. 82/09/00 83N18396

UTTL: Inertial navigation system error model considerations in Kalman filter applications
AUTH: A/HUDDLE, J. R. CORP: Litton Industries, Woodland Hills, Calif. CSS: (Guidance and Control Systems Div.) In AGARD Advan. in the Tech. and Technol. of the Appl. of Nonlinear Filters and Kalman Filters 9 p (SEE N82-29989 20-64)
ABS: The full linear model describing the propagation of error for inertial navigation systems employing the local level, wander azimuth mechanization equations is developed. The model applies to Schuler tuned, space stable or strapdown inertial system instrumentations. For this model, alternative approximate linear models are developed which in different operational applications proved adequate as "design models" for the application of Kalman estimation theory. 82/03/00 82N30002

UTTL: New sensor concepts: Low cost vibrating beam accelerometer
AUTH: A/ALBERT, W. C. CORP: Singer Co., Fairfield, N. J. AFWAL
ABS: Engineering model accelerometers have been assembled and tested to assess their potential for use in future strapped down inertial systems. The accelerometer concept investigated uses vibrating quartz crystal beams as the basic force sensing element. This concept has an inherent digital output and the potential for meeting the performance goals of bias stability of less than 100ug, scale factor stability less than 100ppm, input range at least 10g, bias temperature sensitivity on the order of 1ug/deg C and scale factor temperature sensitivity on the order of 1ppm/deg C. The accelerometer mechanization utilizes two force sensing crystals in a push pull arrangement to enhance the scale factor and cancel non-linear and thermal effects. Test data on engineering units is presented and recommendations for future development tasks are made.

RPT#: AD-A113644 KD-81-27 AFWAL-TR-81-1219 81/12/00 82N28272

UTTL: Study of Strapdown Inertial Optical Systems (SIOS) for future ESA spacecraft, volume 2 CORP: Royal Aircraft Establishment, Farnborough (England).; British Aerospace Dynamics Group, Bristol (England). CSS: (Space Dept.) ESA
ABS: A baseline (Kalman filter) SIOS, consisting of a set of high performance gyros, two or more star mappers and an onboard processor, is described. Centralized and modular data processing are considered. Control systems are specified and the performance of the attitude measurement and control system, using a Kalman filter, is simulated for low orbit Earth pointing cases and for a celestial target mission. Geostationary missions studies assumed the use of a simple constant gain filter and RF sensor, although results with the baseline system are included. The former approach is adequate, but the autonomy of optical systems is attractive. Kalman filter system performance is impressive for an Earth pointing satellite, and the whole system is immune to high noise levels, but geometrical misalignments limit absolute pointing accuracy. Analysis reveals doubt as to whether the Kalman filter is necessary, although its inclusion is not difficult.
RPT#: ESA-CR(P)-1549-VOL-2 81/03/00 82N27354

UTTL: Study of Strapdown Inertial Optical Systems (SIOS) for future ESA spacecraft, volume 1 CORP: Royal Aircraft Establishment, Farnborough (England).; British Aerospace Dynamics Group, Bristol (England). CSS: (Space Dept.) ESA
ABS: A baseline (Kalman filter) SIOS, consisting of a set of high performance gyros, two or more star mappers and an onboard processor, is described. Centralized and modular data processing are considered. Control systems are specified and the performance of the attitude measurement and control system, using a Kalman filter, is simulated for low orbit Earth pointing cases and for a celestial target mission. Geostationary mission studies assumed the use of a simple constant gain filter and RF sensor, although results with the baseline system are included. The former approach is adequate, but the autonomy of optical systems is attractive. Kalman filter system performance is impressive for an Earth pointing satellite, and the whole system is immune to high noise levels, but geometrical misalignments limit absolute pointing accuracy. Analysis reveals doubt as to whether the Kalman filter is necessary, although

its inclusion is not difficult.
RPT#: ESA-CR(P)-1549-VOL-1 81/03/00 82N27353

UTTL: Study on strapdown inertial navigation redundant sensor system
AUTH: A/SHINGU, H. CORP: National Aerospace Lab., Tokyo (Japan).
ABS: An efficient method of increasing the reliability of a strapdown inertial navigator by use of a redundant sensor is described along with a preliminary technique to detect and isolate the sensor failures, and how to determine the tolerance limits of the detection delay. The reliability and the accuracy of various redundant systems using four five and six-sensor are analyzed. It is found that models of nonorthogonal orientation have higher reliability than those of orthogonal orientation using the same number of sensors. If the sensor arrays are optimum, the improvement of accuracy was found to be 13.4%, 22.5%, and 29.3% for four five and six-sensor systems in comparison with conventional three-sensor arrays when all sensors are operating normally. A trail to detect a sensor failure and to find a way to compensate for performance degradation of a system is done by using a set of parity equations. The system is a six-sensor array. The method is one of substituting the integrated values of the sensor data into those equations in order that the detection performance be better. The detection is evaluated as a quantitative relation to the navigational error on the assumption that a redundant system is employed for a mission.
RPT#: NAL-TR-660 ISSN-0389-4010 81/00/00 82N12058

UTTL: Identification and determination of strapdown error-parameters by laboratory testing
AUTH: A/JOOS, D. K.; B/KROGMANN, U. K. CORP: Bodenseewerk Geraetetechnik G.m.b.H., Ueberlingen (West Germany).
In AGARD Advances in Inertial Navigation Systems and Components 37 p (SEE N81-31172 22-04)
ABS: The performance of an inertial navigation system (INS) is largely affected by a number of important error sources, where most of which are related to the instruments used. This particularly applies to strapdown systems. Laboratory test procedures are described which determine static and dynamic parameters of the gyro and accelerometer measurement model. It is shown that a proper rate test and a multiposition test with respect to Earth rate and gravity vector are well suited to ascertain static parameters with sufficient accuracy. Optimal parameter values are retrieved from measured test data applying regression analysis techniques. It is shown how uncertainties in parameter estimates can be determined from actual measurement residues. The verification of major dynamic performance parameters of interest by appropriate test procedures utilizing a three axes test table is shown. Applicability and feasibility of the proposed test procedures are demonstrated utilizing the modular strapdown system. 81/04/00 81N31179

UTTL: Advances in inertial navigation systems and components
AUTH: A/SORG, H. W. CORP: Advisory Group for Aerospace Research and Development, Neuilly-Sur-Seine (France).
RPT#: AGARD-AG-254 ISBN-92-835-1383-5 AD-A101446 81/04/00 81N31172

UTTL: Sensitivity study of strapdown inertial sensors in high performance applications
AUTH: A/RYAN, J. E. CORP: Air Force Inst. of Tech., Wright-Patterson AFB, Ohio. CSS: (School of Engineering.)
ABS: This study uses a computer simulation of a strapdown laser gyro inertial reference system to analyze the errors generated as a result of highly dynamic flight profiles. A stochastic error model using state-of-the-art inertial sensors is developed in detail and implemented in software. SOFE, a generalized simulation program, was used to implement both a Monte Carlo simulation and a covariance analysis. The Monte Carlo method was selected to perform the error analysis. Two highly dynamic flight trajectories were developed using the flight profile generator, PROFGEN. The PROFGEN program itself was modified to include an aircraft roll time constant and a roll-only maneuver. The errors generated in the inertial reference system as a result of these flight trajectories were investigated. Both an error budget and an analysis of the maneuvers inducing these errors were accomplished. Gyro error sources induced the most system error and coupled the dynamics of the flight trajectory into the variations of the error. Misalignment was found to be the major cause of both the accelerometer and gyro induced error. Successive maneuvers were found that reinforced system errors and other maneuvers were found that cancelled these errors. Also, some cases were found where the amount of system error varied with a change in heading.
RPT#: AD-A100825 AFIT/GE/EE/80D-38 80/12/00 81N28078

UTTL: Precision Positioning and Inertial Guidance Sensors: Technology and Operational Aspects CORP: Advisory Group for Aerospace Research and Development. Neuilly-Sur-Seine (France). Symp. held at London, 14-17 Oct. 1980
RPT#: AGARD-CP-298 ISBN-92-835-0287-6 AD-A101019 81/03/00 81N28091

UTTL: Estimation and statistical averaging applied to redundant strapped down inertial sensors for navigation and flight control
AUTH: A/BELL, J. W. CORP: Air Force Wright Aeronautical Labs., Wright-Patterson AFB, Ohio. CSS: (Advanced Aircraft Navigation Section.)
ABS: The concept of providing inertial data to satisfy on-board avionic functions from an integrated, strapped down, redundant inertial sensor reference system is presently receiving attention for military and commercial aircraft applications. Strapped down inertial sensors are well suited for flight control. However, in the highly dynamic environment of high performance aircraft, the present accuracy provided by strapped down inertial reference systems (IRS) is insufficient to meet navigation and weapon delivery requirements. Performance improvement of an IRS employing redundant strapped down inertial sensors of specified ensemble is the subject of this study. Two techniques to improve the performance are considered. One technique is to combine all redundant data from non-failed sensors, through a statistical average, into a orthogonal triac inertial reference frame. This is accomplished by weighted-least-squares averaging. A second technique is the use of an improved gyro and accelerometer output and output rate estimation scheme. Estimation algorithms are developed using Kalman Filter theory and evaluated in a highly dynamic environment. Least-squares averaging of the redundant sensor data can significantly improve the navigation system performance. However, sensor misalignment errors must be minimized such that they are not the dominant sensor error source.
RPT#: AD-A094465 AFWAL-TR-80-1088 80/09/00 81N19133

UTTL: Failure detection and isolation analysis of a redundant strapdown inertial measurement unit
AUTH: A/MOTYKA, P.; B/LANDEY, M.; C/MCKERN, R CORP: Draper (Charles Stark) Lab., Inc., Cambridge, Mass.
ABS: The objective of this study was to define and develop techniques for failure detection and isolation (FDI) algorithms for a dual fail/operational redundant strapdown inertial navigation system are defined and developed. The FDI techniques chosen include provisions for hard and soft failure detection in the context of flight control and navigation. Analyses were done to determine error detection and switching levels for the inertial navigation system, which is intended for a conventional takeoff or landing (CTOL) operating environment. In addition, investigations of false alarms and missed alarms were included for the FDI techniques developed, along with the analyses of filters to be used in conjunction with FDI processing. Two specific FDI algorithms were compared: the generalized likelihood test and the edge vector test. A deterministic digital computer simulation was used to compare and evaluate the algorithms and FDI systems.
RPT#: NASA-CR-165658 R-1414 81/02/00 81N18035

UTTL: Strapdown seeker technology for the terminal guidance of tactical weapons
AUTH: A/EHRICH, R. D.; B/VERGEZ, P. PAA: B/(Air Force Armament Lab., Eglin AFB, Fla.) CORP: Rockwell International Corp., Columbus, Ohio. In AGARD Guidance and Control Aspects of Tactical Air-launched Missiles 15 p (SEE N81-16092 07-15)
ABS: Strapdown or body fixed seekers with sufficient field of view for the terminal guidance of many tactical weapons are now approaching state of the art. Such seekers have a number of advantages over gimballed seekers, including increased reliability and unlimited line of sight rate capability. The major disadvantage is that inertial line of sight rates are not directly available for the implementation of proportional navigation. To form line of sight rates, the seeker output must be combined with inertial sensor measurements. This, however, results in a potential instability due to seeker gain errors. This problem has been minimized by a dither adaptive parameter identification approach for the measurement and correction of seeker errors. Simulation studies indicate the performance of such systems can be comparable to that of gimballed seekers. The basic principles and problems involved with mechanizing proportional navigation with strapdown seekers are considered and performance results for the dither adaptive technique are presented. 80/10/00 81N16094

UTTL: A single gimbal/strapdown inertial navigation system for use on spin stabilized flight test vehicles
AUTH: A/WATTS, A. C.; B/ANDREAS, R. D. CORP: Sandia Labs., Albuquerque, N. Mex.
ABS: A hybrid strapdown inertial navigation system intended for use on spin stabilized flight test vehicles is

described. The configuration of the navigator consists of three floated rate integrating gyros, one of which is used in conjunction with the remaining two operated in a rate gyro mode. Outputs from the two strapdown gyros and three accelerometers are digitized and processed by a high performance computer. The navigation algorithms utilize a direction cosine matrix formulation for the attitude computation implemented in the digital computer. The implementation of this algorithm for the single gimbal configuration is described. An accuracy model and results for a reentry vehicle flight test trajectory are presented. Finally, the flight test performance from launch to reentry is presented.

RPT#: SAND-80-2479C CONF-801211-1 80/00/00 81N16037

UTTL: Inertial navigation and guidance. Citations from the International Aerospace Abstracts data base

AUTH: A/MAUK, S. C. CORP: New Mexico Univ., Albuquerque. CSS: (Technology Application Center.)

ABS: A bibliography containing 263 citations is presented which addresses all aspects of inertial navigation and guidance. Included are articles concerning air navigation, navigation instruments and aids, aircraft guidance, missile control, strapdown inertial guidance, gyroscopes, stabilized platforms, position and instrument errors, error analysis, and accelerometers. Civil, commercial and military applications are covered.

RPT#: NASA-CR-163838 P880-815640 NTIS/PS-79/0825 80/09/00 81N13946

UTTL: A microprocessor application to a strapdown laser gyro navigator

AUTH: A/GIARDINA, C.; B/LUXFORD, E. CORP: Singer-Kearfott, Little Falls, N. J. In NASA, Goddard Space Flight Center Aerospace Appl. of Microprocessors p 73-78 (SEE N81-11644 02-60)

ABS: The replacement of analog circuit control loops for laser gyros (path length control, cross axis temperature compensation loops, dither servo and current regulators) with digital filters residing in microcomputers is addressed. In addition to the control loops, a discussion is given on applying the microprocessor hardware to compensation for coning and skulling motion where simple algorithms are processed at high speeds to compensate component output data (digital pulses) for linear and angular vibration motions. Highlights are given on the methodology and system approaches used in replacing differential equations describing the analog system in terms of the mechanized difference equations of the microprocessor. Standard one for one frequency domain techniques are employed in replacing analog transfer functions by their transform counterparts. Direct digital design techniques are also discussed along with their associated benefits. Time and memory loading analyses are also summarized, as well as signal and microprocessor architecture. Trade offs in algorithm, mechanization, time/memory loading, accuracy, and microprocessor architecture are also given. 80/00/00 81N11655

UTTL: Laser gyroscopes. Citations from the International Aerospace Abstracts data base

AUTH: A/YOUNG, C. G. CORP: New England Research Application Center, Storrs, Conn.

ABS: Laser inertial rotation sensors are detailed in this collection of 146 citations from the world literature. Ring lasers, fiberoptic ring lasers, and laser or optical gyroscopes are designations used and discussed here. Technical problems, such as mode coupling and competition, stray scattering, error sources, and analyses, are treated. The design, engineering, construction, and performance of operational hardware are described.

RPT#: NASA-CR-163650 P880-809130 80/05/00 81N10355

UTTL: Inertial navigation and guidance. Citations from the NTIS data base

AUTH: A/REED, W. E. CORP: National Technical Information Service, Springfield, Va.

ABS: The bibliography cites research reports on the design, development, performance, equipment, and applications of inertial navigation and guidance systems. Reports on strapdown systems are included. This updated bibliography contains 217 abstracts, 20 of which are new entries to the previous edition.

RPT#: P880-812415 NTIS/PS-79/0762 NTIS/PS-78/0735 80/07/00 80N33389

UTTL: The impact of global positioning system on guidance and controls systems design of military aircraft. Volume 2D: Specific study no. 4, gyro accuracy requirements in a strap down inertial navigation system with GPS aiding for RPV missions

AUTH: A/HURRASS, K.; B/WINTER, H. PAA: B/(Inst. fuer Flugfuehrung, Flughafen, Germany); A/(Inst. fuer Flugfuehrung, Flughafen, Germany) CORP: Advisory Group for Aerospace Research and Development, Neuilly-Sur-Seine (France).

ABS: The influence of the NAVSTAR Global Positioning System aiding of a strap-down system on the accuracy

requirements for the gyros was investigated for a remotely piloted vehicle.
RPT#: AGARD-AR-147-VOL-2D AD-A082957 80/02/00 80N23294

UTTL: Methods for strap-down attitude estimation and navigation with accelerometers
AUTH: A/OFFEREINS, R. P.; B/TIERNEGO, M. J. L. CORP: Twente Univ. of Technology, Enschede (Netherlands). CSS: (Dept. of Electrical Engineering.) In AGARD Advan. in Guidance and Control Systems Using Digital Tech. 20 p (SEE N80-14017 05-01)
ABS: Methods are presented for calculating the attitude of a vehicle from the signals of three linear and three angular accelerometers which are rigidly attached to the vehicle. Also course, velocity and position measurements relative to some object can be used. Apart from the attitude, the velocity and position, with respect to this object, are also obtained as output signals. In fire control systems, filters for target position prediction and attitude determination can be combined in this way. 79/08/00 80N14034

UTTL: Development of aiding GPS/strapdown inertial navigation system
AUTH: A/LIANG, D. F.; B/REID, D. B.; C/JOHNSON, R. H.; D/FLETCHER, B. G. PAA: B/(Lapp (Philip A.) Ltd., Toronto); C/(S and S Software Ltd., Ottawa) CORP: Defence Research Establishment, Ottawa, (Ontario). In AGARD Advan. in Guidance and Control Systems Using Digital Tech. 15 p (SEE N80-14017 05-01)
ABS: An overview is presented of the design and development of an integrated multisensor navigation system comprised of a NAVSTAR GPS receiver, an aiding strapdown inertial navigation system (ASIN) and a number of auxiliary sensors, namely, air data and strapdown magnetic sensors. In the present phase, comprehensive software packages were developed to simulate all the subsystems used. A modular and computationally efficient Kalman filtering algorithm was designed and implemented for the integration of the GPS and ASIN. During the course of the development, two techniques were developed. An exact algorithm was derived to transform inertially referenced data into geographic coordinates. Also, a dual channel attitude algorithm was formulated which increases the bandwidth of the attitude computation in the strapdown navigator. Other routines developed include the baro-damping algorithm, auxiliary sensor processing and calibration routines. To provide a baseline level of performance, simulation results were obtained for future flight testing of the hardware. 79/08/00 80N14031

REPORT DOCUMENTATION PAGE			
1. Recipient's Reference	2. Originator's Reference AGARD-LS-133	3. Further Reference ISBN 92-835-0351-1	4. Security Classification of Document UNCLASSIFIED

5. Originator	Advisory Group for Aerospace Research and Development North Atlantic Treaty Organisation 7 rue Ancelle, 92200 Neuilly sur Seine, France
6. Title	ADVANCES IN STRAPDOWN INERTIAL SYSTEMS
7. Presented at	Athens, Greece on 14–15 May 1984; Rome, Italy on 17–18 May 1984; and Copenhagen, Denmark on 21–22 May 1984.

8. Author(s)/Editor(s)	9. Date
Various	April 1984
10. Author's/Editor's Address	**11. Pages**
Various	228

12. Distribution Statement	This document is distributed in accordance with AGARD policies and regulations, which are outlined on the Outside Back Covers of all AGARD publications.

13. Keywords/Descriptors

Inertial guidance	Strapdown systems
Inertial navigation	Aircraft

14. Abstract

This Lecture Series is intended to address the advances in strapdown inertial system technology during the last five years. Areas that are addressed include advances in the strapdown instruments and computational algorithms and the applications to commercial aircraft, remotely piloted vehicles, flight controls, instrumentation, and navigation problems in general. This provides one document which covers the present state-of-the-art in strapdown systems technology.

The material in this publication was assembled to support a Lecture Series under the sponsorship of the Guidance and Control Panel and the Consultant and Exchange Programme of AGARD.

AGARD Lecture Series No.133 Advisory Group for Aerospace Research and Developm nt, NATO ADVANCES IN STRAPDOWN INERTIAL SYSTEMS Published April 1984 228 pages This Lecture Series is intended to address the advances in strapdown inertial system technology during the last five years. Areas that are addressed include advances in strapdown instruments and computational algorithms and the applications to commercial aircraft, remotely piloted vehicles, flight controls, instrumentation, and navigation problems in general. This provides one document which covers the present state-of-the-art in strapdown systems technology. P.T.O.	AGARD-LS-133 Inertial guidance Inertial navigation Strapdown systems Aircraft	AGARD Lecture Series No.133 Advisory Group for Aerospace Research and Development, NATO ADVANCES IN STRAPDOWN INERTIAL SYSTEMS Published April 1984 228 pages This Lecture Series is intended to address the advances in strapdown inertial system technology during the last five years. Areas that are addressed include advances in strapdown instruments and computational algorithms and the applications to commercial aircraft, remotely piloted vehicles, flight controls, instrumentation, and navigation problems in general. This provides one document which covers the present state-of-the-art in strapdown systems technology. P.T.O.	AGARD-LS-133 Inertial guidance Inertial navigation Strapdown systems Aircraft
AGARD Lecture Series No.133 Advisory Group for Aerospace Research and Development, NATO ADVANCES IN STRAPDOWN INERTIAL SYSTEMS Published April 1984 228 pages This Lecture Series is intended to address the advances in strapdown inertial system technology during the last five years. Areas that are addressed include advances in strapdown instruments and computational algorithms and the applications to commercial aircraft, remotely piloted vehicles, flight controls, instrumentation, and navigation problems in general. This provides one document which covers the present state-of-the-art in strapdown systems technology. P.T.O.	AGARD-LS-133 Inertial guidance Inertial navigation Strapdown systems Aircraft	AGARD Lecture Series No.133 Advisory Group for Aerospace Research and Development, NATO ADVANCES IN STRAPDOWN INERTIAL SYSTEMS Published April 1984 228 pages This Lecture Series is intended to address the advances in strapdown inertial system technology during the last five years. Areas that are addressed include advances in strapdown instruments and computational algorithms and the applications to commercial aircraft, remotely piloted vehicles, flight controls, instrumentation, and navigation problems in general. This provides one document which covers the present state-of-the-art in strapdown systems technology. P.T.O.	AGARD-LS-133 Inertial guidance Inertial navigation Strapdown systems Aircraft

The material in this publication was assembled to support a Lecture Series under the sponsorship of the Guidance and Control Panel and the Consultant and Exchange Programme of AGARD on 14–15 May 1984 in Athens, Greece; 17-18 May 1984 in Rome, Italy; and 21–22 May 1984 in Copenhagen, Denmark.

ISBN 92-835-0351-1

The material in this publication was assembled to support a Lecture Series under the sponsorship of the Guidance and Control Panel and the Consultant and Exchange Programme of AGARD on 14–15 May 1984 in Athens, Greece; 17-18 May 1984 in Rome, Italy; and 21–22 May 1984 in Copenhagen, Denmark.

ISBN 92-835-0351-1

The material in this publication was assembled to support a Lecture Series under the sponsorship of the Guidance and Control Panel and the Consultant and Exchange Programme of AGARD on 14–15 May 1984 in Athens, Greece; 17-18 May 1984 in Rome, Italy; and 21–22 May 1984 in Copenhagen, Denmark.

ISBN 92-835-0351-1

The material in this publication was assembled to support a Lecture Series under the sponsorship of the Guidance and Control Panel and the Consultant and Exchange Programme of AGARD on 14–15 May 1984 in Athens, Greece; 17-18 May 1984 in Rome, Italy; and 21–22 May 1984 in Copenhagen, Denmark.

ISBN 92-835-0351-1

AGARD
NATO OTAN
7 RUE ANCELLE · 92200 NEUILLY-SUR-SEINE
FRANCE
Telephone 745.08.10 · Telex 610176

DISTRIBUTION OF UNCLASSIFIED AGARD PUBLICATIONS

AGARD does NOT hold stocks of AGARD publications at the above address for general distribution. Initial distribution of AGARD publications is made to AGARD Member Nations through the following National Distribution Centres. Further copies are sometimes available from these Centres, but if not may be purchased in Microfiche or Photocopy form from the Purchase Agencies listed below.

NATIONAL DISTRIBUTION CENTRES

BELGIUM
Coordonnateur AGARD – VSL
Etat-Major de la Force Aérienne
Quartier Reine Elisabeth
Rue d'Evere, 1140 Bruxelles

CANADA
Defence S
Departm
Ottawa, C

DENMARK
Danish De
Østerbrog
Copenhag

FRANCE
O.N.E.R.A
29 Avenue
92320 Châ

GERMANY
Fachinform
Physik, Mat
Kernforschu
D-7514 Egg

GREECE
Hellenic Air
Research and
Holargos, At

ICELAND
Director of Aviation
c/o Flugrad
Reykjavik

ITALY
Aeronautica Militare
Ufficio del Delegato Nazionale all'AGARD
3, Piazzale Adenauer
Roma/EUR

UNITED KINGDOM
Defence Research Information Centre
Station Square House
St. Mary Cray
Orpington, Kent BR5 3RE

UNITED STATES
National Aeronautics and Space Administration (NASA)
Langley Field, Virginia 23365
Attn: Report Distribution and Storage Unit

THE UNITED STATES NATIONAL DISTRIBUTION CENTRE (NASA) DOES NOT HOLD STOCKS OF AGARD PUBLICATIONS, AND APPLICATIONS FOR COPIES SHOULD BE MADE DIRECT TO THE NATIONAL TECHNICAL INFORMATION SERVICE (NTIS) AT THE ADDRESS BELOW.

PURCHASE AGENCIES

Microfiche or Photocopy
National Technical
Information Service (NTIS)
5285 Port Royal Road
Springfield
Virginia 22161, USA

Microfiche
ESA/Information Retrieval Service
European Space Agency
10, rue Mario Nikis
75015 Paris, France

Microfiche or Photocopy
British Library Lending
Division
Boston Spa, Wetherby
West Yorkshire LS23 7BQ
England

Requests for microfiche or photocopies of AGARD documents should include the AGARD serial number, title, author or editor, and publication date. Requests to NTIS should include the NASA accession report number. Full bibliographical references and abstracts of AGARD publications are given in the following journals:

Scientific and Technical Aerospace Reports (STAR)
published by NASA Scientific and Technical
Information Branch
NASA Headquarters (NIT-40)
Washington D.C. 20546, USA

Government Reports Announcements (GRA)
published by the National Technical
Information Services, Springfield
Virginia 22161, USA

Printed by Specialised Printing Services Limited
40 Chigwell Lane, Loughton, Essex IG10 3TZ

ISBN 92-835-0351-1